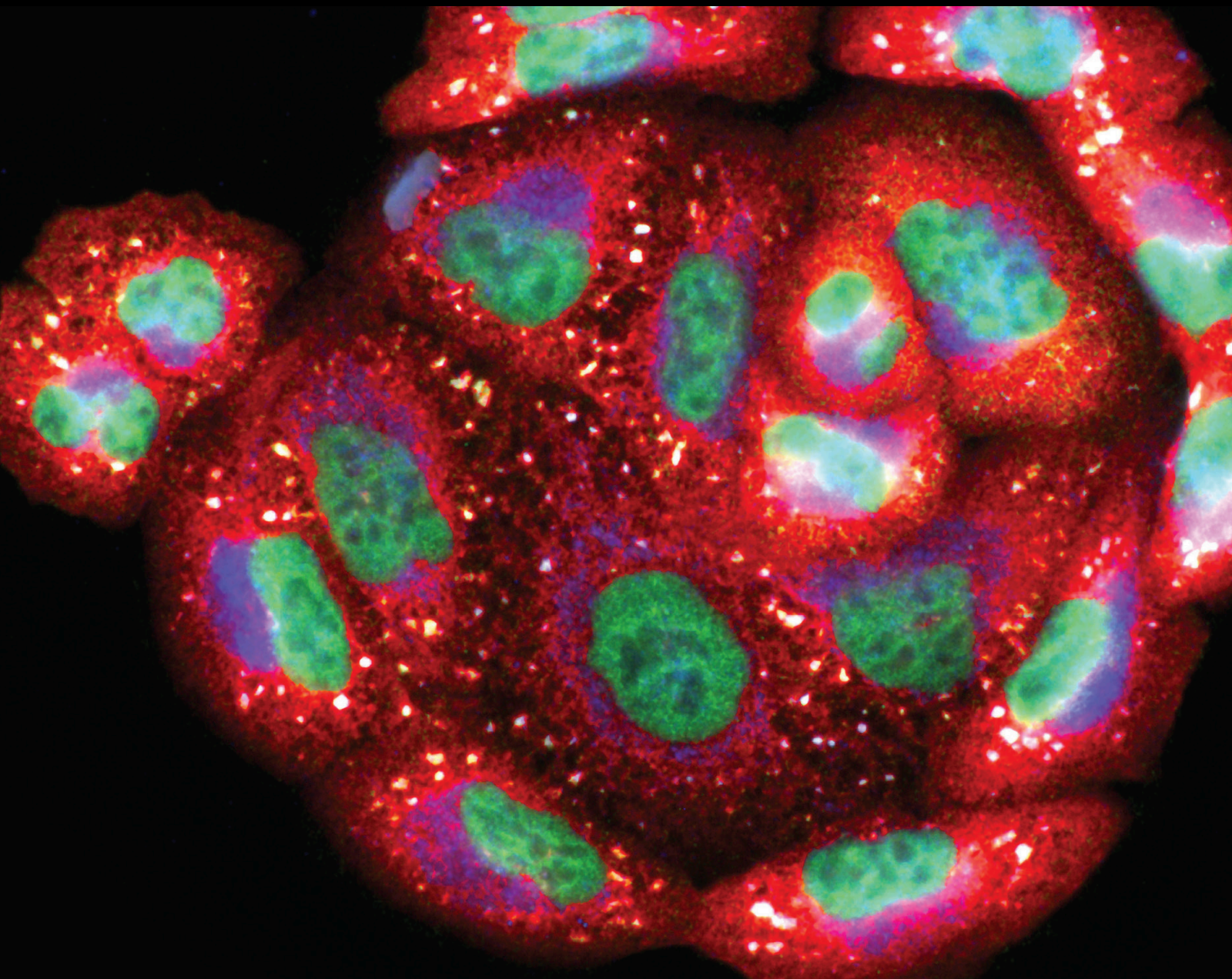


Oxidative Stress and Tissue Repair: Mechanism, Biomarkers, and Therapeutics

Lead Guest Editor: Reggiani Vilela Gonçalves

Guest Editors: Andrea M. A. Costa and Lukasz Grzeskowiak





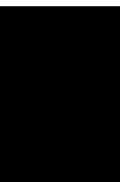
**Oxidative Stress and Tissue Repair:
Mechanism, Biomarkers, and Therapeutics**

Oxidative Medicine and Cellular Longevity

**Oxidative Stress and Tissue Repair:
Mechanism, Biomarkers, and
Therapeutics**

Lead Guest Editor: Reggiani Vilela Gonçalves

Guest Editors: Andrea M. A. Costa and Lukasz
Grzeskowiak



Copyright © 2021 Hindawi Limited. All rights reserved.

This is a special issue published in "Oxidative Medicine and Cellular Longevity" All articles are open access articles distributed under the Creative Commons Attribution License, which permits unrestricted use, distribution, and reproduction in any medium, provided the original work is properly cited.

Chief Editor

Jeannette Vasquez-Vivar, USA

Editorial Board

Ivanov Alexander, Russia
Fabio Altieri, Italy
Fernanda Amicarelli, Italy
José P. Andrade, Portugal
Cristina Angeloni, Italy
Antonio Ayala, Spain
Elena Azzini, Italy
Peter Backx, Canada
Damian Bailey, United Kingdom
Sander Bekeschus, Germany
Ji C. Bihl, USA
Consuelo Borrás, Spain
Nady Braidy, Australia
Ralf Braun, Austria
Laura Bravo, Spain
Amadou Camara, USA
Gianluca Carnevale, Italy
Roberto Carnevale, Italy
Angel Catalá, Argentina
Peter Celec, Slovakia
Giulio Ceolotto, Italy
Shao-Yu Chen, USA
Ferdinando Chiaradonna, Italy
Zhao Zhong Chong, USA
Xinxin Ci, China
Alin Ciobica, Romania
Ana Cipak Gasparovic, Croatia
Giuseppe Cirillo, Italy
Maria R. Ciriolo, Italy
Massimo Collino, Italy
Graziamaria Corbi, Italy
Manuela Corte-Real, Portugal
Mark Crabtree, United Kingdom
Manuela Curcio, Italy
Andreas Daiber, Germany
Felipe Dal Pizzol, Brazil
Francesca Danesi, Italy
Domenico D'Arca, Italy
Sergio Davinelli, Italy
Claudio De Lucia, USA
Yolanda de Pablo, Sweden
Cinzia Domenicotti, Italy
Joël R. Drevet, France
Grégory Durand, France
Anne Eckert, Switzerland
Javier Egea, Spain
Pablo A. Evelson, Argentina
Stefano Falone, Italy
Ioannis G. Fatouros, Greece
Qingping Feng, Canada
Gianna Ferretti, Italy
Giuseppe Filomeni, Italy
Swaran J. S. Flora, India
Teresa I. Fortoul, Mexico
Rodrigo Franco, USA
Joaquin Gadea, Spain
Juan Gambini, Spain
José Luís García-Giménez, Spain
Gerardo García-Rivas, Mexico
Janusz Gebicki, Australia
Alexandros Georgakilas, Greece
Husam Ghanim, USA
Jayeeta Ghose, USA
Rajeshwary Ghosh, USA
Eloisa Gitto, Italy
Daniela Giustarini, Italy
Saeid Golbidi, Canada
Aldrin V. Gomes, USA
Arantxa González, Spain
Tilman Grune, Germany
Chi Gu, China, China
Nicoletta Guaragnella, Italy
Solomon Habtemariam, United Kingdom
Ying Han, China
Eva-Maria Hanschmann, Germany
Tim Hofer, Norway
John D. Horowitz, Australia
Silvana Hrelia, Italy
Juan Huang, China
Stephan Immenschuh, Germany
Maria Isaguliants, Latvia
Luigi Iuliano, Italy
FRANCO J. L, Brazil
Vladimir Jakovljevic, Serbia
Peeter Karihtala, Finland
Kum Kum Khanna, Australia
Neelam Khaper, Canada
Thomas Kietzmann, Finland

Demetrios Kouretas, Greece
Andrey V. Kozlov, Austria
Jean-Claude Lavoie, Canada
Simon Lees, Canada
Qiangqiang Li, China
Xin-Feng Li, China
Jialiang Liang, China
Christopher Horst Lillig, Germany
Paloma B. Liton, USA
Ana Lloret, Spain
Lorenzo Loffredo, Italy
Daniel Lopez-Malo, Spain
Antonello Lorenzini, Italy
Hai-Chun Ma, China
Nageswara Madamanchi, USA
Kenneth Maiese, USA
Marco Malaguti, Italy
Tullia Maraldi, Italy
Reiko Matsui, USA
Juan C. Mayo, Spain
Steven McAnulty, USA
Antonio Desmond McCarthy, Argentina
Bruno Meloni, Australia
Pedro Mena, Italy
Victor M. Mendoza-Núñez, Mexico
Alexandra Miller, USA
Sanjay Misra, USA
Raffaella Molteni, Italy
Maria U. Moreno, Spain
Sandra Moreno, Italy
Trevor A. Mori, Australia
Ryuichi Morishita, Japan
Fabiana Morroni, Italy
Luciana Mosca, Italy
Ange Mouithys-Mickalad, Belgium
Iordanis Mourouzis, Greece
Danina Muntean, Romania
Colin Murdoch, United Kingdom
Pablo Muriel, Mexico
Ryoji Nagai, Japan
Amit Kumar Nayak, India
David Nieman, USA
Hassan Obied, Australia
Julio J. Ochoa, Spain
Pál Pacher, USA
Pasquale Pagliaro, Italy
Valentina Pallottini, Italy




Rosalba Parenti, Italy
Vassilis Paschalis, Greece
Visweswara Rao Pasupuleti, Malaysia
Daniela Pellegrino, Italy
Ilaria Peluso, Italy
Claudia Penna, Italy
Serafina Perrone, Italy
Tiziana Persichini, Italy
Shazib Pervaiz, Singapore
Vincent Pialoux, France
Alessandro Poggi, Italy
Ada Popolo, Italy
Aijuan Qu, China
José L. Quiles, Spain
Zsolt Radak, Hungary
Namakkal Soorappan Rajasekaran, USA
Sid D. Ray, USA
Hamid Reza Rezvani, France
Alessandra Ricelli, Italy
Paola Rizzo, Italy
Francisco J. Romero, Spain
Joan Roselló-Catafau, Spain
H. P. Vasantha Rupasinghe, Canada
Kunihiro Sakuma, Japan
Gabriele Saretzki, United Kingdom
Luciano Saso, Italy
Nadja Schroder, Brazil
Sebastiano Sciarretta, Italy
Ratanesh K. Seth, USA
Xiaolei Shi, China
Cinzia Signorini, Italy
Mithun Sinha, USA
Yi-Rui Sun, China
Carla Tatone, Italy
Frank Thévenod, Germany
Shane Thomas, Australia
Carlo Gabriele Tocchetti, Italy
Angela Trovato Salinaro, Italy
Paolo Tucci, Italy
Rosa Tundis, Italy
Giuseppe Valacchi, Italy
Daniele Vergara, Italy
Victor M. Victor, Spain
László Virág, Hungary
Kai Wang, China
Min-qi Wang, China
Natalie Ward, Australia











Philip Wenzel, Germany
Georg T. Wondrak, USA
Qiongming Xu, China
Sho-ichi Yamagishi, Japan
Liang-Jun Yan, USA
Guillermo Zalba, Spain
Jia Zhang, First Affiliated Hospital of Xi'an
Jiaotong University, Xi'an, Shaanxi Province,
China, China
Ziwei Zhang, China
Yong Zhou, China
Mario Zoratti, Italy

Contents



Oxidative Stress and Tissue Repair: Mechanism, Biomarkers, and Therapeutics

Reggiani Vilela Gonçalves , Andrea M. A. Costa , and Lukasz Grzeskowiak 
Editorial (3 pages), Article ID 6204096, Volume 2021 (2021)





The Estimation of Blood Paramagnetic Center Changes during Burns Management with Biodegradable Propolis-Nanofiber Dressing

Pawel Olczyk , Katarzyna Komosinska-Vassev , Ryszard Krzyminiewski, Janusz Kasperczyk, Pawel Ramos , Bernadeta Dobosz, Olgierd Batoryna, Jerzy Stojko , Mateusz Stojko , Diana Ivanova , Krystyna Olczyk , and Barbara Pilawa 
Research Article (9 pages), Article ID 3675603, Volume 2020 (2020)

Safflor Yellow B Attenuates Ischemic Brain Injury via Downregulation of Long Noncoding AK046177 and Inhibition of MicroRNA-134 Expression in Rats

Chaoyun Wang , Hongzhi Wan, Qiaoyun Wang, Hongliu Sun, Yeying Sun, Kexin Wang, and Chunxiang Zhang 
Research Article (20 pages), Article ID 4586839, Volume 2020 (2020)




Huangbai Liniment Accelerated Wound Healing by Activating Nrf2 Signaling in Diabetes

Jingjing Zhang , Rui Zhou, Changpei Xiang, Qiang Jia , Hongwei Wu , and Hongjun Yang 
Research Article (20 pages), Article ID 4951820, Volume 2020 (2020)




Carbon Monoxide Being Hydrogen Sulfide and Nitric Oxide Molecular Sibling, as Endogenous and Exogenous Modulator of Oxidative Stress and Antioxidative Mechanisms in the Digestive System

Edyta Korbut, Tomasz Brzozowski , and Marcin Magierowski 
Review Article (14 pages), Article ID 5083876, Volume 2020 (2020)






NLRP3 Inflammasome and Its Central Role in the Cardiovascular Diseases

Yeqing Tong , Zhihong Wang, Li Cai, Liangqiang Lin, Jiafa Liu , and Jinquan Cheng 
Review Article (8 pages), Article ID 4293206, Volume 2020 (2020)





Preprotection of Tea Polysaccharides with Different Molecular Weights Can Reduce the Adhesion between Renal Epithelial Cells and Nano-Calcium Oxalate Crystals

Yao-Wang Zhao , Li Liu, Chuang-Ye Li, Hui Zhang, Xin-Yuan Sun , and Jian-Ming Ouyang 
Research Article (13 pages), Article ID 1817635, Volume 2020 (2020)




Exosomal circHIPK3 Released from Hypoxia-Pretreated Cardiomyocytes Regulates Oxidative Damage in Cardiac Microvascular Endothelial Cells via the miR-29a/IGF-1 Pathway

Yan Wang , Ranzun Zhao, Weiwei Liu, Zhenglong Wang, Jidong Rong , Xianping Long, Zhijiang Liu , Junbo Ge , and Bei Shi 
Research Article (28 pages), Article ID 7954657, Volume 2019 (2019)




Potential Role of Nutrient Intake and Malnutrition as Predictors of Uremic Oxidative Toxicity in Patients with End-Stage Renal Disease

Robson E. Silva, Ana C. Simões-e-Silva , Aline S. Miranda , Patrícia B. I. Justino, Máisa R. P. L. Brigagão, Gabriel O. I. Moraes, Reggiani V. Gonçalves , and Rômulo D. Novaes 
Research Article (12 pages), Article ID 7463412, Volume 2019 (2019)








Subacute Testicular Toxicity to Cadmium Exposure Intraperitoneally and Orally

Viviane G. S. Mouro , Ana L. P. Martins, Janaina Silva, Tatiana P. Menezes, Marcos L. M. Gomes, Juraci A. Oliveira, Fabiana C. S. A. Melo , and Sérgio L. P. Matta 
Research Article (14 pages), Article ID 3429635, Volume 2019 (2019)




Radiation-Induced Normal Tissue Damage: Oxidative Stress and Epigenetic Mechanisms

Jinlong Wei, Bin Wang, Huanhuan Wang, Lingbin Meng , Qin Zhao, Xinyu Li, Ying Xin , and Xin Jiang 
Review Article (11 pages), Article ID 3010342, Volume 2019 (2019)




Lipoxin A4 Ameliorates Acute Pancreatitis-Associated Acute Lung Injury through the Antioxidative and Anti-Inflammatory Effects of the Nrf2 Pathway

Wen Ye , Chenlei Zheng, Dinglai Yu , Fan Zhang, Reguang Pan, Xiaofeng Ni, Zhehao Shi, Zhongjing Zhang, Yukai Xiang , Hongwei Sun , Keqing Shi, Bicheng Chen , Qiyu Zhang , and Mengtao Zhou 
Research Article (15 pages), Article ID 2197017, Volume 2019 (2019)



Alcohol Intake and Abnormal Expression of Brf1 in Breast Cancer

Chenghao Huang , Yanmei Zhang , and Shuping Zhong 
Review Article (9 pages), Article ID 4818106, Volume 2019 (2019)




Resveratrol Reverses Thioacetamide-Induced Renal Assault with respect to Oxidative Stress, Renal Function, DNA Damage, and Cytokine Release in Wistar Rats

Seema Zargar , Mona Alonazi, Humaira Rizwana , and Tanveer A. Wani 
Research Article (8 pages), Article ID 1702959, Volume 2019 (2019)


Danhong Injection Alleviates Postoperative Intra-abdominal Adhesion in a Rat Model

Yunhua Wu , Guangbing Wei, Junhui Yu, Zilu Chen, Zhengshui Xu, Rui Shen, Ting Liang, Lu Zheng, Kang Wang, Xuejun Sun , and Xuqi Li 
Research Article (11 pages), Article ID 4591384, Volume 2019 (2019)

miR-200c Modulates the Pathogenesis of Radiation-Induced Oral Mucositis

Jingjing Tao , Mengjing Fan, Difan Zhou, Yiyang Hong, Jing Zhang, Hai Liu, Sherven Sharma, Guanyu Wang , and Qinghua Dong 
Research Article (14 pages), Article ID 2352079, Volume 2019 (2019)

Noncoding RNAs in Cardiac Autophagy following Myocardial Infarction

Annie Turkieh, Henri Charrier, Emilie Dubois-Deruy, Sina Porouchani, Marion Bouvet, and Florence Pinet 
Review Article (6 pages), Article ID 8438650, Volume 2019 (2019)

Hypoxia-Inducible Factor-1 α Knockdown Plus Glutamine Supplementation Attenuates the Predominance of Necrosis over Apoptosis by Relieving Cellular Energy Stress in Acute Pancreatitis

Liang Ji , Xiaoyu Guo , Jiachen Lv , Fan Xiao , Wangjun Zhang , Jie Li , Zhitao Lin , Bei Sun , and Gang Wang 
Research Article (15 pages), Article ID 4363672, Volume 2019 (2019)

Editorial

Oxidative Stress and Tissue Repair: Mechanism, Biomarkers, and Therapeutics

Reggiani Vilela Gonçalves ^{1,2}, Andrea M. A. Costa ³, and Lukasz Grzeskowiak ⁴

¹Animal Biology Department, Federal University of Viçosa, Viçosa, 36570-000 Minas Gerais, Brazil

²Animal Biology and Cellular and Structural Biology Graduate Program, Federal University of Viçosa, Viçosa, 36570-000 Minas Gerais, Brazil

³Morphological Science Graduate Program, State University of Rio de Janeiro, Rio de Janeiro 20950-003, Brazil

⁴Institute of Animal Nutrition, Freie Universität Berlin, Berlin 14195, Germany

Correspondence should be addressed to Reggiani Vilela Gonçalves; reggysvilela@yahoo.com.br

Received 24 December 2020; Accepted 24 December 2020; Published 27 February 2021

Copyright © 2021 Reggiani Vilela Gonçalves et al. This is an open access article distributed under the Creative Commons Attribution License, which permits unrestricted use, distribution, and reproduction in any medium, provided the original work is properly cited.

During the “respiratory burst” in activated leukocytes, the release of reactive oxygen species (ROS) and reactive nitrogen species (RNS) occurs, and these phenomes present a central role in tissue repair [1, 2]. In the inflammatory phase, neutrophils reach the injured area, sending signals for the migration of macrophages that mediate the expression of cytokines, growth factors, reactive oxygen (ROS), and nitrogen species (RNS) [3]. These ROS and RNS generated during inflammation can lead to cell lesions such as membrane disorganization and protein oxidation by altering cellular functions. The balance between ROS production and antioxidant defense is important for efficient tissue repair in organs such as the skin, liver, lungs, kidneys, heart, and testes [4–6]. When the tissue is damaged by reactive species, it is common to observe lipid, protein, and DNA damage, leading to oxidative stress that disables tissue repair [5, 6].

During the chronification process, a persistent activation of the COX way occurs, and neutrophils and macrophages release cytokines and chemokines, which attract more cells to the location of the inflammation and promote oxidative stress in the repairing tissue [7, 8]. The excess of proinflammatory mediators promotes the increase of the peroxide of hydrogen (H₂O₂) and nitric oxide content, which accelerate the peroxidation of the component cells [7, 8]. Therefore, a controlled inflammation process is nec-

essary to avoid persistent tissue damage through the continued action of free radicals and reactive oxygen species (ROS) [7]. Associated with this, we can highlight that the healing environment is usually prooxidant and generally presents a decrease in the synthesis and expression of antioxidant enzymes such as superoxide, glutathione, and catalase, impairing the healing environment [8, 9]. In general, a desirable repairing process results from the balance between the synthesis and degradation of inflammatory mediators and pro- and antioxidant compounds [9, 10].

Antioxidant systems seem to play a crucial role in maintaining the morphological and functional integrity of all microorganisms. Accordingly, disruptors of redox balance (e.g., inductors of oxidative stress or inhibitors of antioxidant molecules) have been proposed as candidates for new healing drugs. Ideally, modulators of redox systems should be able to influence fibroblast migration, proliferation, increased collagen synthesis, and scar tensile strength, a process partially mediated by ROS and RNS catalysis [11, 12]. Interestingly, several drugs and compounds developed for different conditions (e.g., NLRP3, propolis, carbon monoxide, *tea polysaccharides*, *safflor yellow B*, radiation, *Huangbai liniment*, lipoxin A4 ameliorates, resveratrol, and MiR-200c) exhibit antioxidant, anti-inflammatory, and antimicrobial properties. In many cases, these properties are based on the

disruption of cell redox metabolism, a pharmacological effect that opens new venues for drug repurposing and the development of new strategies for the treatment of tissue injury.

This special issue gathers a set of 17 studies in an interdisciplinary platform that addresses the subcellular, cellular, and molecular bases of the metabolism redox associated with the recovery of damaged tissue. This special issue also highlights the continuing effort to understand the redox systems associated with repairing tissues in all levels and understand how the action of different treatments can lead to the increase of antioxidant enzyme levels, such as superoxide dismutase (SOD), catalase (CAT), and glutathione peroxidase (GPx), and consequently accelerate the healing process in different tissues. This issue contains seventeen papers describing different mechanisms involved in tissue repairing in different pathological conditions, which are briefly mentioned below.

Some studies have shown that external agents like alcohol, carbon monoxide, cadmium, and radiation exposition reflect an imbalance between oxidants and antioxidant mechanisms in favour of oxidants capable of provoking tissue damage. These prooxidant mechanisms are related to genetic and epigenetic regulation and can regulate the expression of molecules that can activate signal transduction pathways responsible for inflammation and cause oxidative damage to proteins, lipids, and DNA. The studies in this issue showed that the redox system begins producing free radicals a few hours after exposure and can upregulate several enzymes including nicotinamide adenine dinucleotide phosphate oxidase (NADPH oxidase), lipoxygenases (LOXs), nitric oxide synthase (NOS), and cyclooxygenase (COXs). These enzymes are expressed in specific ways in various cells, tissues, and organs. Normal cells that are exposed to these external agents will give rise to nuclear and mitochondrial DNA damage, which can lead to cell death via processes such as apoptosis and necrosis. Necrosis can trigger the release of inflammatory cytokines such as IL-1, IL-4, IL-13, and other inflammatory mediators, while apoptosis may cause the release of anti-inflammatory cytokines including TGF- β and IL-10.

Considering the development of new drugs and treatments, the studies published in this edition were very broad and addressed different types of therapies in the treatment of injuries in various systems. The use of natural products obtained from plants and animals were more common; among them, we can highlight propolis-nanofiber dressing used for burn treatment and the Huangbai liniment plant compost for accelerated wound healing by Nrf2 activation signalled in diabetes. In one study, Danhong injection was extracted from *Salviae Miltiorrhizae Radix* and *Carthami tinctorii Flos* and showed several positive effects, such as anti-inflammatory, antioxidant, and antiapoptotic, and prevented postoperative adhesion. In another study, resveratrol showed protection against thioacetamide toxicity in rat kidneys with respect to DNA damage, oxidative stress, renal function, and cytokine release.

In addition, two studies analysed the importance of nutrition for oxidative stress in tissues. The former study showed that nutrient intake and malnutrition can act as predictors of oxidative uremic toxicity. Therefore, they provided evidence

that age and sex exhibited a limited association with malnutrition and cardiometabolic risk factors in haemodialysis patients. In addition, these authors showed that serum antioxidant mediators seem to have greater predictive sensitivity to estimate molecular oxidative damage in haemodialysis patients. The latter study evaluated glutamine supplementation for the treatment of acute pancreatitis and showed that the use of glutamine might be promising for the future management of acute pancreatitis by relieving the intracellular energy stress, thereby attenuating the predominance of necrosis over apoptosis. Moreover, one review summarized the role of macroautophagy in the heart following myocardial infarction and showed that some noncoding RNAs and their easy manipulation exposed their potential as new targets for clinical development to treat autophagy-related diseases. Identification of specific cardiac noncoding RNAs that regulate autophagy could be a good opportunity to protect the heart from myocardial infarction injury without affecting the autophagy activity in other organs.

We hope that the readers of this special issue will find these findings interesting and useful to advance the understanding of such a complex and multifaceted theme, suggesting an update for this interesting topic.

Conflicts of Interest

The authors declare that there is no conflict of interest regarding the publication of this special issue.

Acknowledgments

The editorial team is very grateful to the different groups who submitted their scientific findings to this special issue and to the reviewers who kindly provided their time and experience to improve the quality of each study.

Reggiani Vilela Gonçalves
Andrea M.A. Costa
Lukasz Grzeskowiak

References

- [1] M. Cano Sanchez, S. Lancel, E. Boulanger, and R. Nevriere, "Targeting oxidative stress and mitochondrial dysfunction in the treatment of impaired wound healing: a systematic review," *Antioxidants (Basel, Switzerland)*, vol. 7, no. 8, 2018.
- [2] A. Phaniendra, D. B. Jestadi, and L. Periyasamy, "Free radicals: properties, sources, targets, and their implication in various diseases," *Indian journal of clinical biochemistry*, vol. 30, no. 1, pp. 11–26, 2015.
- [3] A. Weidinger and A. V. Kozlov, "Biological activities of reactive oxygen and nitrogen species: oxidative stress versus signal transduction," *Biomolecules*, vol. 5, no. 2, pp. 472–484, 2015.
- [4] D. André-Lévigne, A. Modarressi, M. S. Pepper, and B. Pittet-Cuénod, "Reactive oxygen species and NOX enzymes are emerging as key players in cutaneous wound repair," *International journal of molecular sciences*, vol. 18, no. 10, 2017.
- [5] D. Pitocco, F. Zaccardi, E. di Stasio et al., "Oxidative stress, nitric oxide, and diabetes," *The review of diabetic studies: RDS*, vol. 7, no. 1, pp. 15–25, 2010.

- [6] N. S. Bryan and M. B. Grisham, "Methods to detect nitric oxide and its metabolites in biological samples," *Free Radical Biology and Medicine*, vol. 43, no. 5, pp. 645–657, 2007.
- [7] M. Mittal, M. R. Siddiqui, K. Tran, S. P. Reddy, and A. B. Malik, "Reactive oxygen species in inflammation and tissue injury," *Antioxidants & redox signaling*, vol. 20, no. 7, pp. 1126–1167, 2014.
- [8] A. G. Abdou, A. H. Marae, and H. F. Abd-Elsattar Saif, "Immunohistochemical evaluation of COX-1 and COX-2 expression in keloid and hypertrophic scar," *The American Journal of Dermatopathology*, vol. 36, no. 4, pp. 311–317, 2014.
- [9] I. Marrocco, F. Altieri, and I. Peluso, "Measurement and clinical significance of biomarkers of oxidative stress in humans," *Oxidative medicine and cellular longevity*, vol. 2017, Article ID 6501046, 32 pages, 2017.
- [10] A. Rahal, A. Kumar, V. Singh et al., "Oxidative stress, prooxidants, and antioxidants: the interplay," *BioMed research international*, vol. 2014, Article ID 761264, 19 pages, 2014.
- [11] C. R. A. Nogueira, F. M. Damasceno, M. R. de Aquino-Neto et al., "Doxycycline protects against pilocarpine-induced convulsions in rats, through its antioxidant effect and modulation of brain amino acids," *Pharmacology Biochemistry and Behavior*, vol. 98, no. 4, pp. 525–532, 2011.
- [12] L. S. Altoé, R. S. Alves, M. M. Sarandy, M. Morais-Santos, R. D. Novaes, and R. V. Gonçalves, "Does antibiotic use accelerate or retard cutaneous repair? A systematic review in animal models," *PLOS ONE*, vol. 14, no. 10, article e0223511, 2019.

Research Article

The Estimation of Blood Paramagnetic Center Changes during Burns Management with Biodegradable Propolis-Nanofiber Dressing

Pawel Olczyk ¹, Katarzyna Komosinska-Vassev ², Ryszard Krzyminiewski,³
Janusz Kasperczyk,^{4,5} Pawel Ramos ⁶, Bernadeta Dobosz,³ Olgierd Batoryna,¹
Jerzy Stojko ⁷, Mateusz Stojko ^{4,5}, Diana Ivanova ⁸, Krystyna Olczyk ²
and Barbara Pilawa ⁶

¹Department of Community Pharmacy, Faculty of Pharmaceutical Sciences in Sosnowiec, Medical University of Silesia in Katowice, Sosnowiec, Poland

²Department of Clinical Chemistry and Laboratory Diagnostics, Faculty of Pharmaceutical Sciences in Sosnowiec, Medical University of Silesia in Katowice, Sosnowiec, Poland

³Medical Physics Division, Faculty of Physics, Adam Mickiewicz University, Poznan, Poland

⁴Centre of Polymer and Carbon Materials, Polish Academy of Sciences, Zabrze, Poland

⁵Department of Biopharmacy, School of Pharmacy with the Division of Laboratory Medicine in Sosnowiec, Medical University of Silesia in Katowice, Sosnowiec, Poland

⁶Department of Biophysics, Faculty of Pharmaceutical Sciences in Sosnowiec, Medical University of Silesia in Katowice, Sosnowiec, Poland

⁷Center of Experimental Medicine, Medics 4, Faculty of Medicine in Katowice, Medical University of Silesia in Katowice, Katowice, Poland

⁸Department of Biochemistry, Molecular Medicine and Nutrigenomics, The Faculty of Pharmacy, Medical University of Varna, Varna, Bulgaria

Correspondence should be addressed to Pawel Olczyk; polczyk@sum.edu.pl

Received 1 July 2019; Revised 7 June 2020; Accepted 9 June 2020; Published 29 June 2020

Guest Editor: Reggiani Vilela Gonçalves

Copyright © 2020 Pawel Olczyk et al. This is an open access article distributed under the Creative Commons Attribution License, which permits unrestricted use, distribution, and reproduction in any medium, provided the original work is properly cited.

The evolution of the paramagnetic center system in blood during the healing of skin burn wounds dressed with a biodegradable apitherapeutic nanofiber dressing was examined. The aim of this study was to determine the changes in paramagnetic centers in blood during the influence of apitherapeutic nanofiber dressings on the healing process. The blood samples were tested before burn infliction (day 0) and, respectively, on the 10th and 21st days of the experiment. Paramagnetic centers in the blood of the pig used as the model animal were examined with an X-band (9.3 GHz) electron paramagnetic resonance spectroscopy. The EPR spectra were measured with Bruker spectrometer at 230 K with a modulation frequency of 100 kHz. The EPR lines of the high spin Fe³⁺ in methemoglobin, high spin Fe³⁺ in transferrin, Cu²⁺ in ceruloplasmin, and free radicals were observed in the multicomponent spectra of blood. For the application of the apitherapeutic nanofiber dressing, the amplitudes of the EPR signals of Fe³⁺ in methemoglobin were similar up to 10 days. For the experiment with the apitherapeutic formulation, the heights of EPR signals of Fe³⁺ in transferrin were lower after 10 days and 21 days of therapy, compared to day 0. For the application of the apitherapeutic formulation the signals of Cu²⁺ in ceruloplasmin and free radicals, strongly decreased after 10 days of therapy, and after 21 days it increased to the initial values characteristic for day 0. The apitherapeutic formulation caused that after 21 days the EPR spectrum of Cu²⁺ in ceruloplasmin and free radicals was considerably high. The apitherapeutic formulation interaction after 10 days and after 21 days of therapy resulted in the low EPR lines of Fe³⁺ in methemoglobin. EPR spectra of blood may be useful for presentation of the changes in its paramagnetic centers during the healing process of the burn wounds.

1. Introduction

Propolis represents a complexed, natural raw material, produced, in the region of Eastern Europe by a honeybee, from balsamic substances obtained from buds of, e.g., poplar, birch, willow, alder and chestnut, and resins—among others—possessed from damaged parts of the mentioned trees [1, 2]. Bee glue, however, also contains waxes, essential and aromatic oils, pollen, feathers, dust, bee glandular secretion, and the fragments of beehives [3, 4]. For the first time, Marcucci [5] and Bankova et al. [6] have registered over 300 known substances in discussed unique natural material. The chemical compounds—encompassing the flavonoids, terpenes, and phenolics considered as bioactive markers of propolis are responsible for the pharmaceutical effects including anti-inflammatory, antimicrobial, antitumor, anti-ulcer and anti-HIV, antioxidant, and immunomodulatory activities [7–9]. However, the most important, from the point of view of medicine and pharmacy, is the regenerative action of propolis, which in the course of healing effectively stimulates the expression of the vascular endothelial growth factor and markedly enhances the phenomenon of cellular proliferation through the growth of H3 histone [10–14]. Propolis also enhances the burned tissue repair by stimulation of the wound matrix GAGs (CS/DS and HA) accumulation responsible for granulation, tissue growth, and wound closure [15]. Propolis modulates VN, LN, and HS/HP metabolism, leading to the better regulation of the primary wound healing cellular events, i.e., epidermal cell and keratinocyte migration and proliferation as well as fibroblast activation providing reepithelization and wound closure [16, 17]. Propolis regulates the expression and degradation of collagens types I and III in wound matrix and creates favorable biochemical environment supporting reepithelization [18]. One of the factors determining the corrective action of propolis is its antioxidant potential [19]. Despite the knowledge indicating that propolis inhibits ROS production, blocks peroxidation of LDL, and nitration of proteins, it also enhances the NOS expression and alleviates the NADPH oxidase (NOX) activity. Moreover, bee glue downregulates the damage of the DNA in cultured fibroblasts stimulated by the hydrogen peroxide (H_2O_2), inhibits macrophage apoptosis influencing on glutathione (GSH) and the tumor necrosis factors/nuclear factor kappa B (TNF/NF- κ B) pathway [20]. In this work, the unique application of electron paramagnetic resonance (EPR) spectroscopy to determine paramagnetic centers existing in blood samples taken from the experimental animals, upon therapy by an innovative biodegradable apitherapeutic nanofiber dressing, was performed. The mentioned formulation, obtained using the technique of electrospinning, containing an apitherapeutic agent, was intended for the regeneration of complicated skin wounds. The aforementioned nanofiber dressing creates the favorable environment of the wound, stimulating also reepithelialization, angiogenesis, and biosynthesis of connective tissue components, simultaneously enabling gas exchange between the wound and the environment. This innovation is the subject matter of a patent specification—“P.425636”, and it consists in incorporating a natural raw material with proven antioxi-

dative, anti-inflammatory, immunomodulating, antiviral, anti-neoplastic, antibacterial, antifungal properties, not to mention the fact that it also stimulates the phenomenon of reepithelialization, and it efficiently limits the recovery time of tissue damage. Free radicals contribute to controlling the healing process at the cellular level; however, their precise role in burn wound repair is still little explored. Thus, the different types of paramagnetic centers in blood were searched. The low temperatures were used to detect iron, copper, and free radicals' signals.

2. Experimental

2.1. Tissue Material. 16-week-old, domestic pig was chosen for the evaluation of wound repair because of many similarities between pig and human skin. Eighteen contact burn wounds were inflicted on the right and left flanks of the pig body, according to the methods of Hoekstra et al. [21] and Brans et al. [22]. The experimental animal was housed according to the Good Laboratory Practice (GLP) Standards of Polish Veterinary Law. Blood samples, in three replications, were taken before wounds infliction (day 0) and on postburn days 10th and 21st. The procedure of collection of blood samples for laboratory analysis was based on a marginal ear vein cannulation. After cleaning the surface of the ear, an injection needle was inserted into the lumen of the vessel for sample collection. This procedure was repeated at each collection point [23]. After collection, the blood was stored at low temperature ($-70^{\circ}C$). Thermal injuries were protected with nanofiber apitherapeutic dressings. The experimental protocol was accepted by the Ethics Committee of the Medical University of Silesia in Katowice, Poland (LKE-111/2014).

2.2. Biodegradable Nano-Nonwoven Dressings. Nano-nonwoven wound dressings are made with an electrospinning method using poly(lactide-co-glycolide) containing 85 mole-% of lactidyl and 15 mole-% of glycolidyl comonomer units (PLGA 85:15) [24]. 6 wt-% concentration of the polymer in solution and 1,1,1,3,3,3-hexafluoro-2-propanol as a solvent is used. The electrospinning process consists in producing the polymer fibers in the electric field between the collector with negative electric potential and the spinning nozzle, to which the positive electric potential is applied [25]. The potential difference is adjusted to 27 kV. The distance between the electrodes was set to 15 cm. To obtain the nonwoven mat, 22 ml of the solution is dosed at a rate of 1.5 ml/h [26]. Nonwoven wound dressings containing propolis [4] have been made with an electrospinning method using poly(lactide-co-glycolide) containing: 85 mole-% of lactidyl and 15 mole-% of glycolidyl comonomer units (PLGA 85:15) [24, 27]. A solution of propolis is introduced to the polymer solution and mixed until a homogeneous mixture is obtained. The propolis content is 5 wt-% and 10 wt-%, respectively, to the polymer used. 6 wt-% concentration of the polymer and propolis mixture in a solution and 1,1,1,3,3,3-hexafluoro-2-propanol as a solvent is used. The electrospinning process consists in producing the polymer fibers in the electric field between the collector with negative electric potential and a spinning nozzle, to which

the positive electric potential is applied [25]. The potential difference is adjusted to 27 kV. The distance between the electrodes was set to 15 cm. To obtain the nonwoven mat, 22 ml of solution is dosed at a rate of 1.5 ml/h [26]. The blood samples are placed in the thin-walled tubes with an external diameter of 3 mm and the EPR spectra are measured.

2.3. EPR Measurements. Paramagnetic centers in blood samples were examined by the use of electron paramagnetic resonance spectroscopy (EPR) at low temperature equaled 230 K. This spectroscopic method was chosen, because of the direct experimental procedures providing information about molecules containing unpaired electrons [28]. Energy levels of unpaired electrons in the paramagnetic centers located in the magnetic field are split. Unpaired electrons absorb microwaves of the suitable frequencies, which bring the energy adequate to the distances between the energy levels, and the unpaired electrons go to the higher energy levels. On the way of relaxation processes, the unpaired electrons of the tested paramagnetic centers go back to the lower levels. The absorbed energy of microwaves is measured as the resonance curves, which parameters give information about paramagnetic centers [28, 29]. The important advantages of the EPR method are its nondestructive nature relative to the examined substances [28, 29].

The electron paramagnetic resonance spectra were measured as the first-derivative curves by an X-band (9.3 GHz) EPR spectrometer produced by Bruker (USA). Magnetic modulation of 100 kHz was used. The low microwave power of 7.9 mW was used to avoid microwave saturation of EPR lines. The cryogenic system to low-temperature measurements of Bruker (USA) was used. For the studied blood samples, the following parameters of EPR spectra were analyzed: g-factors and amplitudes (A). Amplitudes (A) of the EPR lines increase with increasing of the amount of paramagnetic centers in the samples [28]. g-Factor depends on the type of paramagnetic centers, which are responsible for the EPR line. g-Values will be calculated from resonance condition according to the formula [28, 29]:

$$g = h\nu/\mu_B B_r. \quad (1)$$

where h is Planck constant, ν is microwave frequency, μ_B is Bohr magneton, and B_r is resonance magnetic field.

The expressions of " $h\nu$ " and " $g\mu_B B_r$ " mean the energy of microwaves and the distance between the energy levels, respectively [28]. Microwave frequency (ν) was directly measured by the Bruker recorder. The B_r values were determined from the electron paramagnetic resonance lines. In the present paper, we followed the same EPR method of examination of paramagnetic centers in the blood as in the previous our work [30] concerning the low-temperature electron paramagnetic resonance application.

3. Results and Discussion

The present study is a continuation of our previous experimental studies concerning the usefulness of a new low-temperature electron paramagnetic resonance technique

for monitoring molecular complexes containing iron Fe^{3+} (methemoglobin, transferrin) or copper Cu^{2+} ions (ceruloplasmin) and free radicals in the blood during healing of burn wounds treated with biodegradable dressings containing poly(lactide-co-glycolide). The obtained results indicated that a more complete assessment of biochemical changes taking place in the process of repairing tissue damage after burn insult is needed, especially in the scope of mechanisms regulating the metabolism of iron and copper ion complexes as well as free radicals in the blood. Followed by EPR technic described in our previous work [30], in this study, we examined the multicomponent electron paramagnetic resonance spectra of the blood during healing taken from the experimental animal, obtained after 1st, 10th, and 21st days of burn treatment with a previously used biodegradable dressings additionally containing pharmacologically active substance of natural origin—propolis.




The evolution of the healing process undergoing three overlapping phases, (1) hemostasis and inflammation, (2) proliferation, and (3) remodelling, has been summarized and presented in Table 1. The effects of management with biodegradable propolis-nanofiber dressing on each would healing stage were also included in this table (Table 1).

For all the tested blood samples, the complex EPR spectra were measured [28, 29]. The EPR spectra of paramagnetic centers in blood for skin before inflicting thermal damages (day 0) and for burned wounds treated with the propolis nanofiber dressing 10 and 21 days of therapy were shown in Figures 1(a)–1(c), respectively. Three lines (signed as I, II, and III) were observed. The line III was a superposition of two signals. Taking into account the earlier results of EPR studies of blood [31], these lines come from high spin Fe^{3+} in methemoglobin (line I), high spin Fe^{3+} in transferrin (line II), and Cu^{2+} in ceruloplasmin and free radicals (line III). The low field signals (line I, line II) of the EPR spectra of blood in the experiment with the dressing containing propolis for day 0 (before burn infliction), 10 days, and 21 days of therapy were presented in Figures 2(a)–2(c), respectively.

The concentration of the individual types of paramagnetic centers in blood changed with time of therapy for propolis nanofiber dressing. This effect was observed with changes in the individual components of the multicomponent EPR spectra of blood. Their heights depended on the time of therapy with the apitherapeutic formulation. The influence of time of therapy on the amplitudes (A) of the high spin Fe^{3+} in methemoglobin (line I), high spin Fe^{3+} in transferrin (line II), and Cu^{2+} in ceruloplasmin and free radicals (line III), in blood for burned skin wounds treated with the mentioned biodegradable dressing, was presented in Figure 3.

For the propolis nanofiber dressing, the amplitudes (A) of the EPR signals of Fe^{3+} in methemoglobin (line I) were similar up to 10 days, and the amplitude (A) of the (line I) for the blood after 10 days of therapy was only slightly lower than the amplitude (A) of this line measured before burn infliction (day 0) (Figure 3). Its value increased after 21 days of therapy (Figure 3). For the experiment with the propolis dressing, the heights of EPR signals of Fe^{3+} in transferrin (line II) were lower after 10 days and 21 days of therapy, compared to day 0 (Figure 3). For the application of the

TABLE 1: Effects of management with biodegradable propolis-nanofiber dressing on each wound healing stage.

Hemostasis and inflammatory phase	Proliferative phase	Tissue remodelling phase
<ul style="list-style-type: none"> (i) Early phase of inflammation begins when the wound develops, lasts 4-6 days (ii) Trauma causes peripheral blood platelets and neutrophils to migrate to the injury, forming a fibrin clot to end bleeding, and the inflammatory stage of the healing cascade begins (iii) Increased free radical formation appears as a result of the local tissue damage and a systemic inflammatory response 	<ul style="list-style-type: none"> (i) Lasts another 3-10 days postinjury (ii) Fibroblasts, endothelial cells and epithelial cells migrate into the wound bed (iii) Granulation tissue formation—fibroblasts proliferate and synthesize new components of extracellular matrix (iv) Angiogenesis—new blood vessels carry oxygen and nutrients necessary for the metabolism and growth of cells, and confer to the granulation tissue its characteristic red, granular appearance (v) Covering the wound (reepithelialization)—epithelial cells migrate from the wound bed or margins 	<ul style="list-style-type: none"> (i) Begins about 21 days postinjury and can continue for a year (ii) Wound contraction and scar tissue formation occurs (iii) Collagen is remodeled from type III to type I cross-linking of collagen reduces scar thickness and makes the skin area of the wound stronger (iv) The wound fully closes (v) The cells that had been used to repair the wound but which are no longer needed are removed by apoptosis
		
<p>Burns management with PLGA 85/15 dressing with 5% propolis</p> <p>Day 0</p> <ul style="list-style-type: none"> (i) Necrosis at the burn induction site and in the wound area from 3 to 15 mm from the edge (ii) Intense redness and swelling around the necrotic area (iii) Exudation, visible tissue at the burn site carbonization 	<p>Burns management with PLGA 85/15 dressing with 5% propolis</p> <p>10th day</p> <ul style="list-style-type: none"> (i) A thin scab not completely covering the wound area (ii) The wound is increasingly covered with a thin layer of epidermis (iii) Bristle growth all over the wound area (iv) No redness around the wound area 	<p>Burns management with PLGA 85/15 dressing with 5% propolis</p> <p>21st day</p> <ul style="list-style-type: none"> (i) The wound covered with pink epidermis, (ii) Significant reduction in the wound surface (iii) Small fragments of the elastic and protruding scab (iv) Regrowth bristles visible at the burn induction site (v) No edema and inflammation around the wound

apitherapeutic formulation, the signals of Cu^{2+} in ceruloplasmin and free radicals (line III) strongly decreased after 10 days of therapy, and after 21 days of therapy it increased slightly over the initial value characteristic for the day before burn infliction (Figure 3). The comparison of the multicomponent EPR spectra of blood may be useful for the presentation of the changes in its paramagnetic centers during the healing process of the burned wounds. Repair of the damaged tissue represents the “fundamental” response to injury, including the replacement of damaged structures with a living tissue that restores the integrity of the skin [32]. In order to modify the wound healing, throughout the reduction or elimination of scarring or to achieve more effective restoration of normal tissue, it is necessary to understand the mechanism of oxidative stress influence on all of the stages of the regeneration process [33–35].

The first phase of wound healing begins immediately upon injury and is dedicated to hemostasis and the formation of a provisional wound matrix. In response to tissue injury, inflammatory cells, including neutrophils, monocytes, and macrophages, are recruited to wounded tissue. Free radicals

released mainly from activated neutrophils contribute to local tissue impairment causing oxidative damage of proteins, lipids, DNA, and RNA [35]. In this way, free radicals are participants in local damage following thermal injury. The acute inflammatory response is followed by the proliferative phase of wound healing, when the wound is rebuilt with new granulation tissue made up of collagen and other extracellular matrix components. The main objective of the repair phase is to achieve protection of the wound’s surface via the formation of granulation tissue and a new epithelial cover and to restore the vascular network to nourish the new tissues. It should be noted that granulation is an oxygen-dependent process [36–38].

Repair of the skin ends with a remodeling phase, which results in wound contraction and scar tissue formation. Collagen is remodeled from type III to type I. Cross-linking of collagen reduces scar thickness and makes the skin area of the wound stronger. Adequate level of oxygen is absolutely essential for the cross-linking process [39–41].

The proposed concept of the role of free radicals in each of the wound healing stage has important implications in

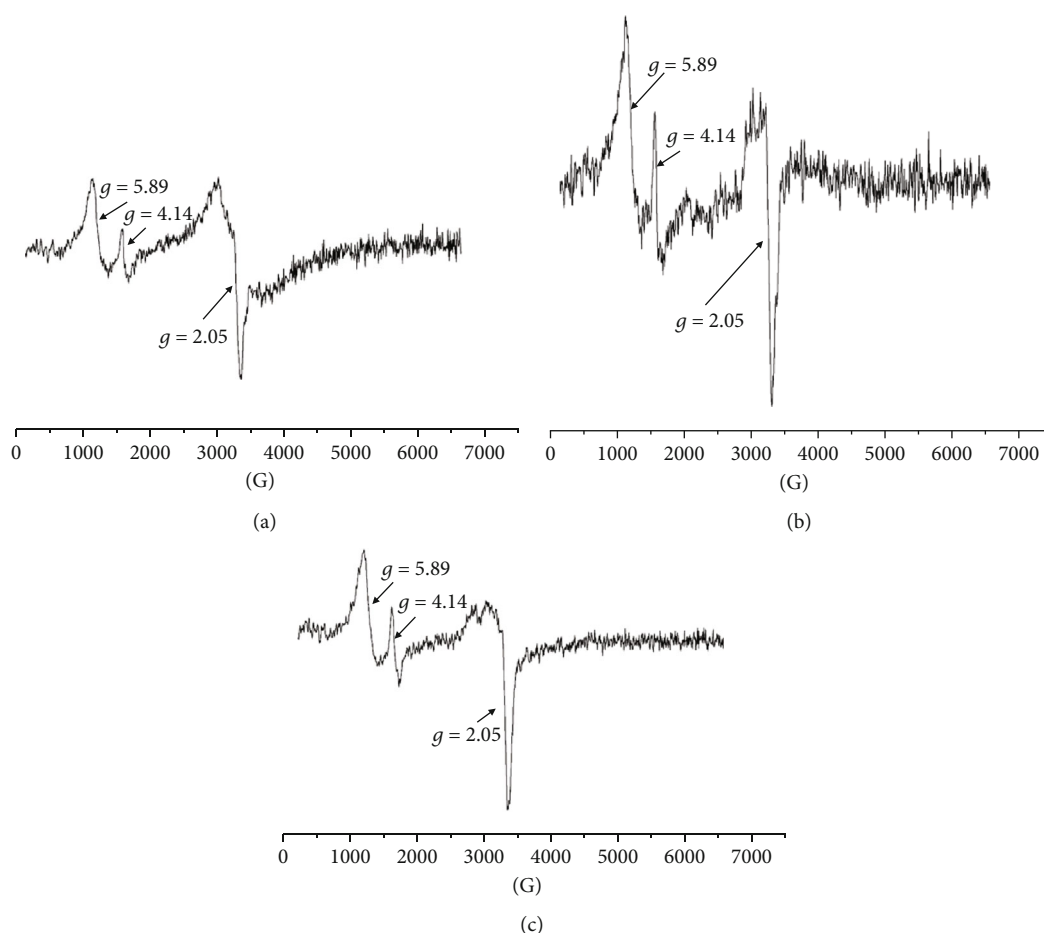


FIGURE 1: The first derivative EPR spectrum of paramagnetic centers: the high spin Fe^{3+} in methemoglobin (line I), high spin Fe^{3+} in transferrin (line II), Cu^{2+} in ceruloplasmin and free radicals (line III), in blood for skin (a) before burn infliction (day 0) and for burned wounds treated with the propolis nanofiber dressing at: (b) 10 and (c) 21 days of therapy. B—magnetic induction.

burn management, indicating that compounds with antioxidant potential, including propolis, can improve the healing of thermal burns.

Except for the formation of free radicals, injury elicits the acute phase response, which increases in hepatic synthesis of proteins, including among others, ceruloplasmin and transferrin. Taking part in the oxidative stress transferrin, ceruloplasmin, and methemoglobin are also involved in iron metabolism [42]. Previously described metal—a vital cofactor for proteins and enzymes involved in energy metabolism, respiration, DNA synthesis, cell cycle arrest, and apoptosis—during oxidative stress processes, acts as a transition metal, which exists in two stable states, Fe^{2+} (electron donor) and Fe^{3+} (electron acceptor) [43]. In the course of wound healing, the mentioned metal is postulated to play a beneficial role in collagen synthesis, while the iron deficiency results in an impaired T cell and phagocyte function during the inflammatory phase, resulting in a subsequent decreased tensile strength [44]. Moreover, during the earliest phase of wound repair, the level of the another estimated indicatory molecule—transferrin (Tf) can be elevated, in response to infection and inflammation, therefore the concentration of Tf usually increases. What is of particular interest, Tf represents the bacteria's growth inhibition factor—essential to

prevent tissue damage [45, 46]. Therefore, reduced transferrin amplitude on the 10th day of the experiment may be caused by the use of iron in the course of the Fenton reaction during the acute phase of wound healing [43]. Last but not least, the increase in transferrin amplitude estimated in blood samples, collected on the 21st day of burns management with the novel apitherapeutic dressing, may be connected with the TFs influence on growth and the formation of extracellular matrix, necessary for the proper regulation of biosynthesis phase of the repair process, manifested by stimulation of the collagen biosynthesis [47] and enhancement of accumulation of dermatan/chondroitin sulfate proteoglycans [48]. Another protein of particular importance not only in case of oxidative stress but also in relation to iron metabolism is methemoglobin (MetHb). The mentioned molecule, containing ferric Fe^{3+} iron rather than ferrous Fe^{2+} one, characterised by the decreased ability to bind oxygen, is reported to be reduced in blood after propolis application [49]. The last-mentioned phenomenon seems to be important due to an oxidative damage of haemoglobin resulting in Heinz body formation. Therefore, methemoglobinemia represents a widely used indicator of oxidant damage of red blood cells, determining functional disturbances of membrane and cytoplasmic structures [50]. Furthermore, according to

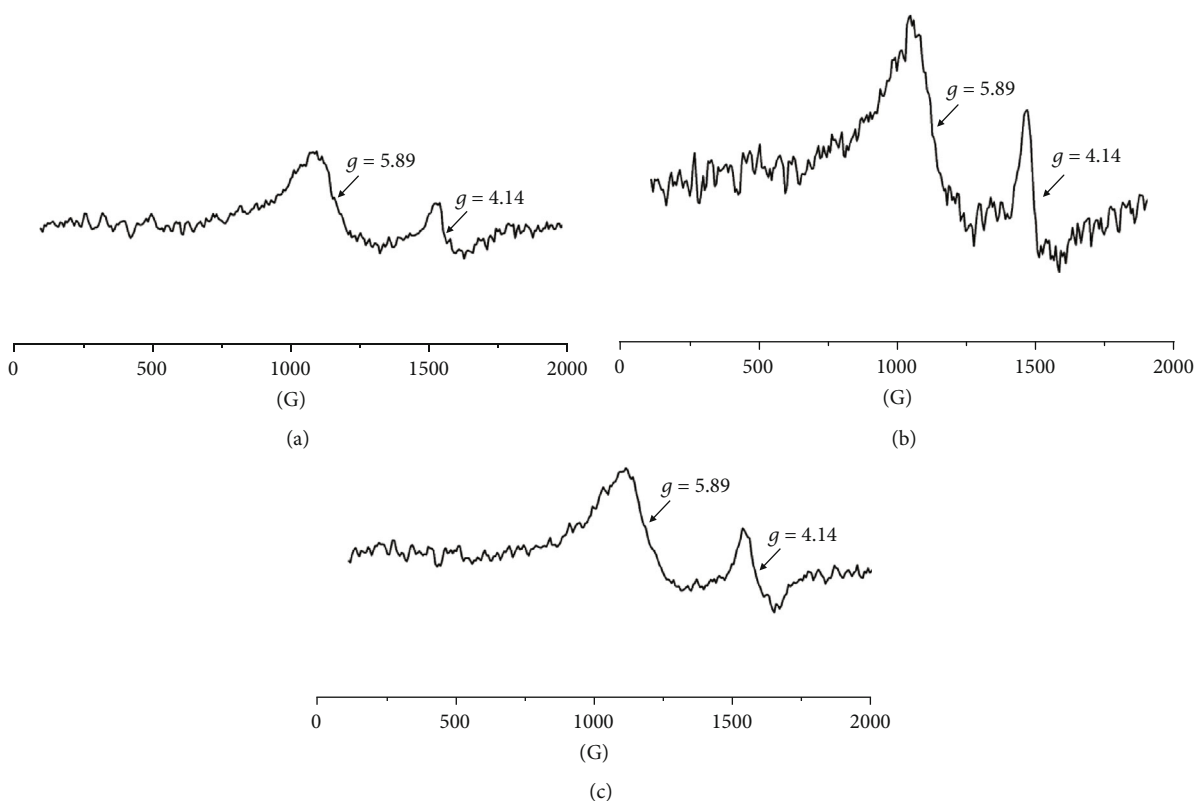


FIGURE 2: The EPR lines of the high spin Fe^{3+} in methemoglobin (line I) and high spin Fe^{3+} in transferrin (line II), in blood for skin (a) before burn infliction (day 0) and for burned wounds treated with the propolis nanofiber dressing on: (b) 10 and (c) 21 days of therapy. B—magnetic induction.

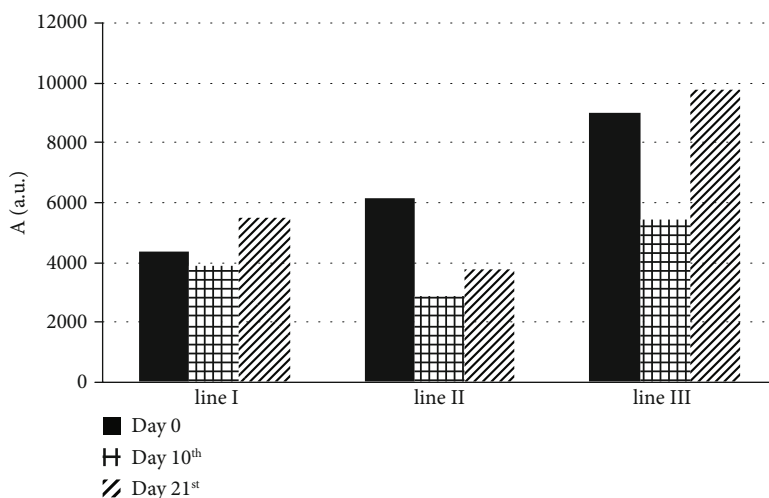


FIGURE 3: The influence of time of therapy for the amplitudes (A) of the high spin Fe^{3+} in methemoglobin (line I), high spin Fe^{3+} in transferrin (line II), and Cu^{2+} in ceruloplasmin and free radicals (line III), in blood for burned skin wounds treated with the propolis. The data, obtained on day 0 (before burn infliction) and, respectively, 10 and 21 days of therapy, were compared.

Moreira et al. [51], propolis was also shown to inhibit the production of methemoglobin under the action of hydrogen peroxide—released by phagocytes to clear tissue debris or kill

the colonizing microorganisms—enhancing the hyaluronan depolymerization [52]. The increase in methemoglobin amplitude found on the final day of the study, remaining in

contradiction with the one stated by Ercis et al. [49], may paradoxically indicate that the time of observation of the impact of the innovative propolis nanofibers on the amplitude of methemoglobin in the sera of experimental animals was too short. Therefore, future observations of the effects of propolis dressing will include an extended period that will probably reveal the overall effect of the proposed propolis formulation on the amplitude of methemoglobin in the blood of experimental animals, qualified for the experimental design of burn wound healing. Moreover, during the above-mentioned phenomenon, the arising wound bed matrix can be protected by the copper and their transporting, acute phase, protein - ceruloplasmin responsible for the catalyzing the ferrous ion into the ferric one [53]. Moreover, ceruloplasmin and copper are crucial for lysyl oxidase and the extracellular cross-linking and maturation of collagen and elastin [54]. Ceruloplasmin—increasing during wound healing—participates in the phospholipid synthesis, necessary for cell membrane creation in the regenerating matrix [52]. However, in the face of oxidative stress reactive oxygen species, including hydrogen peroxide, disrupted copper binding to ceruloplasmin causes a release of the ion responsible for the promotion of oxidative pathology [55]. Therefore, in the course of wound healing particular importance seems to be gained by, the activity of propolis reported to increase the activity of the ceruloplasmin [56, 57]. The last observation seems to confirm the results of the present study experiment, in the course of which, after a previous fall recorded on the 10th day, along with the 21st day of experience, propolis dressing stimulates the increase in ceruloplasmin amplitude, which reaches the values observed at the beginning of the experiment. The evaluation of these molecules, using a unique EPR method, in blood samples of experimental animals may serve to assess the healing effectiveness of the used for the first time, in the experimental burn wounds healing model, the innovative biodegradable dressing containing propolis.

4. Conclusions

The performed electron paramagnetic resonance studies of blood from the organisms in the examples of the skin of burned wounds treated with biodegradable, propolis containing, dressing have pointed out that:

- (1) The high spin Fe^{3+} in methemoglobin, high spin Fe^{3+} in transferrin, and Cu^{2+} in ceruloplasmin and free radicals exist in all the tested blood samples, and they are responsible for their multicomponent EPR spectra
- (2) The amplitudes of the EPR lines, which reflected the concentrations of high spin Fe^{3+} in methemoglobin, high spin Fe^{3+} in transferrin, and Cu^{2+} in ceruloplasmin and free radicals in the blood, depends on the time of therapy
- (3) Paramagnetic centers and free radicals' changes indicate a favorable effect of innovative biodegradable apitherapeutic dressings on burns regeneration, suggesting a pluripotent multifaceted influence of propolis on the prooxidative/antioxidative balance

changes whose components serve a fundamental function in the repair of tissue damages

Data Availability

The WINEPR data used to support the findings of this study have been deposited in the computer that supports an EPR spectrometer produced by Bruker (USA) repository, Medical Physics Division, Faculty of Physics, Adam Mickiewicz University, Poznan, Poland. The contact person is Professor Ryszard Krzyminiewski (rku@amu.edu.pl). The electrospinning method data used to obtain samples of biodegradable, non-woven dressings are patentprotected and so cannot be made freely available. Request for access to these data should be made to Professor Janusz Kasperczyk (jkasperczyk@cmpw-pan.edu.pl) or Mateusz Stojko (mstojko@cmpw-pan.edu.pl).

Conflicts of Interest

The authors declare no conflict of interest.

Acknowledgments

This study was supported by the Medical University of Silesia in Katowice, the grants no. KNW-1-181/N/8/O.

References

- [1] K. Wolska, A. Górka, and A. Adamiak, "Antibacterial properties of propolis," *Advancements of Microbiology*, vol. 55, pp. 343–350, 2016.
- [2] E. Sosin-Bzducha and J. Strzetelski, "P ropolis źródłem flawonoidów korzystnych dla zdrowia i produktywności bydła," *Wiadomości Zootechniczne*, vol. 2, pp. 23–28, 2012.
- [3] A. Oryan, E. Alemzadeh, and A. Moshiri, "Potential role of propolis in wound healing: biological properties and therapeutic activities," *Biomedicine & Pharmacotherapy*, vol. 98, pp. 469–483, 2018.
- [4] B. Kędzia, "Chemical composition of polish propolis. Part I. The initial period of investigations," *Advances in Phytotherapy*, vol. 1, pp. 39–44, 2009.
- [5] M. C. Marcucci, "Propolis-chemical-composition, biological properties and therapeutic activity," *Apidologie*, vol. 26, no. 2, pp. 83–99, 1995.
- [6] V. S. Bankova, S. L. de Castro, and M. C. Marcucci, "Propolis: recent advances in chemistry and plant origin," *Apidologie*, vol. 31, no. 1, pp. 3–15, 2000.
- [7] F. R. S. Corrêa, F. S. Schanuel, N. Moura-Nunes, A. Monte-Alto-Costa, and J. B. Daleprane, "Brazilian red propolis improves cutaneous wound healing suppressing inflammation-associated transcription factor NFκB," *Biomedicine & Pharmacotherapy*, vol. 86, pp. 162–171, 2017.
- [8] S. Huang, C.-P. Zhang, K. Wang, G. Li, and F.-L. Hu, "Recent advances in the chemical composition of propolis," *Molecules*, vol. 19, no. 12, pp. 19610–19632, 2014.
- [9] I. AL-Ani, S. Zimmermann, J. Reichling, and M. Wink, "Antimicrobial activities of European propolis collected from various geographic origins alone and in combination with antibiotics," *Medicines*, vol. 5, no. 1, p. 2, 2018.
- [10] Z. Jastrzębska-Stojko, R. Stojko, A. Rzepecka-Stojko, A. Kabała-Dzik, and J. Stojko, "Biological activity of

- propolis-honey balm in the treatment of experimentally-evoked burn wounds," *Molecules*, vol. 18, no. 11, pp. 14397–14413, 2013.
- [11] A. T. Atayoglu and S. Silici, "Preliminary study on wound healing activity of propolis in albino rats," *International Journal of Innovative Research in Medical Science*, vol. 1, no. 7, 2016.
- [12] M. P. Caley, V. L. C. Martins, and E. A. O'Toole, "Metalloproteinases and wound healing," *Advances in Wound Care*, vol. 4, no. 4, pp. 225–234, 2015.
- [13] L. Rittié, "Cellular mechanisms of skin repair in humans and other mammals," *Journal of Cell Communication and Signaling*, vol. 10, no. 2, pp. 103–120, 2016.
- [14] S. Martinotti and E. Ranzato, "Propolis: a new frontier for wound healing?," *Burns Trauma*, vol. 3, 2015.
- [15] P. Olczyk, K. Komosinska-Vassev, K. Winsz-Szczotka, J. Stojko, K. Klimek, and E. M. Kozma, "Propolis induces chondroitin/dermatan sulphate and hyaluronic acid accumulation in the skin of burned wound," *Evidence Based Complementary and Alternative Medicine*, vol. 2013, pp. 1–8, 2013.
- [16] P. Olczyk, K. Komosińska-Vassev, K. Winsz-Szczotka et al., "Propolis modulates vitronectin, laminin, and heparan sulfate/heparin expression during experimental burn healing," *Journal of Zhejiang University Science B*, vol. 13, no. 11, pp. 932–941, 2012.
- [17] P. Olczyk, K. Komosinska-Vassev, G. Wisowski, L. Mencner, J. Stojko, and E. M. Kozma, "Propolis modulates fibronectin expression in the matrix of thermal injury," *Biomed Research International*, vol. 2014, 10 pages, 2014.
- [18] P. Olczyk, G. Wisowski, K. Komosinska-Vassev et al., "Propolis modifies collagen types I and III accumulation in the matrix of burnt tissue," *Evidence Based Complementary and Alternative Medicine*, vol. 2013, pp. 1–10, 2013.
- [19] J. Kocot, M. Kielczykowska, D. Luchowska-Kocot, J. Kurzepa, and I. Musik, "Antioxidant potential of propolis, bee pollen, and royal jelly: possible medical application," *Oxidative Medicine and Cellular Longevity*, vol. 2018, 29 pages, 2018.
- [20] P. Vit, F. Huq, O. Barth et al., "Use of propolis in cancer research," *British Journal of Medicine and Medical Research*, vol. 8, no. 2, pp. 88–109, 2015.
- [21] M. J. Hoekstra, P. Hupkens, R. P. Dutrieux, M. M. C. Bosch, T. A. Brans, and R. W. Kreis, "A comparative burn wound model in the new Yorkshire pig for the histopathological evaluation of local therapeutic regimens: silver sulfadiazine cream as a standard," *British Journal of Plastic Surgery*, vol. 46, no. 7, pp. 585–589, 1993.
- [22] T. A. Brans, R. P. Dutrieux, M. J. Hoekstra, R. W. Kreis, and J. S. Du Pont, "Histopathological evaluation of scalds and contact burns in the pig model," *Burns*, vol. 20, pp. S48–S51, 1994.
- [23] M. M. Swindle, "Sample collection series blood collection in swine," *Sinclair bio-resources*, pp. 1–4, 2018, <http://www.sinclairresearch.com/assets/sites/2/Blood-Collection-in-Swine.pdf> 01.
- [24] P. Dobrzyński, J. Kasperczyk, H. Janeczek, and M. Bero, "Synthesis of biodegradable copolymers with the use of low toxic zirconium compounds. 1. Copolymerization of glycolide with L-lactide initiated by $Zr(Acac)_4$," *Macromolecules*, vol. 34, no. 15, pp. 5090–5098, 2001.
- [25] Z.-M. Huang, Y.-Z. Zhang, M. Kotaki, and S. Ramakrishna, "A review on polymer nanofibers by electrospinning and their applications in nanocomposites," *Composites Science and Technology*, vol. 63, no. 15, pp. 2223–2253, 2003.
- [26] W. J. Li, C. T. Laurencin, E. J. Caterson, R. S. Tuan, and F. K. Ko, "Electrospun nanofibrous structure: a novel scaffold for tissue engineering," *Journal of Biomedical Materials Research*, vol. 60, no. 4, pp. 613–621, 2002.
- [27] E. Adomavičiūtė, S. Pupkevičiūtė, V. Juškaitė et al., "Formation and investigation of electrospun PLA materials with propolis extracts and silver nanoparticles for biomedical applications," *Journal of Nanomaterials*, vol. 2017, 11 pages, 2017.
- [28] J. E. Wertz and J. R. Bolton, *Electron Spin Resonance: Elementary Theory and Practical Applications*, Chapman and Hall, London, 1986.
- [29] J. A. Weil and J. R. Bolton, *Electron Paramagnetic Resonance: Elementary Theory and Practical Applications (2nd Edition)*, John Wiley & Sons, New York, 2007.
- [30] K. Komosinska-Vassev, P. Olczyk, J. Kasperczyk et al., "EPR spectroscopic examination of different types of paramagnetic centers in the blood in the course of burn healing," *Oxidative Medicine and Cellular Longevity*, vol. 2019, 8 pages, 2019.
- [31] T. Kubiak, R. Krzyminiewski, B. Dobosz, G. Schroeder, J. Kurczewska, and M. Hałupka-Bryl, "A study of magnetite nanoparticles in whole human blood by means of electron paramagnetic resonance," *Acta Bio-Optica et Informatica Medica. Biomedical Engineering*, vol. 21, pp. 9–15, 2015.
- [32] S. A. Eming, P. Martin, and M. Tomic-Canic, "Wound repair and regeneration: mechanisms, signaling, and translation," *Science Translational Medicine*, vol. 6, no. 265, article 265sr6, 2014.
- [33] N. X. Landén, D. Li, and M. Stähle, "Transition from inflammation to proliferation: a critical step during wound healing," *Cellular and Molecular Life Sciences*, vol. 73, no. 20, pp. 3861–3885, 2016.
- [34] T. J. Koh and L. A. DiPietro, "Inflammation and wound healing: the role of the macrophage," *Expert Reviews in Molecular Medicine*, vol. 13, 2011.
- [35] S. Guo and L. A. DiPietro, "Factors affecting wound healing," *Journal of Dental Research*, vol. 89, no. 3, pp. 219–229, 2010.
- [36] J. W. Horton, "Free radicals and lipid peroxidation mediated injury in burn trauma: the role of antioxidant therapy," *Toxicology*, vol. 189, no. 1-2, pp. 75–88, 2003.
- [37] B. Latha and M. Babu, "The involvement of free radicals in burn injury: a review," *Burns*, vol. 27, no. 4, pp. 309–317, 2001.
- [38] J. F. Hansbrough, T. Wikström, M. Braide et al., "Neutrophil activation and tissue neutrophil sequestration in a rat model of thermal injury," *Journal of Surgical Research*, vol. 61, no. 1, pp. 17–22, 1996.
- [39] J. M. Reinke and H. Sorg, "Wound repair and regeneration," *European Surgical Research*, vol. 49, no. 1, pp. 35–43, 2012.
- [40] D. J. Gibson and G. S. Schultz, "Molecular wound assessments: matrix metalloproteinases," *Advances in Wound Care*, vol. 2, no. 1, pp. 18–23, 2013.
- [41] P. A. Ward and G. O. Till, "Pathophysiologic events related to thermal injury of skin," *The Journal of Trauma: Injury, Infection, and Critical Care*, vol. 30, pp. 75–79, 1990.
- [42] G. Cairo, F. Bernuzzi, and S. Recalcati, "A precious metal: iron, an essential nutrient for all cells," *Genes & Nutrition*, vol. 1, no. 1, pp. 25–39, 2006.
- [43] J. A. Wright, T. Richards, and S. K. S. Srail, "The role of iron in the skin and cutaneous wound healing," *Frontiers in Pharmacology*, vol. 5, 2014.

- [44] A. M. Quain and M. N. Khardori, "Nutrition in wound care management: a comprehensive overview," *Wounds*, vol. 27, no. 12, pp. 327–335, 2015.
- [45] M. J. Kotze, D. P. van Velden, S. J. van Rensburg, and R. Erasmus, "Pathogenic mechanisms underlying iron deficiency and iron overload: new insights for clinical application," *Electronic Journal of the International Federation of Clinical Chemistry and Laboratory Medicine*, vol. 2, pp. 108–123, 2009.
- [46] M. Nairz, I. Theurl, D. Wolf, and G. Weiss, "Iron deficiency or anemia of inflammation? Differential diagnosis and mechanisms of anemia of inflammation," *Wiener Medizinische Wochenschrift*, vol. 166, no. 13–14, pp. 411–423, 2016.
- [47] M. Tsunoi, Y. Hakeda, N. Kurihara, N. Maeda, N. Utsumi, and M. Kumegawa, "Effect of transferrin on alkaline phosphatase activity and collagen synthesis in osteoblastic cells derived from newborn mouse calvaria," *Experimental Cell Research*, vol. 153, no. 1, pp. 240–244, 1984.
- [48] S. J. M. Skinner, C. J. Ashby, and G. C. Liggins, "Transferrin stimulates proteoglycan accumulation by fetal lung cells in culture," *Experimental Lung Research*, vol. 15, no. 2, pp. 269–283, 2009.
- [49] K. Ercis, S. Aydoğan, A. T. Atayoğlu, and S. Silici, "Effect of propolis on erythrocyte rheology in experimental mercury intoxication in rats," *Environmental Science and Pollution Research*, vol. 22, no. 16, pp. 12534–12543, 2015.
- [50] A. E. Azab, "Haemato-Protective and Hypolipidemic Effects of Aqueous extract of Libyan propolis against sodium nitrite induced haematotoxicity and hyperlipidemia in Guinea pigs," *Journal of Bioscience and Bioengineering*, vol. 3, no. 4, pp. 22–32, 2015.
- [51] L. L. Moreira, T. Dias, L. G. Dias, M. Rogão, J. P. Da Silva, and L. M. Estevinho, "Propolis influence on erythrocyte membrane disorder (hereditary spherocytosis): a first approach," *Food and Chemical Toxicology*, vol. 49, no. 2, pp. 520–526, 2011.
- [52] M. C. Powanda and E. D. Moyer, "Plasma proteins and wound healing," *Surgery, Gynecology & Obstetrics*, vol. 153, pp. 749–755, 1981.
- [53] V. R. Samyginina, A. V. Sokolov, G. Bourenkov et al., "Ceruloplasmin: macromolecular assemblies with iron-containing acute phase proteins," *PLoS One*, vol. 8, no. 7, article e67145, 2013.
- [54] S. L. M. Dahl, R. B. Rucker, and L. E. Niklason, "Effects of copper and cross-linking on the extracellular matrix of tissue-engineered Arteries," *Cell Transplantation*, vol. 14, no. 6, pp. 367–374, 2017.
- [55] L. Šoltés and G. Kogan, "Catabolism of hyaluronan: involvement of transition metals," *Interdisciplinary Toxicology*, vol. 2, no. 4, pp. 229–238, 2009.
- [56] M. J. Kadhim, A. Los, K. Olszewski, and G. Borsuk, "Propolis in livestock nutrition," *Entomology, Ornithology & Herpetology: Current Research*, vol. 7, no. 1, 2018.
- [57] M. L. Khalil, "Biological activity of bee propolis in health and disease," *Asian Pacific Journal of Cancer Prevention*, vol. 7, no. 1, pp. 22–31, 2006.

Research Article

Safflor Yellow B Attenuates Ischemic Brain Injury via Downregulation of Long Noncoding AK046177 and Inhibition of MicroRNA-134 Expression in Rats

Chaoyun Wang ¹, Hongzhi Wan,² Qiaoyun Wang,² Hongliu Sun,² Yeying Sun,² Kexin Wang,³ and Chunxiang Zhang ⁴

¹Hearing and Speech Institute, Binzhou Medical University, Yantai 264003, China

²School of Pharmaceutical Sciences, Binzhou Medical University, Yantai 264003, China

³Third Class of Senior High School, No. 2 Middle School of Yantai Shandong, Yantai, China

⁴Department of Biomedical Engineering, School of Medicine, University of Alabama at Birmingham, Birmingham, AL, USA

Correspondence should be addressed to Chaoyun Wang; ytwcy@163.com and Chunxiang Zhang; zhangchx999@163.com

Received 8 July 2019; Revised 11 March 2020; Accepted 29 April 2020; Published 4 June 2020

Guest Editor: Reggiani Vilela Gonçalves

Copyright © 2020 Chaoyun Wang et al. This is an open access article distributed under the Creative Commons Attribution License, which permits unrestricted use, distribution, and reproduction in any medium, provided the original work is properly cited.

Stroke breaks the oxidative balance in the body and causes extra reactive oxygen species (ROS) generation, leading to oxidative stress damage. Long noncoding RNAs (lncRNAs) and microRNAs play pivotal roles in oxidative stress-mediated brain injury. Safflor yellow B (SYB) was able to effectively reduce ischemia-mediated brain damage by increasing antioxidant capacity and inhibiting cell apoptosis. In this study, we investigated the putative involvement of lncRNA AK046177 and microRNA-134 (miR-134) regulation in SYB against ischemia/reperfusion- (I/R-) induced neuronal injury. I/R and oxygen-glucose deprivation/reoxygenation (OGD/R) were established *in vivo* and *in vitro*. Cerebral infarct volume, neuronal apoptosis, and protein expression were detected. The effects of SYB on cell activity, cell respiration, nuclear factor erythroid 2-related factor 2 (Nrf2), antioxidant enzymes, and ROS were evaluated. I/R or OGD/R upregulated the expression of AK046177 and miR-134 and subsequently inhibited the activation and expression of CREB, which caused ROS generation and brain/cell injury. SYB attenuated the effects of AK046177, inhibited miR-134 expression, and promoted CREB activation, which in turn promoted Nrf2 expression, and then increased antioxidant capacities, improved cell respiration, and reduced apoptosis. We suggested that the antioxidant effects of SYB were driven by an AK046177/miR-134/CREB-dependent mechanism that inhibited this pathway, and that SYB has potential use in reducing or possibly preventing I/R-induced neuronal injury.

1. Introduction

Stroke is an important cerebrovascular disease that afflicts many people worldwide and frequently causes death or long-term disability [1]. Ischemic stroke is the most common type, accounting for about 80% of all strokes [2, 3]. Brain injury is caused by disruption of blood flow to the brain and is characterized by oxidative stress. In addition, reoxygenation resulting from the restoration of blood flow exacerbates tissue damage [4].

Pathophysiologically, ischemia and reperfusion can inhibit the activity of endogenous antioxidant enzymes and

promote the overproduction of reactive oxygen species (ROS) [5–7]. Previous studies have shown that antioxidants significantly reduce ischemic damage through the inhibition of ROS production [8–11]. Nuclear factor erythroid 2-related factor 2 (Nrf2) is a reduction-oxidation- (redox-) sensitive transcription factor that binds to antioxidant response elements (ARE) and activates the transcription of antioxidant enzymes. Studies have shown that cysteine residues on protein Keap1 are oxidized by ROS, leading to the release and activation of Nrf2 [12, 13]. Thus, Nrf2 is a useful therapeutic target for reducing or preventing ROS damage in the brain following ischemia/reperfusion (I/R) injury. Cyclic

AMP (cAMP) response element-binding protein (CREB) is a leucine zipper transcription factor that inhibits ROS generation and suppresses severe ischemic injury by upregulating brain-derived neurotrophic factor (BDNF) and Bcl-2 [14, 15].

MicroRNAs (miRNAs) are endogenous, short (≈ 22 nucleotides), noncoding single-strand RNAs that regulate gene expression at the posttranscriptional level by influencing the translation of specific target mRNAs. Recent research revealed that a variety of miRNAs play important roles in ischemic injury through the modulation of cellular redox reactions and mitochondrial function [16]. For example, downregulation of miR-134 enhances Bcl-2 expression and alleviates ischemic injury by regulating CREB activity [17].

Long noncoding RNAs (lncRNAs) play key roles in various cellular contexts under both physiological and pathological conditions, and they are involved in diverse biological processes such as RNA processing, modulation of apoptosis and invasion, and chromatin modification [18–20]. AK046177 is a 606-base pair (bp) noncoding RNA sequence derived from a gene sequence (from 116850844 to 116851448) located on chromosome 13.

Safflower yellow is the flavonoid compound extracted from *Carthamus tinctorius* L., which includes the components hydroxysafflor yellow A (HSYA) and safflor yellow B (SYB). It has been shown to effectively reduce oxidative stress-mediated damage [21, 22]. A study by Wang et al. demonstrated that HSYA significantly increases antioxidant enzyme activity by activating the cAMP/PKA signaling pathway [23]. SYB (Figure 1(a)) is a yellow amorphous powder with a purity of more than 98% by HPLC, and it is water soluble and has demonstrated protective effects in neuronal injury models induced by oxidative stress [24, 25]. However, its effect on brain injury induced by I/R remains to be investigated. This study tested whether SYB reduces I/R-mediated brain injury, and evaluated its potential mechanisms by studying changes in the expression of AK046177, miR-134, Nrf2, and CREB.

2. Materials and Methods

2.1. Experimental Design and Cerebral I/R. Male Sprague-Dawley rats (11 months of age), weighing about 350 to 400 g, were purchased from the Experimental Animal Department of Shandong Luye Pharmaceutical Co. Ltd. (Yantai, China). All animals (5 rats per cage) were bred in a temperature-controlled animal facility with a 12 h light/dark cycle.

Animals were randomly assigned to the following 6 groups: sham ($n = 19$), I/R ($n = 19$), I/R+AK046177 siRNA oligo ($n = 19$), I/R+SYB ($n = 19$), I/R+SYB+miR-134 agomir ($n = 19$), and I/R+AK046177 siRNA oligo+miR-134 agomir ($n = 19$).

Rats were anesthetized with 10% chloral hydrate in 0.9% NaCl (300 mg/kg, i.p.) and placed on a 37°C temperature-controlled heating pad. AK046177 siRNAs and miR-134 agomir were synthesized by GenePharma (Shanghai, China). Except for the sham group, all rats from the other groups were treated as follows: every morning at 9 o'clock, 2 ml of

SYB or saline was administered intravenously at a dose of 6 mg/kg continuously for 3 days prior to I/R injury, and 4 μ l of AK046177 siRNA oligo (100 nM) or miR-134 agomir (80 nM) with Lipofectamine was administered via intracerebroventricular infusion half an hour before ischemia

Middle cerebral artery occlusion (MCAO) was performed according to the monofilament method as described by Longa et al. and Macrae [26, 27]. After 1 h of ischemia followed by 23 h of reperfusion, a single experimenter blinded to treatment condition determined the neurological deficit score of each rat according to Longa et al.'s previously validated five-point scale, described below [26]. Following neurological evaluation, rats were decapitated under deep anesthesia and brains were removed. Some whole brains were sectioned and infarct volume was measured by staining with 2,3,5-triphenyl-tetrazolium chloride (TTC; 1.5%). The right part from the same region of the cerebral cortex (the damaged hemisphere for MCAO) and other brain tissues were isolated and stored at -80°C in a freezer. All animals were treated in accordance with the National Institutes of Health Guide for Care and Use of Laboratory Animals (NIH Publications No. 8023, revised 1996). Animal care and experimental procedures were approved by the Ethics Committee on Animal and Human Experimentation of Binzhou Medical University (approval no. 2016077).

2.2. Neurological Tests. After 23 hours of reperfusion, eight rats of each group were subjected to a modified neurological examination designed to evaluate total motor deficit [28]. Briefly, rats were placed on a 10–20 cm horizontal screen, which was rotated from a horizontal to vertical position. The length of time each rat remained on the vertical screen was recorded and scored as 1 point per 5 s, to a maximum of 15 s (3 points). Rats were then placed at the center of a horizontal wooden rod, and the length of time they remained on the rod was recorded and scored as 1 point per 10 s, to a maximum of 30 s (3 points). Rats were placed on a horizontal rope, and the length of time each rat remained on the rope was recorded and scored as 1 point per 2 seconds, to a maximum of 6 s (3 points). A total motor score (TMS) was calculated based on the results of these assessments (maximum 9 points).

2.3. TUNEL Staining. After 23 hours of reperfusion, three rats of every group were anesthetized and intracardially perfused with 4% paraformaldehyde (PFA) in 0.1 M phosphate-buffered saline (PBS; pH 7.4). Following perfusion, the brains were removed and postfixed overnight in 4% PFA at 4°C. The brains were embedded in paraffin and sliced into coronal sections (5 μ m; Leica Biosystems, Wetzlar, Germany). Apoptosis was detected using an *in situ* cell death detection kit (Roche, Germany), in accordance with the manufacturer's protocol. Samples were stained with DAPI for 5 min, following which apoptotic (TUNEL-positive) cells were visualized as localized bright red signals on a black background using a DMR fluorescence microscope (Leica Microsystems, Wetzlar, Germany). An apoptotic index (AI) was determined as the ratio of apoptotic cells to the total number of cells, averaged from 3 sections per animal.

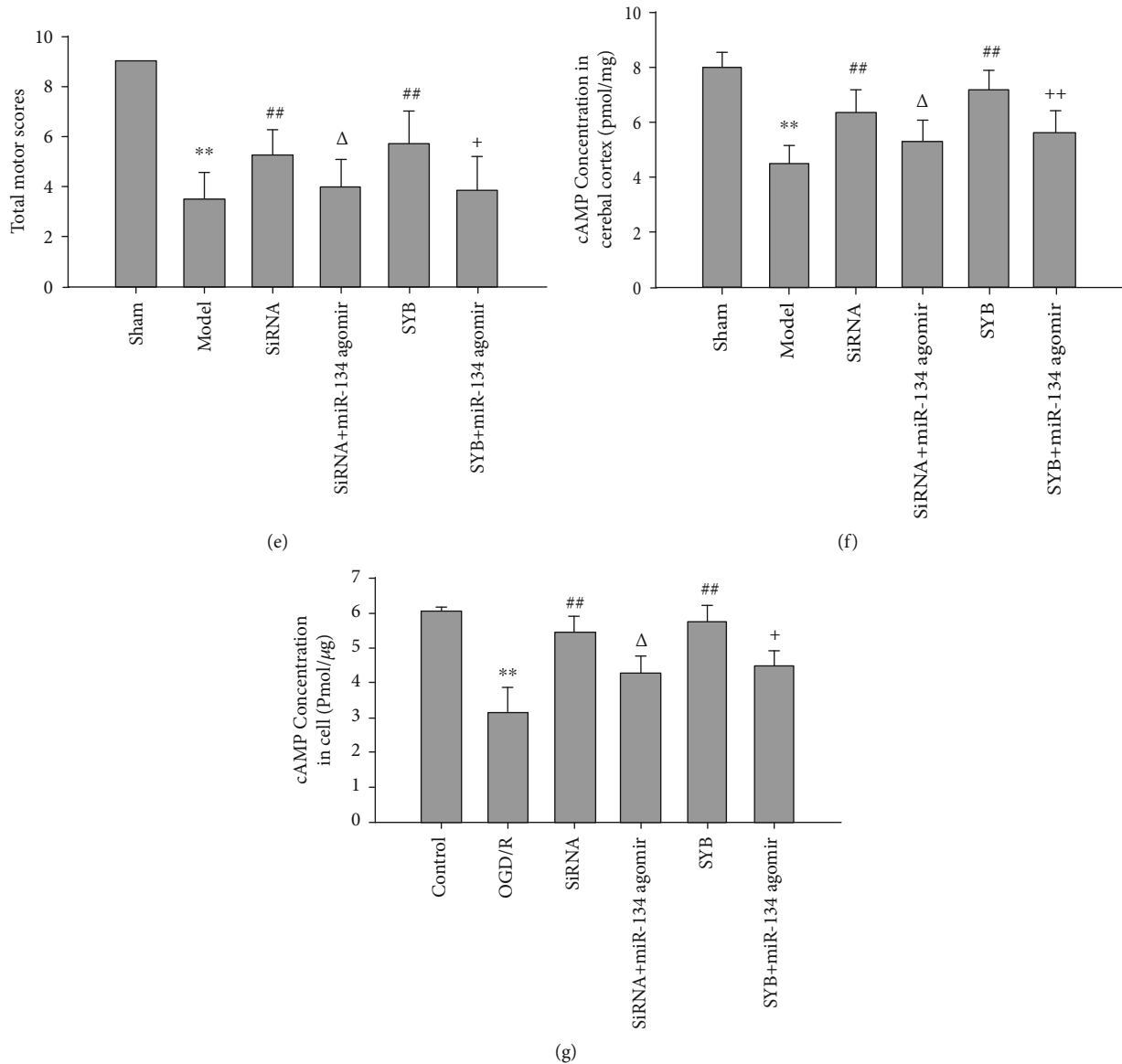


FIGURE 1: Effect of safflor yellow B on neurological deficit score, infarction area, total motor score, and cAMP level. (a) Chemical structure of safflor yellow B. As shown in (b)–(e), rats were divided into six groups: sham, ischemia/reperfusion (I/R), AK046177 siRNA, AK046177 siRNA+miR-134 agomir, SYB, SYB+miR-134 agomir. Except for the sham group, all rats in the other groups had established ischemia for 1 h followed by reperfusion for 23 h. SYB and saline were administrated by tail vein continuously for three days before treatment with I/R, and miR-134 agomir and AK046177 siRNA were given via intracerebroventricular injection. The neurological deficit score of each rat was obtained according to Longa's method. Infarct volumes were measured by staining brain sections with 2,3,5-triphenyltetrazolium chloride. (a) represents pathological changes of cerebral infarction ((a) sham; (b) I/R; (c) AK046177 siRNA; (d) AK046177 siRNA+miR-134 agomir; (e) SYB; (f) SYB+miR-134 agomir). (b) represents neurological deficit scores. (c) represents the infarction area. (d) represents total motor scores ($n = 8$). As shown in (f)–(g), cAMP levels in the cerebral cortex and primary fetal cortical cells were detected using a ^{125}I -radioimmunoassay according to the method described by the manufacturer. Data are presented as mean \pm S.D. ($n = 8$ in tissues; $n = 3$ in cells). One-way ANOVA test was used to determine statistical significance. ** $P < 0.01$ vs. the sham group or the control group, ## $P < 0.01$ vs. the I/R group or the OGD/R group, $\Delta P < 0.05$ or $\Delta\Delta P < 0.01$ vs. the AK046177 siRNA group, and $^+P < 0.05$ or $^{++}P < 0.01$ vs. the SYB group.

2.4. Cell Culture. Primary cortical cells from the cerebral cortex of fetal rats (E16–18) were grown in Dulbecco's Minimal Essential Medium (DMEM) supplemented with 10% (v/v) fetal bovine serum, 1% penicillin/streptomycin, and 3.7 g/l NaHCO_3 . Before the initiation of the experiment, the cells were seeded in dishes and precultured for 3 to 5 days at 37°C in a humidified incubator, with 5% CO_2 and 95%

air. They were then cultured and divided into 7 groups: control, oxygen-glucose deprivation/reoxygenation (OGD/R), AK046177 siRNA (OGD/R+siRNA), AK046177 siRNA+agomiR-134 (OGD/R+siRNA+agomiR-134), SYB (OGD/R+SYB), SYB+agomiR-134 (OGD/R+SYB+agomiR-134), and negative control (OGD/R+NC). All groups excluding the control group were cultured in glucose-free DMEM under

hypoxic conditions (1% O₂/94% N₂/5% CO₂) at 37°C for 4 h. Thereafter, media in all groups was replaced with normal DMEM, and culturing continued for 20 h of reoxygenation under normoxic conditions (95% air/5% CO₂). Cells were pretreated with SYB (final concentration of 0.5 mmol/l), AK046177 siRNA (80 nmol/l), and agomiR-134 (50 nmol/l) for 24 h prior to OGD/R. siRNA, agomiR-134, or control antagomir were transfected into primary cortical cells for 24 h using Lipofectamine RNAiMAX Transfection Reagent (Invitrogen) according to the manufacturer's protocol.

2.5. Assessment of Cell Viability. The 3-(4,5-dimethylthiazol-2-yl)-2,5-diphenyl-tetrazolium bromide (MTT) assay was used to determine cellular mitochondrial dehydrogenase activity in primary cortical cells (2 × 10⁴/ml) cultured in 96-well plates. Dark blue formazan crystals formed in intact cells which were solubilized with dimethyl sulfoxide (DMSO). The absorbance was measured at 490 nm with a microplate reader (Thermo Fisher Scientific, Waltham, MA, USA). Results were expressed as the percentage of MTT reduced, and data were normalized to the absorbance of control cells, considered 100%.

2.6. Measurement of Apoptosis. Primary cortical cells (9 × 10⁵/ml) cultured in 6-well plates were harvested and processed in accordance with the procedure of the Annexin V-FITC Apoptosis Detection Kit (BD Biosciences). Finally, flow cytometry (Epics-XL, Beckman Coulter, USA) was performed to quantify apoptosis. The results are expressed as percent of the control value.

2.7. Measurement of Antioxidative Enzyme Activity and Malondialdehyde Level. In vivo cerebral cortical tissue was dissected and homogenized, and in vitro cells (4 × 10⁵/ml) were harvested and lysed using ultrasound, then centrifuged at 12,000 g for 5 min at 4°C. The supernatants were collected, and the activities of superoxide dismutase (SOD) and glutathione peroxidase (GPx), as well as the malondialdehyde (MDA) concentration, were detected according to the manufacturer's assay kits (Nanjing Jiancheng Bio-Engineering Institute Co., Ltd.).

2.8. Assay of Intracellular Total ROS Levels. Intracellular ROS production in primary cells was assessed by measuring the fluorescence intensity of 2,7-dichlorodihydrofluorescein diacetate (DCFH-DA). After being reoxygenated for 20 h, cells (9 × 10⁵/ml) were treated with 10 μM DCFH-DA in PBS in the dark at 37°C for 30 min, and then washed with PBS to remove excess dye. The level of fluorescence intensity was immediately evaluated at (excitation) 488 nm and (emission) 525 nm with a microplate reader (BioTek Synergy H4, USA).

2.9. Measurement of Intracellular cAMP Concentration. Primary cortical neurons were seeded in 6-well plates, and cells (1 × 10⁶/ml) were subjected to OGD/R, then harvested by centrifugation at 1000 g for 10 min at 4°C. Cerebral cortical tissue and cells were homogenized in 50 mmol/l acetic acid buffer (pH 4.75) and lysed by sonication. The homogenate was centrifuged at 3000 g for 15 min at 4°C. cAMP levels in the supernatant were determined using a ¹²⁵I-radioimmuno-

assay according to the RIA kit instructions (Nuclear Medicine Laboratory of Shanghai University of Traditional Chinese Medicine, Shanghai, PR China).

2.10. Real-Time PCR. The expression levels of AK046177 and miR-134 were analyzed by real-time PCR in both brains and cell cultures after I/R or OGD/R. Total RNA was isolated from 30 mg cerebral cortical tissue or cells (1 × 10⁶/ml) seeded on 6-well plates with TRIzol Reagent (Invitrogen) [29], and reverse transcribed into cDNA using miScript Reverse Transcription Kit (Takara, China). Predesigned PCR primer/probes of miR-134 were obtained from GenePharma (Shanghai, China) for AK046177 and miRNA-134, with β-actin and U6 small nuclear RNA (U6) used as an internal control. Quantitative PCR was conducted as previously described using the TaqMan Assay Kit (Applied Biosystems) [30]. The relative expression levels of AK046177 and miRNA-134 were calculated using the 2^{-ΔΔCT} method [31].

2.11. Observation of Mitochondrial Morphology. Mitochondrial ultrastructure was analyzed using a transmission electron microscope (TEM) (Olympus, Tokyo, Japan). Primary cortical neurons were seeded in a 6-well plate and treated as described as above. After reperfusion, cells (9 × 10⁵/ml) were harvested and fixed in 2.5% (v/v) glutaraldehyde, then collected into a centrifuge tube using a scraper. Samples were fixed in osmic acid, dehydrated by the gradual addition of ethanol, and embedded in epoxy resin. Embedded samples were sectioned into ultraslices, stained with uranyl acetate and lead citrate, and then observed by TEM.

2.12. Measurement of Cell Respiration. Oxygen consumption rate (OCR) was measured using high-resolution respirometry in a 2-channel titration injection respirometer at 37°C (Oxygraph-2k, Oroboros, Innsbruck, Austria), as previously described by Pesta and Gnaiger [32]. Briefly, after reperfusion, cells (1 × 10⁶/ml) were harvested and placed in A and B pools with DMEM. Three readings were taken after the addition of each of the following mitochondrial inhibitors, prior to injection with the subsequent inhibitors. Inhibitors used were oligomycin (2 mg/ml), carbonyl cyanide chlorophenylhydrazine (CCCP; 10 mM), and rotenone (2 mM). OCR was automatically calculated and recorded by a sensor cartridge and Oroboros software.

2.13. Western Blot Analysis. Cerebral cortex tissues or cell cultures (1 × 10⁶/ml) were homogenized with lysis buffer and centrifuged at 12,000 g for 15 min. Forty micrograms of protein from each sample was separated on a SDS/10 and 15% polyacrylamide gel and then transferred to a polyvinylidene difluoride (PVDF) membrane (Millipore, IPVH00010, Bedford, MA, USA). After being blocked with 1% bovine serum albumin for 120 min at 20°C ± 2°C, membranes were incubated with anti-Nrf2 (1:1000; SAB4501984; Sigma-Aldrich), anti-Bcl-2 (1:1000; SAB4500003; Sigma-Aldrich), anti-Bax (1:1000; SAB4502546; Sigma-Aldrich), anti-caspase3 (1:500; ab32042; Abcam), anti-CREB (1:1000; SAB4500441; Sigma-Aldrich), anti-phospho-CREB (pSer¹³³;

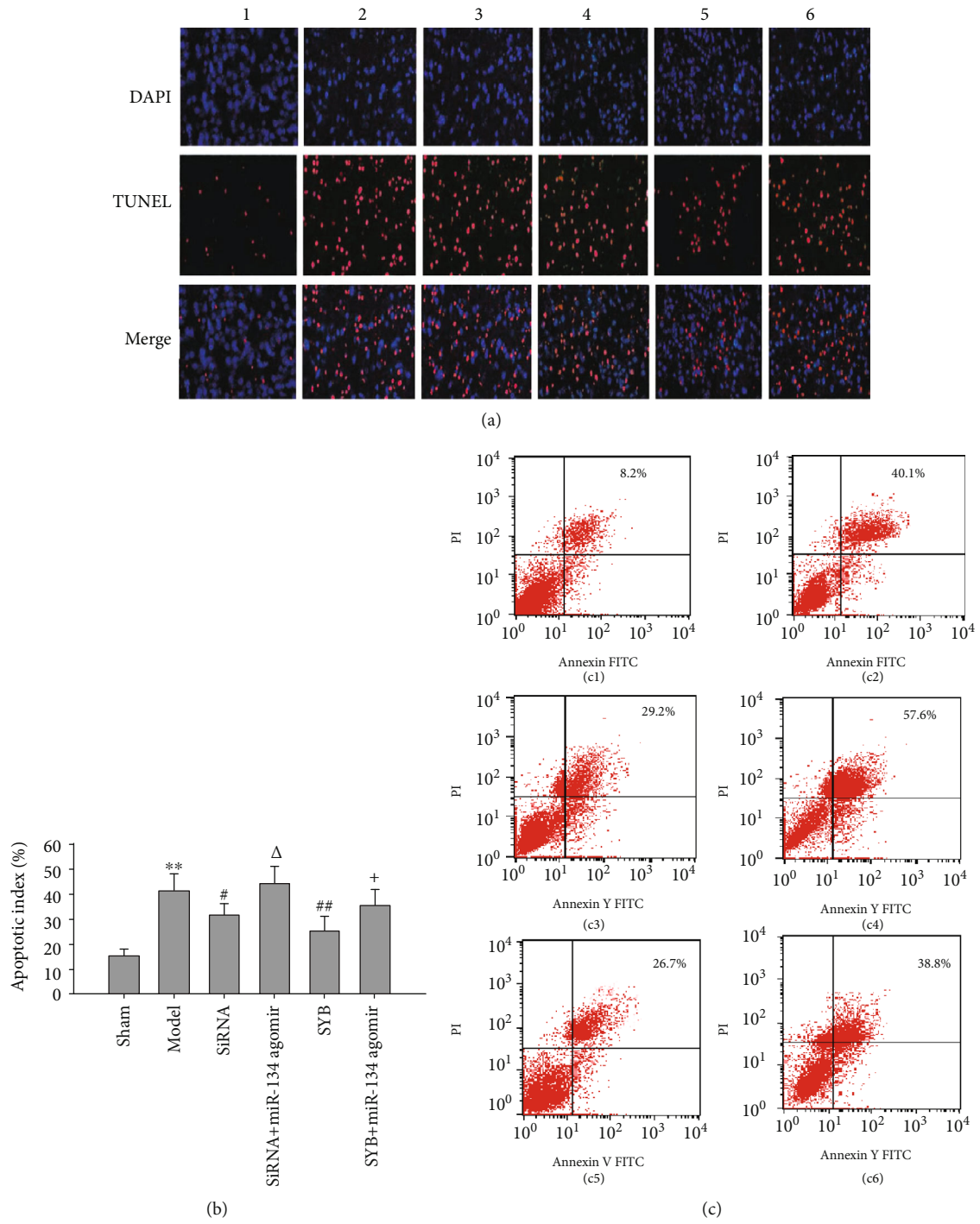


FIGURE 2: Continued.

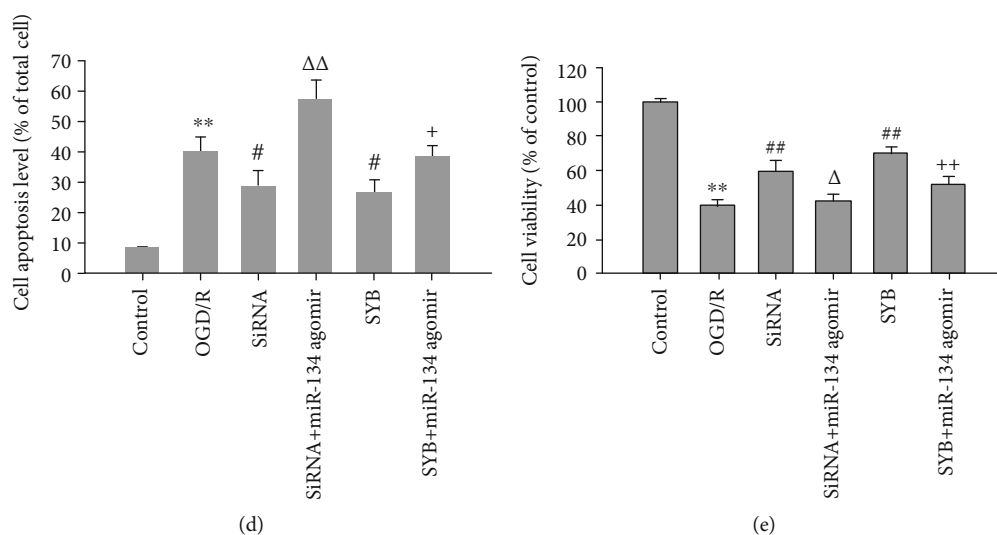


FIGURE 2: Effect of safflor yellow B on TUNEL-positive cells, cell viability, and apoptosis. Rats were divided into six groups: sham, ischemia/reperfusion (I/R), AK046177 siRNA, AK046177 siRNA+miR-134 agomir, SYB, and SYB+miR-134 agomir. (a) Representative images showing TUNEL-positive cells of cerebral cortex in different groups ($\times 200$ magnification; 1, 2, 3, 4, 5, and 6 represent sham, ischemia/reperfusion (I/R), AK046177 siRNA, AK046177 siRNA+miR-134 agomir, SYB, and SYB+miR-134 agomir, respectively). (b) Apoptotic (TUNEL-positive) cells were detected, AI = (number of apoptotic cells/total cell number counted) $\times 100\%$ ($n = 3$). Primary fetal cortical cells were seeded in 96-well and 6-well plates and divided into six groups: control, OGD/R, AK046177 siRNA, AK046177 siRNA+miR-134 agomir, SYB, and SYB+miR-134 agomir. Apart from the control group, all cells in the other groups were cultured in glucose-free DMEM and hypoxic conditions (1% O_2 /94% N_2 /5% CO_2) at $37^\circ C$ for 4 h. Thereafter, all groups' media were replaced with normal DMEM, and culturing continued for 20 h of reoxygenation under normoxic conditions (95% air/5% CO_2). The cells were pretreated with SYB, AK046177, and miR-134 agomir before being exposed to OGD/R. Cell viability was detected by the MTT method. Cell apoptosis was analyzed using flow cytometry. (c1)–(c6) represent control, OGD/R, AK046177 siRNA, AK046177 siRNA+miR-134 agomir, SYB, and SYB+miR-134 agomir, respectively. (d) represents cell apoptosis ($n = 3$). (e) represents cell viability ($n = 8$). Data are presented as mean \pm SD. One-way ANOVA test was used to determine statistical significance. ** $P < 0.01$ vs. the sham group or the control group, # $P < 0.05$ or ## $P < 0.01$ vs. the I/R group or the OGD/R group, $\Delta P < 0.05$ or $\Delta\Delta P < 0.01$ vs. the AK046177 siRNA group, and + $P < 0.05$ or ++ $P < 0.01$ vs. the SYB group.

1:1000; C9102; Sigma-Aldrich), or anti-Nox4 (1:500; ab109225; Abcam) overnight at $4^\circ C$ and washed with TBST (3×15 min). The corresponding horseradish peroxidase (HRP-) conjugated secondary antibody was added and left for 50–60 min at $20^\circ C \pm 2^\circ C$, followed by washing with TBST (3×10 min). Protein bands were visualized using a chemiluminescence reagent (ECL kit; Amersham Corporation, Arlington Heights, CA, USA). The relative density of the protein bands was quantified by densitometry using an Image Acquiring and Analysis System (Leica Com., Germany). β -Actin was used to normalize protein loading. ERK1/2 phosphorylation was calculated as the ratio of normalized arbitrary units (a.u.) of (phosphorylated ERK1/2)/(total ERK1/2).

2.14. Determination of NADPH Oxidase Activity. NADPH oxidase activity was assayed using an Amplitude™ Fluorimetry NADPH Assay Kit (AAT Bioquest, USA) according to the manufacturer's instructions. Primary cortical neurons were seeded in 24-well plates and treated. Rats were treated in vivo as described above. Cells (4×10^5 /ml) and tissues were lysed or homogenized, then centrifuged. The supernatant and NADPH oxidase reaction mixture were incubated at $37^\circ C$ for 2 h. The increase in fluorescence was monitored using a microplate reader (BioTek Synergy H4, USA) at

excitation and emission wavelengths of 540 and 590 nm, respectively.

2.15. Statistical Analysis. Data are presented as mean \pm standard deviation (SD). The statistical analysis of the results was performed via one-way analysis of variance (ANOVA) followed by Student's *t*-test. All analyses were performed using SPSS 10.0 software (SPSS, Inc., San Rafael, CA, USA). Probabilities lower than 5% ($P < 0.05$) were considered statistically significant.

3. Results

3.1. Effect of SYB on Neurological Deficit Score, Infarct Volume, and Motor Function. As shown in Figures 1(b)–1(e), I/R significantly enhanced neurological deficit score and infarcted area and decreased motor scores compared to shams ($P < 0.05$ and $P < 0.01$). Intraventricular injection of AK046177 siRNA or intravenous injection of SYB was able to significantly decrease neurological deficit scores and infarct volume and enhance motor scores ($P < 0.05$ and $P < 0.01$, respectively). In addition, miR-134 agomir was capable of reversing the improvement in neurological deficit score, infarct volume, and motor scores of SYB and AK046177 siRNA ($P < 0.05$ and $P < 0.01$, respectively).

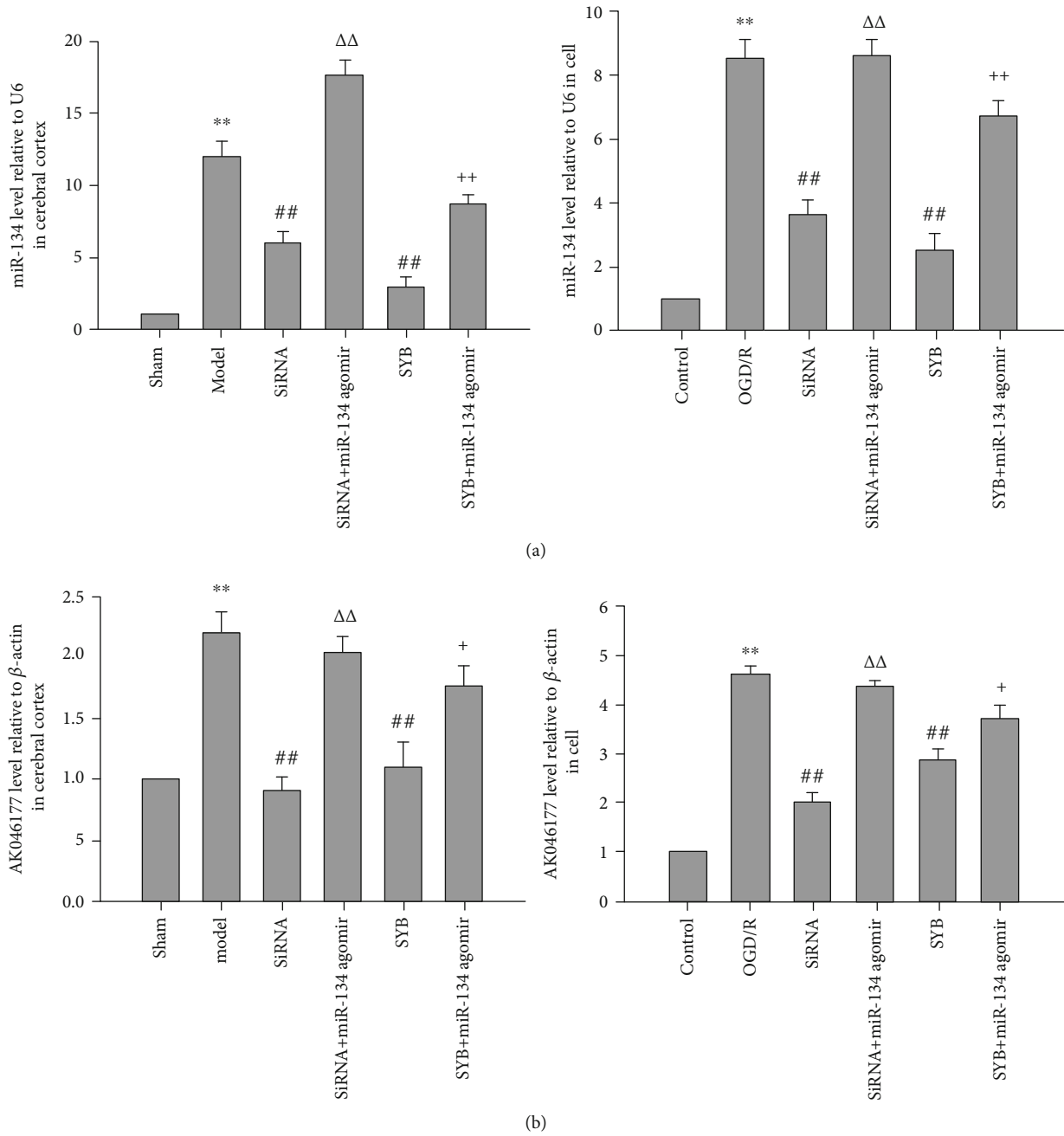


FIGURE 3: Continued.

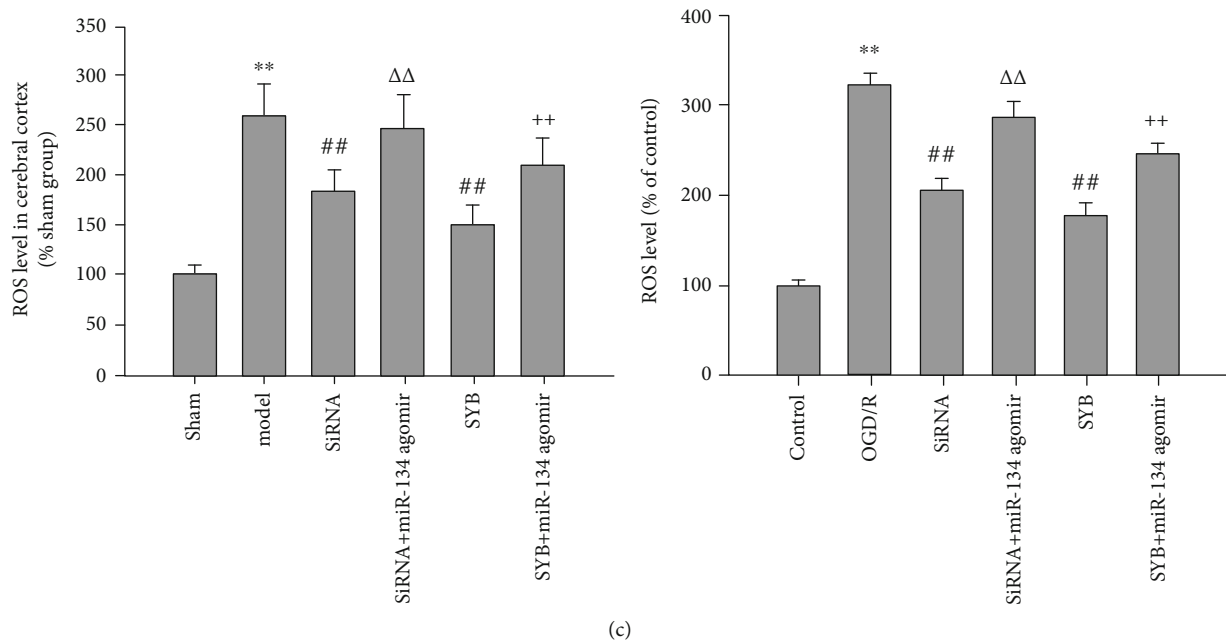


FIGURE 3: Effect of safflor yellow B on ROS level and the expression of AK046177 and miR-134. Rats and primary fetal cortical cells were used to establish the I/R model and the OGD/R model, respectively. After I/R or OGD/R for 24 h, the total RNA of every group was isolated and then reverse transcribed into cDNA. The expression levels of AK046177 and miR-134 were measured by real-time PCR. (a1), (a2), (b1), and (b2) represent miR-134 and AK046177 expression levels in the cerebral cortex and primary fetal cortical cells, respectively. ROS generation was measured according to the procedure of the assay kit provided by the manufacturer. (c1) and (c2) represent ROS levels in the cerebral cortex and the primary fetal cortical cells, respectively. Data are presented as mean \pm SD ($n = 8$ in tissues; $n = 3$ in cells). One-way ANOVA test was used to determine statistical significance. ** $P < 0.01$ vs. the sham group or the control group, ## $P < 0.01$ vs. the I/R group or the OGD/R group, $\Delta\Delta P < 0.01$ vs. the AK046177 siRNA group, and + $P < 0.05$ or ++ $P < 0.01$ vs. the SYB group.

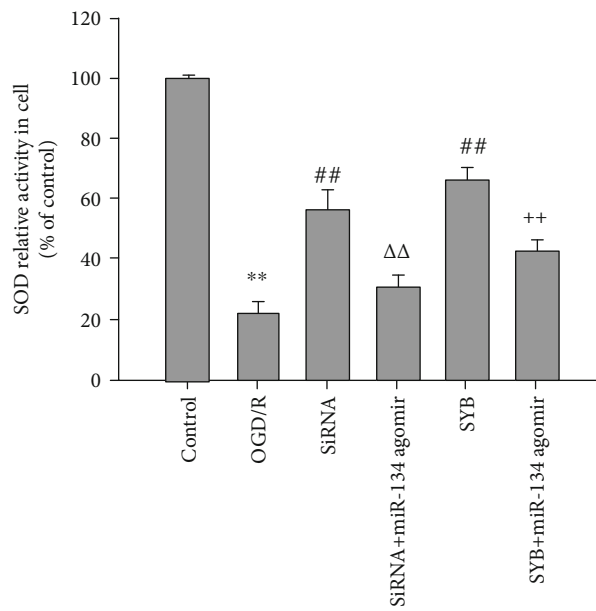
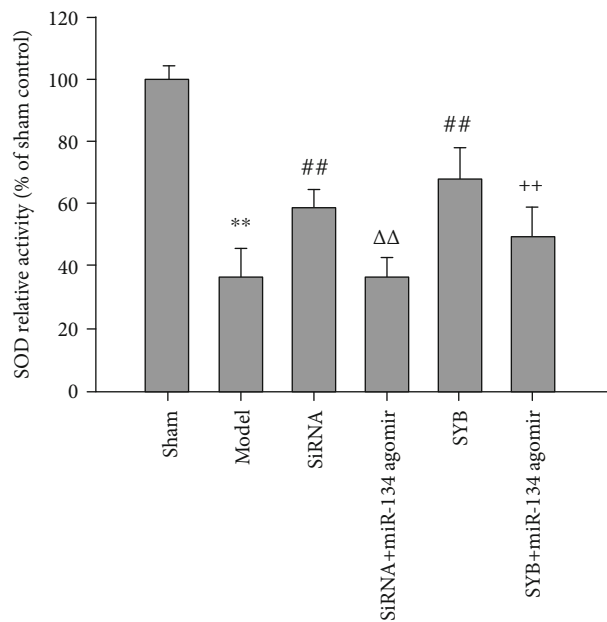
3.2. Effect of SYB on Cell Viability and Apoptosis. I/R and OGD/R produced significant increases in the number of apoptotic cells in vivo ($P < 0.01$; Figures 2(a), 2(b), 2(c1), 2(c2), and 2(d)), as well as significant reductions in cell viability in vitro ($P < 0.01$; Figure 2(e)). This effect was significantly alleviated by AK046177 siRNA and SYB ($P < 0.05$ and $P < 0.01$, respectively; Figures 2(a), 2(b), 2(c3), 2(c5), 2(d), and 2(e)). miR-134 agomir inhibited the protective effect of AK046177 siRNA and SYB and then aggravated I/R- and OGD/R-mediated cell death and damage ($P < 0.05$ and $P < 0.01$, respectively; Figures 2(a), 2(b), 2(c4), 2(c6), 2(d), and 2(e)).

3.3. Effect of SYB on the Intracellular Expression of AK046177 and miR-134 and cAMP Content. As shown in Figures 3(a1), 3(a2), 3(b1), and 3(b2), I/R and OGD/R significantly increased the expression levels of AK046177 and miR-134 ($P < 0.01$), which were decreased by the addition of AK046177 siRNA ($P < 0.01$). SYB effectively attenuated I/R and OGD/R induced increases in the expressions of AK046177 and miR-134 ($P < 0.01$), while the inclusion of miR-134 agomir reversed the SYB-induced attenuation ($P < 0.05$ and $P < 0.01$). Figures 1(f) and 1(g) demonstrate the significant reduction in intracellular cAMP levels caused by I/R and OGD/R; these reductions were further aggravated by miR-134 agomir ($P < 0.05$ and $P < 0.01$, respectively). Following treatment with AK046177 siRNA and SYB, intracellular cAMP levels rose significantly in both the cerebral

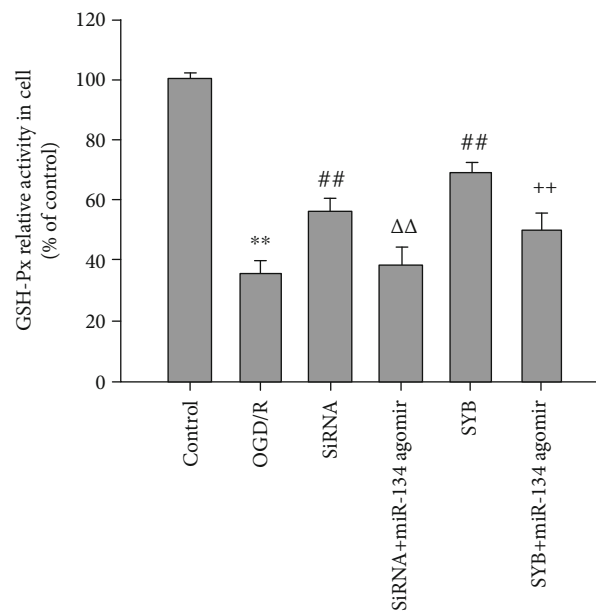
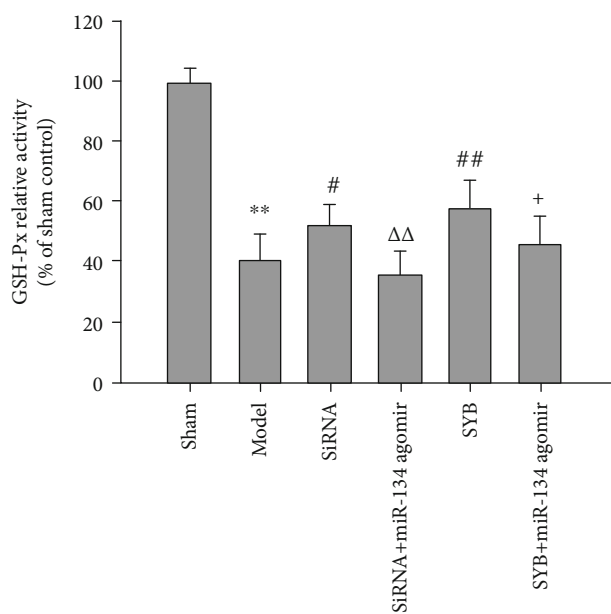
cortex and the primary cultures ($P < 0.05$ and $P < 0.01$). miR-134 agomir significantly reduced the SYB- and AK046177 siRNA-induced increase in intracellular cAMP levels ($P < 0.05$).

3.4. Effect of SYB on SOD and GPx Activities and MDA Levels. As shown in Figures 4(a1), 4(a2), 4(b1), and 4(b2), the activities of SOD and GPx following I/R and OGD/R were reduced ($P < 0.01$), and MDA levels were increased ($P < 0.01$; Figures 4(c1) and 4(c2)) relative to those of the control group. Compared to the I/R or OGD/R groups, SYB significantly increased the activities of SOD and GPx in vitro and in vivo ($P < 0.01$). AK046177 siRNA promoted GPx activity in cells in a manner greater than the effect on SOD activity in vitro and in vivo and GPx activity in vitro ($P < 0.01$). SYB and AK046177 siRNA caused a significant reduction in MDA levels ($P < 0.01$). The effects of SYB and AK046177 siRNA were significantly suppressed by miR-134 agomir ($P < 0.05$ and $P < 0.01$, respectively).

3.5. Effect of SYB on NADPH Oxidase Activity, Nox4 Expression, and ROS Generation. As shown in Figures 5(a1) and 5(a2), compared to the control group, I/R and OGD/R significantly increased NADPH oxidase activity ($P < 0.01$). Compared to the I/R or OGD/R groups, AK046177 siRNA and SYB were capable of significantly abolishing NADPH oxidase activity ($P < 0.01$). After treatment with miR-134 agomir, NADPH oxidase activity in the cerebral cortex and

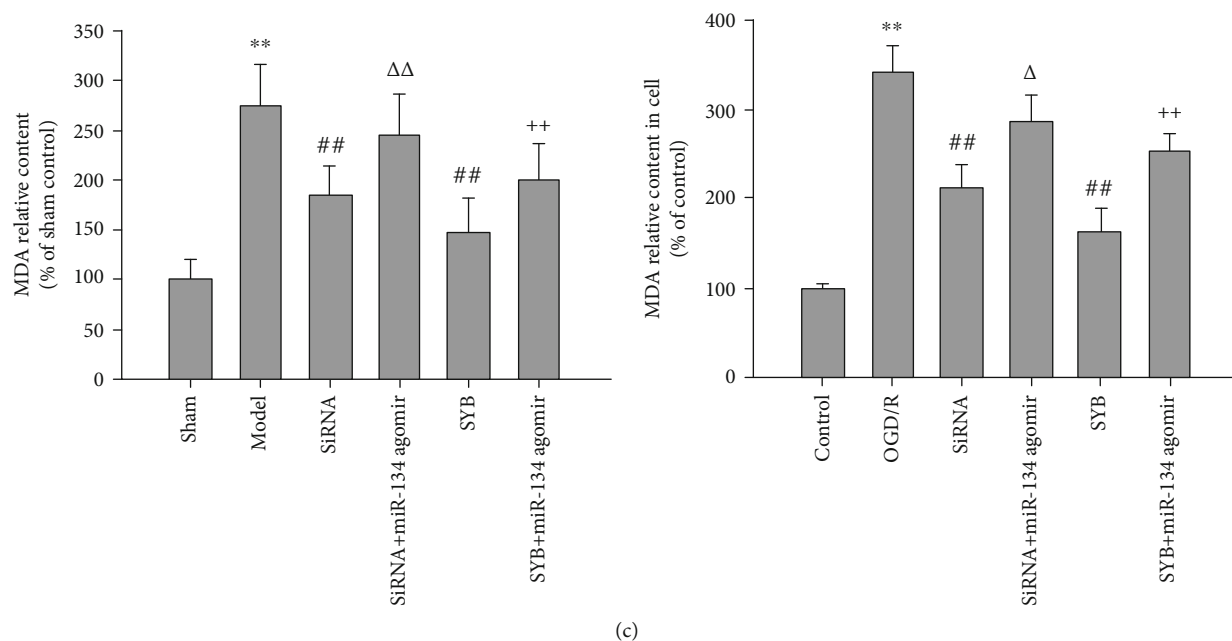


(a)



(b)

FIGURE 4: Continued.



(c)

FIGURE 4: Effect of safflor yellow B on antioxidant enzyme activity and MDA level. Rats and primary fetal cortical cells were used to establish the I/R model and the OGD/R model, respectively. After I/R for 24 h, the cerebral cortex and cells from different groups were collected. The activities of SOD and GSH-Px and the MDA levels in tissues and cells were determined with the spectrophotometrical method according to the procedure described by the assay kit. (a1), (b1), and (c1) represent the activities of SOD and GSH-Px and the MDA level in cerebral cortex tissue. (a2), (b2), and (c2) represent the activities of SOD and GSH-Px and the MDA level in cells. Data are presented as mean \pm SD ($n = 8$ in brain tissues, or $n = 3$ in cells). One-way ANOVA test was used to determine statistical significance. ** $P < 0.01$ vs. the sham group or the control group, # $P < 0.05$ or ## $P < 0.01$ vs. the I/R group or the OGD/R group, $\Delta P < 0.05$ or $\Delta\Delta P < 0.01$ vs. the AK046177 siRNA group, and + $P < 0.05$ or ++ $P < 0.01$ vs. the SYB group.

primary neuronal cultures showed a significant increase relative to the SYB and AK046177 siRNA groups ($P < 0.05$ and $P < 0.01$, respectively).

Nox4 directly reflects NADPH oxidase activity. Our data showed that I/R and OGD/R significantly promoted Nox4 expression relative to the sham and control groups ($P < 0.01$). Both SYB and AK046177 siRNA were able to significantly suppress Nox4 expression, an effect reversed by miR-134 agomir ($P < 0.01$ and $P < 0.05$; Figures 5(b1), 5(b2), 5(c1), and 5(c2)).

ROS levels in cells exposed to OGD/R and cerebral cortex of rats induced by I/R were higher than those of the control group and the sham group ($P < 0.01$; Figures 3(c1) and 3(c2)). This effect was significantly mitigated by AK046177 siRNA and SYB, which also decreased ROS generation relative to the OGD/R group and the sham group ($P < 0.01$). The inhibitory effects of SYB and AK046177 siRNA on ROS generation were significantly ameliorated by miR-134 agomir in vitro ($P < 0.01$).

3.6. Effect of SYB on the Expressions of Nrf2, CREB, pCREB, Caspase3, Bcl-2, and Bax. As seen in Figures 6(a1)–6(e2), the ratio of Bax/Bcl-2 and caspase3 expression in the I/R and OGD/R groups were higher than those in the sham or control groups ($P < 0.01$). AK046177 siRNA and SYB significantly increased Nrf2 expression and the ratio of pCREB/CREB and decreased caspase3 expression and the ratio of Bax/Bcl-2, relative to the I/R and OGD/R groups

($P < 0.01$ and $P < 0.05$). miR-134 agomir reversed these effects, and increased the ratio of Bax/Bcl-2 and caspase3 expression, and reduced the ratio of pCREB/CREB and Nrf2 expression, relative to the AK046177 siRNA and SYB groups ($P < 0.01$ and $P < 0.05$).

3.7. Effect of SYB on Mitochondrial Structure and Cell Respiration. In the control group, the mitochondria were diffused throughout the cell, with an oval or rod-like shape and normal structure (Figure 7(a1)). In OGD/R-treated cells, mitochondria exhibited pathological changes including irregular and swollen shapes, mitochondrial ridge fault, and vesicular mitochondrial clusters, especially adjacent to the cell nucleus (Figure 7(a2)). After treatment with SYB and AK046177 siRNA, an increased number of normal mitochondria were detected (Figures 7(a3) and 7(a5)). miR-134 agomir in addition to SYB and AK046177 siRNA resulted in more irregular and swollen shapes, more mitochondrial cristae fracturing, and severe vacuolization within mitochondria compared to the SYB group (Figures 7(a4) and 7(a6)). Moreover, AK046177 siRNA and SYB were capable of effectively alleviating mitochondrial pathology induced by miR-134 agomir and OGD/R.

OGD/R markedly influenced cellular respiration and decreased the OCR (Figure 7(b)). The OCR in all groups was significantly reduced after treatment with oligomycin. Cells normally increase OCR in response to CCCP in order to maintain the proton gradient and mitochondrial function.

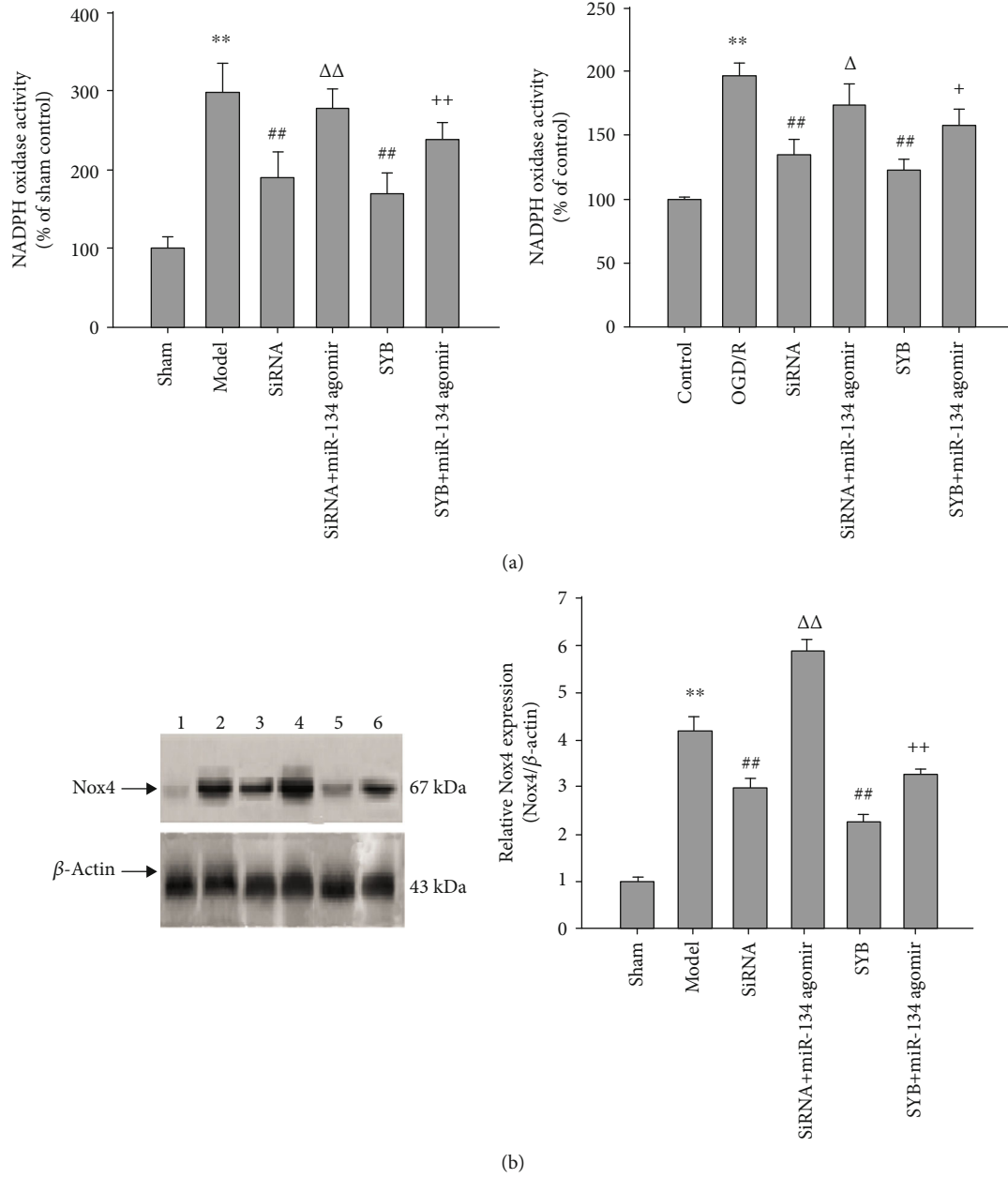
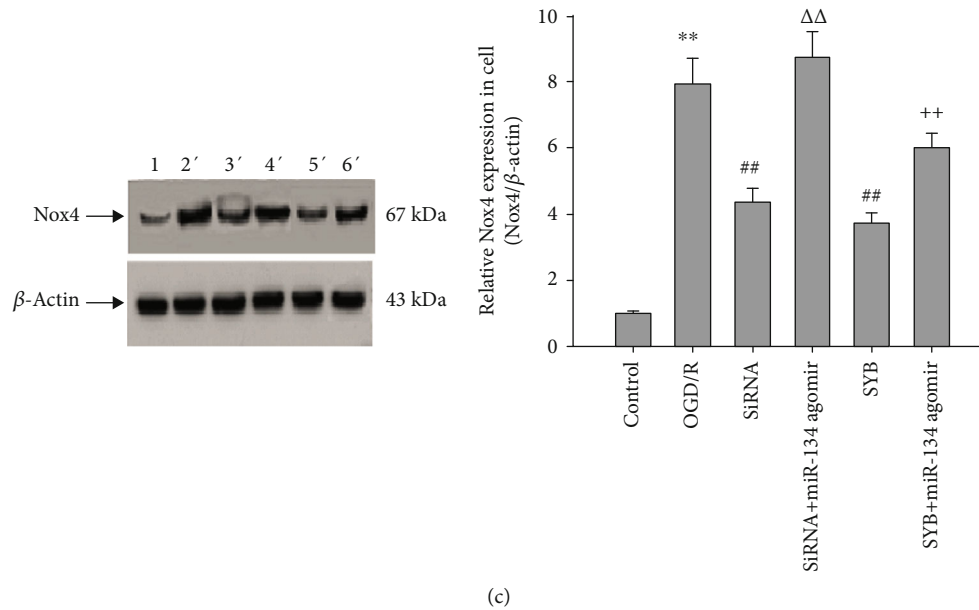


FIGURE 5: Continued.



(c)

FIGURE 5: Effect of safflower yellow B on NADPH oxidase activity and Nox4 expression. Rats and primary fetal cortical cells were used to establish the I/R model and the OGD/R model, respectively. After I/R for 24 h, the cerebral cortex and cells from different groups were collected. NADPH oxidase activity and Nox4 expression was observed using Western blot analysis. (a1) and (a2) represent the NADPH oxidase activity of the cerebral cortex and the primary fetal cortical cells, respectively. (b1) Representative western blots of the cerebral cortex are shown (1, 2, 3, 4, 5, and 6 represent sham, ischemia/reperfusion (I/R), AK046177 siRNA, AK046177 siRNA+miR-134 agomir, SYB, and SYB+miR-134 agomir, respectively). (b2) represents Nox4 expression in the cerebral cortex. (c1) Representative western blots of primary fetal cortical cells are shown (1', 2', 3', 4', 5', and 6' represent control, OGD/R, AK046177 siRNA, AK046177 siRNA+miR-134 agomir, SYB, and SYB+miR-134 agomir, respectively). (c2) represent Nox4 expression in cells. Data are presented as mean \pm SD ($n = 8$ in brain tissues, or $n = 3$ in cells). One-way ANOVA test was used to determine statistical significance. ** $P < 0.01$ vs. the sham group or the control group, ## $P < 0.01$ vs. the I/R group or the OGD/R group, $\Delta P < 0.05$ or $\Delta\Delta P < 0.01$ vs. the AK046177 siRNA group, and + $P < 0.05$ or ++ $P < 0.01$ vs. the SYB group.

However, cells exposed to OGD/R had a smaller increase in OCR after CCCP treatment compared to controls, suggesting that these cells have impaired respiratory capacity. Administration of rotenone, a complex I inhibitor, also inhibited OCR. These data suggest that OGD/R results in the loss of mitochondrial oxidative phosphorylation (OXPHOS) function in primary neurons. Furthermore, AK046177 siRNA and SYB enhanced OCR after CCCP treatment relative to the OGD/R group, suggesting that AK046177 siRNA and SYB were able to improve mitochondrial respiratory capacity. Under OGD/R conditions, miR-134 agomir significantly reduced the OCR increase induced by AK046177 siRNA and SYB and amplified OGD/R-mediated cell injury, resulting in much weaker respiratory capacity.

4. Discussion

lncRNAs may act to upregulate biological processes in various disease states by directly or indirectly interacting with mRNA of the target gene, leading to the modulation of apoptosis and invasion and modification of chromatin [18–20].

MicroRNAs are a type of small noncoding RNA involved in various diseases via their interaction with the mRNA of target genes, which leads to the destabilization and degradation of mRNA [33–35]. Di et al. have shown that a variety of miRNAs are involved in cerebral I/R injury [36]. The brain-specific miR-134 was reported to be differentially

expressed in tissue subjected to MCAO and I/R injury [37]. Previous studies had shown that lncRNAs influenced ischemia-mediated tissue damage via regulation of microRNAs [38–40]. In the present study, we demonstrated that I/R and OGD/R increased the expression levels of miR-134 in the cerebral cortex or primary neuronal cultures and resulted in neuronal damage accompanied by the upregulation of AK046177. Inhibition of AK046177 expression could significantly reduce the expression of miR-134, thereby alleviating I/R- or OGD/R-mediated neuronal injury.

Wang et al.'s studies have shown that SYB was able to effectively inhibit ischemia-induced brain injury [24]. However, the relationship between miR-134 or AK046177 and SYB in cerebral ischemia was unknown. These data confirm that SYB decreases the expression levels of miR-134 and AK046177 and reduces I/R- and OGD/R-induced damage.

Cyclic AMP is an important second messenger involved in many biochemical processes through its ability to regulate protein kinase activity. It is involved in diverse processes such as platelet activation, thrombus formation, inflammatory response, and oxidative stress responses [41–43]. Elevation of intracellular cAMP levels can change the antioxidant capacity of the cells by regulating the phosphorylation of CREB [44]. Thus, CREB has important influences in various diseases [45, 46]. Substantial evidence indicates that CREB plays critical roles in the neuronal responses to ischemia, such that activation and overexpression of CREB significantly

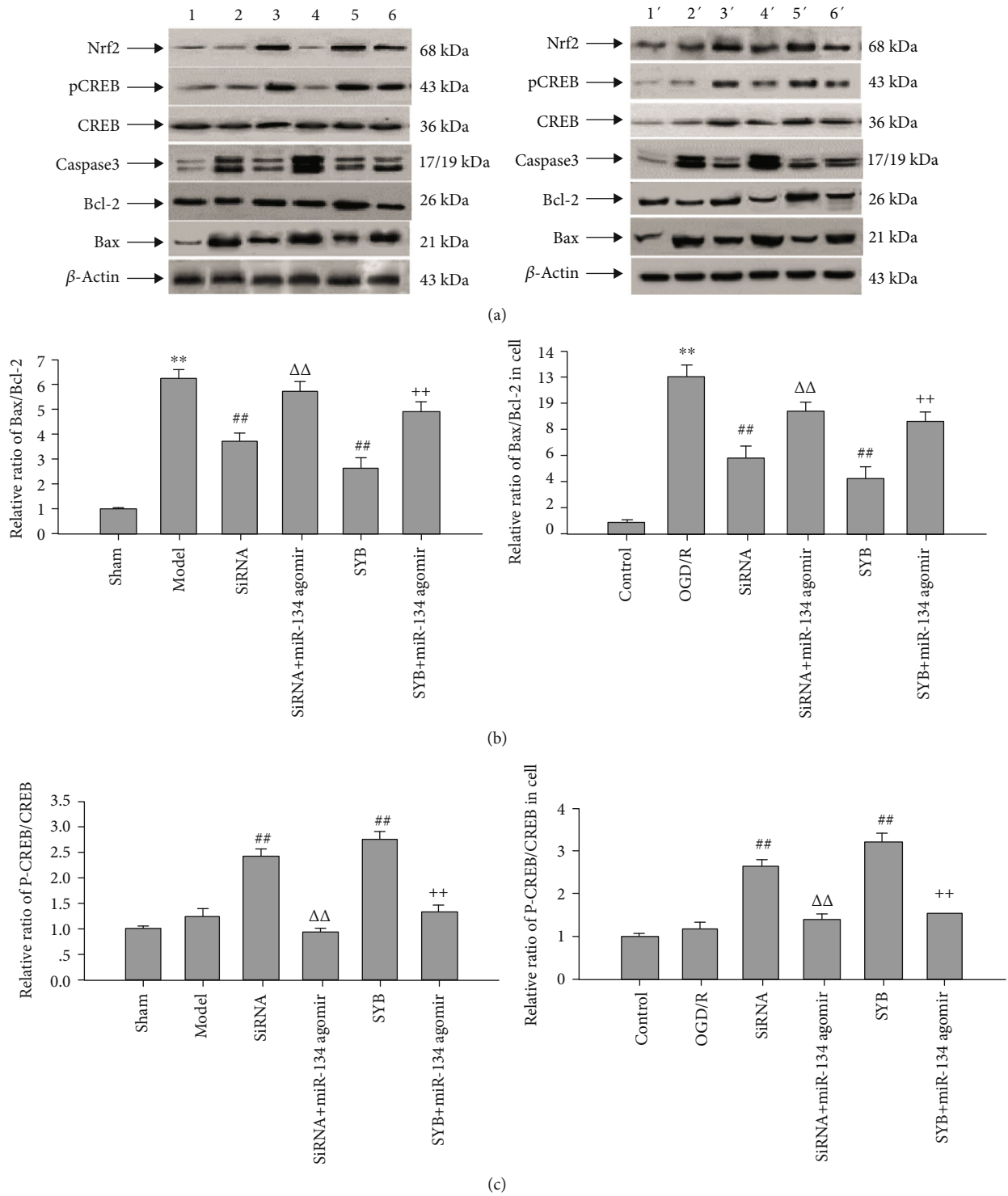


FIGURE 6: Continued.

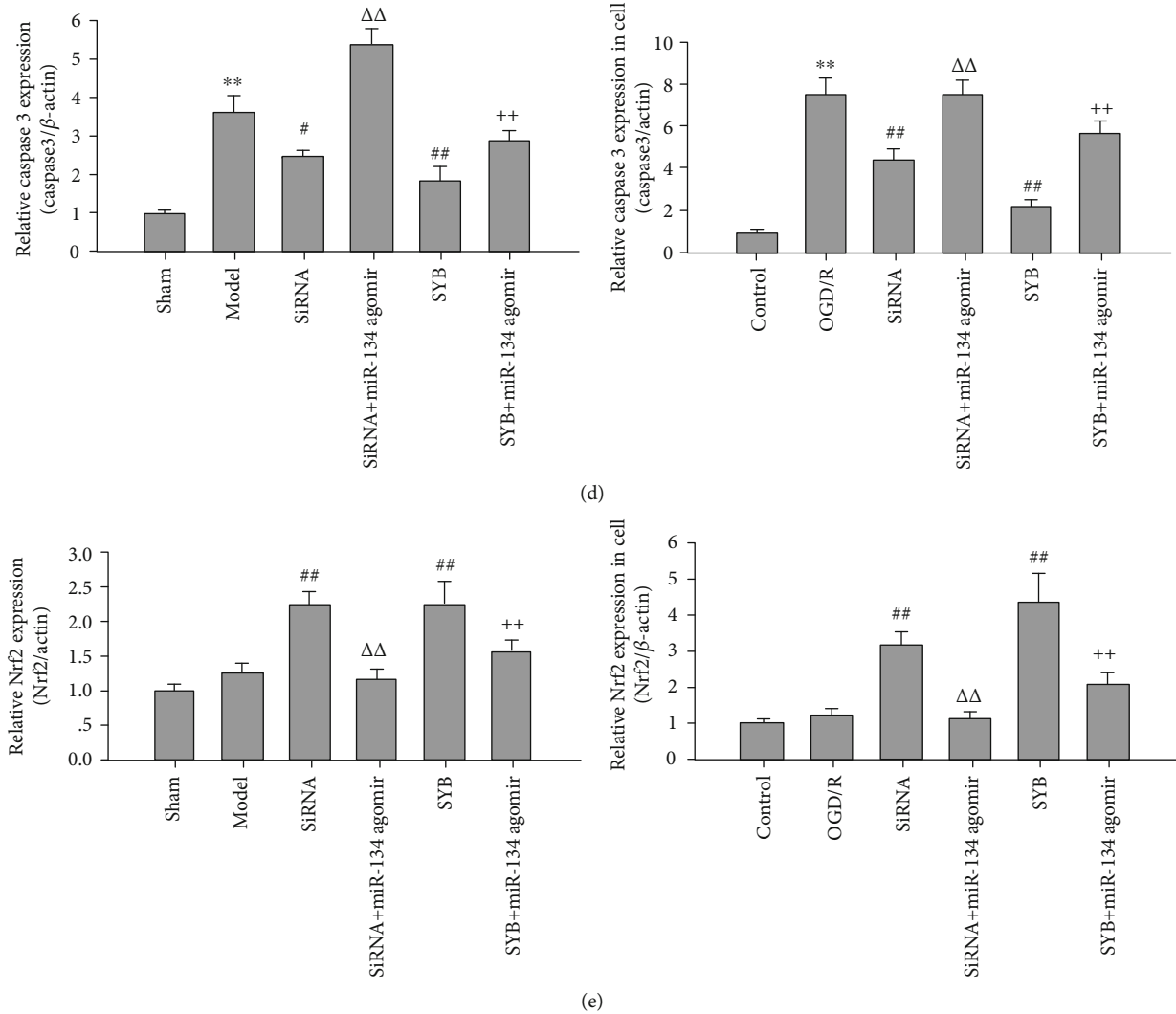


FIGURE 6: Effect of safflor yellow B on target protein expression. Rats and primary fetal cortical cells were used to establish the I/R model and the OGD/R model, respectively. After I/R for 24 h, total protein in the cerebral cortex and cells from different groups were extracted and measured. Thirty micrograms of protein was loaded per lane and separated by SDS-PAGE and transferred to a PVDF membrane. After incubation with secondary antibodies, the expression levels of CREB, pCREB, Bcl-2, Bax, and Nrf2 were visualized using the chemiluminescence method. (a1) and (a2) represent Western blots (1, 2, 3, 4, 5, and 6 represent sham, ischemia/reperfusion (I/R), AK046177 siRNA, AK046177 siRNA+miR-134 agomir, SYB, and SYB+miR-134 agomir, respectively; 1', 2', 3', 4', 5', and 6' represent control, OGD/R, AK046177 siRNA, AK046177 siRNA+miR-134 agomir, SYB, and SYB+miR-134 agomir, respectively). (b1), (c1), (d1), and (e1) represent the relative ratio of Bax/Bcl-2 and pCREB/CREB, caspase3, and Nrf2 expression in the cerebral cortex, respectively. (b2), (c2), (d2), and (e2) represent the relative ratio of Bax/Bcl-2 and pCREB/CREB, caspase3, and Nrf2 expression in cells, respectively. Data are presented as mean \pm SD ($n = 3$). One-way ANOVA test was used to determine statistical significance. ** $P < 0.01$ vs. the sham group or the control group, # $P < 0.05$ or ## $P < 0.01$ vs. the I/R group or the OGD/R group, $\Delta\Delta P < 0.01$ vs. the AK046177 siRNA group, and $\Delta\Delta P < 0.01$ vs. the SYB group.

reduces ischemia-mediated brain injury and increases BDNF and Bcl-2 expression [15, 47]. Mabuchi et al. and Huang et al. showed that miR-134 directly targets the 3'-UTR of CREB mRNA, influences the translation and phosphorylation of CREB, and suppresses BDNF and Bcl-2 expression, leading to apoptosis [47]. Conversely, the activation of miR-134 suppresses the expression of CREB and aggravates tissue or cell injury.

Nrf2 is an important transcription factor that can alleviate oxidative stress-mediated cellular damage by activating

the transcription of antioxidant enzymes. Nguyen et al. demonstrated the potential of Nrf2-mediated transcription to protect the brain from neurodegeneration resulting from oxidative stress [48]. The phosphorylation of CREB also enhances the binding of Nrf2 to its DNA response element [49, 50]. In the present study, we found that I/R and OGD/R induced overexpression of miR-134 and AK046177 and reduced intracellular cAMP levels, which in turn suppressed the expression and phosphorylation of CREB. The result was a further downregulation of Nrf2 and upregulation of Bax

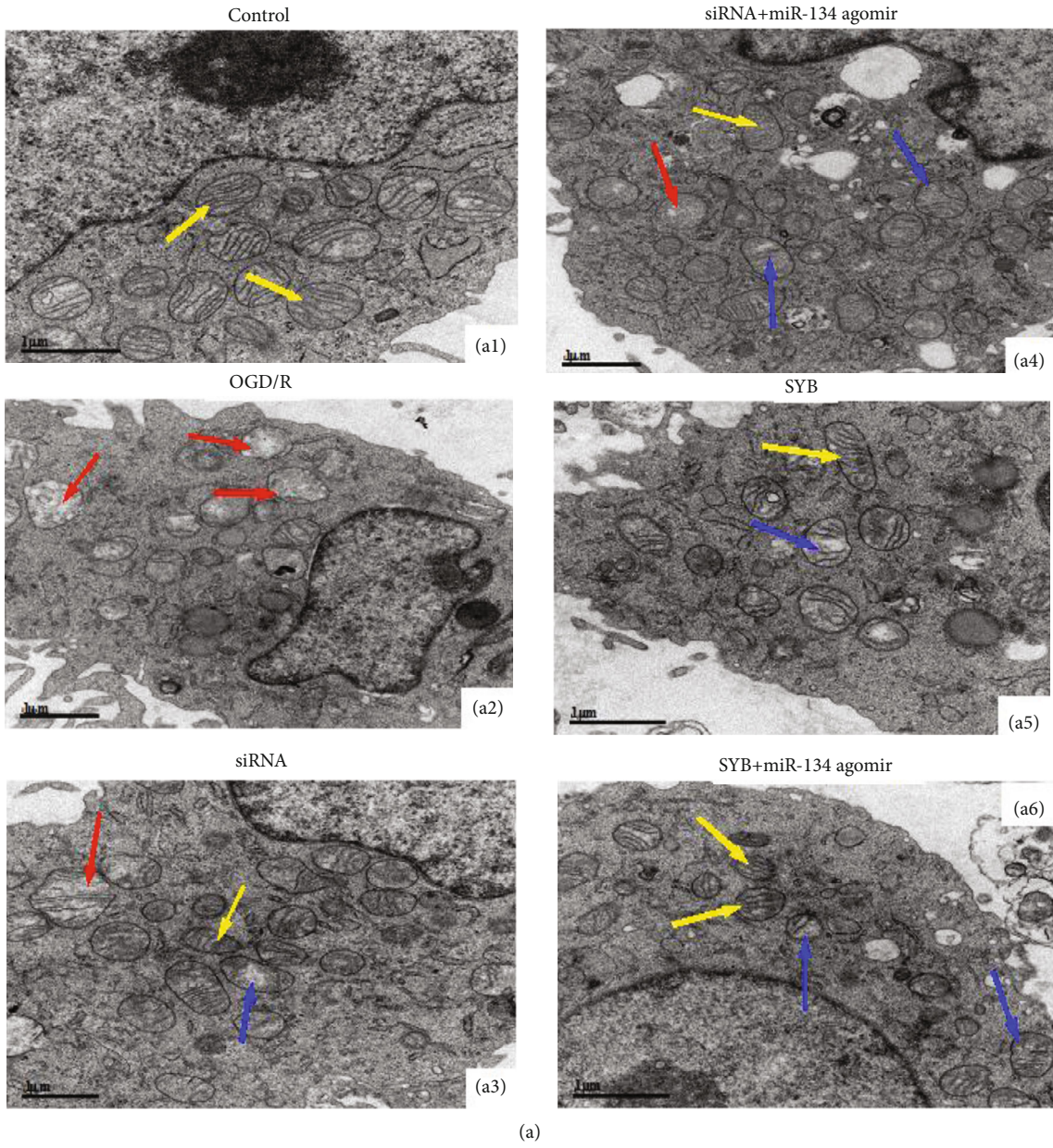


FIGURE 7: Continued.

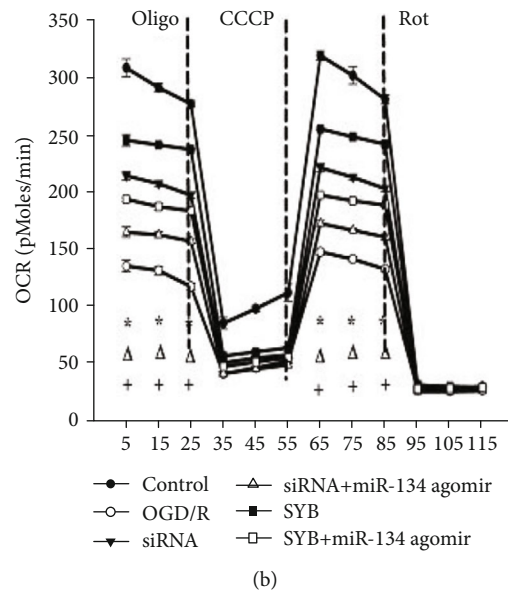


FIGURE 7: Effect of safflor yellow B on mitochondrial structure and cell respiration. Primary fetal cortical cells were seeded in 96-well and 6-well plates and divided into six groups: control, OGD/R, AK046177 siRNA, AK046177 siRNA+miR-134 agomir, SYB, and SYB+miR-134 agomir. The cells were pretreated with the drugs including SYB, AK046177 siRNA, and miR-134 agomir before being dealing with OGD/R. (a1–a6) Mitochondrial structure was evaluated using a transmission electron microscope ($\times 20,000$ magnification, bar $1 \mu\text{m}$) and represent the mitochondria structure of the control group, the OGD/R group, AK046177 siRNA, AK046177 siRNA+miR-134 agomir, SYB, and SYB+miR-134 agomir, respectively. Transmission electron microscope shows normal mitochondrial structure (yellow solid line arrows), and pathological mitochondria with irregular shapes and swollen (red solid line arrow) and vesicular mitochondrial clusters (blue solid line arrow). Cellular oxygen consumption rate (OCR) was measured using an Oxygraph-2k system ($n = 3$ experiments per condition). Data are presented as mean \pm SD ($n = 3$). One-way ANOVA test was used to determine statistical significance. $*P < 0.01$ vs. the control group, $\#P < 0.01$ vs. the OGD/R group, $^{\Delta}P < 0.01$ vs. the AK046177 siRNA group, $^{+}P < 0.01$ vs. the SYB group.

and caspase3, eventually leading to oxidative damage and apoptosis.

Inhibition of AK046177 increased cAMP synthesis and promoted the expression and phosphorylation of CREB, and then stimulated Nrf2 activation and effectively attenuated I/R- or OGD/R-mediated injury by the downregulation of miR-134. Previous studies have shown that the neuroprotective effect of SYB is related to increasing antioxidative enzyme activities, decreasing free radical generation, and regulating Bcl-2/Bax signaling [24], each of which was confirmed in the present study. Moreover, our data demonstrated that SYB also improved cAMP synthesis, and then enhanced the ratio of pCREB/CREB and activated Nrf2 expression via the suppression of overexpressions of AK046177 and miR-134 induced by I/R or OGD/R.

Increased mitochondrial oxidative stress induces mitochondrial dysfunction, which has been linked to a variety of diseases including cardiovascular disease [51, 52]. Mitochondrial dysfunction increases ROS due to electrons escaping from the mitochondrial respiratory chain and interacting with oxygen molecules. ROS destroy mitochondrial membranes and influence cell respiration, facilitate the release of cytochrome C, and promote activation of caspase3, ultimately leading to apoptosis [53, 54].

Nrf2 is a prominent player in supporting the structural and functional integrity of the mitochondria under conditions of stress, and thus plays a crucial role in the maintenance

of cellular redox homeostasis. It regulates the mitochondrial production of ROS and NADPH oxidase [55]. In the present study, we discovered that I/R and OGD/R caused mitochondrial structural damage, such as an increase in mitochondrial volume and the formation of fractured cristae, and increased NADPH oxidase activity. This damage resulted in mitochondrial dysfunction, demonstrated by lower OCR and ROS generation. Both AK046177 siRNA and SYB were able to increase the number of healthy mitochondria, dramatically enhance cellular respiratory function, and inhibit ROS production. However, miR-134 agomir remarkably increased ROS levels by blocking the mitochondrial respiratory chain and reducing the increased activity of antioxidant enzymes related to CREB binding, thereby boosting apoptosis.

5. Conclusion

In this study, SYB protected the brain from I/R-related injury by increasing intracellular cAMP levels, downregulating overexpressions of AK046177 and miR-134, and activating the CREB/Nrf2 pathway. The mechanisms regulating I/R injury are complicated, involving a variety of miRNAs and signaling pathways [35, 56]. We believed that these data only reflected one aspect of the event, and some important proteins may contribute to the understanding of the mechanisms involved in I/R-mediated neuronal injury.

Abbreviations

SYB:	Safflor yellow B
ROS:	Reactive oxygen species
CREB:	Cyclic AMP (cAMP) response element-binding protein
Nrf2:	Nuclear factor erythroid 2-related factor 2
AK046177:	Long noncoding RNA046177
miR-134:	MicroRNA-134
I/R:	Ischemia/reperfusion
OGD/R:	Oxygen-glucose deprivation
cAMP:	Cyclic AMP
ARE:	Antioxidant response elements
BDNF:	Brain-derived neurotrophic factor
DMEM:	Dulbecco's minimal essential medium
MCAO:	Middle cerebral artery occlusion
SOD:	Superoxide dismutase
GPx:	Glutathione peroxidase
MDA:	Malondialdehyde
HSYA:	Hydroxysafflor yellow A
OCR:	Oxygen consumption rate
CCCP:	Carbonyl cyanide chlorophenylhydrazine
OXPHOS:	Oxidative phosphorylation
MTT:	3-(4,5-dimethylthiazol-2-yl)-2,5-diphenyl-tetrazolium bromide.

Data Availability

The data is available on request by asking directly the corresponding author by mail at ytwcy@163.com.

Conflicts of Interest

The authors declared no potential conflicts of interest with respect to the research, authorship, and/or publication of this article.

Authors' Contributions

C.W. conceived and designed the study. H.W., Y.S., K.W., and H.S. performed the apoptosis and cell viability assays, Western blot analysis, and qRT-PCR. H.W., Q.W., and Y.S. observed mitochondrial morphology and cell respiration. H.W., H.S., and Q.W. detected the levels of ROS, MDA, cAMP, and enzyme activity. Q.W., Y.S., C.Z., and H.S. performed the statistical analyses. C.W. and C.Z. wrote the manuscript. Hongzhi Wan contributed equally to this work.

Acknowledgments

This study was supported by the Natural Science Foundation of Shandong Province (ZR2012HM076), the National Natural Science Foundation of China (81530030, 81670398, and 91639102), the Foundation for Outstanding Young Scientist in Shandong Province (BS2014YY049), and the Science and Technology Project of Yantai (2014ZH092).

References

- [1] D. Lloyd-Jones, R. J. Adams, T. M. Brown et al., "Heart disease and stroke statistics—2010 update," *Circulation*, vol. 121, no. 7, pp. e46–e215, 2010.
- [2] T. A. Burke and R. N. Venketasubramanian, "The epidemiology of stroke in the East Asian region: a literature based review," *International Journal of Stroke*, vol. 1, no. 4, pp. 208–215, 2016.
- [3] T. Truelsen, S. Begg, and C. Mathers, "The global burden of cerebrovascular disease," 2006, <https://www.researchgate.net/publication/228551377>.
- [4] E. H. Lo, T. Dalkara, and M. A. Moskowitz, "Mechanisms, challenges and opportunities in stroke," *Nature Reviews Neuroscience*, vol. 4, no. 5, pp. 399–414, 2003.
- [5] M. Y.-T. Globus, R. Busto, B. Lin, H. Schnippering, and M. D. Ginsberg, "Detection of free radical activity during transient global ischemia and recirculation: effects of intraschemic brain temperature modulation," *Journal of Neurochemistry*, vol. 65, no. 3, pp. 1250–1256, 1995.
- [6] C. A. Piantadosi and J. Zhang, "Mitochondrial generation of reactive oxygen species after brain ischemia in the rat," *Stroke*, vol. 27, no. 2, pp. 327–332, 1996.
- [7] L. Ste-Marie, P. Vachon, L. Vachon, C. Bémour, M. C. Guertin, and J. Montgomery, "Hydroxyl radical production in the cortex and striatum in a rat model of focal cerebral ischemia," *The Canadian Journal of Neurological Sciences*, vol. 27, no. 2, pp. 152–159, 2000.
- [8] T. Yamamoto, S. Yuki, T. Watanabe, M. Mitsuka, K. I. Saito, and K. Kogure, "Delayed neuronal death prevented by inhibition of increased hydroxyl radical formation in a transient cerebral ischemia," *Brain Research*, vol. 762, no. 1–2, pp. 240–242, 1997.
- [9] Z. F. Yu, A. J. Bruce-Keller, Y. Goodman, and M. P. Mattson, "Uric acid protects neurons against excitotoxic and metabolic insults in cell culture, and against focal ischemic brain injury in vivo," *Journal of Neuroscience Research*, vol. 53, no. 5, pp. 613–625, 1998.
- [10] H. Imai, H. Masayasu, D. Dewar, D. I. Graham, and I. M. Macrae, "Ebselen protects both gray and white matter in a rodent model of focal cerebral ischemia," *Stroke*, vol. 32, no. 9, pp. 2149–2154, 2001.
- [11] N. Matsumiya, R. C. Koehler, J. R. Kirsch, and R. J. Traystman, "Conjugated superoxide dismutase reduces extent of caudate injury after transient focal ischemia in cats," *Stroke*, vol. 22, no. 9, pp. 1193–1200, 1991.
- [12] J. H. No, Y. B. Kim, and Y. S. Song, "Targeting Nrf2 signaling to combat chemoresistance," *Journal of Cancer Prevention*, vol. 19, no. 2, pp. 111–117, 2014.
- [13] D. D. Zhang and M. Hannink, "Distinct cysteine residues in Keap1 are required for Keap1 dependent ubiquitination of Nrf2 and for stabilization of Nrf2 by chemopreventive agents and oxidative stress," *Molecular and Cellular Biology*, vol. 23, no. 22, pp. 8137–8151, 2003.
- [14] A. Riccio, S. Ahn, C. M. Davenport, J. A. Blendy, and D. D. Ginty, "Mediation by a CREB family transcription factor of NGF-dependent survival of sympathetic neurons," *Science*, vol. 286, no. 5448, pp. 2358–2361, 1999.
- [15] K. Kitagawa, "CREB and cAMP response element-mediated gene expression in the ischemic brain," *The FEBS Journal*, vol. 274, no. 13, pp. 3210–3217, 2007.

- [16] Y. B. Ouyang, C. M. Stary, R. E. White, and R. G. Giffard, "The use of microRNAs to modulate redox and immune response to stroke," *Antioxidants & Redox Signaling*, vol. 22, no. 2, pp. 187–202, 2015.
- [17] W. Huang, X. Liu, J. Cao et al., "miR-134 regulates ischemia/reperfusion injury-induced neuronal cell death by regulating CREB signaling," *Journal of Molecular Neuroscience*, vol. 55, no. 4, pp. 821–829, 2015.
- [18] C. Gong and L. E. Maquat, "lncRNAs transactivate STAU1-mediated mRNA decay by duplexing with 3' UTRs via Alu elements," *Nature*, vol. 470, no. 7333, pp. 284–288, 2011.
- [19] C. Kanduri, "Kcnq1ot1: a chromatin regulatory RNA," *Seminars in Cell & Developmental Biology*, vol. 22, no. 4, pp. 343–350, 2011.
- [20] D. Khaitan, M. E. Dinger, J. Mazar et al., "The melanoma-upregulated long noncoding RNA Spry4-It1 modulates apoptosis and invasion," *Cancer Research*, vol. 71, no. 11, pp. 3852–3862, 2011.
- [21] S. Ramagiri and R. Taliyan, "Neuroprotective effect of hydroxy safflor yellow A against cerebral ischemia-reperfusion injury in rats: putative role of mPTP," *Journal of Basic and Clinical Physiology and Pharmacology*, vol. 27, no. 1, pp. 1–8, 2016.
- [22] J. Cao, Z. Chen, Y. Zhu et al., "Huangqi–Honghua combination and its main components ameliorate cerebral infarction with Qi deficiency and blood stasis syndrome by antioxidant action in rats," *Journal of Ethnopharmacology*, vol. 155, no. 2, pp. 1053–1060, 2014.
- [23] C. Wang, Q. Huang, C. Wang et al., "Hydroxysafflor yellow A suppress oleic acid-induced acute lung injury via protein kinase A," *Toxicology and Applied Pharmacology*, vol. 272, no. 3, pp. 895–904, 2013.
- [24] C. Wang, D. Zhang, G. Li et al., "Neuroprotective effects of safflor yellow B on brain ischemic injury," *Experimental Brain Research*, vol. 177, no. 4, pp. 533–539, 2007.
- [25] C. Wang, H. Ma, S. Zhang, Y. Wang, J. Liu, and X. Xiao, "Safflor yellow B suppresses pheochromocytoma cell (PC12) injury induced by oxidative stress via antioxidant system and Bcl-2/Bax pathway," *Naunyn-Schmiedeberg's Archives of Pharmacology*, vol. 380, no. 2, pp. 135–142, 2009.
- [26] E. Z. Longa, P. R. Weinstein, S. Carlson, and R. Cummins, "Reversible middle cerebral artery occlusion without craniectomy in rats," *Stroke*, vol. 20, no. 1, pp. 84–91, 1989.
- [27] I. M. Macrae, "New models of focal cerebral ischemia," *British Journal of Clinical Pharmacology*, vol. 34, pp. 302–308, 1992.
- [28] D. J. Combs and L. G. D'Alecy, "Motor performance in rats exposed to severe forebrain ischemia: effect of fasting and 1,3-butanediol," *Stroke*, vol. 18, no. 2, pp. 503–511, 1987.
- [29] H. Zhao, R. Wang, Z. Tao et al., "Ischemic postconditioning relieves cerebral ischemia and reperfusion injury through activating T-LAK cell-originated protein kinase/protein kinase B pathway in rats," *Stroke*, vol. 45, no. 8, pp. 2417–2424, 2014.
- [30] Y. B. Ouyang, Y. Lu, S. Yue et al., "miR-181 regulates GRP78 and influences outcome from cerebral ischemia in vitro and in vivo," *Neurobiology of Disease*, vol. 45, no. 1, pp. 555–563, 2012.
- [31] K. J. Livak and T. D. Schmittgen, "Analysis of relative gene expression data using real-time quantitative PCR and the $2^{-\Delta\Delta CT}$ method," *Methods*, vol. 25, no. 4, pp. 402–408, 2001.
- [32] D. Pesta and E. Gnaiger, "High-resolution respirometry: OXPHOS protocols for human cells and permeabilized fibers from small biopsies of human muscle," *Methods in Molecular Biology*, vol. 810, pp. 25–58, 2012.
- [33] D. P. Bartel, "MicroRNAs: genomics, biogenesis, mechanism, and function," *Cell*, vol. 116, no. 2, pp. 281–297, 2004.
- [34] J. T. Mendell and E. N. Olson, "MicroRNAs in stress signaling and human disease," *Cell*, vol. 148, no. 6, pp. 1172–1187, 2012.
- [35] J. Winter, S. Jung, S. Keller, R. I. Gregory, and S. Diederichs, "Many roads to maturity: microRNA biogenesis pathways and their regulation," *Nature Cell Biology*, vol. 11, no. 3, pp. 228–234, 2009.
- [36] Y. Di, Y. Lei, F. Yu, F. Changfeng, W. Song, and M. Xuming, "MicroRNAs expression and function in cerebral ischemia reperfusion injury," *Journal of Molecular Neuroscience*, vol. 53, no. 2, pp. 242–250, 2014.
- [37] C. Liu, Z. Peng, N. Zhang et al., "Identification of differentially expressed microRNAs and their PKC-isoform specific gene network prediction during hypoxic pre-conditioning and focal cerebral ischemia of mice," *Journal of Neurochemistry*, vol. 120, no. 5, pp. 830–841, 2012.
- [38] S. Wang, W. Yu, J. Chen, T. Yao, and F. Deng, "lncRNA MALAT1 sponges miR-203 to promote inflammation in myocardial ischemia-reperfusion injury," *International Journal of Cardiology*, vol. 268, p. 245, 2018.
- [39] S. B. Ong, K. Katwadi, X. Y. Kwek et al., "Non-coding RNAs as therapeutic targets for preventing myocardial ischemia-reperfusion injury," *Expert Opinion on Therapeutic Targets*, vol. 22, no. 3, pp. 247–261, 2018.
- [40] H. Yan, J. Rao, J. Yuan et al., "Long non-coding RNA MEG3 functions as a competing endogenous RNA to regulate ischemic neuronal death by targeting miR-21/PDCD4 signaling pathway," *Cell Death & Disease*, vol. 8, no. 12, p. 3211, 2017.
- [41] E. Fuentes, L. Badimon, J. Caballero et al., "Protective mechanisms of adenosine 5'-monophosphate in platelet activation and thrombus formation," *Thrombosis and Haemostasis*, vol. 111, no. 3, pp. 491–507, 2017.
- [42] M. Ghosh, Y. Xu, and D. D. Pearce, "Cyclic AMP is a key regulator of M1 to M2a phenotypic conversion of microglia in the presence of Th2 cytokines," *Journal of Neuroinflammation*, vol. 13, no. 1, p. 19, 2016.
- [43] S. Saxena, R. E. Rönn, C. Guibentif, R. Moraghebi, and N. B. Woods, "Cyclic AMP signaling through Epac axis modulates human hemogenic endothelium and enhances hematopoietic cell generation," *Stem Cell Reports*, vol. 6, no. 5, pp. 692–703, 2016.
- [44] N. Li, B. Li, T. Brun et al., "NADPH oxidase NOX2 defines a new antagonistic role for reactive oxygen species and cAMP/PKA in the regulation of insulin secretion," *Diabetes*, vol. 61, no. 11, pp. 2842–2850, 2012.
- [45] B. R. Hu, C. M. Fux, M. E. Martone, J. A. Zivin, and M. H. Ellisman, "Persistent phosphorylation of cyclic AMP responsive element-binding protein and activating transcription factor-2 transcription factors following transient cerebral ischemia in rat brain," *Neuroscience*, vol. 89, no. 2, pp. 437–452, 1999.
- [46] K. Tanaka, "Alteration of second messengers during acute cerebral ischemia—adenylate cyclase, cyclic AMP-dependent protein kinase, and cyclic AMP response element binding protein," *Progress in Neurobiology*, vol. 65, no. 2, pp. 173–207, 2001.
- [47] T. Mabuchi, K. Kitagawa, K. Kuwabara et al., "Phosphorylation of cAMP response element-binding protein in

- hippocampal neurons as a protective response after exposure to glutamate in vitro and ischemia in vivo,” *The Journal of Neuroscience*, vol. 21, no. 23, pp. 9204–9213, 2001.
- [48] T. Nguyen, P. Nioi, and C. B. Pickett, “The Nrf2-antioxidant response element signaling pathway and its activation by oxidative stress,” *The Journal of Biological Chemistry*, vol. 284, no. 20, pp. 13291–13295, 2009.
- [49] F. Moosavi, R. Hosseini, L. Saso, and O. Firuzi, “Modulation of neurotrophic signaling pathways by polyphenols,” *Drug Design, Development and Therapy*, vol. 10, pp. 23–42, 2015.
- [50] M. C. Chiang, H. Lin, Y. C. Cheng, C. H. Yen, R. N. Huang, and K. H. Lin, “Beta-adrenoceptor pathway enhances mitochondrial function in human neural stem cells via rotary cell culture system,” *Journal of Neuroscience Methods*, vol. 207, no. 2, pp. 130–136, 2012.
- [51] H. J. Ku, Y. Ahn, J. H. Lee, K. M. Park, and J. W. Park, “IDH2 deficiency promotes mitochondrial dysfunction and cardiac hypertrophy in mice,” *Free Radical Biology & Medicine*, vol. 80, pp. 84–92, 2015.
- [52] M. T. Lin and M. F. Beal, “Mitochondrial dysfunction and oxidative stress in neurodegenerative diseases,” *Nature*, vol. 443, no. 7113, pp. 787–795, 2006.
- [53] J. Z. Li, S. Y. Yu, D. Mo, X. N. Tang, and Q. R. Shao, “Picoside II inhibits hypoxia/reoxygenation-induced cardiomyocyte apoptosis by ameliorating mitochondrial function through a mechanism involving a decrease in reactive oxygen species production,” *International Journal of Molecular Medicine*, vol. 35, no. 2, pp. 446–452, 2015.
- [54] K. M. Hung and M. J. Calkins, “Mitochondrial homeostatic disruptions are sensitive indicators of stress in neurons with defective mitochondrial DNA transactions,” *Mitochondrion*, vol. 31, pp. 9–19, 2016.
- [55] A. T. Dinkova-Kostova and A. Y. Abramov, “The emerging role of Nrf2 in mitochondrial function,” *Free Radical Biology & Medicine*, vol. 88, no. Part B, pp. 179–188, 2015.
- [56] V. P. Nakka, A. Gusain, S. L. Mehta, and R. Raghuram, “Molecular mechanisms of apoptosis in cerebral ischemia: multiple neuroprotective opportunities,” *Molecular Neurobiology*, vol. 37, no. 1, pp. 7–38, 2008.

Research Article

Huangbai Liniment Accelerated Wound Healing by Activating Nrf2 Signaling in Diabetes

Jingjing Zhang ¹, Rui Zhou,^{1,2} Changpei Xiang,² Qiang Jia ³, Hongwei Wu ¹,
and Hongjun Yang ^{1,2}

¹Institute of Chinese Materia Medica, China Academy of Chinese Medical Sciences, Beijing 100700, China

²College of traditional Chinese Medicine, Yunnan University of Traditional Chinese Medicine, Kunming 650500, China

³School of Pharmacy, Shandong University of Traditional Chinese Medicine, Jinan 250355, China

Correspondence should be addressed to Hongjun Yang; hjyang@icmm.ac.cn

Received 17 May 2019; Revised 23 December 2019; Accepted 19 February 2020; Published 26 May 2020

Guest Editor: Reggiani Vilela Gonçalves

Copyright © 2020 Jingjing Zhang et al. This is an open access article distributed under the Creative Commons Attribution License, which permits unrestricted use, distribution, and reproduction in any medium, provided the original work is properly cited.

As a serious complication of diabetes, nonhealing skin ulcer leads to high mortality and disability in diabetic patients. However, limited therapy is available in managing diabetic wounds. In this study, RNA-seq technology was used to systematically investigate the effect of Huangbai (HB) liniment, a traditional Chinese medicine, on the streptozotocin- (STZ-) induced diabetic wound. HB liniment significantly accelerated the wound closure and enhanced the generation of extracellular matrix in diabetic rats, and oxidative stress was identified to play a vital role in HB-mediated wound healing. Importantly, HB liniment activated nuclear factor erythroid-derived 2-like 2 (Nrf2) and its downstream antioxidant genes (e.g., genes involved in glutathione system, thioredoxin system, and GAPDH generation as well as other antioxidant genes), which inhibited oxidative damage and apoptosis. By associating drug targets of HB liniment with Nrf2 and its downstream genes, 54 components in HB liniment were screened out, and the majority was from *Cortex Phellodendri* and *Forsythia suspensa*. Additionally, HB liniment enhanced TGF- β 1 and reduced MMP9 level, accelerating wound healing in diabetes. The *in vitro* experiment showed HB facilitated cell proliferation and inhibited oxidative damage in high glucose-induced HaCaT cells. Our findings provided the experimental evidence for the treatment of diabetic wound with HB, clarified the potential mechanism of HB, and improved our understanding of diabetic wound healing.

1. Introduction

Chronic nonhealing wound is a serious diabetic complication, which leads to severe morbidity and mortality in diabetic population and brings a huge social and economic burden to the world [1, 2]. In the United States alone, it costs as high as \$13 billion to treat diabetic wounds every year. In contrast to the typical sequential emergence of biological process of coagulation, inflammation, proliferation, and remodeling in normal tissue, the normal progression of wound healing is disturbed and delayed in diabetes, resulting in long-term of wound nonunion [3, 4]. Conventional therapies are only effective in the management of diabetic wounds to certain degree, whereas a large number of diabetic wounds still persist, deteriorate, and result in amputation [5]. Notably, a reduced efficiency in diabetic wound healing is usually

accompanied with decreased blood supply, delayed extracellular matrix turnover, reduced wound contraction, repeated infections, and chronic inflammation, which hinders wound healing [4, 6]. Thus, it is urgent to develop an effective therapy to treat diabetic wounds.

Oxidative stress plays a vital role in halting the progression of diabetic wound healing [7, 8]. The oxidative stress in diabetic wounds is characterized by a marked elevation in reactive oxygen species (ROS) levels, as a result of increasing ROS generating pathway and decreasing ROS removing defenses [9]. Overproduced ROS in diabetes damages various macromolecules such as lipids, proteins, and DNA double strands and finally impairs wound healing. Proper oxidative stress has been proved to benefit extracellular matrix (ECM) generation, whereas high ROS levels hinder normal synthesis of ECM and seriously damage existing ECM

[10, 11]. For example, H_2O_2 can disrupt tissue growth, especially collagen production, thus preventing wound closure [12]. In addition, TGF- β 1 signaling is a vital signaling pathway for ECM production and can be interfered by the overproduced ROS. Importantly, high ROS levels promote the generation of matrix metalloproteinases (MMPs), which in turn affect ECM remodeling [13]. Therefore, targeting oxidative stress may be a potential effective therapy for diabetic wound healing.

An increasing number of researchers have demonstrated Traditional Chinese medicine (TCM) is indispensable in the treatment of various disease presentations [14, 15]. Abundant and robust evidences accumulated over time that TCM is effective in its use for diabetic complications [16]. Huangbai liniment (HB) is a standardized medicinal product clinically prescribed for use in wound management and is composed of Cortex Phellodendri, Forsythia suspensa, Lonicera japonica Thunb., Taraxacum mongolicum Hand.-Mazz, and Scolopendridae [17]. Therapeutic benefits of HB liniment have been observed in wound management, including nonhealing diabetic ulcer [18, 19]. These study demonstrated that HB liniment could reduce AGEs and inflammatory factors such as IL-1 β while increasing the secretion of growth factor [20]. However, the mechanism of HB in facilitating diabetic wound healing remains unclear. In this study, the effect of HB on diabetic wound healing was evaluated in STZ-induced iabetic wounds and high glucose-induced cell model, and the mechanism was systematically investigated by using RNA-seq technology.

2. Materials and Methods

2.1. Materials. Streptozotocin (STZ, SigmaS0130) and 4',6-diamidino-2-phenylindole (DAPI) were purchased from Sigma-Aldrich. Huangbai liniment (batch number: 18010111) was kindly provided by Shandong Hanfang Pharmaceutical Co., Ltd (Chinese medicine character: Z10950097). Recombinant human epidermal growth factor derivative for external use (rhEGF) was purchased from Shenzhen Huashengyuan Gene Engineering Development Co., Ltd. The antibodies used in this research were as follows: Ki67 (ab92742), 8-OHdG (sc-66036), Nrf2 (ab137550), NQO1 (ab28947), cleaved caspase 3 (CST, 9664S), TGF- β 1 (ab92486), goat anti-mouse IgG (H+L) (HRP Jackson, 115-035-003), and goat anti-rabbit IgG (H+L) (Jackson, 111-035-003). The malondialdehyde (MDA, A003) was purchased from Nanjing Jiancheng Bioengineering Institute. The ELISA kits of MMP9 (DY-0075) and 8-OHdG (DY-0223) were obtained from Deyi Testing Co., Ltd. Cell Counting Kit-8 (CCK-8) kits were obtained from the Dongren Chemical Technology Co., Ltd. The malondialdehyde ROS (S0033) and GSH (A119) were purchased from Beyotime Biotechnology and Nanjing Jiancheng Bioengineering Institute, respectively.

2.2. In Vivo Animal Study. Male Sprague-Dawley rats (170-200 g) were purchased from the Peking University Health Science Center Experimental Animal Center, Beijing, China ((certificate no. SCXK (Jing) 2009-0017)). All proce-

dures were carried out according to the rules of the Committee on Animal Care and Use published by the Institute of Chinese Materia Medica, China Academy of Chinese Medical Sciences. Rats were housed in a 12-h light/dark cycle facility with a controlled temperature and kept with free access to water and food. Streptozotocin (STZ, 60 mg/kg, i.p.) in sodium citrate buffer (pH 4.5) was used to generate diabetic model according to previous reports [21]. The fasting glucose levels (FGLs) was evaluated 1 and 2 weeks following STZ injection. Rats with FGL more than 16.7 mmol were included for the following experiments. The control animals received the same volume of sodium citrate buffer (pH 4.5) instead. At two weeks after STZ induction, the rats were anesthetized with sodium pentobarbital (50 mg/kg, intraperitoneal injection, i.p.) and then subjected to full-thickness wounds. Two wounds with diameter of 2 cm on the back of rats were made. The rats were randomly allocated to different groups to receive either physiological saline, low dose of Huangbai liniment (STZ+HB-L, equal volume of HB+equal volume of physiological saline, 2 mL/day, topical), high dose of Huangbai liniment STZ+HB-H (original solution, 2 mL/day, topical), or rhEGF (4000 IU/10*10cm², topical) until study end. On the first three days after wound surgery, the wound was covered with double layers of sterile gauze to reduce external irritation and replaced daily. The wounds were photographed at 1, 6, 9, and 13 days after surgical wounds were made. The wound closure photos were analyzed using ImageJ by calculating the percentage of the wound area from the original wound area. After 13 days, skin tissues were collected, half of which were paraffin-embedded for histology, and the other half were used for western blotting, ELISA, and other related experiments.

2.3. In Vitro Cell Experiments. Human immortalized keratinocytes (HaCaT) purchased from National Infrastructure of Cell Line Resource was used for our *in vitro* experiment. Briefly, HaCaT cells were cultured with culture medium which contained DMEM (Gibco, USA) with D-glucose (1 g/L, LG), fetal bovine serum (10%v/v, FBS), and penicillin/streptomycin (100 μ g/mL) at 37°C, and stimulation of HaCaT cells with culture medium containing 4.5 g/L D-glucose DMEM (HG) for 48 hours was used for chronic hyperglycemic cell model. Povidone iodine and quercetin were purchased from Hubei Ketian Pharmaceutical Co., Ltd and National Institutes for Food and Drug Control, respectively. First, HaCaT cells were treated with various concentrations of HB, quercetin, and povidone iodine, respectively, for 48 hours to search the safe concentration. To evaluate the therapeutic effect, cells were treated with HG medium and drugs such as HB (1/50 and 1/5000, dilution), quercetin (1.5625 and 6.25 μ M), and povidone iodine (0.00001% and 0.001%, m/v) at the same time for 48 hours before detection. CCK-8 was used for detecting cell viability with a microplate reader (Molecular Devices, USA).

2.4. Measurement of Malondialdehyde, GSH, ROS, 8-OHdG, and MMP9. Malondialdehyde (MDA) was detected according to the manufacture instrument, using Visible Spectrophotometer 721G (Shanghai Precision Scientific

Instruments Co., Ltd.). And GSH and ROS levels were also performed according to their instruction using a microplate reader (Molecular Devices, USA). The protein extract from the skin tissue was used for the detection of MMP9 and 8-OHdG using commercially available kits. Briefly, plates were immobilized with specific antibody (MMP9 or 8-OHdG) and incubated with protein samples, followed by a secondary antibody conjugated with horseradish peroxidase. The measurement was performed on Beijing DNM-9602G Enzyme Marker Analyzer.

2.5. Western Blotting. The skin tissue was harvested, and protein extraction was performed according to the instruction of Beyotime Protein Assay Kit (P0013, Nanjing, China). After separated on a 10% SDS-PAGE (P0014, China), the protein samples were transferred to a polyvinylidene fluoride membrane (Millipore, IPVH00010), which was blocked with bovine serum albumin (BSA). After that, the primary antibody specific for Nrf2 (ab137550) or NQO1 (ab28947) was added to the membranes and incubated for 24 h at 4°C. The second antibody goat anti-rabbit IgG (H+L) (Jackson, 111-035-003) was loaded, and the signal of the proteins was detected by scanning densitometry.

2.6. Histology and Immunofluorescence Staining. The paraffin tissue section slides with thickness of 5 μm were used for histology and immunofluorescence staining. After deparaffinized, the slides were stained with hematoxylin and eosin (HE) and Masson's trichrome stain following their instructions, respectively. For immunofluorescence (IF) staining, the sections were blocked by 5% (m/v) BSA, after they were permeabilized with 0.5% Triton X-100. Primary antibody was loaded and kept at 4°C overnight. Then Alexa Fluor 488- and Alexa Fluor 647-conjugated secondary antibodies were loaded at room temperature for 1 h. The nuclei were stained with 4',6-diamidino-2-phenylindole (DAPI). The images were visualized using LSM-880 confocal microscope (Carl Zeiss, Oberkochen, Germany). And the real-time collagen growth evaluation was conducted using two-photon microscope (Olympus FV1000) at 6 and 13 days after wound generation.

2.7. Investigation and Analysis of Differentially Expressed Genes Identified by RNA-Seq Technology. The skin tissue was harvested, and the RNA was separated by using Total RNeasy Lysis Reagent (Cat#15596-018, Life Technologies, USA) following its instructions. RNA integrity was quantified with the RNA Nano 6000 Assay Kit using Bioanalyzer 2100 system (Agilent Technologies, CA, USA). The RNA (1 μg) of each sample was used for the following library construction. The RNA sequencing was performed according to the previous research [15]. Briefly, NEBNext® Ultra™ RNA Library Prep Kit was applied to produce the sequencing libraries for Illumina® (NEB, USA). Firstly, purification of mRNA was carried out by using poly-T oligo-grafted magnetic beads before RNA fragmentation was generated. After that, the first strand cDNA was synthesized by using M-MuLV Reverse Transcriptase (RNase H-) and random hexamer primer. And the second strand cDNA was synthesized with RNase

H and DNA polymerase I. The enrichment of cDNA template by PCR was carried out after knot of the adapter and adenylation at the 3' end in the DNA fragment. After purification of PCR results, the library quality was evaluated, and the clustering of samples was performed on TruSeq PE150 Cluster Kit v3-cBot-HS (Illumina) with a cBot Cluster Generation System. Finally, the sequence of the library was carried out by using an Illumina HiSeq 4000 platform with the generation of 150 bp paired-end reads. Novogene Bioinformatics Technology Co., Ltd (Beijing, China) helped to do the sequencing experiment.

Rat reference genome (ensemble release 91) was applied for the transcript assembly and quantification. The numbers of reads were calculated by mapping to every gene with HTseq v0.6.1. Gene expression was obtained by evaluating the fragment number of each kilobase of transcript sequence normalized to every million base pairs which were sequenced and expressed as FPKM. Differential expression of genes was calculated with EdgeR software. The raw data related to HB-mediated protection against STZ-induced diabetic wound was uploaded into <https://www.ncbi.nlm.nih.gov/sra/PRJNA532974> (SRP193129). The differentially expressed genes identified by RNA-seq were analyzed through ClueGO. And the network of "components-drug targets-differentially expressed genes" was constructed with Cytoscape v3.4.0. [22]. Briefly, the drug targets of HB liniment were obtained through BATMAN-TCM, and the downstream differentially expressed genes of Nrf2 and Nfe2l2 were associated with the drug targets by STRING to screen out related drug targets, and the network was constructed through Cytoscape v3.4.0.

2.8. Statistical Analysis. The data was analyzed using one-way ANOVA with Tukey post hoc test through SPSS software, and the data was presented as means \pm SD (standard deviations). * $P < 0.05$ compared with the Con or LG group, * $P < 0.05$ compared with the STZ or HG group was considered as statistical significance.

3. Results

3.1. HB Liniment Accelerated Wound Closure in STZ-Induced Diabetic Rats. The effect of HB liniment on diabetic wound healing was investigated through the evaluation of the wound closure and histology staining. As indicated in Figures 1(b) and 1(c), the wound closure in the STZ group was slower than those of the control group. Both low- and high-dose HB liniments increased the wound closure to the level of the STZ+rhEGF group in STZ-induced diabetic wounds, but it cannot promote wound healing of nondiabetic rats until at 13 days after operation. Additionally, HB liniment and rhEGF treated rats demonstrated a stronger staining than that of the STZ group as indicated by HE staining and Masson staining (Figure 1(d)), indicating improved ECM synthesis and collagen production by HB and rhEGF treatments. These results demonstrated that HB treatment promoted wound healing in STZ-induced diabetic rats.

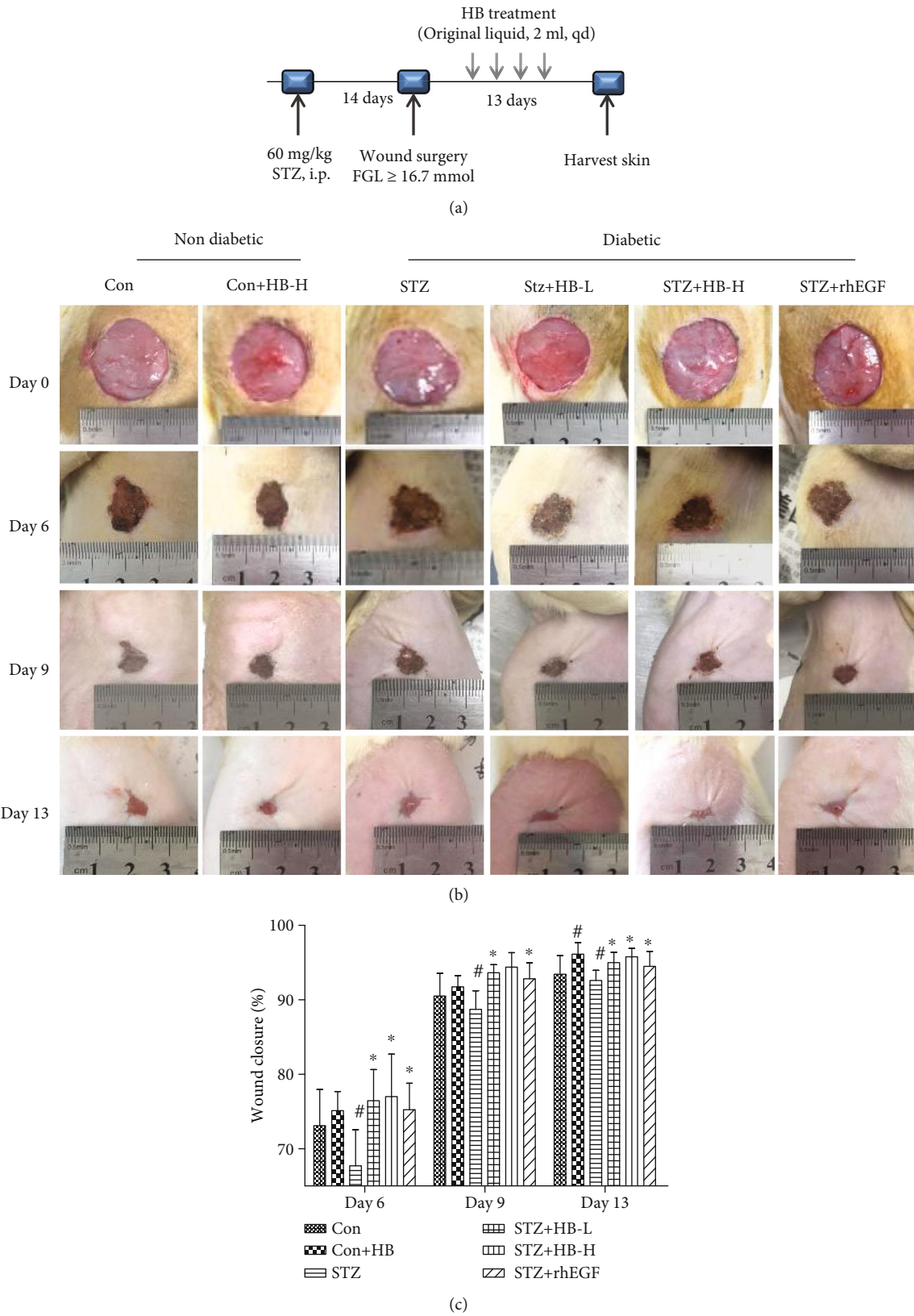


FIGURE 1: Continued.

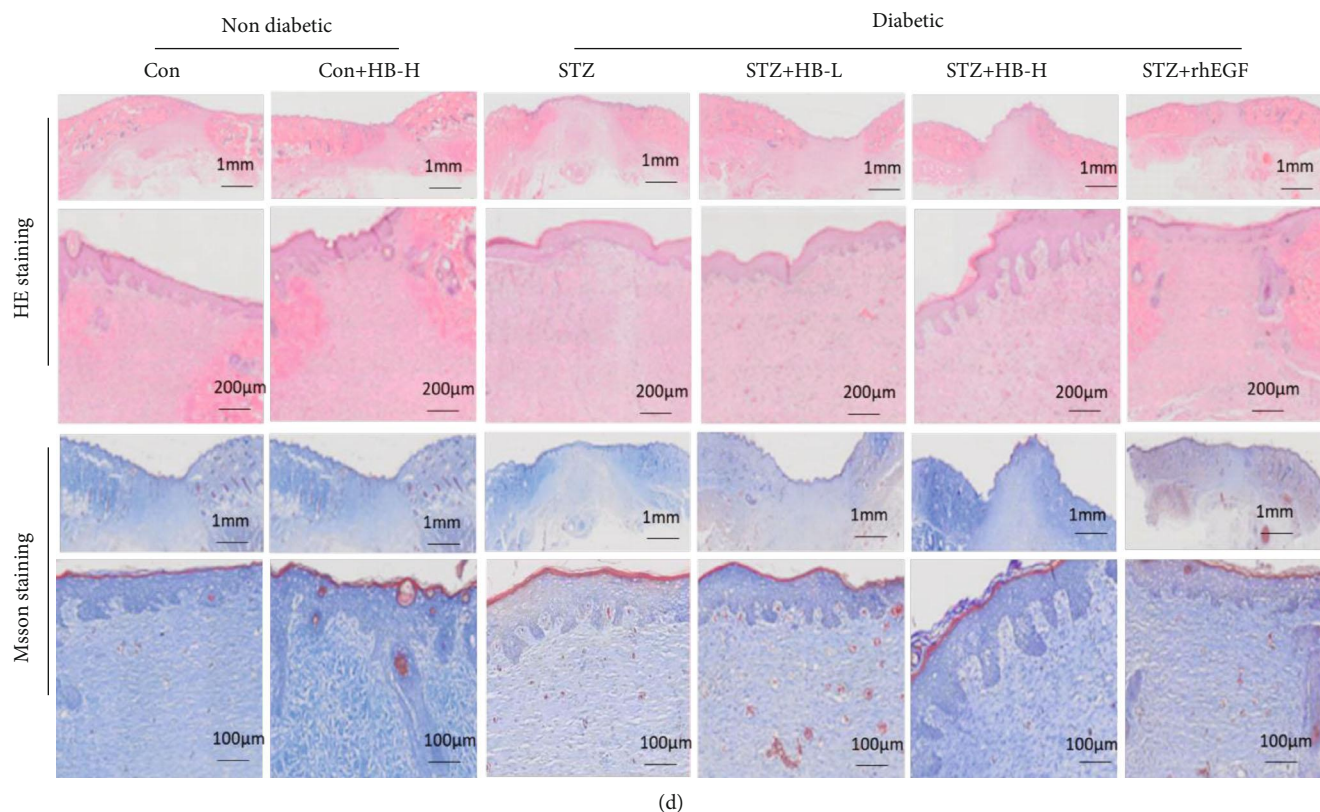


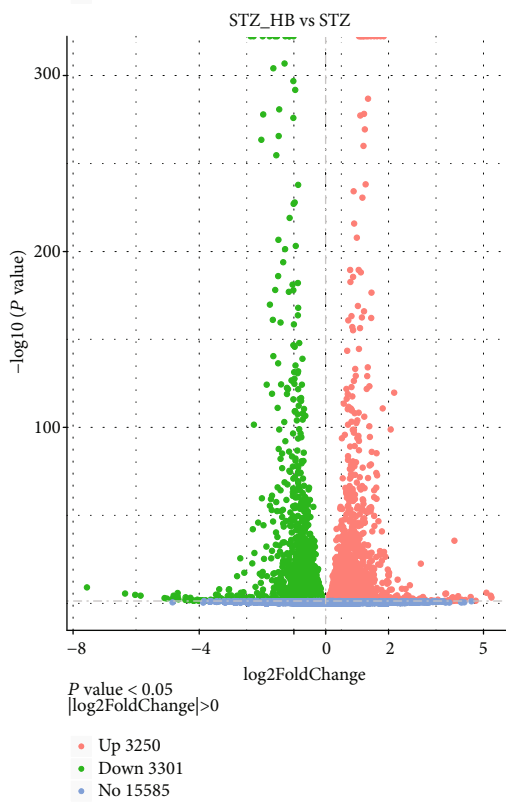
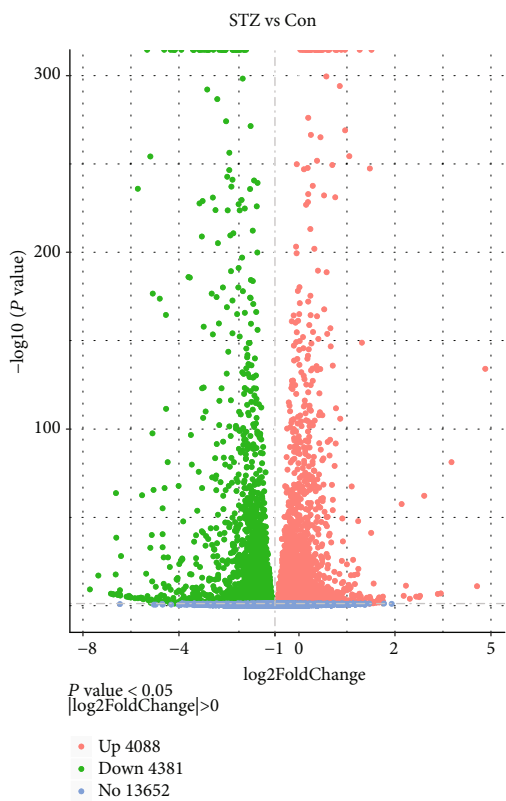
FIGURE 1: HB treatment accelerated wound closure in STZ-induced diabetic model. (a) Schematic showing diabetes induction and wound surgery generation treated with HB liniment for 13 days. (b) Representative photos of wounds healing in different time points with different treatments. (c) Wound closure analyzed by ImageJ ($n = 10$). Data were expressed as mean \pm SD, and significance was expressed as $^{\#}P < 0.05$ vs Con and $^{*}P < 0.05$ vs STZ. (d) Hematoxylin and eosin staining and Masson staining of the wound healing tissues at day 13 after wound surgery.

3.2. The Mechanism of HB-Mediated Wound Healing Was Systematically Investigated by RNA-Seq Technology. To reveal the underlying mechanism, RNA-seq technology was applied to systematically investigate the gene expression after various treatments. In contrast to the control, there were 4088 upregulated and 4381 downregulated genes in the STZ group. HB liniment significantly upregulated 3250 genes and downregulated 3301 genes when compared to the STZ group (Figure 2(a)). And the gene pattern of the STZ+HB group was more similar to the control group rather than the STZ group (Figure 2(b)). Additionally, the DEs between STZ and control were enriched into overrepresented GO terms including “response to oxidative stress,” “cell death response to oxidative stress,” “regulation of cytoskeleton organization,” “cell death,” “apoptotic signaling pathway,” and so on (Figure 3.). Whereas, skin growth-related GO terms such as “skin development,” “regulation of extracellular matrix organization,” “connective tissue development,” and “epithelial cell proliferation” were observed after HB treatment, indicating HB treatment improved wound healing in STZ-induced diabetic model. Importantly, oxidative stress-related GO terms such as “reactive oxygen species metabolic process” and “response to oxidative stress” and cell migration-related GO terms such as “positive regulation of locomotion” and “epithelium migration” were also found in the STZ+HB group. These data indicated oxidative stress

and extracellular matrix secretion may be important factors in HB-mediated wound healing.

3.3. HB Liniment Inhibited Oxidative Damage and Apoptosis in STZ-Induced Diabetic Rats. To verify the antioxidant capacity of HB in diabetic rats, the amount of MDA and 8-OHdG was measured accordingly. As indicated by Figure 4(a), increased oxidative products such as MDA and 8-OHdG were observed in the STZ group. However, the increased MDA and 8-OHdG in the STZ group was reduced by HB and rhEGF treatment. The immunofluorescence staining also confirmed the lower staining of 8-OHdG in the STZ+HB group than that of the STZ group. However, no significance was found between the control group and the Con+HB group (Figure 4(b)). Moreover, cell apoptosis was also repressed by HB liniment and rhEGF as indicated by the less staining of cleaved caspase 3 than that of the STZ group (Figure 4(c)). Taken together, oxidative damage and cell apoptosis were significantly inhibited by HB liniment and rhEGF.

3.4. HB Liniment Activated Nrf2 and Its Downstream Genes in STZ-Induced Diabetic Rats. Since nuclear factor erythroid-derived 2-like 2 (Nrf2) plays as central regulator in the maintenance of redox homeostasis by recognizing antioxidant response element and activates antioxidant genes, the Nrf2 level and its downstream NQO1 were



(a)

FIGURE 2: Continued.

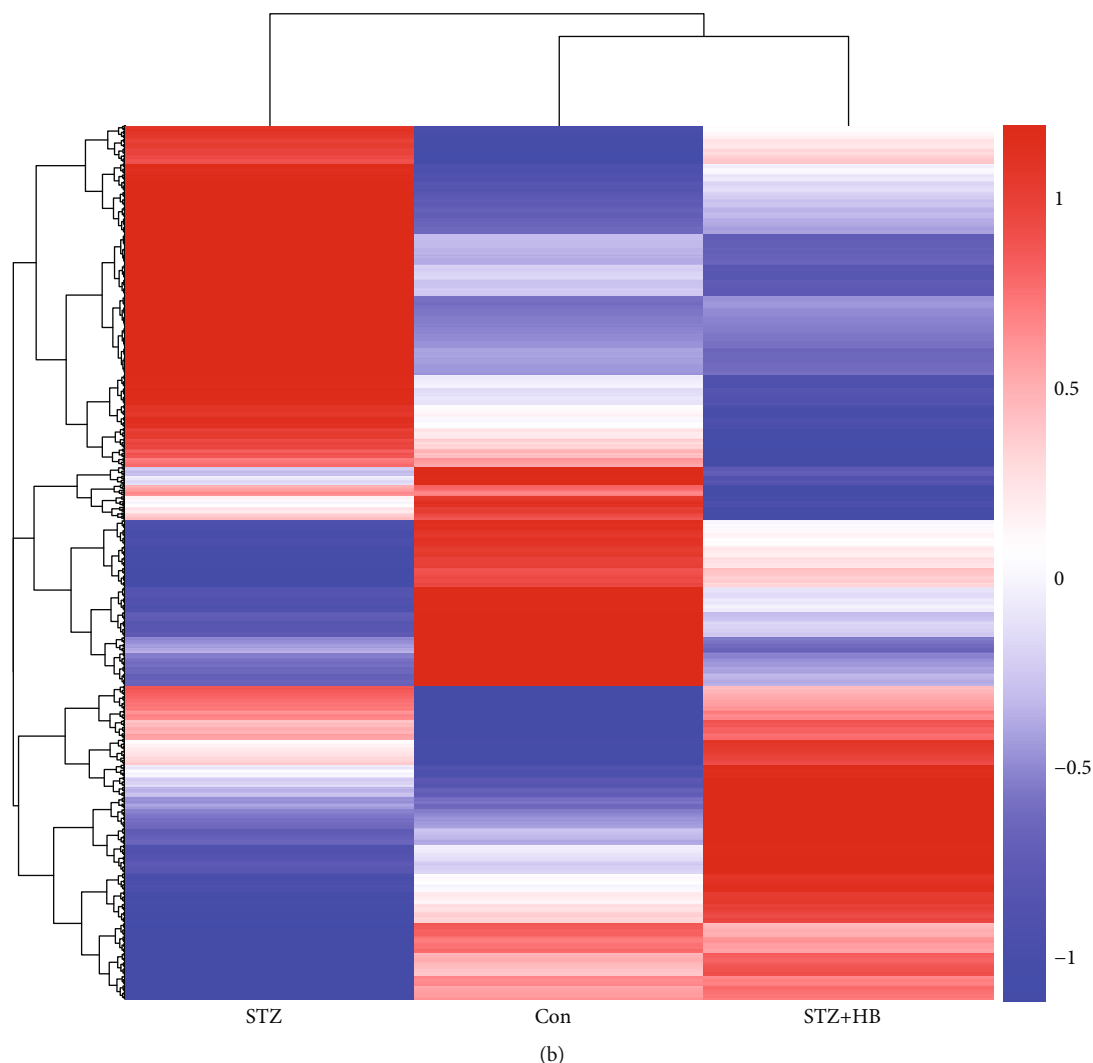


FIGURE 2: Gene expression profiling of HB-mediated wound healing in STZ-induced diabetes. (a) Differentially expressed genes (DEs) in the STZ group compared with the Con group (nondiabetic rats) and HB-treated group compared with the STZ group; upregulated DEs were shown as red dots, and downregulated DEs shown green with no significant genes as blue dots; (b) hierarchical clustering of differentially expressed genes presented as a heat map of different groups.

determined accordingly. As indicated in Figures 5(a) and 5(b), STZ group had an obvious reduction in Nrf2 expression, which was significantly reversed by HB liniment and rhEGF treatment. Importantly, the nuclear staining of Nrf2 in STZ-induced diabetic rats was obviously weak whereas it was enhanced by HB liniment. Additionally, the decreased NQO1 in the STZ group was also enhanced by HB liniment and rhEGF (Figures 5(b) and 5(c)).

To further verify the activity of Nrf2, its downstream DE genes which were involved in resisting oxidative stress were listed in Figure 6. A large number of Nrf2 downstream antioxidant genes such as Gclc, Slc7a11, Glrx5, Ggt1, Glrx3, Gsta4, Gpx1, Prdx1, Srxn1, Txnrd1, Tkt, G6pd, Taldo1, Idh1, Sod1, Sod3, and NQO1 were significantly repressed in the STZ group. Importantly, GSH-based antioxidant genes including Gclc, Gclm, Slc7a11, Glrx5, Ggt1, Glrx3, Gsta4, and Gpx1; Trx-based antioxidant genes including Prdx1, Srxn1, and Txnrd1; NADPH generation-related antioxidant

genes including Me1, Tkt, G6pd, Taldo1, and Idh1, as well as other antioxidant genes including Sod1, Sod3, and NQO1 were all activated by HB liniment. Moreover, a close relationship of Nrf2 and its downstream genes was observed (Figure 6(c)). Thus, HB liniment treatment enhanced Nrf2 and its downstream antioxidant genes to attenuated oxidative damage.

3.5. Identification of Critical Components in HB That Affected Nfe2l2 and Its Downstream Genes by Network Pharmacology Analysis. To identify the components which affected Nfe2l2 and its downstream differentially expressed genes (DEs), drug targets of HB liniment were associated with Nfe2l2 and its downstream DEs and a network of components-drug targets-DE genes was constructed. As indicated by Figure 7, 54 components in HB liniment were identified through 169 drug targets by associating with Nfe2l2 and its downstream DEs. Specifically, 21 components from Cortex

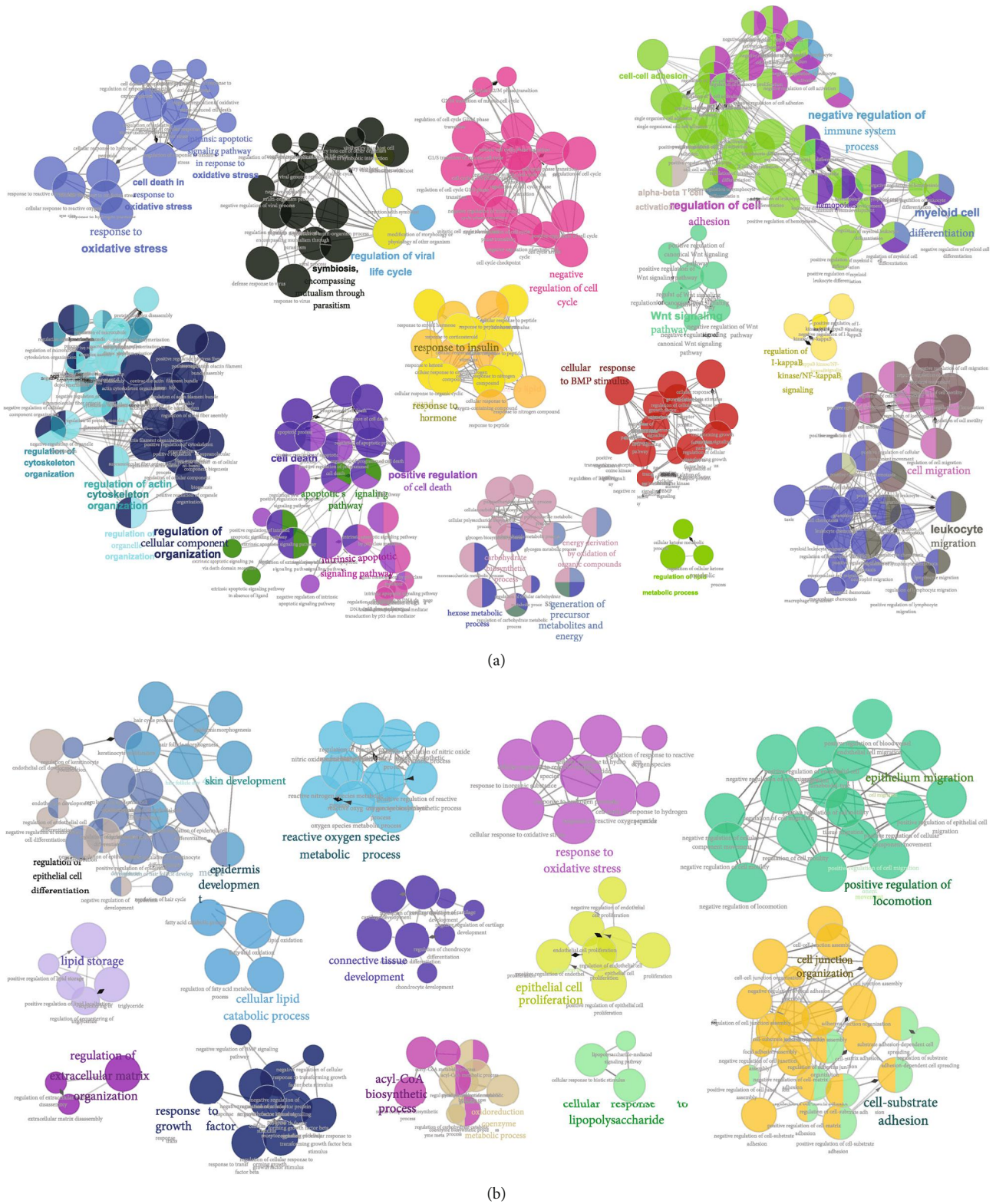


FIGURE 3: Enrichments of differentially expressed genes in HB-mediated wound healing by using ClueGo within Cytoscape software. (a) Enriched biological processes of DEs between the STZ group and the Con group; (b) enriched biological processes of DEs between the STZ+HB group and the STZ group.

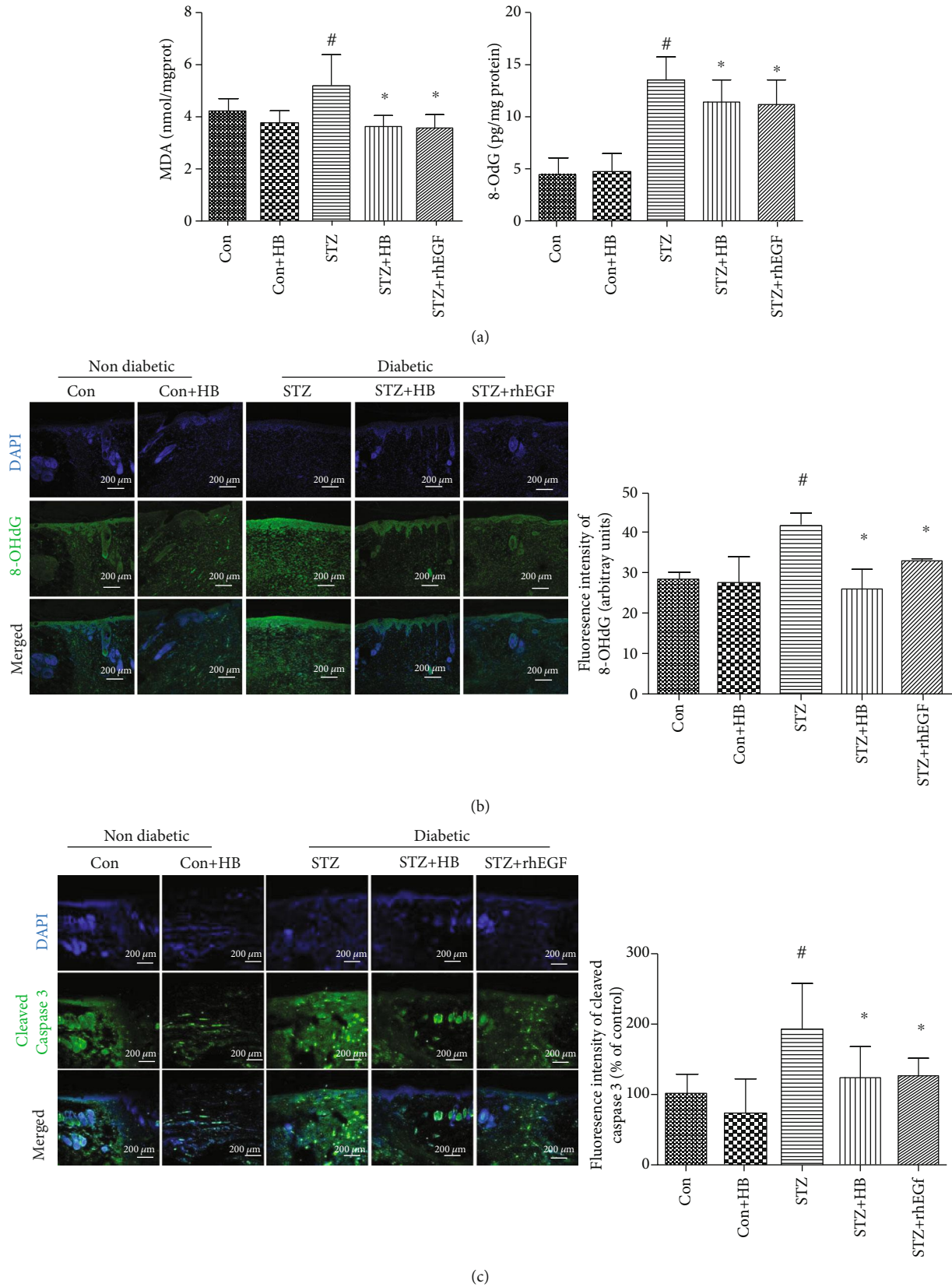
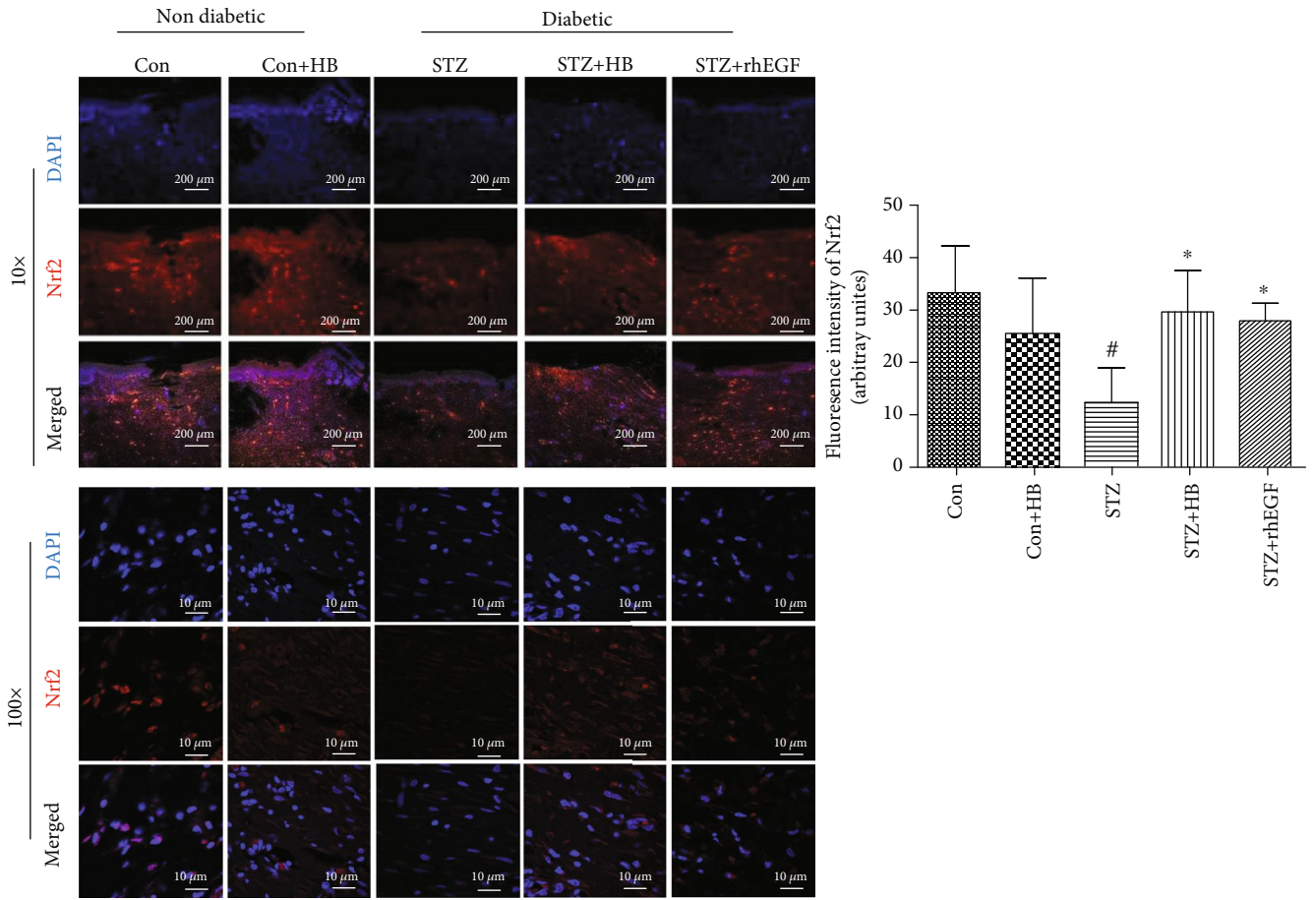
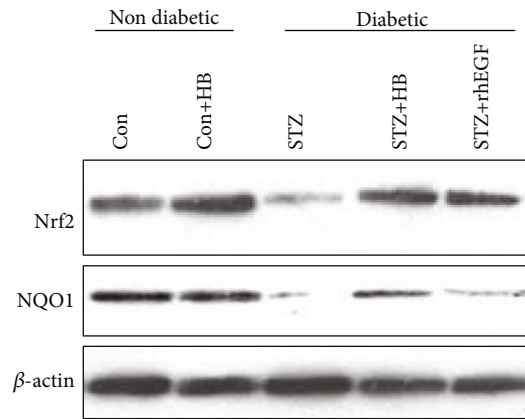


FIGURE 4: HB treatment inhibited oxidative damage and reduced cell apoptosis in diabetic wound model. (a) The level of MDA and 8-OHdG ($n = 6$); (b) immunofluorescence staining of 8-OHdG (green) and its quantitative results ($n = 3 - 5$ animals per group); scale bar: $200 \mu\text{m}$, nucleus (blue); (c) immunofluorescence staining of cleaved caspase 3 (green) and its quantitative results ($n = 3 - 5$ animals per group); scale bar: $200 \mu\text{m}$, nucleus (blue); The data were expressed as mean \pm SD and significance was expressed as $^{\#}P < 0.05$ vs Con and $^*P < 0.05$ vs STZ.



(a)



(b)

FIGURE 5: Continued.

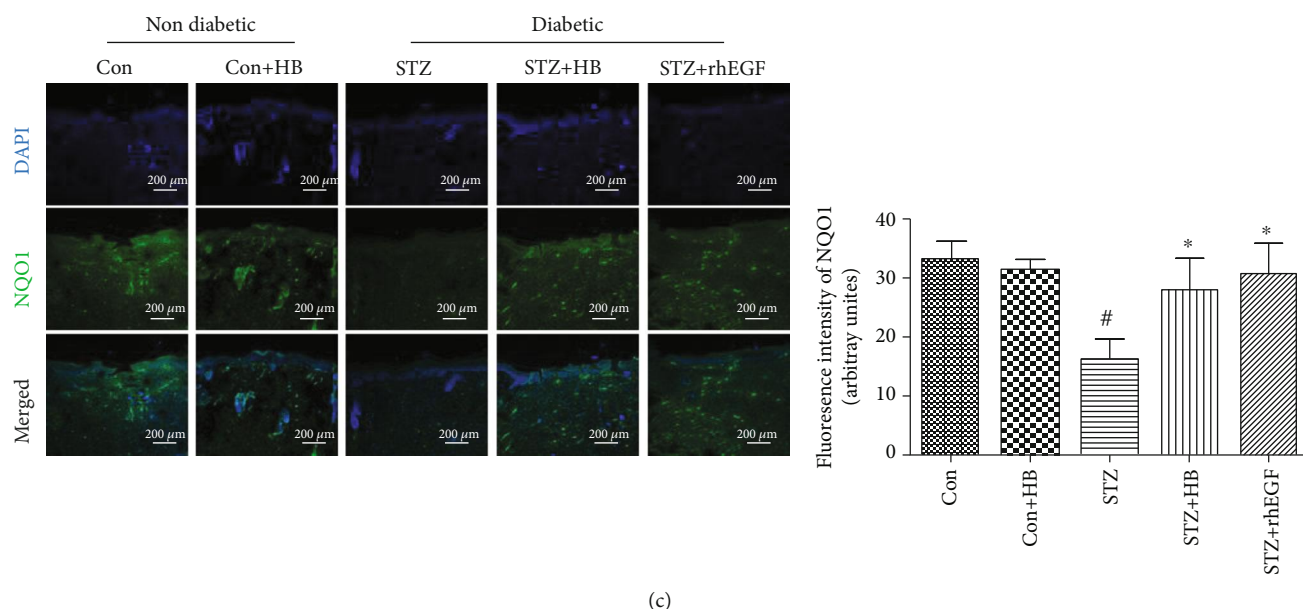


FIGURE 5: HB treatment-activated Nrf2 and its downstream NQO1 in STZ-induced wound model. (a) immunofluorescence staining of Nrf2 (red) and its quantitative results ($n = 3 - 5$ animals per group); nucleus (blue); (b) the representative western blotting results of Nrf2 and NQO1; (c) immunofluorescence staining of cleaved caspase 3 (green) and its quantitative results ($n = 3 - 5$ animals per group); scale bar: $200 \mu\text{m}$, nucleus (blue); the data were expressed as mean \pm SD, and significance was expressed as [#] $P < 0.05$ vs Con and ^{*} $P < 0.05$ vs STZ.

Phellodendri including Cinnamic acid, caffeic acid, Jatrorrhizine, 3,4-dihydroxybenzoic acid, sanleng acid, and 16 other components while 18 components from Forsythia suspensa including suspensine A, hydroxytyrosol, vanillic acid, Succinic acid, and other 14 components were screened out. Additionally, there were 9 components from Taraxacum mongolicum Hand.-Mazz, 5 from Lonicera japonica Thunb, and 7 from Scolopendridae were identified to have an effect on the differentially expressed oxidative genes. Among these identified components, there were several components originated from multiple drugs. For example, Quercetin generated from both Forsythia suspensa, Lonicera japonica Thunb, and Taraxacum mongolicum Hand.-Mazz.

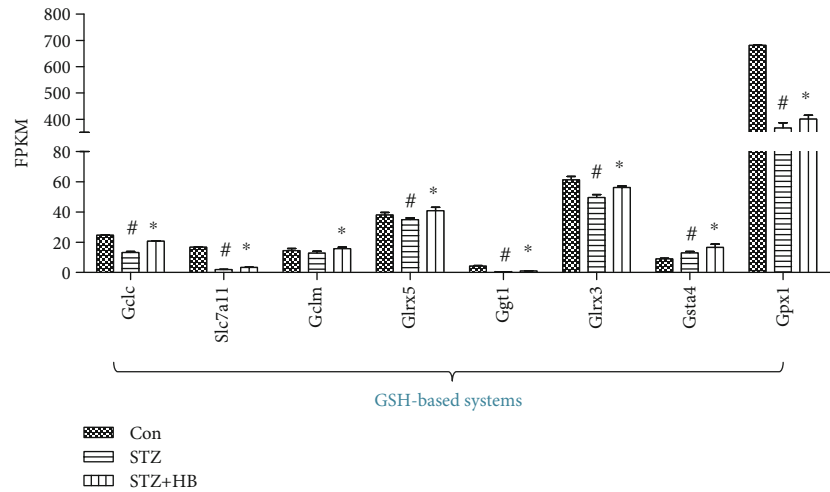
3.6. HB Liniment Modulated the Expression of MMP9 and TGF- β 1 and Improved Collagen Growth. To further reveal the mechanism of HB, TGF- β 1, MMP9 level, and the collagen growth were evaluated accordingly. As indicated by Figure 8, the decreased TGF- β 1 and elevated MMP9 in the STZ group were significantly reversed by HB liniment and rhEGF. The neo-collagen growth at the front of the wound healing was increased by both HB liniment and rhEGF in contrast to the STZ group. These results showed HB liniment and rhEGF enhanced TGF- β 1, reduced MMP9, and improved collagen growth.

3.7. HB Liniment and Quercetin Promoted Cell Proliferation and Decreases Oxidative Damage in HG-Induced Model. To further confirm the mechanism, the effect of HB and quercetin (one of its components), which was reported to have an effect on diabetic wounds, was tested using HaCaT cells. As indicated by Figure 9, HB and quercetin did not inhibit cell viability but enhanced cell proliferation in low-glucose

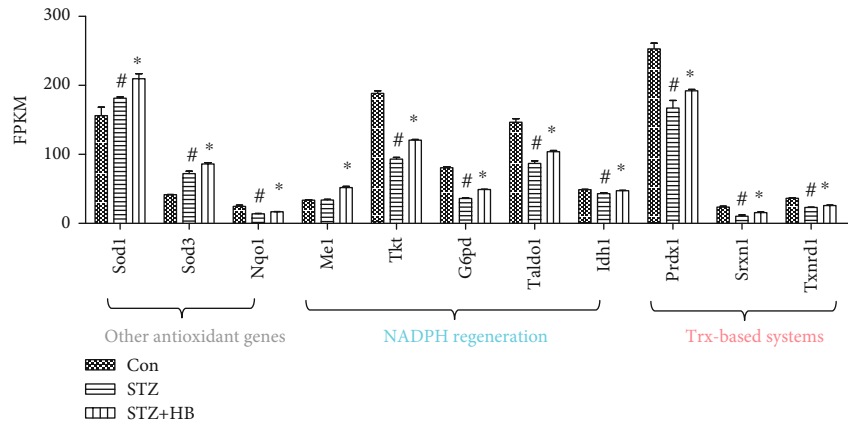
medium. HG stimulation caused a remarkably decrease in cell viability, whereas this was ameliorated by HB, quercetin, and povidone iodine. To confirm the effect of HB on oxidative stress, the levels of ROS and GSH were measured accordingly. HG stimulation led to a significant decrease in GSH level, which was dramatically increased by HB and quercetin. Additionally, the increased ROS level induced by HG was also significantly reduced by HB and quercetin but not by povidone iodine. The positive rate of Ki67 (a cell proliferation marker) was decreased by HG stimulation, which was significantly increased by HB, but not by quercetin or povidone iodine (Figure 9(c)). These data indicated that HB had a good effect in attenuating oxidative damage and promoting cell proliferation.

4. Discussion

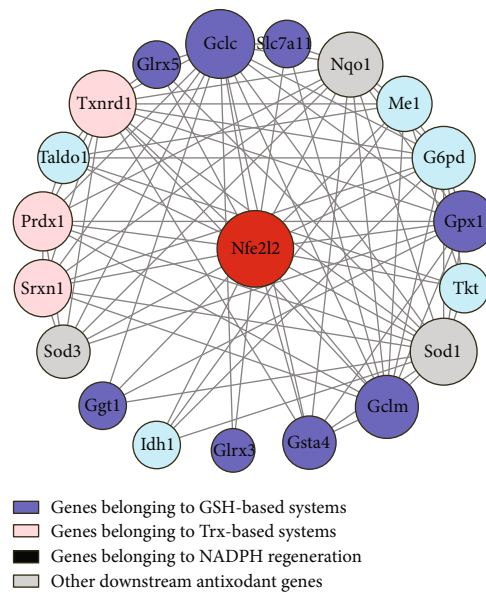
Diabetic wounds cause high mortality and disability in a large number of diabetic patients, whereas there is a limited effective therapy. In this study, the effect of Huangbai (HB) liniment on STZ-induced diabetic wounds was systematically investigated, and the mechanism was revealed. HB liniment significantly accelerated the wound closure and enhanced the generation of extracellular matrix in STZ-induced diabetic rats. By using RNA-seq technology analysis, oxidative stress was identified as a vital process in HB-mediated wound healing. Importantly, the activation of Nrf2 and its downstream genes involved in glutathione system, thioredoxin system, and NADPH generation as well as other antioxidant genes were observed after HB treatment. The activated Nrf2 and its downstream genes developed a stable antioxidant network, contributing to the reduction of oxidative damage and apoptosis (Figure 10). Moreover, HB liniment enhanced



(a)



(b)



(c)

FIGURE 6: HB treatment activated the downstream genes of Nrf2 in diabetic wound model. (a) The downstream genes of Nrf2 involved in GSH-based antioxidant systems ($n=3$); (b) The downstream genes of Nrf2 involved in Trx-based antioxidant systems, GAPDH generation and other antioxidant processes ($n=3$); (c) The network of Nfe2l2 and its downstream DEs constructed by Cytoscape software. The data were expressed as mean \pm SD, and significance was expressed as # $P < 0.05$ vs Con and * $P < 0.05$ vs STZ.

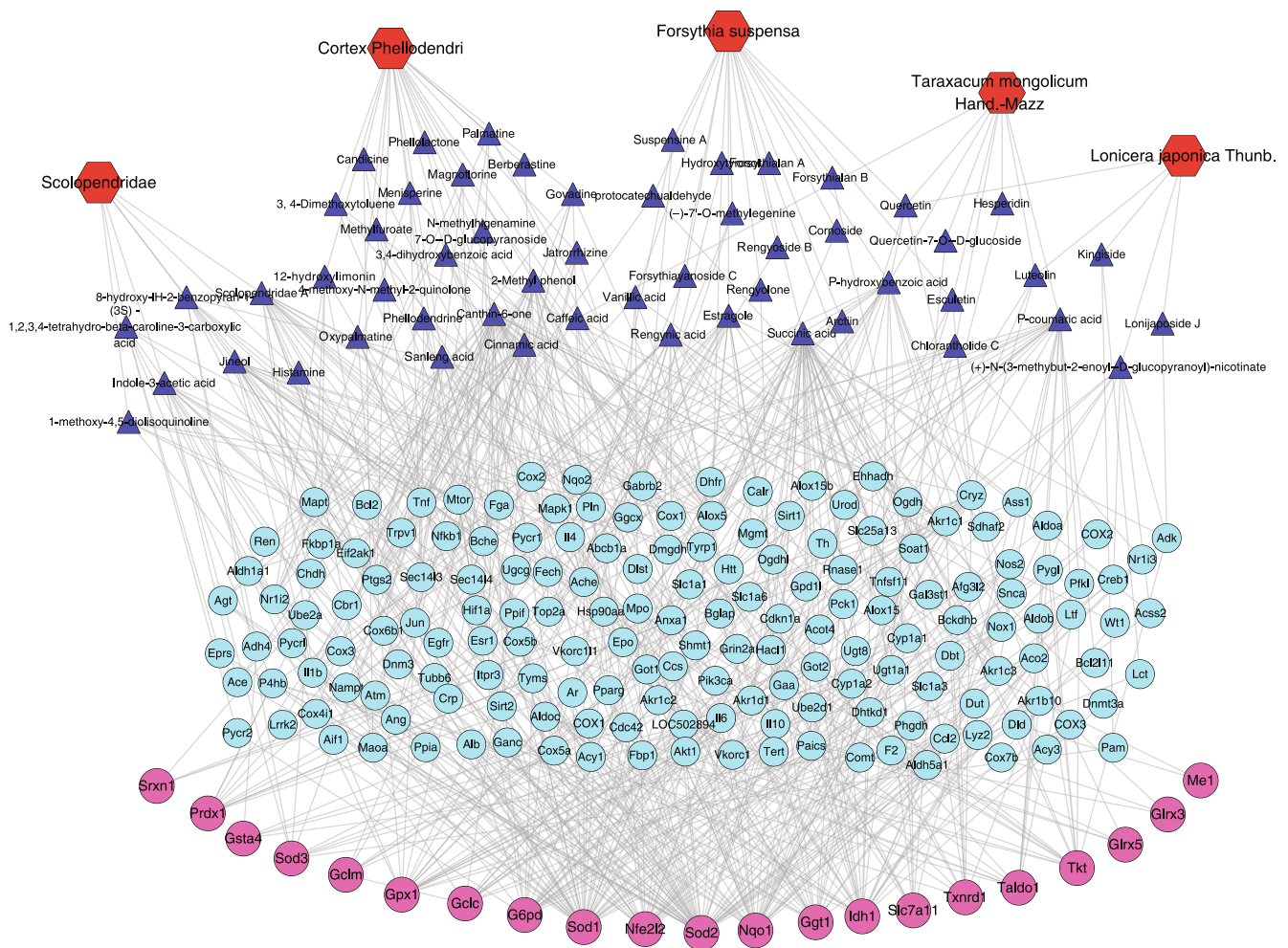


FIGURE 7: The components of HB liniment which affected Nfe2l2 and its downstream differentially expressed genes (DEs) were identified through Network pharmacology analysis. Specifically, 54 components in HB liniment were identified with 21 components from Cortex Phellodendri, 18 components from Forsythia suspensa, 9 components from Taraxacum mongolicum Hand.-Mazz, 5 from Lonicera japonica Thunb., and 7 from Scolopendridae. Some components generated from multiple Chinese medicine. Red hexagons indicated the Chinese medicine, blue triangles indicated the components of HB, blue dots indicated drug targets of components from HB liniment, and red dots indicated Nfe2l2 and its downstream DEs.

TGF- β 1, reduced MMP9 level, and promoted collagen growth, thereby accelerating wound healing in diabetic conditions. The *in vitro* experiment demonstrated the good effect of HB in inhibiting oxidative damage and enhancing cell proliferation. By associating drug targets of HB liniment with Nrf2 and its downstream differentially expressed genes, 54 components were screened out, and the majority of the components was from Cortex Phellodendri and Forsythia suspensa.

Growing evidence has accumulated that redox homeostasis serves a significant role in modulating diabetic wound healing [23]. Overproduced ROS in diabetes damages macromolecules such as lipids, proteins, and DNA double strands, thus results in impaired wound healing and apoptosis. In our study, oxidative stress was identified as a vital process in HB-mediated wound healing (Figure 3), which was subsequently confirmed by decreased high DNA damage (8-OHdG), peroxide products (MDA), and reduced apoptosis in STZ rats. As a central regulator of cellular redox status, Nrf2 is respon-

sible for modulating transcription of cytoprotective and antioxidant genes, which affects the ability of wounds to heal in diabetics [24]. Activation of Nrf2 by its activator or inhibiting its repressor Keap1 alleviated ROS generation, decreased oxidative damage, and accelerated wound closure in diabetes [25, 26]. On the contrary, Nrf2^{-/-} mice was characterized by delayed wound healing [25], indicating the vital role of Nrf2 in facilitating wound closure in diabetes. As consistently demonstrated in our study, hindered Nrf2 activity in diabetes failed to modulate redox homeostasis and resulted in impaired wound closure, whereas the Nrf2 signaling restored by HB treatment inhibited oxidative damage and promoted wound healing. In addition, our results demonstrated the dysfunction of its target genes involved in GSH-based, Trx-based antioxidant systems, as well as NADPH-generating process and other antioxidant genes such as NQO1, Sod1, and Sod3 were also rescued by HB treatment in STZ-induced diabetic wound (Figure 6). Nrf2 activation enhanced expression of Gclc and Gclm which determined the GSH

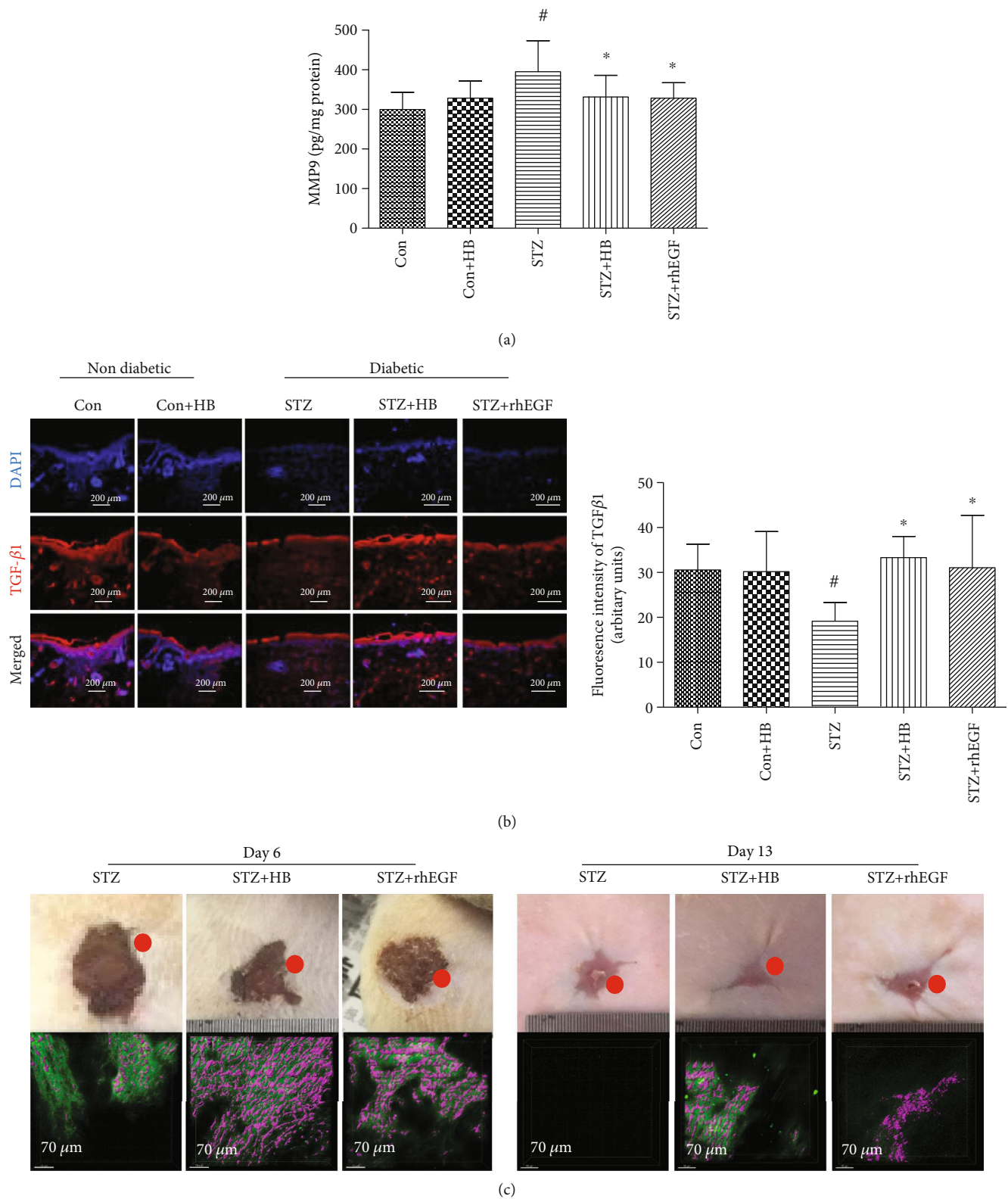
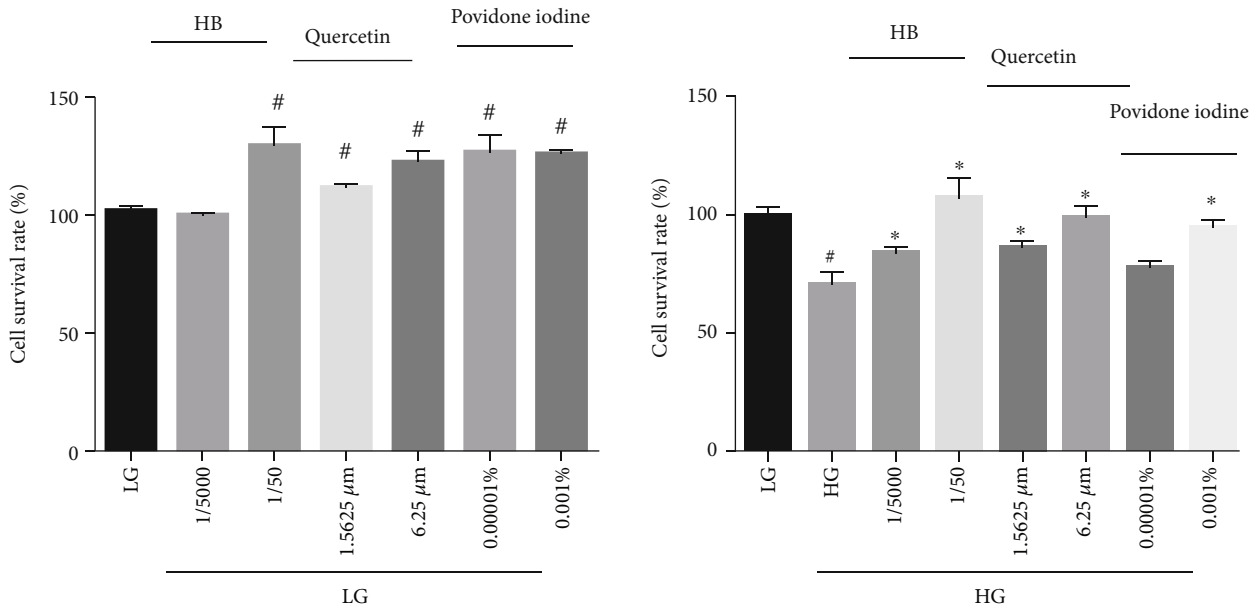
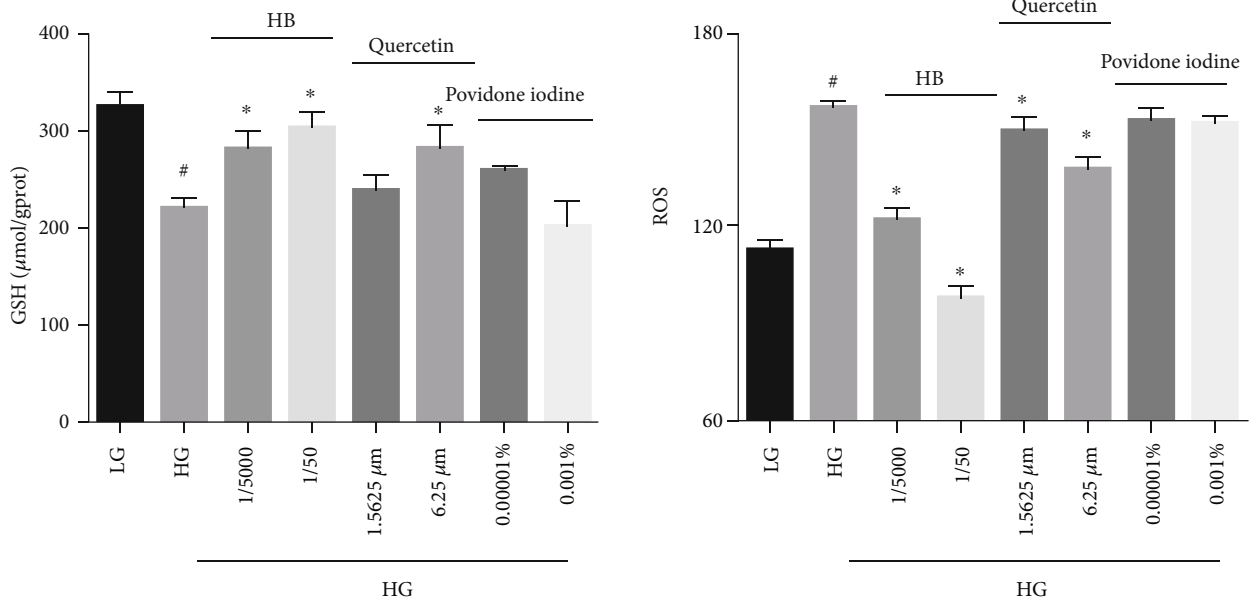


FIGURE 8: HB treatment enhanced TGF- β 1 expression, decreased MMP9 production, and facilitated collagen growth. (a) immunofluorescence staining of TGF- β 1 (red) and its quantitative results ($n = 3 - 5$ animals per group); scale bar: 200 μ m, nucleus (blue); (b) MMP9 level ($n = 6$); (c) New collagen growth observed by using two-photon microscope at days 6 and 13 after wound surgery. The green indicated the background, and the purple indicated the new collagen tissue at the front of the wound healing. The data were expressed as mean \pm SD, and significance was expressed as [#] $P < 0.05$ vs Con and ^{*} $P < 0.05$ vs STZ.

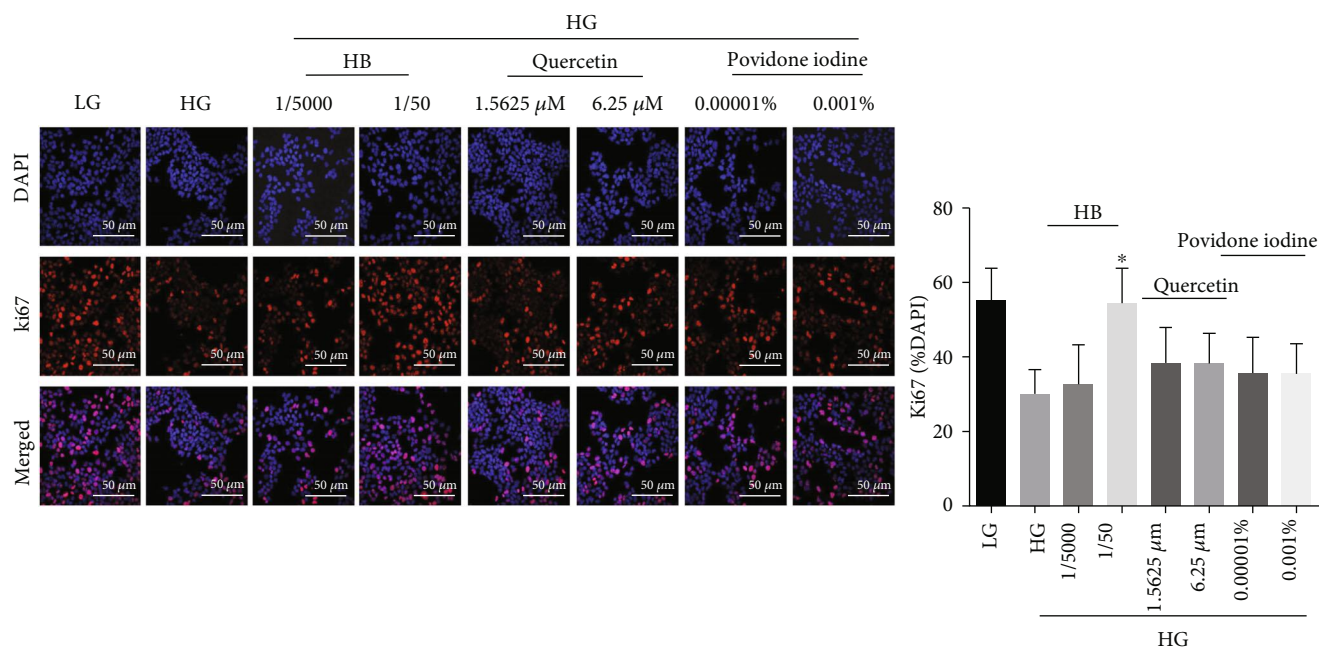


(a)



(b)

FIGURE 9: Continued.



(c)

FIGURE 9: HB facilitated cell proliferation and reduced oxidative damage in HaCaT cells. (a) Cell viability in LG and HG ($n = 6$); (b) the levels of GSH ($n = 3$) and ROS ($n = 6$); (c) immunofluorescence staining of Ki67 (red) and its quantitative result ($n = 3 - 5$ per group), nucleus (blue), scale bar: $50 \mu\text{m}$; the data were expressed as mean \pm SD, and significance was expressed as $^{\#}P < 0.05$ vs LG and $*P < 0.05$ vs HG.

biosynthesis, Gpx1 which helped to decompose H_2O_2 and produce GSSG, and Ggt1 which initiated extracellular glutathione (GSH) breakdown. The elevated levels of GSH-based antioxidant genes maintained GSH homeostasis and ensured that its antioxidant effect was realized [27]. Moreover, Nrf2 activation upregulated gene expression of Txnrd1, Srxn1, and Prdx1, which allowed for the reduction of oxidized thiols in proteins [28]. As a vital reducing resource, NADPH was required for the GSH and Trx regeneration to eliminate excess ROS [29]. The elevated gene expression of Me1, Tkt, Idh1, and Taldo1 by Nrf2 demonstrated the improved function of NADPH generation and maintained GSH- and Trx- based antioxidant function. Thus, the activated Nrf2, together with its downstream genes involved in GSH-based, Trx-based antioxidant systems, as well as NADPH generating process and other antioxidant genes, eliminated ROS, decreased oxidative damage and apoptosis, and accelerated wound healing in diabetes.

The compounds in HB liniment that affected Nfe2l2 and its downstream genes were identified accordingly. Specifically, 54 components from HB liniment were identified to have an effect on Nfe2l2 and its downstream antioxidant genes. Significantly, among the 21 identified components from Cortex Phellodendri, Cinnamic acid [30], caffeic acid [31], Magnoflorine [32, 33], Jatrorrhizine [34], phellodendrine, and 3,4-dihydroxybenzoic acid have proven to reduce oxidative stress. The extract of Forsythia suspensa exhibited a significant antihyperglycemic and antihyperlipidemic effect in the treatment for diabetes by modulating oxidative stress and insulin secretion [35]. The 18 compounds from Forsythia suspensa, including quercetin [36], vanillic acid [37],

Arctiin [38], hydroxytyrosol [39] and Protocatechualdehyde [40], ameliorated oxidative damage. Additionally, Taraxacum mongolicum Hand.-Mazz [41], and its identified components such as p-Coumaric acid and Esculetin [42, 43], as well as Lonicera japonica Thunb., and its identified components such as Luteolin had a beneficial antioxidant effect by removing ROS [44, 45]. Moreover, no studies have shown that Scolopendridae were associated with diabetes, although they have demonstrated to exhibit good antioxidant capacity [46]. In this study, the antioxidant property of HB liniment was observed in the treatment of STZ-induced diabetic wound by using the combination of Cortex Phellodendri, Forsythia suspensa, Lonicera japonica Thunb., Taraxacum mongolicum Hand.-Mazz, and Scolopendridae. In addition, quercetin, which came from three of the five compositions of HB liniment, demonstrated multiple effects in facilitating wound healing [47]. Researches showed it not only has good antibacterial action, similar to other standard drugs (e.g., povidone iodine) [48], but also decreased inflammation, inhibited oxidative damage, and enhanced secretion of VEGF and TGF- β 1, modulated integrin expressions to reduce fibrosis during wound healing [47, 49]. In this study, the effect of HB, quercetin, and povidone iodine on inhibiting oxidative damage was compared in HG-induced HaCaT cell model. It demonstrated that both HB and quercetin had a good effect in inhibiting oxidative damage rather than povidone iodine (Figure 9). Thus, four herbs and Scolopendridae in HB liniment shared some same components, and the 54 identified compounds had a synergistically inhibitive effect on oxidative stress through modulating Nrf2 and its downstream antioxidant genes.

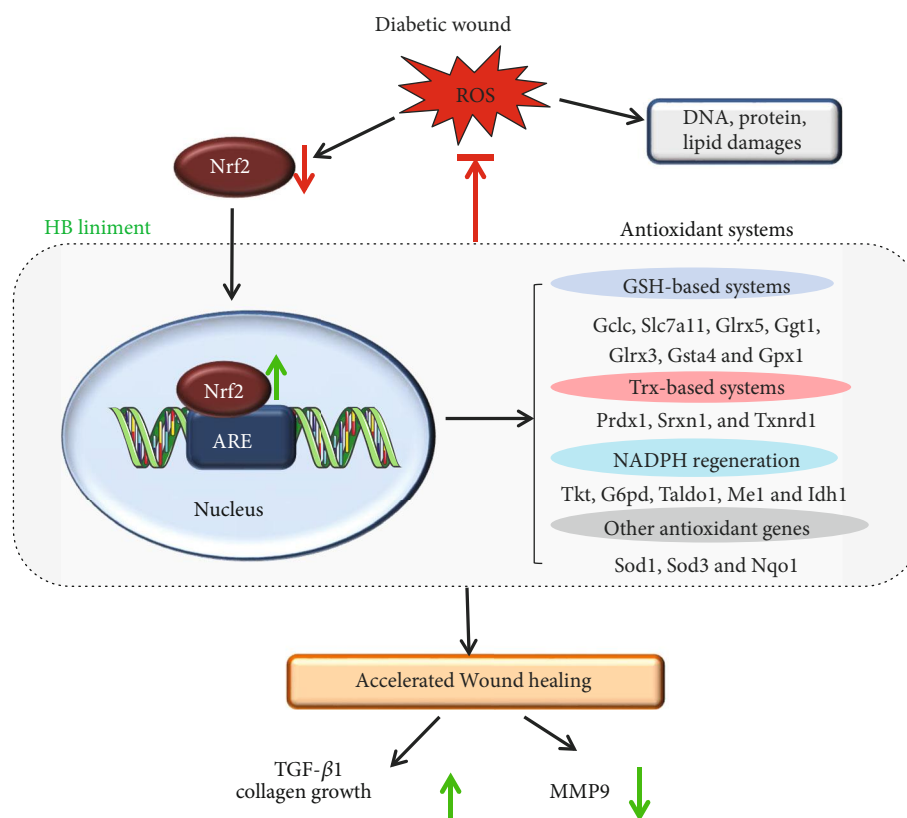


FIGURE 10: Schematic diagram illustrating of the potential mechanism of HB-mediated diabetic wound healing. Reactive oxygen species in diabetic wound caused DNA double strands breakage, lipid peroxide, protein denaturation, and impaired diabetic wound healing. Specifically, Nrf2 and its downstream antioxidant genes were significantly decreased, and wound healing was impaired. In contrast, HB liniment markedly increased Nrf2 level and its downstream genes involved in GSH- and Trx-based systems, NADPH generation, and other antioxidant systems; this led to enhanced antioxidant capacity and decreased oxidative and apoptosis damage. Additionally, these also increased TGF- β 1 and collagen growth while decreased MMP9, which accelerated wound closure in HB-mediated wound healing.

Along with the enhanced antioxidant capacity by HB liniment, an increase in transforming growth factor- β 1 (TGF- β 1) and reduction in matrix metalloproteinase (MMP) contributed to the increased extracellular matrix growth and enhanced wound healing in diabetes. Elevated levels of ROS hinder tissue growth, especially for collagen production and halt wound closure [12], and the interference of ECM production is highlighted through the disruption of TGF- β 1 signaling [10, 11]. Besides, high ROS level affects ECM remodeling through regulating MMPs expression, and ROS production is required for MMPs synthesis [13]. These were consistent with our results that serious oxidative damage in diabetic rats was associated with low ECM synthesis and collagen generation. Delayed wound healing in diabetes is usually characterized with low TGF- β 1 and high MMPs in skin tissue of patients with diabetic foot ulcer [50–52]. TGF- β 1 signaling plays a critical role as the regulator in a series of biological processes of skin regeneration and wound healing, such as angiogenesis and reepithelialization. [53]. MMP9 is responsible for eliminating damaged extracellular matrix and allows for skin tissue remodeling [54]. An overproduction of MMP9 in diabetes causes excessive ECM degradation and results in delayed wound healing [54], but inhibition or knockout of MMP9 promotes diabetic wound healing [55]. This indicates a critical role of MMP9 in treat-

ing diabetic ulcers. Consistent with these research findings, decreased TGF- β 1 and elevated MMP9 were observed in our diabetic wound model, and these were significantly alleviated by HB treatment as indicated by significantly higher TGF- β 1 and reduced MMP9 level. Recent research indicates that Nrf2 activation could promote TGF- β 1 generation and inhibit the overproduction of MMP9 in diabetic wound [25]. Our results demonstrated that elevated TGF- β 1 and decreased MMP9 were associated with the activation of Nrf2 in HB-mediated wound healing.

Taken together, our findings demonstrated activation of Nrf2 by HB liniment accelerated diabetic wound healing. This study provided experiment evidence for topical HB liniment treatment for diabetic wounds and highlighting the effect of activating Nrf2 in diabetic wound healing. However, we only focused on the effect of HB on oxidative damage, whether it had an effect on inflammation, angiogenesis and antibiosis remained further investigation. In addition, the components in HB liniment which really played a role in activating Nrf2 need to be clarified in the future study.

5. Conclusions

In summary, an obvious protective effect of HB treatment against diabetic wound healing was observed, and reduction

in oxidative stress may play a vital role in HB-mediated wound healing. RNA-seq analysis and further experiment suggested that the activation of Nrf2 and its downstream antioxidant genes reduced apoptosis and oxidative damage, thereby improving HB-mediated wound healing. And 54 compounds in HB liniment were identified to have an effect on Nfe2l2 and its downstream genes, which had a synergistically inhibitive effect on oxidative stress. In addition, HB liniment, increased TGF- β 1 level, and reduced MMP9, thereby contributing to the acceleration of diabetic wound healing. Our findings offered experimental evidence of HB liniment in the treatment of diabetic wounds and also improved our understanding of diabetic wound healing, supporting development of Nrf2-based therapy in the treatment of diabetic ulcer.

Data Availability

The data about the RNA-seq analysis was uploaded into NCBI <https://www.ncbi.nlm.nih.gov/sra/PRJNA532974> (SRP193129) which can be downloaded. As for the other data used to support the findings of this study are available from the corresponding author upon request.

Conflicts of Interest

The authors declare that they have no conflicts of interest.

Authors' Contributions

Jingjing Zhang and Rui Zhou contributed equally to this work.

Acknowledgments

The authors would like to acknowledge the financial support from National Key R&D Plan (no. 2017YFC1702605), National Natural Science Foundation of China (no. 81974550), and Fundamental Research Funds for the Central Universities (no. ZZ13-YQ-046). The author would like to thank *Xin Li* for the assistant in the network analysis. The authors disclose that this project was partially funded by Shandong Hanfang Pharmaceutical Co., Ltd, who also provided Huangbai liniment (Chinese medicine character: Z10950097) for this research. The authors promise that the authenticity and conclusions of this study will not be affected by the funding.

Supplementary Materials

Table S1. The RNA-seq data of nondiabetic wound (Con), STZ-induced diabetic wound with or without HB treatment. The gene expressions of different ss were expressed as FPKM and the fold change and false discovery rate (FDR). (*Supplementary Materials*)

References

- [1] V. R. Driver, M. Fabbi, L. A. Lavery, and G. Gibbons, "The costs of diabetic foot: the economic case for the limb salvage team," *Journal of Vascular Surgery*, vol. 52, no. 3, pp. 17S–22S, 2010.
- [2] G. E. Reiber, B. A. Lipsky, and G. W. Gibbons, "The burden of diabetic foot ulcers," *American Journal of Surgery*, vol. 176, no. 2, pp. 5S–10S, 1998.
- [3] R. Blakytyn and E. B. Jude, "Altered molecular mechanisms of diabetic foot ulcers," *The International Journal of Lower Extremity Wounds*, vol. 8, no. 2, pp. 95–104, 2009.
- [4] V. Falanga, "Wound healing and its impairment in the diabetic foot," *Lancet*, vol. 366, no. 9498, pp. 1736–1743, 2005.
- [5] C. Bianchi and S. Del Prato, "Metabolic memory and individual treatment aims in type 2 diabetes—outcome—lessons learned from large clinical trials," *The Review of Diabetic Studies*, vol. 8, no. 3, pp. 432–440, 2011.
- [6] A. K. Arya, R. Tripathi, S. Kumar, and K. Tripathi, "Recent advances on the association of apoptosis in chronic non healing diabetic wound," *World Journal of Diabetes*, vol. 5, no. 6, pp. 756–762, 2014.
- [7] M. Cano Sanchez, S. Lancel, E. Boulanger, and R. Neviere, "Targeting oxidative stress and mitochondrial dysfunction in the treatment of impaired wound healing: a systematic review," *Antioxidants*, vol. 7, no. 8, p. 98, 2018.
- [8] Z. Zhang, Z. Zi, E. E. Lee et al., "Differential glucose requirement in skin homeostasis and injury identifies a therapeutic target for psoriasis," *Nature Medicine*, vol. 24, no. 5, pp. 617–627, 2018.
- [9] F. P. Beserra, A. J. Vieira, L. F. S. Gushiken et al., "Lupeol, a dietary Triterpene, enhances wound healing in streptozotocin-induced hyperglycemic rats with modulatory effects on inflammation, oxidative Stress, and angiogenesis," *Oxidative Medicine and Cellular Longevity*, vol. 2019, Article ID 3182627, 20 pages, 2019.
- [10] T. He, T. Quan, Y. Shao, J. J. Voorhees, and G. J. Fisher, "Oxidative exposure impairs TGF- β pathway via reduction of type II receptor and SMAD3 in human skin fibroblasts," *Age*, vol. 36, no. 3, p. 9623, 2014.
- [11] M. J. Davies, "The oxidative environment and protein damage," *Biochimica et Biophysica Acta*, vol. 1703, no. 2, pp. 93–109, 2005.
- [12] A. E. Loo, Y. T. Wong, R. Ho et al., "Effects of hydrogen peroxide on wound healing in mice in relation to oxidative damage," *PLoS One*, vol. 7, no. 11, 2012.
- [13] B. Hantke, C. Lahmann, K. Venzke et al., "Influence of flavonoids and vitamins on the MMP- and TIMP-expression of human dermal fibroblasts after UVA irradiation," *Photochemical & Photobiological Sciences*, vol. 1, no. 10, pp. 826–833, 2002.
- [14] L. Wang, G. B. Zhou, P. Liu et al., "Dissection of mechanisms of Chinese medicinal formula Realgar-Indigo naturalis as an effective treatment for promyelocytic leukemia," *Proceedings of the National Academy of Sciences of the United States of America*, vol. 105, no. 12, pp. 4826–4831, 2008.
- [15] J. Zhang, F. Guo, J. Wei et al., "An integrated approach to identify critical transcription factors in the protection against hydrogen peroxide-induced oxidative stress by Danhong injection," *Free Radical Biology & Medicine*, vol. 112, pp. 480–493, 2017.
- [16] X. L. Tong, L. Dong, L. Chen, and Z. Zhen, "Treatment of diabetes using traditional Chinese medicine: past, present and future," *The American Journal of Chinese Medicine*, vol. 40, no. 5, pp. 877–886, 2012.

- [17] Committee, CP, *China Pharmacopoeia*, vol. 1, Chemical Industry Press, 2015.
- [18] X. Hou, X. Jun, P. Wang et al., "Analysis on clinical efficacy of compound Huangbai fluid as adjunctive treatment for diabetic foot ulcer," *Chinese Journal of Experimental Traditional Medical Formulae*, vol. 22, no. 4, pp. 159–163, 2016.
- [19] L. You-shan, Z. Qi, and Y. Bo-hua, "Efficacy and safety in a multi-center clinical trial for analyzing compound fluid of cortex phellodendri in the external treatment of diabetic foot ulcers," *Chinese Journal of New Drugs*, vol. 25, no. 20, pp. 2344–2348, 2016.
- [20] L. You-shan and Y. Bo-hua, "Effects of compound fluid of cortex phellodendri on inflammatory cytokines and growth factors in external treatment of diabetic foot ulcer," *Chinese Journal of New Drugs*, vol. 23, no. 10, pp. 1163–1166, 2014.
- [21] H. Zheng, S. A. Whitman, W. Wu et al., "Therapeutic potential of Nrf2 activators in streptozotocin-induced diabetic nephropathy," *Diabetes*, vol. 60, no. 11, pp. 3055–3066, 2011.
- [22] P. Shannon, A. Markiel, O. Ozier et al., "Cytoscape: a software environment for integrated models of biomolecular interaction networks," *Genome Research*, vol. 13, no. 11, pp. 2498–2504, 2003.
- [23] N. T. Moldogazieva, I. M. Mokhosoev, T. I. Mel'nikova, Y. B. Porozov, and A. A. Terentiev, "Oxidative Stress and advanced lipoxidation and glycation end products (ALEs and AGEs) in aging and age-related diseases," *Oxidative Medicine and Cellular Longevity*, vol. 2019, Article ID 3085756, 14 pages, 2019.
- [24] J. D. Hayes and A. T. Dinkova-Kostova, "The Nrf2 regulatory network provides an interface between redox and intermediary metabolism," *Trends in Biochemical Sciences*, vol. 39, no. 4, pp. 199–218, 2014.
- [25] M. Long, M. Rojo de la Vega, Q. Wen et al., "An essential role of NRF2 in diabetic wound healing," *Diabetes*, vol. 65, no. 3, pp. 780–793, 2016.
- [26] M. A. Soares, O. D. Cohen, Y. C. Low et al., "Restoration of Nrf2 signaling normalizes the regenerative niche," *Diabetes*, vol. 65, no. 3, pp. 633–646, 2016.
- [27] L. G. Higgins, M. O. Kelleher, I. M. Eggleston, K. Itoh, M. Yamamoto, and J. D. Hayes, "Transcription factor Nrf2 mediates an adaptive response to sulforaphane that protects fibroblasts in vitro against the cytotoxic effects of electrophiles, peroxides and redox-cycling agents," *Toxicology and Applied Pharmacology*, vol. 237, no. 3, pp. 267–280, 2009.
- [28] J. Lu and A. Holmgren, "The thioredoxin antioxidant system," *Free Radical Biology & Medicine*, vol. 66, pp. 75–87, 2014.
- [29] K. C. Wu, J. Y. Cui, and C. D. Klaassen, "Beneficial role of Nrf2 in regulating NADPH generation and consumption," *Toxicological Sciences*, vol. 123, no. 2, pp. 590–600, 2011.
- [30] E. Pontiki and D. Hadjipavlou-Litina, "Multi-target cinnamic acids for oxidative stress and inflammation: design, synthesis, biological evaluation and modeling studies," *Molecules*, vol. 24, no. 1, p. 12, 2018.
- [31] G. Wang, Z. Lei, Q. Zhong et al., "Enrichment of caffeic acid in peanut sprouts and evaluation of its in vitro effectiveness against oxidative stress-induced erythrocyte hemolysis," *Food Chemistry*, vol. 217, pp. 332–341, 2017.
- [32] T. M. Hung, J. P. Lee, B. S. Min et al., "Magnoflorine from *Coptidis Rhizoma* protects high density lipoprotein during oxidant stress," *Biological & Pharmaceutical Bulletin*, vol. 30, no. 6, pp. 1157–1160, 2007.
- [33] F. Guglielmi, C. Luceri, L. Giovannelli, P. Dolara, and M. Lodovici, "Effect of 4-coumaric and 3,4-dihydroxybenzoic acid on oxidative DNA damage in rat colonic mucosa," *The British Journal of Nutrition*, vol. 89, no. 5, pp. 581–587, 2003.
- [34] T. Luo, X. Y. Shen, S. Li, T. Ouyang, Q. A. Mai, and H. Q. Wang, "The protective effect of jatrorrhizine against oxidative stress in primary rat cortical neurons," *CNS & Neurological Disorders Drug Targets*, vol. 16, no. 5, pp. 617–623, 2017.
- [35] Y. Zhang, F. Feng, T. Chen, Z. Li, and Q. W. Shen, "Antidiabetic and antihyperlipidemic activities of *forsythia suspensa* (Thunb.) vahl (fruit) in streptozotocin-induced diabetes mice," *Journal of Ethnopharmacology*, vol. 192, pp. 256–263, 2016.
- [36] J. Roslan, N. Giribabu, K. Karim, and N. Salleh, "Quercetin ameliorates oxidative stress, inflammation and apoptosis in the heart of streptozotocin-nicotinamide-induced adult male diabetic rats," *Biomedicine & Pharmacotherapy*, vol. 86, pp. 570–582, 2017.
- [37] K. Vinothiya and N. Ashokkumar, "Modulatory effect of vanillic acid on antioxidant status in high fat diet-induced changes in diabetic hypertensive rats," *Biomedicine & Pharmacotherapy*, vol. 87, pp. 640–652, 2017.
- [38] S. Bae, K. Lim, H. Cha et al., "Arctiin blocks hydrogen peroxide-induced senescence and cell death through micro-RNA expression changes in human dermal papilla cells," *Biological Research*, vol. 47, no. 1, p. 50, 2014.
- [39] J. Marhuenda, S. Medina, P. Martínez-Hernández et al., "Melatonin and hydroxytyrosol protect against oxidative stress related to the central nervous system after the ingestion of three types of wine by healthy volunteers," *Food & Function*, vol. 8, no. 1, pp. 64–74, 2017.
- [40] C. Guo, S. Wang, J. Duan et al., "Protocatechualdehyde protects against cerebral ischemia-reperfusion-induced oxidative injury via protein kinase C/Nrf2/HO-1 pathway," *Molecular Neurobiology*, vol. 54, no. 2, pp. 833–845, 2017.
- [41] F. E. Wirngo, M. N. Lambert, and P. B. Jeppesen, "The physiological effects of dandelion (*Taraxacum officinale*) in type 2 diabetes," *The Review of Diabetic Studies*, vol. 13, no. 2-3, pp. 113–131, 2016.
- [42] M. H. Han, C. Park, D. S. Lee et al., "Cytoprotective effects of esculetin against oxidative stress are associated with the upregulation of Nrf2-mediated NQO1 expression via the activation of the ERK pathway," *International Journal of Molecular Medicine*, vol. 39, no. 2, pp. 380–386, 2017.
- [43] P. Stanely Mainzen Prince and A. J. Roy, "p-Coumaric acid attenuates apoptosis in isoproterenol-induced myocardial infarcted rats by inhibiting oxidative stress," *International Journal of Cardiology*, vol. 168, no. 4, pp. 3259–3266, 2013.
- [44] C. Chaowuttikul, C. Palanuvej, and N. Ruangrunsi, "Pharmacognostic Specification, Chlorogenic Acid Content, and *In vitro* Antioxidant Activities of *Lonicera japonica* Flowering Bud," *Pharmacognosy Research*, vol. 9, no. 2, pp. 128–132, 2017.
- [45] S. Kim, Y. W. Chin, and J. Cho, "Protection of cultured cortical neurons by luteolin against oxidative damage through inhibition of apoptosis and induction of heme oxygenase-1," *Biological & Pharmaceutical Bulletin*, vol. 40, no. 3, pp. 256–265, 2017.
- [46] Y. Ren, P. Houghton, and R. C. Hider, "Relevant activities of extracts and constituents of animals used in traditional Chinese medicine for central nervous system effects

- associated with Alzheimer's disease," *The Journal of Pharmacy and Pharmacology*, vol. 58, no. 7, pp. 989–996, 2006.
- [47] N. Polera, M. Badolato, F. Perri, G. Carullo, and F. Aiello, "Quercetin and its natural sources in wound healing management," *Current Medicinal Chemistry*, vol. 26, no. 31, pp. 5825–5848, 2019.
- [48] S. Wang, J. Yao, B. Zhou et al., "Bacteriostatic effect of quercetin as an antibiotic alternative in vivo and its antibacterial mechanism in vitro," *Journal of Food Protection*, vol. 81, no. 1, pp. 68–78, 2018.
- [49] O. M. Ahmed, T. Mohamed, H. Moustafa, H. Hamdy, R. R. Ahmed, and E. Aboud, "Quercetin and low level laser therapy promote wound healing process in diabetic rats _via_ structural reorganization and modulatory effects on inflammation and oxidative stress," *Biomedicine & Pharmacotherapy*, vol. 101, pp. 58–73, 2018.
- [50] E. B. Jude, R. Blakytyn, J. Bulmer, A. J. Boulton, and M. W. Ferguson, "Transforming growth factor-beta 1, 2, 3 and receptor type I and II in diabetic foot ulcers," *Diabetic Medicine*, vol. 19, no. 6, pp. 440–447, 2002.
- [51] Y. Liu, D. Min, T. Bolton et al., "Increased matrix metalloproteinase-9 predicts poor wound healing in diabetic foot ulcers," *Diabetes Care*, vol. 32, no. 1, pp. 117–119, 2009.
- [52] T. Dinh, F. Tecilazich, A. Kafanas et al., "Mechanisms involved in the development and healing of diabetic foot ulceration," *Diabetes*, vol. 61, no. 11, pp. 2937–2947, 2012.
- [53] E. P. Amento and L. S. Beck, "TGF-beta and wound healing," *Ciba Foundation Symposium*, vol. 157, pp. 115–123, 1991.
- [54] S. M. Ayuk, H. Abrahamse, and N. N. Houreld, "The role of matrix metalloproteinases in diabetic wound healing in relation to photobiomodulation," *Journal Diabetes Research*, vol. 2016, article 2897656, 9 pages, 2016.
- [55] M. Gao, T. T. Nguyen, M. A. Suckow et al., "Acceleration of diabetic wound healing using a novel protease-anti-protease combination therapy," *Proceedings of the National Academy of Sciences of the United States of America*, vol. 112, no. 49, pp. 15226–15231, 2015.

Review Article

Carbon Monoxide Being Hydrogen Sulfide and Nitric Oxide Molecular Sibling, as Endogenous and Exogenous Modulator of Oxidative Stress and Antioxidative Mechanisms in the Digestive System

Edyta Korbuc, Tomasz Brzozowski , and Marcin Magierowski 

Department of Physiology, Faculty of Medicine, Jagiellonian University Medical College, 16 Grzegorzeczka Street, 31-531 Krakow, Poland

Correspondence should be addressed to Marcin Magierowski; m.magierowski@uj.edu.pl

Received 24 July 2019; Revised 6 February 2020; Accepted 13 February 2020; Published 15 April 2020

Guest Editor: Reggiani Vilela Gonçalves

Copyright © 2020 Edyta Korbuc et al. This is an open access article distributed under the Creative Commons Attribution License, which permits unrestricted use, distribution, and reproduction in any medium, provided the original work is properly cited.

Oxidative stress reflects an imbalance between oxidants and antioxidants in favor of the oxidants capable of evoking tissue damage. Like hydrogen sulfide (H₂S) and nitric oxide (NO), carbon monoxide (CO) is an endogenous gaseous mediator recently implicated in the physiology of the gastrointestinal (GI) tract. CO is produced in mammalian tissues as a byproduct of heme degradation catalyzed by the heme oxygenase (HO) enzymes. Among the three enzymatic isoforms, heme oxygenase-1 (HO-1) is induced under conditions of oxidative stress or tissue injury and plays a beneficial role in the mechanism of protection against inflammation, ischemia/reperfusion (I/R), and many other injuries. According to recently published data, increased endogenous CO production by inducible HO-1, its delivery by novel pharmacological CO-releasing agents, or even the direct inhalation of CO has been considered a promising alternative in future experimental and clinical therapies against various GI disorders. However, the exact mechanisms underlying behind these CO-mediated beneficial actions are not fully explained and experimental as well as clinical studies on the mechanism of CO-induced protection are awaited. For instance, in a variety of experimental models related to gastric mucosal damage, HO-1/CO pathway and CO-releasing agents seem to prevent gastric damage mainly by reduction of lipid peroxidation and/or increased level of enzymatic antioxidants, such as superoxide dismutase (SOD) or glutathione peroxidase (GPx). Many studies have also revealed that HO-1/CO can serve as a potential defensive pathway against oxidative stress observed in the liver and pancreas. Moreover, increased CO levels after treatment with CO donors have been reported to protect the gut against formation of acute GI lesions mainly by the regulation of reactive oxygen species (ROS) production and the antioxidative activity. In this review, we focused on the role of H₂S and NO molecular sibling, CO/HO pathway, and therapeutic potential of CO-releasing pharmacological tools in the regulation of oxidative stress-induced damage within the GI tract with a special emphasis on the esophagus, stomach, and intestines and also two solid and important metabolic abdominal organs, the liver and pancreas.

1. Introductory Notes

1.1. Oxidative Stress. According to Sies et al., oxidative stress can be defined as an imbalance between oxidants and antioxidants in favor of the oxidants, leading to a disruption of reduction-oxidation (redox) signaling and control and/or molecular damage [1, 2]. Oxidative stress, in terms of its intensity, may be divided into eustress (physiological/positive stress) that plays several beneficial roles in physiological pro-

cesses [1, 2] and excessive oxidative stress (distress/chronic/toxic stress) that may lead to the development and progression of pathological conditions [2–4]. Interestingly, recent reports indicated that oxidative stress can have a dual role in cancer development; on the one hand, it can promote molecular genetic alterations resulting in cancer cell transformation. On the other hand, it is also a necessary anticancer response-activating apoptotic pathway leading to selective cancer cell elimination [5, 6].

Reactive species, such as reactive oxygen species (ROS), nitrogen species (RNS), sulfur species (RSS), or carbonyl species (RCS), have a notable impact on redox signaling and oxidative stress [2, 4]. ROS, the most extensively studied component of oxidative stress, include free radicals such as superoxide radicals ($O_2^{\cdot -}$) or hydroxyl radicals (OH) and nonradical species such as hydrogen peroxide (H_2O_2) or singlet molecular oxygen (1O_2) [2].

Under physiological conditions, production of ROS is highly restricted to specific enzymes that include the NADPH oxidases, xanthine oxidase, uncoupled endothelial nitric oxide synthase (eNOS), and the mitochondrial electron transport chain (mtETC) [7]. In order to protect themselves from ROS, the antioxidant defensive systems based on enzymatic or nonenzymatic components are activated and expressed within the cells. Enzymatic antioxidants, belonging to the first line of cellular defense system, include superoxide dismutase (SOD), catalase (CAT), and glutathione peroxidase (GPx). Nonenzymatic, the second line of defense, include glutathione (GSH) or vitamin E [3, 8]. However, it should be kept in mind that the abovementioned antioxidants may also contribute to oxidative damage. For instance, according to Sies et al., H_2O_2 , an uncharged molecule, performs a major function in the course of oxidative stress rather than free radicals [9]. This is mainly due to its stability and ability to cross the cellular membranes and deliver a redox signal to distant targets [9]. Thus, enzymes such as SOD, catalyzing the conversion of $O_2^{\cdot -}$ to H_2O_2 , may have a dual effect: the first is a classical superoxide scavenger and the second can be the involvement of this enzyme in the regulation of ROS signaling [10].

Gastrointestinal (GI) tract is especially vulnerable to ROS attack due to constant contact with ingested materials and microbial pathogens. Moreover, ROS as well as RNS, such as nitric oxide (NO) and peroxynitrite ($OONO^{\cdot -}$), are excessively produced during inflammatory states developed throughout the *digestive system* [11]. Oxidative stress has been implicated in a variety of major GI tract disorders including peptic ulcers; inflammatory bowel disease (IBD); and gastric, esophageal, and colorectal cancers [5, 12].

1.2. Carbon Monoxide. Carbon monoxide (CO) is a dangerous gas, produced by incomplete combustion of carbon-containing materials. It is tasteless, odorless, and colorless. CO binds to the hemoglobin (Hb) forming carboxyhemoglobin (COHb) with about 210 to 250 times greater affinity than that of oxygen. Such binding reduces the oxygen transportation ability of Hb leading to cellular hypoxia [13]. However, CO is also an endogenously generated gaseous mediator, which is produced during heme degradation *via* the activity of heme oxygenase (HO) enzymes. Currently, three main isoforms of HOs have been described, but only HO-1 and HO-2 have been defined as biologically active. HO-1 is a stress-inducible enzyme which represents a defense mechanism against oxidation and inflammation and is regulated by the transcription factor AP-1 activated by oxidative stress [14]. In contrast to HO-1, the isoform HO-2 is expressed constitutively [15]. Both, HO enzymes cleave the alpha-methylene carbon bond of the porphyrin ring of heme with the involve-

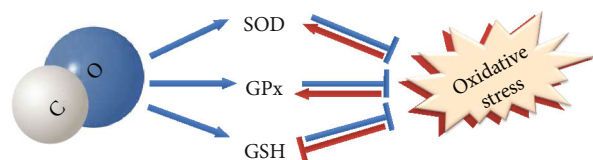


FIGURE 1: Schematic cross-talk between carbon monoxide and antioxidant enzymes. Arrows or blunt ends indicate activation or inhibition, respectively. Blue lines indicate CO-mediated processes; red lines indicate oxidative stress-mediated effects.

ment of NADPH and molecular oxygen to yield equimolar amounts of biliverdin (BV), iron, and CO [16]. It is widely recognized that CO binds to a range of intracellular proteins containing heme prosthetic group, for instance, cytochrome c oxidase, cytochromes P450, myoglobin, guanylate cyclase, catalase, or cystathionine β -synthase (CBS) [16, 17].

It has been reported that endogenous CO-producing enzymes are expressed within the GI tract. Precisely, BV reductase (BVR) with the ability to convert BV to bilirubin and HO-2 are present in mucosal epithelial cells and in the endothelium of intramural vessels of the human gastric fundus [18]. Moreover, these proteins are localized in intramuscular interstitial Cajal cells (ICC) and in intrinsic nerve cell bodies of the submucosal and myenteric plexuses [18]. In rats, HO-2 was identified in gastrin cells of the pyloric glands and in parietal cells of the oxyntic glands [19]. Inducible HO-1 was shown to be expressed in mononuclear cells in the submucosa with minor staining in the epithelial cells of patients with ulcerative colitis [20]. HO-1 is expressed in endothelial cells of the mucous neck region of the gastric mucosa [21]. Moreover, this protein was localized in sinusoidal cells of the rat's liver [21]. Interestingly, pharmacological inhibition of HO by zinc protoporphyrin IX resulted in the attenuation of vasoactive intestinal polypeptide- (VIP-) induced low esophageal sphincter relaxation implying that this enzymatic protein contributes to the regulation of the motor activity of the upper GI tract [22–24].

In the GI tract, the gaseous molecule CO has been shown to exert many physiological functions including its contribution to the mechanism of cell signaling, cytoprotection, regulation of microcirculation, motility, and modulatory effect of pathological events such as inflammation and carcinogenesis [25]. Moreover, exogenous and endogenous CO can be involved in redox signaling and initiate a compensatory expression of antioxidant enzymes and other adaptations to oxidative stress (Figure 1.) [15]. To summarize, the pleiotropic effect of CO, with an emphasis on redox biology, may improve clinical usefulness and applicability of CO-releasing molecules (CO donors) and their implementation in various therapeutic areas in the near future.

1.3. CO and Other Gaseous Mediators in Regulation of Oxidative Stress in the Digestive System. Endogenous CO, similarly to other two gaseous mediators, hydrogen sulfide (H_2S) or nitric oxide (NO), can exert a variety of biologic and physiologic functions which range from the regulation of vascular tone, mitochondrial homeostasis and biogenesis, neurotransmission, the modulation of inflammation,

programmed cell death to cellular proliferation programs [26]. However, CO, unlike NO and H₂S, is not a free radical and does not alternate between different oxidative species; thus, it is considered more biologically stable [25, 27].

Interestingly, according to recently published data, the gaseous mediators CO, H₂S, and NO were shown to play an important role within the GI tract [28, 29]. A large number of studies have focused on the contribution of these gaseous transmitters in the stomach's defensive response against gastric mucosal injury with special emphasis to possible interaction between them. For example, it has been reported that CO-releasing CORM-2, similarly to H₂S released from NaHS, protected gastric mucosa against alendronate-induced damage in the gastric mucosa compromised by oxidation evoked by exposure to chronic mild stress [30]. Both mediators decreased the mRNA expression for nuclear factor κ B (NF- κ B) [30]; however, the direct interaction between the enzymatic pathways of endogenous H₂S and CO still remained insufficiently explained. Interestingly, CO and H₂S donors were demonstrated to reduce aspirin-induced gastric damage and lipid peroxidation observed as documented by an increase in the malondialdehyde (MDA) concentration in the gastric mucosa [31]. Similarly, NO was shown to attenuate nonsteroidal anti-inflammatory drug (NSAID-) induced gastric bleeding [32, 33]. Pretreatment with NaHS and CORM-2 elevated gastric mucosal protein expression for antioxidative GPx but not for SOD [31]. Both molecules caused the antioxidative effects to be dependent on endogenous NO production [31]. Nevertheless, CORM-2-mediated gastroprotection and acceleration of ulcer healing was independent of H₂S biosynthesis while NaHS was not effective when endogenous CO production was pharmacologically inhibited [34, 35]. It is worth to mention that CO and H₂S donors were reported to protect the GI tract against acute oxidative damage induced by ischemia/reperfusion (I/R) injury [36, 37]. However, the NO/constitutive nitric oxide synthase (cNOS) pathway was shown to prevent I/R-induced gastric lesions while the activation of the NO/inducible nitric oxide synthase (iNOS) molecular pathway activity exacerbated this damage [38]. Interestingly, it was observed that H₂S-releasing naproxen (ATB-346) exerted its GI safety as compared with the classic form of this drug in the gastric mucosa compromised by acute experimental stress due to modulation of gastric mucosal HO expression [39]. Taken together, all three gaseous mediators and their pharmacological donors afforded protective activity by the activation of antioxidative activity within the digestive system. However, the precise mechanism of possible interaction between these molecules in the context of oxidative stress modulation and prevention remains to be explained and requires further studies.

1.4. Carbon Monoxide Delivery Systems. There are various pharmacological and chemical tools available with the ability to modulate the concentration of CO *in vitro* and *in vivo*. This could include induction or inhibition of HO activity by hemin or zinc protoporphyrin IX, respectively [13]. However, recent approach has been concentrated on the pharmacological delivery of exogenous CO in a controllable manner

and directly to the target tissue. It is worth to mention that the easiest way seems to be a systemic inhalation of a gas mixture containing CO but this concept is limited due to difficulties with storage and CO delivery in a controlled and directed manner [40–42]. Thus, Motterlini et al. proposed a series of transition metal carbonyls, termed CO-releasing molecules (CORMs) that are able to liberate CO and therefore to provide the direct biological effects to organs and tissues [41]. Being the first identified, the acronym CORM-1 (also known as DMDC) was assigned to dimanganese decacarbonyl (Mn₂(CO)₁₀). CORM-2 acronym was assigned to the tricarbonyldichlororuthenium (II) dimer ((Ru(CO)₃Cl₂)₂) [42]. Both CORM-1 and CORM-2 are soluble in organic solvents. Moreover, CORM-2 and next-generation CORMs contain in their structure heavy metals, such as ruthenium that may potentially restrict their implementation into clinical pharmacology. In addition, the release of CO from these molecules requires photoactivation, as it is in the case of CORM-1 and ligand substitution for CORM-2 [42]. Therefore, novel water-soluble CO delivery molecules were described, tricarbonylchloro (glycinato) ruthenium II (RuCl(glycinato)(CO)₃), termed CORM-3; boron-based compound Na₂H₃BCO₂, named CORM-A1; or recently developed CORM-401 (Mn(CO)₄ [43]) that in contrast to CORM-A1 releases up to three equivalents of CO per mol of the compound [42–44]. Additionally, the new class of organic CO-releasing prodrugs was developed recently [42, 45–47]. These CO prodrugs do not contain heavy metals, have a long half-life, and are able to release CO in a controllable manner. Importantly, few of them are activated to release CO only in contact with specific tissue enzymes, such as esterase and low pH on a click and release basis [42, 45–47]. Interestingly, some of these new compounds were developed as CO releasers in the presence of ROS [43].

2. CO and Oxidation within the Digestive System

2.1. Esophageal Mucosa. Esophageal mucosa is continuously exposed to external noxious agents and therefore is predisposed to epithelial damage [48]. Gastroesophageal reflux disease (GERD) resulting from the influx of the acidic stomach content into the esophagus is considered nowadays the global disease of the upper GI tract leading to the development of esophageal inflammation and oxidation [49]. It has been reported in rat models of reflux esophagitis that pretreatment with antioxidative isorhamnetin decreased esophageal lesion score reducing MDA levels, possibly due to the upregulation of the esophageal HO-1 expression [50]. Additionally, in cultured esophageal epithelial cells (EEC), it has been observed that euptailin prevented indomethacin-induced cytotoxicity and upregulated HO-1 expression due to nuclear translocation of transcription factor nuclear factor erythroid 2-related factor 2 (Nrf2) and the activation of extracellular signal-regulated kinases (ERKs) and phosphatidylinositol-3-kinase (PI3K)/Akt signaling [24, 51]. However, possible involvement of HO and CO and their possible interaction in the regulation of oxidative stress in the esophageal mucosa requires further investigations.

TABLE 1: Antioxidative effects of CO donors in various *in vitro* and *in vivo* experimental models of gastric mucosal injury or gastric cancer.

Experimental model (publication)	CO donor	Dose	Form of application
Ethanol-induced gastric damage mouse model [55]	DMDC	12.5 μ mol/kg	Intraperitoneal injection
↓ Lipid peroxidation, ↑ GSH			
Alendronate-induced gastric damage rat model [56]	DMDC	81 μ mol/kg	Intraperitoneal injection
↓ Lipid peroxidation, ↑ GSH			
Alendronate-induced gastric damage + mild stress rat model [30]	CORM-2	5 mg/kg	Intragastric injection
GPx-1 and SOD-2 gene expression not affected, ↓ NF- κ B gene expression			
Water immersion and restraint stress-induced gastric damage rat model [57]	CORM-2	1 mg/kg	Intragastric injection
↓ Lipid peroxidation, restored activity of gastric mucosal SOD and GSH, and attenuated GPx-1 and SOD-2 gene expression			
Acute aspirin-induced gastric damage rat model [31]	CORM-2	5 mg/kg	Intragastric injection
↓ Lipid peroxidation, ↓ IL-1 β gene expression, restored activity of GPx-1			
Human gastric adenocarcinoma (AGS) cell line [60]	CORM-2	10, 25, 50 μ M	Incubation with medium containing CO
↓ IL-1 β induced IL-8 gene and protein expression, ↓ IL-8 promoter activity, ↓ IL-1 β induced ROS production			

2.2. Gastric Mucosa. Stomach and gastric mucosa are important components of the GI tract, responsible for digestion, GI motility, and early microbial defense [52]. Oxidative stress, induced in response to exogenous gastric mucosal irritants, drugs, and pathogens derived from food intake, is one of the major contributors to the pathogenesis of gastric disorders such as gastritis, gastric ulcers, and gastric cancer and also drug-induced toxicity [53].

Importantly, the HO-1/CO pathway and CO donors has been considered one of protective factors involved in the protection of the gastric mucosa against numerous injuries mediated by oxidative stress. The most important antioxidative effects of CO donors in various *in vitro* and *in vivo* experimental models of gastric mucosa injuries were summarized in Table 1 with special attention paid to the dosages used and the form of pharmacological source of this gaseous molecule.

2.2.1. HCl- and Ethanol-Induced Mucosal Damage. In an animal model of acute gastric mucosal lesions induced by the application of HCl, Ueda et al. have demonstrated that HO-1 mRNA expression level was upregulated and pretreatment with HO-1 inhibitor exacerbated the severity of these lesions [54]. Accordingly, Gomes et al. have evaluated the role of HO-1/BV/CO pathway in gastric mucosal defense against ethanol-induced gastric damage in mice [55]. They revealed the gastroprotective effects of hemin (HO-1 inducer), BV,

and CO donor dimanganese decacarbonyl (DMDC) against the damage induced by this necrotizing agent by a mechanism involving a decrease in free radical production. Moreover, in mice treated with this CO donor, the reduced formation of MDA considered a marker of lipid peroxidation and increased GSH concentrations have been observed in the gastric mucosa with ethanol-induced gastropathy [55].

2.2.2. Drug-Induced Mucosal Damage. Costa et al. have evaluated the gastroprotective effect of HO-1/CO pathway against alendronate-induced gastric damage in rats [56]. In their study, pretreatment with hemin or DMDC reversed the fall in gastric GSH levels and the rise in MDA level elevated after alendronate administration [56]. Thus, they concluded that CO may restore the mechanisms of redox balance and protects the gastric mucosa by the reduction in lipid peroxidation in this experimental model [56]. The question arises whether CO may play an important role in the protection of the gastric mucosa injured by the combination of ulcerogenic factors. Indeed, it has been demonstrated that CO released from CORM-2 is able to protect against alendronate-induced gastric lesions even when the gastric mucosa has previously been exposed to chronic mild stress [30]. In this chronic animal model, CORM-2 did not affect the mRNA expression of antioxidative enzymes GPx-1 and SOD-2 but decreased the expression of mRNA for oxidative marker NF- κ B, upregulated by treatment with alendronate

in the gastric mucosa compromised by stress [30]. In another study [57], CORM-2 restored the activity of gastric mucosal antioxidant enzymes SOD and GSH, both decreased under stress conditions, and attenuated the expression of SOD-2 and GPx-1 mRNA, both markedly increased in the stressed gastric mucosa [57]. Additionally, pretreatment with CORM-2 exhibited beneficial effects in counteracting acute aspirin-induced gastric damage. CORM-2 inhibited gastric mucosal lipid peroxidation and restored antioxidative GPx-1 protein expression impaired by aspirin treatment, thus supporting an important role of CO in the protection of the gastric mucosa against oxidative injury [31]. Interestingly, in the same experimental model, CORM-2 abrogated the expression of proinflammatory cytokine IL-1 β [31]. This pleiotropic cytokine IL-1 β is associated with enhanced metastasis and poor prognosis of gastric cancer and was reported to stimulate the expression of IL-8, another inflammatory cytokine, through mitogen-activated protein (MAP) kinase and ROS signaling [31, 58]. Interestingly, hexacarbonyldicobalt derivative of aspirin considered a CO-releasing aspirin has been reported to decrease the ROS/RNS generation in malignant pleural mesothelioma (MPM) cell lines [59]. Taking into account the antioxidative activity of CO donors against NSAID-induced GI damage, we conclude that the development of novel safer CO-releasing derivatives of these drugs should be considered a new therapeutic option in limiting serious parent NSAID-induced complications which deserve attention of basic scientists and clinical practitioners.

2.2.3. Gastric Cancer In Vitro Models. Besides *in vivo* animal models of ulcerogenesis, *in vitro* studies have been carried out to investigate the role of CO in gastric cancer. Lian et al. [60] have used CORM-2 (10, 25, and 50 μ M) to investigate the effect of CO on IL-1 β -induced expression of IL-8 in human gastric cancer AGS cells. They observed that CORM-2 suppressed IL-1 β -induced IL-8 expression and effectively inhibited IL-1 β -induced ROS production determined by the H₂O₂-sensitive fluorophore DCFDA [60]. These observations support the notion that the antioxidant properties of CO and its ability to inhibit expression of proinflammatory cytokines such as IL-1 β , can contribute, at least in part, to the gastroprotective effect of these gaseous molecules. However, it seems likely that the detailed mechanism by which CO attenuates ROS formation may strongly depend on the chosen experimental model and still remains to be elucidated.

2.3. Intestinal Mucosa. The intestine is responsible for digestion and absorption of nutrients, electrolytes, water, bile salts, and drugs. It also possesses immunological, endocrine, and motility response regulating functions [61]. The increased availability of CO levels in the intestinal compartment beneficially affects a course of various disorders, for example IBD, sepsis, postoperative ileus (POI), and outcomes following intestinal transplant in experimental animal models and preliminary studies in humans. Most of these diseases are directly or indirectly associated with inflammation and/or increased oxidative stress [62]. The most important antioxidative effects of CO donors in various *in vitro* and *in vivo*

experimental models of intestinal mucosa injuries were summarized in Table 2.

2.3.1. IBD. CO/HO-1 pathway and exogenous CO with its immunomodulatory properties and protective activities against oxidative stress reached increased importance due to its beneficial effects observed in the course of chronic intestinal inflammatory diseases, including the most common forms of IBD like ulcerative colitis (UC) and Crohn's disease (CD) [62–65]. For instance, the therapeutic potential of CO was evaluated by Takagi et al. in 2,4,6-trinitrobenzene sulfonic acid- (TNBS-) induced colitis in mice. They observed that increased colonic damage after TNBS administration was inhibited by the pretreatment with inhaled CO. Furthermore, CO significantly attenuated the production of thiobarbituric acid- (TBA-) reactive substances being interpreted in this study as an index of lipid peroxidation [66]. Additionally, Yin et al. examined the role of CORM-2 in a murine model of inflammatory colitis induced by the treatment with dextran sodium sulfate (DSS) [67]. Interestingly, to overcome drawbacks resulting from the poor aqueous solubility of CORM-2 and a very short CO-releasing half-life, a micelles consisting of water-soluble styrene-maleic acid copolymer (SMA) that encapsulated CORM-2 (SMA/CORM-2) were designed. SMA/CORM-2 polymers have shown significant therapeutic and tissue-protective effects, probably through CO released from the micelles evoking antioxidative and anti-inflammatory effects [67].

2.3.2. Systemic Inflammation. Wang et al. have shown that exogenous CO can attenuate inflammatory responses in the small intestine of septic mice induced by cecal ligation and puncture [68]. Administration of CORM-2 significantly attenuated the production of proinflammatory cytokines (IL-1 β and TNF- α) and suppressed lipid peroxidation in the small intestine of septic mice, considerably decreasing the formation of oxidants, and thus reducing the tissue oxidative injury. On the other hand, Liu et al. [69] employed CORM-2 to determine whether they can afford suppression of inflammatory cytokine production and oxidative stress in the small intestine of thermally injured mice. The application of CORM-2 on thermally injured mice decreased the production of IL-1 β , TNF- α , and IL-8 and led to the significant downregulation of intestinal MDA tissue levels [69]. In addition, they also observed that GSH, a key antioxidant, declined significantly as compared to the control group, while treatment with CORM-2 reversed this effect [69]. Since the administration of CORM-2 prevents intestinal GSH depletion, it appears that the protective effect of CO donor involves the activation of an antioxidant defense system in protecting the intestinal tissue against oxidative stress [69]. Taken together, these studies seem to indicate that CORM-2 effectively prevents lipid peroxidation in the small intestine after experimental injury by decreasing the production of oxidants, which in consequence accounts for reduction of tissue oxidative injury.

2.3.3. I/R Injury. The potent clinical CO-inducing protective effects have also been well documented in controlling

TABLE 2: Antioxidative effects of CO donors in various *in vitro* and *in vivo* experimental models of intestinal mucosa injury.

Experimental model (publication)	CO donor	Dose	Form of application
TNBS-induced colitis in mice [70]	CO gas	200 ppm	Inhalation
↓ Lipid peroxidation			
Cecal ligation and puncture-induced sepsis mouse model [68]	CORM-2	8 mg/kg	Intravenous injection
↓ Lipid peroxidation, ↓ IL-1 β production			
Thermally induced small intestine injury mouse model [69]	CORM-2	8 mg/kg	Intravenous injection
↓ Lipid peroxidation, ↓ IL-1 β production, ↓ IL-8 production, and restored activity of GSH			
Cold I/R injury associated with small intestinal transplantation in rats [70]	CO gas	250 ppm	Inhalation
↑ Antioxidant power			
Hindlimb I/R-induced remote intestinal inflammatory response mouse model [71]	CO gas	250 ppm	Inhalation
No protection against intestinal lipid peroxidation			
Surgically induced postoperative ileus mouse model [73]	CORM-3	40 mg/kg	Intraperitoneal injection
↓ Lipid peroxidation			
TNF- α /cycloheximide-induced oxidative stress in the mouse small intestinal epithelial (MODE-K) cell line [74]	CORM-1A	100 μ M	Incubation with medium containing CO
↓ Intracellular ROS level, ↑ GSH			

intestinal I/R injury associated with transplantation. The GI organ damage caused by I/R is a significant problem in a variety of clinical settings usually associated with a high morbidity and mortality. Nakao et al. examined the efficacy of inhaled CO during intestinal cold I/R injury associated with small intestinal transplantation in rats. They observed that perioperative CO inhalation at a low concentration (250 ppm) resulted in the downregulation of several proinflammatory mediators and significantly increased antioxidant response in the intestinal graft, clearly indicating that in the CO-inhaled group less reactive oxygen metabolites were produced [70]. Similarly, Scott et al. suggested that a low dose of inhaled CO (250 ppm) may exhibit potent anti-inflammatory properties by inhibiting the production of pro-inflammatory cytokines [71]. They have also demonstrated a significant increase in ileum lipid peroxidation/oxidative stress following hindlimb I/R in male mice; however, as indicated by elevated MDA and remote intestinal mucosal injury, these events could not be efficiently prevented by a low dose of inhaled CO [71].

2.3.4. *POI*. Transient impairment of gastrointestinal motility, termed *POI*, is a major determinant of recovery after abdom-

inal surgery which leads to increased morbidity and prolonged patient hospitalization [72]. Backer et al. demonstrated that pretreatment with CORM-3 ameliorated the *POI* in surgically operated small intestine in mice. CORM-3 markedly reduced oxidative stress in both the intestinal mucosa and *muscularis propria*. Interestingly, pharmacological HO inhibition partially reversed the protective effects of CORM-3 on inflammation/oxidative stress in the *muscularis propria* and completely abrogated CORM-3-mediated inhibition of the early “oxidative burst” in the intestinal mucosa of *POI*. It has been suggested that this phenomenon might be related to the dysfunction of epithelial barrier and/or the different sources and amounts of ROS generation in the different layers of the intestine, for example, xanthine oxidase in epithelial cells of the mucosa versus NADPH oxidase in residential/infiltrated macrophages of the muscular layer [73]. To address these findings *in vitro*, studies by Babu et al. have proved the inhibitory influence of CO on ROS production in intestinal epithelial cells known to form a semipermeable barrier in the GI tract [74]. During inflammation, this barrier is at risk of damaging the effects of ROS, cytokines and microbial factors, and cytotoxins. In a mouse intestinal epithelial cell line MODE-K, TNF- α /cycloheximide (CHX) was used to induce oxidative

stress as manifested by the increased ROS production and the decreased cellular levels of GSH [74]. These effects were partially prevented by treatment with CORM-A1 and correlated with diminished apoptosis and cell death, suggesting that modulation of ROS/oxidative stress might be considered a primary mode of action responsible for the antiapoptotic and cytoprotective effects of CO [74, 75]. Moreover, CORM-A1 acted solely on NADPH oxidase-derived ROS without major influence on the mtETC [76]. Nevertheless, the chemical characteristics of different CORMs have a nonnegligible effect on cellular regulation of ROS sources. As an example, Babu et al. revealed that the cytoprotective effect of water-soluble CORM-401 mitigates NADPH oxidase-derived ROS, whereas lipid-soluble CORM-2 interferes with both NADPH oxidase- and mitochondria-derived ROS to protect MODE-K cells from TNF- α /CHX-induced cell death [44, 76].

2.3.5. Colon Cancer In Vitro Models. It is widely known that ROS induces DNA damages and different genetic disorders that are critical causes of cancers including colorectal cancer [77]. Dijkstra et al. have observed that in the human colon carcinoma DLD-1 cell line, HO-1 is strongly activated by various oxidative stress-inducing factors, including thiol-modifying agent diethylmaleate (DEM) and the lipid peroxidation end product: 4-hydroxy-nonenal (4-HNE) [14]. Interestingly, they have demonstrated a switch from a NF- κ B-regulated to an activator protein 1- (AP-1-) regulated stress response, which may be controlled by HO-1-derived CO [14].

2.4. Liver. The liver plays a crucial role in all metabolic processes and detoxifies endogenous compounds and xenobiotics, as a part of the digestive system. Therefore, this organ remains at the high risk of oxidative injury caused by the production of ROS. Oxidative stress has been considered a key factor causing liver damage induced by a variety of chemical and nonchemical agents, including alcohol, drugs, hepatic viral infections, and nutritional components, which in turn causes progression of hepatic injury, liver fibrosis, cirrhosis, and in some cases hepatocellular carcinoma [78–81]. These highly reactive species can be responsible for hepatic I/R injury occurring during surgical procedures such as liver resection and liver transplantation [82, 83]. The most important antioxidative effects of CO donors in various *in vivo* and *in vitro* experimental models of liver injury were summarized in Table 3.

2.4.1. I/R Injury. Recently, the HO-1/CO system has been investigated as a potential mechanism for protection against oxidative stress and hepatic injury in numerous experimental models [84]. Brugger et al. provided evidence that CO inhalation (250 ppm) or administration of methylene chloride (MC) can reduce hepatic lipid peroxidation, reestablish total hepatic glutathione and glutathione disulfide (GSH/GSSG) ratio, and reduce hepatocellular injury in a murine model of bilateral hindlimb I/R [85]. The inhalation of CO during the reperfusion period and the oral gavage of MC caused a significant increase in COHb content. Moreover, these authors have attributed the observed reduction in hepatic ROS formation following CO administration to the inhi-

bition of NADPH oxidase caused by this gaseous molecule [85].

Beneficial effects of CO were also observed by Lee and colleagues [86] in liver grafts initiated by cold preservation and augmented by reperfusion. They have shown using an *in vitro* model that exposure to 20% CO-containing medium for 6 h inhibited ROS generation in Kupffer cells (KC) under hypothermic condition with an upregulation of HSP70 protein [86]. Moreover, pretreatment with inhaled CO (250 ppm, for 24 h before liver graft retrieval) upregulated hepatic HSP70 protein expression and caused significant inhibition of cold I/R injury after liver transplantation *in vivo* [86]. It was demonstrated that CO bound to red blood cells (CO-RBC) exhibited the potential to protect hepatic cytochrome P450 protein, maintaining its ability to exert resuscitative effect in a rat model of hemorrhagic shock. This beneficial effect was attributed to the inactivation of KC resulting in the suppression of ROS production [87]. On the other hand, Kato have shown that exogenous supplementation with a low dose of bilirubin, an antioxidant bile pigment, rather than CO could be a crucial factor that significantly reduces oxidative stress and ameliorates I/R-induced hepatobiliary dysfunction in rats [88].

The signaling pathway by which CO can protect liver tissues against I/R-injury was studied by Kim et al. [89]. It has been reported that inhaled CO (250 ppm) attenuated liver damage *via* ROS-dependent Akt signaling and by the inhibition of glycogen synthase kinase 3 β (GSK-3 β) through Ser9 phosphorylation in the murine model of hepatic warm I/R-induced injury [89]. Moreover, CO ameliorated hepatic I/R injury by the regulation of miR-34a/Sirtin1 pathway known to modulate inflammation and apoptosis in response to oxidative stress [90]. These data strongly support the conclusion that increased bioavailability of CO by treatment with CO donors could be the promising preventive strategy against I/R injury after liver transplantation and may provide novel clinical opportunity in the management of liver disorders due to CO exerting antioxidative and anti-inflammatory properties.

2.4.2. Alcoholic and Nonalcoholic Liver Damage. Besides important protective role against I/R injury, CO also conferred substantial prevention against alcoholic liver damage [91]. In adult male Balb/c mice treated with ethanol or incubated with ethanol primary rat hepatocytes, CO derived from HO-1 or released from CORM-2 exerted a substantial antioxidant action against oxidative damage in these experimental models of hepatic injury. This CO-induced protection was mainly manifested by suppressed lipid peroxidation, normalized GSH concentration, and SOD activity [91]. Furthermore, Upadhyay et al. investigated the therapeutic potential of CORM-A1 in acetaminophen- (APAP-) induced liver injury in mice [79]. They showed elevated levels of serum transaminases, depleted hepatic GSH, and hepatocyte necrosis after APAP treatment [79]. On the contrary, in mice injected with CORM-A1 after APAP administration, the reduction in serum transaminases, preservation of hepatic GSH, and attenuation of hepatocyte necrosis have been observed. Interestingly, mice that received a lethal dose of

TABLE 3: Antioxidative effects of CO donors in various *in vitro* and *in vivo* experimental models of liver injury.

Experimental model (publication)	CO donor	Dose	Form of application
Hindlimb I/R-induced systemic inflammation mouse model [85]	CO gas or MC	250 ppm or 5.8 μ mol/kg	Inhalation or orally
↓ Lipid peroxidation, ↓ inhibition of NADPH oxidase, and restored GSH/GSSG ratio			
Liver transplantation- (LTx-) induced I/R injury rat model/Kupffer cells isolated from the liver [86]	CO gas	20% CO-saturated culture medium	Incubation with medium containing CO
↓ ROS generation, ↑ HSP 70 protein expression			
Hemorrhagic shock and resuscitation rat model/Kupffer cells isolated from the liver [87]	CO gas	Gently bubbling CO gas through the RBC resuscitative fluid	Infusion of resuscitative fluids
↓ ROS generation			
Hepatic warm I/R injury mouse model [89]	CO gas	250 ppm	Inhalation
↑ ROS-dependent PI3 K/Akt activation, ↓ inhibition of GSK3 β through Ser9 phosphorylation			
Ethanol-induced liver damage mouse model or primary rat hepatocytes [91]	CORM-2	8 mg/kg or 20 μ mol/l	Tail vein injection or incubation with medium containing CO
↓ Lipid peroxidation, restored GSH level, and restored SOD level			
APAP-induced liver injury in mice [79]	CORM-1A	20 mg/kg	Intraperitoneal injection
↑ Nrf2 gene upregulation, ↑ ARE gene upregulation, and restored GSH level			
HFHF diet-induced hepatic steatosis in mice [92]	CORM-1A	2 mg/kg/day	Intraperitoneal injection
↑ Nrf2 activation, ↑ ARE gene upregulation, and ↑ ATP production			
GalN/LPS-induced acute liver mouse model [94]	CO gas	First at a dose of 15 ml/kg, and then 6 h later, 8 ml/kg	Intraperitoneal injection
↓ Lipid peroxidation, restored GSH level, and restored SOD level			
Primary rat or mouse hepatocytes and Hep3B cells [96]	CO gas	250 ppm	Incubation with medium containing CO
↓ Apoptosis, ↓ endogenous antioxidant ascorbic acid, ↓ antioxidant power, ↑ ROS generation, ↑ Akt phosphorylation, and ↓ I κ B degradation (= ↑ NF- κ B activation)			
HepG2 cells [95]	CORM-2	80 μ M for 6 h	CO-saturated stock solutions
↑ Nrf2 activation, ↑ HO-1 expression			
Tert-butyl hydroperoxide- (t-BHP-) treated HepG2 cells [79]	CORM-A1	100 μ M	Incubation with medium containing CO
↓ ROS generation, ↑ Nrf2 activation			
Rat liver mitochondria [98]	CO gas	50 ppm for 1, 2, or 7 days	Inhalation
↓ GSH/GSSG ratio, ↑ activation of MMP, and ↑ mitochondrial SOD-2			
Mouse liver mitochondria [99]	CO solution	10 μ M	Swelling buffer
↓ Inhibition of MPP, ↑ mitochondrial ROS generation			
PA-treated HepG2 cells [92]	CORM-1A	100 μ M	Incubation with medium containing CO
↑ Nrf2 activation, ↑ ARE gene upregulation ↓ mitochondrial ROS generation, and ↑ activation of mitochondrial membrane potential			

APAP died but those cotreated with CORM-A1 showed a 50% survival [79]. Additionally, CORM-A1 prevented hepatic steatosis in high-fat high-fructose (HFHF) diet fed mice, used as a model of nonalcoholic steatohepatitis (NASH) [92]. The beneficial effects of CORM-A1 in HFHF fed mice were associated with improved lipid homeostasis, Nrf2 activation, upregulation of antioxidant-responsive (ARE) genes, and increased ATP production [92].

The effects of HO-1 and its enzymatic activity products CO, BV, and iron/ferritin were also assessed in a mouse model of inflammatory liver damage induced by bacterial wall cytotoxin lipopolysaccharide (LPS) and hepatocyte-specific transcription inhibitor D-galactosamine (GalN). It has been shown that oral administration of the MC or BV was effective in the protection of hepatic damage in mice, prolonged their survival, and reduced the expression of proinflammatory cytokines (TNF- α , IFN- γ) [93]. Moreover, when GalN/LPS were administered to induce acute liver damage, the intraperitoneal injection of exogenous CO gas improved the survival rate of mice and attenuated hepatocellular damage. Exogenous CO administration markedly reduced MDA concentrations and restored SOD and GSH levels, thus inhibiting lipid peroxidation, which might considerably contribute to the mechanism of CO-mediated hepatoprotection [94].

2.4.3. Hepatocyte In Vitro Models. The important role of CO in the maintenance of hepatic function in both physiological and pathophysiological conditions was also demonstrated in multiple *in vitro* studies. For instance, Lee et al. have suggested that CO induces Nrf2 activation *via* MAP kinase signaling pathways, thereby prompting an increase in HO-1 expression in HepG2 cells [95]. Similarly, Upadhyay et al. have revealed that CORM-A1 (10-100 μ M) facilitated nuclear translocation of Nrf2, reduced oxidative stress, up-regulated ARE genes, and prevented GSH depletion promoting cell viability in HepG2 cells treated with tert-butyl hydroperoxide (t-BHP), known to cause oxidative stress-mediated hepatocyte injury [79]. Moreover, Kim et al. [96] have determined whether the effects of CO are dependent on modulation of ROS signaling in primary rat- or mouse-derived hepatocytes and Hep3B cells. They found that CO treatment (250 ppm) triggered a low level of ROS production in hepatocytes *in vitro*, considered an adaptive response leading to an increase in cell viability, in combination with Akt phosphorylation and I κ B degradation (required for NF- κ B activation) [96]. This finding generated in cultured hepatocytes indicates the existence of another survival pathway, possibly parallel to Nrf2 activation [97]. Moreover, exogenous CO failed to increase ROS production in respiration-deficient Hep3B cells, suggesting that the mitochondria are the source of CO-induced ROS generation in this model [96].

2.4.4. Liver Mitochondria. Recently, the possible contribution of mitochondria as the molecular targets of CO has been suggested [92, 96, 98]. These key organelles for cell energy supply play a crucial role in the initiation and progression of many diseases following oxidative stress-induced damage [98]. Piantadosi et al. revealed that exposure to gaseous CO (50 ppm) for 1, 3, or 7 days induced hypoxia-sensitive protein

expression for hypoxia-inducible factor 1 α (HIF-1 α), HO-1, and SOD-2 in rat liver mitochondria [98]. CO was shown to induce a profound early mitochondrial oxidative stress manifested by a decrease in GSH/GSSG ratio and the activation of the mitochondrial pore transition (MPT) [98]. On the other hand, Queiroga et al. have demonstrated that low concentrations of CO (10 μ M) may inhibit mitochondrial membrane permeabilization (MMP) in isolated mouse liver mitochondria *in vitro*, possibly by preventing mitochondrial swelling, mitochondrial depolarization, and the opening of a nonspecific pore through inner membrane [99]. In addition, CO increased mitochondrial ROS generation that is essential for signaling of MMP inhibition, although not enough to induce the damage [99]. Moreover, CORM-A1 significantly ameliorated mitochondrial function in palmitic acid- (PA-) treated HepG2 cells *via* Nrf2 translocation and activation of cytoprotective gene expression. Furthermore, in PA-treated cells, CORM-A1 improved mitochondrial oxidative stress, mitochondrial membrane potential, and rescued mitochondrial biogenesis [92].

The abovementioned findings appear to indicate that CO may have a dual role in oxidative stress and its pro- or antioxidant effects depend on the dosage, route of administration, the exposure duration, and cell type.

2.5. Pancreas. The pancreas is an important organ for proper nutrient metabolism that consists of exocrine cells producing digestive enzymes and endocrine cells responsible for generation of pancreatic hormones. Malfunction of the exocrine part can lead to the development of pancreatitis and even pancreatic cancer [100, 101]. The most important antioxidative effects of CO donors in various *in vivo* and *in vitro* experimental models of pancreatic injury were summarized in Table 4.

2.5.1. Acute Pancreatitis. Sato et al. have analyzed protein expression of the heme oxygenase in a rat model of acute pancreatitis showing that the expression of HO-1 in the pancreas *in vivo* was enhanced. Oxidative stress also elevated HO-1 expression level in murine islet (LTC3) and rat acinar (AR42J) pancreatic cells. These findings indicate that HO-1 may act as a potential inflammatory biomarker and a crucial defense mechanism against oxidative stress in acute pancreatitis [102]. It is noteworthy that ROS are possible regulators of pancreatic injury development. They may activate NF- κ B that regulates gene expression of numerous inflammatory markers [40, 101]. Chen et al. have demonstrated that CORM-2-releasing CO exerts beneficial effects on severe acute pancreatitis in rats. Of note, CORM-2 not only reduced the serum levels of proinflammatory TNF- α and IL-1 β but also suppressed pancreatic tissue mRNA expression of TNF- α and IL-1 β , whereas anti-inflammatory cytokine IL-10 was considerably increased. Interestingly, CORM-2 was also found to suppress NF- κ B binding activity which might testify for the protective, anti-inflammatory, and antioxidative effects of CO in this experimental model [103]. Similarly, Nuhn et al. have demonstrated that treatment with HO-1 metabolites has a beneficial influence on severity and survival of acute necrotizing pancreatitis in rats induced by

TABLE 4: Antioxidative effects of CO donors in various *in vitro* and *in vivo* experimental models of pancreatic injury.

Experimental model (publication)	CO donor	Dose	Form of application
Retrograde infusion of sodium taurocholate-induced severe acute pancreatitis rat model [103]	CORM-2	8 mg/kg	Intravenous injection
↓ NF-κB activity			
Retrograde injection of sodium taurocholate-induced acute necrotizing pancreatitis rat model [104]	MC	500 mg/kg	Orally
↓ NF-κB activity			
Choline-deficient ethionine-supplemented diet-induced acute pancreatitis mouse model [105]	CO-HbV	1,000 mg Hb/kg	Via tail vein
↓ Oxidative stress			

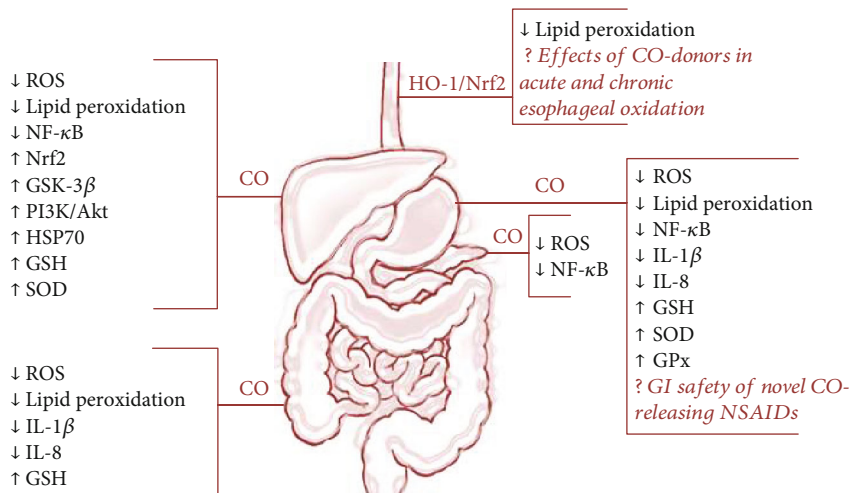


FIGURE 2: Pleiotropic effects of HO-1/CO pathway against oxidative stress in the digestive system.

retrograde intraductal injection of sodium taurocholate [104]. Biliverdin hydrochloride (BV-HCl), the CO donor MC, or iron-chelating desferrioxamine (DFO) was used in this model [104]. All HO-1 metabolites showed protective effects on the severity of pancreatitis accompanied by the diminished pancreatic NF-κB activity [104]. In turn, Nagao et al. have examined the therapeutic efficacy of CO-bound Hb vesicle (CO-HbV), a CO carrier, against severe acute pancreatitis in mice that were fed with a choline-deficient ethionine-supplemented diet. A CO-HbV treatment significantly reduced mice mortality with experimental acute pancreatitis by inhibiting the systemic release of proinflammatory cytokines, neutrophil infiltration, and locally oxidative injuries to the pancreatic tissue [105]. Therefore, the administration of HO-1 products, including CO, seems to decrease oxidative stress and attenuate the inflammatory changes in acute pancreatitis.

2.5.2. Autoimmune Diseases. Interestingly, CO was also identified as a potential therapeutic molecule for the treatment of diseases related to pancreas autoimmune diseases, such as

type 1 diabetes. Recently, Nicolic et al. have shown that CORM-A1 suppressed the incidence and the severity of immunoinflammatory and autoimmune diabetes in experimental mouse models of type 1 diabetes [106]. Moreover, Li et al. revealed that the upregulation of HO-1 decreased superoxide ($O_2^{\cdot -}$) generation and increased CO release and bilirubin formation in the pancreas of nonobese diabetic mice [107]. Taken together, these results indicate that enhanced HO-1 activity associated with increased production of CO can significantly counteract the diabetic complications [107].

3. Summary

As presented in this review, the gaseous molecule CO plays an essential physiological role exhibiting beneficial pleiotropic effects in the maintenance of GI tract integrity and the mechanism of GI mucosal defense (Figure 2). Bioavailability of CO released from its donors seems to depend on many factors, such as dosage of this CO donor, the exposure time, and mechanism of its release by particular donors. Different CO

sources may give rise to distinct and complex responses in different parts of the digestive system.

Nevertheless, according to an evidence-based medicine, the major mechanism of the beneficial action of this gaseous molecule depends upon cell oxidative metabolism, modulation of ROS generation, and antioxidative activity as reflected by the expression and activity of antioxidant enzymes (SOD, GSH) and molecular anti-inflammatory pathways such as NF- κ B or Nrf-2 in the digestive system.

4. Future Perspectives

Due to its antioxidative and anti-inflammatory properties, CO released from its pharmacological donors or produced endogenously due to HO-1 activity seems to open new treatment modalities of GI tract disorders by exerting a strong protective potential which warrants its possible implementation in digestive system pharmacology. Detailed mechanism of CO-mediated gastroprotection against gastric mucosal I/R injury and possible DNA oxidation with special emphasis on the modulation of mitochondrial activity by this gas still remains unexplained. Moreover, novel ROS-sensitive CO prodrugs are promising tools for further investigation, perhaps in the treatment and prevention of various digestive system pathologies such as colitis, gastric mucosal injuries, postsurgical complications, and esophagitis [43]. Therefore, despite scientific evidence of its efficacy in the protection of mucosal components of digestive system, the detailed molecular mechanisms by which endogenous CO or CO-releasing donors exert antioxidative, gastroprotective, and/or therapeutic effects in the digestive system still require further studies. This could include interaction with nitric oxide or hydrogen sulfide.

Conflicts of Interest

None is declared.

Acknowledgments

M.M. received research grant from the National Science Centre Poland (UMO-2016/23/D/NZ4/01913). M.M. received financial support from the Foundation for Polish Science (START 62.2018).

References

- [1] H. Sies, "Oxidative stress: a concept in redox biology and medicine," *Redox Biology*, vol. 4, pp. 180–183, 2015.
- [2] H. Sies, C. Berndt, and D. P. Jones, "Oxidative stress," *Annual Review of Biochemistry*, vol. 86, pp. 715–748, 2017.
- [3] G. Pizzino, N. Irrera, M. Cucinotta et al., "Oxidative stress: harms and benefits for human health," *Oxidative Medicine and Cellular Longevity*, vol. 2017, Article ID 8416763, 13 pages, 2017.
- [4] V. I. Lushchak, "Free radicals, reactive oxygen species, oxidative stress and its classification," *Chemico-Biological Interactions*, vol. 224, pp. 164–175, 2014.
- [5] A. Takaki, S. Kawano, D. Uchida, M. Takahara, S. Hiraoka, and H. Okada, "Paradoxical roles of oxidative stress response in the digestive system before and after carcinogenesis," *Cancers*, vol. 11, no. 2, p. 213, 2019.
- [6] J. Liu and Z. Wang, "Increased oxidative stress as a selective anticancer therapy," *Oxidative Medicine and Cellular Longevity*, vol. 2015, Article ID 294303, 12 pages, 2015.
- [7] S. Dikalov, "Cross talk between mitochondria and NADPH oxidases," *Free Radical Biology & Medicine*, vol. 51, no. 7, pp. 1289–1301, 2011.
- [8] O. M. Ighodaro and O. A. Akinloye, "First line defence antioxidants-superoxide dismutase (SOD), catalase (CAT) and glutathione peroxidase (GPX): their fundamental role in the entire antioxidant defence grid," *Alexandria Journal of Medicine*, vol. 54, no. 4, pp. 287–293, 2018.
- [9] H. Sies, "Hydrogen peroxide as a central redox signaling molecule in physiological oxidative stress: oxidative eustress," *Redox Biology*, vol. 11, pp. 613–619, 2017.
- [10] Y. Wang, R. Branicky, A. Noe, and S. Hekimi, "Superoxide dismutases: dual roles in controlling ROS damage and regulating ROS signaling," *The Journal of Cell Biology*, vol. 217, no. 6, pp. 1915–1928, 2018.
- [11] Y. J. Kim, E. H. Kim, and K. B. Hahm, "Oxidative stress in inflammation-based gastrointestinal tract diseases: challenges and opportunities," *Journal of Gastroenterology and Hepatology*, vol. 27, no. 6, pp. 1004–1010, 2012.
- [12] A. Bhattacharyya, R. Chattopadhyay, S. Mitra, and S. E. Crowe, "Oxidative stress: an essential factor in the pathogenesis of gastrointestinal mucosal diseases," *Physiological Reviews*, vol. 94, no. 2, pp. 329–354, 2014.
- [13] L. Wu and R. Wang, "Carbon monoxide: endogenous production, physiological functions, and pharmacological applications," *Pharmacological Reviews*, vol. 57, no. 4, pp. 585–630, 2005.
- [14] G. Dijkstra, H. Blokzijl, L. Bok et al., "Opposite effect of oxidative stress on inducible nitric oxide synthase and haem oxygenase-1 expression in intestinal inflammation: anti-inflammatory effect of carbon monoxide," *The Journal of Pathology*, vol. 204, no. 3, pp. 296–303, 2004.
- [15] C. A. Piantadosi, "Carbon monoxide, reactive oxygen signaling, and oxidative stress," *Free Radical Biology & Medicine*, vol. 45, no. 5, pp. 562–569, 2008.
- [16] C. A. Piantadosi, "Biological chemistry of carbon monoxide," *Antioxidants & Redox Signaling*, vol. 4, no. 2, pp. 259–270, 2002.
- [17] W. A. Pryor, K. N. Houk, C. S. Foote et al., "Free radical biology and medicine: it's a gas, man!," *American Journal of Physiology. Regulatory, Integrative and Comparative Physiology*, vol. 291, no. 3, pp. R491–R511, 2006.
- [18] E. E. Colpaert, J.-P. Timmermans, and R. A. Lefebvre, "Immunohistochemical localization of the antioxidant enzymes biliverdin reductase and heme oxygenase-2 in human and pig gastric fundus," *Free Radical Biology and Medicine*, vol. 32, no. 7, pp. 630–637, 2002.
- [19] Y. Hu, M. Yang, N. Ma, H. Shinohara, and R. Semba, "Contribution of carbon monoxide-producing cells in the gastric mucosa of rat and monkey," *Histochemistry and Cell Biology*, vol. 109, no. 4, pp. 369–373, 1998.
- [20] T. Takagi, Y. Naito, K. Mizushima et al., "Increased intestinal expression of heme oxygenase-1 and its localization in patients with ulcerative colitis," *Journal of Gastroenterology and Hepatology*, vol. 23, Supplement 2, pp. S229–S233, 2008.

- [21] G. Bekyarova, M. Tzaneva, and M. Hristova, "Heme oxygenase-1 expression in gastric mucosa and liver after burns: preliminary immunohistochemical study," *Journal of Interdisciplinary Histopathology*, vol. 1, no. 5, p. 246, 2013.
- [22] S. Rattan, Y. P. Fan, and S. Chakder, "Mechanism of inhibition of VIP-induced LES relaxation by heme oxygenase inhibitor zinc protoporphyrin IX," *The American Journal of Physiology*, vol. 276, no. 1, pp. G138–G145, 1999.
- [23] Y. P. Fan, S. Chakder, and S. Rattan, "Inhibitory effect of zinc protoporphyrin IX on lower esophageal sphincter smooth muscle relaxation by vasoactive intestinal polypeptide and other receptor agonists," *The Journal of Pharmacology and Experimental Therapeutics*, vol. 285, no. 2, pp. 468–474, 1998.
- [24] M. Chang, J. Xue, V. Sharma, and A. Habtezion, "Protective role of hemeoxygenase-1 in gastrointestinal diseases," *Cellular and Molecular Life Sciences*, vol. 72, no. 6, pp. 1161–1173, 2015.
- [25] J. L. Wallace, A. Ianaro, and G. de Nucci, "Gaseous mediators in gastrointestinal mucosal defense and injury," *Digestive Diseases and Sciences*, vol. 62, no. 9, pp. 2223–2230, 2017.
- [26] R. Motterlini and R. Foresti, "Biological signaling by carbon monoxide and carbon monoxide-releasing molecules," *American Journal of Physiology. Cell Physiology*, vol. 312, no. 3, pp. C302–C313, 2017.
- [27] G. Farrugia and J. H. Szurszewski, "Carbon monoxide, hydrogen sulfide, and nitric oxide as signaling molecules in the gastrointestinal tract," *Gastroenterology*, vol. 147, no. 2, pp. 303–313, 2014.
- [28] K. Magierowska, T. Brzozowski, and M. Magierowski, "Emerging role of carbon monoxide in regulation of cellular pathways and in the maintenance of gastric mucosal integrity," *Pharmacological Research*, vol. 129, pp. 56–64, 2018.
- [29] F. Shen, C. S. Zhao, M. F. Shen, Z. Wang, and G. Chen, "The role of hydrogen sulfide in gastric mucosal damage," *Medical Gas Research*, vol. 9, no. 2, pp. 88–92, 2019.
- [30] M. Magierowski, K. Magierowska, J. Szmyd et al., "Hydrogen sulfide and carbon monoxide protect gastric mucosa compromised by mild stress against alendronate injury," *Digestive Diseases and Sciences*, vol. 61, no. 11, pp. 3176–3189, 2016.
- [31] M. Magierowski, M. Hubalewska-Mazgaj, K. Magierowska et al., "Nitric oxide, afferent sensory nerves, and antioxidative enzymes in the mechanism of protection mediated by tricarbonyldichlororuthenium(II) dimer and sodium hydrosulfide against aspirin-induced gastric damage," *Journal of Gastroenterology*, vol. 53, no. 1, pp. 52–63, 2018.
- [32] A. Lanas, "Role of nitric oxide in the gastrointestinal tract," *Arthritis Research & Therapy*, vol. 10, article S4, Supplement 2, 2008.
- [33] K. V. S. Nemmani, S. V. Mali, N. Borhade et al., "NO-NSAIDs: gastric-sparing nitric oxide-releasable prodrugs of non-steroidal anti-inflammatory drugs," *Bioorganic & Medicinal Chemistry Letters*, vol. 19, no. 18, pp. 5297–5301, 2009.
- [34] M. Magierowski, K. Magierowska, M. Hubalewska-Mazgaj et al., "Interaction between endogenous carbon monoxide and hydrogen sulfide in the mechanism of gastroprotection against acute aspirin-induced gastric damage," *Pharmacological Research*, vol. 114, pp. 235–250, 2016.
- [35] M. Magierowski, K. Magierowska, M. Hubalewska-Mazgaj et al., "Cross-talk between hydrogen sulfide and carbon monoxide in the mechanism of experimental gastric ulcers healing, regulation of gastric blood flow and accompanying inflammation," *Biochemical Pharmacology*, vol. 149, pp. 131–142, 2018.
- [36] M. Magierowski, K. Magierowska, M. Hubalewska-Mazgaj et al., "Exogenous and endogenous hydrogen sulfide protects gastric mucosa against the formation and time-dependent development of ischemia/reperfusion-induced acute lesions progressing into deeper ulcerations," *Molecules*, vol. 22, no. 2, p. 295, 2017.
- [37] K. Magierowska, E. Korbut, M. Hubalewska-Mazgaj et al., "Oxidative gastric mucosal damage induced by ischemia/reperfusion and the mechanisms of its prevention by carbon monoxide-releasing tricarbonyldichlororuthenium (II) dimer," *Free Radical Biology & Medicine*, vol. 145, pp. 198–208, 2019.
- [38] A. Kobata, T. Kotani, Y. Komatsu, K. Amagase, S. Kato, and K. Takeuchi, "Dual action of nitric oxide in the pathogenesis of ischemia/reperfusion-induced mucosal injury in mouse stomach," *Digestion*, vol. 75, no. 4, pp. 188–197, 2007.
- [39] M. Magierowski, K. Magierowska, M. Surmiak et al., "The effect of hydrogen sulfide-releasing naproxen (ATB-346) versus naproxen on formation of stress-induced gastric lesions, the regulation of systemic inflammation, hypoxia and alterations in gastric microcirculation," *Journal of Physiology and Pharmacology*, vol. 68, no. 5, pp. 749–756, 2017.
- [40] J. Y. Seo, H. Kim, J. T. Seo, and K. H. Kim, "Oxidative stress induced cytokine production in isolated rat pancreatic acinar cells: effects of small-molecule antioxidants," *Pharmacology*, vol. 64, no. 2, pp. 63–70, 2002.
- [41] R. Motterlini, J. E. Clark, R. Foresti, P. Sarathchandra, B. E. Mann, and C. J. Green, "Carbon monoxide-releasing molecules," *Circulation Research*, vol. 90, no. 2, pp. E17–E24, 2002.
- [42] X. Ji, Z. Pan, C. Li et al., "Esterase-sensitive and pH-controlled carbon monoxide prodrugs for treating systemic inflammation," *Journal of Medicinal Chemistry*, vol. 62, no. 6, pp. 3163–3168, 2019.
- [43] Z. Pan, J. Zhang, K. Ji, V. Chittavong, X. Ji, and B. Wang, "Organic CO prodrugs activated by endogenous ROS," *Organic Letters*, vol. 20, no. 1, pp. 8–11, 2018.
- [44] D. Babu, G. Leclercq, R. Motterlini, and R. A. Lefebvre, "Differential effects of CORM-2 and CORM-401 in murine intestinal epithelial MODE-K cells under oxidative stress," *Frontiers in Pharmacology*, vol. 8, 2017.
- [45] Z. Pan, V. Chittavong, W. Li et al., "Organic CO prodrugs: structure-CO-release rate relationship studies," *Chemistry*, vol. 23, no. 41, pp. 9838–9845, 2017.
- [46] X. Ji, C. Zhou, K. Ji et al., "Click and release: a chemical strategy toward developing gasotransmitter prodrugs by using an intramolecular Diels-Alder reaction," *Angewandte Chemie International Edition*, vol. 55, no. 51, pp. 15846–15851, 2016.
- [47] X. Ji, K. Ji, V. Chittavong, B. Yu, Z. Pan, and B. Wang, "An esterase-activated click and release approach to metal-free CO-prodrugs," *Chemical Communications*, vol. 53, no. 59, pp. 8296–8299, 2017.
- [48] R. C. Orlando, "The integrity of the esophageal mucosa. Balance between offensive and defensive mechanisms," *Best Practice & Research. Clinical Gastroenterology*, vol. 24, no. 6, pp. 873–882, 2010.
- [49] N. Yoshida, "Inflammation and oxidative stress in gastroesophageal reflux disease," *Journal of Clinical Biochemistry and Nutrition*, vol. 40, no. 1, pp. 13–23, 2007.

- [50] G. Liu, C. Jiang, D. Li et al., "Isorhamnetin alleviates esophageal mucosal injury in a chronic model of reflux esophagitis," *European Journal of Pharmacology*, vol. 864, p. 172720, 2019.
- [51] H. J. Song, C. Y. Shin, T. Y. Oh, Y. S. Min, E. S. Park, and U. D. Sohn, "Eupatilin with heme oxygenase-1-inducing ability protects cultured feline esophageal epithelial cells from cell damage caused by indomethacin," *Biological & Pharmaceutical Bulletin*, vol. 32, no. 4, pp. 589–596, 2009.
- [52] R. H. Hunt, M. Camilleri, S. E. Crowe et al., "The stomach in health and disease," *Gut*, vol. 64, no. 10, pp. 1650–1668, 2015.
- [53] H. Suzuki, T. Nishizawa, H. Tsugawa, S. Mogami, and T. Hibi, "Roles of oxidative stress in stomach disorders," *Journal of Clinical Biochemistry and Nutrition*, vol. 50, no. 1, pp. 35–39, 2012.
- [54] K. Ueda, T. Ueyama, K. Yoshida et al., "Adaptive HNE-Nrf2-HO-1 pathway against oxidative stress is associated with acute gastric mucosal lesions," *American Journal of Physiology. Gastrointestinal and Liver Physiology*, vol. 295, no. 3, pp. G460–G469, 2008.
- [55] A. S. Gomes, G. G. Gadelha, S. J. Lima et al., "Gastroprotective effect of heme-oxygenase 1/biliverdin/CO pathway in ethanol-induced gastric damage in mice," *European Journal of Pharmacology*, vol. 642, no. 1-3, pp. 140–145, 2010.
- [56] N. R. D. Costa, R. O. Silva, L. A. D. Nicolau et al., "Role of soluble guanylate cyclase activation in the gastroprotective effect of the HO-1/CO pathway against alendronate-induced gastric damage in rats," *European Journal of Pharmacology*, vol. 700, no. 1-3, pp. 51–59, 2013.
- [57] S. Kwiecien, K. Magierowska, M. Magierowski et al., "Role of sensory afferent nerves, lipid peroxidation and antioxidative enzymes in the carbon monoxide-induced gastroprotection against stress ulcerogenesis," *Journal of Physiology and Pharmacology*, vol. 67, no. 5, pp. 717–729, 2016.
- [58] Y. S. Hwang, M. Jeong, J. S. Park et al., "Interleukin-1beta stimulates IL-8 expression through MAP kinase and ROS signaling in human gastric carcinoma cells," *Oncogene*, vol. 23, no. 39, pp. 6603–6611, 2004.
- [59] I. Zanellato, I. Bonarrigo, M. Ravera, E. Gabano, R. Gust, and D. Osella, "The hexacarbonyldicobalt derivative of aspirin acts as a CO-releasing NSAID on malignant mesothelioma cells," *Metallomics*, vol. 5, no. 12, pp. 1604–1613, 2013.
- [60] S. Lian, Y. Xia, T. T. Ung et al., "Carbon monoxide releasing molecule-2 ameliorates IL-1 β -induced IL-8 in human gastric cancer cells," *Toxicology*, vol. 361-362, pp. 24–38, 2016.
- [61] G. Gasbarrini, M. Montalto, L. Santoro et al., "Intestine: organ or apparatus?," *Digestive Diseases*, vol. 26, no. 2, pp. 92–95, 2008.
- [62] S. J. Gibbons, P. J. Verhulst, A. Bharucha, and G. Farrugia, "Review article: carbon monoxide in gastrointestinal physiology and its potential in therapeutics," *Alimentary Pharmacology & Therapeutics*, vol. 38, no. 7, pp. 689–702, 2013.
- [63] Y. Naito, T. Takagi, and T. Yoshikawa, "Heme oxygenase-1: a new therapeutic target for inflammatory bowel disease," *Alimentary Pharmacology and Therapeutics*, vol. 20, no. s1, Supplement 1, pp. 177–184, 2004.
- [64] A. M. Westbrook, A. Szakmary, and R. H. Schiestl, "Mechanisms of intestinal inflammation and development of associated cancers: lessons learned from mouse models," *Mutation Research/Reviews in Mutation Research*, vol. 705, no. 1, pp. 40–59, 2010.
- [65] R. A. Hegazi, K. N. Rao, A. Mayle, A. R. Sepulveda, L. E. Otterbein, and S. E. Plevy, "Carbon monoxide ameliorates chronic murine colitis through a heme oxygenase 1-dependent pathway," *The Journal of Experimental Medicine*, vol. 202, no. 12, pp. 1703–1713, 2005.
- [66] T. Takagi, Y. Naito, K. Mizushima et al., "Inhalation of carbon monoxide ameliorates TNBS-induced colitis in mice through the inhibition of TNF- α expression," *Digestive Diseases and Sciences*, vol. 55, no. 10, pp. 2797–2804, 2010.
- [67] H. Yin, J. Fang, L. Liao, H. Nakamura, and H. Maeda, "Styrene-maleic acid copolymer-encapsulated CORM2, a water-soluble carbon monoxide (CO) donor with a constant CO-releasing property, exhibits therapeutic potential for inflammatory bowel disease," *Journal of Controlled Release*, vol. 187, pp. 14–21, 2014.
- [68] X. Wang, J. Cao, B. W. Sun, D. D. Liu, F. Liang, and L. Gao, "Exogenous carbon monoxide attenuates inflammatory responses in the small intestine of septic mice," *World Journal of Gastroenterology*, vol. 18, no. 40, pp. 5719–5728, 2012.
- [69] D. M. Liu, B. W. Sun, Z. W. Sun, Q. Jin, Y. Sun, and X. Chen, "Suppression of inflammatory cytokine production and oxidative stress by CO-releasing molecules-liberated CO in the small intestine of thermally-injured mice," *Acta Pharmacologica Sinica*, vol. 29, no. 7, pp. 838–846, 2008.
- [70] A. Nakao, K. Kimizuka, D. B. Stolz et al., "Carbon monoxide inhalation protects rat intestinal grafts from ischemia/reperfusion injury," *The American Journal of Pathology*, vol. 163, no. 4, pp. 1587–1598, 2003.
- [71] J. R. Scott, M. A. Cukiernik, M. C. Ott et al., "Low-dose inhaled carbon monoxide attenuates the remote intestinal inflammatory response elicited by hindlimb ischemia-reperfusion," *American Journal of Physiology. Gastrointestinal and Liver Physiology*, vol. 296, no. 1, pp. G9–G14, 2009.
- [72] S. H. van Bree, A. Nemethova, C. Cailotto, P. J. Gomez-Pinilla, G. Matteoli, and G. E. Boeckxstaens, "New therapeutic strategies for postoperative ileus," *Nature Reviews. Gastroenterology & Hepatology*, vol. 9, no. 11, pp. 675–683, 2012.
- [73] O. De Backer, E. Elinck, B. Blanckaert, L. Leybaert, R. Motterlini, and R. A. Lefebvre, "Water-soluble CO-releasing molecules reduce the development of postoperative ileus via modulation of MAPK/HO-1 signalling and reduction of oxidative stress," *Gut*, vol. 58, no. 3, pp. 347–356, 2009.
- [74] D. Babu, S. J. Soenen, K. Raemdonck et al., "TNF- α /cycloheximide-induced oxidative stress and apoptosis in murine intestinal epithelial MODE-K cells," *Current Pharmaceutical Design*, vol. 18, no. 28, pp. 4414–4425, 2012.
- [75] D. Babu, R. Motterlini, and R. A. Lefebvre, "CO and CO-releasing molecules (CO-RMs) in acute gastrointestinal inflammation," *British Journal of Pharmacology*, vol. 172, no. 6, pp. 1557–1573, 2015.
- [76] D. Babu, G. Leclercq, V. Goossens et al., "Antioxidant potential of CORM-A1 and resveratrol during TNF- α /cycloheximide-induced oxidative stress and apoptosis in murine intestinal epithelial MODE-K cells," *Toxicology and Applied Pharmacology*, vol. 288, no. 2, pp. 161–178, 2015.
- [77] H. Liu, X. Liu, C. Zhang et al., "Redox imbalance in the development of colorectal cancer," *Journal of Cancer*, vol. 8, no. 9, pp. 1586–1597, 2017.
- [78] F. Yan, Q. Y. Zhang, L. Jiao et al., "Synergistic hepatoprotective effect of *Schisandrae* lignans with *Astragalus*

- polysaccharides on chronic liver injury in rats,” *Phytomedicine*, vol. 16, no. 9, pp. 805–813, 2009.
- [79] K. K. Upadhyay, R. N. Jadeja, J. M. Thadani et al., “Carbon monoxide releasing molecule A-1 attenuates acetaminophen-mediated hepatotoxicity and improves survival of mice by induction of Nrf2 and related genes,” *Toxicology and Applied Pharmacology*, vol. 360, pp. 99–108, 2018.
- [80] D. Singh, W. C. Cho, and G. Upadhyay, “Drug-induced liver toxicity and prevention by herbal antioxidants: an overview,” *Frontiers in Physiology*, vol. 6, p. 363, 2016.
- [81] M. Farzaei, M. Zobeiri, F. Parvizi et al., “Curcumin in liver diseases: a systematic review of the cellular mechanisms of oxidative stress and clinical perspective,” *Nutrients*, vol. 10, no. 7, p. 855, 2018.
- [82] H. K. Eltzschig and T. Eckle, “Ischemia and reperfusion—from mechanism to translation,” *Nature Medicine*, vol. 17, no. 11, pp. 1391–1401, 2011.
- [83] H. Jaeschke and B. L. Woolbright, “Current strategies to minimize hepatic ischemia-reperfusion injury by targeting reactive oxygen species,” *Transplantation Reviews*, vol. 26, no. 2, pp. 103–114, 2012.
- [84] M. Bauer and I. Bauer, “Heme oxygenase-1: redox regulation and role in the hepatic response to oxidative stress,” *Antioxidants & Redox Signaling*, vol. 4, no. 5, pp. 749–758, 2002.
- [85] J. Brugger, M. A. Schick, R. W. Brock et al., “Carbon monoxide has antioxidative properties in the liver involving p38 MAP kinase pathway in a murine model of systemic inflammation,” *Microcirculation*, vol. 17, no. 7, pp. 504–513, 2010.
- [86] L. Y. Lee, T. Kaizu, H. Toyokawa et al., “Carbon monoxide induces hypothermia tolerance in Kupffer cells and attenuates liver ischemia/reperfusion injury in rats,” *Liver Transplantation*, vol. 17, no. 12, pp. 1457–1466, 2011.
- [87] S. Ogaki, K. Taguchi, H. Maeda et al., “Kupffer cell inactivation by carbon monoxide bound to red blood cells preserves hepatic cytochrome P450 via anti-oxidant and anti-inflammatory effects exerted through the HMGB1/TLR-4 pathway during resuscitation from hemorrhagic shock,” *Biochemical Pharmacology*, vol. 97, no. 3, pp. 310–319, 2015.
- [88] Y. Kato, M. Shimazu, M. Kondo et al., “Bilirubin rinse: a simple protectant against the rat liver graft injury mimicking heme oxygenase-1 preconditioning,” *Hepatology*, vol. 38, no. 2, pp. 364–373, 2003.
- [89] H. J. Kim, Y. Joe, J. S. Kong et al., “Carbon Monoxide Protects against Hepatic Ischemia/Reperfusion Injury via ROS-Dependent Akt Signaling and Inhibition of Glycogen Synthase Kinase 3 β ,” *Oxidative Medicine and Cellular Longevity*, vol. 2013, Article ID 306421, 11 pages, 2013.
- [90] H. J. Kim, Y. Joe, J. K. Yu et al., “Carbon monoxide protects against hepatic ischemia/reperfusion injury by modulating the miR-34a/SIRT1 pathway,” *Biochimica et Biophysica Acta*, vol. 1852, no. 7, pp. 1550–1559, 2015.
- [91] Y. Li, C. Gao, Y. Shi et al., “Carbon monoxide alleviates ethanol-induced oxidative damage and inflammatory stress through activating p38 MAPK pathway,” *Toxicology and Applied Pharmacology*, vol. 273, no. 1, pp. 53–58, 2013.
- [92] K. K. Upadhyay, R. N. Jadeja, H. S. Vyas et al., “Carbon monoxide releasing molecule-A1 improves nonalcoholic steatohepatitis via Nrf2 activation mediated improvement in oxidative stress and mitochondrial function,” *Redox Biology*, vol. 28, article 101314, 2020.
- [93] G. Sass, S. Seyfried, M. Parreira Soares et al., “Cooperative effect of biliverdin and carbon monoxide on survival of mice in immune-mediated liver injury,” *Hepatology*, vol. 40, no. 5, pp. 1128–1135, 2004.
- [94] Z. Wen, Y. Liu, F. Li, and T. Wen, “Low dose of carbon monoxide intraperitoneal injection provides potent protection against GalN/LPS-induced acute liver injury in mice,” *Journal of Applied Toxicology*, vol. 33, no. 12, pp. 1424–1432, 2013.
- [95] B. S. Lee, J. Heo, Y. M. Kim et al., “Carbon monoxide mediates heme oxygenase 1 induction via Nrf2 activation in hepatoma cells,” *Biochemical and Biophysical Research Communications*, vol. 343, no. 3, pp. 965–972, 2006.
- [96] H. S. Kim, P. A. Loughran, J. Rao, T. R. Billiar, and B. S. Zuckerman, “Carbon monoxide activates NF- κ B via ROS generation and Akt pathways to protect against cell death of hepatocytes,” *American Journal of Physiology. Gastrointestinal and Liver Physiology*, vol. 295, no. 1, pp. G146–G152, 2008.
- [97] I. Bellezza, A. L. Mierla, and A. Minelli, “Nrf2 and NF- κ B and their concerted modulation in Cancer pathogenesis and progression,” *Cancers*, vol. 2, no. 2, pp. 483–497, 2010.
- [98] C. A. Piantadosi, M. S. Carraway, and H. B. Suliman, “Carbon monoxide, oxidative stress, and mitochondrial permeability pore transition,” *Free Radical Biology & Medicine*, vol. 40, no. 8, pp. 1332–1339, 2006.
- [99] C. S. F. Queiroga, A. S. Almeida, P. M. Alves, C. Brenner, and H. L. A. Vieira, “Carbon monoxide prevents hepatic mitochondrial membrane permeabilization,” *BMC Cell Biology*, vol. 12, no. 1, p. 10, 2011.
- [100] A. Bastidas-Ponce, K. Scheibner, H. Lickert, and M. Bakhti, “Cellular and molecular mechanisms coordinating pancreas development,” *Development*, vol. 144, no. 16, pp. 2873–2888, 2017.
- [101] J. Pereda, L. Sabater, L. Aparisi et al., “Interaction between cytokines and oxidative stress in acute pancreatitis,” *Current Medicinal Chemistry*, vol. 13, no. 23, pp. 2775–2787, 2006.
- [102] H. Sato, R. C. Siow, S. Bartlett et al., “Expression of stress proteins heme oxygenase-1 and -2 in acute pancreatitis and pancreatic islet betaTC3 and acinar AR42J cells,” *FEBS Letters*, vol. 405, no. 2, pp. 219–223, 1997.
- [103] P. Chen, B. Sun, H. Chen et al., “Effects of carbon monoxide releasing molecule-liberated CO on severe acute pancreatitis in rats,” *Cytokine*, vol. 49, no. 1, pp. 15–23, 2010.
- [104] P. Nuhn, T. Mitkus, G. O. Ceyhan et al., “Heme oxygenase 1-generated carbon monoxide and biliverdin attenuate the course of experimental necrotizing pancreatitis,” *Pancreas*, vol. 42, no. 2, pp. 265–271, 2013.
- [105] S. Nagao, K. Taguchi, H. Sakai et al., “Carbon monoxide-bound hemoglobin vesicles ameliorate multiorgan injuries induced by severe acute pancreatitis in mice by their anti-inflammatory and antioxidant properties,” *International Journal of Nanomedicine*, vol. 11, pp. 5611–5620, 2016.
- [106] I. Nikolic, T. Saksida, K. Mangano et al., “Pharmacological application of carbon monoxide ameliorates islet-directed autoimmunity in mice via anti-inflammatory and anti-apoptotic effects,” *Diabetologia*, vol. 57, no. 5, pp. 980–990, 2014.
- [107] M. Li, S. Peterson, D. Husney et al., “Interdiction of the diabetic state in NOD mice by sustained induction of heme oxygenase: possible role of carbon monoxide and bilirubin,” *Antioxidants & Redox Signaling*, vol. 9, no. 7, pp. 855–863, 2007.

Review Article

NLRP3 Inflammasome and Its Central Role in the Cardiovascular Diseases

Yeqing Tong ^{1,2}, Zhihong Wang,³ Li Cai,^{4,5} Liangqiang Lin,² Jiafa Liu ¹,
and Jinquan Cheng ^{2,6}

¹Center for Disease Control and Prevention, 430079 Hubei, China

²Key Laboratory of Molecular Biology of Guangdong Province, Center for Disease Control and Prevention, Shenzhen 518055, China

³Department of Neurology, Shenzhen NO. 2 People's Hospital, The First Affiliated Hospital of Shenzhen University, Shenzhen 518035, China

⁴Wuhan Center for Disease Control and Prevention, Wuhan 430015, China

⁵School of Health Sciences, Wuhan University, Wuhan 430071, China

⁶School of Public Health and Primary Care, The Chinese University of Hong Kong, Shatin Hong Kong, China

Correspondence should be addressed to Jiafa Liu; l_jiafa@163.com and Jinquan Cheng; c_jinquan@163.com

Received 29 July 2019; Revised 26 March 2020; Accepted 31 March 2020; Published 15 April 2020

Guest Editor: Reggiani Vilela Gonçalves

Copyright © 2020 Yeqing Tong et al. This is an open access article distributed under the Creative Commons Attribution License, which permits unrestricted use, distribution, and reproduction in any medium, provided the original work is properly cited.

Background/Aims. NLRP3 inflammasome, an inflammasome which consists of nucleotide-binding oligomerization domain- (Nod-) like receptor3 (NLRP3) scaffold, apoptosis-associated speck-like protein (ASC) containing a CARD adaptor, and pro-caspase-1, is assembled after the cytoplasmic leucine-rich repeats (LRRs) of NLRP3 sense pathogens or danger signals. In recent years, the role of inflammasome in cardiovascular diseases has attracted mounting attention, and the in-depth study of its mechanism is gradually clear. **Materials.** The NLRP3 inflammasome controls the activation of the proteolytic enzyme caspase-1. Caspase-1 in turn regulates the maturation of the proinflammatory cytokines IL-1 β and IL-18, which leads to an inflammatory response. We made a mini-review on the association of regulatory mechanisms of NLRP3 inflammasome with the development of cardiovascular diseases systematically based on the recent research studies. **Discussion.** The inflammasome plays an indispensable role in the development of atherosclerosis, coronary heart diseases (CHD), and heart ischemia-reperfusion (I/R) injury, and NLRP3 inflammasome may become a new target for the prevention and treatment of cardiovascular diseases. Effective regulation of NLRP3 may help prevent or even treat cardiovascular diseases. **Conclusion.** This mini-review focuses on the association of regulatory mechanisms of NLRP3 inflammasome with the development of cardiovascular diseases, which may supply some important clues for future therapies and novel drug targets for cardiovascular diseases.

1. Introduction

The inflammasome, a multiprotein complex macromolecular intracellular protein which supplies the platform for promoting the maturation of inflammatory cytokines, could promote the maturation of inflammatory cytokines, such as IL-1 β and IL-18 [1–5]. These cytokines are extremely powerful molecules with myriad functions that are widely and rapidly induced in the cardiovascular diseases upon infection, trauma, or stress. Therefore, inflammasome is likely to control the inflammation in the development of cardiovascular diseases [6–8]. NLRP3 inflammasome, the most typically inflamma-

some which could be activated by crystal or particle pathogen damage-associated molecular patterns (PAMPs) and ischemic hypoxia danger-associated molecular patterns (DAMPs), can promote the secretion of IL-1 β and IL-18 [9–11]. Through these mechanisms, it promotes atherosclerosis (AS), coronary heart diseases (CHD), heart ischemia-reperfusion (I/R) injury, and so on [12]. Thus, NLRP3 inflammasome may play a critical role in the cardiovascular diseases physiopathology and act as a proinflammatory mediator; it has become the focus of researchers in recent years. Researches on the role of NLRP3 inflammasome in the cardiovascular diseases are on the focus stage and have made a lot of great progress.

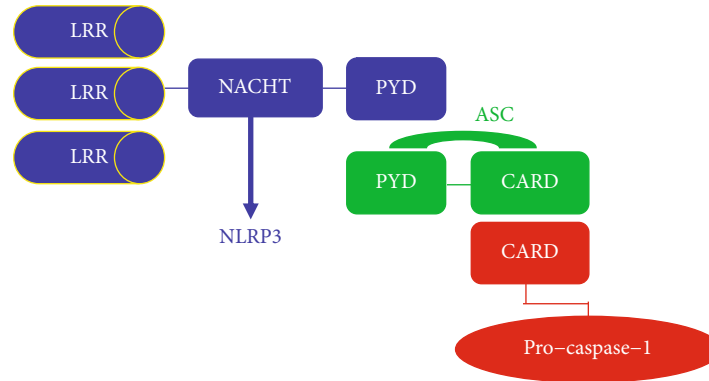


FIGURE 1: Structure of NLRP3 inflammasome.

However, a number of questions deserve further investigation. How the NLRP3 inflammasome is involved in other cardiovascular diseases, such as hypertension, arrhythmia, and heart failure, remains not very clear. In addition, the exact molecular mechanisms by which NLRP3 inflammasome is activated should also be further examined, too. Whether this complex protein is biochemically and genetically regulated or not may be a new focus in the coming years. Clinical trials have confirmed that IL-1 β and its receptor antagonist could be used to treat a variety of cardiovascular diseases [13, 14], and the widely used drug glyburide played a crucial role in the treatment of cardiovascular diseases through the inhibition of the NLRP3 inflammasome [15]. Thus, investigations into NLRP3 inflammasome will shed light on the pathogenesis of cardiovascular diseases and provide critical clues for seeking new targets for clinical cardiovascular diseases drug development.

Despite the potential significance of NLRP3 inflammasome in the pathogenesis of several diseases, emerging evidence suggests that NLRP3 inflammasome events are associated with cardiovascular diseases conditions. Details on the activation mechanism of the NLRP3 inflammasome by a variety of stimulators have yet to be systematically reported [16]. In view of its importance and value in cardiovascular diseases, we systematically reviewed the recent research advances in NLRP3 inflammasome, particularly its specialized role in the cardiovascular diseases. In this review, we summarized the role of NLRP3 in inflammatory response and discussed the relationship between NLRP3 and cardiovascular diseases. We also provided insights into new treatment strategies for targeting NLRP3 inflammasome, as well as the upstream and downstream components of NLRP3 in alleviating cardiovascular diseases.

2. Structure of NLRP3 Inflammasome

NLRP3, the main component of the NLRP3 inflammasome which consists of N-terminal and C-terminal function structural domain, was known as a novel inflammatory gene [13, 17, 18]. The structure of NLRP3 inflammasome is described in Figure 1.

The N-terminal domain includes the hot protein pyrin domain (PYD), the caspase-associated recruitment domain (CARD), and the nucleotide-binding oligomerization domain

(NOD/NACHT); the C-terminal domain includes the leucine-rich repeat (LRR) which provides a bracket to identify pathogen-associated patterns and other ligands. When ligands are identified by LRR, the NOD structure domain rearranges and triggers its biological effects [13, 19].

NLRP3 inflammasome, a new inflammasome which oligomerizes upon activation, is constituted by NLRP3, ASC, and pro-caspase-1 [20]. First and foremost, its activation will result in the recruitment of ASC through homotypic PYD-PYD interactions. Secondly, ASC forms large speck-like structures and recruits pro-caspase-1 via CARD-CARD contact, leading to the autocatalytic activation of caspase-1 [21]. Finally, activated caspase-1 converts the inactive pro-IL-1 β and pro-IL-18 into their activated and secreted forms, mediating the subsequent responses.

3. Mechanisms of NLRP3 Inflammasome Activation

NLRP3 inflammasome is assembled and activated in certain classical types of mechanisms such as the lysosome destabilization, the K⁺ efflux, and Ca²⁺ mobilization as well as the ROS; the mechanisms of NLRP3 Inflammasome activation are described in Figure 2.

3.1. The Lysosome Destabilization Mediating Activation Pathway. The activated pathway mediated by the lysosome destabilization is mainly to activate caspase-1 to process the proinflammatory cytokines interleukin- (IL-) 1 β and IL-18. The studies found that urea, cholesterol crystal, and aseptic materials were swallowed into the intracellular to destroy the stability of lysosome membrane and then activate the lysosomal proteases and caspase-1, further activate NLRP3 inflammasome, and promote the process of proinflammatory cytokines interleukin- (IL-) 1 β and IL-18 damaging the body [22].

3.2. The K⁺ Efflux- and Ca²⁺ Mobilization-Mediated Activation Pathway. The K⁺ efflux- and Ca²⁺ mobilization-mediated pathway may play a critical role in triggering the NLRP3 inflammasome activation. It can be activated by two pathways: (1) The purinergic 2X7 receptor (P2X7R) is in the upstream of NLRP3 activation. The extracellular ATP is involved in the formation of P2X7R which triggers the K⁺ efflux. K⁺ efflux results in low K⁺ concentrations in

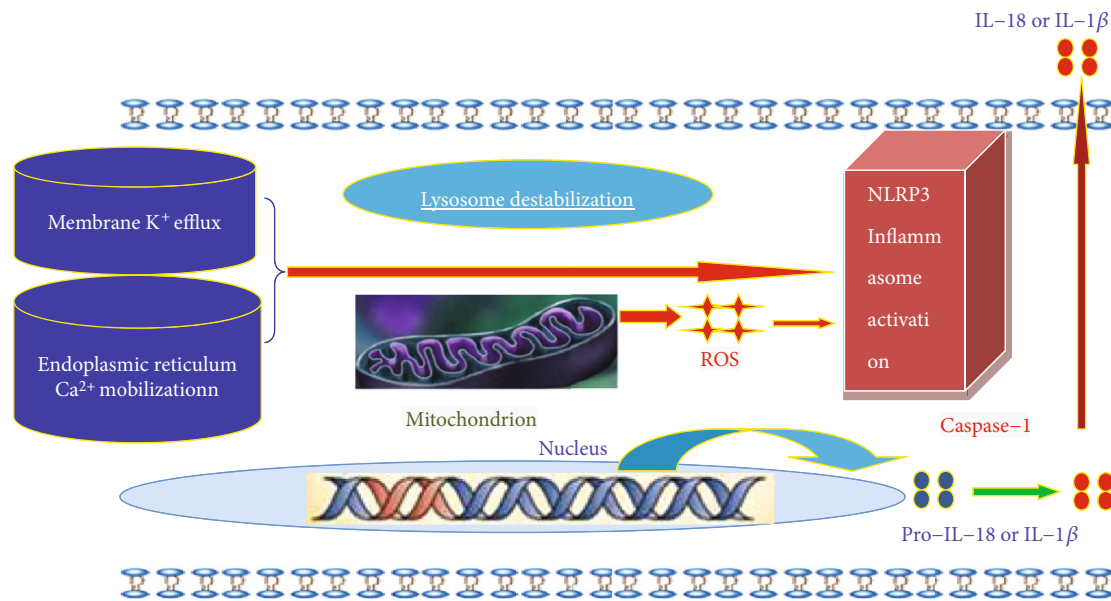


FIGURE 2: Mechanisms of NLRP3 inflammasome activation.

the intracellular environment, leading to mitochondrial dysfunction, apoptosis, and the subsequent release of ROS and oxidative mtDNA, which can activate the NLRP3 inflammasome [23, 24]. (2) In response to ATP and other stimuli, Ca²⁺ released from endoplasmic reticulum storage or the extracellular space can trigger mitochondrial damage, which can also activate NLRP3 inflammasome [25].

3.3. The ROS-Mediated Activation Pathway. Reactive oxygen species (ROS), a powerful oxidant which is mainly produced by the mitochondria, could trigger oxidative stress and activate NLRP3 inflammasome [26]. The complex of thioredoxin and thioredoxin-interacting protein (TXNIP) could dissociate in the high ROS level circumstance. The subsequent binding of TXNIP and NLRP3 leads to the activation of TXNIP-NLRP3 inflammasome and recruitment of ASC and pro-caspase-1 as well as the formation of the active inflammasome complex [27]. Studies have found that reducing the damage of mitochondria by regulating mitochondrial autophagy could inhibit ROS from inducing NLRP3 inflammasome activation. Absence of autophagy will increase the activation of the NLRP3 inflammasome dramatically.

Mitochondrial dysfunction acts in the upstream of NLRP3 activation by providing ROS to trigger NLRP3 oligomerization or by inducing α -tubulin acetylation to relocate mitochondria to the proximity of NLRP3 [28]. In addition, mitochondria work as a platform for inflammasome assembly. Mitochondrial function may also depend on the downstream of NLRP3 activation. While the molecular mechanisms of mitochondrial dysfunction associated with NLRP3 activation are still unclear, they might be involved in the perturbation of mitochondria by K⁺ efflux and subsequent intracellular disequilibrium [29]. Thus, mitochondria ROS and NLRP3 machinery appear to be closely interwoven at multiple levels.

4. The Role of NLRP3 Inflammasomes in the Cardiovascular Diseases

Activation of the NLRP3 inflammasome by these mechanisms has been discovered in various disorders, including metabolic syndrome, type 2 diabetes, atherosclerosis, gout, reperfusion injury of the heart, neurodegeneration, such as Alzheimer's disease, chronic kidney diseases, and more, and more studies suggest that NLRP3 inflammasome is involved in the development of cardiovascular diseases.

4.1. The Association between NLRP3 Inflammasome and Coronary Heart Diseases (CHD). NLRP3 plays a very important role in the early stage of CHD. Low-density lipoprotein (LDL) promotes a cholesterol crystal to deposit in the vessel wall. Then, the macrophages phagocytize the lipoprotein and turn themselves into foam cells. Foam cells are activated by the following mechanisms to initiate inflammatory cycle reaction: (1) The macrophages phagocytize lysosome and then lysosomes are damaged and release ROS and protease to activate NLRP3 [30, 31]. (2) The TLR- (Toll-like receptor-) 12/TLR-4 located in the capsular identifies minimally oxidized LDL and free fatty acids and raises the myeloid differentiation primary response gene 88 and interferon TIR domain-containing adapter-inducing interferon beta (TRIF) to induce nuclear factor-kappa B (NF- κ B). NF- κ B promotes intracellular NLRP3 gene and IL-1 β precursor expression to promote inflammation [32]. (3) The proinflammatory factors induce macrophage, neutrophil, lymphocyte, vascular smooth muscle cell infiltration and activation causing cell death and the accumulation of extracellular cholesterol and cellulose and promoting calcium phosphate crystallization deposition. The deposited crystallization calcium further breaks the lysosome of macrophages [33]. (4) The IL-1 β raises mononuclear cells to activate platelets and promotes the release of themselves [34, 35]. (5) The activated macrophages can generate IL-18 causing more vascular smooth

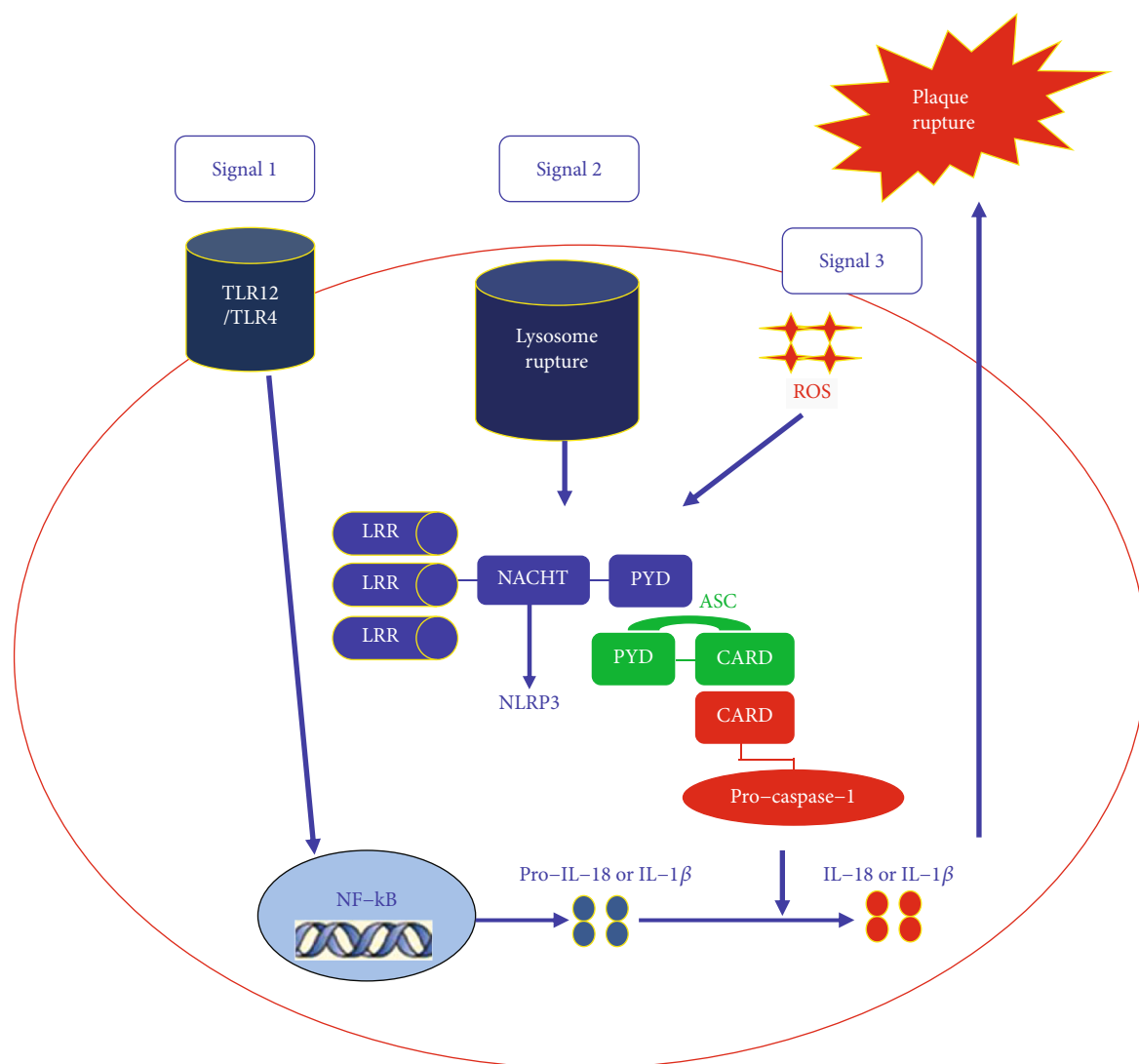


FIGURE 3: The association between NLRP3 inflammasomes and coronary heart diseases (CHD) in macrophages.

muscle cell necrosis and releasing the organization metalloproteinases to reduce the stability of the plaques [36]. The above mechanisms form the cycle reaction could make plaque size more big and plaque stability more serious. The detailed association between NLRP3 inflammasome and CHD is described in Figure 3.

4.2. The Association between NLRP3 Inflammasome and Myocardial Ischemia/Reperfusion (I/R) Injury. Inflammation plays a key role in the pathophysiology of the I/R injury [37, 38]; however, the mechanism how myocardial I/R induces inflammation remains unclear. Recent evidence indicates that a sterile inflammatory response triggered by tissue damage is mediated through a multiple-protein complex called the NLRP3 inflammasome. Inflammatory response is initiated by the detection of PAMPs and/or DAMPs via extracellular and intracellular pattern recognition receptors [39, 40]. The inflammasome is an initial sensor for danger signals in myocardial I/R injury. Kawaguchi et al. have found that inflammasome activation in cardiac fibroblasts was crucially

involved in the initial inflammatory response after myocardial I/R injury [41]. NLRP3 inflammasome was formed by I/R, and its subsequent activation of inflammasomes led to IL-1 β production, resulting in inflammatory responses such as inflammatory cell infiltration and cytokine expression in the heart [42]. The activated NLRP3 inflammasome could integrate ASC to activate caspase-1. In mice deficient in apoptosis-associated speck-like adaptor protein and caspase-1, these inflammatory responses and subsequent injuries, including infarct development, myocardial fibrosis, and dysfunction, were markedly diminished [43–45]. Bone marrow transplantation experiments with apoptosis-associated speck-like adaptor protein-deficient mice revealed that NLRP3 inflammasome activation in bone marrow cells and myocardial resident cells such as cardiomyocytes or cardiac fibroblasts plays a crucial role in myocardial I/R injury [41]. The *in vitro* experiments revealed that hypoxia/reoxygenation stimulated by NLRP3 inflammasome activation in cardiac fibroblasts and hypoxia/reoxygenation-induced activation was mediated through reactive oxygen

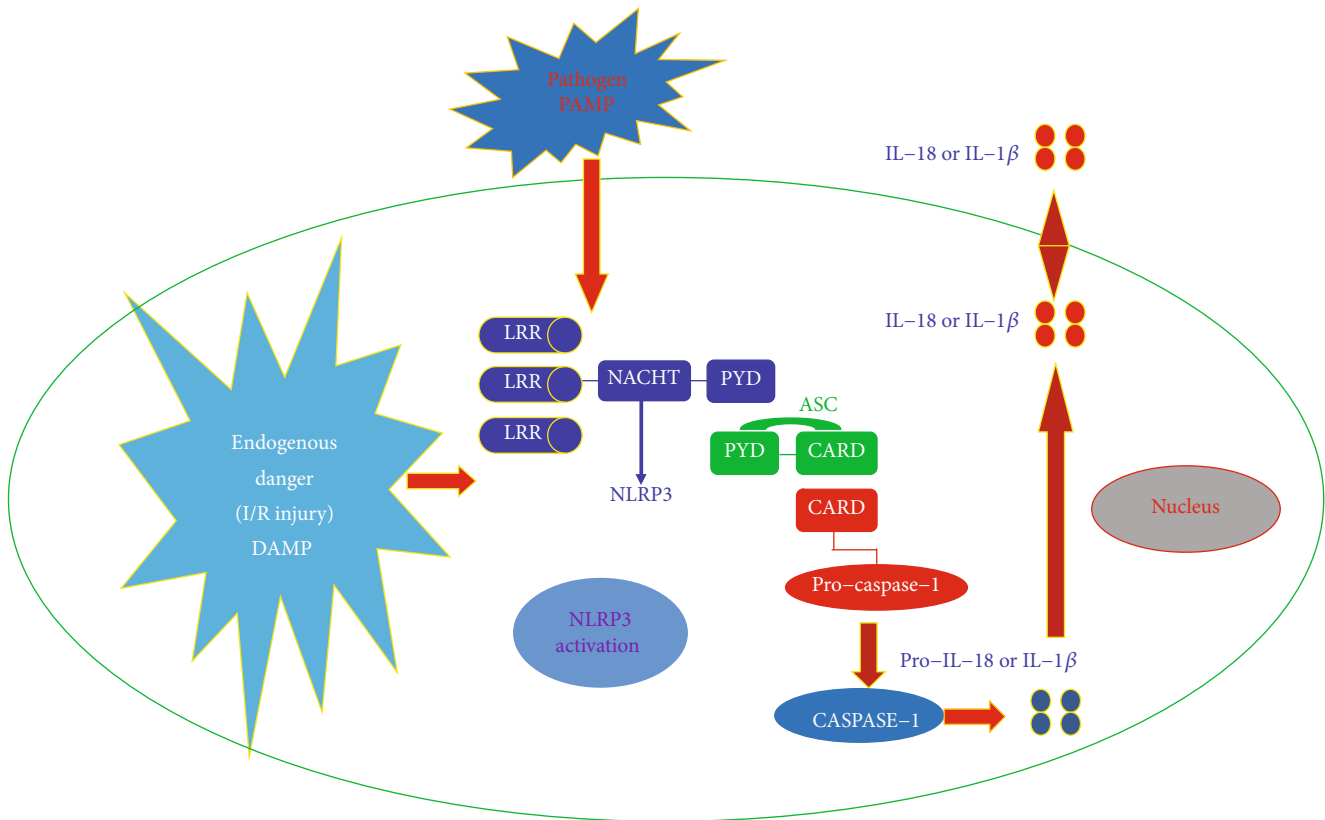


FIGURE 4: The association between NLRP3 inflammasome and myocardial ischemia/reperfusion (I/R) injury in cardiomyocytes.

species production and potassium efflux [46, 47]. All of these suggested that NLRP3 inflammasome was one of the most important molecular basis for the initial inflammatory response after I/R. Its activation in cardiac fibroblasts was essential for myocardial I/R injury, so it maybe a potential novel therapeutic target for preventing myocardial I/R injury [48–51]. The detailed association between NLRP3 inflammasome and myocardial I/R injury is described in Figure 4.

4.3. The Association between NLRP3 Inflammasome and Heart Failure. Inflammation is associated with cardiac remodeling and heart failure, but how it is initiated in response to nonischemic interventions in the absence of cell death is still not very clear. Activation of the NLRP3 inflammasome triggers inflammatory gene expression in cardiomyocytes. These responses could provide signals for macrophage recruitment, fibrosis, and myocardial dysfunction in the heart. These studies suggests targeting early inflammatory responses induced by NLRP3 inflammasome-associated signal can prevent the progression to heart failure [52, 53]. The *in vivo* study also had shown that Tet2 deficiency in hematopoietic cells is associated with greater cardiac dysfunction in murine models of heart failure as a result of elevated IL-1 β signaling. Individuals with TET2-mediated clonal hematopoiesis may have greater risk of developing heart failure and respond better to IL-1 β -NLRP3 inflammasome inhibition [54].

5. Discussion and Conclusion

To sum up, these previous results have a number of therapeutic implications. NLRP3 inflammasome could identify a large number of bacteria, viruses, and some endogenous signals that activate caspase-1 and induce production and secretion of IL-1 β and IL-18. Numerous studies have confirmed that the NLRP3 played a vital role in the atherosclerosis and occurrence of cardiovascular diseases [3, 30, 41]. Based on the activation mode of NLRP3, inhibiting NLRP3 inflammasome activation may have beneficial effects in preventing the damage mediated by the sterile inflammatory response in cardiovascular diseases such as CHD and MI. Preventing pathological NLRP3 inflammasome from activation may provide some insight into the future prevention and treatment of cardiovascular diseases [1, 3, 10]. Currently, the most promising treatments for inhibiting NLRP3 are anti-IL-1, inhibition of caspase-1, and P2X7 receptors antagonist [47–49].

Targeting against the assembly and activity of the NLRP3 inflammasome is a potential and novel therapy for inflammasome-associated diseases, especially for cardiovascular diseases [55–60]. Some studies have indicated that blocking S194 phosphorylation can prevent NLRP3 inflammasome activation. Inhibiting NLRP3 phosphorylation could be an effective treatment for NLRP3-related diseases [61]. In addition, other studies have shown that the NLRP3 NACHT domain molecule may be the target for drug development against cardiovascular diseases. Blocking ATP

hydrolysis could inhibit NLRP3 activation and inflammasome formation [62, 63].

Further research on the NLRP3 activation mechanisms and more sophisticated animal experiments as well as clinical trials of molecular targeted agents on NLRP3 are needed to better shed light on the association between NLRP3 inflammasome and cardiovascular diseases, as well as the complicated roles of inflammasome in cardiovascular diseases precisely.

Conflicts of Interest

The authors declare no conflicts of interest.

Authors' Contributions

Yeqing Tong, Zhihong Wang, and Li Cai contributed equally to this work.

Acknowledgments

This study was supported by funds (81302497 and 81573237) from the National Natural Science Foundation of China, Hubei Natural Science Foundation (No. 2013CFB056, 2016CFB403, and 2017ADC061), Hubei Province's young talent program (20171102), Hubei Province's young top medical talent program (20191229), and China Postdoctoral Scientific Foundation (No. 2014M550394 and 2015T80807).

References

- [1] S. Y. Yu, L. Tang, G. J. Zhao, and S. H. Zhou, "Statin protects the heart against ischemia-reperfusion injury via inhibition of the NLRP3 inflammasome," *International Journal of Cardiology*, vol. 229, pp. 23-24, 2017.
- [2] S. Bleda, J. de Haro, C. Varela, A. Ferruelo, and F. Acin, "Elevated levels of triglycerides and vldl-cholesterol provoke activation of nlrp1 inflammasome in endothelial cells," *International Journal of Cardiology*, vol. 220, pp. 52-55, 2016.
- [3] S. Toldo, C. Marchetti, A. G. Mauro et al., "Inhibition of the NLRP3 inflammasome limits the inflammatory injury following myocardial ischemia-reperfusion in the mouse," *International Journal of Cardiology*, vol. 209, pp. 215-220, 2016.
- [4] X. Liu, Z. Zhang, J. Ruan et al., "Inflammasome-activated gasdermin D causes pyroptosis by forming membrane pores," *Nature*, vol. 535, no. 7610, pp. 153-158, 2016.
- [5] L. Vande Walle, D. Jiménez Fernández, D. Demon et al., "Does caspase-12 suppress inflammasome activation?," *Nature*, vol. 534, no. 7605, pp. E1-E4, 2016.
- [6] D. S. El-Agamy, H. H. Almaramhy, N. Ahmed, B. Bojan, W. D. Alrohily, and M. A. Elkablawy, "Anti-inflammatory effects of vardenafil Against cholestatic liver damage in mice: a mechanistic study," *Cellular Physiology and Biochemistry*, vol. 47, no. 2, pp. 523-534, 2018.
- [7] K. B. Shah, A. G. Mauro, M. Flattery, S. Toldo, and A. Abbate, "Formation of the inflammasome during cardiac allograft rejection," *International Journal of Cardiology*, vol. 201, pp. 328-330, 2015.
- [8] Q. Hu, B. Wei, L. Wei et al., "Sodium tanshinone IIA sulfonate ameliorates ischemia-induced myocardial inflammation and lipid accumulation in Beagle dogs through NLRP3 inflammasome," *International Journal of Cardiology*, vol. 196, pp. 183-192, 2015.
- [9] M. H. Liu, "FGF-21 alleviates diabetes-associated vascular complications: Inhibiting NF- κ B/NLRP3 inflammasome-mediated inflammation?," *International Journal of Cardiology*, vol. 185, pp. 320-321, 2015.
- [10] B. Tang, G. X. Chen, M. Y. Liang, J. P. Yao, and Z. K. Wu, "Ellagic acid prevents monocrotaline-induced pulmonary artery hypertension via inhibiting NLRP3 inflammasome activation in rats," *International Journal of Cardiology*, vol. 180, pp. 134-141, 2015.
- [11] H. Zhang, S. Chen, M. Zeng et al., "Apelin-13 administration protects against LPS-induced acute lung injury by inhibiting NF- κ B pathway and NLRP3 inflammasome activation," *Cellular Physiology and Biochemistry*, vol. 49, no. 5, pp. 1918-1932, 2018.
- [12] Q. Su, L. Li, Y. Sun, H. Yang, Z. Ye, and J. Zhao, "Effects of the TLR4/Myd88/NF- κ B signaling pathway on NLRP3 inflammasome in coronary microembolization-induced myocardial injury," *Cellular Physiology and Biochemistry*, vol. 47, no. 4, pp. 1497-1508, 2018.
- [13] V. Compan, F. Martín-Sánchez, A. Baroja-Mazo et al., "Apoptosis-associated speck-like protein containing a CARD forms specks but does not activate caspase-1 in the absence of NLRP3 during macrophage swelling," *Journal of Immunology*, vol. 194, no. 3, pp. 1261-1273, 2015.
- [14] W. Q. Huang, P. Wei, R. Q. Lin, and F. Huang, "Protective effects of microRNA-22 against endothelial cell injury by targeting NLRP3 through suppression of the inflammasome signaling pathway in a rat model of coronary heart disease," *Cellular Physiology and Biochemistry*, vol. 43, no. 4, pp. 1346-1358, 2017.
- [15] P. Tang, R. Zhu, W. P. Ji et al., "The NLRP3/Caspase-1/Interleukin-1 β axis is active in human lumbar cartilaginous endplate degeneration," *Clinical Orthopaedics and Related Research*, vol. 474, no. 8, pp. 1818-1826, 2016.
- [16] Z. Fan, M. Lu, C. Qiao, Y. Zhou, J. H. Ding, and G. Hu, "MicroRNA-7 enhances subventricular zone neurogenesis by inhibiting NLRP3/caspase-1 axis in adult neural stem cells," *Molecular Neurobiology*, vol. 53, no. 10, pp. 7057-7069, 2016.
- [17] X. S. Ren, Y. Tong, L. Ling et al., "NLRP3 gene deletion attenuates angiotensin II-induced phenotypic transformation of vascular smooth muscle cells and vascular remodeling," *Cellular Physiology and Biochemistry*, vol. 44, no. 6, pp. 2269-2280, 2018.
- [18] J. Qi, X. J. Yu, X. L. Shi et al., "NF- κ B blockade in hypothalamic paraventricular nucleus inhibits high-salt-induced hypertension through NLRP3 and caspase-1," *Cardiovascular Toxicology*, vol. 16, no. 4, pp. 345-354, 2016.
- [19] Q. Zhang, W. Yu, S. Lee, Q. Xu, A. Naji, and A. D. le, "Bisphosphonate induces osteonecrosis of the jaw in diabetic mice via NLRP3/caspase-1-dependent IL-1 β mechanism," *Journal of Bone and Mineral Research*, vol. 30, no. 12, pp. 2300-2312, 2015.
- [20] M. Muroi and K. Tanamoto, "Zinc- and oxidative property-dependent degradation of pro-caspase-1 and NLRP3 by ziram in mouse macrophages," *Toxicology Letters*, vol. 235, no. 3, pp. 199-205, 2015.
- [21] F. Madouri, N. Guillou, L. Fauconnier et al., "Caspase-1 activation by NLRP3 inflammasome dampens IL-33-dependent house dust mite-induced allergic lung inflammation," *Journal of Molecular Cell Biology*, vol. 7, no. 4, pp. 351-365, 2015.

- [22] M. A. Katsnelson, K. M. Lozada-Soto, H. M. Russo, B. A. Miller, and G. R. Dubyak, "NLRP3 inflammasome signaling is activated by low-level lysosome disruption but inhibited by extensive lysosome disruption: roles for K^+ efflux and Ca^{2+} influx," *American Journal of Physiology-Cell Physiology*, vol. 311, no. 1, pp. C83–C100, 2016.
- [23] C. J. Groß, R. Mishra, K. S. Schneider et al., " K^+ Efflux-independent NLRP3 inflammasome activation by small molecules targeting mitochondria," *Immunity*, vol. 45, no. 4, pp. 761–773, 2016.
- [24] R. Muñoz-Planillo, P. Kuffa, G. Martínez-Colón, B. L. Smith, T. M. Rajendiran, and G. Núñez, " K^+ efflux is the common trigger of NLRP3 inflammasome activation by bacterial toxins and particulate matter," *Immunity*, vol. 38, no. 6, pp. 1142–1153, 2013.
- [25] S. Lacroix-Lamandé, M. Fanton d'Andon, E. Michel et al., "Downregulation of the Na/K-ATPase pump by leptospiral glycolipoprotein activates the NLRP3 inflammasome," *Journal of Immunology*, vol. 188, no. 6, pp. 2805–2814, 2012.
- [26] J. Wu, X. Li, G. Zhu, Y. Zhang, M. He, and J. Zhang, "The role of resveratrol-induced mitophagy/autophagy in peritoneal mesothelial cells inflammatory injury via NLRP3 inflammasome activation triggered by mitochondrial ROS," *Experimental Cell Research*, vol. 341, no. 1, pp. 42–53, 2016.
- [27] H. Shi, Z. Zhang, X. Wang et al., "Inhibition of autophagy induces IL-1 β release from ARPE-19 cells via ROS mediated NLRP3 inflammasome activation under high glucose stress," *Biochemical and Biophysical Research Communications*, vol. 463, no. 4, pp. 1071–1076, 2015.
- [28] S. Yang, C. Xia, S. Li, L. du, L. Zhang, and R. Zhou, "Defective mitophagy driven by dysregulation of rheb and KIF5B contributes to mitochondrial reactive oxygen species (ROS)-induced nod-like receptor 3 (NLRP3) dependent proinflammatory response and aggravates lipotoxicity," *Redox Biology*, vol. 3, pp. 63–71, 2014.
- [29] J. Tschopp and K. Schroder, "NLRP3 inflammasome activation: the convergence of multiple signalling pathways on ROS production?," *Nature Reviews. Immunology*, vol. 10, no. 3, pp. 210–215, 2010.
- [30] J. He, Y. Yang, and D.-Q. Peng, "Monosodium urate (MSU) crystals increase gout associated coronary heart disease (CHD) risk through the activation of NLRP3 inflammasome," *International Journal of Cardiology*, vol. 160, no. 1, pp. 72–73, 2012.
- [31] M. E. Heid, P. A. Keyel, C. Kamga, S. Shiva, S. C. Watkins, and R. D. Salter, "Mitochondrial reactive oxygen species induces NLRP3-dependent lysosomal damage and inflammasome activation," *Journal of Immunology*, vol. 191, no. 10, pp. 5230–5238, 2013.
- [32] S. Y. Chuang, C. H. Yang, C. C. Chou, Y. P. Chiang, T. H. Chuang, and L. C. Hsu, "TLR-induced PAI-2 expression suppresses IL-1 β processing via increasing autophagy and NLRP3 degradation," *Proceedings of the National Academy of Sciences of the United States of America*, vol. 110, no. 40, pp. 16079–16084, 2013.
- [33] H. Ahn, J. Kim, E. B. Jeung, and G. S. Lee, "Dimethyl sulfoxide inhibits NLRP3 inflammasome activation," *Immunobiology*, vol. 219, no. 4, pp. 315–322, 2014.
- [34] M. Aloï, L. Tromba, G. di Nardo et al., "Premature subclinical atherosclerosis in pediatric inflammatory bowel disease," *The Journal of Pediatrics*, vol. 161, no. 4, pp. 589–594.e1, 2012.
- [35] R. Alten, J. Gomez-Reino, P. Durez et al., "Efficacy and safety of the human anti-IL-1 β monoclonal antibody canakinumab in rheumatoid arthritis: results of a 12-week, Phase II, dose-finding study," *BMC Musculoskeletal Disorders*, vol. 12, no. 1, p. 153, 2011.
- [36] F. Zheng, S. Xing, Z. Gong, W. Mu, and Q. Xing, "Silence of NLRP3 suppresses atherosclerosis and stabilizes plaques in apolipoprotein E-deficient mice," *Mediators of Inflammation*, vol. 2014, Article ID 507208, 8 pages, 2014.
- [37] H.-Y. Kim, S.-J. Kim, and S.-M. Lee, "Activation of NLRP3 and AIM2 inflammasomes in Kupffer cells in hepatic ischemia/reperfusion," *The FEBS Journal*, vol. 282, no. 2, pp. 259–270, 2015.
- [38] Y. Qi, M. Zhao, Y. Bai et al., "Retinal ischemia/reperfusion injury is mediated by Toll-like receptor 4 activation of NLRP3 inflammasomes," *Investigative Ophthalmology & Visual Science*, vol. 55, no. 9, pp. 5466–5475, 2014.
- [39] Y. Liu, K. Lian, L. Zhang et al., "TXNIP mediates NLRP3 inflammasome activation in cardiac microvascular endothelial cells as a novel mechanism in myocardial ischemia/reperfusion injury," *Basic Research in Cardiology*, vol. 109, no. 5, p. 415, 2014.
- [40] P. J. Bakker, L. M. Butter, N. Claessen et al., "A tissue-specific role for Nlrp3 in tubular epithelial repair after renal ischemia/reperfusion," *The American Journal of Pathology*, vol. 184, no. 7, pp. 2013–2022, 2014.
- [41] M. Kawaguchi, M. Takahashi, T. Hata et al., "Inflammasome activation of cardiac fibroblasts is essential for myocardial ischemia/reperfusion injury," *Circulation*, vol. 123, no. 6, pp. 594–604, 2011.
- [42] M. Moriyama, I. Y. Chen, A. Kawaguchi et al., "The RNA- and TRIM25-binding domains of influenza virus NS1 protein are essential for suppression of NLRP3 inflammasome-mediated Interleukin-1 β secretion," *Journal of Virology*, vol. 90, no. 8, pp. 4105–4114, 2016.
- [43] F. T. Cero, V. Hillestad, I. Sjaastad et al., "Absence of the inflammasome adaptor ASC reduces hypoxia-induced pulmonary hypertension in mice," *American Journal of Physiology-Lung Cellular and Molecular Physiology*, vol. 309, no. 4, pp. L378–L387, 2015.
- [44] K. M. Boini, T. Hussain, P. L. Li, and S. S. Koka, "Trimethylamine-N-oxide instigates NLRP3 inflammasome activation and endothelial dysfunction," *Cellular Physiology and Biochemistry*, vol. 44, no. 1, pp. 152–162, 2018.
- [45] H. Li, S. Zhang, F. Li, and L. Qin, "NLRX1 attenuates apoptosis and inflammatory responses in myocardial ischemia by inhibiting MAVS-dependent NLRP3 inflammasome activation," *Molecular Immunology*, vol. 76, pp. 90–97, 2016.
- [46] M. Takahashi, "NLRP3 inflammasome as a novel player in myocardial infarction," *International Heart Journal*, vol. 55, no. 2, pp. 101–105, 2014.
- [47] W. M. C. Jong and C. J. Zuurbier, "A role for NLRP3 inflammasome in acute myocardial ischaemia-reperfusion injury?," *Cardiovascular Research*, vol. 99, no. 1, p. 226, 2013.
- [48] G. Lordén, I. Sanjuán-García, N. de Pablo et al., "Lipin-2 regulates NLRP3 inflammasome by affecting P2X7 receptor activation," *Journal of Experimental Medicine*, vol. 214, no. 2, pp. 511–528, 2017.
- [49] M. Karmakar, M. A. Katsnelson, G. R. Dubyak, and E. Pearlman, "Neutrophil P2X₇ receptors mediate NLRP3 inflammasome-dependent IL-1 β secretion in response to ATP," *Nature Communications*, vol. 7, no. 1, article 10555, 2016.

- [50] M. Takahashi, "Role of NLRP3 Inflammasome in cardiac inflammation and remodeling after myocardial infarction," *Biological & Pharmaceutical Bulletin*, vol. 42, no. 4, pp. 518–523, 2019.
- [51] S. Toldo and A. Abbate, "The NLRP3 inflammasome in acute myocardial infarction," *Nature Reviews Cardiology*, vol. 15, no. 4, pp. 203–214, 2018.
- [52] N. J. Byrne, N. Matsumura, Z. H. Maayah et al., "Empagliflozin blunts worsening cardiac dysfunction associated with reduced NLRP3 (nucleotide-binding domain-like receptor protein 3) inflammasome activation in heart failure," *Circulation: Heart Failure*, vol. 13, no. 1, article e006277, 2020.
- [53] T. Suetomi, A. Willeford, C. S. Brand et al., "Inflammation and NLRP3 inflammasome activation initiated in response to pressure overload by Ca^{2+} /calmodulin-dependent protein kinase II δ signaling in cardiomyocytes are essential for adverse cardiac remodeling," *Circulation*, vol. 138, no. 22, pp. 2530–2544, 2018.
- [54] S. Sano, K. Oshima, Y. Wang et al., "Tet2-mediated clonal hematopoiesis accelerates heart failure through a mechanism involving the IL-1 β /NLRP3 inflammasome," *Journal of the American College of Cardiology*, vol. 71, no. 8, pp. 875–886, 2018.
- [55] P. Hong, R. N. Gu, F. X. Li et al., "NLRP3 inflammasome as a potential treatment in ischemic stroke concomitant with diabetes," *Journal of Neuroinflammation*, vol. 16, no. 1, p. 121, 2019.
- [56] A. G. Mauro, A. Bonaventura, and A. Abbate, "Drugs to inhibit the NLRP3 inflammasome: not always on target," *Journal of Cardiovascular Pharmacology*, vol. 74, no. 3, pp. 225–227, 2019.
- [57] C. J. Zuurbier, "NLRP3 inflammasome in cardioprotective signaling," *Journal of Cardiovascular Pharmacology*, vol. 74, no. 4, pp. 271–275, 2019.
- [58] W. Zhou, C. Chen, Z. Chen et al., "NLRP3: a novel mediator in cardiovascular disease," *Journal of Immunology Research*, vol. 2018, Article ID 5702103, 8 pages, 2018.
- [59] L. E. Pavillard, F. Marín-Aguilar, P. Bullon, and M. D. Cordero, "Cardiovascular diseases, NLRP3 inflammasome, and western dietary patterns," *Pharmacological Research*, vol. 131, pp. 44–50, 2018.
- [60] R. Mastrocola, M. Aragno, G. Alloatti, M. Collino, C. Penna, and P. Pagliaro, "Metaflammation: tissue-specific alterations of the NLRP3 inflammasome platform in metabolic syndrome," *Current Medicinal Chemistry*, vol. 25, no. 11, pp. 1294–1310, 2018.
- [61] N. Song, Z. S. Liu, W. Xue et al., "NLRP3 phosphorylation is an essential priming event for inflammasome activation," *Molecular Cell*, vol. 68, no. 1, pp. 185–197.e6, 2017.
- [62] X. Huang, Z. Feng, Y. Jiang et al., "VSIG4 mediates transcriptional inhibition of Nlrp3 and IL-1 β in macrophages," *Science Advances*, vol. 5, no. 1, article eaau7426, 2019.
- [63] R. C. Coll, J. R. Hill, C. J. Day et al., "MCC950 directly targets the NLRP3 ATP-hydrolysis motif for inflammasome inhibition," *Nature Chemical Biology*, vol. 15, no. 6, pp. 556–559, 2019.

Research Article

Preprotection of Tea Polysaccharides with Different Molecular Weights Can Reduce the Adhesion between Renal Epithelial Cells and Nano-Calcium Oxalate Crystals

Yao-Wang Zhao ¹, Li Liu,¹ Chuang-Ye Li,¹ Hui Zhang,² Xin-Yuan Sun ²,
and Jian-Ming Ouyang ²

¹Department of Urology, Hunan Children's Hospital, Changsha 410007, China

²Institute of Biomineralization and Lithiasis Research, Jinan University, Guangzhou 510632, China

Correspondence should be addressed to Yao-Wang Zhao; yw508@sina.com and Jian-Ming Ouyang; toyjm@jnu.edu.cn

Received 17 July 2019; Accepted 19 November 2019; Published 6 January 2020

Guest Editor: Reggiani Vilela Gonçalves

Copyright © 2020 Yao-Wang Zhao et al. This is an open access article distributed under the Creative Commons Attribution License, which permits unrestricted use, distribution, and reproduction in any medium, provided the original work is properly cited.

Crystal adhesion is an important link in the formation of kidney stones. This study investigated and compared the adhesion differences between nano-calcium oxalate monohydrate (COM) and human renal proximal tubule epithelial (HK-2) cells before and after treatment with tea polysaccharides (TPSs) TPS0, TPS1, TPS2, and TPS3 with molecular weights of 10.88, 8.16, 4.82, and 2.31 kDa, respectively. TPS treatment effectively reduced the damage of COM to HK-2 cells, thereby resulting in increased cell activity, decreased release of lactate dehydrogenase, cell morphology recovery, decreased level of reactive oxygen species, increased mitochondrial membrane potential, increased lysosomal integrity, decreased expression of adhesion molecule osteopontin and eversion of phosphatidylserine, and decreased crystal adhesion. Among the TPSs, TPS2 with moderate molecular weight had the best protective effect on cells and the strongest effect on the inhibition of crystal adhesion. Thus, TPS2 may be a potential anticalculus drug.

1. Introduction

Tea is one of the most popular drinks in the world [1] and has many variations, such as green, black, oolong, and Pu'er tea. Numerous studies have shown that tea has many properties, as follows: antioxidant property, cholesterol-lowering property, inhibition of hypertension, inhibition of blood coagulation, dissolution of fibrinogen, reduction of endothelin levels, activation of GSH-Px, protection of LDL oxidation, prevention of cardiovascular disease, and anticancer property [2–6]. Different concentrations (0.00078–5 µg/mL) of black tea extract (BTE) have toxic effects on human colon cancer cells (HT-29), human breast cancer cells (MCF-7), and human alveolar cancer cells (A549) and have no effect on normal cells (NIH-3T3) [4]. BTE can induce DNA strand breakage and oxidative damage in HT-29 and MCF-7 cancer cells. San Cheang et al. [5] prevented the increase of ER stress markers and reactive oxygen species (ROS) levels and the

downregulation of Hcy metabolic enzymes in the aortae of Ang II-infused rats through BT treatment. Fei et al. [6] observed that the water extract of Pu'er tea, BT, and green tea increased the lifespan of worms, postponed Aβ-induced progressive paralysis of Alzheimer's disease in transgenic worms, and improved the tolerance of worms to oxidative stress induced by heavy metal Cr⁶⁺.

The main component of kidney stones is calcium oxalate (CaOx) [7]. The antistone effect of tea has become the focus of researchers [8–11]. Alhaji herbal tea prevents the formation of CaOx kidney stones at high concentrations of calcium and oxalate ions [8]. *Blumea balsamifera* (sambong) tea can form small stones that can be easily eliminated through urination because of the decrease in surface free energy and increase in nucleation rate [9]. Rode et al. [10] showed that the prevalence of CaOx monohydrate (COM) stones immensely decreases among green tea drinkers in a population of 273 hypercalciuric stone formers. Chen et al.

[11] evaluated 13842 subjects with kidney stones through ultrasound and observed that the amounts of daily tea consumption are 119.2 ± 306.8 and 131.7 ± 347.3 mL in groups with and without renal stone disease, respectively. Daily tea consumption ≥ 240 mL (two cups) is associated with a low risk of renal stone disease. These beneficial effects of tea are attributed to its active ingredients, as follows: polysaccharides (PSs), polyphenols, alkaloids, amino acids, vitamins, and inorganic elements [12]. However, the antistone mechanism of tea PSs (TPSs) has not been fully elucidated.

In our previous study [13], we investigated the antioxidant activities of four green TPSs with different molecular weights (10.88 (TPS0), 8.16 (TPS1), 4.82 (TPS2), and 2.31 kDa (TPS3)) and their repair of damaged human renal proximal tubule epithelial (HK-2) cells. Four TPSs repaired mitochondria, lysosomes, and intracellular DNA in HK-2 cells, and TPS2 had the strongest ability.

The prevention of kidney stones is more important than clinical treatment [14–16]. In our previous studies, we have found that polysaccharides extracted from green tea [13, 17] and *Porphyra yezoensis* [18] have the ability of repairing damaged renal epithelial cells. The cells repaired by polysaccharide inhibited the adhesion of CaOx crystals and promoted the endocytosis of the adherent crystals. Cell repair is to repair damaged renal epithelial cells so as to prevent the formation of kidney stones, which is a passive treatment method. However, for undamaged cells, protecting cells from oxidative damage of urine crystallites or oxalic acid *in vivo* in advance is an active effective method to prevent kidney stone formation, and its clinical value is greater than that of passive repair. TPSs with good antioxidant capacity may protect cells and increase their ability to resist oxidative damage. On this basis, this study investigated the adhesion of CaOx crystals to renal epithelial cells before and after protection by TPSs with different molecular weights, in order to provide insights into the active prevention of the formation of kidney stones and investigation of new antistone drugs.

2. Experimental Methods

2.1. Reagents and Instruments. Tea polysaccharide (TPS0) was provided by Shaanxi Ciyuan Biological Co., Ltd. and its molecular weight is 10.88 kDa. The degradation of polysaccharides was performed as previously described [13, 17]. The molecular weights of TPS1, TPS2, and TPS3 were 8.16, 4.82 and 2.31 kDa, respectively.

Calcium oxalate monohydrate (COM) was synthesized according to the previous reference [19]. SEM and XRD indicate that it is a target crystal with a size of about 100 nm.

Human kidney proximal tubular epithelial (HK-2) cells were purchased from the Shanghai Cell Bank, Chinese Academy of Sciences (Shanghai, China). Fetal bovine serum and cell culture medium (DMEM-F12) were purchased from HyClone Biochemical Products Co. Ltd. (Beijing, China). A cell proliferation assay kit (Cell Counting Kit-8, CCK-8) was purchased from Dojindo Laboratory (Kumamoto, Japan). Acridine orange (AO), hematoxylin and eosin staining kit, reactive oxygen detection kit (DCFH-DA), lactate dehydrogenase (LDH) kit, 5,5',6,6'-tetrachloro-1,1',3,3'

-tetraethylbenzimi-dazolylcarbocyanine iodide (JC-1), osteopontin primary antibody (OPN), rabbit anti-rat (FITC-IgG), Annexin V-FITC/PI apoptosis detection kit, cell membrane red fluorescent probe (DiI), and 4',6-diamidino-2-phenylindole (DAPI) were all purchased from Shanghai Beyotime Bio-Tech Co., Ltd. (Shanghai, China). The paraformaldehyde and ethanol are of analytical grade (Guangzhou Chemical Reagent Factory).

The apparatus included a laser confocal microscope (LSM510 META DuoScan, ZEISS, Germany), optical microscope (OLYMPUS, CKX41, Japan), microplate reader (SafireZ, Tecan, Switzerland), multifunction microplate detector (Synergy H1M, BioTek, USA), and flow cytometer (BD FACSAria, USA).

2.2. Cell Culture and Experimental Model. According to our previous study [17], HK-2 cells were cultured in a DMEM-F12 culture medium containing 10% fetal bovine serum and 100 U/mL penicillin-100 μ g/mL streptomycin antibiotics with pH 7.4 at 37°C in a 5% CO₂ humidified environment. Upon reaching an 80%–90% confluent monolayer, cells were blown gently after trypsin digestion to form cell suspension for the following cell experiment.

Cell suspension with a cell concentration of 1×10^5 cells/mL was inoculated with 200 μ L, 1 mL, and 2 mL/well in 96-, 12-, and 6-well plates, respectively, and incubated in DMEM-F12 culture medium for 24 h. The cells were divided into three groups:

- (1) Normal control group, in which only a serum-free culture medium was added
- (2) Damage control group, in which a serum-free culture medium with 200 μ g/mL COM was added and incubated for 6 h
- (3) Protection group, in which the crystal was pretreated with 80 μ g/mL tea polysaccharide for 1 h, then the serum-free medium of 200 μ g/mL COM was added to the cell for 6 h

2.3. Cell Viability Detection by CCK-8. The experimental model is the same as in Section 2.2. After reaching the time, add 10 μ L of CCK-8 reagent to each well of the 96-well plate and incubate for 4 h. The OD values were measured using a microplate reader instrument at 450 nm to detect the repair capacity of polysaccharides.

2.4. Lactate Dehydrogenase (LDH) Release Assay. Divide the cells into the following groups:

- (1) Cell-free medium (background blank wells)
- (2) Untreated cell wells for subsequent lysis (sample maximum enzyme activity control wells)
- (3) Normal control group, in which only a serum-free culture medium was added
- (4) Damage control group, in which a serum-free culture medium with 200 μ g/mL COM was added and incubated for 6 h

- (5) Protection group, in which the crystal was pretreated with 80 $\mu\text{g}/\text{mL}$ tea polysaccharide for 1 h, then the serum-free medium of 200 $\mu\text{g}/\text{mL}$ COM was added to the cell for 6 h

After the damage was completed, each group of 96-well plates was assayed for OD using a microplate reader according to the LDH kit test method to determine the repair ability of the polysaccharide. The specific operation is as follows: add 60 μL LDH detection working solution to each well, mix well, and incubate in the dark (about 25°C) for 30 minutes (can be wrapped in aluminum foil and placed in a horizontal shaker or shaken on a rocking bed). Absorbance was then measured at 490 nm. Dual-wavelength measurements are performed using any wavelength of 600 nm or greater than 600 nm as the reference wavelength. The measured absorbance of each group should subtract the absorbance of the background blank control wells. The result was calculated as follows: LDH release (%) = (absorbance of the treated sample – absorbance of the sample control well) / (absorbance of the cell's maximum enzyme activity – absorbance of the sample control well) \times 100.

2.5. Hematoxylin and Eosin (HE) Staining. According to our previous study [13], cell morphology was observed by HE staining. The experimental model is the same as in Section 2.2. After the treatment time, the cells of the 12-well plate were fixed with 4% paraformaldehyde for 15 min at room temperature. Then, the cells were stained with hematoxylin stain and incubated for 15 min. Then, cells were washed with distilled water for 2 minutes to remove excess stain. After that, the cells were stained with eosin staining solution for 5 min. The cells were washed with distilled water for 2 minutes to remove excess eosin. After treatment, the cells in the 12-well plate were observed under the optical micro-

scope: the cell nucleus was stained purple or blue and the cytoplasm was stained pink or red.

2.6. Reactive Oxygen Species (ROS) Detection. According to our previous study [13], the ROS level was analyzed by DCFH-DA staining. The experimental model is the same as in Section 2.2. After reaching the incubation time, the cells were then stained with 500 μL DCFH-DA with a dilution ratio of 1 : 1000 in a serum-free medium and incubated for 30 min, then washed twice with PBS; the slides of cells in the 12-well plate were observed with a fluorescence microscope and the fluorescence intensity of cells in the 96-well plate was detected with a multifunction microplate detector.

2.7. Measurement of Mitochondrial Membrane Potential ($\Delta\Psi\text{m}$). According to our previous study [13], the $\Delta\Psi\text{m}$ was analyzed by JC-1 staining. The experimental model is the same as in Section 2.2. After reaching the incubation time, the supernatant was aspirated and the cells were washed twice with PBS. Finally, the samples were stained with JC-1 for 15 min. Then, the cells were washed twice with PBS. The cells in the 12-well plate were observed with an optical microscope, and the fluorescence intensity of cells in the 96-well plate was detected with a multifunction microplate detector.

2.8. Lysosomal Integrity Assay. According to our previous study [13], the lysosomal integrity was detected by fluorescence staining. After the cells were then loaded with 5 $\mu\text{g}/\text{mL}$ AO in DMEM for 15 min, the experimental model is the same as Section 2.2. After the damage is finished, the 12-well plate was observed with a fluorescence microscope and the 96-well plate was detected with a microplate reader with excitation at 485 nm and emission at 530 (green cytoplasmic AO) and 620 nm (red lysosomal AO).

$$\text{Normal lysosomal integrity} = \frac{\text{total red fluorescence intensity}}{\text{total green fluorescence intensity}}, \quad (1)$$

$$\text{Lysosomal integrity} = \frac{\text{total red fluorescence intensity}}{\text{total green fluorescence intensity} \times \text{normal lysosomal integrity}}.$$

2.9. Osteopontin (OPN) Expression Detection. According to our previous study [17], the OPN expression was detected by fluorescence staining. The experimental model is the same as Section 2.2. After reaching the damage time, 4% paraformaldehyde was added to fix the cells for 10 min. Subsequently, the sheep serum was added for 20 min. The first antibody of OPN (1 : 100) was dropped into this sample, and it was laid still overnight at 4°C. After that, the cells were rinsed three times with PBS before the addition of FITC-IgG (1 : 100) in the dark. The cells were rinsed three times with PBS again after the incubation for 0.5 h at 37°C. Finally, the cells were stained with DAPI. The 12-well plate was observed

using a laser confocal fluorescence microscope. The color of the nucleus was blue, the OPN was green.

2.9.1. Quantitative Detection of OPN. Referring to the above method, a 96-well plate was used to quantitatively detect the fluorescence intensity with a multifunctional microplate reader.

2.10. Phosphatidylserine (PS) Eversion Detection. According to our previous study [18], the PS eversion was detected by flow cytometry. The experimental model is the same as in Section 2.2. After the damage time was completed, 100 μL

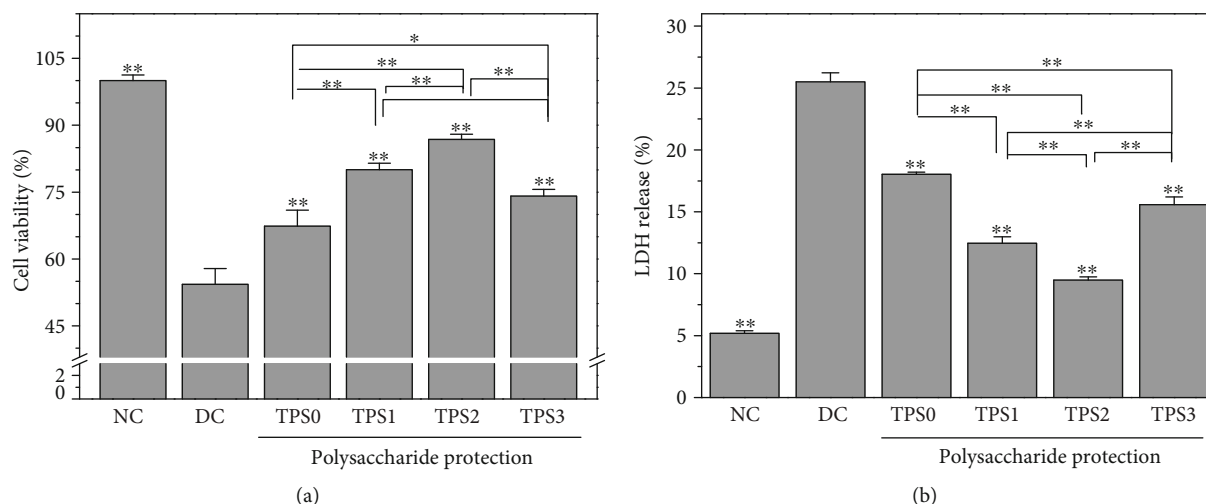


FIGURE 1: Effect of nano-COM crystals on HK-2 cell viability (a) and LDH release (b) before and after TPS protection. NC: normal control group; DC: damage control group. Polysaccharide concentration: 80 $\mu\text{g}/\text{mL}$; protection time: 1 h. Nano-COM concentration: 200 $\mu\text{g}/\text{mL}$; crystal damage time: 6 h. Compared with DC group, * $p < 0.05$ indicates a significant difference; ** $p < 0.01$ indicates a very significant difference.

of binding buffer and 10 μL of FITC-labeled Annexin V were added, and the cells were kept in the dark for 30 min at room temperature. After treatment, the cells of the 6-well plate were detected by flow cytometry.

2.11. Observation of Crystal Adhesion by SEM. According to our previous study [18], the crystal adhesion was observed by SEM. The experimental group is the same as in Section 2.2. After cells are incubated with crystals for 6 h, they are fixed at 4° with 2.5% glutaraldehyde for 24 h, washed 3 times with PBS solution, dehydrated with gradient ethanol (30%, 50%, 70%, 90%, and 100%), dried at the critical point of CO_2 , and sprayed with gold. Cell morphology and crystal adhesion were observed under SEM.

2.12. Quantitative Analysis of the Percentage of Cells Adhered by Crystals by Flow Cytometry. According to our previous study [18], the percentage of cells with adhered crystals was assessed by flow cytometry. The experimental model is the same as in Section 2.2. The 6-well plate was precooled for 30 min at 4°C, then 200 $\mu\text{g}/\text{mL}$ FITC-labeled nano-COM crystals was added. After 6 h at 4°C, the cells were cultured and washed twice with cold PBS, and the percentage of cells adhering to the crystals was detected by flow cytometry.

2.13. Statistical Analysis. Experimental data were expressed as mean \pm SD from at least three independent experiments. The experimental results were statistically analyzed using SPSS 13.0 software, and Tukey test was used to analyze the differences between the mean of each experimental group and the control group. If $p < 0.05$, there was significant difference; if $p < 0.01$, the difference was extremely significant; and if $p > 0.05$, there was no significant difference.

3. Results

3.1. Cell Viability and Lactate Dehydrogenase (LDH) Release. The toxicity of COM crystals to HK-2 cells before and after

treatment of TPSs (TPS0, TPS1, TPS2, and TPS3) with molecular weights of 10.88, 8.16, 4.82, and 2.31 kDa, respectively, was compared. The changes of cell viability are shown in Figure 1(a). After 6 h incubation with nano-COM crystals, cell viability significantly decreased (54.34%). COM treatment attenuated the toxicity of COM crystals to cells. TPS2 had the strongest protective ability, and the cell viability of TPS0, TPS1, TPS2, and TPS3 protection groups was 67.35%, 80.03%, 86.80%, and 74.13%, respectively.

LDH release is used as an important indicator of cell membrane integrity and is widely used in cytotoxicity assays [20]. Figure 1(b) shows the effect of COM crystals on LDH release from HK-2 cells before and after treatment with four TPSs. LDH release of the TPS protection group (9.48%–18.03%) was greater than that of the normal group (5.18%) but smaller than that of the damage group (25.50%), thereby indicating that the damage of HK-2 cells caused by nano-COM can be significantly inhibited by TPSs.

3.2. Cell Morphology. Figure 2 shows the effect of nano-COM crystals on the morphology of HK-2 cells before and after treatment of TPSs. The nucleus of normal cells is uniform, and the connection between the cells is complete. After damage of COM crystals for 6 h, the number of cells significantly decreased, the nucleus was pyknotic, the morphology was disordered, and the connection among cells was destroyed. However, the degree of cell damage was reduced after TPS treatment. The number of cells in the protection group was significantly higher than that in the damage group. The number of nucleated cells was less than in the injury group.

3.3. ROS Level. Figure 3 shows the effect of nano-COM crystals on ROS levels of HK-2 cells before and after TPS treatment. ROS fluorescence of the normal group was low. ROS fluorescence significantly increased after damage, thereby indicating the elevated ROS level. ROS fluorescence intensity of the protection group was between those of the normal and

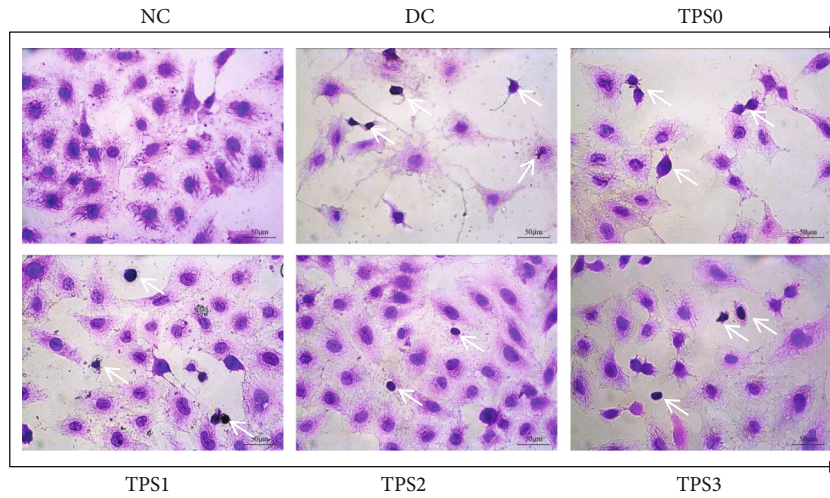


FIGURE 2: Effect of nano-COM crystals on the morphology of HK-2 cells before and after TPS protection. The white arrow is the condensed nuclei. The experimental conditions are the same as in Figure 1.

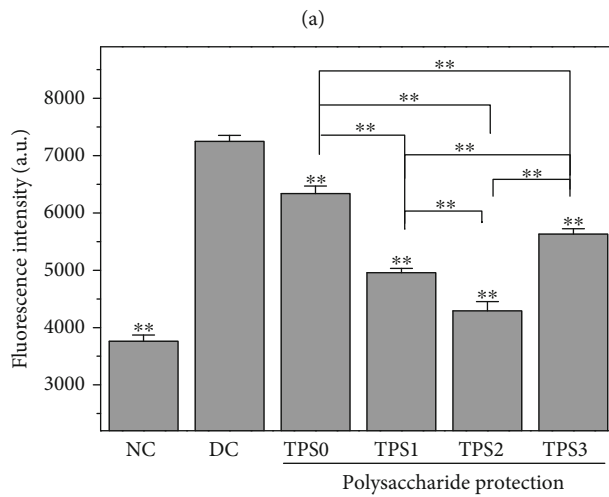
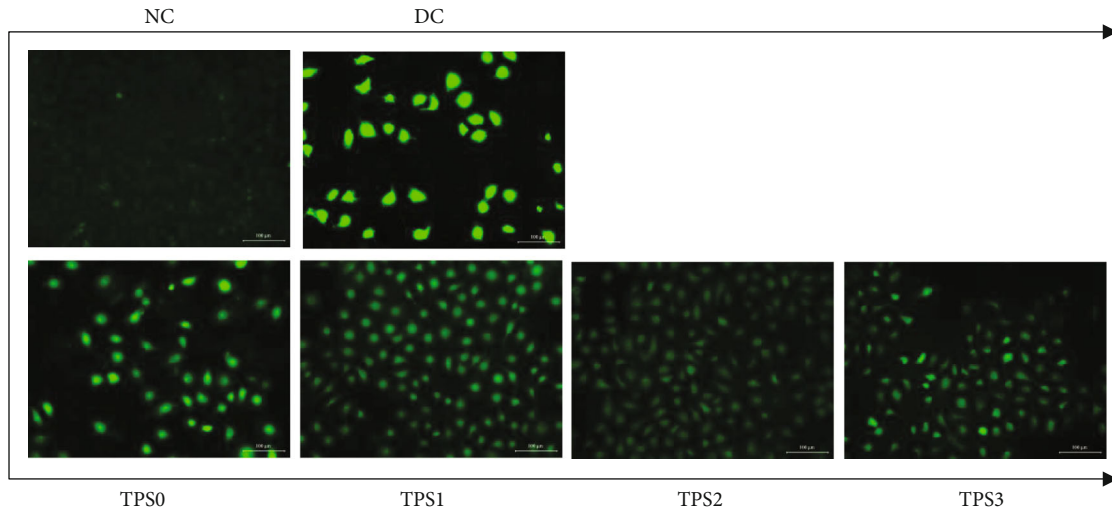


FIGURE 3: Effect of nano-COM crystals on ROS levels of HK-2 cells before and after TPS protection: (a) fluorescence observation; (b) quantitative histogram. Experimental conditions are the same as in Figure 1.

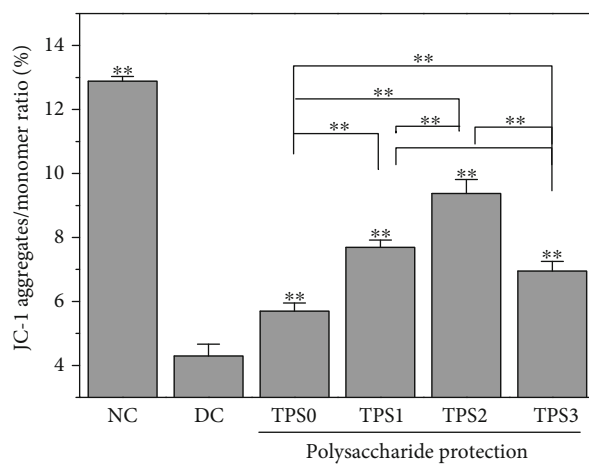
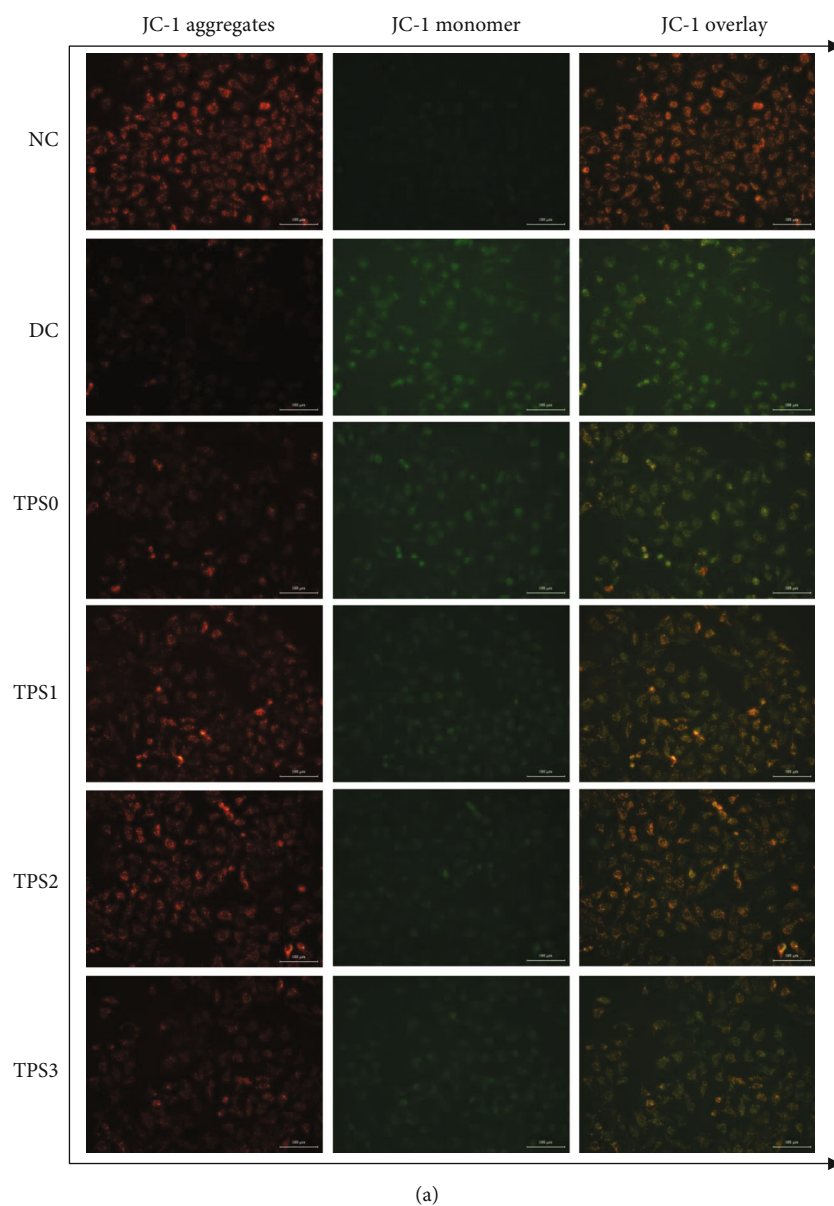


FIGURE 4: Effect of nano-COM crystals on mitochondrial membrane potential of HK-2 cells before and after TPS protection: (a) fluorescence microscopy; (b) quantitative histogram. Experimental conditions are the same as in Figure 1.

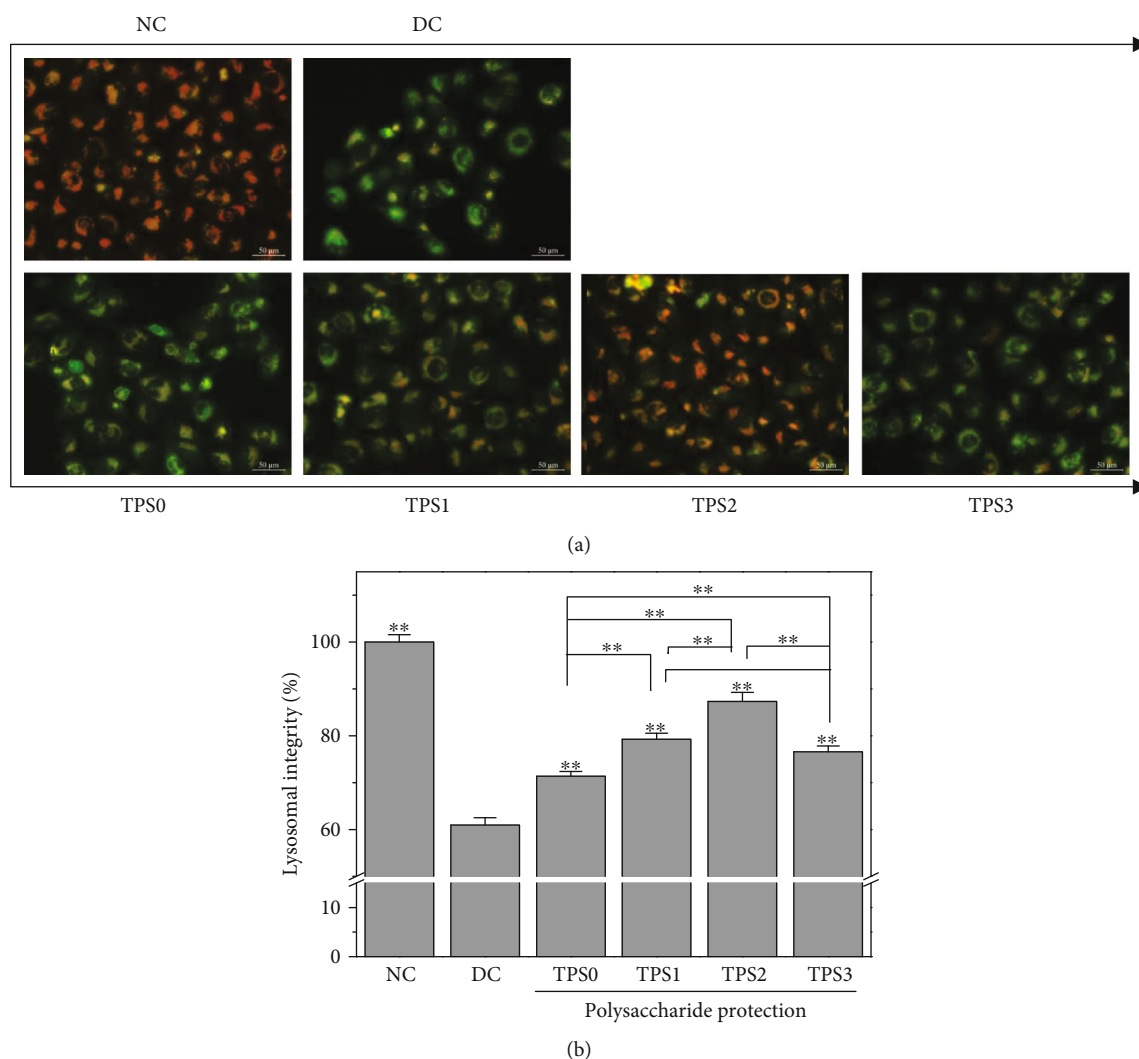


FIGURE 5: Effect of nano-COM crystals on the lysosomal integrity of HK-2 cells before and after TPS protection: (a) fluorescence observation; (b) quantitative histogram. Experimental conditions are the same as in Figure 1.

injury groups, indicating that TPSs can protect cells from damage. The fluorescence intensity quantification results (Figure 3(b)) are consistent with the results of fluorescence microscopy.

3.4. Mitochondrial Membrane Potential ($\Delta\Psi_m$). Figure 4 shows the $\Delta\Psi_m$ change of HK-2 cells before and after TPS treatment. $\Delta\Psi_m$ of normal group cells was high, and the fluorescent probe molecule JC-1 was aggregated in the matrix of the mitochondria to form a polymer (J-aggregates), thereby producing red fluorescence. $\Delta\Psi_m$ of damaged cells significantly decreased, and JC-1 mainly existed as a monomer, which produced green fluorescence. TPS treatment inhibited the decrease of $\Delta\Psi_m$ caused by COM crystals. $\Delta\Psi_m$ of protected cells was between those of the normal and injury groups. TPS2 had the strongest protective ability among the TPSs.

3.5. Lysosomal Integrity. Weak basic acridine orange can enter the lysosome through the cell membrane. It combines

with acid hydrolase to produce orange-red fluorescence and emits a green fluorescence in the cytoplasm. The integrity of lysosomes can be detected by measuring the intensity ratio of red and green fluorescence [21]. Low amount of red fluorescence indicates more severe lysosomal damage and higher degree of cell necrosis.

As shown in Figure 5, the lysosomal integrity of the normal group was 100.01% and that of the damage group was reduced to 60.97%. The lysosomal integrity of the cells in the protection group improved and reached 71.38%–87.32%.

3.6. Osteopontin (OPN) Expression. Figure 6 shows the effect of COM crystals on OPN expression of HK-2 cells before and after TPS treatment. The green fluorescence of the normal group was not obvious, whereas in the injury group was significantly enhanced, thereby indicating that OPN expression of damaged cells significantly increased. OPN expression on the cell surface after TPS treatment was higher than that of the normal group but less than that of the injury group, and OPN expression of the TPS2 group was the least. At

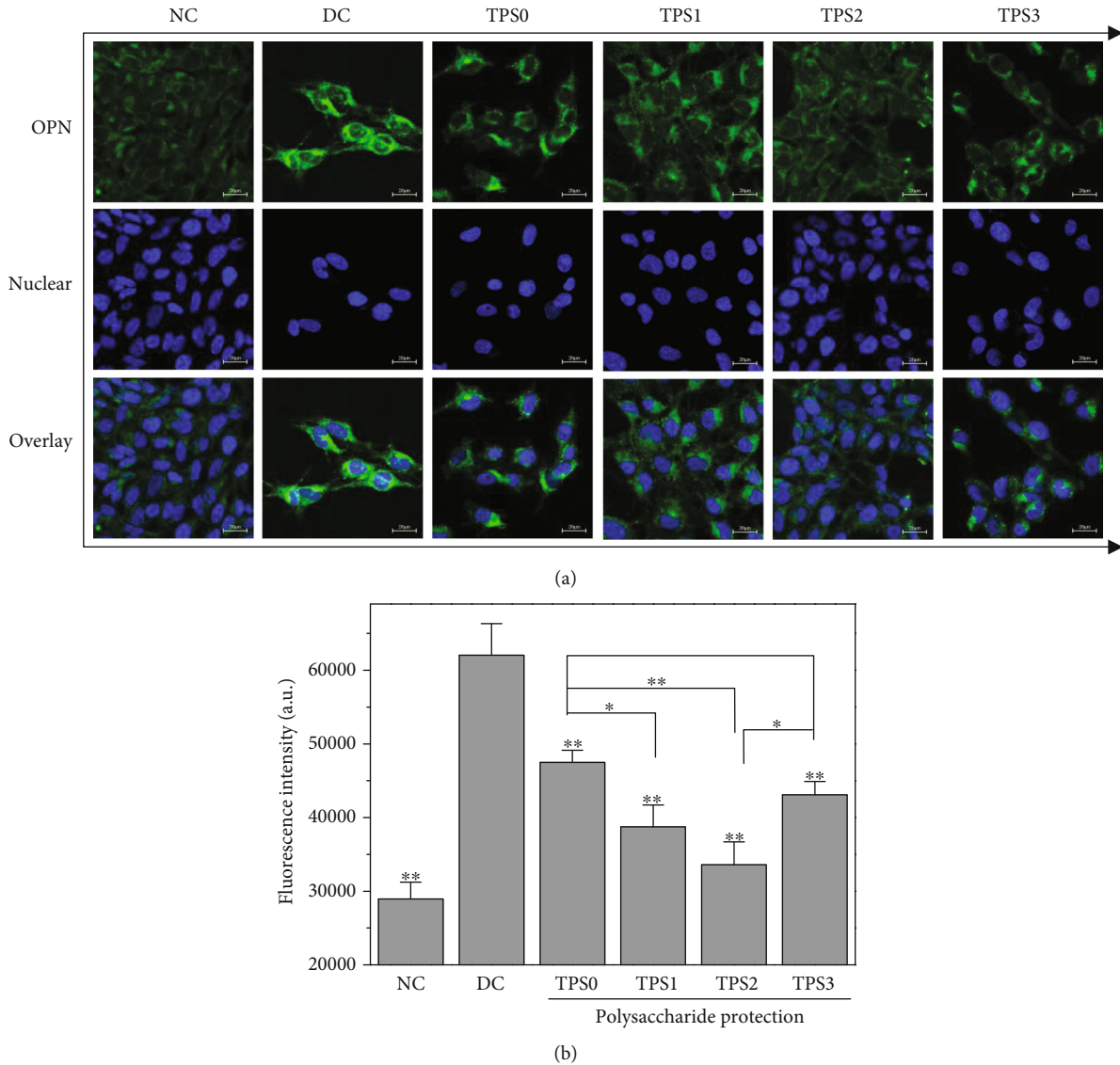


FIGURE 6: Effect of nano-COM crystals on OPN expression in HK-2 cells before and after TPS protection: (a) fluorescence observation; (b) quantitative histogram. Experimental conditions are the same as in Figure 1.

the same time, the nuclei of the normal group were round, the nuclei of the injury group were deformed, and the nuclei of the protection group were mostly round and partially deformed. These results were consistent with the cell morphology observation in Figure 2.

The quantitative detection results of OPN expression (Figure 6(b)) were consistent with the qualitative observations. The OPN average fluorescence intensity of the normal group was approximately 29000, whereas it increased to 62000 in the injury group. The average fluorescence intensities of protection groups (47500, 38700, 33600, and 43000) were between those of the normal and injury groups.

3.7. PS Eversion. Figure 7 shows the effect of COM crystals on the cell surface PS eversion before and after TPS treatment. The amount of PS eversion in the normal group was low (1.67%), and it significantly increased (27.8%) in the injury

group. PS eversions of protected cells were 15.9%, 12.8%, 10.6%, and 14.2%, and these values were between those of the normal and injury groups.

3.8. SEM Observation of Adherent Crystals on Cell Surface.

Figure 8 shows the SEM images of the adhesion of COM crystals on the cells before and after TPS treatment with different molecular weights. Few COM crystals adhered to the surface of normal cells. Damaged cells showed decreased morphology, and many crystals were found on the surface of these cells, thereby causing serious crystal aggregation. The cell morphology in TPS protection groups gradually recovered, and the adhesion amount and aggregation degree of crystals on the cell surface were lower than those in the damage group. For the TP2 protection group, its cell morphology recovered similar to normal cells with few adhered crystals, although the adhered crystals did not aggregate.

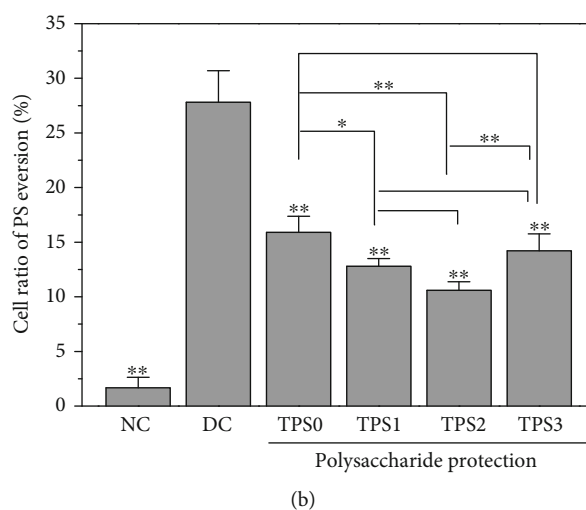
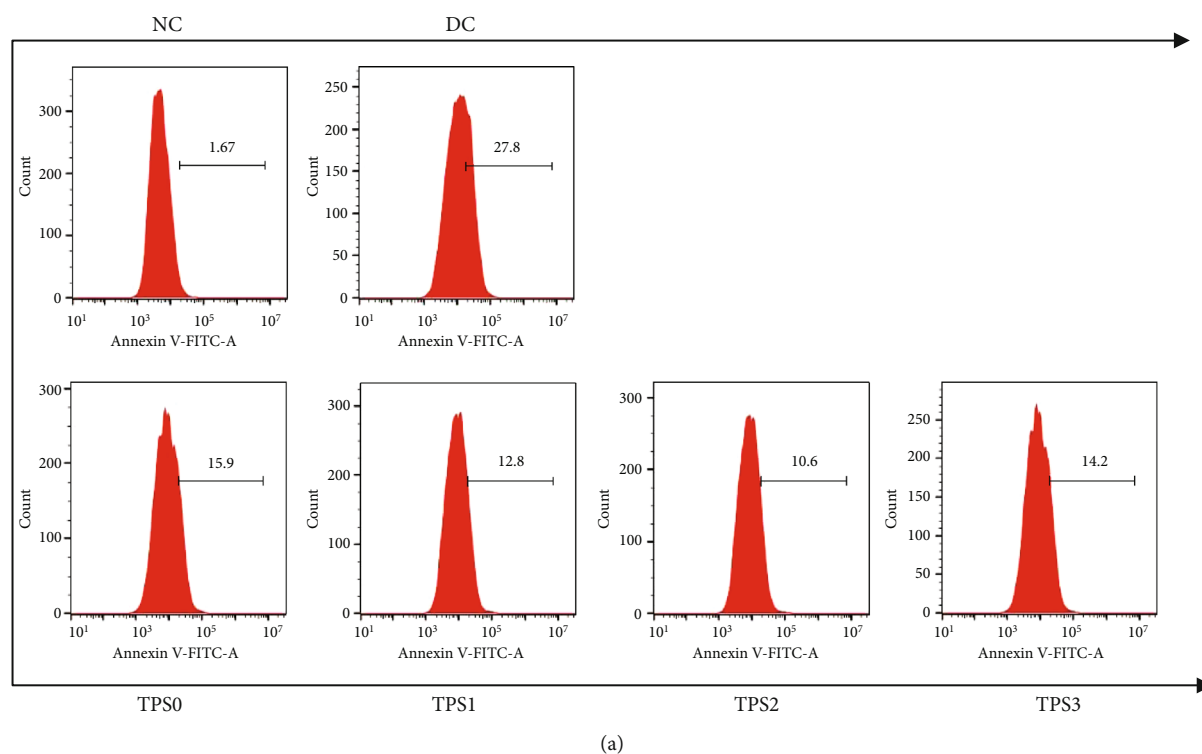


FIGURE 7: Effect of nano-COM crystals on the PS valgus of HK-2 cells before and after TPS protection: (a) quantitative histogram; (b) statistical histogram. Experimental conditions are the same as in Figure 1.

3.9. Percentage of Adhered Cells to Crystals. Figure 8 shows the percentage of adhered cells to crystals before and after TPS treatment. The percentage of cells in the injury group was 48.7%, whereas the percentage of cells in TPS0, TPS1, TPS2, and TPS3 groups were 42.8%, 25.4%, 21.6%, and 31.4%, respectively (Figure 9(b)). In other words, TPS treatment can inhibit the adhesion of COM crystals to cells.

4. Discussion

4.1. Reduction of Cytotoxicity of COM Crystals after Treatment of TPSs with Different Molecular Weights. Renal epithelial cell damage is a key factor that leads to the forma-

tion of kidney stones. Normal kidney tissues have an effective antioxidant defense system, such as superoxide dismutase (SOD) and other enzymes that can remove free radicals and their metabolites and protect the body from oxidative damage. In the pathological state, excessive free radicals produced in the body cause oxidative damage to kidney tissues, leading to the formation of diseases, such as kidney stones [22]. TPSs have good antioxidant capacity, and TPS treatment can improve the ability of renal epithelial cells to resist oxidative damage [23, 24].

The results showed that TPSs protected HK-2 cells from damage caused by nano-COM crystals by reducing ROS production. After the TPS treatment, mitochondrial membrane

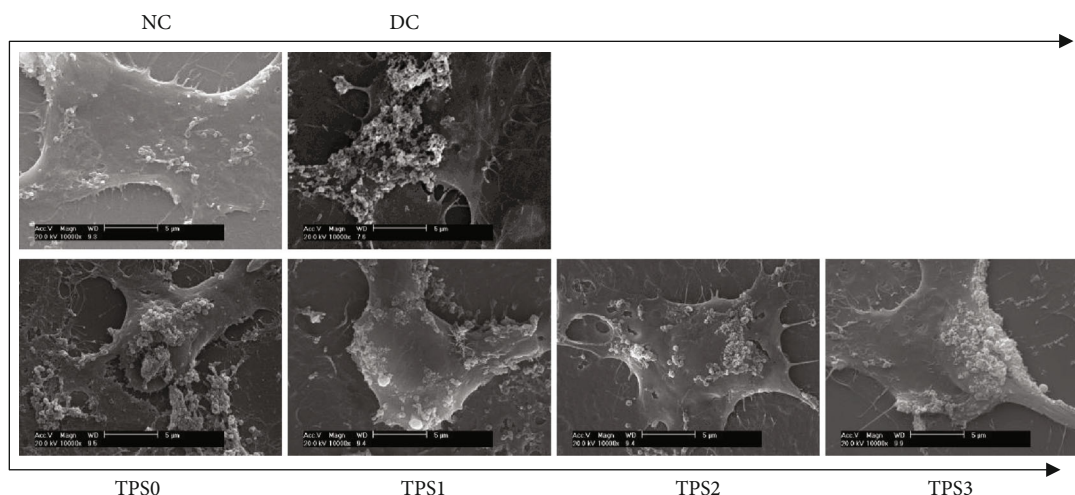


FIGURE 8: SEM images of nano-COM crystal adhesion on cells before and after TPS protection with different molecular weights. Experimental conditions are the same as those in Figure 1.

potential and lysosomal integrity improved, cell membrane damage was reduced, and cell morphology was repaired.

Many studies have demonstrated the protective effect of PSs on cells. For example, Jia et al. [14] observed that low-molecular weight (7 kDa) fucoidan could protect renal function and tubular cells from albumin overload caused by injury and inhibit the increase of ROS levels. Li et al. [15] showed that *Lycium barbarum* PS (LBP-4a) exhibits protective effects against renal damage induced by KBrO_3 . Its mechanism was closely correlated with the reduction in lipid peroxidation levels and the increase in the activities of antioxidant enzymes in kidney tissues, which alleviated DNA damage and increased mitochondrial membrane potentials in renal cells. Zhang et al. [16] showed that the viability and morphology of rat bone marrow endothelial progenitor cells decrease after thrombin damage, and *Astragalus* PS (APS) inhibited this damage.

The molecular weight of TPSs affected their protective effect on HK-2 cells. The cell membrane cannot be crossed when the molecular weights of the TPSs were large (e.g., 10.88 kDa of TPS0) [25, 26]. However, the hydrogen chain was weak, and the active helical structure was not formed because of the short sugar chain [27, 28] when the molecular weight of TPSs was small (such as 2.31 kDa of TPS3), thereby leading to a decrease in the protective effect. Thus, TPS2 with moderate molecular weight (4.82 kDa) was the most active. The molecular weight ranges of different PSs that show strong biological activity differ because of their monosaccharide composition, acidic group species, and content. For example, Yuan et al. [29] demonstrated that all purified PSs obtained from *Ligusticum chuanxiong* Hort (LCA, LCB, and LCC at approximately 2.83×10^4 , 1.23×10^4 , and 6.31×10^4 Da, respectively) exhibit antioxidant properties and cytotoxicity. Among these, LCB had the highest antioxidant and cytotoxic activity. You et al. [30] investigated the protective effects of *Lentinus edodes* PSs with molecular weights of 25.5, 306.2, and 605.4 kDa on D-galactose-induced oxidative stress-induced myocardial cells in mice

and showed that PSs with medium molecular weight have the strongest protective effect.

4.2. Inhibition of Adhesion of COM Crystals to HK-2 Cells after TPS Treatment. Crystallites are common compared with stones, thereby suggesting that crystal adhesion is the key to the formation of kidney stones [31, 32]. Crystallites are excreted in urine rather than adhering to renal epithelial cells and do not form kidney stones. Urine crystallites adhere to the surface of renal epithelial cells and grow or aggregate on the cell surface to form large-sized crystals, which lead to the formation of kidney stones [33].

The risk of stone formation increases, because cell damage promotes cell adhesion to CO crystals. For example, the adhesion of COM crystals to the surface of normal Madin-Darby canine kidney (MDCK) cells is $0.2 \pm 0.03 \mu\text{g}/\text{cm}^2$, and the surface of damaged MDCK increases to $3.90 \pm 0.35 \mu\text{g}/\text{cm}^2$, in which >90% of COM crystals adhere to damaged cells. After the repair of damaged cells, adhesion is reduced to $0.16 \pm 0.02 \mu\text{g}/\text{cm}^2$ [34].

After TPS treatment, the expression of negatively charged adhesion molecules, such as OPN (Figure 6) and PS (Figure 7), is inhibited due to the inhibition of cell damage [35, 36], thereby reducing the adhesion of nanocrystals (Figures 7 and 9). Veena et al. [37] found that fucoidan can protect the kidney of mice with high oxalic aciduria from damage; increase the activity of SOD, CAT, and GPX; prevent renal cell membrane damage; inhibit the adhesion of CO crystals; and reduce the deposition of CO crystals in mice.

The acid group-rich TPSs can adsorb on the surface of COM crystals, thereby increasing the absolute value of zeta potential on the crystal surface and reducing the adhesion of crystals to the surface of negatively charged cell surface. Verkoelen et al. [38] observed that natural glycosaminoglycans and semisynthetic PSs can inhibit the binding of COM crystals to the monolayers of MDCK cells. de Cógáin et al. [39] confirmed that the extract of *Costus arabicus* L. (*C. arabicus*), which contains a PS as its active ingredient, has no effect on

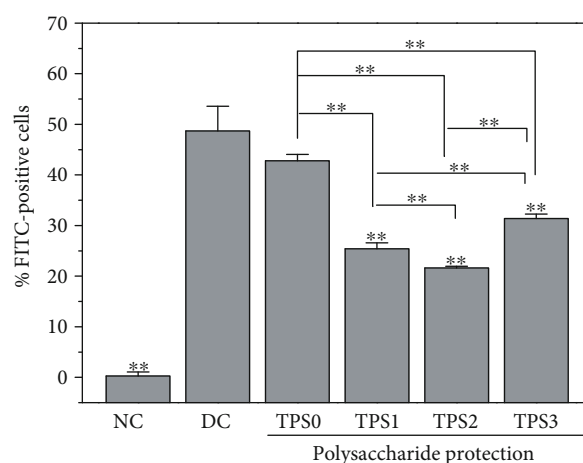
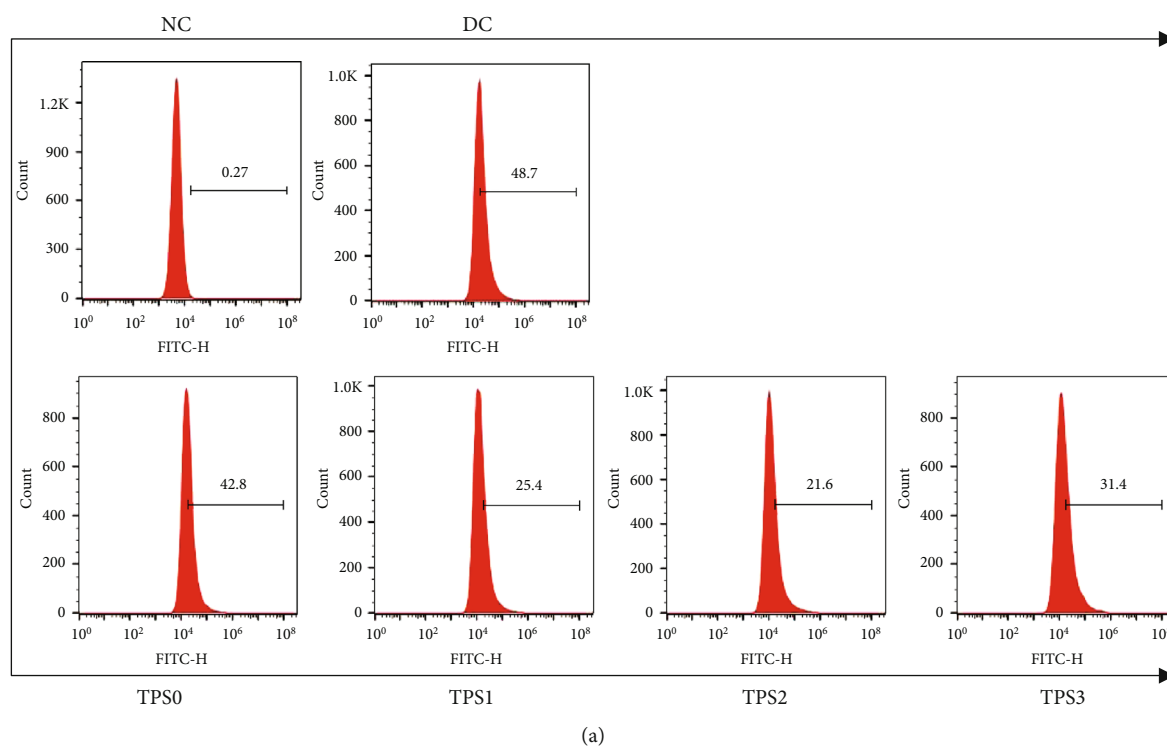


FIGURE 9: Percentage of cells adhering to nano-COM crystals before and after TPS protection: (a) quantitative histogram; (b) statistical histogram. Experimental conditions are the same as in Figure 1.

the pretreatment of MDCK cells on crystal adhesion, and the pretreatment of COM crystals can significantly reduce crystal adhesion in a concentration-dependent manner. The adhesion amount was 0.95 ± 0.12 when the concentration of *C. arabicus* was $1 \mu\text{g}/\text{mL}$ compared with the normal group, and the adhesion amount decreased to 0.37 ± 0.1 when the concentration increased to $1000 \mu\text{g}/\text{mL}$. This condition was similar to the inhibitory effect of heparin in the positive control group.

Figure 10 shows the inhibition model of adhesion of HK-2 cells to nano-COM crystals after TPS treatment. TPS treatment can reduce the zeta potential of the crystal surface and the amount of exposed Ca^{2+} , thereby inhibiting the adhesion of crystals to negatively charged cells on the surface. In addition,

PSs can inhibit cell membrane damage by eliminating excess ROS, increasing mitochondrial membrane potential, improving lysosomal integrity, repairing cell morphology, reducing OPN expression, inhibiting PS eversion, and inhibiting crystal adhesion.

5. Conclusion

Treatment with TPSs with different molecular weights can inhibit the damage of nano-COM crystals to HK-2 cells, improve cell viability, reduce LDH release, restore cell morphology, reduce ROS level, improve mitochondrial membrane potential, improve lysosomal integrity, reduce OPN

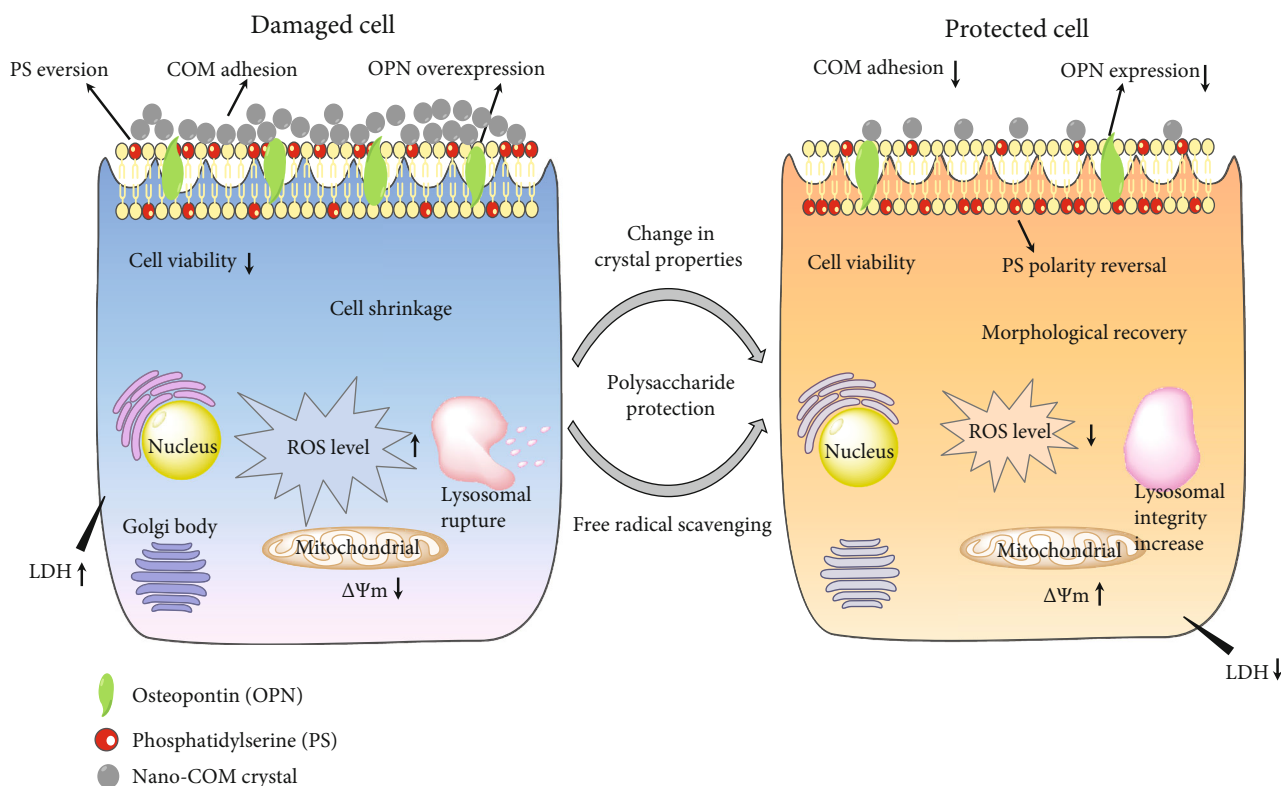


FIGURE 10: Inhibition of adhesion of HK-2 cells to nano-COM crystals by TPS protection.

expression, inhibit PS eversion, and reduce crystal adhesion. The protective effect of TPSs is related to their molecular weight. TPS2 with moderate molecular weight has the best protective effect and is a potential drug for preventing stones.

Data Availability

All the data supporting the results are shown in the paper and can be obtained from the corresponding authors.

Conflicts of Interest

The authors declare that they have no competing interests.

Acknowledgments

This work was granted by the National Natural Science Foundation of China (Nos. 21975105 and 21701050) and the Natural Science Foundation of Hunan Province (No. 2017JJ2139). We thank the Scientific Research Platform of Hunan Key Laboratory of Emergency Medicine for Children (2018TP1028).

References

[1] A. Acquaviva, A. Jones, G. R. Dennis, R. A. Shalliker, and A. Soliven, "Phenolic profiling of complex tea samples via simultaneous multiplexed detection employing reaction flow HPLC columns and colorimetric post column derivatisation," *Microchemical Journal*, vol. 138, pp. 533–539, 2018.

[2] J. Petimar, É. O'Reilly, H. O. Adami et al., "Coffee, tea, and caffeine intake and amyotrophic lateral sclerosis mortality in a pooled analysis of eight prospective cohort studies," *European Journal of Neurology*, vol. 26, no. 3, pp. 468–475, 2019.

[3] M. Xu, J. Wang, and L. Y. Zhu, "The qualitative and quantitative assessment of tea quality based on E-nose, E-tongue and E-eye combined with chemometrics," *Food Chemistry*, vol. 289, pp. 482–489, 2019.

[4] K. Koňariková, M. Ježovičová, J. Keresteš, H. Gbelcová, Z. Ďuračková, and I. Žitňanová, "Anticancer effect of black tea extract in human cancer cell lines," *Springerplus*, vol. 4, no. 1, article 127, 2015.

[5] W. San Cheang, C. Y. Ngai, Y. Y. Tam et al., "Black tea protects against hypertension-associated endothelial dysfunction through alleviation of endoplasmic reticulum stress," *Scientific Reports*, vol. 5, no. 1, article 10340, 2015.

[6] T. Y. Fei, J. Fei, F. Huang et al., "The anti-aging and anti-oxidation effects of tea water extract in *Caenorhabditis elegans*," *Experimental Gerontology*, vol. 97, pp. 89–96, 2017.

[7] S. R. Khan, M. S. Pearle, W. G. Robertson et al., "Kidney stones," *Nature Reviews Disease Primers*, vol. 2, no. 1, article 16008, 2016.

[8] H. Mosta'anzade, E. Honarmand, M. Khalilian, and A. Mozafari, "Prevention and treatment of calcium oxalate kidney stones using Alhaji herbal tea," *Avicenna Journal of Phytomedicine*, vol. 5, pp. 107–108, 2015.

[9] C. M. Montealegre and R. L. De Leon, "*Blumea balsamifera* (sambong) tea as a therapeutic drink for calcium oxalate stones," *MATEC Web of Conferences*, vol. 62, article 02002, 2016.

[10] J. Rode, D. Bazin, A. Dessombz et al., "Daily green tea infusions in hypercalciuric renal stone patients: no evidence for

- increased stone risk factors or oxalate-dependent stones,” *Nutrients*, vol. 11, no. 2, p. 256, 2019.
- [11] H. Y. Chen, J. S. Wu, Y. F. Chang et al., “Increased amount and duration of tea consumption may be associated with decreased risk of renal stone disease,” *World Journal of Urology*, vol. 37, no. 2, pp. 379–384, 2019.
- [12] J. E. Chen, H. J. Feng, and H. R. Zhang, “Effects of active ingredients in black tea, green tea and oolong tea on antioxidant capability,” *Food Science*, vol. 30, no. 3, pp. 62–64, 2009.
- [13] X.-Y. Sun, J.-M. Wang, J.-M. Ouyang, and L. Kuang, “Antioxidant activities and repair effects on oxidatively damaged HK-2 cells of tea polysaccharides with different molecular weights,” *Oxidative Medicine and Cellular Longevity*, vol. 2018, Article ID 5297539, 17 pages, 2018.
- [14] Y. L. Jia, Y. Sun, L. Weng et al., “Low molecular weight fucoidan protects renal tubular cells from injury induced by albumin overload,” *Scientific Reports*, vol. 6, article 31759, 2016.
- [15] J. Li, M. Shi, B. Ma, Y. Zheng, R. Niu, and K. Li, “Protective effects of fraction 4a of polysaccharides isolated from *Lycium barbarum* against KBrO_3 -induced renal damage in rats,” *Food & Function*, vol. 8, no. 7, pp. 2566–2572, 2017.
- [16] X. X. Zhang, K. N. Yao, L. H. Ren, T. Chen, and D. G. Yao, “Protective effect of *Astragalus* polysaccharide on endothelial progenitor cells injured by thrombin,” *International Journal of Biological Macromolecules*, vol. 82, pp. 711–718, 2016.
- [17] Y. W. Zhao, D. Guo, C. Y. Li, and J. M. Ouyang, “Comparison of the adhesion of calcium oxalate monohydrate to HK-2 cells before and after repair using tea polysaccharides,” *International Journal of Nanomedicine*, vol. 14, pp. 4277–4292, 2019.
- [18] H. Zhang, X. Y. Sun, and J. M. Ouyang, “Effects of *Porphyrizyzoensis* Polysaccharide with different molecular weights on the adhesion and endocytosis of nanocalcium oxalate monohydrate in repairing damaged HK-2 cells,” *ACS Biomaterials Science & Engineering*, vol. 5, no. 8, pp. 3974–3986, 2019.
- [19] X. Y. Sun, J. M. Ouyang, A. J. Liu, Y. M. Ding, Y. B. Li, and Q. Z. Gan, “Preparation, characterization, and in vitro cytotoxicity of COM and COD crystals with various sizes,” *Materials Science and Engineering: C*, vol. 57, pp. 147–156, 2015.
- [20] Y. Jin, K. X. Liu, J. Y. Peng et al., “*Rhizoma Dioscoreae* Nipponica polysaccharides protect HUVECs from H_2O_2 -induced injury by regulating PPAR γ factor and the NADPH oxidase/ROS-NF- κ B signal pathway,” *Toxicology Letters*, vol. 232, no. 1, pp. 149–158, 2015.
- [21] Z. M. Liu, Y. Xiao, W. Chen et al., “Calcium phosphate nanoparticles primarily induce cell necrosis through lysosomal rupture: the origination of material cytotoxicity,” *Journal of Materials Chemistry B*, vol. 2, no. 22, pp. 3480–3489, 2014.
- [22] Y. H. Peng, C. Yang, X. L. Shi et al., “Sirt3 suppresses calcium oxalate-induced renal tubular epithelial cell injury via modification of FoxO3a-mediated autophagy,” *Cell Death & Disease*, vol. 10, no. 2, article 34, 2019.
- [23] J. D. Pressly, S. M. Mustafa, A. H. Adibi et al., “Selective cannabinoid 2 receptor stimulation reduces tubular epithelial cell damage after renal ischemia-reperfusion injury,” *The Journal of Pharmacology and Experimental Therapeutics*, vol. 364, no. 2, pp. 287–299, 2018.
- [24] N. Arulkumaran, S. Pollen, E. Greco et al., “Renal tubular cell mitochondrial dysfunction occurs despite preserved renal oxygen delivery in experimental septic acute kidney injury,” *Critical Care Medicine*, vol. 46, no. 4, article e318, e325 pages, 2018.
- [25] L. S. Huang, X. Y. Sun, Q. Gui, and J. M. Ouyang, “Effects of plant polysaccharides with different carboxyl group contents on calcium oxalate crystal growth,” *CrystEngComm*, vol. 19, no. 32, pp. 4838–4847, 2017.
- [26] D. Guo, K. Yu, X. Y. Sun, and J. M. Ouyang, “Structural characterization and repair mechanism of *Gracilaria lemaneiformis* sulfated polysaccharides of different molecular weights on damaged renal epithelial cells,” *Oxidative Medicine and Cellular Longevity*, vol. 2018, Article ID 7410389, 15 pages, 2018.
- [27] Y. H. Sun, X. L. Chen, Z. Q. Cheng et al., “Degradation of polysaccharides from *Grateloupia filicina* and their antiviral activity to avian leucosis virus subgroup j,” *Marine Drugs*, vol. 15, no. 11, p. 345, 2017.
- [28] K. I. Berker, B. Demirata, and R. Apak, “Determination of total antioxidant capacity of lipophilic and hydrophilic antioxidants in the same solution by using ferric–ferricyanide assay,” *Food Analytical Methods*, vol. 5, no. 5, pp. 1150–1158, 2012.
- [29] J. F. Yuan, Z. Q. Zhang, Z. C. Fan, and J. X. Yang, “Antioxidant effects and cytotoxicity of three purified polysaccharides from *Ligusticum chuanxiong* Hort.,” *Carbohydrate Polymers*, vol. 74, no. 4, pp. 822–827, 2008.
- [30] R. You, K. Wang, J. Liu, M. Liu, L. Luo, and Y. Zhang, “A comparison study between different molecular weight polysaccharides derived from *Lentinus edodes* and their antioxidant activities in vivo,” *Pharmaceutical Biology*, vol. 49, no. 12, pp. 1298–1305, 2011.
- [31] S. R. Khan, “Renal tubular damage/dysfunction: key to the formation of kidney stones,” *Urological Research*, vol. 34, no. 2, pp. 86–91, 2006.
- [32] X. Sheng, M. D. Ward, and J. A. Wesson, “Adhesion between molecules and calcium oxalate crystals: critical interactions in kidney stone formation,” *Journal of the American Chemical Society*, vol. 125, no. 10, pp. 2854–2855, 2003.
- [33] Q. Z. Gan, X. Y. Sun, and J. M. Ouyang, “Adhesion and internalization differences of COM nanocrystals on Vero cells before and after cell damage,” *Materials Science and Engineering: C*, vol. 59, no. 1, pp. 286–295, 2016.
- [34] C. F. Verkoelen, B. G. Van Der Boom, A. B. Houtsmuller, F. H. Schröder, and J. C. Romijn, “Increased calcium oxalate monohydrate crystal binding to injured renal tubular epithelial cells in culture,” *American Journal of Physiology-Renal Physiology*, vol. 274, no. 5, pp. F958–F965, 1998.
- [35] A. George and A. Veis, “Phosphorylated proteins and control over apatite nucleation, crystal growth and inhibition,” *Chemical Reviews*, vol. 108, no. 11, pp. 4670–4693, 2008.
- [36] B. Grohe, J. O’Young, D. A. Ionescu et al., “Control of calcium oxalate crystal growth by face-specific adsorption of an osteopontin phosphopeptide,” *Journal of the American Chemical Society*, vol. 129, no. 48, pp. 14946–14951, 2007.
- [37] C. K. Veena, A. Josephine, S. P. Preetha, P. Varalakshmi, and R. Sundarapandiyam, “Renal peroxidative changes mediated by oxalate: the protective role of fucoidan,” *Life Sciences*, vol. 79, no. 19, pp. 1789–1795, 2006.
- [38] C. F. Verkoelen, J. C. Romijn, L. C. Cao, E. R. Boevé, W. C. De Bruijn, and F. H. Schroder, “Crystal-cell interaction inhibition by polysaccharides,” *Journal of Urology*, vol. 155, no. 2, pp. 749–752, 1996.
- [39] M. R. de Cógáin, M. P. Linnes, H. J. Lee et al., “Aqueous extract of *Costus arabicus* inhibits calcium oxalate crystal growth and adhesion to renal epithelial cells,” *Urolithiasis*, vol. 43, no. 2, pp. 119–124, 2015.

Research Article

Exosomal circHIPK3 Released from Hypoxia-Pretreated Cardiomyocytes Regulates Oxidative Damage in Cardiac Microvascular Endothelial Cells via the miR-29a/IGF-1 Pathway

Yan Wang ¹, Ranzun Zhao,¹ Weiwei Liu,¹ Zhenglong Wang,¹ Jidong Rong ¹,
Xianping Long,¹ Zhijiang Liu ¹, Junbo Ge ², and Bei Shi ¹

¹Department of Cardiology, Affiliated Hospital of Zunyi Medical University, Zunyi 563000, China

²Department of Cardiology, Shanghai Institute of Cardiovascular Diseases, Zhongshan Hospital, Fudan University, Shanghai 200032, China

Correspondence should be addressed to Bei Shi; shibei2147@163.com

Received 11 July 2019; Accepted 21 October 2019; Published 5 December 2019

Guest Editor: Reggiani Vilela Gonçalves

Copyright © 2019 Yan Wang et al. This is an open access article distributed under the Creative Commons Attribution License, which permits unrestricted use, distribution, and reproduction in any medium, provided the original work is properly cited.

Background/Aims. Circular RNAs (circRNAs) are a class of endogenous noncoding RNAs that regulate gene expression in eukaryotes. Recently, exosomes from cardiomyocytes (CMs) have been found to facilitate cell proliferation and survival by transporting various bioactive molecules, including circRNA. However, the functions of exosomal circRNAs are not clear. The present research is aimed at determining whether circHIPK3 released from hypoxia-pretreated CMs is transferred into cardiac microvascular endothelial cells (CMVECs) by exosomes and becomes functionally active in the CMVECs under oxidative stress conditions. **Methods.** Quantitative polymerase chain reactions were conducted to detect the expression pattern of circHIPK3 in CMVECs under oxidative stress. Annexin V-FITC/propidium iodide (PI) staining assays, TUNEL assays, ROS assays, and Western blot analysis were conducted to detect the role of exosomal circHIPK3 in CMVEC function in vitro. Luciferase activity assays and RNA immunoprecipitation studies were conducted in vitro to reveal the mechanism of circHIPK3-mediated CMVEC function. **Results.** circHIPK3 expression was significantly upregulated in hypoxic exosomes (HPC-exos) compared with normoxic exosomes (Nor-exos). Moreover, HPC-exos induced stronger antioxidant effects than Nor-exos. The silencing or overexpression of circHIPK3 changed CMVEC survival under oxidative conditions in vitro. Furthermore, circHIPK3 silencing in HPC-exos abrogated the protective effects of HPC-exos in CMVECs, as shown by increased levels of apoptosis, ROS, MDA, and proapoptotic proteins. circHIPK3 acted as an endogenous miR-29a sponge to sequester and inhibit miR-29a activity, which led to increased IGF-1 expression. The ectopic expression of miR-29a mimicked the effect of circHIPK3 silencing in CMVECs in vitro. **Conclusions.** circHIPK3 in HPC-exos plays a role in CMVECs under oxidative conditions through miR-29a-mediated IGF-1 expression, leading to a decrease in oxidative stress-induced CMVECs dysfunction. These data suggest that the exosomal circRNA in CMs is a potential target to control CMVECs dysfunction under oxidative conditions.

1. Introduction

Microcirculatory dysfunction is an important etiological component of ischemia-reperfusion injury [1]. Oxidative stress caused by a surge in the generation of reactive oxygen species (ROS) during reoxygenation can disrupt microvascular integrity [2], consequently decreasing the oxygen and nutrients supplied to cardiac cells. Cardiac microvascular endothelial cells (CMVECs) play an obligatory role in regu-

lating and maintaining cardiac function by forming connections and constituting the continuous endothelium between the circulation and cardiomyocytes (CMs) [3, 4]. The response of CMVECs to ROS impacts heart function via changes in endothelial barrier function that subsequently disrupt tissue blood flow. To ensure sufficient blood supply to deprived areas [5], it is important to explore powerful strategies to protect CMVECs from oxidative stress. The maintenance of microvascular anatomic and functional integrity

after ischemia-reperfusion injury is a highly controlled mechanism that involves communication between the different cell types in the heart [6]. Typically, some level of direct communication is established between CMs and CMVECs. The close contact between CMs and CMVECs allows for the transfer of oxygen and metabolic information from CMs to CMVECs [7]. Thus, the elucidation of the crosstalk between CMs and CMVECs may open completely new avenues for protecting CMVECs from oxidative injury.

Exosomes, as one of cell-derived vesicles, are involved in cell-to-cell signaling and may influence processes in target cells because they can merge with and then release their contents into target cells [8]. In recent years, a large number of studies have shown the role of exosomes in different cell types and different stress conditions, such as glucose starvation [9], inflammation [10, 11], and hypoxic/ischemic preconditioning [12, 13], and indicated that exosomes induce completely different outcomes in recipient cells. Similar to many other types of cells, CMs can release exosomes, and changes in the roles of these vesicles have been related to changes in pathophysiological conditions [14, 15]. Recently, exosomes were found to be released from CMs obtained under ischemic conditions and to promote angiogenesis [16]. Hypoxic preconditioning (HPC) is widely used to simulate *in vivo* ischemic preconditioning (IPC) in cell culture models. HPC may enhance cellular tolerance to ROS [17]. As shown in our previous studies, miR-214, also known as “exosomal shuttle RNA,” is shuttled between cells following HPC and regulates apoptosis in target cells [13, 18]. Circular RNAs (circRNAs) are enriched and stable in exosomes [19] and can be transferred into target cells [20, 21]. However, the functions of exosomal circRNAs remain to be elucidated.

circRNAs are a novel class of noncoding RNAs that are characterized by covalently closed loop structures with neither 5' to 3' polarity nor a polyadenylated tail. circRNAs are expressed in a tissue-specific and developmental stage-specific manner [22]. Emerging evidence shows that circRNAs are implicated in a wide range of physiological and pathological processes, such as cell survival, growth, differentiation, and metastasis. circRNAs also regulate gene expression by acting as miRNA sponges, RNA-binding protein sequestering agents, or nuclear transcriptional regulators [23]. Several lines of evidence indicate that circRNAs are aberrantly expressed in several vascular diseases and cancers [20, 23]. For example, circRNA-MYLK can regulate the VEGFA/VEGFR2 axis by sponging miR-29a and plays a critical role in the progression of bladder carcinoma [24]. As a particularly abundant circRNA [25], circHIPK3 has been verified to be involved in regulating apoptosis, proliferation, migration, and angiogenesis by sponging different miRNAs [26–29]. However, whether circHIPK3 expression in cardiomyocyte exosomes (CMs-exos) is sensitive to hypoxic stimulation and whether circHIPK3 can be shuttled from CMs to CMVECs by exosomes remains unknown. Additionally, the regulatory roles of exosomal circHIPK3 that act as “miRNA sponges” in CMVECs are not yet elucidated. In the present study, we demonstrated that circHIPK3 can be shuttled by exosomes released from CMs pretreated with hypoxia and regulated the H₂O₂-induced dysfunction of CMVECs *in vitro*.

2. Materials and Methods

2.1. Animals. C57BL/6J mice (male and female, approximately 3 weeks old, 22–25 g) were provided and fed at Zunyi Medical University (Zunyi, China). All mice were kept in an air-conditioned room with a constant temperature of 21–22°C and had access to food and water in separated clean cages under a 12-hour light/dark cycle. All experimental procedures were performed according to the “Guide for the Care and Use of Laboratory Animals” in China and were approved by the local Experimental Animal Care and Use Committee.

2.2. CM Culture and Hypoxia Preconditioning. Primary cultures of neonatal mouse CMs were prepared as previously described [30] with minor modifications. Briefly, 1- to 2-day-old mice were euthanized after performing heparinization for 5–10 min. The hearts were carefully excised after quickly removing the connective tissue and atria. The ventricles were minced by eye scissors and digested with phosphate-buffered saline (PBS) containing 0.03% trypsin and 0.04% collagenase type II (Sigma) until the tissue fragments disappeared. Subsequently, a differential attachment technique was adopted to purify neonatal mouse CMs by removing cardiac fibroblasts. The resulting fraction was resuspended in a complete medium containing 10% Dulbecco's modified Eagle's medium (DMEM; Gibco) with fetal bovine serum (FBS), 1% L-glutamine, 0.1 mmol/L 5-Brdu, 1% sodium pyruvate, and 1% penicillin-streptomycin and placed in a culture flask for 90 min at 37°C. Afterwards, the cardiac fibroblasts were attached to the dishes, and the CMs remained suspended in the medium. The CMs were then seeded at a density of 1×10^6 cells per well in culture flasks at 37°C in the presence of 20% O₂, 5% CO₂, and 75% N₂. The CMs were then stained with cardiac troponins T (cTnT) together with 1 mg/ml 4',6-diamidino-2-phenylindole (DAPI) (Invitrogen). Then, fluorescence microscopy (Olympus) was used to observe those cells.

The cells were stimulated with hypoxia [31]. Approximately 5×10^6 CMs were separately incubated in complete media (DMEM) with 10% FBS under a 94% N₂, 5% CO₂, and 1% O₂ gas mixture in a Galaxy® 48 R incubator (Eppendorf/Galaxy Corporation, USA) at 37°C for 0 h, 6 h, 12 h, or 24 h. CM viability was analyzed with CCK-8 assays according to the manufacturer's instructions.

2.3. CMVEC Culture and Establishment of the H₂O₂ Oxidative Stress Model. The isolation of CMVECs was performed according to a published protocol [32]. Briefly, C57BL/6J mice were sacrificed, and the hearts were dissected into ≈ 1 mm³ pieces. The heart samples were then digested by the addition of 0.1% collagenase II (Sigma) until the tissue blocks disappeared (approximately 30 min), followed by 0.25% trypsin-EDTA (Sigma) for 10 min at 37°C. Subsequently, the CMVECs were collected by filtrating and centrifugation (1000 xg for 10 min), resuspended in 20% FBS (Gibco)-M199 medium (HyClone) containing 50 μ g/ml heparin and 75 μ g/ml endothelial cell growth supplement (BD Biosciences), and plated in a culture flask. After 48 h, the CMVECs were cultured in a complete medium containing

20% FBS. Microscopy and flow cytometry (FCM) were adopted to identify CMVECs. Cells were incubated with the following fluorochrome-conjugated primary antibodies: anti-CD31-FITC, anti-CD34-FITC, and anti-vWF-FITC (BioLegend). CMVECs between 3 and 5 passages were used for subsequent experiments. These CMVECs were exposed to 200 μ M H₂O₂ for 3 h to establish the oxidative stress conditions for subsequent experiments [33].

2.4. Purification and Identification of CMs-Exosomes. The CMs exosome extraction procedures were performed as previously described [18]. Briefly, 50 ml of conditioned culture medium containing 10% exosome-depleted FBS/DMEM was used to culture CMs, and the CMs were subjected to normoxic or hypoxic conditions for 12 h. Then, the media were collected for sequential centrifugation (Optima XPN-100 ultracentrifuge; Beckman Coulter SW 41 Ti rotor) at 10,000 g for 35 min to remove cell debris, dead cells, and microvesicles. The supernatant was centrifuged at 100,000 xg for 70 min with an ultracentrifuge. Then, the exosome particles were collected and resuspended in PBS to wash, followed by another ultracentrifugation at 100,000 g for 70 min. The final particles were collected and resuspended in 200 μ l of PBS and stored at -80°C. The amount of CMs-exos was determined by a bicinchoninic acid (BCA) protein assay kit (Pierce). These exosomes were directly observed under a transmission electron microscope (TEM, Hitachi H7500, Tokyo, Japan) and identified by Western blotting with anti-CD63, anti-CD9, and anti-Alix antibodies (Abcam). The absolute exosome size distribution was analyzed by nanoparticle tracking analysis (NTA) (NanoSight NS300 Malvern, UK). Three recordings were performed for each sample.

2.5. Internalization of DiI-Labeled Exosomes into CMVECs. Exosomes were internalized by target cells as previously described, which allow the contents of exosomes to be released into target cells [34]. Briefly, 1 μ M DiI lipophilic dye (Invitrogen) was used to label exosomes. After incubating at 37°C for 30 min, those DiI-labeled exosomes (300 μ g/ml) were added to the CMVEC culture medium for 24 h. The CMVECs were then stained with 1 mg/ml DAPI (Invitrogen) for 5 min. Finally, cell fluorescence was observed by using a fluorescence microscope (Olympus) to provide.

2.6. 5-Ethynyl-20-deoxyuridine (EdU) Incorporation Assay. A Cell-Light EdU DNA Cell Proliferation Kit (RiboBio, Guangzhou, China) was adopted to detect the proliferation of CMVECs according to the manufacturer's protocol. After incubation with 50 mM 5-ethynyl-20-deoxyuridine (EdU) for 2 h, the CMVECs were collected and fixed in 4% paraformaldehyde and stained with Apollo Dye Solution for proliferating cells. The fluorescence intensity of cells was analyzed by FCM.

2.7. RNA Fluorescence In Situ Hybridization (RNA-FISH). RNA fluorescence in situ hybridization (RNA-FISH) assays were conducted using FITC- or Cy3-labeled RNA probes targeted to circHIPK3 or miR-29a. After prehybridization (1x PBS/0.5% Triton X-100), CMVECs were hybridized overnight with RNA probes in the hybridization buffer

(40% formamide, 10% dextran sulfate, 1x Denhardt's solution, 4x saline-sodium citrate (SSC), 10 mM dichlorodiphenyltrichloroethane (DDT), 1 mg/ml yeast transfer RNA, and 1 mg/ml sheared salmon sperm DNA). Cell nuclei were counterstained with DAPI, and fluorescence images were acquired.

2.8. Dual Luciferase Reporter Assay. CMVECs were seeded into 96-well plates in triplicate at a density of 5×10^3 cells per well 24 h before transfection. The circHIPK3 sequences containing wild-type miR-29a binding sites were synthesized and inserted into the pmirGLO luciferase vector (GeneCreate, Wuhan, China), and an empty vector was used as a control. The cells were cotransfected with a mixture of firefly luciferase reporter vector, pRL-TK vector (Renilla luciferase control reporter vector) (Promega), and miR-29a mimics or negative control by using Lipofectamine 2000. In addition, 200 ng of pmirGLO-IGF-1-WT or pmirGLO-IGF-1-Mut reporter plasmids was cotransfected into cells with 50 nM miR-29a mimics using Lipofectamine 2000. Cells were harvested 48 h after transfection, and luciferase reporter assays were performed using a dual luciferase reporter assay system (Promega, Madison, WI) according to the manufacturer's instructions. Relative luciferase activity was normalized to the Renilla luciferase internal control.

2.9. RNA Immunoprecipitation (RIP). CMVECs were washed twice in ice-cold PBS. Approximately 1×10^7 cells were collected and resuspended in an equal volume of RNA immunoprecipitation (RIP) lysis buffer (approximately 100 ml) plus protease and RNase inhibitors. The supernatant was collected after centrifugation (10000 xg for 5 min at 4°C, $\times 2$), and the cell lysates were incubated with 1800 μ l of RIP buffer (containing protease and RNA enzyme inhibitors). Magnetic beads conjugated with mouse anti-Argonaute2 (AGO2) antibody (Millipore, Billerica, MA, USA) or negative control mouse IgG (Millipore, Billerica, MA, USA) were also added to the cell lysates with rotation at 4°C overnight. Samples were washed with 500 μ l of RIP Wash Buffer 1 with rotation at 4°C for 15 min, followed by another wash with 500 μ l of RIP Wash Buffer 2 (both containing RNA enzyme inhibitors and protease inhibitors). The supernatant was collected, and 200 μ l of freshly NaHCO₃ was added with rotation at 4°C for 15 min twice. The supernatant was collected, and the RNA was extracted using TRIzol and analyzed by RT-PCR or qRT-PCR to identify the presence of circRNA-HIPK3 and miR-29a.

2.10. Cell Transfection. CMs or CMVECs were transfected at approximately 80% confluence using a lentiviral construct (HANBIO, China) according to the manufacturer's protocol. Some of those lentiviral constructs were empty (LV), and some carried synthesized circHIPK3 (LV-circHIPK3), small interfering RNAs (Sigma) targeting circHIPK3 (LV-sircHIPK3), or linear HIPK3 (LV-silineHIPK3). In addition, an miR-29a inhibitor, miR-29a mimics, and negative controls were all synthesized by RiboBio (Guangzhou, China) and transfected into CMVECs by using Lipofectamine 2000 (Invitrogen, USA) according to the manufacturer's

TABLE 1: PCR primer sequence, siRNA sequence, shRNA target sequence, and FISH probe sequence.

Primer sequence	
circHIPK3	F: 5'-GGATCGGCCAGTCATGTATC-3' R: 5'-ACCGCTTGGCTCTACTTTGA-3'
miR-29a	RT: GTCGTATCCAGTGCCTGTCGTGGAGTC GGCAATTGCACTGGATACGACTAACCGAT F: ACACTCCAGCTGGGTAGCACCATCTGAAAT R: TGGTGTCTGGAGTCG
U6	RT: 5'-AACGCTTCACGAATTTGCGT-3' F: 5'-CTCGCTTCGGCAGCACA-3' R: 5'-AACGCTTCACGAATTTGCGT-3'
IGF-1	F: 5'-CATCTCTTCTACCTGGCACTCTG-3' R: 5'-TTGGTCCACACACGAACTGAA-3'
GAPDH	F: 5'-GTCAAGGCTGAGAACGGGAA-3' R: 5'-AAATGAGCCCCAGCCTTCTC-3'
β -Actin	F: 5'-TTGTTACAGGAAGTCCCTTGCC-3' R: 5'-ATGCTATCACCTCCCCTGTGTG-3'
siRNA sequence	circHIPK3 siRNA 5'-TAGAAGACCATGGGGGATA-3' linearHIPK3 siRNA 5'-GCUGAUUGAUGCAGAUUUA-3'
FISH probe:	
circHIPK3	5'-TGGGTAGACCAAGACTTGTGAGGCCATACCTGTAGTACCGAGA-3'
miR-29a	5'-TAACCGATTTTCAGATGGTGCTA-3'

instructions. CMVEC functions and gene expression were evaluated 48 h after transfection. The sequence information is listed in Table 1.

2.11. RNase R Treatment. Actinomycin D (2 mg/ml) or DMSO (Sigma-Aldrich, St. Louis, MO, USA) were added to the culture medium to assess the stability of circHIPK3 and its linear isoform. For RNase R treatment, approximately 2 μ g of total RNA was incubated with or without 3 μ g RNase R (Epicenter Technologies, USA) at 37°C for 30 min. The resulting RNAs were subsequently purified using an RNeasy MinElute Cleaning Kit (Qiagen), and the expression levels of circHIPK3 were determined by qRT-PCR.

2.12. Real-Time qPCR. Total RNA was isolated from cell lysates using TRIzol reagent (Life Technologies, Carlsbad, CA). The cDNAs of mRNA and circRNA were synthesized by using PrimeScript RT Master Mix (Takara, Dalian, China) from 500 ng of RNA. Real-time PCR analyses were performed using SYBR Premix Ex Taq II (Takara). In particular, the divergent primers annealing to the distal ends of circRNA were used to determine the abundance of circRNA. For the absolute quantification of circHIPK3, the purified PCR product amplified from the cDNA corresponding to the circHIPK3 sequence was serially diluted to generate a standard curve. Stem-loop RT-qPCR TaqMan MicroRNA assays (Life

Technologies) were used to detect the amount of miRNA. GAPDH or U6 was detected as the internal reference. All primer sequences were designed and synthesized by RiboBio (Guangzhou, China). The primers are listed in Table 1. Gene expression was quantified using the $2^{-\Delta\Delta Ct}$ method.

2.13. Flow Cytometric Analysis. The apoptosis of CMVECs was determined by FCM using Annexin V-FITC/propidium iodide (PI) staining assay kits (Solarbio, China) according to the manufacturer's instructions, as previously reported [1]. CMVEC apoptosis was analyzed via a FACSCalibur flow cytometer (BD Biosciences, USA). The results are expressed as the percentage of apoptotic cells among all the cells.

Intracellular ROS production was determined by dihydroethidium (DHE) staining (Sigma, USA), followed by FCM [35] according to the manufacturer's instructions. Briefly, cells were incubated with MitoSOX reagent (2.5 mmol/l, Invitrogen) for 30 min at 37°C, washed twice with PBS, trypsinized, and centrifuged. The cell fluorescence intensity was analyzed by FCM.

2.14. Assessment of Intracellular SOD and MDA Levels In Vitro. CMVECs were harvested by centrifugation, and the supernatants were removed. The remaining cells were washed with PBS twice and lysed in lysis buffer for 30 min at 4°C. Following centrifugation, the supernatant was used

to detect the activity of superoxide dismutase (SOD) and the level of malondialdehyde (MDA) by using different assay kits (Nanjing Jiancheng Bioengineering Institute, China), as mentioned in the protocols. The BCA test was used to quantify proteins.

2.15. The Terminal Deoxynucleotidyl Transferase-Mediated dUTPbiotin Nick End Labeling (TUNEL) Assay. CMVECs were previously seeded on poly-l-lysine-treated coverslips. Fixed cells were stained using a terminal deoxynucleotidyl transferase-mediated dUTPbiotin nick end labeling (TUNEL) kit according to the manufacturer's instructions (Click-iT Plus TUNEL Kit, Thermo Fisher), and cell nuclei were stained with DAPI, as previously reported [18]. For quantification, the TUNEL-positive cells were counted in at least five randomly chosen visual fields in three independent samples under a fluorescence microscope (Olympus). The total number of cells was counted using DAPI staining, and the average ratio of TUNEL-positive cells was calculated.

2.16. Western Blot Analysis. Western blot analysis of total protein from CMVECs was performed as previously described [29]. The protein extracts were separated by SDS-polyacrylamide gel electrophoresis (SDS-PAGE) and transferred onto polyvinylidene difluoride (PVDF) membranes. After blocking overnight in a nonfat milk solution, the membranes were probed with primary antibodies against proteins such as IGF-1, Bcl-2, Bax, procaspase-3, cleaved caspase-3, β -actin, or GAPDH. The PVDF membranes were incubated with horseradish peroxidase-conjugated secondary antibodies for 1 h, followed by incubation with enhanced chemiluminescence reagent (Amersham Biosciences, USA). Immunoreactivity was visualized by a ChemiDoc MP system.

2.17. Statistical Analysis. The data were processed with the SPSS 21.0 statistical package (IBM, Armonk, NY, USA). Measurement data were normally distributed, and the results are expressed as the mean \pm standard deviation. Multiple groups were compared using one-way analysis of variance (ANOVA), followed by least significant difference (LSD) or Dunnett's T3 post hoc test for multiple comparisons. In addition, differences were considered significant at $P < 0.05$.

3. Results

3.1. Exosomes Derived from Hypoxia-Pretreated CMs Are Transferred to CMVECs and Protect CMVECs from Oxidative Damage. CMs were obtained [30] by using previously published methods. Immunofluorescence staining showed that the CMs expressed cTnT (Figure 1(a)). Next, we used a CCK-8 assay to examine the response of the CMs to hypoxia for 0, 6, 12, or 24 h. The cell viability remained $>90\%$ after hypoxia for 6 h and was not significantly different between normoxic and hypoxic conditions, while hypoxia for 12 h significantly increased cell viability ($P < 0.05$). However, the cell viability was significantly reduced ($P < 0.05$) after hypoxia for 24 h compared with normoxic conditions (Figure 1(b)). Therefore, we adopted the 12 h hypoxia pretreatment as the optimized treatment time.

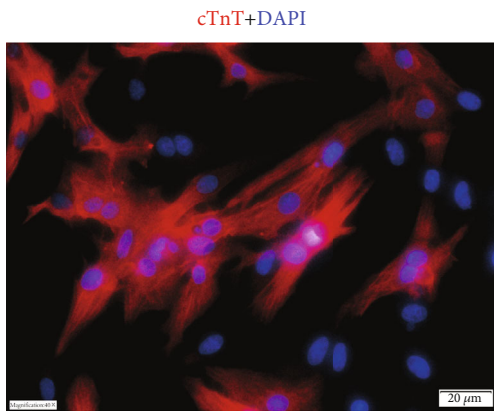
The characteristic cobblestone morphology of CMVECs was observed under a light microscope (Figure 1(c)). FCM was used to analyze CMVECs for blood cell and endothelial markers (CD31, CD34, and vWF) [36]. The results indicated that CMVECs were positive for CD31, CD34, and vWF (Figure 1(c)).

Exosomes were isolated from conditioned media by ultracentrifugation after CMs were cultured under hypoxic or normoxic conditions. To evaluate whether hypoxia modulates the profile of exosomes released by CMs, we used TEM and NTA to assess the number, size, and morphology of the exosomes. TEM showed that the exosomes exhibited a round morphology with a cup-like shape and were approximately 30–160 nm in diameter, and the profiles of the exosomes secreted from the two groups were similar (Figure 1(d)). NTA analysis confirmed the purity of particles was approximately 90% and suggested a physically homogeneous population; the mean hydrodynamic diameter for both normoxic exosomes (Nor-exos) and hypoxic exosomes (HPC-exos) was 151 nm. The presence of the surface markers CD63, CD9, and Alix typically enriched in exosomes was detected by Western blotting in CM-exos (Figure 1(e)), which indicated that the isolation procedure gave rise to a population of vesicles highly enriched in exosomes even after the CMs were exposed to hypoxia.

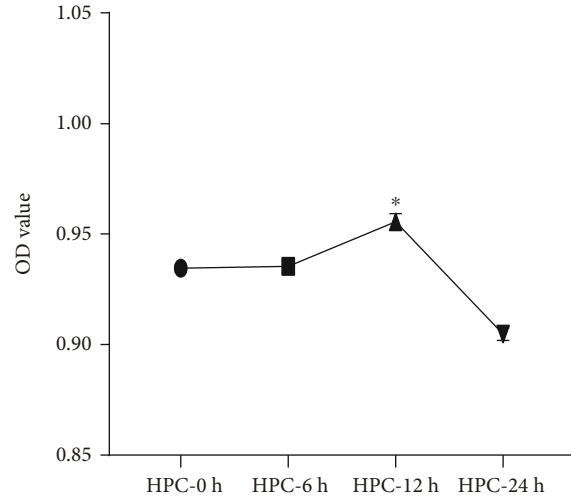
Exosome internalization is one of the mechanisms for cargo delivery to recipient cells [34]. In this study, we labeled exosomes with DiI and evaluated the internalization of exosomes into CMVECs. After the labeled CM-exos (300 $\mu\text{g}/\text{ml}$) were incubated with CMVECs for 24 h and counterstained with DAPI to visualize the nuclei, the fluorescence image showed that red fluorescence emission localized in the cytoplasm of the CMVECs, which indicated successful internalization of DiI-labeled exosomes by CMVECs (Figure 1(f)). Additionally, the quantification of cell proliferation with different concentrations of exosomes incubated under oxidative conditions showed that treatment of CMVECs with 300 $\mu\text{g}/\text{ml}$ HPC-exos 24 h could significantly improve cell proliferation. Above 300 $\mu\text{g}/\text{ml}$, the cell viability did not significantly increase with increasing exosome concentration (Figures 1(g) and 1(h)). Therefore, we adopted the 300 $\mu\text{g}/\text{ml}$ CM-exos treatment for 24 h as the exosome treatment condition in the subsequent experiments.

To establish an in vitro model of CMVEC apoptosis, H_2O_2 (50, 100, 200, and 300 μM) was selected to stimulate CMVECs for 3 h. The FCM results indicated that after 3 h of incubation, H_2O_2 could induce cell apoptosis in a concentration-dependent manner ($P < 0.05$). Exposure to 200 μM H_2O_2 for 3 h resulted in the apoptosis of 72.49% of CMVECs, which was significantly higher ($P < 0.05$) than the apoptosis observed under control conditions (Figures 2(a) and 2(b)), and most of the detected apoptosis events were early apoptotic cells. Therefore, we chose 200 μM H_2O_2 for 3 h to induce apoptosis in subsequent experiments.

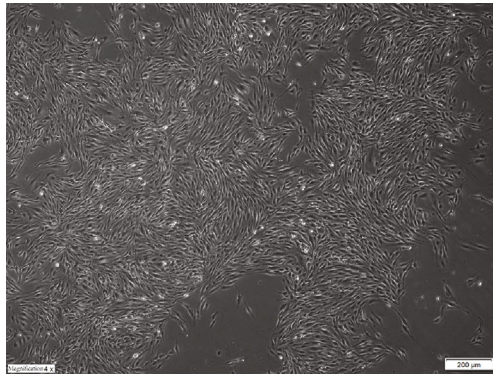
To investigate the regulatory effects of CM-exos on CMVECs under oxidative stress, we evaluated the impact of Nor-exos and HPC-exos on the capacity of cells to respond to oxidative stress. CMVECs ($>1 \times 10^9$) were cultured with Nor-exos or HPC-exos (300 $\mu\text{g}/\text{ml}$) for 24 h and then



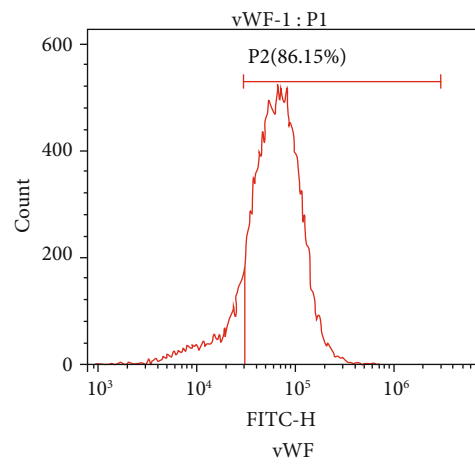
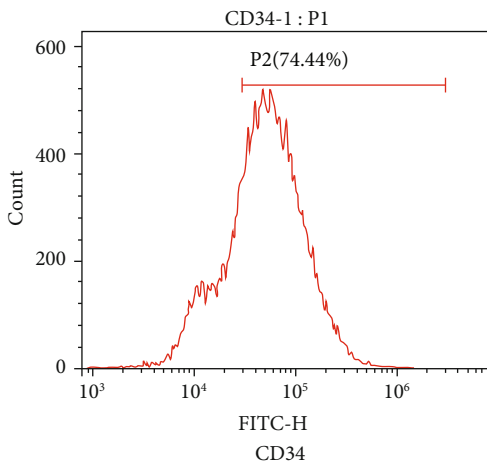
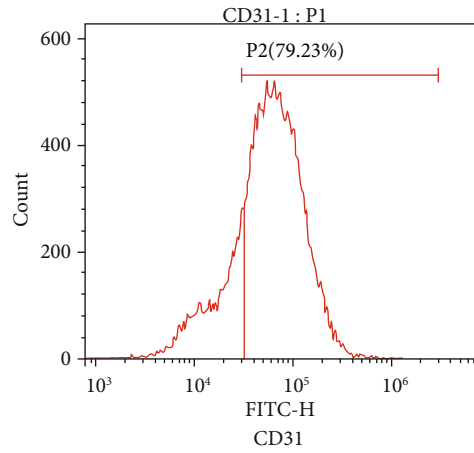
(a)



(b)



CMVECs



(c)

FIGURE 1: Continued.

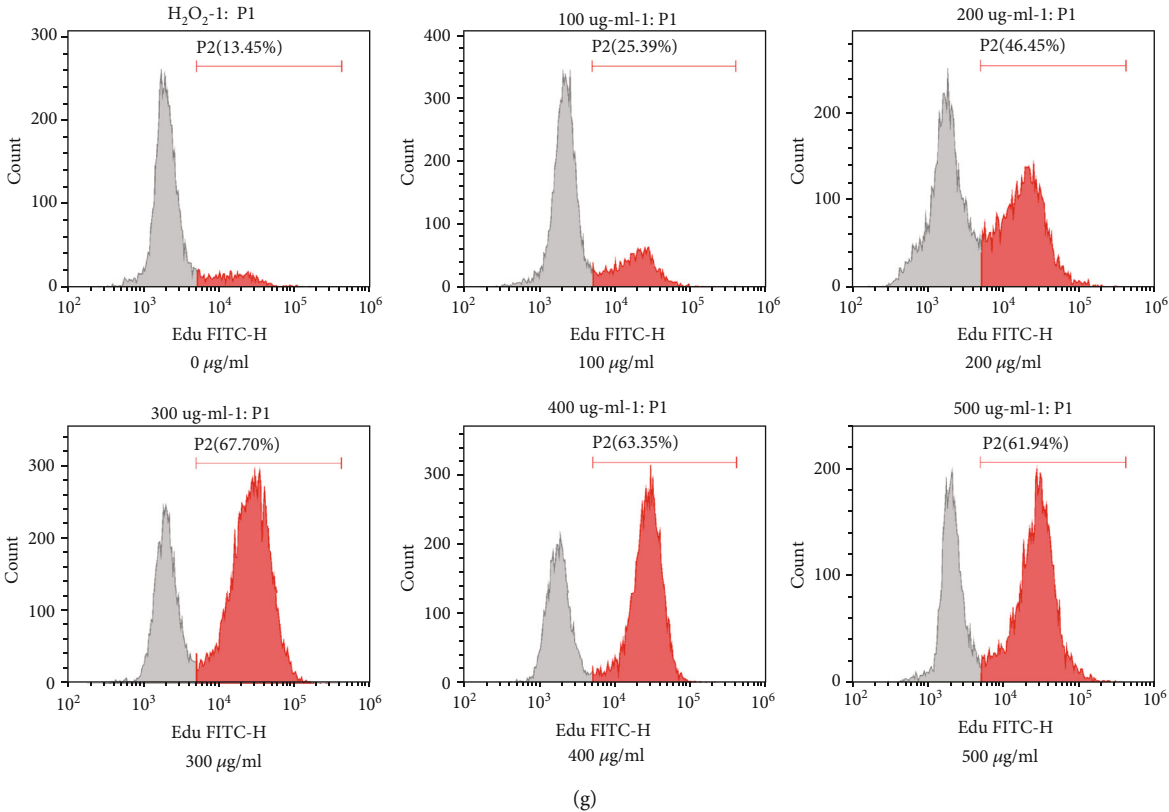
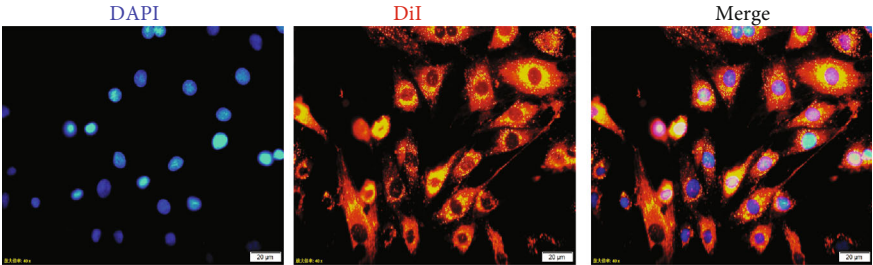
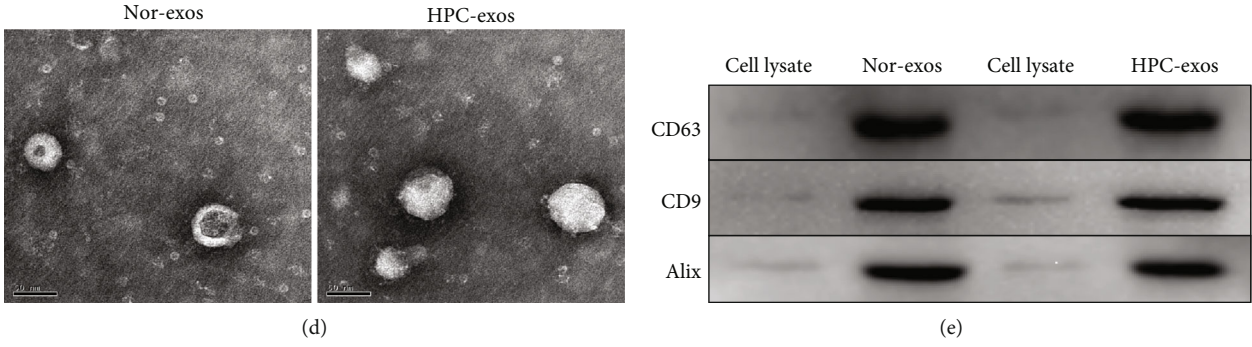


FIGURE 1: Continued.

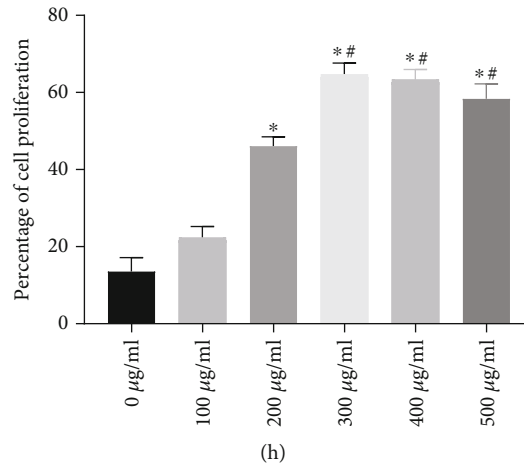


FIGURE 1: Characterization of CMs, CMVECs, exosomes, and cellular internalization. (a) Purified CMs were double stained for cTnT (red) and DAPI (blue) and observed under a fluorescence microscope (Olympus, Japan). (b) The CCK-8 assay showed that hypoxia pretreatment for 12 h significantly increased cell viability. (c) A confluent endothelial monolayer with cobblestone morphology was observed by inverted microscopy. The typical surface antigens of CMVECs, CD31, CD34, and vWF were detected by FMC. (d) Transmission electron microscopy analysis of CM-exos in two groups. Scale bar = 100 nm. (e) Western blotting of the exosome markers CD63, CD9, and Alix. (f) Fluorescence photomicrographs showing internalized DiI-labeled CM-exos (red) in DAPI-labeled CMVECs (blue). Scale bar = 20 μ m. (g) Representative dot plots of cell proliferation after EdU staining. (h) Quantitative analysis of proliferative cells. $n = 3$; * $P < 0.05$ compared with 0 μ g/ml; # $P < 0.05$ compared with 200 μ g/ml.

exposed to H_2O_2 (200 μ M) for 3 h to induce oxidative stress. The FCM results indicated significantly higher apoptosis rates and ROS production levels in the H_2O_2 -treated group than in the control group. The CMVECs pretreated with CM-exos exhibited a significantly decreased percentage of apoptotic cells and reduced ROS production. Moreover, compared with Nor-exos pretreatment, HPC-exos pretreatment significantly improved the viability of CMVECs subjected to oxidative stress, suggesting that HPC-exos can be more protective than Nor-exos (Figures 2(c)–2(f)). Intracellular MDA and SOD levels, which reflect oxidation levels, were also detected by an assay kit. As shown in Figures 2(g) and 2(h), compared with the H_2O_2 group and the Nor-exos group, the HPC-exos group had decreased MDA levels and increased SOD activity. Next, we examined whether exosomes protected CMVECs against H_2O_2 -induced DNA fragmentation. As shown in Figures 2(i) and 2(j), the percentage of TUNEL-positive cells was significantly increased in the H_2O_2 -treated group compared with the control group. Furthermore, the percentage of TUNEL-positive cells was significantly reduced in the Nor-exos-treated group and the HPC-exos-treated group, compared with the H_2O_2 group. Moreover, HPC-exos induced more regulatory effects than the Nor-exos group. The levels of cell apoptosis-related genes, such as procaspase-3, cleaved caspase-3, Bax, and Bcl-2, were also detected by Western blotting. Not surprisingly, compared with H_2O_2 -treated cells, HPC-exos-treated cells displayed substantially decreased levels of cleaved caspase-3 and Bax and increased levels of Bcl-2 (Figures 2(k) and 2(l)). Collectively, these results indicate that HPC-exos might exert a strong protective effect against H_2O_2 -induced oxidative damage in CMVECs.

3.2. Exosomal circHIPK3 Derived from Hypoxia-Pretreated CMs Induces the Protection of Oxidative Injury in CMVECs. circRNA can be transferred into target cells by exosomes [21]. Exosomes derived from CMs cultured under hypoxic conditions have a greater reparative capacity than exosomes from normal cells. It is important to investigate the content of circRNA with potential biological functions in exosomes released under certain hypoxic conditions. circBase retrieval revealed that the HIPK3 host gene might produce 20 circRNAs in the human genome and 3 circRNAs in the mouse genome. One circRNA (mmu_circ_0001052) from the HIPK3 host gene in mice was identified in endothelial cells followed by RNase R treatment and could regulate endothelial proliferation and vascular dysfunction [29]. qRT-PCR assays revealed that circHIPK3 was significantly upregulated in HPC-exos compared with Nor-exos (Figure 3(a)). circHIPK3 expression was also detected in CMVECs after pretreatment with HPC-exos or Nor-exos (Figure 3(b)). qRT-PCR analysis revealed that circHIPK3 levels were substantially downregulated in CMVECs treated with H_2O_2 compared with control CMVECs. Compared with Nor-exos pretreatment, HPC-exos pretreatment significantly rescued the circHIPK3 levels of CMVECs subjected to oxidative stress, suggesting the existence of a possible negative connection between circHIPK3 and H_2O_2 -induced oxidative damage in CMVECs.

We next investigated the role of circHIPK3 in CMVECs. First, we conducted gain-of-function and loss-of-function analyses of circHIPK3 and determined whether circHIPK3 alone was sufficient to protect CMVECs from oxidative damage. Cells were transfected with the circHIPK3 expression lentiviral vector (LV-circHIPK3), siRNA-circHIPK3 expression lentiviral vector (LV-sircHIPK3), or lentiviral vector

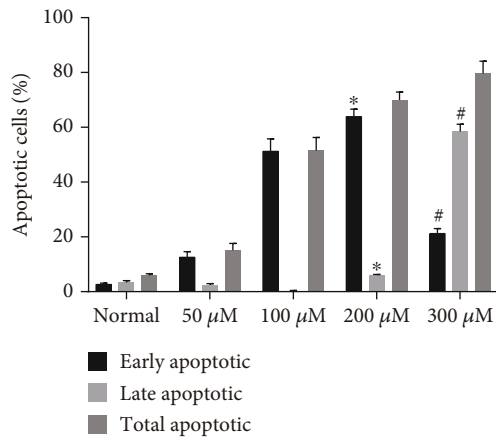
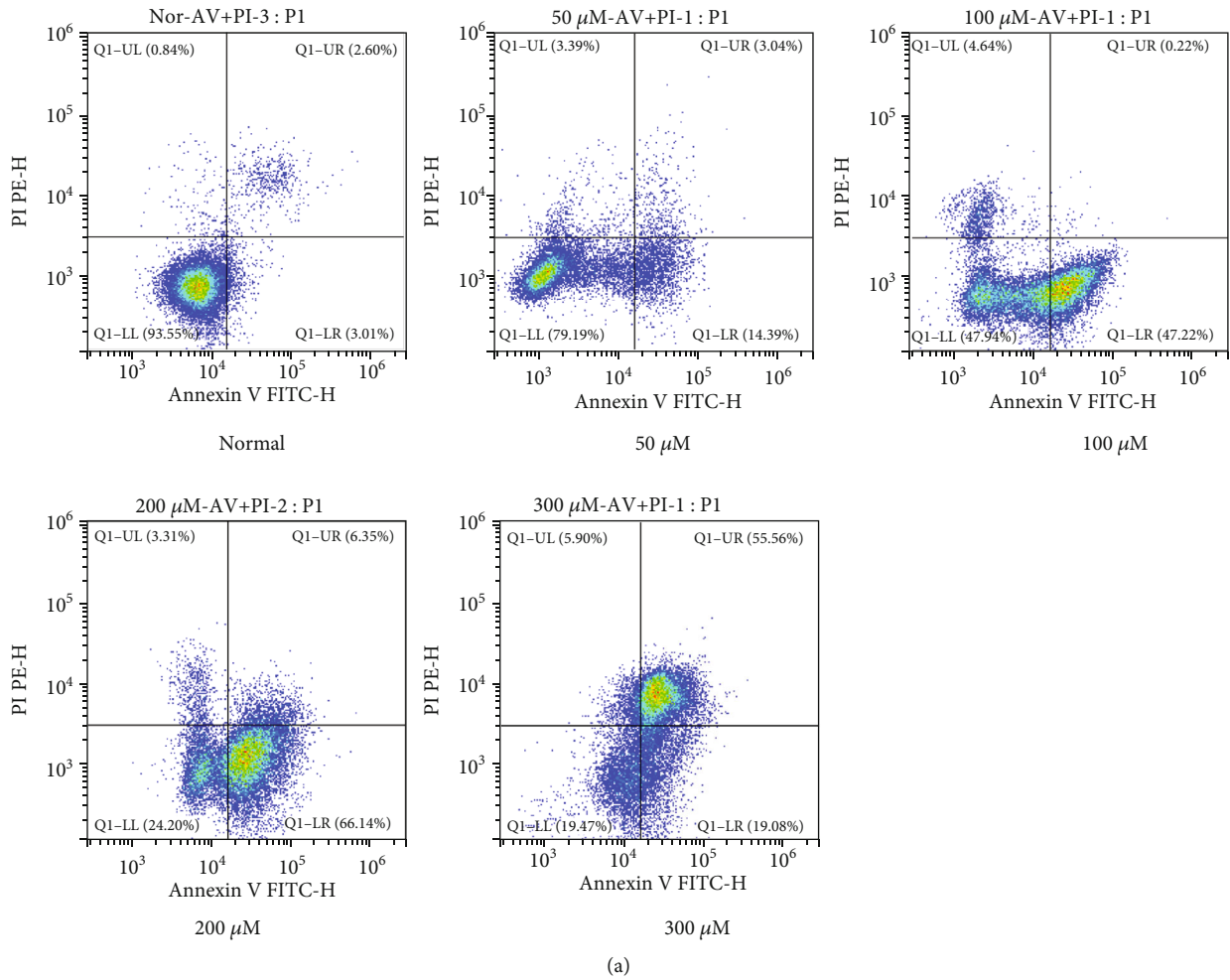
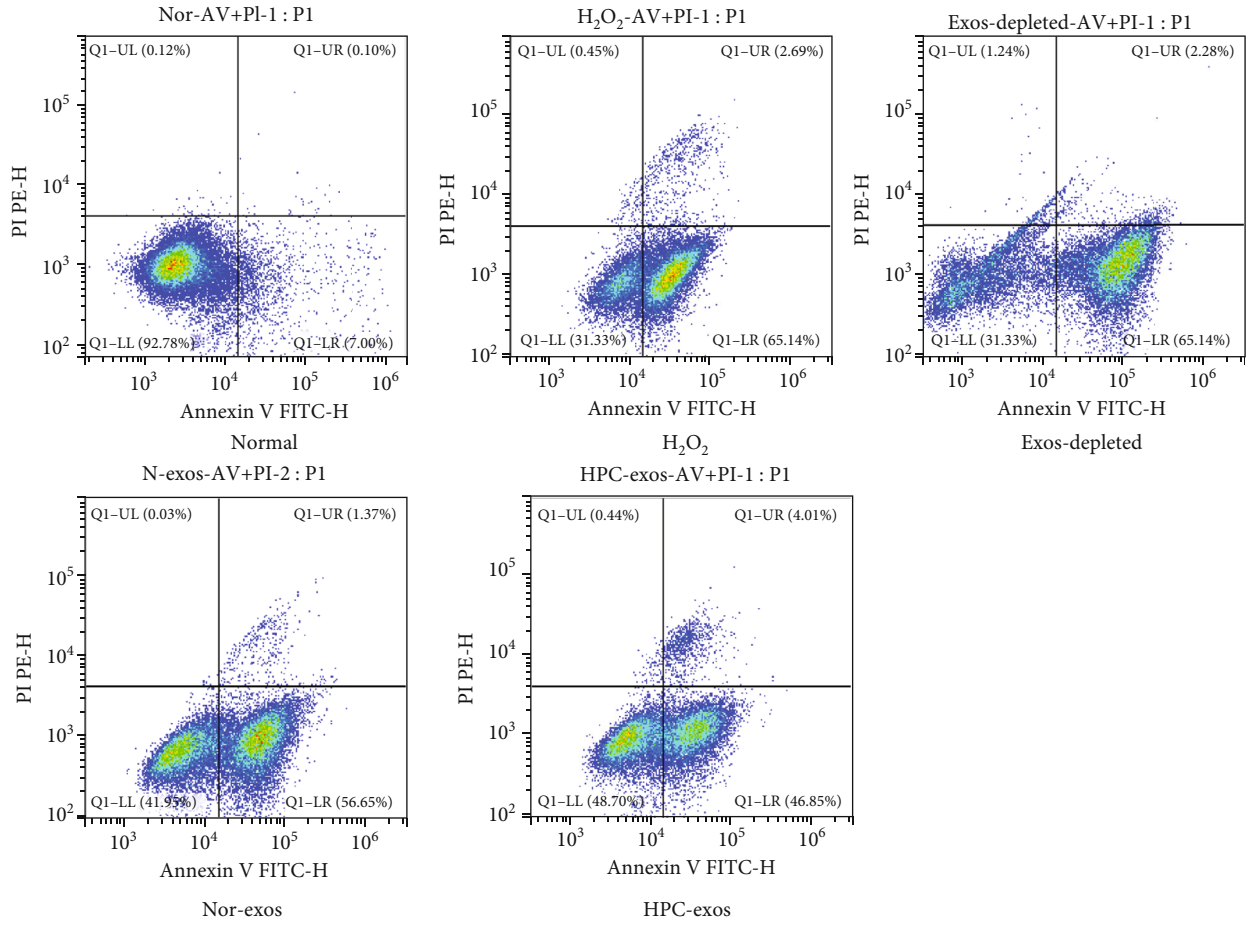
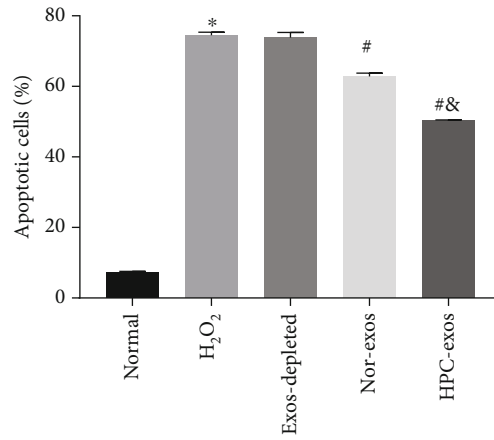


FIGURE 2: Continued.

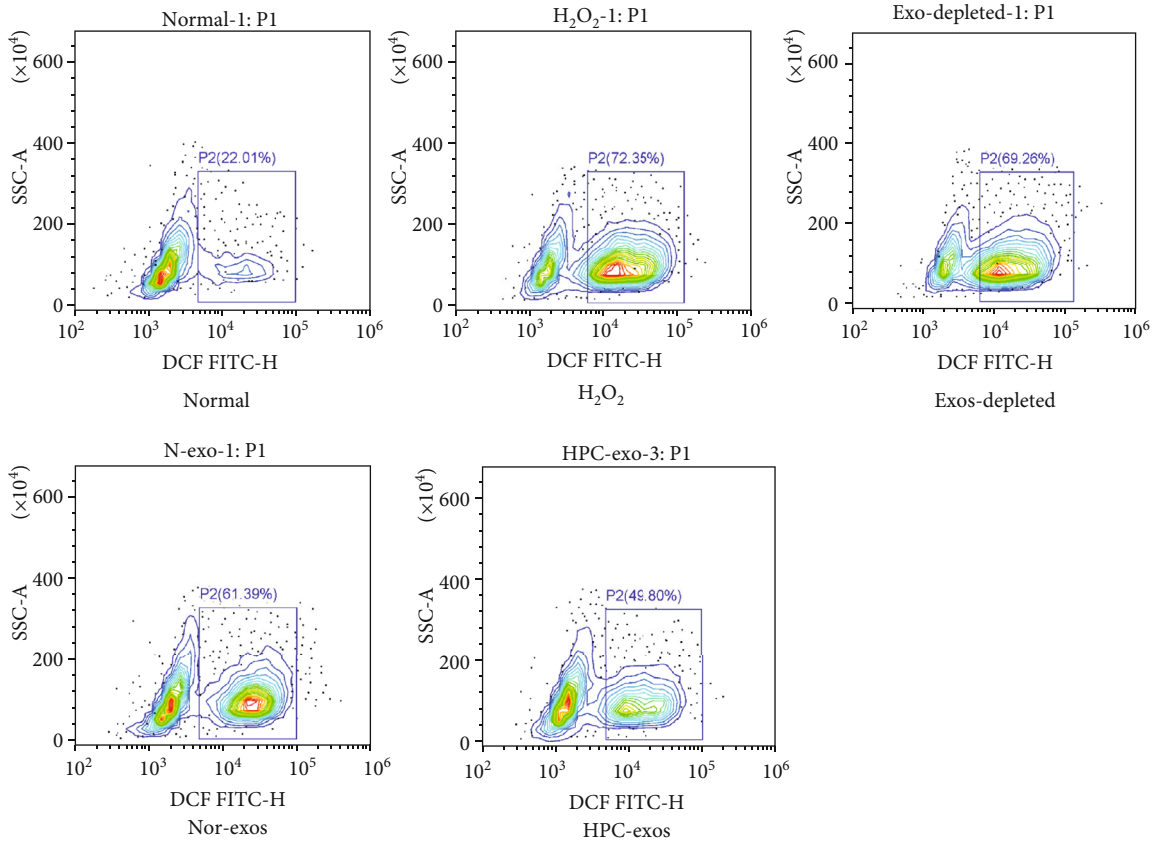


(c)

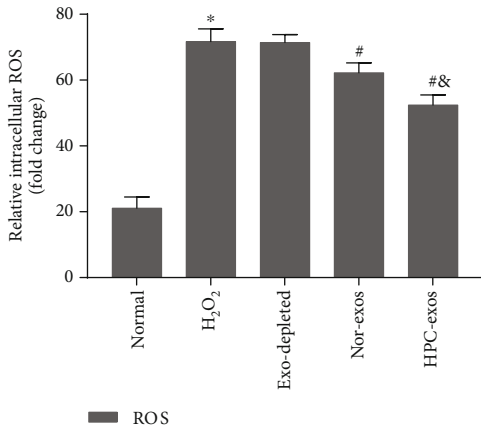


(d)

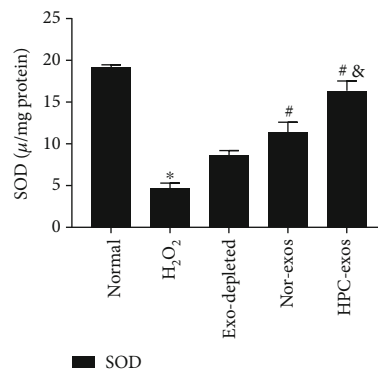
FIGURE 2: Continued.



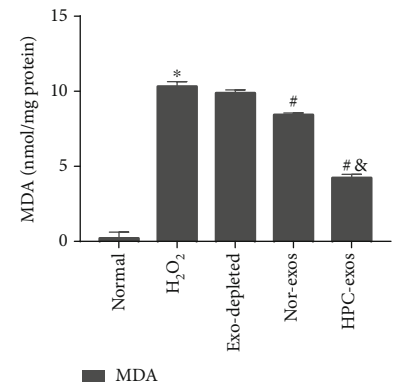
(e)



(f)



(g)



(h)

FIGURE 2: Continued.

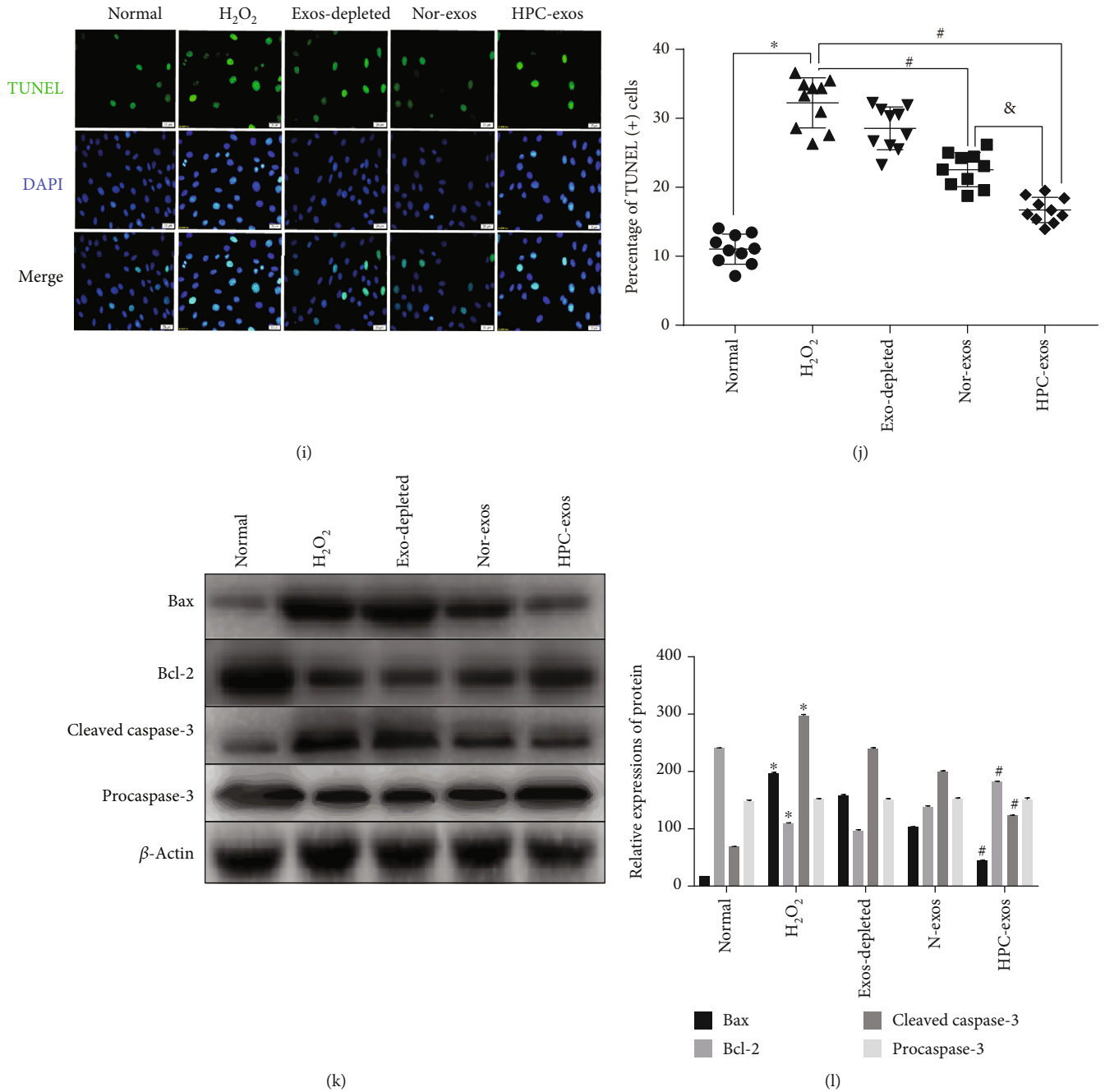


FIGURE 2: Exosomes released from hypoxia-pretreated CMs protect CMVECs from oxidative stress injury. CMVECs were pretreated with CM-exos (300 $\mu\text{g}/\text{ml}$) for 24 h before incubation with 200 μM H_2O_2 for 3 h and then subjected to analysis. (a) Representative dot plots of cell apoptosis after Annexin V/PI dual staining are shown. The left upper quadrant (% gated) shows necrotic cells (Annexin V $^-$ /PI $^+$); the upper right quadrant (% gated) shows late apoptotic cells (Annexin V $^+$ /PI $^+$); the lower left quadrant (% gated) shows live cells (Annexin V $^-$ /PI $^-$); and the lower right quadrant (% gated) shows early apoptotic cells (Annexin V $^+$ /PI $^-$). (b) The percentage of apoptotic cells represents total apoptotic cells, including both early and late apoptotic cells; $n = 3$. (c) Representative dot plots of cell apoptosis after Annexin V/PI dual staining are shown. (d) The percentage of apoptotic cells represents both early and late apoptotic cells; $n = 3$. (e) The intracellular ROS level was determined by FCM. The P2 percentage indicates the proportion of cells with increased ROS production, with signals above background 2',7'-dichlorofluorescein (DCF) fluorescence levels. (f) Quantitative analysis of ROS levels; $n = 3$. (g) Graph represents SOD levels; $n = 9$. (h) Graph represents MDA levels; $n = 9$. (i) Representative immunofluorescence of TUNEL (green) and DAPI (blue) staining and merged images. Photos were randomly captured using a fluorescence microscope. Scale bar = 20 μm . (j) The panel shows the percentage of TUNEL-positive cells; $n = 6$. (k) Apoptosis-related genes, such as procaspase-3, cleaved caspase-3, Bax, and Bcl-2, were detected by immunoblotting. (l) Quantitative analysis of the apoptosis-related proteins; $n = 3$. * $P < 0.05$ compared with the control group; # $P < 0.05$ compared with the H_2O_2 group; & $P < 0.05$ compared with the Nor-exos group.

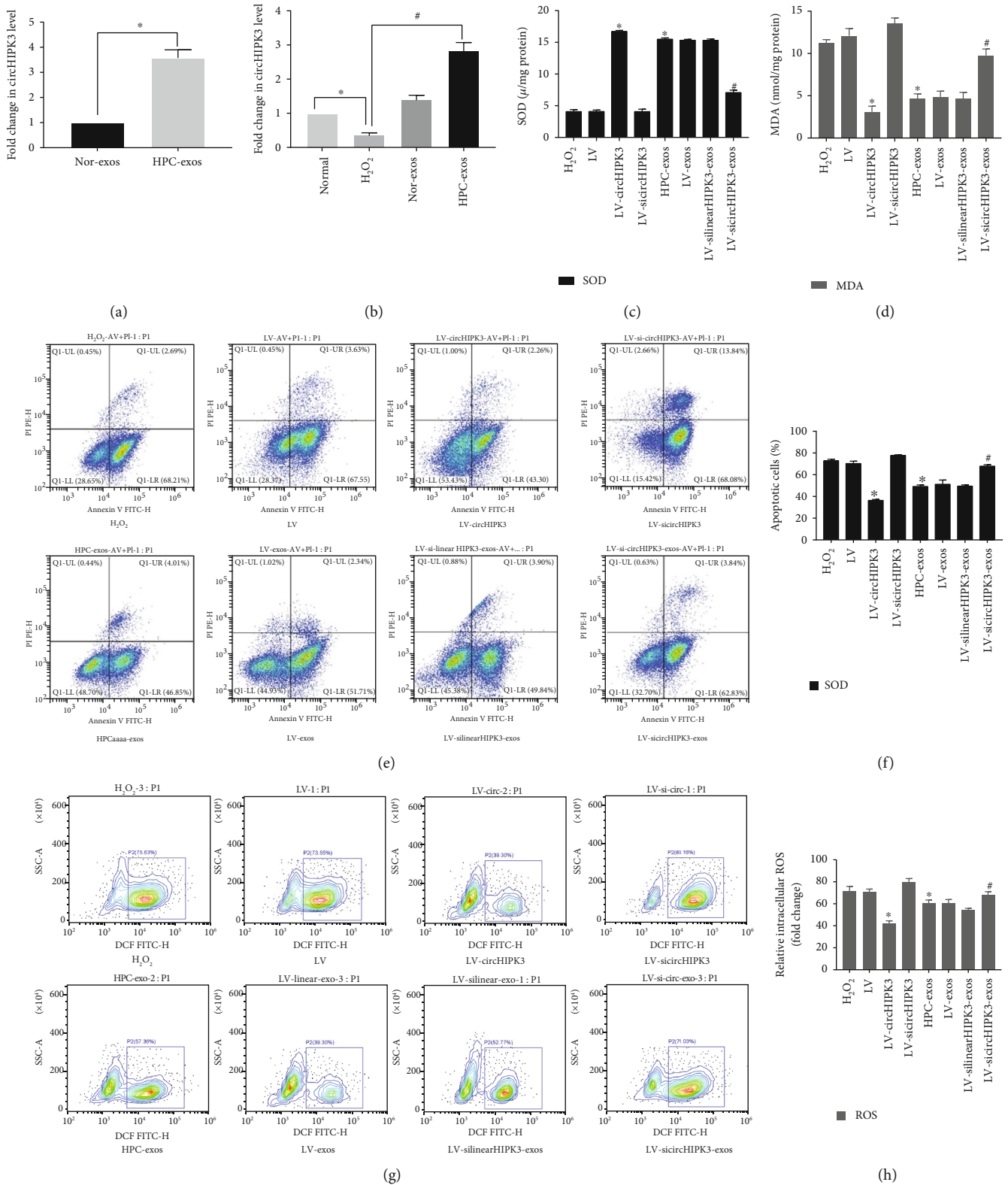


FIGURE 3: Continued.

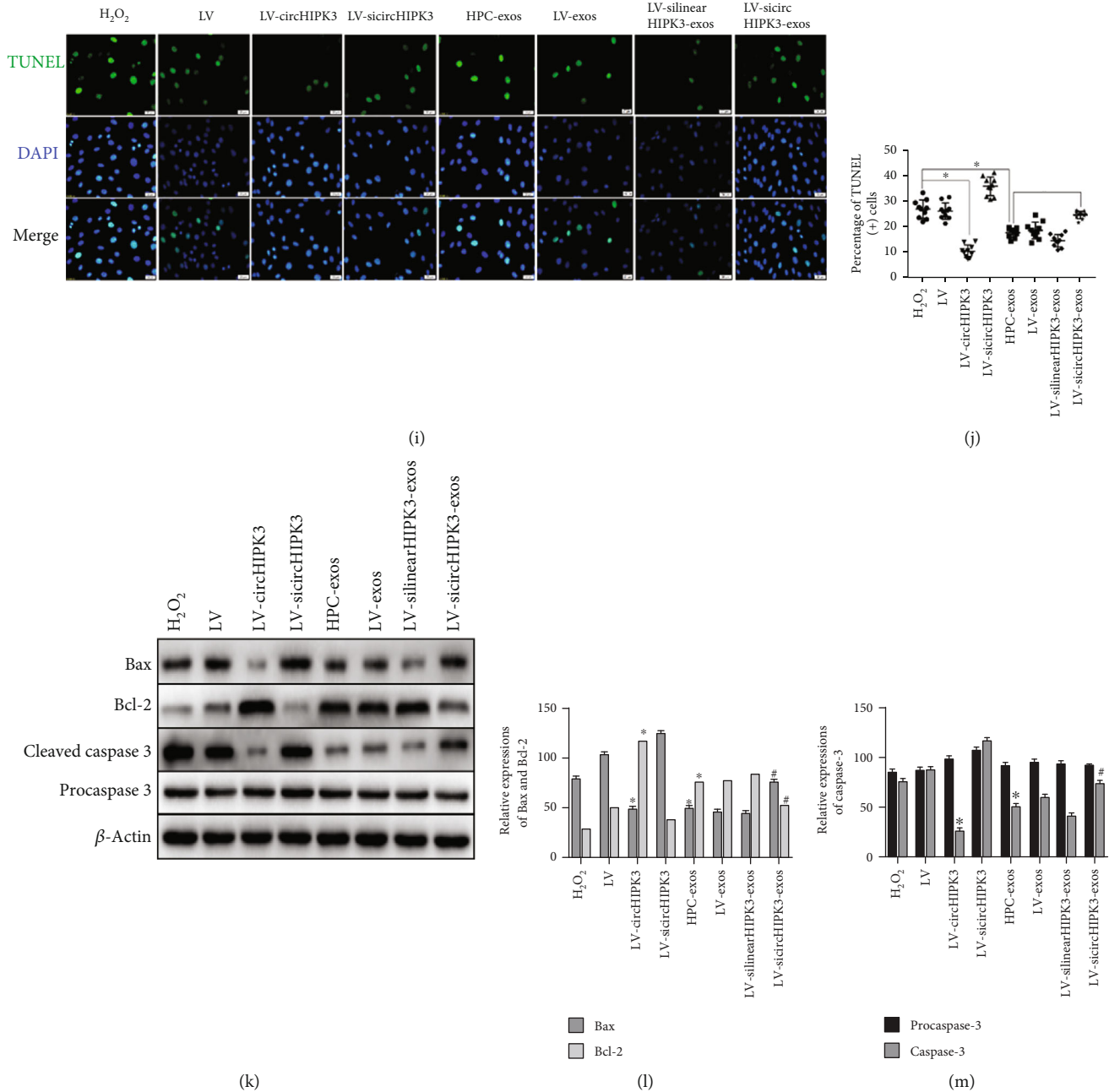


FIGURE 3: Exosomes derived from circHIPK3-enriched CMs exert an antioxidant effect on CMVECs under oxidative stress. CMVECs were transfected with negative control, circHIPK3, or circHIPK3 siRNA for 48 h. Exosomes were isolated from CMs transfected with negative control siRNA, linear circHIPK3 siRNA, and circHIPK3 siRNA and then incubated under hypoxic conditions. These exosomes were cocultured with CMVECs for 24 h and then processed under oxidative stress conditions for 2 h. (a) qRT-PCR analysis of circHIPK3 expression in exosomes after different treatments; $n = 9$. (b) qRT-PCR analysis of circHIPK3 expression in CMVECs after different treatments; $n = 9$. (c) Graph represents SOD levels; $n = 9$. (d) Graph represents MDA levels; $n = 9$. (e) Representative dot plots of cell apoptosis after Annexin V/PI dual staining are shown. (f) The percentage of apoptotic cells represents both early and late apoptotic cells; $n = 3$. (g) The intracellular ROS level was determined by FCM. The P2 percentage indicates the proportion of cells with increased ROS production, with signals above background 2',7'-dichlorofluorescein (DCF) fluorescence levels. (h) Quantitative analysis of the ROS levels; $n = 3$. (i) Representative immunofluorescence of TUNEL (green) and DAPI (blue) staining and merged images. Photos were randomly captured using a fluorescence microscope. Scale bar = 20 μm . (j) The panel shows the percentage of TUNEL-positive cells; $n = 6$. (k) Apoptosis-related genes, such as procaspase-3, cleaved caspase-3, Bax, and Bcl-2, were detected by immunoblotting. (l, m) Quantitative analysis of the apoptosis-related proteins; $n = 3$. * $P < 0.05$ compared with the H₂O₂ group; # $P < 0.05$ compared with the HPC-exos group.

empty vector (LV). In CMVECs under oxidative conditions, circHIPK3 overexpression significantly decreased apoptosis and oxidative status (including ROS, SOD, and MDA) (Figures 3(c)–3(j)), upregulated the antiapoptotic protein Bcl-2, and downregulated the proapoptotic proteins Bax and cleaved caspase-3 (Figures 3(k)–3(m)). Additionally, siRNAs were designed for circHIPK3 silencing (LV-sircHIPK3), which was verified to significantly downregulate circHIPK3 expression [29]. FCM analysis and TUNEL assays revealed that compared with H₂O₂ treatment, siRNA transfection did not markedly affect CMVECs apoptosis or ROS production (Figures 3(c)–3(h)). LV-sircHIPK3 clearly increased the levels of MDA and the proapoptotic proteins Bax and cleaved caspase-3 and decreased SOD production and the antiapoptotic protein Bcl-2; the LV-sircHIPK3 and H₂O₂ treatment groups were not significantly different (Figures 3(i)–3(k)).

To further determine whether the effects of HPC-exos on CMVECs are dependent on circHIPK3 and not linear HIPK3, the impact of linearHIPK3 or circHIPK3 loss-of-function in HPC-exos was determined. CMs were pretreated with negative control siRNA, linear HIPK3 siRNA, or circHIPK3 siRNA for 48 h. After transfection, the cells were incubated under hypoxic conditions for 12 h, and their exosomes (named LV-exos, LV-silinearHIPK3-exos, and LV-sircHIPK3-exos) were collected. Then, the exosomes were cocultured with CMVECs. Interestingly, LV-sircHIPK3-exos but not LV-exos or LV-silinearHIPK3-exos could partially neutralize the protective effect of HPC-exos; compared with the HPC-exos group, the LV-sircHIPK3-exos group displayed increased apoptosis and ROS production (Figures 3(c)–3(m)). qRT-PCR analysis of circHIPK3 expression revealed that compared with CMVECs treated with H₂O₂, CMVECs pretreated with HPC-exos or transfected with circHIPK3 had significantly increased circHIPK3 levels, whereas circHIPK3 siRNA-pretreated CMVECs displayed a further decrease in circHIPK3 expression under oxidative stress. Interestingly, compared with the HPC-exos group, CMVECs pretreated with LV-sircHIPK3-exos had significantly decreased circHIPK3 levels. In contrast, linear HIPK3 siRNA had no effect on regulating circHIPK3 expression (Figure 4(a)). These data confirmed the antioxidant function of circHIPK3 and suggested that rescuing downregulated circHIPK3 expression in CMVECs with HPC-exos is a potential strategy for protecting CMVECs from oxidative stress injury.

3.3. circHIPK3 Abundantly Sponges miR-29a in CMVECs. Stable transcripts with many miRNA-binding sites may function as miRNA sponges. circHIPK3 was mainly expressed in the cytoplasm of CMVECs. A previous study demonstrated that circHIPK3 could act as a miR-29a sponge and regulate cell growth [37]. We thus investigated the regulatory relationship between miR-29 and circHIPK3 expression levels in CMVECs. qRT-PCR showed that there was no significant change in the expression of miR-29a in each group (Figure 4(b)). If circHIPK3 indeed interact with miR-29a, circHIPK3 and miR-29a should be coexpressed in CMVECs. FISH assays showed that circHIPK3 and miR-29a were colo-

calized in the cytoplasm (Figure 4(c)). Next, we carried out luciferase reporter assays and demonstrated that the overexpression of miR-29a significantly decreased the luciferase activity of the vector containing the complete circHIPK3 sequence but did not affect the luciferase activity of the empty vector in CMVECs (Figure 4(d)). Furthermore, the AGO2 protein is a core component of the RNA-induced silencing complex (RISC) that binds miRNA complexes to target mRNAs or circRNAs. We conducted anti-AGO2 RIP in CMVECs transiently overexpressing miR-29a to pull down circHIPK3 using anti-AGO2 antibodies or control IgG, followed by RT-qPCR analysis. We observed increased enrichment of circHIPK3 in the miR-29a-captured fraction compared to the IgG fraction in RIP (Figures 4(e) and 4(f)), suggesting that miR-29a could directly target circHIPK3 in an AGO2-dependent manner. The above results implied that circHIPK3 can bind miR-29a but cannot change the expression of miR-29a.

3.4. miR-29a Upregulation in CMVECs Promotes Cell Apoptosis and Increases ROS Levels by Targeting IGF-1 In Vitro. To investigate the role of miR-29a in CMVECs, miR-29a gain-of-function and loss-of-function treatments were used to evaluate apoptosis and ROS status in CMVECs. The data showed that compared with the H₂O₂ treatment, the overexpression of miR-29a induced apoptosis and increased ROS levels, but the difference was not statistically significant. However, the inhibition of miR-29a significantly protected CMVECs from apoptosis and oxidative stress injury following H₂O₂ insult (Figures 5(a)–5(d)). The levels of apoptosis-related genes were also detected by Western blotting. The proapoptotic genes cleaved caspase-3 and Bax were substantially decreased, and the antiapoptotic gene Bcl-2 was significantly increased in the inhibitor group compared with the H₂O₂ group (Figures 5(e)–5(l)). Subsequently, we searched the miRanda database to predict miR-29a targets. As shown in Figure 5(h), the 3' untranslated region (3'-UTR) of IGF-1 contains two putative binding motifs of miR-29a. Increasing evidence indicates that IGF-1 is involved in the inhibition of apoptosis through cellular signal transduction and metabolic mechanisms [38, 39]. In addition, miR-29a has been shown to regulate the apoptosis of MCs by repressing the expression of IGF-1 [40]. Luciferase reporter assays were performed to verify that IGF-1 is a target of miR-29a in CMVECs. The data showed that compared to that of miR-NC, the transfection of miR-29a mimics could reduce the activity of a luciferase reporter carrying the wild-type IGF-1-3'UTR (Figures 5(i) and 5(j)). Furthermore, the miR-29a mimics significantly increased and the miR-29a inhibitor significantly decreased miR-29a expression in CMVECs (Figure 5(k)). We also found that miR-29a mimics significantly reduced IGF-1 mRNA levels, whereas the miR-29a inhibitor induced the opposite effect in CMVECs (Figure 5(l)). Western blot showed that miR-29a downregulation markedly promoted IGF-1 expression, while the upregulation of miR-29a clearly reduced IGF-1 levels (Figures 5(m) and 5(n)). These results indicated that miR-29a could target IGF-1 and negatively regulate its expression

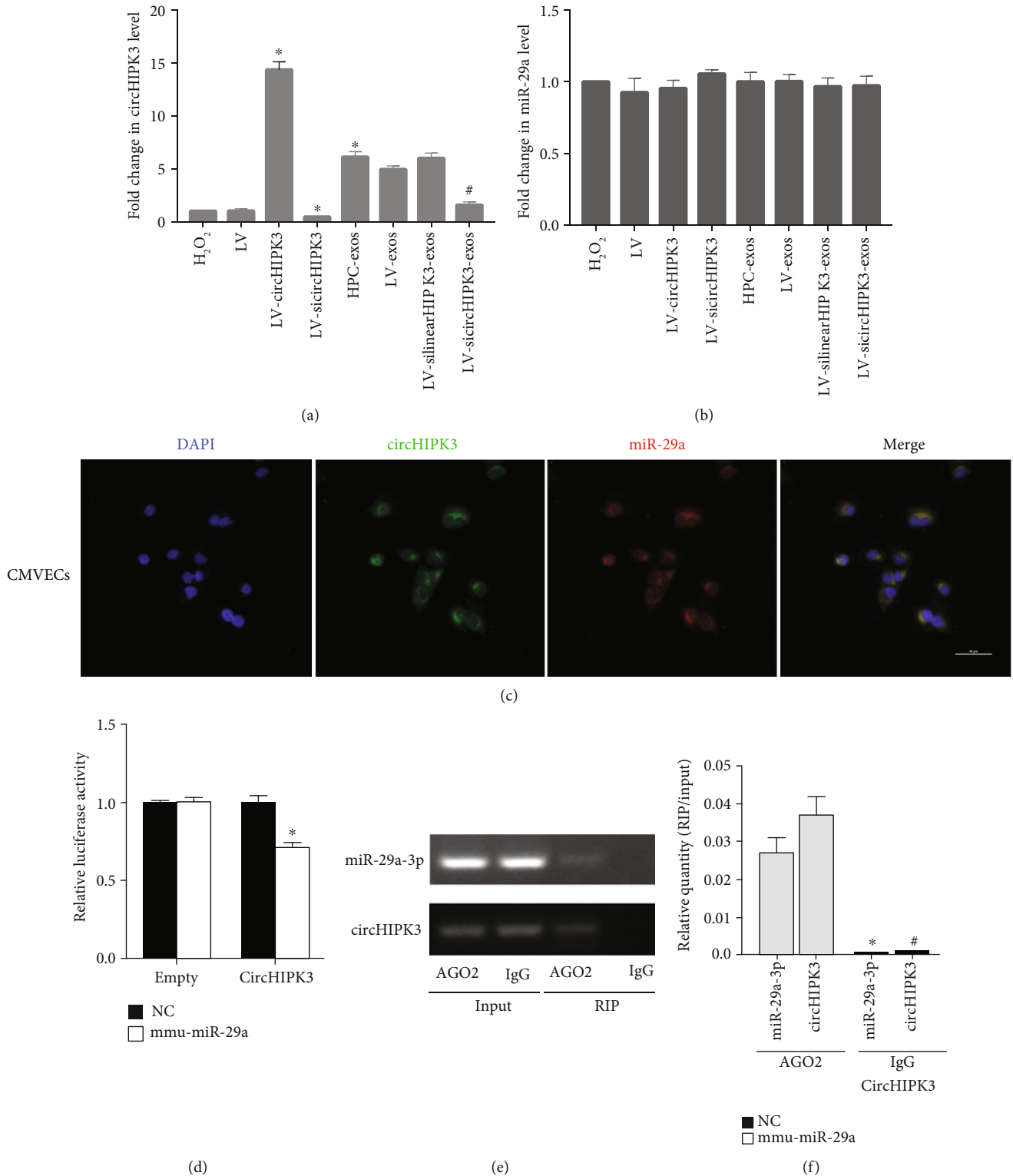
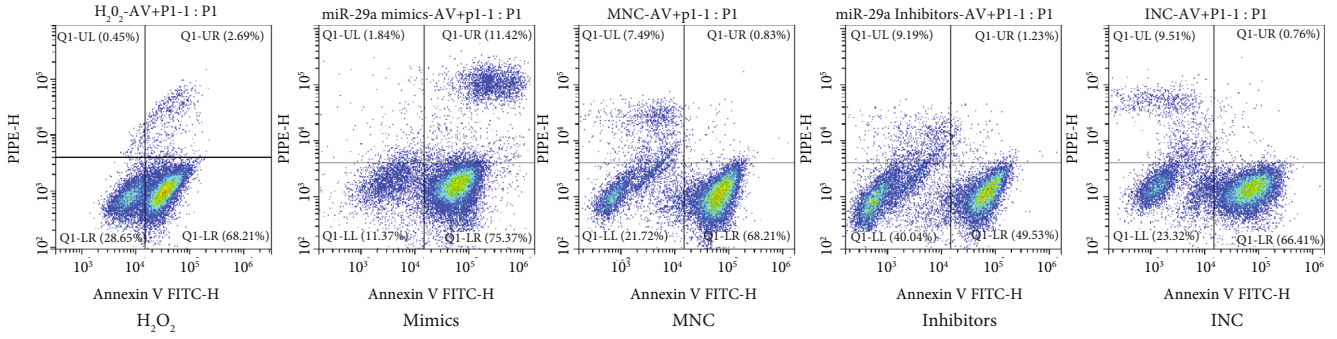
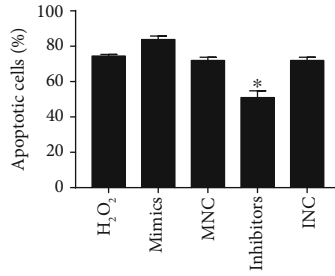


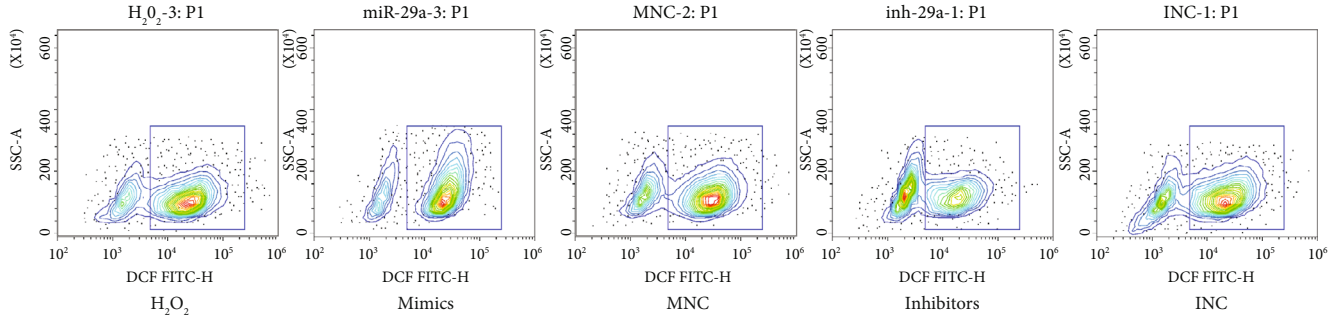
FIGURE 4: circHIPK3 directly binds to miR-29a. (a) qRT-PCR analysis of the expression of circHIPK3 in CMVECs after different treatments; $n = 9$; * $P < 0.05$ compared with the H₂O₂ group; * $P < 0.05$ compared with the HPC-exos group. (b) qRT-PCR analysis of the expression of miR-29a in CMVECs after different treatments. (c) FISH for circHIPK3 (green) and miR-29a (red) was detected in CMVECs. Scale bar = 50 μ m. (d) The relative luciferase activities were analyzed by cotransfection with miR-29a mimics or miR-NC and luciferase reporter vectors pmirGLO-circHIPK3-WT or pmirGLO-circHIPK3-empty. $n = 3$, * $P < 0.05$ compared with the empty group. (e, f) Anti-AGO2 RIP was performed in CMVECs transfected with miR-29a mimics or circHIPK3, followed by RT-PCR and qRT-PCR to detect miR-29a and circHIPK3. $n = 9$; * $P < 0.05$ compared with the miR-29a-3p-AGO2 group. # $P < 0.05$ compared with the circHIPK3-AGO2 group.



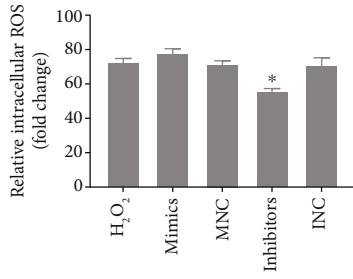
(a)



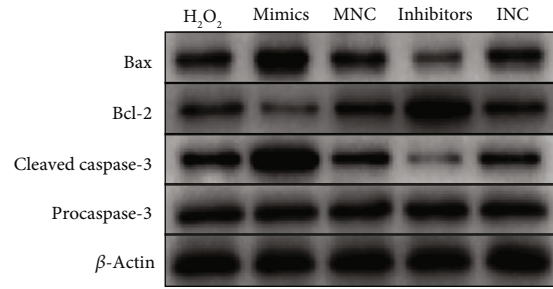
(b)



(c)



(d)



(e)

FIGURE 5: Continued.

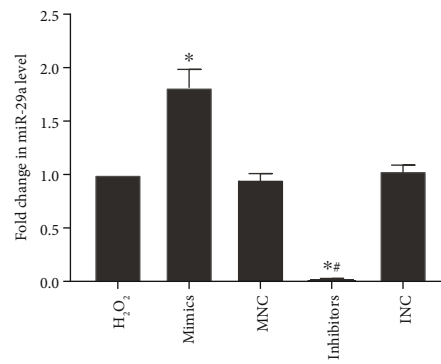
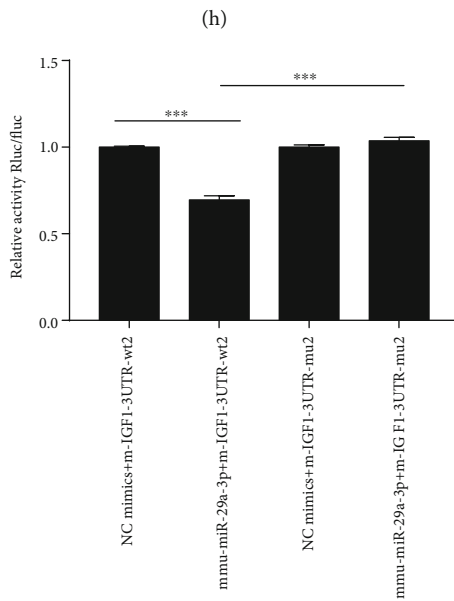
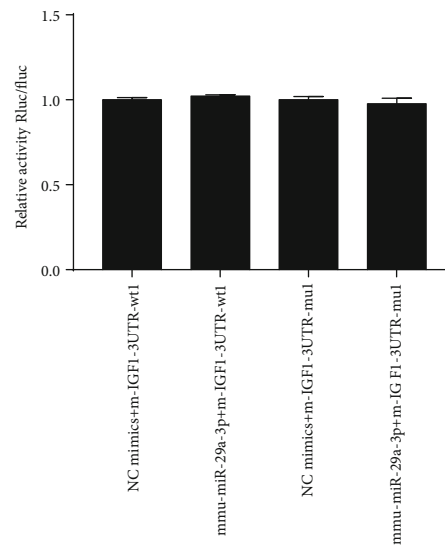
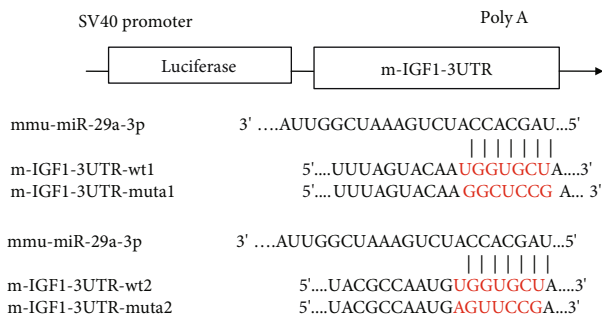
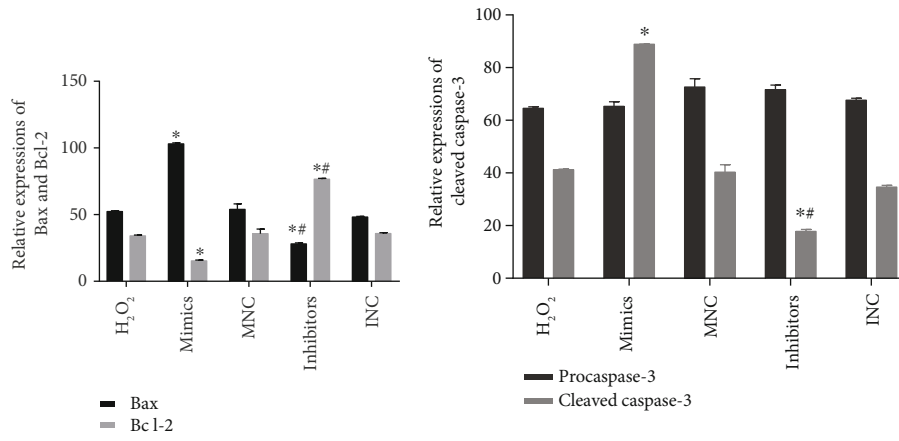


FIGURE 5: Continued.

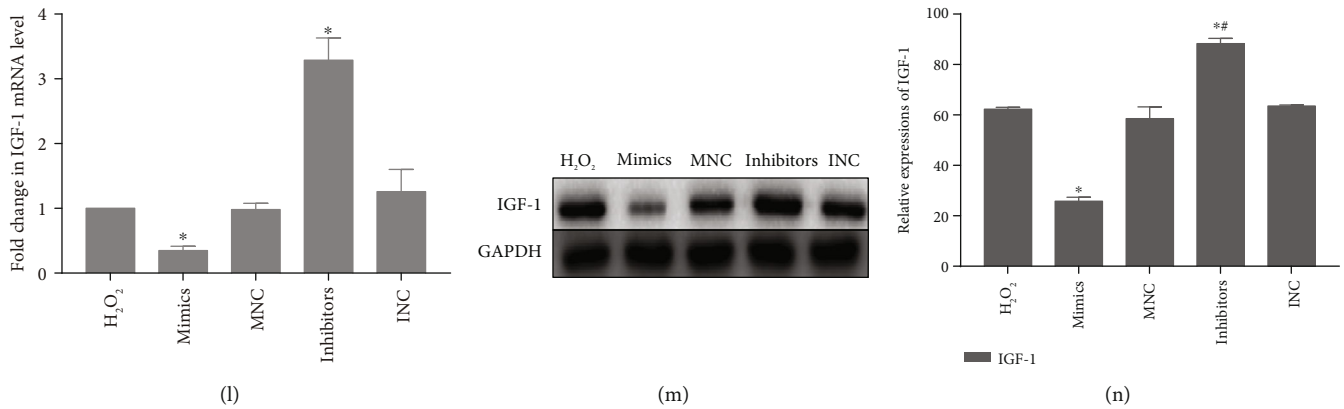


FIGURE 5: Overexpression of miR-29a promotes apoptosis through targeting IGF-1 in CMVECs. (a) Representative dot plots of cell apoptosis after Annexin V/PI dual staining are shown. (b) The percentage of apoptotic cells represents both early and late apoptotic cells; $n = 3$. (c) The intracellular ROS level was determined by FCM. The P2 percentage indicates the proportion of cells with increased ROS production, with signals above the background 2',7'-dichlorofluorescein (DCF) fluorescence levels. (d) Quantitative analysis of the ROS levels; $n = 3$. (e) Apoptosis-related genes, such as procaspase-3, cleaved caspase-3, Bax, and Bcl-2, were detected by immunoblotting. (f, g) Quantitative analysis of the apoptosis-related proteins; $n = 3$. (h) A schematic diagram of the putative binding between IGF-1 and miR-29a. (i, j) The relative luciferase activities were analyzed by cotransfecting miR-29a mimics or miR-NC and the luciferase reporter vectors pmirGLO-LGF-1-Mut or pmirGLO-IGF-1-WT. (k) qRT-PCR analysis of miR-29a expression in CMVECs after different treatments; $n = 9$. (l) qRT-PCR analysis of IGF-1 mRNA expression in CMVECs after different treatments; $n = 9$. (m) IGF-1 protein expression was detected by immunoblotting. (n) Quantitative analysis of IGF-1 protein expression; $n = 3$. * $P < 0.05$ compared with the H₂O₂ group; # $P < 0.05$ compared with the mimics group; *** $P < 0.05$ compared with the NC-mimics-IGF1-WT group; **** $P < 0.05$ compared with the Mmu-mimics-IGF1-WT group.

and that miR-29a could promote oxidative damage in CMVECs partially through targeting IGF-1.

3.5. Exosomal circHIPK3 Derived from Hypoxia-Pretreated CMs Induces Protection from Oxidative Injury via miR-29a/IGF-1 in CMVECs. To investigate whether HPC-exos regulated oxidative damage in CMVECs by targeting IGF-1 via miR-29a sponging, we transfected CMVECs with miR-29a mimics, inhibitor, or negative control RNA. 48 h after transfection, HPC-exos were added to CMVECs for 24 h, and then the CMVECs were exposed to oxidative stress for 3 h. Compared with the H₂O₂ group, the HPC-exos group displayed substantially reduced apoptosis, whereas the HPC-exos+mimics group had significantly elevated apoptosis and the HPC-exos+inhibitor group had significantly decreased apoptosis (Figures 6(a) and 6(b)). The production of ROS was measured to further confirm the antioxidant ability of HPC-exos. The ROS production of the HPC-exos+mimics group was dramatically increased compared with that of the HPC-exos group. In contrast, ROS was further decreased in the HPC-exos+inhibitor group compared with the HPC-exos group in CMVECs, and the difference was statistically significant (Figures 6(c) and 6(d)). The percentage of TUNEL-positive cells was significantly increased in the HPC-exos+mimics group compared with the HPC-exos group. Furthermore, the percentage of TUNEL-positive cells was significantly decreased in the HPC-exos+inhibitor group compared with the HPC-exos group (Figures 6(e) and 6(f)). Apoptosis-related proteins were then detected by Western blotting. Indeed, compared with the H₂O₂-treated cells, cells treated with HPC-exos or HPC-exos+miR-29a inhibitor displayed substantially decreased expression of the proapoptotic proteins cleaved caspase-3 and Bax and increased expression

of the antiapoptotic protein Bcl-2. However, cells treated with HPC-exos+miR-29a mimics displayed the opposite results; caspase-3 and Bax levels were increased while Bcl-2 levels were decreased in the HPC-exos+mimics group compared with the H₂O₂ group (Figures 6(g)–6(i)). Next, IGF-1 protein levels were detected by Western blotting. In CMVECs exposed to H₂O₂, the IGF-1 protein levels of the HPC-exos+mimics and HPC-exos+inhibitor groups were downregulated and upregulated, respectively, compared with that of the HPC-exos group (Figures 6(j) and 6(k)). These data suggested that HPC-exos function as antioxidants to regulate CMVECs via the miR-29a/IGF-1 axis.

To identify whether the circHIPK3 in HPC-exos regulates CMVECs oxidative damage and IGF-1 expression by inhibiting miR-29a, we performed rescue experiments. Similar to the previous experiments in this study, CMVECs were transfected with miR-29a mimics, inhibitor, or negative control RNA. Forty-eight hours after transfection, circHIPK3-exos were added to CMVECs for 24 h, and then CMVECs were exposed to oxidative stress for 3 h. As shown in Figures 7(a) and 7(b), the CMVEC apoptosis induced by circHIPK3 knockdown in HPC-exos was rescued by the miR-29a inhibitor but intensified by the miR-29a mimics. Furthermore, in vitro oxidative damage (including ROS, SOD, and MDA) was increased with the combination of exosomal circHIPK3 silencing and miR-29a overexpression compared with circHIPK3 knockdown in HPC-exos alone. In addition, we also found that oxidative stress in CMVECs was suppressed with the combined knockdown of miR-29a in CMVECs and circHIPK3 in HPC-exos compared with exosomal circHIPK3 silencing alone (Figures 7(c)–7(k)). In addition, we did not observe a marked increase in miR-29a levels following circHIPK3 knockdown in HPC-exos;

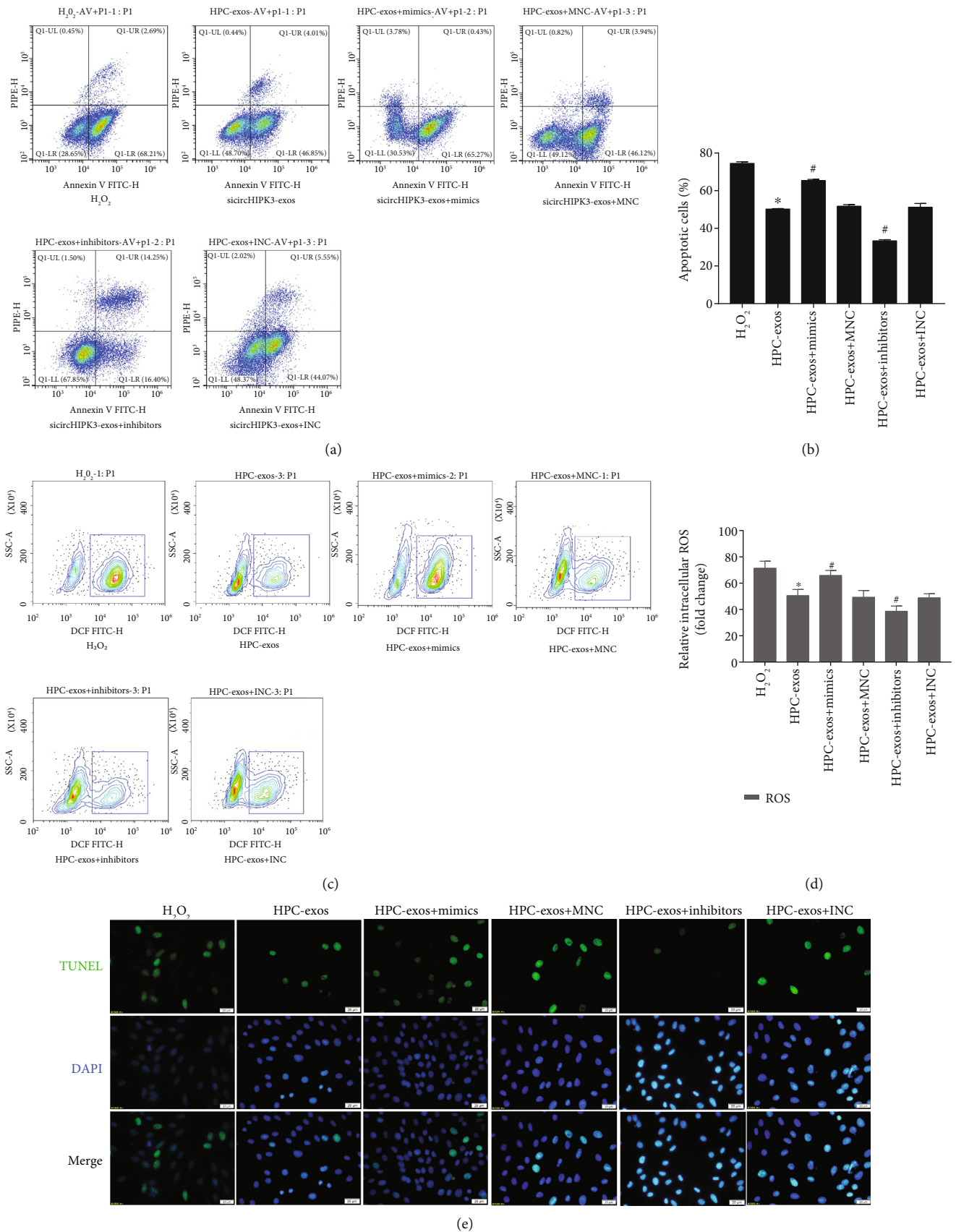


FIGURE 6: Continued.

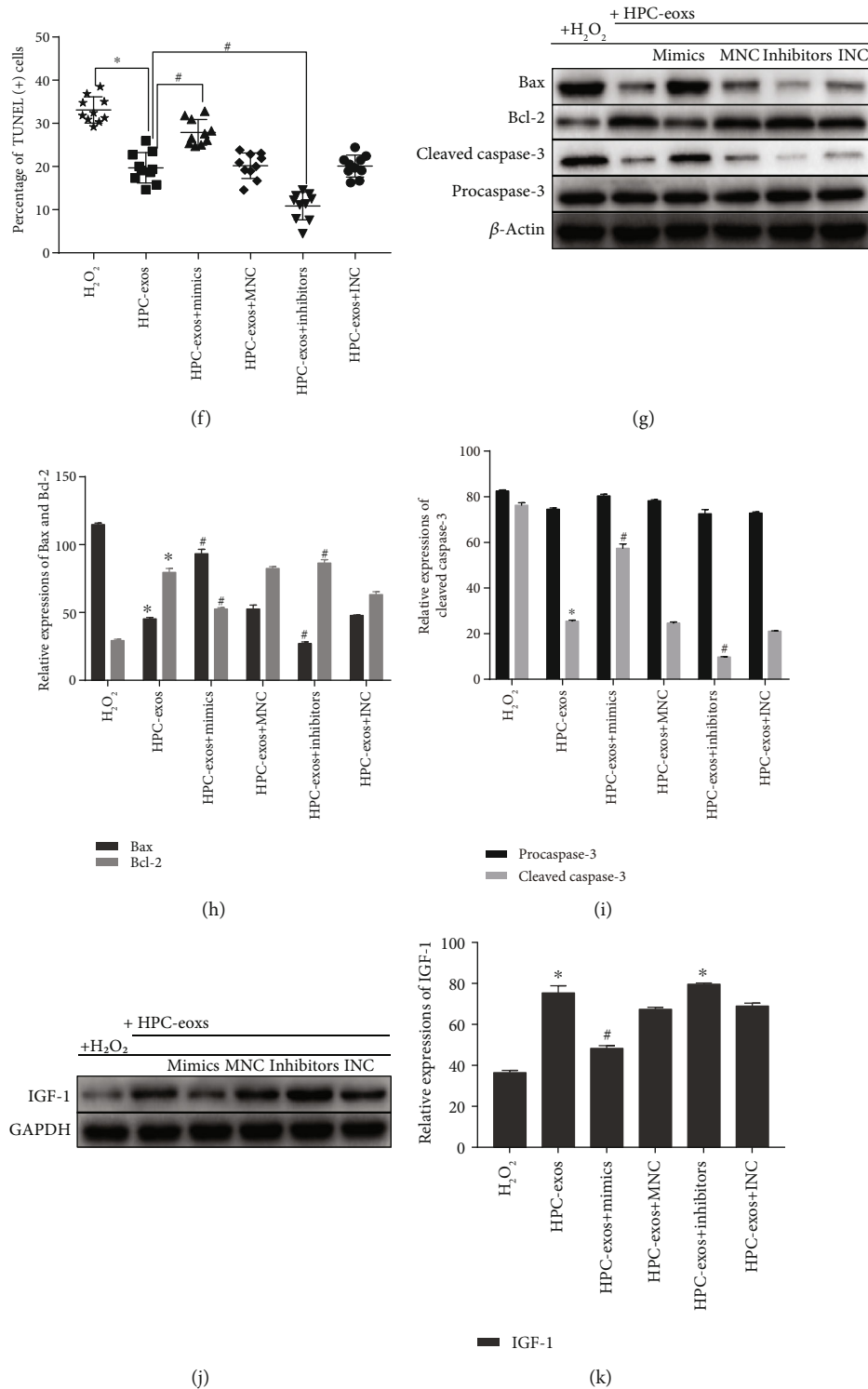


FIGURE 6: HPC-exos protect against oxidative injury via miR-29a/IGF-1 in CMVECs. (a) Representative dot plots of cell apoptosis after Annexin V/PI dual staining are shown. (b) The percentage of apoptotic cells represents both early and late apoptotic cells; $n = 3$. (c) The intracellular ROS level was determined by FCM. The P2 percentage indicates the proportion of cells with increased ROS production, with signals above the background 2',7'-dichlorofluorescein (DCF) fluorescence levels. (d) Quantitative analysis of ROS levels; $n = 3$. (e) Representative immunofluorescence of TUNEL (green) and DAPI (blue) staining and merged images. Photos were randomly captured using a fluorescence microscope. Scale bar = $20 \mu m$. (f) The panel shows the percentage of TUNEL-positive cells; $n = 6$. (g) Apoptosis-related genes, such as procaspase-3, cleaved caspase-3, Bax, and Bcl-2, were detected by immunoblotting. (h, i) Quantitative analysis of the apoptosis-related proteins; $n = 3$. (j) IGF-1 protein expression was detected by immunoblotting. (k) Quantitative analysis of IGF-1 protein expression; $n = 3$. * $P < 0.05$ compared with the H_2O_2 group; # $P < 0.05$ compared with the HPC-exos group.

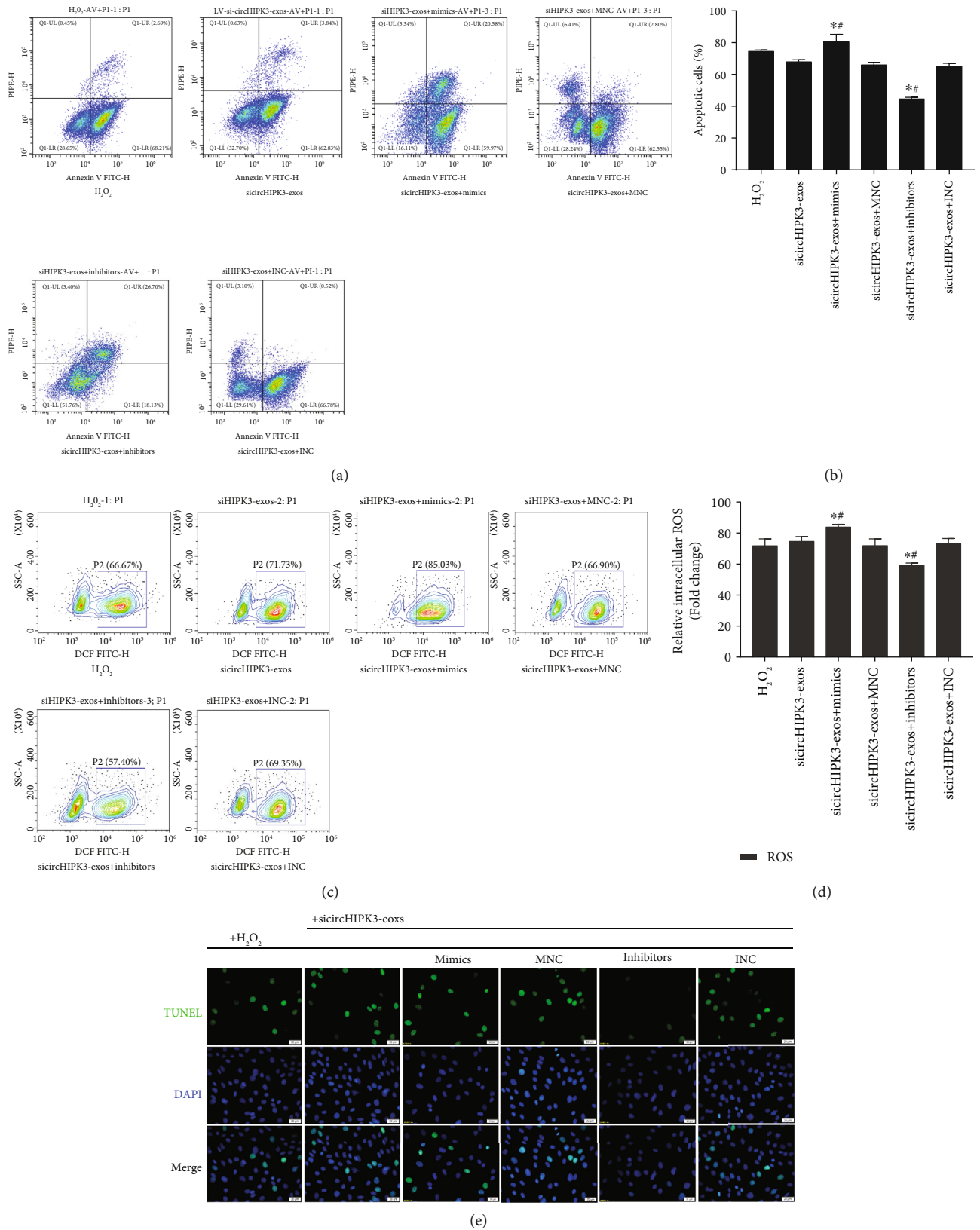


FIGURE 7: Continued.

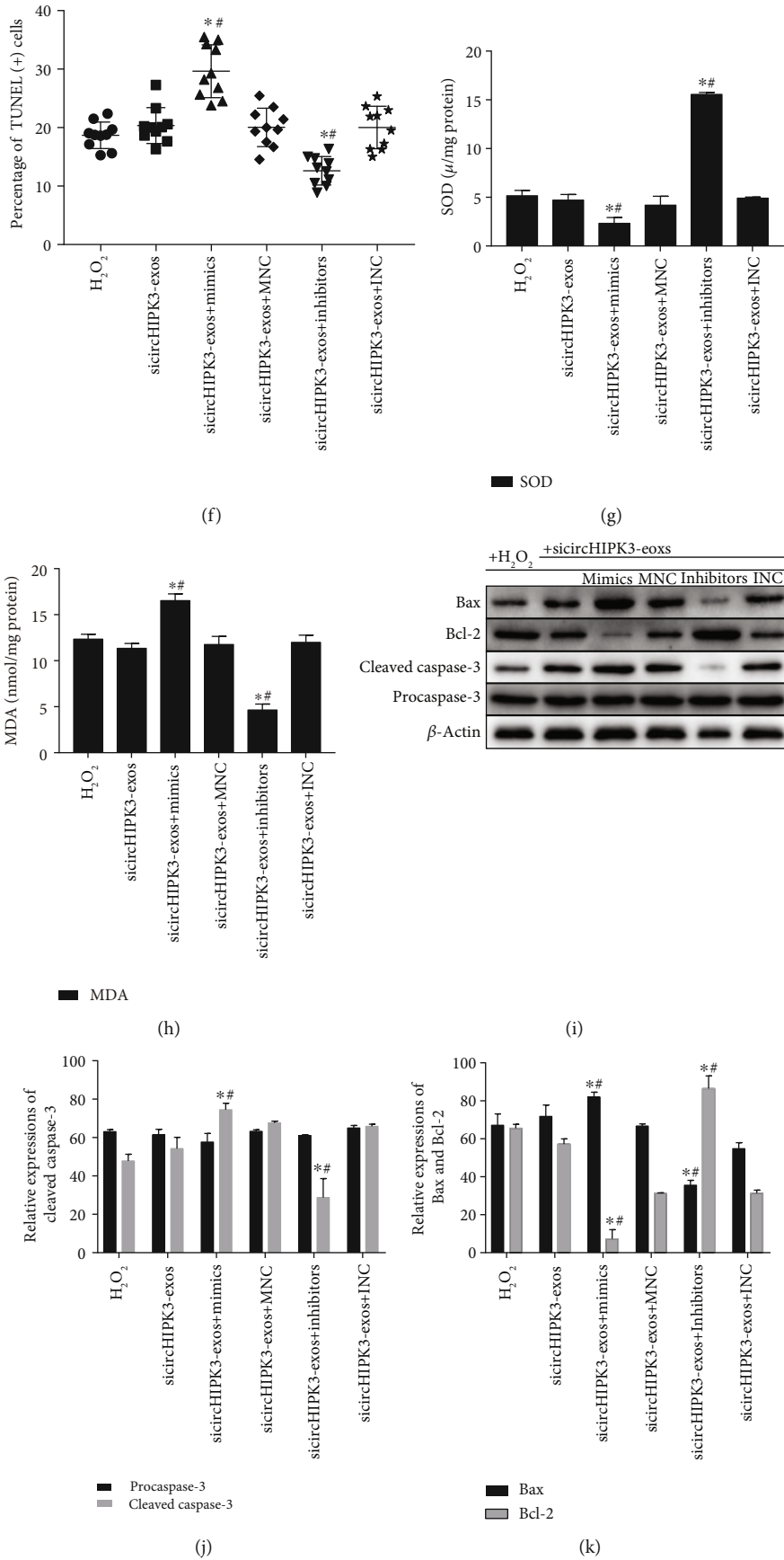


FIGURE 7: Continued.

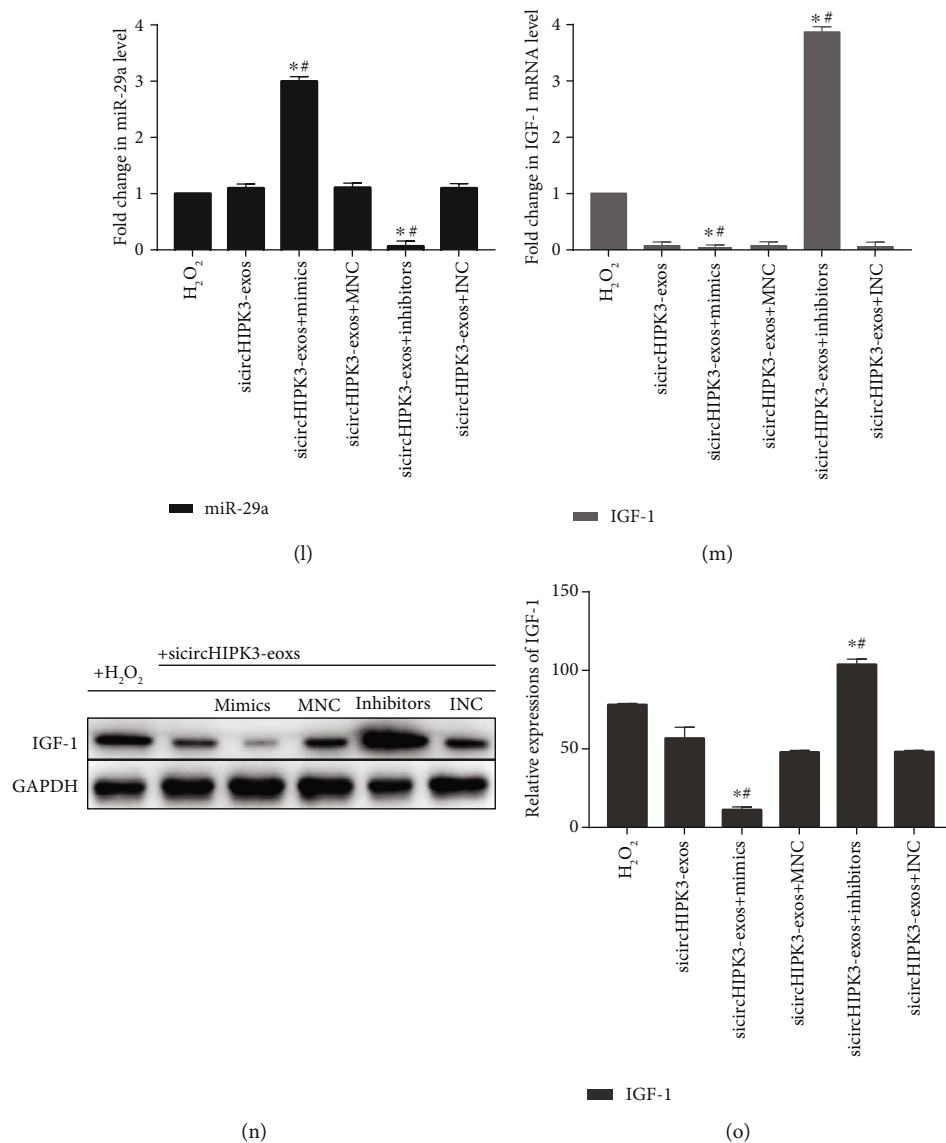


FIGURE 7: Exosomal circHIPK3 derived from hypoxia-pretreated CMs induces protection from oxidative injury via miR-29a/IGF-1 in CMVECs. (a) Representative dot plots of cell apoptosis after Annexin V/PI dual staining are shown. (b) The percentage of apoptotic cells represents both early and late apoptotic cells; $n = 3$. (c) The intracellular ROS level was determined by FCM. The P2 percentage indicates the proportion of cells with increased ROS production, with signals above background 2',7'-dichlorofluorescein (DCF) fluorescence levels. (d) Quantitative analysis of ROS levels; $n = 3$. (e) Representative immunofluorescence staining of TUNEL (green) and DAPI (blue) staining and merged images. Photos were randomly captured using a fluorescence microscope. Scale bar = 20 μm . (f) The panel shows the percentage of TUNEL-positive cells; $n = 6$. (g) Graph represents SOD levels; $n = 9$. (h) Graph represents MDA levels; $n = 9$. (i) Apoptosis-related genes, such as procaspase-3, cleaved caspase-3, Bax, and Bcl-2, were detected by immunoblotting. (j, k) Quantitative analysis of the apoptosis-related proteins; $n = 3$. (l) qRT-PCR analysis of miR-29a expression in CMVECs after different treatments. (m) qRT-PCR analysis of IGF-1 mRNA expression in CMVECs after different treatments. (n) IGF-1 protein was detected by immunoblotting. (o) Quantitative analysis of IGF-1 protein; $n = 3$. * $P < 0.05$ compared with the H₂O₂ group; # $P < 0.05$ compared with the sicircHIPK3-exos group.

moreover, the miR-29a mimics significantly increased and the miR-29a inhibitor significantly decreased miR-29a expression in CMVECs (Figure 7(l)). However, the mRNA and protein levels of IGF-1 were significantly decreased in the sicircHIPK3 and sicircHIPK3+mimic groups (Figures 7(l)–7(o)). Interestingly, the suppression of IGF-1 by sicircHIPK3-exos or miR-29a mimics could also be rescued by the addition of the miR-29a inhibitor (Figures 7(l)–7(o)). These data suggested that HPC-exosomal circHIPK3

regulate oxidative damage in CMVECs via the miR-29a/IGF-1 axis.

4. Discussion

circRNAs have recently gained attention due to their key roles in the regulation of gene expression and human diseases. In exosomes, circRNAs are enriched and stable [19] and can be transferred into target cells [20, 21]. However,

few exosomal circRNAs have been explored, especially under certain pathological conditions. In this study, we investigated the role of exosomal circHIPK3 released from CMs pretreated with hypoxia in maintaining cardiac microvascular endothelial cell function. Mechanistically, circHIPK3 in HPC-exos acts as an endogenous miR-29a sponge to inhibit miR-29a activity, thereby leading to increased IGF-1 expression and regulating oxidative damage in CMVECs *in vitro*.

Compared to damage to CMs, damage to microvasculature and microendothelial cells in the context of ischemic cardiomyopathy has unfortunately been a neglected topic in the past 30 years [41]. Oxidative stress-related complications in CMVECs after myocardial ischemia are the major cause of heart dysfunction [42]. Considering the central role of microcirculation in the exchange of oxygen and metabolites between blood and CMs [43], it is important to provide protection for microvasculature from oxidative injury. Recently, studies examining the intercellular interactions between the different cell types in the heart have provided new insight into the regulatory mechanism of CMVEC dysfunction. The close contact between CMs and CMVECs allows exosomes to transfer from CMs to CMVECs [12], which may represent completely new avenues for the regulation of oxidative damage in CMVECs.

Exosomes, as the beneficial paracrine signals generated by different cell types, carry functional messages and play an essential role in cell-to-cell communication under both physiological and pathophysiological conditions [44]. HPC is widely used to enhance cellular tolerance to oxidative stress [17]. Importantly, HPC enhanced the benefit of CMs-exos in an animal myocardial infarction model and led to an increased proangiogenic effect of exosomes [16]. In this study, cell viability analysis showed that 12 h was the appropriate length for hypoxia preconditioning in CMs. We obtained exosome vesicles (round, 30 ± 100 nm) from the media of conditioned CMs and confirmed these vesicles by detecting the expression of specific surface markers. The number, size, and morphology of exosomes were not changed after exposure to hypoxia. Furthermore, the exosomes could be internalized by CMVECs, which indicates that these exosomes may play roles in CMVECs by transferring cargo. H_2O_2 induces oxidative stress, which may cause cell damage [45]. We established an *in vitro* oxidative stress model with different concentrations of H_2O_2 to simulate the microenvironment of infarcted myocardium. Given that $200 \mu M$ H_2O_2 induced the most apoptosis (up to 72.49%) among the tested concentrations and relatively low necrosis in CMs, we chose $200 \mu M$ H_2O_2 pretreatment for 3 h to establish an *in vitro* model of oxidative stress. Furthermore, cell proliferation measurements of cells incubated with different concentrations of exosomes under hypoxic conditions showed that $300 \mu g/ml$ could significantly improve the proliferation of CMVECs pretreated with H_2O_2 . We have shown that the exosomes generated by CMs under hypoxic conditions increase the survival of CMVECs to a greater extent than exosomes from normoxic cells.

Exosomes contain specific proteins, RNA, ncRNA (including circRNA, lncRNA, and miRNA), and lipids.

Recently, reports have demonstrated that the transfer of unique exosome-derived miRNAs and circRNAs to recipient cells is an alternative mechanism that allows for gene-based communication between cells, in addition to the classical mechanisms, including direct cell-cell contact or chemical receptor-mediated events [13, 20]. In recent years, circRNAs have emerged as novel regulators in the pathogenesis of several ocular diseases, including retinal vascular dysfunction in diabetes retinopathy [29] and physiological neuronal apoptosis in developing rat retina [46]. In addition, circRNA is dynamically regulated after cells are exposed to hypoxia [47]. circRNA HIPK3, originating from exon 2 of the HIPK3 gene, is highly conserved in different cell lines and tissues [26, 37]. circBase retrieval revealed that the HIPK3 host gene might produce 20 circRNAs in the human genome and 3 circRNAs in the mouse genome. One circRNA (mmu_circ_0001052) from the HIPK3 host gene in mice was identified in endothelial cells after RNase R treatment and could increase endothelial proliferation and vascular dysfunction [29]. However, another study demonstrated a contrasting role of circHIPK3; the overexpression of circHIPK3 inhibits the migration, invasion, and angiogenesis of human invasive bladder cancer T24T and UMUC3 cells [26]. Here, we found that hypoxia preconditioning significantly upregulates circHIPK3 expression in CM-exos and that H_2O_2 significantly downregulates circHIPK3 expression in CMVECs. We thus hypothesized that circHIPK3 downregulation is responsible for H_2O_2 -induced CMVEC dysfunction. In addition, HPC-exos could induce circHIPK3 upregulation and protect CMVECs from apoptosis and oxidative damage, which prompted us to further investigate the function of circHIPK3. We show that the overexpression of circHIPK3 alone was sufficient to protect CMVECs from oxidative damage, whereas circHIPK3 knockdown further increased the apoptosis, ROS level, and MDA level of CMVECs, implying that decreased circHIPK3 levels in CMVECs promote the dysfunction of CMVECs under oxidative stress. Furthermore, the knockdown of circHIPK3, but not linear HIPK3, in HPC-exos increased the apoptosis and oxidative stress of CMVECs. Taken together, the circHIPK3 from HPC-exos mediates CMVEC protection.

circRNAs have emerged as promising novel regulators of gene expression through a complicated network involving mRNAs, miRNAs, and proteins [48]. A previous study showed that circHIPK3 sponged to 18 sites of 9 miRNAs (miR-124, miR-152, miR-193a, miR-29a, miR-29b, miR-338, miR-379, miR-584, and miR-654) [37]. miR-29a, a well-known angiogenesis suppressor, was proposed to participate in the process of apoptosis and proliferation in endotheliocytes [49–51]. In our experiment, we showed that the mRNA levels of miR-29a were not influenced by the overexpression or knockdown of circHIPK3. This result occurred because circRNA acts as an endogenous miRNA sponge to adsorb miRNA and inhibit miRNA activity, instead of degrading miRNA [29]. In addition, FISH assays showed that circHIPK3 and miR-29a were colocalized in the cytoplasm of CMVECs. The dual luciferase reporter assay showed that circHIPK3 binds to miR-29a. Furthermore, increased circHIPK3 expression could lead to a binding platform for

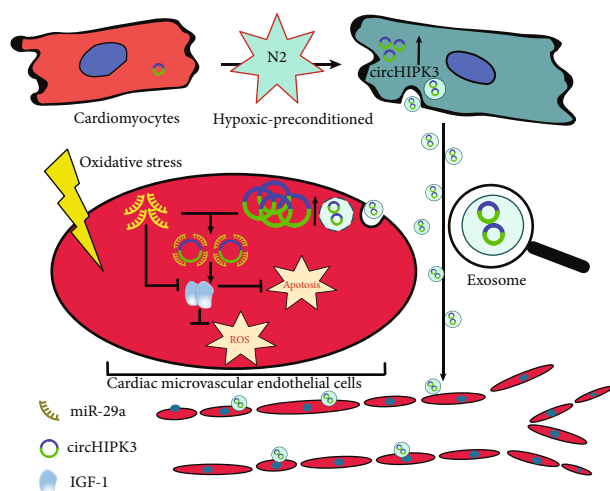


FIGURE 8: A schematic cartoon of the circHIPK3/miR-29g/IGF-1 axis in CMVECs. In CMs, circHIPK3 is upregulated by hypoxia pretreatment. Then, circHIPK3 is internalized by CMVECs through exosomes. In CMVECs, circHIPK3 sponges additional endogenous miR-29a to sequester and inhibit miR-29a activity, thereby leading to increased IGF-1 expression, which regulates oxidative damage in cardiac microvascular endothelial cells.

AGO2 and function as a miRNA sponge for miR-29a. These results further suggest that circHIPK3 can specifically bind to miR-29a.

Canonically, miRNAs can either retard the translation or induce the degradation of target mRNA and then decrease the expression of the corresponding protein by incomplete or complete base pairing to the 3'UTR of target mRNA [52]. Many targets of miR-29a have been identified, such as VEGF in gastric carcinoma [49] and MCL1 in anaplastic large cell lymphomas [53]. We demonstrate that IGF-1, which is of vital significance in the maintenance of CMVECs, is a newly discovered direct target of miR-29a in CMVECs. The miR-29a-induced imbalance in IGF-1 expression may promote damage accumulation and attenuate the protective effect of IGF-1. We established in vitro miR-29a gain-of-function and loss-of-function models to assess the effect of miR-29a on oxidative damage. In agreement with previous studies [38], our data also indicated that the miR-29a inhibitor significantly inhibited CMVEC oxidative stress injury and alleviated apoptosis; moreover, these inhibitory effects were strikingly similar to the overexpression of circHIPK3. We also found that upregulated miR-29a levels effectively decreased IGF-1 mRNA and protein expression, while downregulated miR-29a levels significantly increased IGF-1 protein expression. In addition, a dual luciferase reporter assay showed that miR-29a binds to IGF-1. miR-29a mimics abrogated the HPC-exos-mediated repressive effects though increasing apoptosis and ROS under oxidative conditions in vitro. In contrast, transfection of the miR-29a inhibitor significantly decreased apoptosis and oxidative damage in CMVECs. Furthermore, the high level of circHIPK3 in HPC-exos is a sink for miR-29a and releases the inhibitory effect of miR-29a on IGF-1. The rescue experiments also

showed that the reduced protection from oxidative damage induced by circHIPK3 knockdown in HPC-exos could be rescued by the miR-29a inhibitor and intensified by the miR-29a mimics. Furthermore, the suppression of IGF-1 by sicircHIPK3-exos could also be rescued after miR-29a inhibition. This regulatory mechanism provides a novel insight into microvascular dysfunction.

In conclusion, we observed circHIPK3 upregulation in HPC-exos. Our results demonstrated that the circHIPK3 in CMs-exos could influence the survival of CMVECs by sponging endogenous miR-29a to sequester and reduce miR-29a activity, thus resulting in the increased expression of the miR-29a-targeted gene IGF-1 (Figure 8). This study shed light on a potentially new targeted method to regulate CMVECs dysfunction using an exosomal ncRNA-based approach. Additional in vivo studies are warranted to further confirm that CMs-exos pretreated with hypoxia have similar effects on the survival of CMVECs. Notably, CMs-exos contain various types of circRNA, including circHIPK3; moreover, circHIPK3 targets more than one miRNA, and IGF-1 is not the only protein downstream of miR-29a. Furthermore, the upstream signaling mechanism that causes the change in circHIPK3 expression is also worth exploring.

Data Availability

The data used to support the findings of this study are included within the article.

Conflicts of Interest

The authors declare that there is no conflict of interest regarding the publication of this paper.

Authors' Contributions

Yan Wang and Ranzun Zhao contributed equally to this work.

Acknowledgments

This work was supported by grants from the National Natural Science Foundation of China (Grant no. 81760042 and Grant no. 81860061).

References





- [1] F. Yu, Y. Liu, and J. Xu, "Pro-BDNF contributes to hypoxia/reoxygenation injury in myocardial microvascular endothelial cells: roles of receptors p75^{NTR} and sortilin and activation of JNK and caspase 3," *Oxidative Medicine and Cellular Longevity*, vol. 2018, Article ID 3091424, 11 pages, 2018.
- [2] R. Wang, Q. Yang, X. Wang et al., "FoxO3 α -mediated autophagy contributes to apoptosis in cardiac microvascular endothelial cells under hypoxia," *Microvascular Research*, vol. 104, pp. 23–31, 2016.
- [3] D. L. BRUTSAERT, "Cardiac endothelial-myocardial signaling: its role in cardiac growth, contractile performance, and

- rhythmicity,” *Physiological Reviews*, vol. 83, no. 1, pp. 59–115, 2003.
- [4] Y. Fujita and A. Kawamoto, “Stem cell-based peripheral vascular regeneration,” *Advanced Drug Delivery Reviews*, vol. 120, pp. 25–40, 2017.
- [5] C. Seiler, M. Stoller, B. Pitt, and P. Meier, “The human coronary collateral circulation: development and clinical importance,” *European Heart Journal*, vol. 34, no. 34, pp. 2674–2682, 2013.
- [6] Y. Tian and E. E. Morrisey, “Importance of myocyte-nonmyocyte interactions in cardiac development and disease,” *Circulation Research*, vol. 110, no. 7, pp. 1023–1034, 2012.
- [7] A. K. Brzezinska, D. Merkus, and W. M. Chilian, “Metabolic communication from cardiac myocytes to vascular endothelial cells,” *American Journal of Physiology. Heart and Circulatory Physiology*, vol. 288, no. 5, pp. H2232–H2237, 2005.
- [8] N. A. Garcia, J. Moncayo-Arandi, P. Sepulveda, and A. Diez-Juan, “Cardiomyocyte exosomes regulate glycolytic flux in endothelium by direct transfer of GLUT transporters and glycolytic enzymes,” *Cardiovascular research*, vol. 109, no. 3, pp. 397–408, 2016.
- [9] N. A. Garcia, I. Ontoria-Oviedo, H. González-King, A. Diez-Juan, and P. Sepúlveda, “Glucose starvation in cardiomyocytes enhances exosome secretion and promotes angiogenesis in endothelial cells,” *PLoS One*, vol. 10, no. 9, article e0138849, 2015.
- [10] N. Genneback, U. Hellman, L. Malm et al., “Growth factor stimulation of cardiomyocytes induces changes in the transcriptional contents of secreted exosomes,” *Journal of Extracellular Vesicles*, vol. 2, no. 1, article 20167, 2013.
- [11] E. Hirsch, D. Hilfiker-Kleiner, J. L. Balligand et al., “Interaction of the heart and its close and distant neighbours: report of the meeting of the ESC working groups myocardial function and cellular biology,” *Cardiovascular Research*, vol. 99, no. 4, pp. 595–599, 2013.
- [12] S. M. Davidson, J. A. Riquelme, Y. Zheng, J. M. Vicencio, S. Lavandero, and D. M. Yellon, “Endothelial cells release cardioprotective exosomes that may contribute to ischaemic preconditioning,” *Scientific Reports*, vol. 8, no. 1, p. 15885, 2018.
- [13] B. Shi, Y. Wang, R. Zhao, X. Long, W. Deng, and Z. Wang, “Bone marrow mesenchymal stem cell-derived exosomal miR-21 protects C-kit+ cardiac stem cells from oxidative injury through the PTEN/PI3K/Akt axis,” *PLoS One*, vol. 13, no. 2, article e0191616, 2018.
- [14] D. A. Chistiakov, A. N. Orekhov, and Y. V. Bobryshev, “Cardiac extracellular vesicles in normal and infarcted heart,” *International Journal of Molecular Sciences*, vol. 17, no. 1, p. 63, 2016.
- [15] X. Loyer, I. Zlatanova, C. Devue et al., “Intra-cardiac release of extracellular vesicles shapes inflammation following myocardial infarction,” *Circulation Research*, vol. 123, no. 1, pp. 100–106, 2018.
- [16] T. M. Ribeiro-Rodrigues, T. L. Laundos, R. Pereira-Carvalho et al., “Exosomes secreted by cardiomyocytes subjected to ischaemia promote cardiac angiogenesis,” *Cardiovascular Research*, vol. 113, no. 11, pp. 1338–1350, 2017.
- [17] J. H. Barrington, B. C. R. Christmas, O. R. Gibson et al., “Hypoxic air inhalation and ischemia interventions both elicit preconditioning which attenuate subsequent cellular stress in vivo following blood flow occlusion and reperfusion,” *Frontiers in Physiology*, vol. 8, p. 560, 2017.
- [18] Y. Wang, R. Zhao, D. Liu et al., “Exosomes derived from miR-214-enriched bone marrow-derived mesenchymal stem cells regulate oxidative damage in cardiac stem cells by targeting CaMKII,” *Oxidative Medicine and Cellular Longevity*, vol. 2018, Article ID 4971261, 21 pages, 2018.
- [19] X. O. Zhang, H. B. Wang, Y. Zhang, X. Lu, L. L. Chen, and L. Yang, “Complementary sequence-mediated exon circularization,” *Cell*, vol. 159, no. 1, pp. 134–147, 2014.
- [20] Y. Dou, D. J. Cha, J. L. Franklin et al., “Circular RNAs are down-regulated in KRAS mutant colon cancer cells and can be transferred to exosomes,” *Scientific Reports*, vol. 6, no. 1, p. 37982, 2016.
- [21] E. Lasda and R. Parker, “Circular RNAs co-precipitate with extracellular vesicles: a possible mechanism for circRNA clearance,” *PLoS One*, vol. 11, no. 2, article e0148407, 2016.
- [22] S. Werfel, S. Nothjunge, T. Schwarzmayr, T. M. Strom, T. Meitinger, and S. Engelhardt, “Characterization of circular RNAs in human, mouse and rat hearts,” *Journal of Molecular and Cellular Cardiology*, vol. 98, pp. 103–107, 2016.
- [23] K. Wang, B. Long, F. Liu et al., “A circular RNA protects the heart from pathological hypertrophy and heart failure by targeting miR-223,” *European Heart Journal*, vol. 37, no. 33, pp. 2602–2611, 2016.
- [24] Z. Zhong, M. Huang, M. Lv et al., “Circular RNA MYLK as a competing endogenous RNA promotes bladder cancer progression through modulating VEGFA/VEGFR2 signaling pathway,” *Cancer Letters*, vol. 403, pp. 305–317, 2017.
- [25] D. Liang and J. E. Wilusz, “Short intronic repeat sequences facilitate circular RNA production,” *Genes & Development*, vol. 28, no. 20, pp. 2233–2247, 2014.
- [26] Y. Li, F. Zheng, X. Xiao et al., “CircHIPK3 sponges miR-558 to suppress heparanase expression in bladder cancer cells,” *EMBO reports*, vol. 18, no. 9, pp. 1646–1659, 2017.
- [27] N. Liu, J. Zhang, L. Y. Zhang, and L. Wang, “CircHIPK3 is upregulated and predicts a poor prognosis in epithelial ovarian cancer,” *European Review for Medical and Pharmacological Sciences*, vol. 22, no. 12, pp. 3713–3718, 2018.
- [28] X. Liu, B. Liu, M. Zhou et al., “Circular RNA HIPK3 regulates human lens epithelial cells proliferation and apoptosis by targeting the miR-193a/CRYAA axis,” *Biochemical and Biophysical Research Communications*, vol. 503, no. 4, pp. 2277–2285, 2018.
- [29] K. Shan, C. Liu, B.-H. Liu et al., “Circular noncoding RNA HIPK3 mediates retinal vascular dysfunction in diabetes mellitus,” *Circulation*, vol. 136, no. 17, pp. 1629–1642, 2017.
- [30] X. Wang, Y. Liu, L. Xiao et al., “Hyperoside protects against pressure overload-induced cardiac remodeling via the AKT signaling pathway,” *Cellular Physiology and Biochemistry*, vol. 51, no. 2, pp. 827–841, 2018.
- [31] Y. Cheng, P. Zhu, J. Yang et al., “Ischaemic preconditioning-regulated miR-21 protects heart against ischaemia/reperfusion injury via anti-apoptosis through its target PDCD4,” *Cardiovascular Research*, vol. 87, no. 3, pp. 431–439, 2010.
- [32] F. M. Marelli-Berg, E. Peek, E. A. Lidington, H. J. Stauss, and R. I. Lechler, “Isolation of endothelial cells from murine tissue,” *Journal of Immunological Methods*, vol. 244, no. 1–2, pp. 205–215, 2000.
- [33] W. Xuan, B. Wu, C. Chen et al., “Resveratrol improves myocardial ischemia and ischemic heart failure in mice by antagonizing the detrimental effects of fractalkine,” *Critical Care Medicine*, vol. 40, no. 11, pp. 3026–3033, 2012.

- [34] T. Ma, Y. Chen, Y. Chen et al., "MicroRNA-132, delivered by mesenchymal stem cell-derived exosomes, promote angiogenesis in myocardial infarction," *Stem Cells International*, vol. 2018, Article ID 3290372, 11 pages, 2018.
- [35] T. Hao, J. Li, F. Yao et al., "Injectable fullerene/alginate hydrogel for suppression of oxidative stress damage in brown adipose-derived stem cells and cardiac repair," *ACS Nano*, vol. 11, no. 6, pp. 5474–5488, 2017.
- [36] Y. Zhou, Y. Zhang, F. Gao et al., "N-n-butyl haloperidol iodide protects cardiac microvascular endothelial cells from hypoxia/reoxygenation injury by down-regulating Egr-1 expression," *Cellular Physiology and Biochemistry*, vol. 26, no. 6, pp. 839–848, 2010.
- [37] Q. Zheng, C. Bao, W. Guo et al., "Circular RNA profiling reveals an abundant circHIPK3 that regulates cell growth by sponging multiple miRNAs," *Nature Communications*, vol. 7, no. 1, 2016.
- [38] L. Wang, X. Niu, J. Hu et al., "After myocardial ischemia-reperfusion, miR-29a, and Let7 could affect apoptosis through regulating IGF-1," *BioMed Research International*, vol. 2015, Article ID 245412, 7 pages, 2015.
- [39] R. Troncoso, C. Ibarra, J. M. Vicencio, E. Jaimovich, and S. Lavandero, "New insights into IGF-1 signaling in the heart," *Trends in Endocrinology and Metabolism*, vol. 25, no. 3, pp. 128–137, 2014.
- [40] C. Han, X. Chen, R. Zhuang, M. Xu, S. Liu, and Q. Li, "miR-29a promotes myocardial cell apoptosis induced by high glucose through down-regulating IGF-1," *International Journal of Clinical and Experimental Medicine*, vol. 8, no. 8, pp. 14352–14362, 2015.
- [41] R. A. P. Weir, C. A. Murphy, C. J. Petrie et al., "Microvascular obstruction remains a portent of adverse remodeling in optimally treated patients with left ventricular systolic dysfunction after acute myocardial infarction," *Circulation: Cardiovascular Imaging*, vol. 3, no. 4, pp. 360–367, 2010.
- [42] C. Hewson, D. Capraro, J. Burdach, N. Whitaker, and K. V. Morris, "Extracellular vesicle associated long non-coding RNAs functionally enhance cell viability," *Non-coding RNA Research*, vol. 1, no. 1, pp. 3–11, 2016.
- [43] H. Zhou, S. Hu, Q. Jin et al., "Mff-dependent mitochondrial fission contributes to the pathogenesis of cardiac microvasculature ischemia/reperfusion injury via induction of mROS-mediated cardiolipin oxidation and HK2/VDAC1 disassociation-involved mPTP opening," *Journal of the American Heart Association*, vol. 6, no. 3, 2017.
- [44] X. Dai, C. Chen, Q. Yang et al., "Exosomal circRNA_100284 from arsenite-transformed cells, via microRNA-217 regulation of EZH2, is involved in the malignant transformation of human hepatic cells by accelerating the cell cycle and promoting cell proliferation," *Cell Death & Disease*, vol. 9, no. 5, p. 454, 2018.
- [45] A. J. Kattoor, N. V. K. Pothineni, D. Palagiri, and J. L. Mehta, "Oxidative stress in atherosclerosis," *Current Atherosclerosis Reports*, vol. 19, no. 11, p. 42, 2017.
- [46] J. Han, L. Gao, J. Dong, J. Bai, M. Zhang, and J. Zheng, "The expression profile of developmental stage-dependent circular RNA in the immature rat retina," *Molecular Vision*, vol. 23, pp. 457–469, 2017.
- [47] J. N. Boeckel, N. Jaé, A. W. Heumüller et al., "Identification and characterization of hypoxia-regulated endothelial circular RNA," *Circulation Research*, vol. 117, no. 10, pp. 884–890, 2015.
- [48] L. L. Chen, "The biogenesis and emerging roles of circular RNAs," *Nature Reviews. Molecular Cell Biology*, vol. 17, no. 4, pp. 205–211, 2016.
- [49] H. Zhang, M. Bai, T. Deng et al., "Cell-derived microvesicles mediate the delivery of miR-29a/c to suppress angiogenesis in gastric carcinoma," *Cancer Letters*, vol. 375, no. 2, pp. 331–339, 2016.
- [50] P. Jia, H. Cai, X. Liu et al., "Long non-coding RNA H19 regulates glioma angiogenesis and the biological behavior of glioma-associated endothelial cells by inhibiting microRNA-29a," *Cancer Letters*, vol. 381, no. 2, pp. 359–369, 2016.
- [51] C. Zhou, Q. Y. Zou, H. Li et al., "Preeclampsia downregulates microRNAs in fetal endothelial cells: roles of miR-29a/c-3p in endothelial function," *The Journal of Clinical Endocrinology and Metabolism*, vol. 102, no. 9, pp. 3470–3479, 2017.
- [52] D. de Rie, The FANTOM Consortium, I. Abugessaisa et al., "An integrated expression atlas of miRNAs and their promoters in human and mouse," *Nature Biotechnology*, vol. 35, no. 9, pp. 872–878, 2017.
- [53] C. Desjobert, M. H. Renalier, J. Bergalet et al., "MiR-29a down-regulation in ALK-positive anaplastic large cell lymphomas contributes to apoptosis blockade through MCL-1 overexpression," *Blood*, vol. 117, no. 24, pp. 6627–6637, 2011.

Research Article

Potential Role of Nutrient Intake and Malnutrition as Predictors of Uremic Oxidative Toxicity in Patients with End-Stage Renal Disease

Robson E. Silva,^{1,2} Ana C. Simões-e-Silva ,³ Aline S. Miranda ,⁴ Patrícia B. I. Justino,² Máisa R. P. L. Brigagão,⁵ Gabriel O. I. Moraes,⁵ Reggiani V. Gonçalves ,⁶ and Rômulo D. Novaes ⁵

¹School of Medicine, Federal University of Alfenas, Alfenas, 37130-001 Minas Gerais, Brazil

²University Hospital Alzira Velano, Alfenas, 37132-202 Minas Gerais, Brazil

³Department of Pediatrics, Faculty of Medicine, Federal University of Minas Gerais, Belo Horizonte, 30130-100 Minas Gerais, Brazil

⁴Department of Morphology, Federal University of Minas Gerais, Belo Horizonte, 31270-910 Minas Gerais, Brazil

⁵Institute of Biomedical Sciences, Federal University of Alfenas, Alfenas, 37130-001 Minas Gerais, Brazil

⁶Department of Animal Biology, Federal University of Viçosa, Viçosa, 36570-000 Minas Gerais, Brazil

Correspondence should be addressed to Rômulo D. Novaes; romuonovaes@yahoo.com.br

Received 6 June 2019; Revised 25 September 2019; Accepted 4 October 2019; Published 29 November 2019

Academic Editor: Steven McAnulty

Copyright © 2019 Robson E. Silva et al. This is an open access article distributed under the Creative Commons Attribution License, which permits unrestricted use, distribution, and reproduction in any medium, provided the original work is properly cited.

Oxidative stress is an important risk factor for cardiovascular disease and death in hemodialysis (HD) patients. However, whether biochemical and nutritional markers might be useful to stratify HD patients according to the risk of oxidative damage remains unclear. We investigated whether low-cost and easily available parameters such as the profile of nutrients intake, nutritional status, and antioxidant defenses can predict lipid and protein oxidation in HD patients. Forty-nine HD patients (women = 20, men = 29), ranging from 18 to 65 years of age (73.5%) were submitted to biochemical and nutritional analysis. At least 93.9% of HD patients had malnutrition. A patient's stratification according to nutritional risk was highly coherent with anthropometric parameters and nutrients intake, which were complementarily used as markers of malnutrition. Nutritional stratification was unable to reveal differences in the oxidative status. On the other hand, carbohydrate and zinc intake, serum zinc (Zn), glutathione peroxidase (GPx) activity, total antioxidant capacity (TAC), and nonprotein antioxidants (npAC) in serum were predictive markers of lipid ($R^2 = 0.588$, $P < 0.001$) and protein ($R^2 = 0.581$, $P < 0.001$) oxidation. Interestingly, GPx activity, TAC, and npAC exhibited good (>80% < 90%) or excellent (>90%) accuracy to estimate lipid oxidation ($P \leq 0.01$). Regarding the prediction of protein oxidation, GPx activity and TAC presented regular accuracy (>70% < 80%), and Zn serum levels exhibited good sensitivity ($P \leq 0.01$). Herein, we provided evidence that clinical characteristics relevant to predict different levels of lipid and protein oxidation in HD patients can be easily obtained, during routine hospital visits by means of the combined analyses of biochemical and nutritional parameters.

1. Introduction

End-stage renal disease (ESRD) and renal replacement therapy are closely associated with chronic inflammation, metabolic imbalance, decreased dietary intake, and nutritional derangements, which can be termed as protein energy wasting (PEW) [1]. Imbalance in protein metabolism is the most pronounced biochemical disturbance of patients at

ESRD. This alteration in protein metabolism is multifactorial and can be linked to reduced protein and energy intake, systemic inflammation, resistance to anabolic hormones including insulin and growth hormones, and direct loss of amino acids in the dialysate [2].

Metabolic imbalance and accumulation of uremic toxins are associated with the onset and progression of nutritional changes in ESRD patients [3]. Considering the marked

catabolic component in patients undergoing hemodialysis (HD) [4], biochemical and nutritional analyses are critical to monitor physiological parameters and to identify the occurrence of PEW [5]. Thus, a broad biochemical and nutritional screening might be useful to stratify patients at risk, to define personalized interventions, and to evaluate therapeutic efficacy in ESRD patients. Although several tools are available for the nutritional assessment of HD patients, there is no gold standard method [6]. The combined use of nutritional markers has been recommended to improve the prediction of morbidity and mortality risks associated with ESRD [6]. Subjective global assessments (SGA) and anthropometric and biochemical methods are the main clinical tools applied in nutritional assessment of HD patients [7]. However, it is not well understood whether and which nutritional assessment methods will accurately predict the oxidative stress in HD patients.

Malnutrition and inflammation associated with intense lipid, protein, and DNA oxidation are common manifestations in HD patients [8]. There is evidence that redox imbalance and oxidative molecular damage are early findings associated to classical causes of chronic kidney disease (CKD), including diabetes mellitus (DM), arterial hypertension (AH), and atherosclerosis [8]. Oxidative stress may contribute to CKD onset and progression to ESRD by promoting renal ischemia, inflammation, cell death, and glomerular morphofunctional damage [9]. Due to the accumulation of uremic toxins, oxidative stress becomes more intense in ESRD, playing a relevant role in the pathogenesis of cardiovascular complications in HD patients [10]. In addition, ESRD patients exhibit 15 to 30 times higher mortality risk due to cardiovascular events than the general population [11].

Although biochemical evaluation of oxidative status might be relevant for the prognosis and therapeutic approach of HD patients [2, 9], it is still unclear which characteristics of these patients are related to oxidative status and can be predictors of oxidative molecular damage. Therefore, the aim of this study was to evaluate whether the profile of nutrient intake, nutritional status, and antioxidant defenses can be useful to predict lipid and protein oxidation in HD patients.

2. Patients and Methods

2.1. Study Design and Sample Size. This is a cross-sectional study with all adult ESRD patients of both sexes under HD in the renal replacement therapy center of our institution. Patients of both sexes that agreed to participate in the study and signed the free consent term were included. The exclusion criteria were as follows: (i) patients who refuse to participate in the study, (ii) presence of cognitive deficit (evaluated by the Mini Mental State Examination) that makes the application of the questionnaires difficult [12], (iii) patients submitted to renal transplantation during the last 6 months, (iv) neoplastic disease, (v) change in dialysis modality during the last 3 months, (vi) newly implanted catheters, (vii) hemodynamic instability, and (ix) patients with physical incapacity to stay in a standing position for anthropometric evaluation. It is worth mentioning that no

patient was excluded based on the abovementioned criteria. Thus, all patients ($n = 49$) undergoing hemodialysis from a renal replacement therapy center were included in this study.

2.2. Study Protocol and Ethical Issues. The same nephrologist and nutritionist who were responsible for the clinical follow-up of the patients performed all data collection. The data were recorded during the first two of the three HD sessions, weakly performed by each patient in the renal replacement therapy center. In the first session, the general characteristics of the patients (i.e., age, sex, comorbidities, time on hemodialysis, smoking, alcohol intake, and Kt/V) were collected from the medical record (weekly updated) and confirmed with all patients, when appropriate. The nutritional assessment was also performed in the first week session to ensure a more detailed food recall, which considered food intake in a typical week, including weekends. To avoid the influence of the HD procedure on blood parameters, blood samples were collected using Gel SST II Advance Vacutainer® tubes (Becton Dickinson, San Jose, CA, USA) immediately before the second session (48 h after the first HD session). Immediately after this session, the anthropometric parameters were recorded to avoid the influence of water retention on body composition. All measurements were performed in triplicate, and the mean values were calculated. The study was conducted in accordance with the guidelines of the Declaration of Helsinki and approved by the Institutional Ethics Committee in Human Research (protocol 1.767.706).

2.3. Urea, Creatinine, and Hemoglobin Blood Levels. Urea and creatinine were analyzed by spectrophotometry using commercial diagnostic colorimetric kits (Invitro, Itaboraí, MG, Brazil). Hemoglobin was quantified in a hematological analyzer by using high-grade human reagents (Sysmex, XE-2100, Sao Paulo, SP, Brazil). The urea reduction ratio (URR) after dialysis was estimated according the relation $URR = ([U_{pre} - U_{post}]/U_{pre}) * 100\%$. The dialysis dose was calculated by the Kt/V equation: $Kt/V = -\ln(R - 0.008 \times t) + (4 - 3.5 \times R) 0.55 \times UF/V$, where R is U_{post}/U_{pre} , t is the duration of the session in hours, $-\ln$ is the natural logarithm negative, UF is the weight loss in kilograms, and V is the volume of urea distribution in liters.

2.4. Nutritional Status and Malnutrition Assessment. Malnutrition was investigated in all subjects from a multilevel clinical and nutritional screening, including (i) modified global subjective assessment (mGSA) for HD patients [7], (ii) global objective assessment (GOA) for HD patients [13], and (iii) anthropometric measures obtained after HD session (dry weight (kg), height (cm), waist, hip and arm circumferences, and skinfold thickness (triceps, biceps, subscapular, and suprailiac)) according to standardized protocols [14–17]. Waist circumference was measured at the expiratory phase from the abdominal point with the largest circumference. Waist circumference was classified according to the cut-off points described by the World Health Organization [16]. Hip circumference was evaluated without tissue compression at the most protuberant point in the horizontal alignment between hips and buttocks [17]. From the waist/hip ratio

(WHR), the risk of cardiovascular disease was estimated considering recommended cut-off points [16]. Waist/height ratio (WHtR) was measured by the ratio between the WC (cm) and the height (cm) [18]; conicity index (CNI) was calculated using the equation $CNI = WC (m)/0.109 (\text{weight [kg]}/\text{height [m]})^{1/2}$ [19], and body adiposity index (BAI) was calculated as $BAI = [HC (cm)/\text{height [m]} (\text{height [m]})^{1/2} - 18$ [20].

Skinfold thickness was measured in triplicate by means of the skinfold caliper with precision from 0 to 60 mm, a scale of 1 mm, and a constant pressure of 10 g/mm² (Lange, Ann Arbor, MI, USA) [21]. Arm circumference was analyzed with the upper limbs parallel to the trunk, and the midpoint between the scapula acromion and the olecranon was used as reference for the measures. The reference values of U.S. Hanes were used to evaluate the adequacy of our arm circumference results [22]. Arm fat area [22], muscle circumference [23], and adjusted-arm muscle area [24, 25] were calculated from the results of triceps skinfold thickness and arm circumference. Body fat percentage was estimated considering the sum of four skinfolds' thickness ($\Sigma 4ST = \text{suprailiac} + \text{biceps} + \text{triceps} + \text{subscapular}$) [26, 27].

2.5. Cut-Off Points of Malnutrition. Malnutrition was classified according to the objective criteria for each method: (i) mGSA: 9–23 points = mild malnutrition/nutritional risk, 24–31 points = moderate malnutrition, 32–39 points = severe malnutrition, and ≥ 40 points = very serious malnutrition [28]; (ii) GOA: ≥ 7 points = mild malnutrition/nutritional risk, 13–18 points = moderate malnutrition, and ≥ 19 points = severe malnutrition; (iii) BMI: $< 18.5 \text{ kg/m}^2$ for adults [16] and $< 22 \text{ kg/m}^2$ for the elderly [28]; (iv) arm circumference (AC): arm muscle circumference and triceps skinfold thickness: 50th percentile as reference according age and sex (classification: $< 70\%$ = severe malnutrition, 70–80% = moderate malnutrition, and 80–90% = mild malnutrition) [13]; (v) Waist circumference (WC): ≥ 80 cm for women and ≥ 94 for men = high risk, ≥ 88 cm for women and ≥ 102 for men = very high risk of metabolic complications [16]; (vi) adjusted arm muscle area (AAMA): < 15 th percentile as reference according to age and sex (classification: < 5 th percentile = severe malnutrition and mild/moderate malnutrition $\pm > 5$ th and < 15 th [22]; (vii) arm fat area (AFA): < 25 th percentile [29], admitting the 25th percentile for age and sex [22].

2.6. Dietary and Nutrient Intake Assessment. A standardized 24-hour food record was used to collect information about dietary intake [30]. We used the standardized technique described by the authors, in which the respondent was stimulated to remember the food they consumed the day before. During the evaluation, all patients were instructed to record daily drink and food intake. Dietary intake data were analyzed by using DietBox software to estimate energy and nutrient consumption. This software uses the Brazilian Table databases Food Composition 2011-TACO [31], Composition Table of the Brazilian Institute of Geography and Statistics (IBGE, Brazil), and Food Composition Table Tucunduva [32], with more than 5 thousand registered foods. Detailed

instructions were given to all patients to record all dietary habits including additions and amount (i.e., sugar, salt, and oils), supplementations (i.e., vitamin and mineral), cooking method, and type and brand names of industrial foods. Conventional measures such as cups, spoons, and bowls, as well as portion sizes (small, medium, and large), were defined and recorded to help the nutritional analysis [25]. Daily food consumption was estimated as frequency \times portion \times size for each consumed food item. Nutrient intake was evaluated according to two Brazilian nutritional composition tables [31, 33] or to an international reference table (USDA, 2017), when the nutritional information was unavailable in Brazilian tables [34]. Daily nutrient intake was compared with the recommendations provided by the US National Institute of Health [35].

2.7. Iron, Manganese, Selenium, and Zinc Serum Levels. Iron was analyzed by spectrophotometry using a commercial diagnostic colorimetric kit (Invitro, Itaboraí, MG, Brazil). Manganese, selenium, and zinc were quantified by atomic absorption spectrophotometry [36]. Serum samples (500 μl) were dried at 70°C, digested (30 min) in glass tubes with 750 μl concentrated HNO_3 and 250 μl HClO_4 (70%) using a plate heater, where the temperature was gradually increased from 70°C to 90°C. After digestion, the samples were diluted in deionized water (5 mL) and filtered. Iron, zinc, and selenium concentrations were determined using an atomic absorption spectrophotometer (Varian 220FS SpectrAA, Palo Alto, California, USA). Solutions with known content of these minerals were used as standard. The mineral content was normalized by protein levels in serum.

2.8. Lipid and Protein Oxidation. Lipid oxidation was estimated from malondialdehyde quantification by high-performance liquid chromatography (HPLC). Briefly, serum samples were separated on a 250 mm \times 4.6 mm i.d. VC-ODS RP18 column with 50:50 (v/v) 25 mM phosphate buffer (pH 6.5). Methanol was used as the mobile phase with a flow rate of 0.8 ml min⁻¹. Fluorometric detection was performed at wavelengths of 532 nm excitation and 553 nm emission using a RF-10AXL detector coupled to the HPLC system (Shimadzu Scientific Instruments, Kyoto, Japan) to ensure the sensitivity for low concentrations of MDA (TBA)₂ adduct. Tetraethoxypropane was processed in the same way as the serum samples and was applied to calibrate the peak of MDA-TBA [37].

Protein oxidation was estimated by the quantification of protein carbonyl (PCn) serum levels. Protein carbonyl was measured by forming labeled protein hydrazone derivatives, using 2,4-dinitrophenylhydrazine, which were quantified at 370 nm in a spectrophotometer (Biochrom Libra 522, Berlin, Germany) [38]. The carbonyl content was determined considering the molar absorption coefficient of 21,000 M⁻¹ cm⁻¹ and expressed as nmol mg protein⁻¹ [39]. MDA and PCn results were normalized by protein levels, which were measured by the Bradford method [40].

2.9. Enzymatic Antioxidant Defenses. Erythrocytes were obtained after blood centrifugation at 1800 g, 5°C for 10

minutes. The erythrocytes' glutathione peroxidase (GPx) activity was measured by enzymatic assay using a colorimetric commercial kit (Cayman Chemical, Ann Arbor, MI). The assay was based on two coupled reactions: (i) reduction of hydrogen peroxide (H_2O_2) to water by GPx, with the conversion of reduced glutathione (GSH) to oxidized glutathione (GSSH), and (ii) GSH recovery from GSSH catalyzed by glutathione reductase, with NADPH oxidation to $NADP^+$. In this reaction, absorbance decay at 340 nm is directly proportional to GPx activity, expressed in nmol/ml/minute [25].

2.10. Total and Nonprotein Antioxidant Capacity. Total and nonprotein antioxidant defenses in serum were analyzed by using a commercial colorimetric biochemical kit, according to the manufacturer's instructions (TAC Assay Kit, Sigma Aldrich, Milwaukee, USA). The method is based on Cu^{2+} conversion to Cu^+ by both small molecules and proteins. Small antioxidant molecules were isolated from protein antioxidants by using a chemical mask, which prevents Cu^{2+} reduction by proteins. The antioxidant capacity (mM) was analyzed in a spectrophotometer at 570 nm and estimated from a standard curve using trolox as the antioxidant reference.

2.11. Statistical Analysis. Data were expressed as the frequencies, mean, and standard deviation or median, depending on the variable's distribution, which was analyzed by the D'Agostino-Pearson test. The difference between the frequency of malnutrition for the different anthropometric and biochemical markers, according to sex and age, was analyzed using Pearson's chi-squared or Fisher's exact tests. Student's *t*-test or Mann-Whitney *U* test was applied to compare body composition, nutrient intake, and biochemical data according the nutritional stratification obtained from GOA. Macronutrient intake was adjusted by body mass, and micronutrients were adjusted by daily energy intake according the residual method [41]. The association between protein and lipid oxidation with nutritional intake and blood antioxidants was analyzed by Pearson's correlation coefficient and multiple linear regression. The receiver operator characteristic (ROC) curve was analyzed using 50% of data distribution (median) as cut-off for lipid and protein oxidation. The discriminative potential of ROC statistics was classified as excellent (>90%), good (>80% < 90%), regular (>70% < 80%), weak (>60% < 70%), or inadequate (<60%). Values of $P \leq 0.05$ were considered statistically significant in all tests.

3. Results

The investigated sample was mostly composed of individuals ranging from 18 to 65 years of age (73.5%, men = 49% and women = 24.5%), with a mean weight of 66.69 ± 15.38 kg (CV = 0.20). Systemic arterial hypertension alone (77.6%) and diabetes mellitus (12.3%) were the main causes of ESRD. The frequency of alcohol intake was low (6.1%), and the mean time in HD was 4.09 ± 2.77 years. Predialysis urea concentration was higher in men rather than in women ($P < 0.05$). Most patients (65.3%) presented $Kt/V \geq 1.2$. Sex exerted

no significant impact on postdialysis urea, hemoglobin, creatinine, and urea reduction rate (Table 1).

From all anthropometric parameters analyzed, cardiometabolic risk and malnutrition indicated by WC and WHR were significantly associated with sex and age ($P < 0.05$), and AAMA was significantly associated with age groups ($P < 0.05$), but not sex ($P > 0.05$). Women and elderly patients exhibited higher frequency of the increased risk of metabolic complications indicated by WC and WHR. Cardiometabolic and malnutrition risks estimated from BMI, AC, AFA, mGSA, and GOA were similarly distributed according to sex and age groups ($P > 0.05$). Considering all patients, high prevalence of mild or moderate malnutrition was identified from mGSA (93.9%) and GOA (98.0%) (Table 2).

The estimative of malnutrition obtained from GOA was closely correlated with anthropometric evaluation. When the patients were stratified by the risk of malnutrition according to GOA, almost all anthropometric parameters analyzed, except biceps skinfolds thickness and lean mass $\Sigma 4ST$, were significantly reduced in patients with moderate malnutrition compared with patients with nutritional risk/mild malnutrition ($P < 0.05$) (Table 3).

In general, energy-adjusted vitamin and mineral dietary intake was significantly increased in patients with moderate malnutrition compared with patients with nutritional risk/mild malnutrition ($P < 0.05$), while vitamin C intake was drastically reduced in patients with moderate malnutrition than those with nutritional risk/mild malnutrition ($P < 0.05$). Manganese and vitamin C intake was similar in both groups ($P > 0.05$) (Table 4).

Protein and lipid peroxidation, as well as the levels of plasmatic antioxidant mediators, were similar in both groups, independent of malnutrition classification by GOA ($P > 0.05$) (Table 5).

Considering the similar status redox in both groups stratified by GOA, lipid and protein oxidation was correlated with nutritional intake (only carbohydrate and zinc) and plasmatic antioxidants for all patients. Carbohydrate intake was directly correlated with MDA and PCn levels ($P < 0.05$), while zinc intake and serum levels, GPx activity, TAC, and npAC were inversely correlated with MDA and PCn ($P < 0.05$) (Table 6).

When the variables correlated with MDA and PCn were applied in multiple linear regression models, 58.8% of MDA and of 58.1% PCn variability were predicted by carbohydrate and zinc intake, GPx activity, TAC, and npAC ($P < 0.05$). Carbohydrate intake was the best independent predictor of lipid oxidation ($P < 0.05$) and together with TAC was consistent predictors of protein oxidation ($P < 0.05$) (Table 7).

ROC curve analysis was used to evaluate the accuracy of nutrient intake and plasma antioxidant concentrations to predict MDA and PCn levels in HD patients. Complementary to multiple linear regression analysis, serum zinc, GPx activity, TAC, and npAC were the most sensitive markers (good [>80% < 90%] or excellent [>90%] sensitivity) to predict lipid oxidation ($P < 0.05$). While serum zinc exhibited good sensitivity, GPx activity and TAC were markers with

TABLE 1: General characteristics of the patients in hemodialysis.

Variables	Total (<i>n</i> = 49)	Women (<i>n</i> = 20)	Men (<i>n</i> = 29)	<i>P</i> value
Age, <i>n</i> (%)				
>18 < 65	36 (73.5)	12 (24.5)	24 (49.0)	0.104
≥65	13 (26.5)	8 (16.3)	5 (10.2)	
Weight (kg), mean ± S.D.	66.69 ± 15.32	62.23 ± 15.07	70.00 ± 14.92	0.085
Comorbidities, <i>n</i> (%)				
SAH	38 (77.6)	15 (30.6)	23 (46.9)	0.373
DM+SAH	7 (14.3)	2 (4.1)	5 (10.2)	
Others*	4 (8.2)	3 (6.1)	1 (2.0)	
Smoking, <i>n</i> (%) (cigars/day)				
Yes	7 (14.3) 20	2 (4.1) 15	5 (10.2) 5	0.684
No	42 (85.7)	18 (36.7)	24 (49.0)	
Alcohol intake, <i>n</i> (%) (g/day)				
Yes	3 (6.1) 50	0 (0)	3 (6.1) 50	0.260
No	46 (93.9)	20 (40.8)	26 (53.1)	
Time in hemodialysis (months), mean ± S.D.	4.09 ± 2.77	3.91 ± 1.48	4.23 ± 3.50	0.275
Urea predialysis (mg/dl), mean ± S.D.	82.92 ± 19.96	75.71 ± 15.11	81.52 ± 21.67	0.026
Urea postdialysis (mg/dl), mean ± S.D.	22.08 ± 10.18	21.24 ± 11.04	22.74 ± 9.62	0.406
Creatinine (mg/dl), mean ± S.D.	8.14 ± 2.34	7.45 ± 2.11	8.67 ± 2.41	0.072
Hemoglobin (g/dl), mean ± S.D.	11.23 ± 1.95	10.81 ± 1.55	11.57 ± 2.18	0.181
Urea reduction rate (%), mean ± S.D.	72.97 ± 11.49	71.64 ± 13.95	74.01 ± 9.29	0.484
<i>Kt/V</i> , <i>n</i> (%)				
<1.2	17 (34.7)	8 (16.3)	9 (18.4)	0.555
≥1.2	32 (65.3)	12 (24.5)	20 (40.8)	

DM: diabetes mellitus; SAH: systemic arterial hypertension; other comorbidities = hypothyroidism, systemic lupus erythematosus, and hepatitis C; Kt/V — K = urea clearance dialyzer, t = treatment time, V = volume of distribution of urea; S.D.: standard deviation of the mean. *P* values represent the result of Pearson's chi-squared test or Fisher's exact test for categorical variables and Student's *t*-test or Mann-Whitney *U* test for continuous variables. *P* values in bold indicate the statistical difference among the groups stratified by sex ($P \leq 0.05$).

regular sensitivity (>70% < 80%) to predict protein oxidation ($P < 0.05$) (Table 8).

4. Discussion

We evaluated cardiometabolic risk factors and nutritional status in HD patients, emphasizing the association between nutritional status and oxidative stress markers. Demographic, clinical, and laboratory data of our HD patients were comparable to previous reports [42]. Accordingly, our group of patients was predominantly composed of males, and hypertension was the most common etiology of ESRD. Considering that hypertension is a potentially preventable and/or treatable condition, it is worrying that this disease is still a primary etiological agent of CKD [43].

In the current study, we identified a low frequency of alcohol intake and smoking, and most patients (73.5%) were submitted to HD for two or more years. In 65.3% cases, we identified adequate and efficient dialysis dose [44], a relevant finding since a close correlation between HD dose, patient morbidity, and mortality has been reported [44]. Although signs and symptoms are relevant in patient monitoring, they are not enough to indicate the dose of dialysis. Accordingly, the quality of HD can be measured by Kt/V , which consider urea levels, duration of HD session, and body mass. From this method, a dose of HD can be appropriately estimated for patients who undergo three sessions per week, in which values of Kt/V above 1.2 are interpreted as efficient doses of HD [45].

TABLE 2: Cardiometabolic and malnutrition risk in hemodialysis patients by gender and age.

Variables	Total (<i>n</i> = 49), <i>n</i> (%)	Women (<i>n</i> = 20), <i>n</i> (%)*	Men (<i>n</i> = 29), <i>n</i> (%)*	<i>P</i> value	Adult (<i>n</i> = 29), <i>n</i> (%)*	Elderly (<i>n</i> = 20), <i>n</i> (%)*	<i>P</i> value
BMI							
Underweight	4 (8.2)	1 (2.0)	3 (6.1)		3 (6.12)	1 (2.0)	
Normal weight	25 (51)	11 (22.4)	14 (28.6)	0.080	12 (24.5)	13 (26.5)	0.262
Overweight	20 (40.8)	8 (16.3)	12 (24.5)		14 (28.6)	6 (12.2)	
WC							
Adequate	34 (69.4)	9 (18.4)	25 (51)	0.002	25 (86.2)	9 (45)	0.002
Inadequate	15 (30.6)	11 (22.4)	4 (8.2)		4 (13.8)	11 (55)	
WHR							
No risk	31 (63.2)	5 (10.2)	25 (51.3)	<0.001	24 (48.9)	10 (20.4)	0.014
Risk	19 (36.8)	15 (30.6)	4 (8.1)		5 (10.2)	10 (20.4)	
AC							
Adequate nutrition	32 (65.3)	15 (30.6)	17 (34.7)		20 (40.8)	12 (24.5)	
Mild malnutrition	9 (18.3)	2 (4)	7 (14.3)	0.545	7 (14.3)	2 (4)	0.132
Moderate malnutrition	7 (14.3)	3 (6.1)	4 (8.1)		2 (4)	5 (10.2)	
Severe malnutrition	1 (2.1)	0 (0)	1 (2.1)		0 (0)	1 (2.1)	
AAMA							
Adequate nutrition	26 (53)	14 (28.5)	12 (24.5)		18 (36.7)	8 (16.3)	
Mild/moderate malnutrition	16 (32.6)	6 (12.2)	10 (20.4)	0.035	6 (12.2)	10 (20.4)	0.098
Severe malnutrition	7 (14.4)	0 (0)	7 (14.3)		5 (10.2)	2 (8.1)	
AFA							
Adequate nutrition	20 (40.8)	9 (18.3)	11 (22.4)		12 (24.5)	8 (16.3)	
Mild malnutrition	23 (46.9)	9 (18.3)	14 (28.6)	0.856	11 (22.4)	12 (24.5)	0.068
Moderate malnutrition	6 (12.3)	2 (4.0)	4 (8.1)		6 (12.2)	0 (0)	
mGSA, <i>n</i> (%)							
Appropriate	3 (6.1)	1 (2)	2 (6.9)	0.517	2 (4)	1 (2.0)	0.785
Risk/mild malnutrition	46 (93.9)	19 (38.7)	27 (93.1)		27 (55.1)	19 (38.7)	
GOA							
Appropriate	1(2.0)	1 (2.0)	0 (0)		1 (2.0)	0 (0)	
Risk/mild malnutrition	30 (61.2)	14 (28.5)	16 (32.6)	0.447	20 (40.8)	10 (20.4)	0.222
Moderate	18 (36.8)	5 (10.2)	13 (26.5)		8 (16.3)	10 (20.4)	

BMI: body mass index; WC: waist circumference; WHR: waist-hip ratio; AC: arm circumference; AAMA: adjusted-arm muscle area; AFA: fat arm area; mGSA: modified global subjective assessment; GOA: global objective assessment. *In the total sample, *P* values in bold indicated significant association of sex or age with cardiometabolic and malnutrition risk analyzed by Pearson's chi-squared test or Fisher's exact test.

Anthropometric parameters were limited predictors of malnutrition compared with mGSA and GOA, which showed high validity, reliability, and reproducibility to diagnose malnutrition in HD patients [46]. We identified that the high risk of malnutrition was homogeneously distributed in both age and gender groups, a finding in line with the high prevalence (18-70%) of malnutrition in ESRD patients undergoing HD [47]. To date, there is no consensus or guidelines on desirable or ideal anthropometric measures for HD patients [48]. In the absence of specific evidence, cut-off points applied to the general adult population have been used to identify malnutrition and to stratify HD patients in groups exposed to distinct cardiometabolic risk factors [48]. In addition to the standard biochemical monitoring adopted in HD centers, nutritional evaluation provides a simple, low-cost, and rapid estimation of the clinical condition of HD patients. Anthropometric and nutritional parameters, including BMI,

WC, WHR, fat mass, and macro- and micronutrient intake, are closely related with the risk of death by cardiovascular events in the general population [47]. However, these relations are not obvious and are highly complex in HD patients due to metabolic imbalance associated with kidney failure and accumulation of uremic toxins [49].

Anthropometrical parameters may have diverse impact in healthy individuals when compared to ESRD patients. For instance, high values of body adiposity and BMI frequently are related to cardiovascular events in healthy individuals, whereas in ESRD patients under HD, slightly high BMI values have been associated with increased survival rates in a 12-month follow-up [14, 48]. In addition, patients who are in the upper 10 percentile of body weight for height have the highest monthly survival rates [50]. Conversely, patients in maintenance dialysis in the lower 50th percentile of body weight-for-height clearly exhibited reduced survival rates

TABLE 3: Anthropometric, body composition, and biochemical variables of hemodialysis patients ($n = 48^*$) stratified according to the global objective assessment (GOA).

Variables	Nutritional risk/mild malnutrition ($n = 30$)	Moderate malnutrition ($n = 18$)	<i>P</i> value
BMI (kg/m^2)	27.81 \pm 5.28	20.14 \pm 2.22	<0.001
AC (cm)	30.78 \pm 3.55	23.30 \pm 6.39	<0.001
AMA (cm^2)	51.43 \pm 16.98	39.00 \pm 11.44	0.002
AFA (cm^2)	22.57 \pm 11.92	10.60 \pm 5.01	<0.001
Biceps ST (mm)	10.28 \pm 6.34	6.93 \pm 3.47	0.062
Suprailiac ST (mm)	14.14 \pm 6.26	7.60 \pm 3.76	<0.001
Triceps ST (mm)	16.45 \pm 7.25	10.00 \pm 5.73	0.005
Subscapular ST (mm)	17.59 \pm 7.91	9.40 \pm 5.33	<0.001
WC (cm)	97.78 \pm 13.18	74.97 \pm 16.73	<0.001
HC (cm)	101.40 \pm 11.41	87.13 \pm 5.38	<0.001
WHR	0.96 \pm 0.09	0.88 \pm 0.10	0.013
WHtR	0.60 \pm 0.09	0.45 \pm 0.09	<0.001
CNI	60.17 \pm 12.99	39.93 \pm 10.57	<0.001
BAI	30.91 \pm 7.74	22.87 \pm 3.34	<0.001
Fat mass Σ 4ST (kg)	20.61 \pm 6.75	9.98 \pm 5.04	<0.001
Lean mass Σ 4ST (kg)	52.52 \pm 12.11	46.13 \pm 8.36	0.075

BMI: body mass index; AC: arm circumference; AMA: arm muscle are; AFA: arm fat area; ST: skinfold thickness; WC: waist circumference; HC: hip circumference; WHR: waist-hip ratio; WHtR: waist-height ratio; CNI: conicity index; BAI: body adiposity index; Σ 4ST: sum of four skinfolds thickness. *One patient with adequate nutrition in GOA was excluded. Values expressed as the mean \pm standard deviation. *P* values in bold indicate statistical difference among the groups stratified according to GOA ($P \leq 0.05$).

[51]. Although normal weight or overweight was identified in the present study, the classification of underweight from BMI and malnutrition from mGSA and GOA provided an interesting tool to stratify HD patients in risk groups, an information that might be potentially relevant in clinical decision-making.

Currently, instruments such as mGSA and GOA are often underestimated in the assessment of HD patients [30]. These tools provide a classification system that can identify malnutrition by combining multiple indicators in the nutritional assessment [30]. Herein, a mild or moderate malnutrition status was identified in most patients by means of mGSA and GOA. mGSA is a complete and validated quantitative method for nutritional diagnosis in patients under dialysis, which is related with morbidity and mortality risk in this population [52]. GOA has the same function as mGSA; however, it has been considered more specific than mGSA to assess the nutritional status in HD patients [52]. These tools have often been used in combination with complementary anthropometric and biochemical assessment methods [52], whose diagnostic and prognostic relevance for HD patients requires further clarification.

Interestingly, marked anthropometric divergences were observed when HD patients were stratified according to the nutritional status obtained from GOA. This finding suggested that robust results and a more consistent nutritional evaluation could be obtained combining these tools. Anthropometric measures are valid and clinically useful indicators of the protein energy nutritional status of patients on maintenance dialysis [49], providing together with the biochemical

analysis a more comprehensive estimation of the catabolic condition in CKD patients [14]. Considering that protein metabolism is profoundly impaired in HD patients, parameters such as muscle area, diameter, and circumference are used to estimate muscle mass, total lean mass, and somatic protein pool. Although clear cut-off points are not available, significant changes in these measurements may indicate a decline in nutritional state, which should be considered in the management of HD patient [53].

As unbalanced nutritional intake by HD patients is often reported [47], the evaluation of dietary macro- and micronutrients is highly relevant for the diagnosis of malnutrition [47]. A divergent profile of nutrient intake was clearly observed when HD patients were stratified according to GOA. Except for manganese and vitamin E, the ingestion of all macro- and micronutrients analyzed was increased in patients with moderate malnutrition. This result seems to be opposed to the anthropometric findings and the nutritional classification obtained from GOA. However, this apparent divergence indicates that the characterization of nutritional status should not be limited to assessing the dietary intake profile [46], since the metabolic imbalance and the catabolic status of HD patients should also be taken into account [4]. In this way, GOA becomes even more relevant, since biochemical parameters are additionally used as indicators of the catabolic state in this population [46]. As nutrient intake is not always associated with the diagnosis of malnutrition from anthropometric data and mGSA, dietary recall is a complementary tool in the assessment of HD patients [46].

TABLE 4: Energy-adjusted vitamin and mineral dietary intake[†] by hemodialysis patients ($n = 48^*$) stratified according to the global objective assessment (GOA).

Variables	Nutritional risk/mild malnutrition ($n = 30$)	Moderate malnutrition ($n = 18$)	P value	DR [§]
Dietary intake (g/kg) ^a	14.19 ± 5.03	34.00 ± 36.5	<0.001	(-)
Energy intake (kcal/kg) ^a	16.40 ± 6.73	75.78 ± 150.09	<0.001	(-)
Carbohydrate (g/kg/d) ^a	1.96 ± 0.81	6.34 ± 8.67	<0.001	45-65% EI
Lipid (g/kg/d)	0.59 ± 0.35	4.46 ± 13.31	0.002	20-30% EI
Protein (g/kg/d)	0.82 ± 0.41	2.59 ± 4.98	0.009	0.8-1.6
Iron (mg/d)	8.81 ± 2.14	17.71 ± 7.33	<0.001	8-18
Manganese (μg/d)	1.24 ± 0.65	1.83 ± 1.33	0.137	11
Selenium (μg/d)	73.26 ± 47.07	162.52 ± 94.87	<0.001	55
Zinc (mg/d)	6.70 ± 2.97	19.86 ± 10.91	<0.001	8-11
Vitamin C (mg/d)	120.00 ± 134.23	49.88 ± 46.18	0.029	75-90
Vitamin E (mg/d)	7.60 ± 3.83	7.89 ± 2.60	0.793	15

[†]Data obtained from a 24-hour dietary recall interview. *One patient with adequate nutrition in GOA was excluded. [§]DR: daily recommendation according U.S. National Institutes of Health. ^(c)Based on the basal metabolic rate and the level of physical activity. EI: energy intake. ^{a,b}Data adjusted by ^abody mass and ^bresidual method. Values expressed as the mean ± standard deviation. P values in bold indicate statistical difference among the groups stratified according to GOA ($P \leq 0.05$).

TABLE 5: Oxidative stress markers and antioxidant defenses in blood samples of hemodialysis patients ($n = 48^*$) according global objective assessment (GOA).

Variables	Nutritional risk/mild malnutrition ($n = 30$)	Moderate malnutrition ($n = 18$)	P value
<i>Molecular oxidation</i>			
PCn (nmol/mg pt)	63.55 ± 95.15	81.29 ± 148.58	0.400
MDA (μg/mol pt) × 10 ⁻⁸	4.31 ± 2.77	3.77 ± 2.65	0.729
<i>Antioxidant defenses</i>			
TAC (mM)	1.65 ± 0.14	1.66 ± 0.16	0.911
npAC (mM)	1.14 ± 0.16	1.09 ± 0.14	0.332
GPx (nmol/[ml/min.])	559.66 ± 62.13	533.56 ± 52.92	0.287
<i>Pro- and antioxidant minerals</i>			
Iron (μg/l)	506.40 ± 253.6	549.90 ± 291.8	0.584
Zinc (μg/l)	60.39 ± 14.28	68.26 ± 15.66	0.457
Selenium (μg/l)	54.41 ± 17.11	61.29 ± 22.05	0.240
Manganese (μg/l)	0.89 ± 0.21	0.97 ± 0.20	0.489

*One patient with adequate nutrition in GOA was excluded. PCn: carbonyl proteins; MDA: malondialdehyde; TAC: total antioxidant capacity; npAC: nonprotein antioxidant capacity; GPx: glutathione peroxidase activity. *One patient with adequate nutrition in GOA was excluded. Values expressed as the mean ± standard deviation. P values indicate no statistical difference among the groups stratified according to GOA ($P > 0.05$).

The adequate nutrient intake is favorable to attenuate the catabolic profile of HD patients, which seems to be associated with a sustained proinflammatory and prooxidant status triggered by the accumulation of uremic toxins [46]. The accumulation of oxidative tissue damage is directly associated with the development and progression of CKD [3], as well as with an increased risk of death by cardiovascular events in patients with ESRD [54]. The balance between pro- and antioxidant molecules seems to be a relevant indicator of cardiometabolic risk in CKD patients [54]. However, the association between nutritional profile and oxidative status remains to be fully investigated in HD patients. Interestingly, our findings revealed that the nutritional stratification from

GOA was unable to identify divergences in antioxidant mediators and lipid and protein oxidation. The anthropometric data were irrelevant indicators of molecular oxidation, when the patients were analyzed together. On the other hand, lipid and protein oxidation was directly correlated with carbohydrate intake and inversely correlated with zinc intake, GPx activity, TAC, and npAC serum levels. Taken together, these variables were able to explain 58% and 59% of the variability in protein and lipid oxidation, respectively.

The correlation between carbohydrate intake and molecular oxidation is consistent with the dietary adjustments adopted in the treatment of HD patients [3]. Based on the fact that proteins are the main sources of uremic toxins,

TABLE 6: Correlation between body mass-adjusted carbohydrate dietary intake, energy-adjusted zinc dietary intake, and enzymatic and nonenzymatic blood molecules.

Variables	Coefficient (<i>R</i>)	<i>P</i> value
<i>MDA</i> ($\mu\text{g/mol pt}$)		
CHO dietary intake (g/kg/d)	0.5220	0.0002
Zinc dietary intake (mg/d)*	-0.3139	0.0358
Serum zinc ($\mu\text{g/L}$)	-0.375	0.0111
GPx (nmol/[ml/min.])	-0.5713	<0.0001
TAC (mM)	-0.5204	0.0002
npAC (mM)	-0.4555	0.0017
<i>PCn</i> (nmol/mg pt)		
CHO dietary intake (g/kg/d)	0.4930	0.0005
Zinc dietary intake (mg/d)*	-0.3161	0.0344
Serum zinc ($\mu\text{g/l}$)	-0.402	0.0062
GPx (nmol/[ml/min.])	-0.5756	<0.0001
TAC (mM)	-0.5380	0.0001
npAC (mM)	-0.4452	0.0022

*Values adjusted by the residual method. MDA: malondialdehyde; PCn: protein carbonyl; CHO: carbohydrate; GPx: glutathione peroxidase; TAC: total antioxidant capacity; npAC: nonprotein antioxidant capacity. *P* values in bold indicate significant correlation of MDA and PCn with nutrient intake and plasmatic antioxidants ($P \leq 0.05$).

TABLE 7: Multiple linear regression model with malondialdehyde (MDA) and protein carbonyl (PCn) as dependent variables.

Variables	β coefficient	<i>P</i> value
<i>MDA</i> ($\mu\text{g/mol pt}$) as dependent		
CHO (g/kg)	0.0000000410	0.003
Zinc dietary intake (mg/d)*	-0.0000000116	0.098
Serum zinc ($\mu\text{g/l}$)	0.00000000539	0.763
GPx (nmol/[ml/min.])	-0.00000000259	0.127
TAC (mM)	-0.00000132	0.074
npAC (mM)	0.000000690	0.912
$R^2 = 0.588$ ($P < 0.001$)		
<i>PCn</i> (nmol/mg pt) as dependent		
CHO dietary intake (g/kg/d)	8.075	<0.004
Zinc dietary intake (mg/d/d)*	-2.460	0.094
Serum zinc ($\mu\text{g/l}$)	0.916	0.807
GPx (nmol/[ml/min.])	-0.532	0.136
TAC (mM)	-312.209	0.045
npAC (mM)	48.377	0.711
$R^2 = 0.581$ ($P < 0.001$)		

*Values adjusted by the residual method. CHO: carbohydrate; GPx: glutathione peroxidase; TAC: total antioxidant capacity; npAC: nonprotein antioxidant capacity. Equations obtained from multiple linear regression analysis: PCn (nmol/mg pt) = $779.887 + (8.075 * \text{CHO}) - (2.460 * \text{DZinc}) + (0.916 * \text{SZinc}) - (0.532 * \text{GPx}) - (312.209 * \text{TAC}) + (48.377 * \text{npAC})$. MDA ($\mu\text{g/mol pt}$) = $0.00000357 + (0.0000000410 * \text{CHO}) - (0.0000000116 * \text{DZinc}) + (0.00000000539 * \text{SZinc}) - (0.00000000259 * \text{GPx}) - (0.00000132 * \text{TAC}) + (0.000000690 * \text{npAC})$. *P* values in bold indicate statistical significance for individual predictors in the regression models ($P \leq 0.05$).

protein intake should be highly adjusted in HD patients [55]. About 1.2 to 1.3 g/kg/day is recommended for patients under maintenance dialysis [55]. Of note, manipulation of diet composition is required until achieving a neutral or positive nitrogen balance [52, 56]. Accordingly, due to disturbance in lipid metabolism and increased cardiovascular risk in HD patients [10], the enhanced intake of carbohydrate rather than that of lipids is often recommended to obtain energy-adjusted diets [3]. Apart from the fact that this adjustment seems to be quite necessary, high carbohydrate intake (i.e., glycemic load and glycemic index) has been associated with systemic inflammation and oxidative stress in HD patients [9, 57], independently of the body composition [57].

Patients under HD are also instructed to avoid water and mineral excess in their meals to limit interdialytic weight gain [56]. As a consequence, the diet is often restricted in antioxidant-rich foods, which may potentiate the associated nutritional deficiencies [4]. Although no divergences in mineral serum levels have been identified, the values of iron, manganese, selenium, and zinc are close to the lower limit estimated for the general population [58, 59]. Among these minerals, only Zn presented significant sensitivity to predict lipid and protein oxidation. Zn is an essential trace mineral often depleted in HD patients. Reduced levels of this mineral are a risk factor for increased oxidative stress in this population [57]. It has also been reported that there is a correlation between Zn levels and Cu/Zn ratio in serum with the nutritional, redox, and inflammatory status in patients under dialysis [60]. A cohort study showed that reduced Zn levels were associated with lipid peroxidation and inflammation, acting as strong predictors of cardiovascular death in HD patients [61]. Zn supplementation is proved to be efficient in restoring Zn serum levels and reducing inflammation and protein catabolic state in patients undergoing HD [61]. Considering the diagnostic, prognostic, and therapeutic potential of Zn in this population, the nutritional evaluation of Zn dietary intake might be relevant to identify and correct micronutrient deficiencies [60].

Minerals such as manganese and selenium are also essential cofactors of antioxidant enzymes; however, these elements were unable to predict molecular oxidation in our patients. Nevertheless, GPx activity, TAC, and npAC were sensitive markers of lipid and protein oxidative damage. Reduction of TAC, glutathione, and GPx activity is often reported in this population [3]. In general, increased molecular oxidation has been partially attributed to deficiencies in antioxidant defenses, which develop at early stages of CKD and worsen as renal dysfunction and the accumulation of uremic toxins exacerbate [3]. Nonprotein mediators, such as vitamins C and E, are also involved in TAC [62]. While vitamin C intake was adequate, we observed a reduction of vitamin E intake in HD patients compared with the recommendations for the general population [20]. This finding corroborates with the reduced antioxidant-rich food intake in CKD patients, which is correlated with decreased enzymatic and nonprotein antioxidant defenses and increased oxidative stress measured in blood samples [60]. As the severity of renal disease seems to be associated with the magnitude of these changes, it is quite reasonable to hypothesize that

TABLE 8: Comparison between the areas under the ROC curve of malondialdehyde (MDA) and protein carbonyl (PCn) in relation to body mass-adjusted carbohydrate dietary intake, energy-adjusted zinc dietary intake, and blood antioxidant parameters.

Test result	AUC	SEM	CI (95%)	P value
<i>MDA (μg/mol pt)</i>				
CHO (g/kg/d)	0.5737	0.1010	0.3757–0.7718	0.4328
Zinc dietary intake (mg/d)*	0.5253	0.09796	0.3333–0.7174	0.7874
Serum zinc (μg/L)	0.9954	0.00624	0.9832–1.008	<0.0001
GPx (nmol/[ml/min.])	0.9055	0.04995	0.8076–1.003	<0.0001
TAC (mM)	0.9608	0.02535	0.9111–1.011	<0.0001
npAC (mM)	0.8018	0.06524	0.6740–0.9297	0.0013
<i>PCn (nmol/mg pt)</i>				
CHO (g/kg/d)	0.5455	0.08794	0.3731–0.7179	0.6015
Zinc dietary intake (mg/d)*	0.5632	0.08736	0.3920–0.7345	0.4675
Serum zinc (μg/l)	0.8913	0.04949	0.7943–0.9883	<0.0001
GPx (nmol/[ml/min.])	0.7806	0.06761	0.6481–0.9132	0.0012
TAC (mM)	0.7115	0.08034	0.5540–0.8690	0.0151
npAC (mM)	0.6581	0.08248	0.4964–0.8198	0.0693

*Values adjusted by the residual method. CHO: carbohydrate; GPx: glutathione peroxidase; TAC: total antioxidant capacity; npAC: nonprotein antioxidant capacity; AUC: area under the curve; SEM: mean standard error; CI: confidence interval. Values of *P* in bold indicate statistical significance of AUC obtained from individual predictors of MDA and PCn levels ($P \leq 0.05$).

imbalance in redox metabolism may be both a cause and a consequence of CKD [54, 60]. However, it is not a consensus whether supplementation with antioxidant vitamins and minerals may modify the cardiometabolic risk in HD patients [62].

Herein, we provided evidence that age and sex exhibited a limited association with malnutrition and cardiometabolic risk factors in HD patients. By using mGSA and GOA, we found a high prevalence of malnutrition. Moreover, a patient's stratification according to the nutritional risk obtained from GOA was highly consistent with the anthropometric parameters and nutrient intake, complementarily used as markers of malnutrition. Although this stratification was unable to reveal differences in the oxidative status, carbohydrate and Zn dietary intake, GPx activity, TAC, npAC, and Zn serum levels were predictive markers of lipid and protein oxidation. Thus, serum antioxidant mediators seem to have a greater predictive sensitivity to estimate molecular oxidative damage in HD patients.

Data Availability

The data used to support the findings of this study are included within the article.

Conflicts of Interest

The authors declare that there are no conflicts of interest.

Acknowledgments

This work was supported by the following Brazilian agencies: Fundação do Amparo à Pesquisa do Estado de Minas Gerais (FAPEMIG, processes APQ-01895-16 and PPM-00077-18) and Conselho Nacional de Desenvolvimento

Científico e Tecnológico (CNPq, processes 303972/2017-3, 305093/2017-7, and 423594/2018-4). This study was financed in part by the Coordenação de Aperfeiçoamento de Pessoal de Nível Superior (CAPES), Brazil (Finance Code 001).

References




- [1] D. Fouque, K. Kalantar-Zadeh, J. Kopple et al., "A proposed nomenclature and diagnostic criteria for protein-energy wasting in acute and chronic kidney disease," *Kidney International*, vol. 73, no. 4, pp. 391–398, 2008.
- [2] J. J. Carrero, P. Stenvinkel, L. Cuppari et al., "Etiology of the protein-energy wasting syndrome in chronic kidney disease: a consensus statement from the International Society of Renal Nutrition and Metabolism (ISRNM)," *Journal of Renal Nutrition*, vol. 23, no. 2, pp. 77–90, 2013.
- [3] A. P. Epifânio, K. P. Balbino, S. M. Ribeiro, S. C. Franceschini, and H. H. Hermsdorff, "Clinical-nutritional, inflammatory and oxidative stress predictors in hemodialysis mortality: a review," *Nutrition Hospitalaria*, vol. 35, pp. 461–468, 2018.
- [4] M. Bossola, E. di Stasio, A. Viola et al., "Dietary intake of trace elements, minerals, and vitamins of patients on chronic hemodialysis," *International Urology and Nephrology*, vol. 46, no. 4, pp. 809–815, 2014.
- [5] T. A. Ikizler, "Optimal nutrition in hemodialysis patients," *Advances in Chronic Kidney Disease*, vol. 20, no. 2, pp. 181–189, 2013.
- [6] F. G. Bigogno, R. L. Fetter, and C. M. Avesani, "Applicability of subjective global assessment and malnutrition inflammation score in the assessment of nutritional status on chronic kidney disease," *Jornal Brasileiro de Nefrologia*, vol. 36, no. 2, pp. 236–240, 2014.
- [7] M. Ruperto, F. J. Sánchez-Muniz, and G. Barril, "Predictors of protein-energy wasting in haemodialysis patients: a cross-

- sectional study,” *Journal of Human Nutrition and Dietetics*, vol. 29, no. 1, pp. 38–47, 2016.
- [8] R. Zafar, “A new insight into pathogenesis of cardiovascular diseases: stress induced lipid mediated, vascular diseases,” *Journal of Cardiovascular Diseases and Diagnosis*, vol. 3, pp. 2–21, 2015.
- [9] V. Liakopoulos, S. Roumeliotis, X. Gorny, E. Dounousi, and P. R. Mertens, “Oxidative stress in hemodialysis patients: a review of the literature,” *Oxidative Medicine and Cellular Longevity*, vol. 2017, Article ID 3081856, 22 pages, 2017.
- [10] G. Boudouris, I. I. Verginadis, Y. V. Simos et al., “Oxidative stress in patients treated with continuous ambulatory peritoneal dialysis (CAPD) and the significant role of vitamin C and e supplementation,” *International Urology and Nephrology*, vol. 45, no. 4, pp. 1137–1144, 2013.
- [11] S. Said and G. T. Hernandez, “The link between chronic kidney disease and cardiovascular disease,” *Journal of Nephro-pathology*, vol. 3, no. 3, pp. 99–104, 2014.
- [12] S. M. D. Brucki, R. Nitrini, P. Caramelli, P. H. F. Bertolucci, and I. H. Okamoto, “Suggestions for utilization of the mini-mental state examination in Brazil,” *Arquivos de Neuro-Psiquiatria*, vol. 61, no. 3B, pp. 777–781, 2003.
- [13] M. C. Riella and C. Martins, *Nutrição e o Rim*, Guanabara Koogan, Rio de Janeiro, 1st edition, 2001.
- [14] National Kidney Foundation, “K/DOQI - clinical practice guidelines for nutrition in chronic renal failure,” *American Journal of Kidney Diseases*, vol. 35, pp. S1–140, 2000.
- [15] D. B. Jelliffe, *Evaluacion del Estado de Nutrición de la Comunidad. Série de Monografias*, Ginebra: Organización Mundial de la Salud, 1968.
- [16] World Health Organization (WHO), “Physical status: the use and interpretation of anthropometry. Report of a WHO expert committee. WHO technical report series no. 854. Pp. 452. (WHO, Geneva, 1995.) Swiss Fr 71.00,” *Journal of Biosocial Science*, vol. 30, no. 1, pp. 135–144, 1995.
- [17] A. C. G. Duarte, *Avaliação Nutricional: Aspectos Clínicos e Laboratoriais*, Atheneu, 2007.
- [18] F. de Carvalho Vidigal, A. Q. Ribeiro, N. Babio, J. Salas-Salvadó, and J. Bressan, “Prevalence of metabolic syndrome and pre-metabolic syndrome in health professionals: LATINMETS Brazil study,” *Diabetology and Metabolic Syndrome*, vol. 7, no. 1, article 3, pp. 1–9, 2015.
- [19] R. Valdez, “A simple model-based index of abdominal adiposity,” *Journal of Clinical Epidemiology*, vol. 44, no. 9, pp. 955–956, 1991.
- [20] R. N. Bergman, D. Stefanovski, T. A. Buchanan et al., “A better index of body adiposity,” *Obesity*, vol. 19, no. 5, pp. 1083–1089, 2011.
- [21] National Research Council (US) Committee on Technological Options to Improve the Nutritional Attributes of Animal Products, *Designing Foods: Animal Product Options in the Marketplace*, Washington: National Academy Press, 1988.
- [22] A. R. Frisancho, “New norms of upper limb fat and muscle areas for assessment of nutritional status,” *American Journal of Clinical Nutrition*, vol. 34, no. 11, pp. 2540–2545, 1981.
- [23] J. M. Gurney and D. B. Jelliffe, “Arm anthropometry in nutritional assessment: nomogram for rapid calculation of muscle circumference and cross-sectional muscle and fat areas,” *American Journal of Clinical Nutrition*, vol. 26, no. 9, pp. 912–915, 1973.
- [24] S. B. Heymsfield, C. McManus, J. Smith, V. Stevens, and D. W. Nixon, “Anthropometric measurement of muscle mass: revised equations for calculating bone-free arm muscle area,” *The American Journal of Clinical Nutrition*, vol. 36, no. 4, pp. 680–690, 1982.
- [25] K. B. F. Barbosa, A. C. P. Volp, J. L. Marques-Rocha et al., “Modulators of erythrocyte glutathione peroxidase activity in healthy adults: an observational study,” *Redox Report*, vol. 19, no. 6, pp. 251–258, 2014.
- [26] P. M. G. Pereira, G. A. da Silva, G. M. Santos, E. L. Petroski, and A. A. R. Gerales, “Development and validation of anthropometric equations to estimate appendicular muscle mass in elderly women,” *Nutrition Journal*, vol. 12, no. 1, article 670, 2013.
- [27] J. V. G. A. Durnin and J. Womersley, “Body fat assessed from total body density and its estimation from skinfold thickness: measurements on 481 men and women aged from 16 to 72 years,” *British Journal of Nutrition*, vol. 32, no. 1, pp. 77–97, 1973.
- [28] T. Vos, R. M. Barber, B. Bell et al., “Global, regional, and national incidence, prevalence, and years lived with disability for 301 acute and chronic diseases and injuries in 188 countries, 1990–2013: a systematic analysis for the Global Burden of Disease Study 2013,” *The Lancet*, vol. 386, no. 9995, pp. 743–800, 2015.
- [29] K. P. Balbino, A. P. S. Epifânio, S. M. R. Ribeiro, L. D. M. da Silva, M. G. Gouvea, and H. H. M. Hermsdorff, “Comparison between direct and indirect methods to diagnose malnutrition and cardiometabolic risk in haemodialysis patients,” *Journal of Human Nutrition and Dietetics*, vol. 30, no. 5, pp. 646–654, 2017.
- [30] L. A. Barufaldi, A. Abreu Gde, G. V. Veiga et al., “Software to record 24-hour food recall: application in the study of cardiovascular risks in adolescents,” *Brazilian Journal of Epidemiology*, vol. 19, no. 2, pp. 464–468, 2016.
- [31] Núcleo de Estudos e Pesquisas em Alimentação (NEPA/UNICAMP), *Tabela Brasileira de Composição de Alimentos*, NEPA-UNICAMP, Campinas, Brazil, 4th edition, 2011.
- [32] S. T. Philippi, *Table of Food Composition: Support for Nutritional Decision*, Manole, São Paulo, 5th edition, 2016.
- [33] S. T. Philippi, *Table of Food Composition: Support for Nutritional Decision*, Manole, Barueri, SP, 3th edition, 2012.
- [34] P. G. Cocate, A. J. Natali, A. . Oliveira et al., “Red but not white meat consumption is associated with metabolic syndrome, insulin resistance and lipid peroxidation in Brazilian middle-aged men,” *European Journal of Preventive Cardiology*, vol. 22, no. 2, pp. 223–230, 2013.
- [35] National Institute of Health (NIH) - Office of Dietary Supplements, “Dietary supplement fact sheets,” 2018, <https://ods.od.nih.gov/factsheets/list-all/>.
- [36] G. D. Christian, “Medicine, trace elements, and atomic absorption spectroscopy,” *Analytical Chemistry*, vol. 41, no. 1, pp. 24A–40A, 1969.
- [37] R. K. Brown and F. J. Kelly, “Peroxides and other products,” in *Free Radicals: A Practical Approach*, N. A. Punchard and F. J. Kelly, Eds., pp. 119–131, Oxford University Press, New York, NY, USA, 1996.
- [38] R. L. Levine, D. Garland, C. N. Oliver et al., “[49] Determination of carbonyl content in oxidatively modified proteins,” *Methods in Enzymology*, vol. 186, pp. 464–478, 1990.

- [39] A. Z. Reznick and L. Packer, “[38] Oxidative damage to proteins: spectrophotometric method for carbonyl assay,” *Methods in Enzymology*, vol. 233, pp. 357–363, 1994.
- [40] M. M. Bradford, “A rapid and sensitive method for the quantitation of microgram quantities of protein utilizing the principle of protein-dye binding,” *Analytical Biochemistry*, vol. 72, no. 1-2, pp. 248–254, 1976.
- [41] J. J. Rhee, E. Cho, and W. C. Willett, “Energy adjustment of nutrient intakes is preferable to adjustment using body weight and physical activity in epidemiological analyses,” *Public Health Nutrition*, vol. 17, no. 5, pp. 1054–1060, 2014.
- [42] J. J. Carrero, M. Hecking, I. Ulas, L. Sola, and B. Thomas, “Chronic kidney disease, gender, and access to care: a global perspective,” *Seminars in Nephrology*, vol. 37, no. 3, pp. 296–308, 2017.
- [43] T. Vos, C. Allen, M. Arora et al., “Global, regional, and national incidence, prevalence, and years lived with disability for 310 diseases and injuries, 1990–2015: a systematic analysis for the Global Burden of Disease Study 2015,” *The Lancet*, vol. 388, no. 10053, pp. 1545–1602, 2016.
- [44] R. C. Sesso, A. A. Lopes, F. S. Thomé, J. R. Lugon, and C. T. Martins, “Brazilian chronic dialysis survey 2016,” *Brazilian Journal of Nephrology*, vol. 39, no. 3, pp. 261–266, 2017.
- [45] G. Breitsameter, A. E. Figueiredo, and D. S. Kochhann, “Cálculo de Kt/V em hemodiálise: comparação entre fórmulas,” *Brazilian Journal of Nephrology*, vol. 34, no. 1, pp. 22–26, 2012.
- [46] A. A. C. Morais, M. A. T. Silva, J. Faintuch et al., “Correlation of nutritional status and food intake in hemodialysis patients,” *Clinics*, vol. 60, no. 3, pp. 185–192, 2005.
- [47] R. Dukkipati and J. D. Kopple, “Causes and prevention of protein-energy wasting in chronic kidney failure,” *Seminars in Nephrology*, vol. 29, no. 1, pp. 39–49, 2009.
- [48] K. Odagiri, I. Mizuta, M. Yamamoto, Y. Miyazaki, H. Watanabe, and A. Uehara, “Waist to height ratio is an independent predictor for the incidence of chronic kidney disease,” *PLoS One*, vol. 9, no. 2, article e88873, 2014.
- [49] N. J. M. Cano, M. Miolane-Debouit, J. Léger, and A. E. Heng, “Assessment of body protein: energy status in chronic kidney disease,” *Seminars in Nephrology*, vol. 29, no. 1, pp. 59–66, 2009.
- [50] J. D. Kopple, X. Zhu, N. L. Lew, and E. G. Lowrie, “Body weight-for-height relationships predict mortality in maintenance hemodialysis patients,” *Kidney International*, vol. 56, no. 3, pp. 1136–1148, 1999.
- [51] J. Lee, J. Y. Choi, Y. K. Kwon et al., “Changes in serum metabolites with the stage of chronic kidney disease: comparison of diabetes and non-diabetes,” *Clinica Chimica Acta*, vol. 459, pp. 123–131, 2016.
- [52] M. C. Riella, “Nutritional evaluation of patients receiving dialysis for the management of protein-energy wasting: what is old and what is new?,” *Journal of Renal Nutrition*, vol. 23, no. 3, pp. 195–198, 2013.
- [53] K. G. J. V. Wilkens, “Medical nutrition therapy for renal disorders,” in *Krause’s Food, Nutrition, and Diet Therapy*, M. L. Kathleen and E.-S. Sylvia, Eds., pp. 921–958, Saunders Elsevier, 2008.
- [54] D. Elkabbaj, A. Bahadi, Y. Cherrah, M. Errasfa, and R. Eljaoudi, “Impact of improving quality of dialysis fluid on oxidative stress and lipid profile in hemodialysis patients,” *ISRN Nephrology*, vol. 2013, Article ID 717849, 5 pages, 2013.
- [55] M. Wolfson, “Management of protein and energy intake in dialysis patients,” *Journal of the American Society of Nephrology*, vol. 10, no. 10, pp. 2244–2247, 1999.
- [56] M. Maraj, B. Kuśnierz-Cabala, P. Dumnicka et al., “Malnutrition, inflammation, atherosclerosis syndrome (MIA) and diet recommendations among end-stage renal disease patients treated with maintenance hemodialysis,” *Nutrients*, vol. 10, no. 1, p. 69, 2018.
- [57] C. Limkunakul, M. B. Sundell, B. Pouliot, A. J. Graves, A. Shintani, and T. A. Ikizler, “Glycemic load is associated with oxidative stress among prevalent maintenance hemodialysis patients,” *Nephrology, Dialysis, Transplantation*, vol. 29, no. 5, pp. 1047–1053, 2014.
- [58] M. Rügauer, J. Klein, and J. D. Kruse-Jarres, “Reference values for the trace elements copper, manganese, selenium, and zinc in the serum / plasma of children, adolescents, and adults,” *Journal of Trace Elements in Medicine and Biology*, vol. 11, no. 2, pp. 92–98, 1997.
- [59] J. Carmona-Fonseca, “Selenium in serum and plasma: epidemiology and reference values,” *Pan American Journal of Public Health*, vol. 28, no. 5, pp. 388–398, 2010.
- [60] N. Sahni, K. L. Gupta, S. V. Rana, R. Prasad, and A. K. Bhalla, “Intake of antioxidants and their status in chronic kidney disease patients,” *Journal of Renal Nutrition*, vol. 22, no. 4, pp. 389–399, 2012.
- [61] J. C. Lobo, M. B. Stockler-Pinto, N. E. Farage et al., “Reduced plasma zinc levels, lipid peroxidation, and inflammation biomarkers levels in hemodialysis patients: implications to cardiovascular mortality,” *Renal Failure*, vol. 35, no. 5, pp. 680–685, 2013.
- [62] R. Deicher, F. Ziai, C. Bieglmayer, M. Schillinger, and W. H. Hörl, “Low total vitamin C plasma level is a risk factor for cardiovascular morbidity and mortality in hemodialysis patients,” *Journal of the American Society of Nephrology*, vol. 16, no. 6, pp. 1811–1818, 2005.

Research Article

Subacute Testicular Toxicity to Cadmium Exposure Intraperitoneally and Orally

Viviane G. S. Mouro ¹, Ana L. P. Martins,¹ Janaina Silva,¹ Tatiana P. Menezes,¹ Marcos L. M. Gomes,² Juraci A. Oliveira,¹ Fabiana C. S. A. Melo ³,
and Sérgio L. P. Matta ^{1,3}

¹Department of General Biology, Federal University of Viçosa, Viçosa, MG 36570-900, Brazil

²Department of Structural Biology, Federal University of Triângulo Mineiro, Uberaba, MG 38025-180, Brazil

³Department of Animal Biology, Federal University of Viçosa, Viçosa, 36570-900 MG, Brazil

Correspondence should be addressed to Viviane G. S. Mouro; vivianemouro@yahoo.com and Sérgio L. P. Matta; smatta@ufv.br

Received 8 April 2019; Revised 7 August 2019; Accepted 24 October 2019; Published 25 November 2019

Academic Editor: Maria R. Ciriolo

Copyright © 2019 Viviane G. S. Mouro et al. This is an open access article distributed under the Creative Commons Attribution License, which permits unrestricted use, distribution, and reproduction in any medium, provided the original work is properly cited.

The toxic effects of cadmium (Cd) on reproductive parameters are widely described in the literature. Experimental models often make use of the intraperitoneal route (*i.p.*), although human intoxication occurs preferentially by the oral route and can be continuous. However, little is known about the effect of Cd administration routes on the testicular structure. Thus, this study investigated the testicular impact of Cd exposure comparing both *i.p.* and oral routes, both single dose (SD), in addition to the oral route in fractional doses (FD). Swiss adult male mice received CdCl₂ 1.5 mg/kg *i.p.*, 30 mg/kg oral SD, and 4.28 mg/kg oral FD for 7 consecutive days. The Cd bioaccumulation was observed in all routes, mainly in the oral FD route. The concentrations of testicular Ca and Cu decreased in all animals exposed to Cd, while Zn and Mn decreased only in the *i.p.* route. Testicular SOD activity was reduced in both routes of oral administration, while CAT increased in the *i.p.* route, and GST increased in all animals exposed to Cd. Changes in the tubular parameters and cell viability were observed in both routes of Cd administration but were more intense in the oral route, mainly in the FD. Serum testosterone concentration was reduced in both routes of oral administration. Tubular damage, such as the vacuolization of the seminiferous epithelium, germ cell detachment, and seminiferous tubule degeneration, occurred in all groups exposed to Cd. Therefore, the oral Cd administration presented greater potential to promote testicular damage, mainly when the metal was given in a fractionated way.

1. Introduction

Cadmium (Cd) is a nonessential metal that can contaminate by occupational and nonoccupational exposure. Occupational exposure is associated with paint, plastic, glass, metal alloy production, and mining activities [1]. Nonoccupational exposure can occur by the ingestion of food and water containing the metal and bioaccumulation in plants and aquatic organisms [2]. Other forms of contamination are inhalation of cigarette smoke or air pollution caused by forest fires, mining areas, and metal refining industries [3].

It is known that Cd exposure can affect organs, such as the liver, lung, and kidneys, and the testicles are particularly

sensitive to toxicity mediated by this pollutant [4, 5]. Changes in testicular structure due to Cd intoxication include damage to germ and Sertoli cells, as well as degeneration and testicular necrosis [4, 6, 7], since this metal leads to the rupture of the blood-testis barrier [8, 9].

When ingested, Cd is absorbed in the duodenum by the divalent metal receptor (DMT-1), which absorbs microminerals [10, 11]. This competition may reduce the concentration of essential minerals, such as magnesium (Mg), iron (Fe), zinc (Zn), selenium (Se), and copper (Cu), which are important for the development and maintenance of spermatogenesis [6]. The aforementioned minerals act as cofactors of antioxidant enzymes, such as superoxide dismutase

[12], and a reduction of mineral levels increases reactive oxygen species (ROS) concentrations, which is also a mechanism of Cd toxicity.

Matovic et al. [13] have shown that, when Cd is administered through intraperitoneal injection (*i.p.*) (1.5 mg/kg) and at the corresponding oral dose (30 mg/kg), both in single doses, a severe acute hepatic intoxication is observed in the *i.p.* route. However, Mouro et al. [14] found that testicular damage after Cd exposure was more intense in the oral single dose (24 mg/kg) compared to the *i.p.* (1.2 mg/kg) route in the subchronic evaluation. The authors did not observe histomorphometric changes in the testicular tissue, at the used doses, in the subacute evaluation. However, it is still unknown whether the dose, route, and frequency of administration (*i.p.* or oral, single or fractionated doses) cause similar testicular damage. Therefore, the present study is aimed at verifying if Cd exposure, by oral and *i.p.* single dose and fractionated oral route, may lead to the same changes in testicular reproductive parameters in adult mice in the subacute evaluation after Cd exposure.

2. Material and Methods

2.1. Animal Model. Twenty Swiss adult male mice (8 weeks old) were maintained under controlled illumination (12-12 h light/dark) and ambient temperature ($21 \pm 1^\circ\text{C}$). Water and feed, standard rodent diet, were offered *ad libitum*. The experimental procedures were approved by the Ethics Committee on Animal Use of the Federal University of Viçosa (protocol 058/2016) and were performed in accordance with the guidelines issued by the National Council for the Control of Animal Experimentation (CONCEA).

2.2. Experimental Design and Tissue Collection. After 1 month of adaptation, the mice were randomized in four experimental groups ($n = 5$ animals/group): one control group and three groups exposed to Cd. The control group received distilled water by gavage, while the other groups received a solution of cadmium chloride (CdCl_2 , Sigma, St Louis, MO, USA) at the following concentrations: 1.5 mg/kg (0.92 mg Cd/kg) *i.p.* single dose (*i.p.* SD), 30 mg/kg (18.33 mg Cd/kg) orally by gavage single dose (oral SD), and 4.29 mg/kg/day (2.62 mg Cd/kg/day) orally by gavage for seven consecutive days (fractionated dose, oral FD). After one week, both groups exposed to oral Cd received a total of 30 mg/kg CdCl_2 . The dose of 1.5 mg/kg of CdCl_2 was chosen based on a previous study carried out by our laboratory (unpublished data). The oral dose of 30 mg/kg was chosen because Cd absorption into duodenal cells is approximately 5% of that which was orally ingested [15–17]. Thus, this dose corresponds to 1.5 mg/kg *i.p.* Furthermore, this amount is considered a safe standard rate of absorption after Cd exposure [3].

The 7-day period was adopted to observe subacute effects induced by Cd exposition before a possible rehabilitation process could change the degree of damage [4]. On the 8th day of the experiment, the animals were anesthetized (sodium thiopental 30 mg/kg *i.p.*) and euthanized by deepening the anesthesia (sodium thiopental, 150 mg/kg *i.p.*)

followed by cardiac puncture and exsanguination. The testes were collected, dissected, and weighed.

The left testis of each animal was immersed in Karnovsky fixative solution, in which approximately half of each testis was destined for histological evaluation and cell viability whereas the other half was used to determine the dosage of Cd and microminerals. The right testis of each animal was frozen (-80°C) for assessment of oxidative and nitrosative stress markers.

2.3. Cadmium Bioaccumulation and Micromineral Levels. Samples of the testis designated to this were weighed in an analytical balance (0.0001 g; BEL Mark 210A) and dried (70°C), until the dry weight was constant. The dried samples were placed in Erlenmeyer flasks with 1.5 mL of concentrated nitric acid (HNO_3) and 0.5 mL of perchloric acid (HClO_4 , 70%). Afterward, they were transferred to the hot plate. The temperature was gradually raised to 90°C so that the samples had a complete digestion. Then, the samples were diluted in deionized water in a 10 mL volumetric flask and filtered using filter papers. The concentrations of cadmium (Cd), zinc (Zn), calcium (Ca), magnesium (Mn), manganese (Mg), copper (Cu), and iron (Fe) were determined using an atomic absorption spectrophotometer (SpectrAA 220FS Varian) [14].

2.4. Assessment of Oxidative and Nitrosative Stress Markers. The frozen testes were homogenized with potassium phosphate buffer (pH 7.4, 0.1 M) containing 1 M EDTA, in the proportion of 100 mg of tissue for 1 mL of buffer, followed by centrifugation at 3000 g (6200 rpm) for 10 min. The analyses were performed in the supernatant and in duplicate.

The superoxide dismutase (SOD) activity was determined by the pyrogallol method, which is based on the ability of SOD to catalyze the superoxide radical (O^{2-}) reaction in hydrogen peroxide (H_2O_2), monitored at 570 nm in a microplate spectrophotometer (PowerWave X) [18]. The catalase (CAT) activity was assayed according to Dieterich et al. [19], by measuring the decomposition rate of H_2O_2 for 60 seconds, in a spectrophotometer, at 240 nm. The glutathione S-transferase (GST) activity was estimated spectrophotometrically, at 340 nm [20], and calculated through the formation of 1-chloro-2,4-dinitrobenzene (CDNB) conjugate.

For determining MDA levels, the samples were placed to react with thiobarbituric acid reactive substance (TBARS) solution (15% trichloroacetic acid, 0.375% thiobarbituric acid, and HCl 0.25 N) for 40 min in a water bath (90°C). TBARS formation was monitored at 535 nm in a microplate spectrophotometer (PowerWave X) [21]. Tissue levels of NO were indirectly determined by the quantification of nitrite/nitrate levels through of the standard Griess reaction [22]. Briefly, the testicular samples were placed with an equal volume of Griess reagent (1% sulfanilamide, 0.1% naphthylethylenediamine hydrochloride, and 2.5% H_3PO_4), at room temperature, for 10 min. The absorbance was measured spectrophotometrically at 570 nm. The nitrite concentration was calculated with reference to the standard curve (0.0610 to 125 μM) of sodium nitrite (NaNO_2).

2.5. Histological Preparation. The left testis was immersed in Karnovsky fixative solution (4% paraformaldehyde: 4% glutaraldehyde in phosphate buffer 0.1 mol L^{-1} , pH 7.4) [23] for 24 hours. The samples were dehydrated in crescent ethanol series and embedded in glycol methacrylate (Historesin, Leica Microsystems, Nussloch, Germany). Semiserial sections ($3 \mu\text{m}$) were obtained using a rotatory microtome (RM2255, Leica Biosystems, Nussloch, Germany), with at list $40 \mu\text{m}$ between sections. Then, the histological slides were stained with toluidine blue/sodium borate (1%). The digital images were obtained using a light-field photomicroscope (Olympus BX-53, Tokyo, Japan) connected to a digital camera (Olympus DP73, Tokyo, Japan). Finally, the histomorphometric assessment was performed using ImageJ® (National Institute of Health, USA) software.

2.6. Testicular Histopathology. For the histopathological evaluation of the testis, the proportion of normal and pathological seminiferous tubules was estimated by counting 200 random tubules per animal. The pathological tubules were separated as follows: mild pathologies (vacuolization and germinal epithelial detachment) and severe pathologies (absence of germ cells and/or Sertoli cells). This procedure was adapted from the Johnsen index [24].

2.7. Testicular Cell Viability. Histological slides containing testicular sections of $1 \mu\text{m}$ were stained with acridine orange (AO; green) and propidium iodide (PI; red) for evaluating cellular morphological changes [25]. AO is a vital dye that stains both live (viable) and dead (nonviable) cells, while PI stain only stains cells that have lost their membrane integrity. Therefore, the cellular classification was based on nuclear condensation and fragmentation as well as membrane integrity [25].

Viable cells stained by AO exhibit intact green nuclei, while nonviable cells costained by AO and PI show a dense yellow/orange/red nucleus due to chromatin condensation and the degree of loss membrane integrity [26]. Digital images were obtained using the EVOS FL photomicroscope (Life Technologies, Carlsbad, Canada) and evaluated using ImageJ® image analysis software (Media Cybernetics, Silver Spring, MD). A total area of $30 \times 10^4 \mu\text{m}^2$ per testis was used to calculate the percentage of nonviable germ cells within the seminiferous tubules [27].

2.8. Histomorphometric Evaluation of Seminiferous Tubules. The gonadosomatic index (GSI) was determined according to Amann [28] using the following equation: $\text{GSI} = \text{TW}/\text{BW} \times 100$, in which TW is the testes weight and BW is the body weight. The weight of the testicular parenchyma (PW) was considered the weight of the testis without albuginea. The parenchymosomatic index (PSI) was calculated as follows: $\text{PSI} = \text{TW}/\text{BW} \times 100$.

The proportion among the components that constitute the testicular parenchyma was obtained using square grids placed over digital images (100x magnification). A total of 2,660 intersection points were counted per animal classifying those that were on seminiferous tubules and their components (tunica propria, seminiferous epithelium, and lumen)

and interstitial tissue. The percentage of each component was determined by the following equation: volume density (%) = (number of points in the tubule or intertubule/2,660 points in total) $\times 100$. The volume (mL) of each component was obtained by the following equation: (%tubule or intertubule \times testicular parenchyma weight)/100 [29]. Considering that the density of the mammalian testis is about 1 [30], the mass of the testicle is equal to its volume.

The tubulesomatic (TSI) and epithelium somatic (ESI) indexes were also estimated using the following equations, respectively: $\text{TSI} = \text{STV}/\text{BW} \times 100$, in which STV is the seminiferous tubule volume and BW is the body weight [28], and $\text{ESI} = \text{SEV}/\text{BW} \times 100$, so that SEV is the seminiferous epithelium volume.

The seminiferous tubule diameter (STD) was considered the mean of 20 random circular seminiferous tubule cross sections from each animal regardless the tubule stage because the tubular diameter does not change in adult male mice throughout the seminiferous epithelium cycle [31]. These tubule cross sections were also used to obtain the seminiferous epithelium height (SEH), which was considered as the mean of two diametrically opposed measurements made from the tunica propria to the tubular lumen. The lumen diameter was calculated subtracting the two heights of the seminiferous epithelium from STD [32].

The seminiferous tubule area (STAr) was determined using the following equation: $\text{STAr} = \pi R^2$, in which R is the tubule radius. The lumen area (LAr) was calculated by the following equation: $\text{LAr} = \text{LR}^2$, where LR is the luminal radius. The epithelium area (EAr) was obtained by subtracting STAr from LAr. The area results were expressed as square millimeter (mm^2). The tubule epithelium ratio (TER) was obtained by dividing the STAr by the EAr [14].

The seminiferous tubule length (STL) was estimated using the following equation: $\text{STL} = \text{STV}/\pi R^2$ (STV is the seminiferous tubule volume, πR^2 is the tubule area, and $R = \text{diameter}/2$) [33]. Afterward, the STL values were divided by the testicular weight to obtain the seminiferous tubule length per gram of testis (STL/g).

2.9. Intertubular Histomorphometry Histomorphometric Evaluation of Intertubule. The proportion among the intertubular components (Leydig cell nucleus and cytoplasm, blood vessels, lymphatic space, macrophages, and connective tissue) was calculated after counting 1,000 intersection points, per animal, over the intertubular compartment. The following equation was used to calculate the percentage of such components: the percentage of each intertubular component = number of points on the component $\times 100/1000$ (total points). The following equation was applied to calculate the volume (mL) of each component: (percentage of the element in the testes \times testicular parenchyma weight)/100 [34].

The diameter of the Leydig cell nucleus was considered the mean of 30 nuclear diameters per animal (400x magnification), which had characteristic perinuclear chromatin and evident nucleoli. Nuclear (NV) and cytoplasmic volumes (CV) ($\text{NV} = 4/3(\pi R^3)$, $R = \text{nuclear diameter}/2$, and $\text{CV} = \% \text{cytoplasm} \times \text{NV}/\% \text{nucleus}$, respectively) were calculated,

followed by the calculation of the single Leydig cell volume ($LV = NV + CV$, in μm^3) [34].

The volume occupied by the Leydig cells in the testis was determined as follows: percentage of Leydig cells in the testicular parenchyma \times parenchyma weight of the testes/100. Afterward, the volume occupied by Leydig cells in the testis was divided by the testicular weight to obtain the volume that the Leydig cells occupy per gram of testis [14].

The total number of Leydig cells in the testes was determined using the following equation: volume occupied by Leydig cells in the testicular parenchyma (μm^3)/Leydig cell individual volume (μm^3). The total number of Leydig cells per gram of testis was calculated using the following equation: volume that the Leydig cell occupies per gram of testis (μm^3)/volume of one Leydig cell (μm^3). The Leydigomatic index (LSI) was calculated using the following equation: $LSI = \text{total volume of Leydig cell in the testicular parenchyma}/\text{BW} \times 100$, in which BW is the body weight [32].

2.10. Serum Testosterone Quantification. The blood was collected during anesthesia by cardiac puncture and centrifuged at $419 \times g$ for 15 min. The serum was stored in microtubes and frozen at -20°C . The serum testosterone was quantified by chemiluminescent assay, using the Access testosterone reagent kit, suitable for the Access 2 Immunoassay System (Beckman Coulter, Brea, CA).

2.11. Statistical Analysis. The percentage values were converted into sine arc to increase the statistical analysis accuracy [35]. Normal distribution was investigated by Shapiro-Wilk's test. The results obtained from the quantitative evaluations were assessed by the analysis of variance (ANOVA), followed by the Student-Newman-Keuls (SNK) post hoc method, using Statistica 7.0 program. The differences were considered significant when $p \leq 0.05$. Data were expressed as mean \pm standard deviation of the mean (SEM).

3. Results

3.1. Cadmium Bioaccumulation and Micromineral Levels. The concentration of testicular Cd increased in all routes of administration of the metal compared to the control, mainly in the oral FD, while Ca and Cu decreased in all groups exposed to Cd (Figure 1, $p \leq 0.05$). The concentration of manganese (Mn) and zinc (Zn) decreased in animals that received Cd *i.p.* SD in comparison to the control and oral FD groups, similar to the oral SD (Figure 1, $p \leq 0.05$).

3.2. Oxidative Status Analyses. SOD activity decreased in the animals that received oral Cd in both routes of administration. CAT activity increased in relation to the control group only in the animals that received Cd *i.p.*, similar to the oral routes. The activity of GST increased in *i.p.* and oral SD routes in relation to the control group (Figure 2, $p \leq 0.05$). However, the activity of this enzyme did not differ between the groups that received Cd. MDA and NO levels were not altered by Cd exposure (Figure 2, $p > 0.05$).

3.3. Biometric Parameters. Testicular and parenchyma weights decreased in animals that received oral Cd in both routes of administration (Table 1, $p \leq 0.05$). There were no changes either in body weight or in gonadosomatic and parenchymosomatic indexes in all experimental groups (Table 1, $p > 0.05$).

3.4. Testicular Histopathology. The changes in tissue architecture observed in animals exposed to Cd include degeneration of the seminiferous tubules with absence of germ cells and generalized vacuolization of the seminiferous epithelium (Figure 3). Therefore, the percentage of seminiferous tubules with mild and severe pathologies increased in all animals exposed to Cd (Figure 4, $p \leq 0.05$).

3.5. Germ Cell Viability. Animals exposed to Cd showed increased proportions of cells with initial damage, evidenced by the overlap of acridine orange and propidium iodide (merge), and positive propidium iodide cells (Figure 3). However, this percentage was higher in animals in which Cd was administered orally in both single and fractionated doses (Figure 4, $p \leq 0.05$).

3.6. Tubular Histomorphometry. The percentage and volume of the lumen increased in the animals that received Cd *i.p.* SD (Tables 2 and 3, $p \leq 0.05$). However, the lumen volume decreased in animals treated with Cd oral SD compared to the control group but was similar to Cd oral FD (Table 3, $p \leq 0.05$). The percentage of the epithelium decreased in animals exposed to Cd *i.p.* SD (Table 2, $p \leq 0.05$). However, the epithelium volume was reduced only in animals exposed to Cd oral FD compared to the control group, similar to the groups exposed to Cd. The epithelium height decreased in the Cd oral FD group in relation to the control and Cd oral SD groups (Table 3, $p \leq 0.05$).

The volume of seminiferous tubules was reduced in animals in which Cd was administered orally in both single and fractionated doses (Table 3, $p \leq 0.05$). The tubule epithelium ratio increased in animals exposed to Cd oral FD in relation to the other experimental groups (Table 3, $p \leq 0.05$). The other tubular morphometric parameters did not change after Cd exposure in both routes (Table 3, $p > 0.05$).

3.7. Intertubular Histomorphometry. The intertubular volume decreased in the animals that received Cd oral FD compared to Cd *i.p.* SD (Table 4, $p \leq 0.05$). The percentage of connective tissue was higher in animals exposed to Cd oral SD, while their volume increased in these same animals, compared to the control and Cd oral FD groups (Table 4, $p \leq 0.05$). The percentage of macrophages increased in all routes of Cd exposure, while the volume increased in both forms of oral administration (Table 4, $p \leq 0.05$). The blood vessel volume decreased when Cd was offered orally SD compared to the control animals and those that received Cd *i.p.* SD ($p \leq 0.05$), but it was similar to the oral FD group (Table 4, $p > 0.05$). The percentage of the Leydig cytoplasm increased in animals that received Cd *i.p.* in comparison to the other experimental groups (Table 4, $p \leq 0.05$). The percentage of the Leydig nucleus was higher in the animals that received Cd orally SD when compared to the control

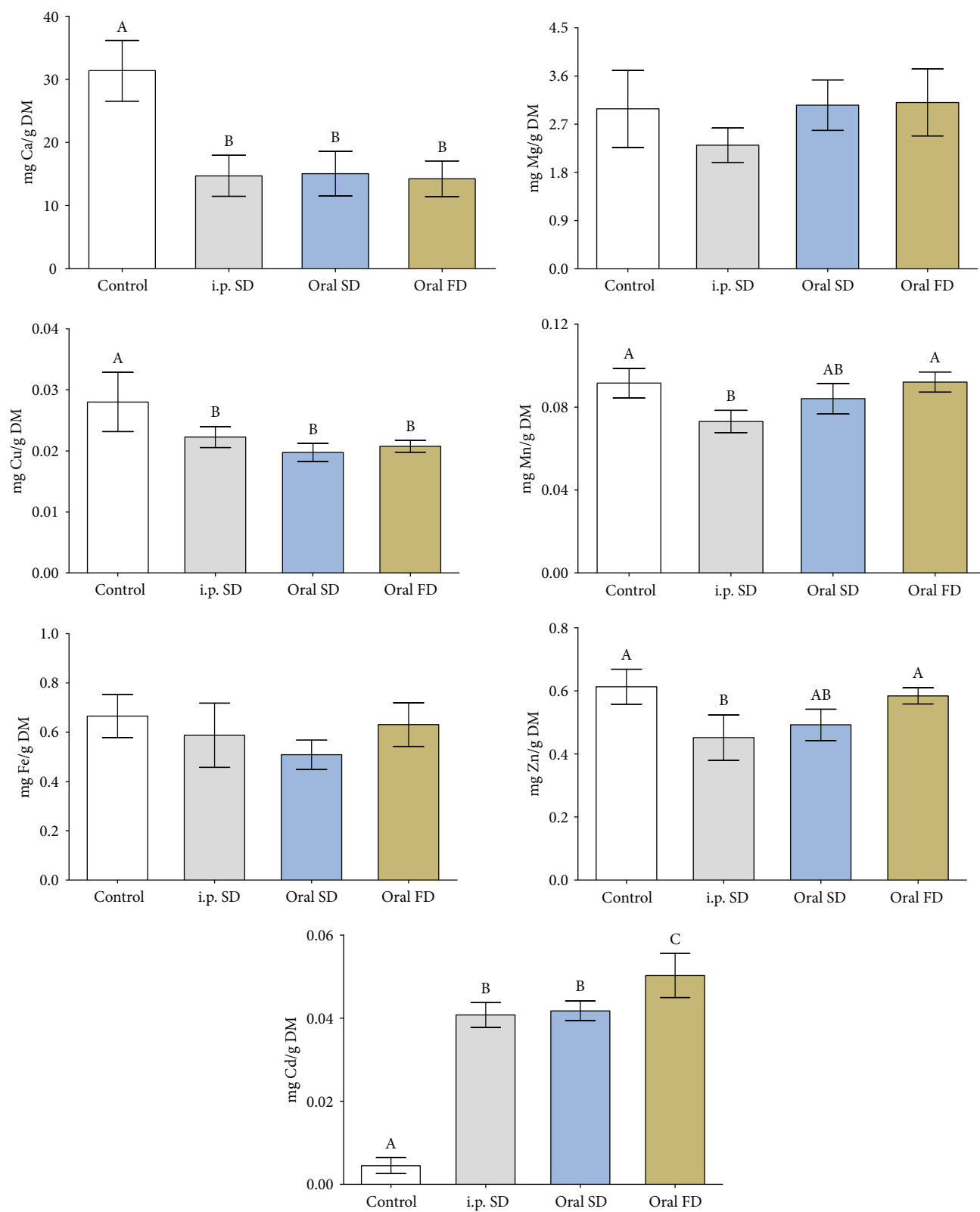


FIGURE 1: Levels of cadmium and testicular essential minerals (g/DM) of mice exposed to cadmium chloride (CdCl_2). Control: distilled water; i.p. SD: CdCl_2 intraperitoneal single dose; oral SD: CdCl_2 oral single dose; oral FD: CdCl_2 oral fractionated dose; DM: dry mass; Ca: calcium; Mg: magnesium; Cu: copper; Mn: manganese; Fe: iron; Zn: zinc; Cd: cadmium. (A, B) Different letters indicate significant differences by the Student-Newman-Keuls test ($p \leq 0.05$).

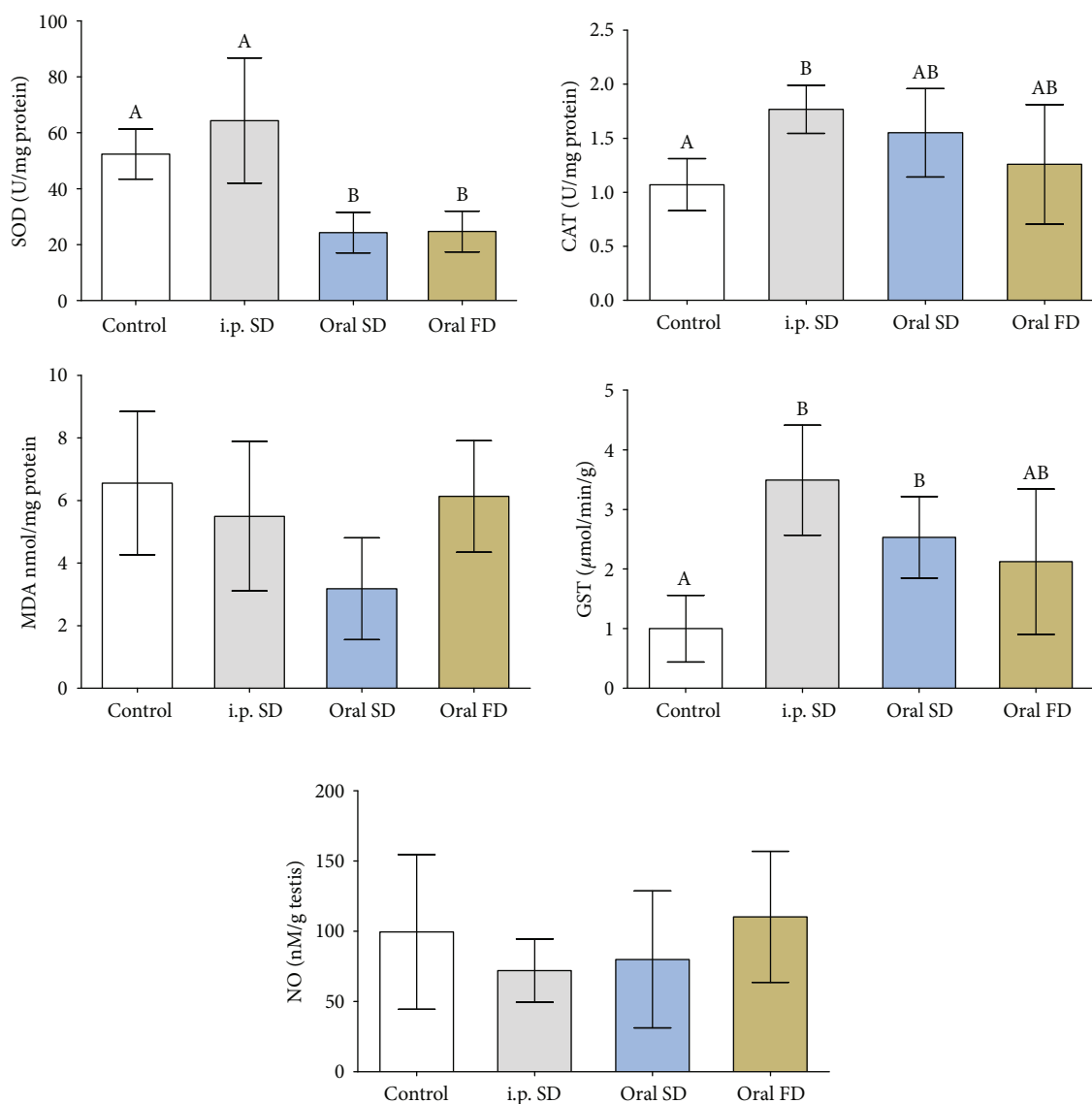


FIGURE 2: Activity of antioxidant enzymes, oxidative stress marker, and nitric oxide levels of mice exposed to cadmium chloride (CdCl_2). Control: distilled water; i.p. SD: CdCl_2 intraperitoneal single dose; oral SD: CdCl_2 oral single dose; oral FD: CdCl_2 oral fractionated dose; SOD: superoxide dismutase; CAT: catalase; GST: glutathione S-transferase; MDA: malondialdehyde; NO: nitric oxide. (A, B) Different letters indicate significant differences by the Student-Newman-Keuls test ($p \leq 0.05$).

TABLE 1: Body and testicular biometry of mice exposed to cadmium chloride (CdCl_2) ($n = 5$ animals/group).

	Control	i.p. SD	Oral SD	Oral FD
Body weight (g)	38.10 ± 0.47	39.60 ± 4.00	33.71 ± 4.30	36.57 ± 4.20
Testicular weight (g)	0.220 ± 0.020 ^a	0.216 ± 0.017 ^a	0.188 ± 0.016 ^b	0.181 ± 0.013 ^b
Parenchyma weight (g)	0.202 ± 0.017 ^a	0.206 ± 0.022 ^a	0.175 ± 0.021 ^b	0.171 ± 0.011 ^b
Albuginea weight (g)	0.018 ± 0.009	0.010 ± 0.005	0.013 ± 0.007	0.010 ± 0.004
GSI (%)	0.58 ± 0.06	0.55 ± 0.02	0.57 ± 0.11	0.50 ± 0.07
PSI (%)	0.53 ± 0.05	0.52 ± 0.02	0.53 ± 0.11	0.47 ± 0.07

Mean ± SDM (standard deviation of the mean); control: distilled water; i.p. SD: CdCl_2 intraperitoneal single dose; oral SD: CdCl_2 oral single dose; oral FD: CdCl_2 oral fractionated dose; GSI: gonadosomatic index; PSI: parenchymosomatic index. ^{ab}Different letters in the same row, for each evaluated time, indicate significant differences by the Student-Newman-Keuls test ($p \leq 0.05$).

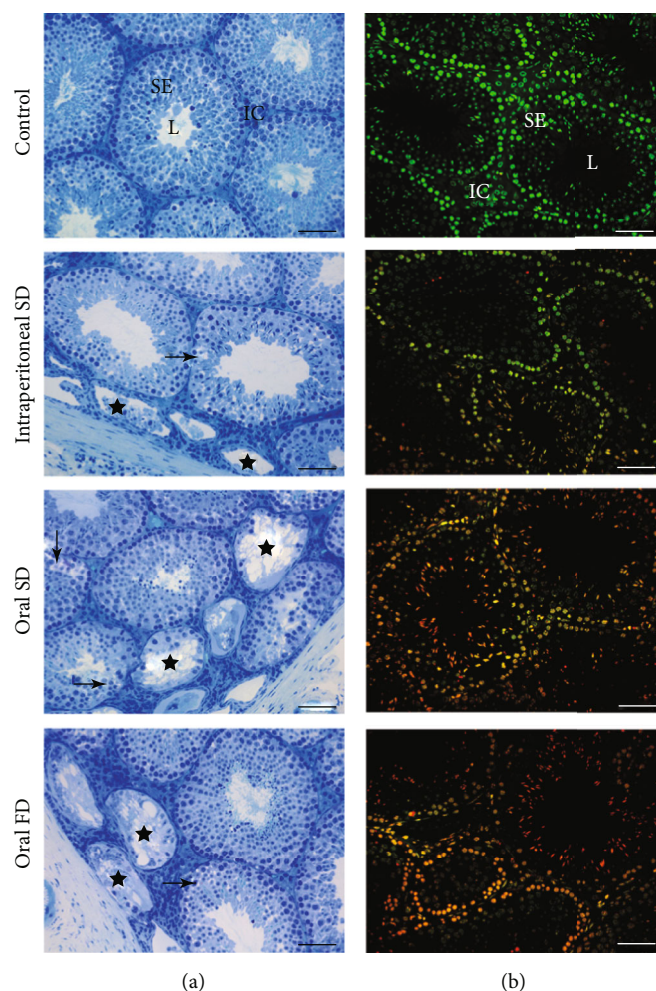


FIGURE 3: Photomicrographs of testicular sections from control and of mice exposed to cadmium chloride (CdCl_2). On (A), sections show the tubular compartment composed of a seminiferous epithelium (SE) and lumen (L) and an intertubular compartment (IC) analyzed under light microscopy with toluidine blue. Arrows: vacuolated germinal epithelium (mild pathology); stars: degenerate seminiferous tubules (severe pathology). On (B), sections of seminiferous epithelium analyzed under epifluorescence microscopy using the fluorochrome dye acridine orange (AO; green) and propidium iodide (PI; red). Viable cells (green) and nonviable cells with initial damage (orange) and positive propidium iodide cells (red). Control: distilled water; intraperitoneal SD: CdCl_2 intraperitoneal single dose; oral SD: CdCl_2 oral single dose; oral FD: CdCl_2 oral fractionated dose; SE: seminiferous epithelium; L: lumen; IC: intertubular compartment. Bars = 60 μm .

(Table 4, $p \leq 0.05$). The Leydig cytoplasm volume decreased when Cd was administered orally FD compared to the control and Cd *i.p.* groups (Table 4, $p \leq 0.05$). However, the administration of Cd via *i.p.* increased the cytoplasmic volume of Leydig cells (Table 4, $p \leq 0.05$) in relation to the other experimental groups.

There were no changes in the stereological parameters of Leydig cells, such as nuclear diameter, cytoplasmic and nuclear volumes, and cell numbers in animals exposed to Cd (Supplementary Table 1, $p > 0.05$).

3.8. Serum Testosterone Quantification. The concentration of serum testosterone decreased in animals exposed to oral Cd (Supplementary Table 1, $p \leq 0.05$). Animals receiving Cd *i.p.* did not show any change in serum testosterone concentration (Supplementary Table 1, $p > 0.05$).

4. Discussion

Cadmium exposure led to reduction in testicular and parenchyma weights in animals receiving Cd oral SD and FD. However, body weight did not change in both evaluated routes. Cupertino et al. [6] did not observe changes in biometric parameters of rats receiving 1.2 mg/kg of CdCl_2 in a single dose and evaluated after 7 days, as well as in mice receiving 2 mg/kg for 7 consecutive days [36], both by the *i.p.* route. On the other hand, rats receiving 1.2 mg/kg of CdCl_2 *i.p.* showed reduction in testicular weight [7]. Differently from the present study, rats receiving 50 mg/kg of CdCl_2 by the oral route, 3 times a week for 15 days, showed no change in body and testicular biometric parameters [37]. According to the authors, this finding is indicative of nonoccurrence of general toxicity of Cd, and this may present

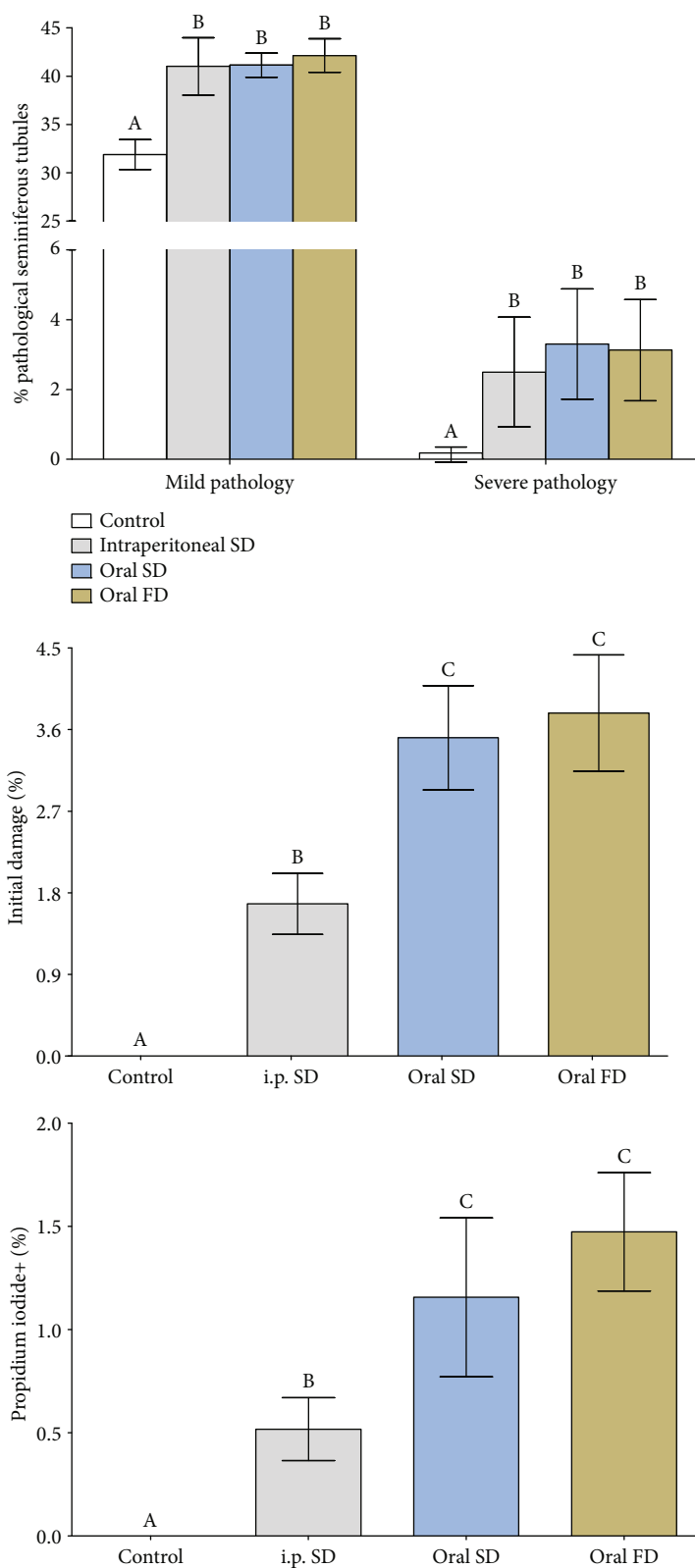


FIGURE 4: Percentage of pathological seminiferous tubules and cell damage of mice exposed to cadmium chloride (CdCl₂). Control: distilled water; intraperitoneal SD: CdCl₂ intraperitoneal single dose; oral SD: CdCl₂ oral single dose; oral FD: CdCl₂ oral fractionated dose. (A, B) Different letters indicate significant differences by the Student-Newman-Keuls test ($p \leq 0.05$).

TABLE 2: Volumetric density of the tubular compartment of mice exposed to cadmium chloride (CdCl₂) (*n* = 5 animals/group).

	Control	i.p. SD	Oral SD	Oral FD
Tubule (%)	88.80 ± 0.41	87.75 ± 1.52	88.12 ± 1.10	88.74 ± 1.07
Epithelium (%)	64.72 ± 1.21 ^a	61.12 ± 1.72 ^b	65.32 ± 1.65 ^a	63.98 ± 2.14 ^a
Tunica propria (%)	10.75 ± 0.22	10.38 ± 0.84	10.49 ± 0.60	10.65 ± 0.71
Lumen (%)	13.33 ± 1.05 ^a	16.25 ± 1.09 ^b	12.31 ± 1.91 ^a	14.11 ± 0.94 ^a
TSI (%)	0.47 ± 0.05	0.46 ± 0.02	0.47 ± 0.09	0.42 ± 0.06
ESI (%)	0.34 ± 0.03	0.32 ± 0.02	0.35 ± 0.07	0.30 ± 0.04

Mean ± SDM (standard deviation of the mean); control: distilled water; i.p. SD: CdCl₂ intraperitoneal single dose; oral SD: CdCl₂ oral single dose; oral FD: CdCl₂ oral fractionated dose; TSI: tubulesomatic index; ESI: epithelium somatic index. ^{ab}Different letters in the same row, for each evaluated time, indicate significant differences by the Student-Newman-Keuls test (*p* ≤ 0.05).

TABLE 3: Morphometry and stereology of tubular compartment of mice exposed to cadmium chloride (CdCl₂) (*n* = 5 animals/group).

	Control	i.p. SD	Oral SD	Oral FD
<i>Volume (mL)</i>				
Tubule	0.179 ± 0.015 ^a	0.181 ± 0.021 ^a	0.154 ± 0.016 ^b	0.151 ± 0.010 ^b
Epithelium	0.130 ± 0.010 ^a	0.126 ± 0.014 ^{ab}	0.115 ± 0.014 ^{ab}	0.109 ± 0.008 ^b
Tunica propria	0.022 ± 0.002	0.021 ± 0.003	0.018 ± 0.003	0.018 ± 0.002
Lumen	0.027 ± 0.004 ^a	0.034 ± 0.005 ^b	0.021 ± 0.001 ^c	0.024 ± 0.002 ^{ac}
Tubular diameter (μm)	225.11 ± 9.04	222.41 ± 11.36	226.81 ± 11.0	215.27 ± 14.86
Lumen diameter (μm)	74.19 ± 3.89	75.42 ± 6.39	80.21 ± 5.31	83.23 ± 7.70
Epithelium height (μm)	150.92 ± 6.86 ^a	146.99 ± 11.10 ^{ab}	146.60 ± 5.88 ^a	132.04 ± 10.77 ^b
STAr (mm ²)	0.0398 ± 0.0032	0.0389 ± 0.0040	0.0404 ± 0.0039	0.0365 ± 0.0050
LAr (mm ²)	0.0043 ± 0.0004	0.0045 ± 0.0007	0.0051 ± 0.0007	0.0053 ± 0.0010
EAr (mm ²)	0.0355 ± 0.0029	0.0344 ± 0.0038	0.0354 ± 0.0033	0.0311 ± 0.0044
TER	1.12 ± 0.01 ^a	1.13 ± 0.03 ^a	1.14 ± 0.01 ^a	1.17 ± 0.03 ^b
STL (m)	4.50 ± 0.31	4.71 ± 0.85	3.83 ± 0.38	4.20 ± 0.58
STL/g (m/g)	20.58 ± 2.28	21.68 ± 2.60	20.42 ± 2.23	23.24 ± 3.07

Mean ± SDM (standard deviation of the mean); control: distilled water; i.p. SD: CdCl₂ intraperitoneal single dose; oral SD: CdCl₂ oral single dose; oral FD: CdCl₂ oral fractionated dose; STAr: seminiferous tubule area; LAr: lumen area; EAr: epithelium area; TER: tubule epithelium ratio; STL: seminiferous tubule length; STL/g: seminiferous tubule length per gram of testis. ^{ab}Different letters in the same row, for each evaluated time, indicate significant differences by the Student-Newman-Keuls test (*p* ≤ 0.05).

greater toxicity when administered by the *i.p.* route. However, the results of the present study suggest that the oral route presents greater toxicity than the *i.p.* route.

The accumulation of Cd was demonstrated by the higher concentration of this metal in the testis of animals exposed to oral FD. The greater accumulation in this route may be related to the daily administration of the metal, which maintains the continuous absorption throughout the experimental period.

According to Hentze et al. [10], Cd can compete with minerals for the divalent metal transporter (DMT-1) located in the duodenum, which has specificity for Fe, Zn, and Mg, and reduce the absorption of these minerals. This transporter has been reported to be expressed in cells of the seminiferous epithelium (Sertoli and germ cells) of the adult animals, and its expression is associated with the stages of the seminiferous tubule [38]. However, in the present study, the *i.p.* route was more effective in reducing the concentration of minerals

than the oral route. Therefore, the effects of this competition could not be observed in the oral administration route.

In the present study, we observed no changes in testicular Fe concentration in animals after *i.p.* and oral Cd exposure. Differently, mice receiving 25 mg/kg of CdCl₂, once a week for 35 days, showed a reduction in testicular Fe concentration [39]. In another study, these authors also observed reduction in this mineral in animals receiving 50 mg/kg of CdCl₂ once a week for 60 days [40]. According to the authors, the Cd exposure leads to the expulsion of testicular Fe, which leads to its decreased concentration. However, in both studies, the time of Cd exposure was higher than in the present study.

Cd has the ability to compete with Cu at the site of membrane and cytoplasmic proteins [6]. The reduced Cu concentration in both routes of administration may be related to this competition capacity. In addition, the route did not affect the testicular concentration of this mineral, since the concentration of Cu decreased in both routes of Cd exposure. It is

TABLE 4: Volumetric density and volume of intertubular compartment in the testes of mice exposed to cadmium chloride (CdCl₂) (*n* = 5 animals/group).

	Control	i.p. SD	Oral SD	Oral FD
<i>Volumetric density (%)</i>				
Intertubule	11.20 ± 0.41	12.25 ± 1.50	11.88 ± 1.12	11.26 ± 1.07
Connective tissue	0.70 ± 0.19 ^a	0.92 ± 0.17 ^a	1.36 ± 0.25 ^b	0.94 ± 0.17 ^a
Lymphatic space	0.92 ± 0.43	0.42 ± 0.24	0.56 ± 0.11	0.87 ± 0.51
Blood vessel	1.92 ± 0.48	1.79 ± 0.42	1.22 ± 0.41	1.51 ± 0.42
Macrophage	0.23 ± 0.02 ^a	0.50 ± 0.21 ^b	0.78 ± 0.20 ^b	0.60 ± 0.19 ^b
Leydig cytoplasm	6.09 ± 0.53 ^{ab}	7.06 ± 1.05 ^b	6.22 ± 0.37 ^a	5.84 ± 0.23 ^a
Leydig nucleus	1.33 ± 0.25 ^a	1.56 ± 0.25 ^{ab}	1.74 ± 0.18 ^b	1.50 ± 0.18 ^{ab}
Leydig cell	7.42 ± 0.75	8.62 ± 1.30	7.96 ± 0.54	7.34 ± 0.35
<i>Volume (mL)</i>				
Intertubule	0.023 ± 0.001 ^{ab}	0.025 ± 0.002 ^a	0.022 ± 0.005 ^{ab}	0.019 ± 0.002 ^b
Connective tissue	0.0014 ± 0.0004 ^a	0.0019 ± 0.0003 ^{ab}	0.0024 ± 0.0006 ^b	0.0016 ± 0.0003 ^a
Lymphatic space	0.0019 ± 0.0009	0.0009 ± 0.0005	0.0010 ± 0.0003	0.0015 ± 0.0009
Blood vessel	0.0038 ± 0.0008 ^a	0.0037 ± 0.0009 ^a	0.0022 ± 0.0010 ^b	0.0026 ± 0.0008 ^{ab}
Macrophage	0.0005 ± 0.0001 ^a	0.0010 ± 0.0005 ^{ab}	0.0014 ± 0.0004 ^b	0.0010 ± 0.0003 ^b
Leydig cytoplasm	0.0123 ± 0.0014 ^a	0.0144 ± 0.0014 ^b	0.0110 ± 0.0018 ^{ac}	0.099 ± 0.0005 ^c
Leydig nucleus	0.0027 ± 0.0004	0.0032 ± 0.0004	0.0031 ± 0.0006	0.0025 ± 0.0003
Leydig cell	0.0150 ± 0.0016 ^a	0.0176 ± 0.0017 ^b	0.0141 ± 0.0024 ^a	0.0124 ± 0.0007 ^a

Mean ± SDM (standard deviation of the mean); control: distilled water; i.p. SD = CdCl₂ intraperitoneal single dose; oral SD: CdCl₂ oral single dose; oral FD: CdCl₂ oral fractionated dose. ^{ab}Different letters in the same row, for each evaluated time, indicate significant differences by the Student-Newman-Keuls test (*p* ≤ 0.05).

known that Cu, together with Zn and Mn, works as a cofactor of SOD [12]. Thus, the lower concentration of this mineral may be related to the reduced SOD activity in the oral route of Cd administration, with induced oxidative stress [41]. The reduction in testicular SOD activity after Cd exposure related to increased oxidative stress has already been described [42–44]. The reduced enzyme activity may have been caused by excess of the superoxide radical in the oral route, with consequent enzymatic saturation [45] or by inactivation of enzymatic functional groups [42, 46, 47]. In addition, imbalance of essential minerals may lead to altered SOD expression [48]. However, although they are SOD cofactors, Zn and Mn reduction in animals receiving Cd *i.p.* SD did not result in loss of enzymatic activity.

Increased CAT activity in *i.p.* SD also indicates the occurrence of oxidative stress due to the higher production of H₂O₂ by SOD in this route, to be decomposed through CAT. In addition, according to Cupertino et al. [6], increased CAT activity in animals exposed to Cd may be a demonstration of the attempt to protect the tissue against changes caused by the metal.

GST belongs to the second antioxidant defense line, whose function is the detoxification of xenobiotics, with consequent protection against the oxidative stress [49], besides the detoxification of peroxidized lipids [45]. The increase in testicular MDA concentration associated with reduction of GSH [36, 50, 51] and GST [12], after Cd exposure, is indicative of lipid peroxidation and oxidative stress. As in the present study, the MDA concentration did not change; the treatment may not have promoted lipid peroxidation. The

increased GST shows that this enzyme activity was not impaired by Cd.

Chemical similarities between Cd and Ca atoms make it possible for Cd to replace Ca in binding proteins [52]. Thus, the reduced concentration of testicular Ca found in both administration routes may be related to its replacement by Cd. Thus, the replacement of Ca in the cellular junctions can lead to the destabilization and consequent rupture of the blood-testis barrier [53]. Previous studies have shown that mice exposed to Cd presented a decreased number of proteins that form the blood-testis barrier, such as cadherins, catenins, occludin, and claudin-11 [8, 54]. Thus, changes in the proteins present in the barrier can be harmful to the germinal epithelium [9]. Therefore, the higher percentage of tubular pathologies found in animals exposed to Cd, in both administration routes, may be related to the low concentration of Ca and the bioaccumulation of Cd.

Changes in morphometric parameters, such as reduced tubule and epithelial volumes and decreased epithelial height, associated with increased tubule epithelium ratio (TER) in animals receiving Cd oral route fractions, may indicate loss of the germinative epithelium [6, 7]. Such loss may be due to the destabilization of the blood-testis barrier caused by the reduced Ca concentration [8, 9]. According to França and Russell [31], the loss of germ cells leads to changes in morphometry and decline in quantitative parameters, as observed in the present study. Thus, it is suggested that the reduced height of the epithelium, associated with increased TER, may lead to spermatogenic capacity loss. The reduced volume of the seminiferous tubule in the oral route, besides

being related to the lower testicle weight of these animals, may also be associated with the smaller epithelium volume in the oral FD route, which contributed to the reduction of epithelial height. The higher percentage of positive propidium iodide cells, especially in the oral route, may also be related to loss of germ cell viability and consequent loss of the epithelium [27].

Considering the oral FD route, the greater intensity of changes in tubular morphometry may be related to the higher Cd accumulation and not to oxidative stress. Dodson et al. [55] challenge the paradigm that oxidative stress and ROS generation are the main causes of pathologies. The authors showed that low doses of arsenic (As) cause proteostasis and not oxidative stress in cell culture. In addition, Wang et al. [56] reported that excessive Cd exposure can lead to cellular changes due to Cd accumulation. According to the authors, the cells perform autophagy as a form of defense. However, autophagy is intensified when there is metal accumulation, and tissue damage can be observed due to the large amount of cells in the process of cell death [56]. Thus, the greatest tubular damage found in the oral FD route may be related to increased Cd accumulation in the testis of these animals, with consequent loss of the germinal epithelial cells due to increased autophagy and destabilization of the blood-testis barrier. However, further studies should be performed to confirm this process.

The results found by Sharma and Kaur [57] corroborate the findings of the present study. The authors observed that mice exposed to small doses (0.1 mg/kg) of CdCl₂ *i.p.* daily, for 15 and 30 days, showed greater alteration in testicular histology compared to those exposed to 2 mg/kg *i.p.* in a single dose and evaluated after 15 and 30 days of exposure. Cupertino et al. [6] reported vacuolization of germ cells and reduced tubule and epithelial volumes in rats receiving 1.2, 1.4, 1.8, and 2.2 mg/kg of CdCl₂ in a single dose *i.p.*, in addition to tubular obstruction in those receiving at least 1.4 mg/kg. These same authors observed increased testicular Cd concentration in all animals exposed to the metal. However, unlike the present study, the authors reported higher germinative epithelium loss, especially in animals that received 1.8 and 2.2 mg/kg of CdCl₂, to increased testicular concentration of Ca and consequent dystrophic calcification. Predes et al. [4, 58] also observed disorganized seminiferous tubules, besides reduced testicular weight of Wistar rats receiving a single dose of 1.2 mg/kg CdCl₂ *i.p.* and evaluated after 7 days. The authors observed reduced tubular diameter after 56 days of metal exposure, which gives evidence of the progression of tubular alterations caused by Cd, and spermatogenesis impairment.

The increased percentage and volume of the lumen associated with reduced percentage of the epithelium observed in animals that received Cd *i.p.* did not lead to changes in the other tubular parameters. Since proportion is a spot analysis and the values obtained are used to determine the global parameters of the organ, it is concluded that the *i.p.* route did not cause the same intensity of toxicity shown by the oral route in the tubular parameters.

The increased percentage of connective tissue was significant only in animals that received Cd oral SD, although its

proportion was also higher in other Cd-administrated groups. It is known that the presence of macrophages induces the synthesis of collagen via fibroblasts [59]. Thus, the greater proportion of connective tissue may be associated with an increased percentage of macrophages in animals exposed to Cd. In addition, the excess fibers can impair the communication between tubular and intertubular compartments and damage the spermatogenesis. Testicular fibrosis caused by Cd exposure is already known [60], as well as the increased percentage of macrophages [61].

The increased percentage of the Leydig cell nucleus in the oral SD route, along with the increased cytoplasmic percentage and cytoplasmic and cell volumes in *i.p.* SD administration, may be due to the onset of the necrotic cell death process. According to Majno and Joris [62], cells in necrosis show increased volume due to the destabilization of the plasma membrane, followed by rupture and cell death. Although no decrease was observed in the number of Leydig cells, in the oral route, the serum concentration of testosterone decreased. Thus, the reduction in serum testosterone concentration may be due to morphometric changes in Leydig cells, which suggests the steroidogenic impairment of this route, compared to the *i.p.* route. Such loss may have increased the intensity of the tubular changes found in the oral route.

The oral FD route presented greater intensity of testicular morphometric changes and lower oxidative stress. The lower oxidative stress may have occurred due to the adaptation to ROS generation caused by continuous exposure to Cd. This adaptive mechanism is reported in patients with β -thalassemia in order to maintain homeostasis due to Fe overload [63], in pancreatic β -cells after As exposure [64], and in zebrafish after fluoroquinolone exposure [65]. Thus, it is suggested that the testis also has an oxidative adaptive mechanism in case of continuous exposure to Cd. However, the possible adaptation to stress conditions was not effective in tissue protection. Thus, we believe that continuous and low-dose exposure of Cd causes serious damage on the testis compared to single-dose exposure of this metal.

5. Conclusion

The subacute exposure leads to the bioaccumulation of this metal, regardless of the route of administration, although it is more significant in the oral fractionated route. The route of administration does not affect the reduction of testicular Ca and Cu, whereas the *i.p.* route reduces Mn and Zn concentration. SOD activity decreases only when the metal is administered orally. Changes in the tubular parameters and cell viability are observed in both routes, but it is more intense in the oral route, mainly when fractionated. Serum testosterone concentration decreases when Cd is given orally. The lower serum testosterone concentration may be related to the decreased testicular and parenchyma weights and increased intensity of morphological damage in the testis of animals receiving oral Cd, mainly in the fractionated dose. Thus, the oral administration of Cd showed greater testicular damage potential, mainly when the metal is administered in a fractionated dose.

Data Availability

The data used to support the findings of this study are available from the corresponding author upon request.

Disclosure

This work was based on a PhD thesis entitled “Ação antioxidante do açaí (*Euterpe oleracea* mart.) frente ao estresse oxidativo induzido pelo cádmio no testículo de camundongos adultos,” developed at the Federal University of Viçosa, Brazil, 2018, by Viviane Gorete Silveira Mouro as the first author.

Conflicts of Interest

The authors indicate no potential conflicts of interest.

Acknowledgments

This work was supported by Universidade Federal de Viçosa (UFV), Coordenação de Aperfeiçoamento de Pessoal de Nível Superior (CAPES), and Conselho Nacional de Desenvolvimento Científico e Tecnológico (CNPq), Brazil.

Supplementary Materials

Supplementary Table 1: Leydig cell morphometry of mice exposed to cadmium chloride (CdCl₂) ($n = 5$ animals/group). (*Supplementary Materials*)

References

- [1] P. Gao, S. Liu, W. Ye et al., “Assessment on the occupational exposure of urban public bus drivers to bioaccessible trace metals through resuspended fraction of settled bus dust,” *Science of The Total Environment*, vol. 508, pp. 37–45, 2015.
- [2] M. P. Waalkes, “Cadmium carcinogenesis,” *Mutation Research*, vol. 533, no. 1-2, pp. 107–120, 2003.
- [3] S. Satarug, S. H. Garrett, M. A. Sens, and D. A. Sens, “Cadmium, environmental exposure, and health outcomes,” *Environmental Health Perspectives*, vol. 118, no. 2, pp. 182–190, 2010.
- [4] F. de Souza Predes, M. A. S. Diamante, and H. Dolder, “Testis response to low doses of cadmium in Wistar rats,” *International Journal of Experimental Pathology*, vol. 91, no. 2, pp. 125–131, 2010.
- [5] H. Y. Jung, D. W. Seo, C. O. Hong, J. Y. Kim, S. Y. Yang, and K. W. Lee, “Nephroprotection of plantamajoside in rats treated with cadmium,” *Environmental Toxicology and Pharmacology*, vol. 39, no. 1, pp. 125–136, 2015.
- [6] M. do Carmo Cupertino, R. D. Novaes, E. C. Santos et al., “Cadmium-induced testicular damage is associated with mineral imbalance, increased antioxidant enzymes activity and protein oxidation in rats,” *Life Sciences*, vol. 175, pp. 23–30, 2017.
- [7] M. C. Cupertino, R. D. Novaes, E. C. Santos et al., “Differential Susceptibility of Germ and Leydig Cells to Cadmium-Mediated Toxicity: Impact on Testis Structure, Adiponectin Levels, and Steroidogenesis,” *Oxidative Medicine and Cellular Longevity*, vol. 2017, Article ID 3405089, 11 pages, 2017.
- [8] L. Minutoli, A. Micali, A. Pisani et al., “Flavocoxid protects against cadmium-induced disruption of the blood-testis barrier and improves testicular damage and germ cell impairment in mice [corrected],” *Toxicological Sciences*, vol. 148, no. 1, pp. 311–329, 2015.
- [9] F. Squadrito, A. Micali, M. Rinaldi et al., “Polydeoxyribonucleotide, an adenosine-A2A receptor agonist, preserves blood testis barrier from cadmium-induced injury,” *Frontiers in Pharmacology*, vol. 7, 2017.
- [10] M. W. Hentze, M. U. Muckenthaler, and N. C. Andrews, “Balancing acts: molecular control of mammalian iron metabolism,” *Cell*, vol. 117, no. 3, pp. 285–297, 2004.
- [11] D. Y. Ryu, S. J. Lee, D. W. Park, B. S. Choi, C. D. Klaassen, and J. D. Park, “Dietary iron regulates intestinal cadmium absorption through iron transporters in rats,” *Toxicology Letters*, vol. 152, no. 1, pp. 19–25, 2004.
- [12] A. Djuric, A. Begic, B. Gobeljic et al., “Oxidative stress, bioelements and androgen status in testes of rats subacutely exposed to cadmium,” *Food and Chemical Toxicology*, vol. 86, pp. 25–33, 2015.
- [13] V. Matović, A. Buha, Z. Bulat et al., “Route-dependent effects of cadmium/cadmium and magnesium acute treatment on parameters of oxidative stress in rat liver,” *Food and Chemical Toxicology*, vol. 50, no. 3-4, pp. 552–557, 2012.
- [14] V. G. S. Mouro, V. A. Siman, J. da Silva et al., “Cadmium induced testicular toxicity in mice: subacute and subchronic route-dependent effects,” *Biological Trace Element Research*, pp. 1–17, 2019.
- [15] P. L. Goering, M. P. Waalkes, and C. D. Klaassen, “Toxicology of cadmium,” in *Toxicology of Metals*, R. A. Goyer and M. G. Cherian, Eds., pp. 189–214, Springer-Verlag, New York, 1995.
- [16] S.-H. Oh, B.-H. Lee, and S.-C. Lim, “Cadmium induces apoptotic cell death in WI 38 cells via caspase-dependent Bid cleavage and calpain-mediated mitochondrial Bax cleavage by Bcl-2-independent pathway,” *Biochemical Pharmacology*, vol. 68, no. 9, pp. 1845–1855, 2004.
- [17] ATSDR, “Toxicological Profile for Cadmium,” in *Agency for Toxic Substances and Disease Registry*, U.S. Department of Health and Human Services, Atlanta, GA, 2012.
- [18] S. Sarban, A. Kocyigit, M. Yazar, and U. E. Isikan, “Plasma total antioxidant capacity, lipid peroxidation, and erythrocyte antioxidant enzyme activities in patients with rheumatoid arthritis and osteoarthritis,” *Clinical Biochemistry*, vol. 38, no. 11, pp. 981–986, 2005.
- [19] S. Dieterich, U. Bieligg, K. Beulich, G. Hasenfuss, and J. Prestle, “Gene expression of antioxidative enzymes in the human heart: increased expression of catalase in the end-stage failing heart,” *Circulation*, vol. 101, no. 1, pp. 33–39, 2000.
- [20] W. H. Habig, M. J. Pabst, and W. B. Jakoby, “Glutathione S-transferases: the first enzymatic step in mercapturic acid formation,” *The Journal of Biological Chemistry*, vol. 249, no. 22, pp. 7130–7139, 1974.
- [21] J. A. Buege and S. D. Aust, “[30] microsomal lipid peroxidation,” *Methods in Enzymology*, vol. 52, pp. 302–310, 1978.
- [22] D. Ricart-Jané, M. Llobera, and M. D. López-Tejero, “Anticoagulants and other preanalytical factors interfere in plasma nitrate/nitrite quantification by the Griess method,” *Nitric Oxide*, vol. 6, no. 2, pp. 178–185, 2002.
- [23] M. J. Karnovsky, “A Formaldehyde-Glutaraldehyde Fixative of High Osmolality for Use in Electron Microscopy,” *The Journal of Cell Biology*, vol. 27, pp. 1A–149A, 1965.

- [24] S. G. Johnsen, "Testicular biopsy score count—a method for registration of spermatogenesis in human testes: normal values and results in 335 hypogonadal males," *Hormones*, vol. 1, no. 1, pp. 2–25, 1970.
- [25] B. R. Giri and B. Roy, "Cysticercus fasciolaris infection induced oxidative stress and apoptosis in rat liver: a strategy for host-parasite cross talk," *Parasitology Research*, vol. 115, no. 7, pp. 2617–2624, 2016.
- [26] O. H. Lowry, N. J. Rosebrough, A. L. Farr, and R. J. Randall, "Protein measurement with the Folin phenol reagent," *The Journal of Biological Chemistry*, vol. 193, no. 1, pp. 265–275, 1951.
- [27] G. D. de Almeida Lima, M. N. Sertorio, A. C. F. Souza et al., "Fertility in male rats: disentangling adverse effects of arsenic compounds," *Reproductive Toxicology*, vol. 78, pp. 130–140, 2018.
- [28] R. P. Amann, "Sperm production rates," in *The Testis*, A. D. Johnson and W. R. Gomes, Eds., Academic Press, New York, 1970.
- [29] F. C. S. A. Melo, S. L. P. Matta, T. A. R. Paula, M. L. M. Gomes, and L. C. Oliveira, "The effects of *Tynnanthus fasciculatus* (Bignoniaceae) infusion on testicular parenchyma of adult Wistar rats," *Biological Research*, vol. 43, no. 4, pp. 445–450, 2010.
- [30] L. Johnson and W. B. Neaves, "Age-related changes in the Leydig cell population, seminiferous tubules, and sperm production in stallions," *Biology of Reproduction*, vol. 24, no. 3, pp. 703–712, 1981.
- [31] L. R. França and L. D. Russell, "The testis of domestic mammals," in *Male Reproduction - a Multidisciplinary Overview*, F. Martinez-Garcia and J. Regadera, Eds., pp. 198–219, Churchill Communications, Madrid, 1998.
- [32] V. G. S. Mouro, T. P. Menezes, G. D. A. Lima et al., "How bad is aluminum exposure to reproductive parameters in rats?," *Biological Trace Element Research*, vol. 183, no. 2, pp. 314–324, 2018.
- [33] J. Attal, M. Courot, C. Richetin, and C. Pisselet, "Développement testiculaire et établissement de la SPERMATOGENÈSE chez le taureau," *Annales de Biologie Animale, Biochimie, Biophysique*, vol. 3, no. 3, pp. 219–241, 1963.
- [34] L. D. Russel, R. A. Ettlin, A. P. S. Hikim, and E. D. Clegg, *Histological and Histopathological Evaluation of the Testis*, Cache River Press, Clearwater, Florida, 1990.
- [35] S. L. P. Matta, D. A. R. Vilela, H. P. Godinho, and L. R. França, "The goitrogen 6-n-propyl-2-thiouracil (PTU) given during testis development increases Sertoli and germ cell numbers per cyst in fish: the tilapia (*Oreochromis niloticus*) model," *Endocrinology*, vol. 143, no. 3, pp. 970–978, 2002.
- [36] R. Li, X. Luo, L. Li et al., "The protective effects of melatonin against oxidative stress and inflammation induced by acute cadmium exposure in mice testis," *Biological Trace Element Research*, vol. 170, no. 1, pp. 152–164, 2016.
- [37] S. O. Abarikwu, P. D. Olufemi, C. J. Lawrence, F. C. Wekere, A. C. Ochulor, and A. M. Barikuma, "Rutin, an antioxidant flavonoid, induces glutathione and glutathione peroxidase activities to protect against ethanol effects in cadmium-induced oxidative stress in the testis of adult rats," *Andrologia*, vol. 49, no. 7, article e12696, 2017.
- [38] K. P. Griffin, D. T. Ward, W. Liu, G. Stewart, I. D. Morris, and C. P. Smith, "Differential expression of divalent metal transporter DMT1 (Slc11a2) in the spermatogenic epithelium of the developing and adult rat testis," *American Journal of Physiology. Cell Physiology*, vol. 288, no. 1, pp. C176–C184, 2005.
- [39] S. O. Abarikwu, A. F. S. Wokoma, C. J. Mgbudom-Okah, S. I. Omeodu, and R. Ohanador, "Effect of Fe and Cd co-exposure on testicular steroid metabolism, morphometry, and spermatogenesis in mice," *Biological Trace Element Research*, vol. 190, no. 1, pp. 109–123, 2019.
- [40] S. O. Abarikwu, S. Oruitemeka, I. A. Uwadileke et al., "Oral administration of cadmium depletes intratesticular and epididymal iron levels and inhibits lipid peroxidation in the testis and epididymis of adult rats," *Journal of Trace Elements in Medicine and Biology*, vol. 48, pp. 213–223, 2018.
- [41] K. B. Jacobson and J. E. Turner, "The interaction of cadmium and certain other metal ions with proteins and nucleic acids," *Toxicology*, vol. 16, no. 1, pp. 1–37, 1980.
- [42] U. R. Acharya, M. Mishra, J. Patro, and M. K. Panda, "Effect of vitamins C and E on spermatogenesis in mice exposed to cadmium," *Reproductive Toxicology*, vol. 25, no. 1, pp. 84–88, 2008.
- [43] A. M. Al-Attar, "Antioxidant effect of vitamin E treatment on some heavy metals-induced renal and testicular injuries in male mice," *Saudi Journal of Biological Sciences*, vol. 18, no. 1, pp. 63–72, 2011.
- [44] S. A. E.-M. Bashandy, E. A. A. Omara, H. Ebaid, M. M. Amin, and M. S. Soliman, "Role of zinc as an antioxidant and anti-inflammatory to relieve cadmium oxidative stress induced testicular damage in rats," *Asian Pacific Journal of Tropical Biomedicine*, vol. 6, no. 12, pp. 1056–1064, 2016.
- [45] R. J. Aitken and S. D. Roman, "Antioxidant systems and oxidative stress in the testes," *Oxidative Medicine and Cellular Longevity*, vol. 1, no. 1, 24 pages, 2008.
- [46] E. Casalino, G. Calzaretto, C. Sblano, and C. Landriscina, "Molecular inhibitory mechanisms of antioxidant enzymes in rat liver and kidney by cadmium," *Toxicology*, vol. 179, no. 1–2, pp. 37–50, 2002.
- [47] C. C. Spiazzi, V. Manfredini, F. E. Barcellos da Silva et al., "γ-Oryzanol protects against acute cadmium-induced oxidative damage in mice testes," *Food and Chemical Toxicology*, vol. 55, pp. 526–532, 2013.
- [48] P. I. Oteiza, V. N. Adonaylo, and C. L. Keen, "Cadmium-induced testes oxidative damage in rats can be influenced by dietary zinc intake," *Toxicology*, vol. 137, no. 1, pp. 13–22, 1999.
- [49] E. Casalino, C. Sblano, V. Landriscina, G. Calzaretto, and C. Landriscina, "Rat liver glutathione S-transferase activity stimulation following acute cadmium or manganese intoxication," *Toxicology*, vol. 200, no. 1, pp. 29–38, 2004.
- [50] M. H. Arafa, N. S. Mohammad, and H. H. Atteia, "Fenugreek seed powder mitigates cadmium-induced testicular damage and hepatotoxicity in male rats," *Experimental and Toxicologic Pathology*, vol. 66, no. 7, pp. 293–300, 2014.
- [51] M. Erbogaa, M. Kanter, C. Aktas et al., "Anti-apoptotic and anti-oxidant effects of caffeic acid phenethyl ester on cadmium-induced testicular toxicity in rats," *Biological Trace Element Research*, vol. 171, no. 1, pp. 176–184, 2016.
- [52] A. Martelli, E. Rousselet, C. Dycke, A. Bouron, and J.-M. Moulis, "Cadmium toxicity in animal cells by interference with essential metals," *Biochimie*, vol. 88, no. 11, pp. 1807–1814, 2006.
- [53] W. C. Prozialeck and P. C. Lamar, "Interaction of cadmium (Cd²⁺) with a 13-residue polypeptide analog of a putative

- calcium-binding motif of E-cadherin," *Biochimica et Biophysica Acta*, vol. 1451, no. 1, pp. 93–100, 1999.
- [54] C.-h. Wong, D. D. Mruk, W.-y. Lui, and C. Y. Cheng, "Regulation of blood-testis barrier dynamics: an in vivo study," *Journal of Cell Science*, vol. 117, no. 5, pp. 783–798, 2004.
- [55] M. Dodson, M. R. de la Vega, B. Harder et al., "Low-level arsenic causes proteotoxic stress and not oxidative stress," *Toxicology and Applied Pharmacology*, vol. 341, no. 341, pp. 106–113, 2018.
- [56] Y.-J. Wang, J. Yan, F. Yin et al., "Role of autophagy in cadmium-induced testicular injury," *Human & Experimental Toxicology*, vol. 36, no. 10, pp. 1039–1048, 2017.
- [57] S. Sharma and S. Kaur, "Histopathological effects of acute and chronic doses of cadmium on testes of albino mice," *Journal of Experimental Zoology, India*, vol. 15, no. 1, pp. 107–111, 2012.
- [58] F. de Souza Predes, M. A. S. Diamante, M. A. Foglio, and H. Dolder, "Effects of *Arctium lappa* on cadmium-induced damage to the testis and epididymis of adult Wistar rats," *Biological Trace Element Research*, vol. 173, no. 2, pp. 362–371, 2016.
- [59] T. A. Wynn and L. Barron, "Macrophages: master regulators of inflammation and fibrosis," *Seminars in Liver Disease*, vol. 30, no. 3, pp. 245–257, 2010.
- [60] M. C. Cupertino, *Danos oxidativos e histológicos crônicos causados pelo cádmio no fígado e na espermatogênese de ratos. M.Sc.Dissertation*, Universidade Federal de Viçosa,, Viçosa, MG, 2012.
- [61] R. P. Leite, R. S. Wada, J. C. Monteiro, F. S. Predes, and H. Dolder, "Protective effect of guaraná (*Paullinia cupana* var. *sorbilis*) pre-treatment on cadmium-induced damages in adult Wistar testis," *Biological Trace Element Research*, vol. 141, no. 1–3, pp. 262–274, 2011.
- [62] G. Majno and I. Joris, "Apoptosis, oncosis, and necrosis. An overview of cell death," *The American journal of pathology*, vol. 146, no. 1, pp. 3–15, 1995.
- [63] N. Somparn, A. Prawan, L. Senggunprai et al., "Cellular adaptation mediated through Nrf2-induced glutamate cysteine ligase up-regulation against oxidative stress caused by iron overload in β -thalassemia/HbE patients," *Free Radical Research*, vol. 53, no. 7, pp. 791–799, 2019.
- [64] C. M. Carmean and S. Seino, "Braving the element: pancreatic β -Cell dysfunction and adaptation in response to arsenic exposure," *Frontiers in Endocrinology*, vol. 10, pp. 1–14, 2019.
- [65] P. Sehonova, N. Tokanova, N. Hodkovicova et al., "Oxidative stress induced by fluoroquinolone enrofloxacin in zebrafish (*Danio rerio*) can be ameliorated after a prolonged exposure," *Environmental Toxicology and Pharmacology*, vol. 67, pp. 87–93, 2019.

Review Article

Radiation-Induced Normal Tissue Damage: Oxidative Stress and Epigenetic Mechanisms

Jinlong Wei,¹ Bin Wang,¹ Huanhuan Wang,¹ Lingbin Meng¹,² Qin Zhao,¹ Xinyu Li,¹ Ying Xin¹,³ and Xin Jiang¹

¹Department of Radiation Oncology, The First Hospital, Jilin University, Changchun 130021, China

²Department of Internal Medicine, Florida Hospital, Orlando, FL 32803, USA

³Key Laboratory of Pathobiology, Ministry of Education, Jilin University, Changchun 130021, China

Correspondence should be addressed to Ying Xin; xinyu@jlu.edu.cn and Xin Jiang; jiangx@jlu.edu.cn

Received 7 July 2019; Revised 23 October 2019; Accepted 24 October 2019; Published 12 November 2019

Guest Editor: Reggiani Vilela Gonçalves

Copyright © 2019 Jinlong Wei et al. This is an open access article distributed under the Creative Commons Attribution License, which permits unrestricted use, distribution, and reproduction in any medium, provided the original work is properly cited.

Radiotherapy (RT) is currently one of the leading treatments for various cancers; however, it may cause damage to healthy tissue, with both short-term and long-term side effects. Severe radiation-induced normal tissue damage (RINTD) frequently has a significant influence on the progress of RT and the survival and prognosis of patients. The redox system has been shown to play an important role in the early and late effects of RINTD. Reactive oxygen species (ROS) and reactive nitrogen species (RNS) are the main sources of RINTD. The free radicals produced by irradiation can upregulate several enzymes including nicotinamide adenine dinucleotide phosphate oxidase (NADPH oxidase), lipoxygenases (LOXs), nitric oxide synthase (NOS), and cyclooxygenases (COXs). These enzymes are expressed in distinct ways in various cells, tissues, and organs and participate in the RINTD process through different regulatory mechanisms. In recent years, several studies have demonstrated that epigenetic modulators play an important role in the RINTD process. Epigenetic modifications primarily contain noncoding RNA regulation, histone modifications, and DNA methylation. In this article, we will review the role of oxidative stress and epigenetic mechanisms in radiation damage, and explore possible prophylactic and therapeutic strategies for RINTD.

1. Introduction

Cancer is one of the most challenging diseases in modern times. In 2015, China reported about 4.2 million new cancer cases and 2.8 million cancer-related deaths [1]. Radiotherapy (RT) is currently one of the leading therapeutic approaches for several cancers; however, it carries the potential to cause injury to normal tissue, with both short-term and long-term side effects. In recent years, studies have shown that the oxidation/reduction (redox) system was associated with several types of damage after radiation exposure [2]. In addition, the redox system is related to epigenetic regulation and can regulate the expression of microRNAs (miRNAs) and other molecules, thus playing a role in sustained oxidative damage after radiation [3].

Cells and tissues are composed of about 80% or more water, and most of the radiation damage occurs due to the

radiolysis of water, which induces the production of reactive oxygen species (ROS) and reactive nitrogen species (RNS) [4]. ROS and RNS are the main sources of radiation-induced normal tissue damage (RINTD). The generation of ROS induces molecular changes and causes oxidative damage to proteins, lipids, and DNA. It can also activate signal transduction pathways and early-response transcription factors [5]. The redox system plays an important role in acute radiation damage and is responsible for some radiation-induced early and late effects including inflammation, out-of-field effects, fibrosis, bystander effects, and others [6–9].

In recent years, several studies have demonstrated that epigenetic modulators play an important role in normal tissue damage, after redox-induced ionizing radiation. Epigenetic modifications are made up of the heritable changes in the expression of the gene that do not influence the sequence of the DNA. In mammals, epigenetic modifications primarily

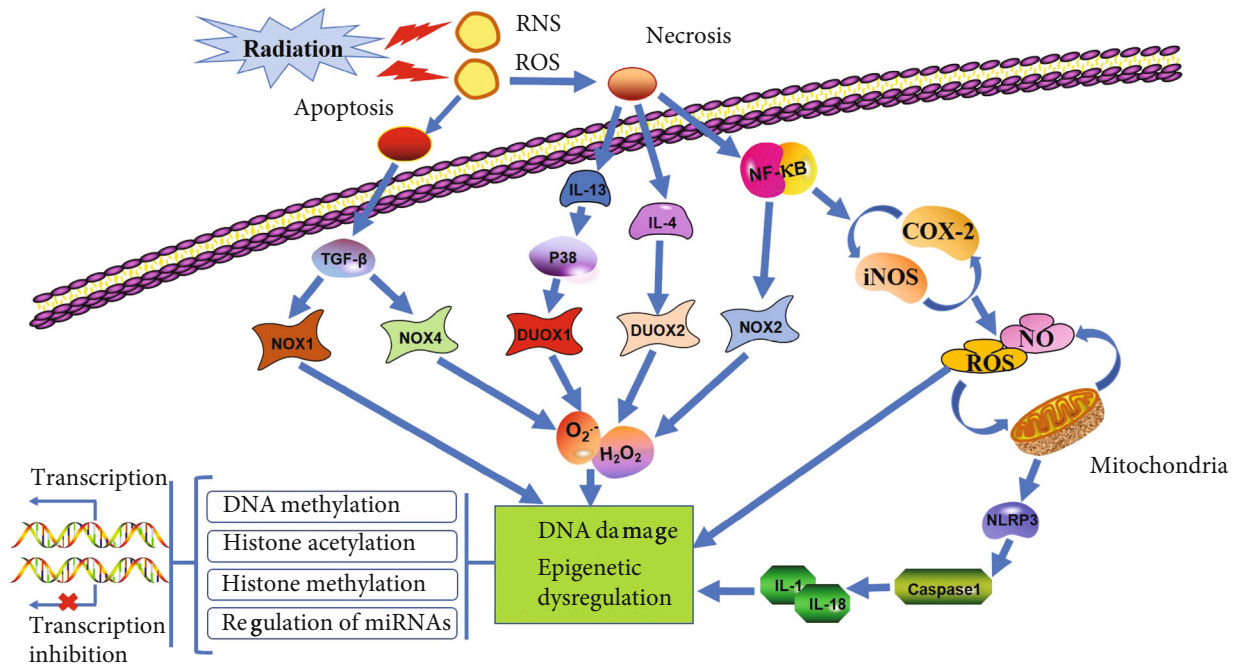


FIGURE 1: The mechanisms of redox system activation, inflammation response, and epigenetic regulation following exposure to radiation.

contain noncoding RNA regulation, histone modifications (methylation, phosphorylation, and acetylation), and DNA methylation. Epigenetic changes can be reversible and can easily respond to natural bioactive dietary compounds [10]. Afanas'ev et al. has reported that free radicals such as NO and ROS can regulate and control the epigenetic processes [11]. In addition, the regulation of some miRNAs may decrease or increase the oxidative damage [11].

In regard to the damage caused by RT, treatment strategies are still lacking. Here, we review the role of oxidative stress and epigenetic mechanisms in radiation damage to explore possible therapeutic strategies for RINTD.

2. Oxidative Stress

Oxidative stress is involved in the development of many diseases including RINTD. The redox system plays an important role in the early and late effects of RINTD [12]. When cells are exposed to radiation, they immediately form free radicals with a half-life of nanoseconds. The redox system begins producing free radicals a few hours after exposure, with the potential to last for years [13, 14]. The free radicals produced by ionizing radiation can upregulate several enzymes, including nicotinamide adenine dinucleotide phosphate oxidase (NADPH oxidase), lipoxygenases (LOXs), nitric oxide synthase (NOS), and cyclooxygenases (COXs). Their effects on mitochondrial function are distinct. These enzymes are expressed in specific ways in various cells, tissues, and organs (Figure 1).

2.1. NADPH Oxidases. NADPH oxidase (NOX) is thought to be a membrane-bound oxidoreductase. It can transfer electrons from NADPH to the oxygen molecules. In addition, some subtypes of these enzymes have been found in cells

[12]. NADPH oxidase enzymes such as DUOX1, DUOX2, and NOX1-5 are the most crucial subtypes. They participate in the process of respiratory chain rupture after radiation [15]. These enzymes have the ability to transfer electrons across the plasma membrane and produce superoxide and other downstream ROS. However, the tissue distribution and activation mechanisms of the individual members of the NOX family are undoubtedly different [16]. In addition, many inflammatory cytokines and chemokines such as TGF- β , TNF- α , IL-1, and IFN- γ are involved in the NOX system activation [17]. NADPH oxidase enzymes play a key role in acute and chronic oxidative stress in bystander and directly irradiated cells [18]. Also, it has been shown that the expression of NOX2 and NOX4 can be upregulated in nontargeted tissues [19].

NOX1 is the first homolog of NOX2 described (then called gp91^{phox}) [20, 21]. NOX1 can be expressed in a variety of cells including endothelial cells in the uterus, prostate, and placenta, as well as osteoclasts. It can also be expressed in some malignant tumors including colon cancer and melanoma [22–24]. Choi et al. reported that the NOX1-specific inhibitor can limit radiation-induced collagen deposition and fibroblastic changes in the endothelial cells, thereby alleviating pulmonary fibrosis induced by radiation [25]. In addition, the production of ROS was significantly decreased after inhibition of NOX1.

NOX2 is considered the prototype of the NADPH oxidase. A report by Kim et al. confirmed that NOX2 was involved in radiation-induced salivary gland damage. After 56 days of exposure to 18 Gy radiation, the expression of the NOX2 gene in the salivary glands of rats was significantly increased. In addition, the apoptotic genes such as caspase-9 and MAPKs, including p-38 and JNK, participate in NOX2 signaling cascades [26]. Experiments

conducted by Narayanan et al. demonstrated that irradiation of human lung fibroblasts generated $O_2^{\bullet-}$ and H_2O_2 with alpha particles. The plasma membrane-bound NOX2 is responsible for the production of $O_2^{\bullet-}$ and H_2O_2 [27]. Datta et al. confirmed that long-range mitochondrial dysfunction and the increased NADPH oxidase, including NOX1 and NOX2 activity, are the main factors for radiation-induced continuous oxidative stress in the intestinal epithelial cells [28].

NOX3 was first described in the year 2000 based on its similarity to the sequences of other NOX subtypes [29], although the function of the protein was first studied in 2004 [30, 31]. At present, the study of NOX3 in radiation damage is limited. Shin et al. confirmed that the expression of NOX3 was upregulated after the irradiation of the oral mucosa of rats. The increased expression of NOX3 is thought to be related to the necrotic inflammatory exudate and oral mucosa ulcers [32].

NOX4 was initially thought to be an NADPH oxidase homolog, highly expressed in the kidney [33, 34]. Pazhani-samy et al. found that systemic irradiation in mice can selectively induce sustained oxidative stress in hematopoietic stem cells (HSCs), at least in part, by the upregulation of NOX4. The increased production of ROS by NOX in HSCs can mediate radiation-induced hematopoietic genomic instability [35]. The experimental results of Wang et al. showed that systemic irradiation selectively induces chronic oxidative stress in HSCs, at least in part by the upregulation of NOX4 expression, thereby giving rise to the induction of HSC senescence and residual bone marrow damage [36]. In addition, the TGF- β -NOX4 pathway may be responsible for the continuous production of ROS/NO and the subsequent genomic instability after bone marrow irradiation [37].

NOX5, found in the lymphoid and testis, contains an N-terminal extension with three EF hands, and it can produce superoxide dismutase and conduct H^+ ions when intracellular free Ca^{2+} increases [38–40]. NOX5 may participate in Ca^{2+} -activated, redox-dependent processes of spermatozoa and lymphocytes including cytokine secretion, cell proliferation, and sperm-oocyte fusion [41]. Weyemi et al. showed that the two members of NADPH oxidase, NOX4 and NOX5, participated in the process of radiation-induced DNA damage in human primary fibroblasts.

Currently, there is a small amount of evidence supporting the role of DUOX1/DUOX2 in chronic oxidative stress. Both DUOX1 and DUOX2 are highly expressed in the thyroid gland [42, 43]. Furthermore, DUOX1 can be found in the prostate and airway epithelia [44–47]. DUOX2 has been described in the salivary gland, airway epithelia, prostate, rectal mucosa, duodenum, cecum, and colon [44–49]. Ameziane-El-Hassani et al. demonstrated that radiation-induced DUOX1-dependent H_2O_2 production by NADPH oxidase was delayed in a dose-dependent manner for several days. In addition, p38 MAPK, which was activated after irradiation, can increase DUOX1 through the expression of IL-13, giving rise to sustained DNA damage and growth stagnation [50]. Wu and Doroshov showed that IL-4/IL-13 can induce the expression of DUOX2/DUOX2A and the production of ROS in human colon and pancreatic cancer cells,

which in turn may be related to the occurrence of inflammatory gastrointestinal malignancies [51]. There are some studies that have shown the upregulation of DUOX1 and DUOX2 in the lung and heart. Some radioprotectors and antioxidants such as melatonin, metformin, and selenium have been shown to reduce the expression of these genes following exposure to ionizing radiation, relieving the heart damage and lung damage caused by radiation [52–56]. However, the relationship between DUOX2 expression and radiation-induced carcinogenesis has not been established and demands further verification.

2.2. COX-2. Cyclooxygenase-2 (COX-2), an isoform of cyclooxygenase, is responsible for the time-dependent and localized production of prostaglandins (PGs) at inflammatory sites [57], including tissues exposed to ionizing radiation. COX-2 plays a crucial role in the inflammatory response that converts arachidonic acid released by membrane phospholipids into PGs. In addition, ROS production is a standard secondary byproduct of arachidonic acid metabolism in the synthesis of PGE2 [58]. Several studies have shown that increased COX-2 expression is related to radiation toxicity after the irradiation of organs, such as the lungs, heart, kidneys, intestines, colon, and the brain [59, 60]. Other studies have reported that COX-2 is involved in the pathogenesis of vascular damage, atherosclerosis, and fibrosis induced by ionizing radiation [61]. Cheki et al. demonstrated that celecoxib, an inhibitor of COX-2, can decrease dermal inflammation, MCP-1 mRNA expression, and radiation-induced skin reactions [62]. In addition, several studies have investigated the role of nonsteroidal anti-inflammatory drugs (NSAIDs) as an inhibitor of COX on radiation damage in the lung and joints [63–65]. Clinically approved inhibitors are represented by NSAIDs like aspirin or ibuprofen and by selective COX-2 inhibitors such as celecoxib [60].

2.3. LOXs. LOXs are enzymes that dioxygenate unsaturated fatty acids, which can initiate lipoperoxidation of the membrane, synthesize signaling molecules, or induce cell structural and metabolic changes [66]. Currently, the role of LOX in radiation damage has been reported. Matyshevskaja et al. demonstrated that activated LOX is involved in the production of ROS after exposure and plays an important role in the process of radiation-induced DNA fragmentation in lymphocytes [67]. Another experimental study showed that LOX was activated immediately after exposure to thymocytes. High LOX activity was observed in cells within an hour after irradiation. In addition, radiation-induced generation of lipid peroxides may be a factor in LOX activation [68]. In another study, Halle et al. showed that chronic adventitial inflammation, vasa vasorum expansion, and 5-LOX upregulation are involved in radiation-induced arterial damage in cancer survivors. In previously irradiated arterial segments, the expression of 5-LOX was increased in exogenous macrophages surrounding vascular dilatation [69].

2.4. Nitric Oxide. Under conditions of stress, including inflammation, inducible nitric oxide synthase (iNOS) was thought to be the primary source of nitric oxide (NO) and

played an important role in carcinogenesis and the oxidative stress process. NO is generated by macrophages under the stimulation of inflammation through the iNOS enzyme, and it can interact with the mitochondria-derived superoxide to further produce peroxynitrite [70]. iNOS enzymes play a key role in the radiation damage via posttranslational regulation of the BER pathway of DNA repair. The main effect of NO is nitroacetylation of 8-xoguanine glycosylase (Ogg1). Ogg1 inhibition by NO can result in increased accumulation of oxidative DNA lesions [71, 72]. Malaviya et al. noted that iNOS is involved in radiation-induced lung damage. In addition, there are complex interactions between oxidative and nitrosative stress, as well as inflammatory pathways that mediate lung damage after radiation [73]. In another study, the inhibitors of iNOS such as aminoguanidine and N-nitro-L-arginine methyl ester have been shown to reduce radiation-induced lung damage [74, 75]. In a study by Ohta et al., increased levels of NO were directly related to the radiation dose, and NO levels increased in the first few hours after receiving the radiation [76].

The role of NO in the radiation-induced bystander effect has been explored. The peculiarity of NO as a redox signaling molecule is partly due to its hydrophobic properties and relative stability [77]. The hydrophobicity of NO allows it to diffuse through the cytoplasm and plasma membrane, allowing this kind of signaling molecule to readily diffuse from irradiated cells to bystander cells without the involvement of gap junction intercellular communication. NO generated in the irradiated tissues can mediate cellular regulation through posttranslational modification of many regulatory proteins [78]. Ghosh et al. have shown that activated iNOS in irradiated cells are crucial to the bystander response. In addition, lipopolysaccharide-induced iNOS activity and the production of NO after irradiation increased bystander cell DNA damage [79, 80]. Han et al. showed that within 30 min of low-dose alpha-particle irradiation, NO played an important role in the process of DNA double-strand breaks in bystander cells [81].

2.5. Oxidative Stress and Inflammation. Inflammatory responses are thought to play an important role in redox activation. Normal cells that are directly exposed to irradiation or ROS will give rise to nuclear and mitochondrial DNA damages, which can lead to cell death via processes such as mitotic catastrophe, apoptosis, and necrosis [82]. Necrosis can trigger the release of inflammatory cytokines such as IL-1, IL-4, IL-13, and other inflammatory mediators, while apoptosis may cause the release of anti-inflammatory cytokines including TGF- β and IL-10 [83, 84]. ROS are the main cause of RINTD. The continuous formation of ROS after IR exposure can be the source of radiosensitivity of the T lymphocytes and other cells [85]. Moreover, ROS can activate the NF- κ B signaling pathway along with proinflammatory cytokines. NF- κ B plays a key role in chronic inflammatory diseases after RT [86]. Inflammatory cytokines and growth factors can give rise to a variety of signaling cascades, such as NADPH oxidase, COX-2, and iNOS [87]. It has also been reported that COX-2 is an important gene which can mediate the subsequent inflammatory responses [88]. Mitochondria

is thought to be an energy and free radical reservoir. In normal conditions, antioxidant defense systems neutralize superoxide and form free radicals and protect cells from oxidative damage resulting from mitochondrial activity [89]. However, mitochondrial dysfunction and apoptosis can be induced by ROS, pro-IL-1 β , iNOS, and inflammatory responses. Also, studies have shown that the ROS-derived NOX system participated in mitochondrial dysfunction and in the subsequent production of ROS in this organelle [90]. Next, the damaged mitochondria will release ROS and activate the nucleotide-binding domain and the leucine-rich-repeat-containing family pyrin 3 (NLRP3) inflammasome pathway [91]. The activation of the NLRP3 inflammasome is the platform of caspase-1 activation. Finally, it will lead to the secretion of proinflammatory cytokines IL-18 and IL-1 β [92]. Recent experiments and studies have shown that the upregulation of the NLRP3 inflammasome has a big impact on radiation damage [93–96]. Chronic inflammatory processes can exist for ages after irradiation, and the immune system does not suppress them. This is related to chronic oxidative damage giving rise to the genomic instability and impaired normal tissue function [97].

2.6. Oxidative Stress and Cellular Senescence. Cellular senescence can be induced by ionizing radiation. Radiation-induced senescence is mainly one of the mechanisms in radiation-induced pathological changes. Radiation-induced cellular senescence is thought to be caused by p53 activation, which is associated with a radiation-induced double-strand DNA break [98]. However, the exact mechanism of inducing cellular senescence is still unclear, but the involvement of ROS has been widely reported [99, 100]. The study of Kobashigawa et al. suggested that the delayed increase of intracellular oxidative stress levels plays a key role in the process of radiation-induced cellular senescence by p53 accumulation [101]. Sakai et al. showed that NOX4 can mediate the production of ROS in radiation-induced senescent cells and lead to normal tissue damage after irradiation through recruitment of inflammatory cells and intensification of tissue inflammation [102].

3. Epigenetic Mechanisms

3.1. Epigenetics and Cancer. Cancer is commonly thought to be caused by genetic alterations including deletions, insertions, mutations, recombination, copy number gains, single-nucleotide polymorphisms, and genomic instability [103, 104]. The latest evidence suggests that cancer may occur without changes in the nucleotide sequence, by means of alleged epigenetic alterations. Combinational crosstalk between epigenetic alterations and genetics has been known to play a role in the development, progression, and recurrence of cancer [105]. Miousse et al. reported that epigenetic alterations are among the driving forces of irradiation-induced carcinogenesis, by observing long interspersed nucleotide element 1 DNA methylation changes in the mouse hematopoietic system after irradiation [106].

Epigenetic dysregulation including increased activity of histone deacetyltransferases (HDACs), DNA methyltransferases

TABLE 1: The epigenetic regulation in radiation-induced normal tissue damage.

Epigenetic mechanisms	Irradiation organ	Epigenetic functions	Target genes/proteins	Damage effects	Reference
DNA methylation	Brain	Increased expression of DNMT1 and 3a	Increased expression of TET1 and TET3 proteins	Radiation-induced cognitive dysfunction	Acharya et al. [116]
	Thymus	Decreased expression of DNMT1, 3a, and 3b	Decrease in the levels of methyl-binding proteins MeCP2 and MBD2	Increased the risk of radiation-induced leukemia and thymic lymphoma	Pogribny et al. [119]
	Human breast cancer cells (MDA-MB-231)	Decreased DNMT1 expression	Downregulation of RB1 expression	DNA damage and apoptosis	Antwih et al. [118]
	Brain	Decreased expression of DNMT1, 3a, and 3b	Decrease in the levels of methyl-binding protein MeCP2	Bystander effect in the spleen	Koturbash et al. [120]
Histone methylation	Intestine	Increased expression of histone H3 methylation	—	Radiation-induced intestinal damage	Herberg et al. [124]
Histone acetylation	Skin	Inhibition of HDAC activity	—	Radiation-induced skin damage and carcinogenesis	Zhang et al. [125]
Regulation of miRNAs	Hematopoietic system	Upregulation of miR-30a-3p, miR-30c-5p, etc.	—	Radiation-induced hematopoietic damage	Acharya et al. [129]
	Lung	Upregulation of miR-19a-3p, miR-144-5p, and miR-144-3p	—	Radiation-induced lung injury	Gao et al. [135]
	Spleen	Increased expression of miR-34a	Upregulation of gene p53	Radiation-induced spleen damage	Ghosh et al. [137]
	Hematopoietic and osteoblast cells	Increased expression of miR-30c	Suppression of gene REDD1	Radiation-induced hematopoietic and osteoblast cell damage	Li et al. [131]

(DNMTs), and changes in the noncoding RNA expression, can give rise to changes in gene transcription and expression, which regulate cell cycle, cell differentiation and proliferation, and apoptosis [107, 108]. Yi et al. showed that the combined action of DNMT and HDAC inhibitors could stagnate the cell cycle at the G2/M phase and suppress the growth of endometrial cancer by upregulating E-cadherin and downregulating Bcl-2 [107]. Choi et al. noted that DNMTs including DNMT3A, DNMT3B, and DNMT1 are overexpressed in the hepatocellular carcinoma compared with noncancerous liver samples [109]. One such study has demonstrated that HDAC5 can promote glioma cell proliferation by upregulating the expression of Notch 1 at both the mRNA and the protein level [110]. In addition, HDAC5 can also promote human HCC cell proliferation by upregulating the expression of Six1 [111]. Epigenetic regulation, as a molecular target for cancer prevention and therapy, has aroused wide interest. For example, some studies showed that (-)-epigallocatechin-3-gallate, a main component of green tea, could possibly bind with the DNMTs, reducing the methylation activity of cancer cells through epigenetic mechanisms, and thus leading to cancer prevention

or treatment [112, 113]. At present, there is increasing evidence that targeting epigenetic modifications is an effective cancer prevention strategy.

3.2. Epigenetics and RINTD. In recent years, the relationship between epigenetic mechanisms and radiation damage has been studied extensively [114–116]. Currently, epigenetic mechanisms such as DNA methylation and miRNA and histone modifications are reported to be associated with radiation damage. These mechanisms are summarized in Table 1.

3.2.1. DNA Methylation. DNA methylation is a crucial means of epigenetic modification, which primarily occurs in the CPG islands of the gene promoter regions. Multiple DNMT functions are required to establish and maintain DNA methylation patterns [117]. Therapeutic radiation can give rise to biological responses to confront the subsequent DNA damage and genomic stress, to avoid cell death. Antwih et al. showed that the DNA methylation response to radiation is parallel to the classical biological responses to radiation. The differential methylation level of DNA repair, cell cycle, and apoptosis pathways varied with different radiation doses

[118]. Fractionated low-dose radiation exposure has been reported to cause the accumulation of DNA damage and profound alterations in DNA methylation in the murine thymus. This could be the source of the risk of radiation-induced leukemia and thymic lymphoma [119].

Acharya et al. showed that neuroepigenetic mechanisms played an important role in affecting the functional and structural changes in the brain and in cognition after irradiation. In irradiated mice with cognitive impairment, 5-hydroxymethylcytosine and 5-methylcytosine were detected in the region of the hippocampus consistent with increased levels of Ten Eleven Translocation- (TET-) 1, TET3, and DNMT3a. DNMT3a and TET enzymes including TET1 and TET3 are related to addiction behavior and memory formation. In addition, they found an obvious improvement in the epigenetic effects of irradiation by inhibiting methylation using 5-iodotubercidin [116]. Koturbash et al. demonstrated the role of epigenetic effects in maintaining the long-term, persistent bystander effect in the spleen, *in vivo*. After localized cranial irradiation for 24 h and 7 months, the levels of methyltransferases DNMT3a, DNMT3b, and DNMT1 and methyl-binding protein MeCP2 in the spleen tissue were significantly decreased [120].

The above results indicate that radiation can cause changes in DNA methylation to modify and regulate the expression of related genes and proteins, thus causing the corresponding tissue and organ damage. Future research is essential to confirm the role of DNA methylation in radiation-induced normal tissue damage. In addition, DNA methylation can be used as a target to prevent and treat radiation damage in the future.

3.2.2. Histone Modifications. Histone modification is rarely studied in radiation-induced normal tissue damage. Most reports have focused on the regulatory role of histone modification in radiation approaches for killing tumor cells [121–123]. Histone modifications include methylation, phosphorylation, and acetylation. Herberg et al. showed that mismatch repair-deficiency leads to genome-wide changes in histone H3 methylation profiles prior to tumorigenesis. Analogous changes constitute a lasting epigenetic feature of radiation-induced DNA damage [124]. Zhang et al. showed that solar-simulated ultraviolet radiation can influence both histone acetyltransferase and HDAC activities causing decreased histone acetylation. This could be the main cause for radiation-induced skin DNA damage [125]. Further research is needed to verify the role of histone modifications in radiation damage.

3.2.3. Regulation of miRNAs. miRNAs combined with mRNAs can lead to posttranscriptional degradation or repression [126]. It is well known that the role of miRNAs in ROS production and oxidative stress is to increase the superoxide level by suppressing antioxidant enzymes. A good example is the upregulation of miR-21 in both targeted and bystander cells. MiR-21, which is triggered by TGF- β , can inhibit SOD2 gene expression, giving rise to a decrease in the activity of SOD2 and damage to irradiated and bystander cells by superoxide [3, 127]. In addition, the SOD activity and

glutathione level were inhibited which have been revealed in nontargeted lung tissues [128]. Many studies have shown a link between miRNA regulation and RINTD. miRNAs can play an important role in the early evaluation of radiation-induced hematopoietic damage, as functional dosimeters of radiation [129, 130]. Li et al. also demonstrated that miR-30c plays a key role in radiation-induced hematopoietic and osteoblast cell damage, possibly by regulating the expression of the gene REDD1 [131].

Another study by Li et al. reported that the isomer of vitamin E, delta-tocotrienol, can inhibit radiation-induced miR-30 and protect human and mice CD34⁺ cells from radiation damage by inhibiting IL-1 β -induced NF- κ B/miR-30 signaling [132].

Radiation-induced lung damage includes chronic fibrosis and acute pneumonia [133]. miRNAs have been reported in many diseases including those with lung involvement [134]. Gao et al. showed that miR-19a-3p, miR-144-5p, and miR-144-3p are upregulated in rats 2 weeks after thorax irradiation [135]. Recently, Xie et al. also studied the response of lung miRNA expression to radiation-induced lung damage in rats [136]. miRNAs may serve as biomarkers for early stages of radiation-induced lung damage.

Radiation-induced spleen damage has also been reported in recent years. Ghosh et al. reported that whole-body radiation exposure resulted in higher expression of miRNAs in the spleen tissue on day 4 and on day 250. In addition, the vitamin E analog gamma-tocotrienol can modulate radiation-induced miRNA expression in the mouse spleen, preventing radiation damage to the spleen [137].

Collectively, miRNAs can serve as promising candidates for radiation biodosimetry. In addition, the prevention and treatment of RINTD through miRNA regulation may have a promising future.

4. Conclusions

In summary, oxidative stress responses and epigenetic mechanisms play important roles in RINTD. The redox system and various oxidases upregulated by free radicals and generated by radiation, including NADPH oxidase, LOXs, NOS, and COXs, participated in RINTD through different regulatory mechanisms. ROS and NOS produced by inflammatory cells and mitochondria are involved in oxidative damage to bystander cells and untargeted tissues. In addition, a variety of inflammatory factors including the NLRP3 inflammasome play an important role in radiation-induced oxidative stress damage. Epigenetic mechanisms such as DNA methylation, regulation of miRNAs, and histone modifications have been extensively studied in recent years in relation to RINTD. New progress has been made in the field of radiation damage treatment through the regulation of epigenetic mechanisms. With a further understanding of oxidative stress and epigenetic regulatory mechanisms, we hope to better explore the preventive and therapeutic strategies in RINTD in the future.

Conflicts of Interest

The authors report no conflicts of interest in this work.

Authors' Contributions

Jinlong Wei and Bin Wang contributed equally to this work.

Acknowledgments

We would like to thank Editage (<http://www.editage.cn>) for English language editing. This work was supported in part by grants from the National Natural Science Foundation of China (grant no. 81570344 to Ying Xin), the Norman Bethune Program of Jilin University (grant no. 2015225 to Ying Xin and no. 2015203 to Xin Jiang), and the Science and Technology Foundation of Jilin Province (grant no. 20180414039GH to Ying Xin and no. 20190201200JC to Xin Jiang).

References

- [1] W. Chen, R. Zheng, P. D. Baade et al., "Cancer statistics in China, 2015," *CA: A Cancer Journal for Clinicians*, vol. 66, no. 2, pp. 115–132, 2016.
- [2] D. R. Spitz, E. I. Azzam, J. J. Li, and D. Gius, "Metabolic oxidation/reduction reactions and cellular responses to ionizing radiation: a unifying concept in stress response biology," *Cancer Metastasis Reviews*, vol. 23, no. 3-4, pp. 311–322, 2004.
- [3] Y. Jiang, X. Chen, W. Tian, X. Yin, J. Wang, and H. Yang, "The role of TGF-beta1-miR-21-ROS pathway in bystander responses induced by irradiated non-small-cell lung cancer cells," *British Journal of Cancer*, vol. 111, no. 4, pp. 772–780, 2014.
- [4] E. Vorotnikova, R. A. Rosenthal, M. Tries, S. R. Doctrow, and S. J. Brauhut, "Novel synthetic SOD/catalase mimetics can mitigate capillary endothelial cell apoptosis caused by ionizing radiation," *Radiation Research*, vol. 173, no. 6, pp. 748–759, 2010.
- [5] P. Dent, A. Yacoub, P. B. Fisher, M. P. Hagan, and S. Grant, "MAPK pathways in radiation responses," *Oncogene*, vol. 22, no. 37, pp. 5885–5896, 2003.
- [6] M. Najafi, A. Shirazi, E. Motevaseli et al., "The melatonin immunomodulatory actions in radiotherapy," *Biophysical Reviews*, vol. 9, no. 2, pp. 139–148, 2017.
- [7] R. Yahyapour, D. Shabeeb, M. Cheki et al., "Radiation protection and mitigation by natural antioxidants and flavonoids: implications to radiotherapy and radiation disasters," *Current Molecular Pharmacology*, vol. 11, no. 4, pp. 285–304, 2018.
- [8] R. Yahyapour, E. Motevaseli, A. Rezaeyan et al., "Mechanisms of radiation bystander and non-targeted effects: implications to radiation carcinogenesis and radiotherapy," *Current Radiopharmaceuticals*, vol. 11, no. 1, pp. 34–45, 2018.
- [9] R. Yahyapour, A. Salajegheh, A. Safari et al., "Radiation-induced non-targeted effect and carcinogenesis; implications in clinical radiotherapy," *Journal of Biomedical Physics & Engineering*, vol. 8, no. 4, pp. 435–446, 2018.
- [10] S. M. Meeran, A. Ahmed, and T. O. Tollefsbol, "Epigenetic targets of bioactive dietary components for cancer prevention and therapy," *Clinical Epigenetics*, vol. 1, no. 3-4, pp. 101–116, 2010.
- [11] I. Afanas'ev, "Mechanisms of superoxide signaling in epigenetic processes: relation to aging and cancer," *Aging and Disease*, vol. 6, no. 3, pp. 216–227, 2015.
- [12] R. Yahyapour, E. Motevaseli, A. Rezaeyan et al., "Reduction-oxidation (redox) system in radiation-induced normal tissue injury: molecular mechanisms and implications in radiation therapeutics," *Clinical and Translational Oncology*, vol. 20, no. 8, pp. 975–988, 2018.
- [13] F. Sieber, S. A. Muir, E. P. Cohen et al., "High-dose selenium for the mitigation of radiation injury: a pilot study in a rat model," *Radiation Research*, vol. 171, no. 3, pp. 368–373, 2009.
- [14] W. Zhao and M. E. Robbins, "Inflammation and chronic oxidative stress in radiation-induced late normal tissue injury: therapeutic implications," *Current Medicinal Chemistry*, vol. 16, no. 2, pp. 130–143, 2009.
- [15] G. R. Drummond, S. Selemidis, K. K. Griendling, and C. G. Sobey, "Combating oxidative stress in vascular disease: NADPH oxidases as therapeutic targets," *Nature Reviews Drug Discovery*, vol. 10, no. 6, pp. 453–471, 2011.
- [16] K. Bedard and K. H. Krause, "The NOX family of ROS-generating NADPH oxidases: physiology and pathophysiology," *Physiological Reviews*, vol. 87, no. 1, pp. 245–313, 2007.
- [17] A. Panday, M. K. Sahoo, D. Osorio, and S. Batra, "NADPH oxidases: an overview from structure to innate immunity-associated pathologies," *Cellular & Molecular Immunology*, vol. 12, no. 1, pp. 5–23, 2015.
- [18] K. Mortezaee, N. H. Goradel, P. Amini et al., "NADPH oxidase as a target for modulation of radiation response; implications to carcinogenesis and radiotherapy," *Current Molecular Pharmacology*, vol. 12, no. 1, pp. 50–60, 2019.
- [19] M. Najafi, A. Shirazi, E. Motevaseli et al., "Melatonin modulates regulation of NOX2 and NOX4 following irradiation in the lung," *Current Clinical Pharmacology*, vol. 14, 2019.
- [20] B. Bánfi, A. Maturana, S. Jaconi et al., "A mammalian H⁺ channel generated through alternative splicing of the NADPH oxidase homolog NOH-1," *Science*, vol. 287, no. 5450, pp. 138–142, 2000.
- [21] Y. A. Suh, R. S. Arnold, B. Lassegue et al., "Cell transformation by the superoxide-generating oxidase Mox1," *Nature*, vol. 401, no. 6748, pp. 79–82, 1999.
- [22] Z. Sun and F. Liu, "Association of Nox1 and vinculin with colon cancer progression," *Cancer Investigation*, vol. 31, no. 4, pp. 273–278, 2013.
- [23] F. Liu, A. M. Gomez Garcia, and F. L. Meyskens Jr., "NADPH oxidase 1 overexpression enhances invasion via matrix metalloproteinase-2 and epithelial-mesenchymal transition in melanoma cells," *The Journal of Investigative Dermatology*, vol. 132, no. 8, pp. 2033–2041, 2012.
- [24] X. J. Fu, Y. B. Peng, Y. P. Hu, Y. Z. Shi, M. Yao, and X. Zhang, "NADPH oxidase 1 and its derived reactive oxygen species mediated tissue injury and repair," *Oxidative Medicine and Cellular Longevity*, vol. 2014, Article ID 282854, 10 pages, 2014.
- [25] S. H. Choi, M. Kim, H. J. Lee, E. H. Kim, C. H. Kim, and Y. J. Lee, "Effects of NOX1 on fibroblastic changes of endothelial cells in radiation-induced pulmonary fibrosis," *Molecular Medicine Reports*, vol. 13, no. 5, pp. 4135–4142, 2016.
- [26] J. H. Kim, K. M. Kim, M. H. Jung et al., "Protective effects of alpha lipoic acid on radiation-induced salivary gland injury in rats," *Oncotarget*, vol. 7, no. 20, pp. 29143–29153, 2016.

- [27] P. K. Narayanan, E. H. Goodwin, and B. E. Lehnert, " α particles initiate biological production of superoxide anions and hydrogen peroxide in human cells," *Cancer Research*, vol. 57, no. 18, pp. 3963–3971, 1997.
- [28] K. Datta, S. Suman, B. V. S. Kallakury, and A. J. Fornace, "Exposure to heavy ion radiation induces persistent oxidative stress in mouse intestine," *PLoS One*, vol. 7, no. 8, article e42224, 2012.
- [29] H. Kikuchi, M. Hikage, H. Miyashita, and M. Fukumoto, "NADPH oxidase subunit, gp91(phox) homologue, preferentially expressed in human colon epithelial cells," *Gene*, vol. 254, no. 1-2, pp. 237–243, 2000.
- [30] B. Bánfi, B. Malgrange, J. Knisz, K. Steger, M. Dubois-Dauphin, and K. H. Krause, "NOX3, a superoxide-generating NADPH oxidase of the inner ear," *The Journal of Biological Chemistry*, vol. 279, no. 44, pp. 46065–46072, 2004.
- [31] R. Paffenholz, R. A. Bergstrom, F. Pasutto et al., "Vestibular defects in head-tilt mice result from mutations in Nox3, encoding an NADPH oxidase," *Genes & Development*, vol. 18, no. 5, pp. 486–491, 2004.
- [32] Y. S. Shin, H. A. Shin, S. U. Kang et al., "Effect of epicatechin against radiation-induced oral mucositis: in vitro and in vivo study," *PLoS One*, vol. 8, no. 7, article e69151, 2013.
- [33] M. Geiszt, J. B. Kopp, P. Várnai, and T. L. Leto, "Identification of renox, an NAD(P)H oxidase in kidney," *Proceedings of the National Academy of Sciences of the United States of America*, vol. 97, no. 14, pp. 8010–8014, 2000.
- [34] A. Shiose, J. Kuroda, K. Tsuruya et al., "A novel superoxide-producing NAD(P)H oxidase in kidney," *The Journal of Biological Chemistry*, vol. 276, no. 2, pp. 1417–1423, 2001.
- [35] S. K. Pazhanisamy, H. Li, Y. Wang, I. Batinic-Haberle, and D. Zhou, "NADPH oxidase inhibition attenuates total body irradiation-induced haematopoietic genomic instability," *Mutagenesis*, vol. 26, no. 3, pp. 431–435, 2011.
- [36] Y. Wang, L. Liu, S. K. Pazhanisamy, H. Li, A. Meng, and D. Zhou, "Total body irradiation causes residual bone marrow injury by induction of persistent oxidative stress in murine hematopoietic stem cells," *Free Radical Biology & Medicine*, vol. 48, no. 2, pp. 348–356, 2010.
- [37] H. Zhang, Y. A. Wang, A. Meng et al., "Inhibiting TGFbeta1 has a protective effect on mouse bone marrow suppression following ionizing radiation exposure in vitro," *Journal of Radiation Research*, vol. 54, no. 4, pp. 630–636, 2013.
- [38] B. Bánfi, F. Tirone, I. Durussel et al., "Mechanism of Ca^{2+} activation of the NADPH oxidase 5 (NOX5)," *The Journal of Biological Chemistry*, vol. 279, no. 18, pp. 18583–18591, 2004.
- [39] G. Cheng, Z. Cao, X. Xu, E. van Meir, and J. D. Lambeth, "Homologs of gp91phox: cloning and tissue expression of Nox3, Nox4, and Nox5," *Gene*, vol. 269, no. 1-2, pp. 131–140, 2001.
- [40] N. Salles, I. Szanto, F. Herrmann et al., "Expression of mRNA for ROS-generating NADPH oxidases in the aging stomach," *Experimental Gerontology*, vol. 40, no. 4, pp. 353–357, 2005.
- [41] B. Bánfi, G. Molnár, A. Maturana et al., "A Ca^{2+} -activated NADPH oxidase in testis, spleen, and lymph nodes," *The Journal of Biological Chemistry*, vol. 276, no. 40, pp. 37594–37601, 2001.
- [42] X. De Deken, D. Wang, M. C. Many et al., "Cloning of two human thyroid cDNAs encoding new members of the NADPH oxidase family," *The Journal of Biological Chemistry*, vol. 275, no. 30, pp. 23227–23233, 2000.
- [43] C. Dupuy, R. Ohayon, A. Valent, M. S. Noël-Hudson, D. Dème, and A. Virion, "Purification of a novel flavoprotein involved in the thyroid NADPH oxidase. Cloning of the porcine and human cdnas," *The Journal of Biological Chemistry*, vol. 274, no. 52, pp. 37265–37269, 1999.
- [44] R. Forteza, M. Salathe, F. Miot, R. Forteza, and G. E. Conner, "Regulated hydrogen peroxide production by Duox in human airway epithelial cells," *American Journal of Respiratory Cell and Molecular Biology*, vol. 32, no. 5, pp. 462–469, 2005.
- [45] C. Schwarzer, T. E. Machen, B. Illek, and H. Fischer, "NADPH oxidase-dependent acid production in airway epithelial cells," *The Journal of Biological Chemistry*, vol. 279, no. 35, pp. 36454–36461, 2004.
- [46] M. Geiszt, J. Witt, J. Baffi, K. Lekstrom, and T. L. Leto, "Dual oxidases represent novel hydrogen peroxide sources supporting mucosal surface host defense," *The FASEB Journal*, vol. 17, no. 11, pp. 1502–1504, 2003.
- [47] D. Wang, X. de Deken, M. Milenkovic et al., "Identification of a novel partner of duox: EFP1, a thioredoxin-related protein," *The Journal of Biological Chemistry*, vol. 280, no. 4, pp. 3096–3103, 2005.
- [48] C. Dupuy, M. Pomerance, R. Ohayon et al., "Thyroid oxidase (THOX2) gene expression in the rat thyroid cell line FRTL-5," *Biochemical and Biophysical Research Communications*, vol. 277, no. 2, pp. 287–292, 2000.
- [49] R. A. El Hassani, N. Benfares, B. Caillou et al., "Dual oxidase2 is expressed all along the digestive tract," *American Journal of Physiology-Gastrointestinal and Liver Physiology*, vol. 288, no. 5, pp. G933–G942, 2005.
- [50] R. Ameziane-El-Hassani, M. Talbot, M. C. de Souza Dos Santos et al., "NADPH oxidase DUOX1 promotes long-term persistence of oxidative stress after an exposure to irradiation," *Proceedings of the National Academy of Sciences of the United States of America*, vol. 112, no. 16, pp. 5051–5056, 2015.
- [51] Y. Wu and J. H. Doroshov, "Abstract 5358: IL-4/IL-13 induce Duox2/DuoxA2 expression and reactive oxygen production in human pancreatic and colon cancer cells," *Cancer Research*, vol. 74, Supplement 19, pp. 5358–5358, 2014.
- [52] R. Azmoonfar, P. Amini, H. Saffar et al., "Metformin protects against radiation-induced pneumonitis and fibrosis and attenuates upregulation of dual oxidase genes expression," *Advanced Pharmaceutical Bulletin*, vol. 8, no. 4, pp. 697–704, 2018.
- [53] P. Amini, S. Kolivand, H. Saffar et al., "Protective effect of selenium-L-methionine on radiation-induced acute pneumonitis and lung fibrosis in rat," *Current Clinical Pharmacology*, vol. 14, no. 2, pp. 157–164, 2019.
- [54] S. Kolivand, P. Amini, H. Saffar et al., "Selenium-L-methionine modulates radiation injury and Duox1 and Duox2 upregulation in rat's heart tissues," *Journal of Cardiovascular and Thoracic Research*, vol. 11, no. 2, pp. 121–126, 2019.
- [55] A. Aliasgharzadeh, B. Farhood, P. Amini et al., "Melatonin attenuates upregulation of Duox1 and Duox2 and protects against lung injury following chest irradiation in rats," *Cell Journal*, vol. 21, no. 3, pp. 236–242, 2019.
- [56] B. Farhood, A. Aliasgharzadeh, P. Amini et al., "Radiation-induced dual oxidase upregulation in rat heart tissues: protective effect of melatonin," *Medicina*, vol. 55, no. 7, p. 317, 2019.

- [57] J. Y. Fu, J. L. Masferrer, K. Seibert, A. Raz, and P. Needleman, "The induction and suppression of prostaglandin H2 synthase (cyclooxygenase) in human monocytes," *The Journal of Biological Chemistry*, vol. 265, no. 28, pp. 16737–16740, 1990.
- [58] J. Song, Y. Wei, Q. Chen, and D. Xing, "Cyclooxygenase 2-mediated apoptotic and inflammatory responses in photodynamic therapy treated breast adenocarcinoma cells and xenografts," *Journal of Photochemistry and Photobiology B*, vol. 134, pp. 27–36, 2014.
- [59] D. Wang and R. N. Dubois, "The role of COX-2 in intestinal inflammation and colorectal cancer," *Oncogene*, vol. 29, no. 6, pp. 781–788, 2010.
- [60] M. Laube, T. Kniess, and J. Pietzsch, "Development of antioxidant COX-2 inhibitors as radioprotective agents for radiation therapy—a hypothesis-driven review," *Antioxidants*, vol. 5, no. 2, p. 14, 2016.
- [61] A. Rezaeyan, G. H. Haddadi, M. Hosseinzadeh, M. Moradi, and M. Najafi, "Radioprotective effects of hesperidin on oxidative damages and histopathological changes induced by X-irradiation in rats heart tissue," *Journal of Medical Physics*, vol. 41, no. 3, pp. 182–191, 2016.
- [62] M. Cheki, R. Yahyapour, B. Farhood et al., "COX-2 in radiotherapy: a potential target for radioprotection and radiosensitization," *Current Molecular Pharmacology*, vol. 11, no. 3, pp. 173–183, 2018.
- [63] T. A. Zykova, F. Zhu, X. Zhai et al., "Resveratrol directly targets COX-2 to inhibit carcinogenesis," *Molecular Carcinogenesis*, vol. 47, no. 10, pp. 797–805, 2008.
- [64] P. Rao and E. E. Knaus, "Evolution of nonsteroidal anti-inflammatory drugs (NSAIDs): cyclooxygenase (COX) inhibition and beyond," *Journal of Pharmacy & Pharmaceutical Sciences*, vol. 11, no. 2, pp. 81s–110s, 2008.
- [65] D. Citrin, A. P. Cotrim, F. Hyodo, B. J. Baum, M. C. Krishna, and J. B. Mitchell, "Radioprotectors and mitigators of radiation-induced normal tissue injury," *The Oncologist*, vol. 15, no. 4, pp. 360–371, 2010.
- [66] M. Maccarrone, "Lipoxygenases, apoptosis, and the role of antioxidants," in *Photoprotection, Photoinhibition, Gene Regulation, and Environment*, B. Demmig-Adams, W. W. Adams, and A. K. Mattoo, Eds., vol. 21 of *Advances in Photosynthesis and Respiration*, pp. 321–332, Springer, Dordrecht, 2006.
- [67] O. P. Matyshevskaia, V. N. Pastukh, and V. A. Solodushko, "Inhibition of lipoxygenase activity reduces radiation-induced DNA fragmentation in lymphocytes," *Radiatsionnaia Biologiya, Radioecologiya*, vol. 39, no. 2-3, pp. 282–286, 1999.
- [68] O. E. Grichenko, A. C. Pushin, V. V. Shaposhnikova, M. K. H. Levitman, and N. Korystov Iu, "Analysis of 15-lipoxygenase activity in irradiated thymocytes," *Izvestiya Akademii Nauk. Seriya Biologicheskaya*, vol. 5, pp. 517–521, 2004.
- [69] M. Halle, T. Christersdottir, and M. Back, "Chronic adventitial inflammation, vasa vasorum expansion, and 5-lipoxygenase up-regulation in irradiated arteries from cancer survivors," *The FASEB Journal*, vol. 30, no. 11, pp. 3845–3852, 2016.
- [70] F. Aktan, "iNOS-mediated nitric oxide production and its regulation," *Life Sciences*, vol. 75, no. 6, pp. 639–653, 2004.
- [71] M. Najafi, E. Motevaseli, A. Shirazi et al., "Mechanisms of inflammatory responses to radiation and normal tissues toxicity: clinical implications," *International Journal of Radiation Biology*, vol. 94, no. 4, pp. 335–356, 2018.
- [72] M. Jaiswal, N. LaRusso, R. A. Shapiro, T. R. Billiar, and G. J. Gores, "Nitric oxide-mediated inhibition of DNA repair potentiates oxidative DNA damage in cholangiocytes," *Gastroenterology*, vol. 120, no. 1, pp. 190–199, 2001.
- [73] R. Malaviya, A. J. Gow, M. Francis, E. V. Abramova, J. D. Laskin, and D. L. Laskin, "Radiation-induced lung injury and inflammation in mice: role of inducible nitric oxide synthase and surfactant protein D," *Toxicological Sciences*, vol. 144, no. 1, pp. 27–38, 2015.
- [74] Y. Nozaki, Y. Hasegawa, A. Takeuchi et al., "Nitric oxide as an inflammatory mediator of radiation pneumonitis in rats," *The American Journal of Physiology*, vol. 272, 4 Part 1, pp. L651–L658, 1997.
- [75] C. Tsuji, S. Shioya, Y. Hirota et al., "Increased production of nitrotyrosine in lung tissue of rats with radiation-induced acute lung injury," *American Journal of Physiology-Lung Cellular and Molecular Physiology*, vol. 278, no. 4, pp. L719–L725, 2000.
- [76] S. Ohta, S. Matsuda, M. Gunji, and A. Kamogawa, "The role of nitric oxide in radiation damage," *Biological & Pharmaceutical Bulletin*, vol. 30, no. 6, pp. 1102–1107, 2007.
- [77] J. S. Beckman and W. H. Koppenol, "Nitric oxide, superoxide, and peroxynitrite: the good, the bad, and ugly," *American Journal of Physiology-Cell Physiology*, vol. 271, no. 5, pp. C1424–C1437, 1996.
- [78] V. A. Yakovlev, "Role of nitric oxide in the radiation-induced bystander effect," *Redox Biology*, vol. 6, pp. 396–400, 2015.
- [79] S. Ghosh, D. K. Maurya, and M. Krishna, "Role of iNOS in bystander signaling between macrophages and lymphoma cells," *International Journal of Radiation Oncology, Biology, Physics*, vol. 72, no. 5, pp. 1567–1574, 2008.
- [80] V. A. Yakovlev, "Nitric oxide-dependent downregulation of BRCA1 expression promotes genetic instability," *Cancer Research*, vol. 73, no. 2, pp. 706–715, 2013.
- [81] W. Han, L. Wu, S. Chen et al., "Constitutive nitric oxide acting as a possible intercellular signaling molecule in the initiation of radiation-induced DNA double strand breaks in non-irradiated bystander cells," *Oncogene*, vol. 26, no. 16, pp. 2330–2339, 2007.
- [82] J. Pugin, "How tissue injury alarms the immune system and causes a systemic inflammatory response syndrome," *Annals of Intensive Care*, vol. 2, no. 1, p. 27, 2012.
- [83] B. Frey, M. Rückert, L. Deloch et al., "Immunomodulation by ionizing radiation-impact for design of radio-immunotherapies and for treatment of inflammatory diseases," *Immunological Reviews*, vol. 280, no. 1, pp. 231–248, 2017.
- [84] Y. Shen, X. Jiang, L. Meng, C. Xia, L. Zhang, and Y. Xin, "Transplantation of bone marrow mesenchymal stem cells prevents radiation-induced artery injury by suppressing oxidative stress and inflammation," *Oxidative Medicine and Cellular Longevity*, vol. 2018, Article ID 5942916, 13 pages, 2018.
- [85] Y. Ogawa, T. Kobayashi, A. Nishioka et al., "Radiation-induced reactive oxygen species formation prior to oxidative DNA damage in human peripheral T cells," *International Journal of Molecular Medicine*, vol. 11, no. 2, pp. 149–152, 2003.
- [86] K. Mortezaee, M. Najafi, B. Farhood, A. Ahmadi, D. Shabeeb, and A. E. Musa, "NF- κ B targeting for overcoming tumor

- resistance and normal tissues toxicity,” *Journal of Cellular Physiology*, vol. 234, no. 10, pp. 17187–17204, 2019.
- [87] V. Bours, G. Bonizzi, M. Bentires-Alj et al., “NF- κ B activation in response to toxic and therapeutical agents: role in inflammation and cancer treatment,” *Toxicology*, vol. 153, no. 1-3, pp. 27–38, 2000.
- [88] S. M. Meeran, S. Akhtar, and S. K. Katiyar, “Inhibition of UVB-induced skin tumor development by drinking green tea polyphenols is mediated through DNA repair and subsequent inhibition of inflammation,” *The Journal of Investigative Dermatology*, vol. 129, no. 5, pp. 1258–1270, 2009.
- [89] M. A. Packer and M. P. Murphy, “Peroxynitrite formed by simultaneous nitric oxide and superoxide generation causes cyclosporin-A-sensitive mitochondrial calcium efflux and depolarisation,” *European Journal of Biochemistry*, vol. 234, no. 1, pp. 231–239, 1995.
- [90] R. A. Kowluru and M. Mishra, “Oxidative stress, mitochondrial damage and diabetic retinopathy,” *Biochimica et Biophysica Acta (BBA) - Molecular Basis of Disease*, vol. 1852, no. 11, pp. 2474–2483, 2015.
- [91] F. Ortiz, D. Acuña-Castroviejo, C. Doerrier et al., “Melatonin blunts the mitochondrial/NLRP3 connection and protects against radiation-induced oral mucositis,” *Journal of Pineal Research*, vol. 58, no. 1, pp. 34–49, 2015.
- [92] J. C. Leemans, S. L. Cassel, and F. S. Sutterwala, “Sensing damage by the NLRP3 inflammasome,” *Immunological Reviews*, vol. 243, no. 1, pp. 152–162, 2011.
- [93] R. Han, D. Wu, S. Deng, T. Liu, T. Zhang, and Y. Xu, “NLRP3 inflammasome induces pyroptosis in lung tissues of radiation-induced lung injury in mice,” *Xi Bao Yu Fen Zi Mian Yi Xue Za Zhi*, vol. 33, no. 9, pp. 1206–1211, 2017.
- [94] D. Shin, G. Lee, S. H. Sohn et al., “Regulatory T cells contribute to the inhibition of radiation-induced acute lung inflammation via bee venom phospholipase A2 in mice,” *Toxins*, vol. 8, no. 5, p. 131, 2016.
- [95] S. H. Sohn, J. M. Lee, S. Park et al., “The inflammasome accelerates radiation-induced lung inflammation and fibrosis in mice,” *Environmental Toxicology and Pharmacology*, vol. 39, no. 2, pp. 917–926, 2015.
- [96] Y. G. Liu, J. K. Chen, Z. T. Zhang et al., “NLRP3 inflammasome activation mediates radiation-induced pyroptosis in bone marrow-derived macrophages,” *Cell Death & Disease*, vol. 8, no. 2, article e2579, 2017.
- [97] R. Yahyapour, P. Amini, S. Rezapoor et al., “Targeting of inflammation for radiation protection and mitigation,” *Current Molecular Pharmacology*, vol. 11, no. 3, pp. 203–210, 2018.
- [98] K. Suzuki, I. Mori, Y. Nakayama, M. Miyakoda, S. Kodama, and M. Watanabe, “Radiation-induced senescence-like growth arrest requires TP53 function but not telomere shortening,” *Radiation Research*, vol. 155, no. 1, pp. 248–253, 2001.
- [99] N. J. Linford, S. E. Schriener, and P. S. Rabinovitch, “Oxidative damage and aging: spotlight on mitochondria,” *Cancer Research*, vol. 66, no. 5, pp. 2497–2499, 2006.
- [100] S. E. Schriener, N. J. Linford, G. M. Martin et al., “Extension of murine life span by overexpression of catalase targeted to mitochondria,” *Science*, vol. 308, no. 5730, pp. 1909–1911, 2005.
- [101] S. Kobashigawa, G. Kashino, H. Mori, and M. Watanabe, “Relief of delayed oxidative stress by ascorbic acid can suppress radiation-induced cellular senescence in mammalian fibroblast cells,” *Mechanisms of Ageing and Development*, vol. 146-148, pp. 65–71, 2015.
- [102] Y. Sakai, T. Yamamori, Y. Yoshikawa et al., “NADPH oxidase 4 mediates ROS production in radiation-induced senescent cells and promotes migration of inflammatory cells,” *Free Radical Research*, vol. 52, no. 1, pp. 92–102, 2018.
- [103] J. S. You and P. A. Jones, “Cancer genetics and epigenetics: two sides of the same coin?,” *Cancer Cell*, vol. 22, no. 1, pp. 9–20, 2012.
- [104] M. Verma, D. Seminara, F. J. Arena, C. John, K. Iwamoto, and V. Hartmuller, “Genetic and epigenetic biomarkers in cancer: improving diagnosis, risk assessment, and disease stratification,” *Molecular Diagnosis & Therapy*, vol. 10, no. 1, pp. 1–15, 2006.
- [105] M. Verma, “Cancer control and prevention: nutrition and epigenetics,” *Current Opinion in Clinical Nutrition and Metabolic Care*, vol. 16, no. 4, pp. 376–384, 2013.
- [106] I. R. Miousse, J. Chang, L. Shao et al., “Inter-strain differences in LINE-1 DNA methylation in the mouse hematopoietic system in response to exposure to ionizing radiation,” *International Journal of Molecular Sciences*, vol. 18, no. 7, p. 1430, 2017.
- [107] T. Z. Yi, J. Li, X. Han et al., “DNMT inhibitors and HDAC inhibitors regulate E-cadherin and Bcl-2 expression in endometrial carcinoma in vitro and in vivo,” *Chemotherapy*, vol. 58, no. 1, pp. 19–29, 2012.
- [108] N. Reichert, M. A. Choukrallah, and P. Matthias, “Multiple roles of class I HDACs in proliferation, differentiation, and development,” *Cellular and Molecular Life Sciences*, vol. 69, no. 13, pp. 2173–2187, 2012.
- [109] M. S. Choi, Y. H. Shim, J. Y. Hwa et al., “Expression of DNA methyltransferases in multistep hepatocarcinogenesis,” *Human Pathology*, vol. 34, no. 1, pp. 11–17, 2003.
- [110] Q. Liu, J.-M. Zheng, J.-K. Chen et al., “Histone deacetylase 5 promotes the proliferation of glioma cells by upregulation of Notch 1,” *Molecular Medicine Reports*, vol. 10, no. 4, pp. 2045–2050, 2014.
- [111] G. W. Feng, L. D. Dong, W. J. Shang et al., “HDAC5 promotes cell proliferation in human hepatocellular carcinoma by up-regulating Six1 expression,” *European Review for Medical and Pharmacological Sciences*, vol. 18, no. 6, pp. 811–816, 2014.
- [112] M. Z. Fang, Y. Wang, N. Ai et al., “Tea polyphenol (–)-epigallocatechin-3-gallate inhibits DNA methyltransferase and reactivates methylation-silenced genes in cancer cell lines,” *Cancer Research*, vol. 63, no. 22, pp. 7563–7570, 2003.
- [113] A. S. Tsao, D. Liu, J. Martin et al., “Phase II randomized, placebo-controlled trial of green tea extract in patients with high-risk oral premalignant lesions,” *Cancer Prevention Research*, vol. 2, no. 11, pp. 931–941, 2009.
- [114] C. Weigel, P. Schmezer, C. Plass, and O. Popanda, “Epigenetics in radiation-induced fibrosis,” *Oncogene*, vol. 34, no. 17, pp. 2145–2155, 2015.
- [115] C. Weigel, M. R. Veldwijk, C. C. Oakes et al., “Epigenetic regulation of diacylglycerol kinase α promotes radiation-induced fibrosis,” *Nature Communications*, vol. 7, no. 1, article 10893, 2016.
- [116] M. M. Acharya, A. A. D. Baddour, T. Kawashita et al., “Epigenetic determinants of space radiation-induced cognitive dysfunction,” *Scientific Reports*, vol. 7, no. 1, article 42885, 2017.

- [117] H. Denis, M. N. Ndlovu, and F. Fuks, "Regulation of mammalian DNA methyltransferases: a route to new mechanisms," *EMBO Reports*, vol. 12, no. 7, pp. 647–656, 2011.
- [118] D. A. Antwi, K. M. Gabbara, W. D. Lancaster, D. M. Ruden, and S. P. Zietske, "Radiation-induced epigenetic DNA methylation modification of radiation-response pathways," *Epigenetics*, vol. 8, no. 8, pp. 839–848, 2013.
- [119] I. Pogribny, I. Koturbash, V. Tryndyak et al., "Fractionated low-dose radiation exposure leads to accumulation of DNA damage and profound alterations in DNA and histone methylation in the murine thymus," *Molecular Cancer Research*, vol. 3, no. 10, pp. 553–561, 2005.
- [120] I. Koturbash, A. Boyko, R. Rodriguez-Juarez et al., "Role of epigenetic effectors in maintenance of the long-term persistent bystander effect in spleen in vivo," *Carcinogenesis*, vol. 28, no. 8, pp. 1831–1838, 2007.
- [121] H. D. Halicka, X. Huang, F. Traganos, M. A. King, W. Dai, and Z. Darzynkiewicz, "Histone H2AX phosphorylation after cell irradiation with UV-B: relationship to cell cycle phase and induction of apoptosis," *Cell Cycle*, vol. 4, no. 2, pp. 339–345, 2005.
- [122] B. Maroschik, A. Gürtler, A. Krämer et al., "Radiation-induced alterations of histone post-translational modification levels in lymphoblastoid cell lines," *Radiation Oncology*, vol. 9, no. 1, p. 15, 2014.
- [123] S. Matsuda, K. Furuya, M. Ikura, T. Matsuda, and T. Ikura, "Absolute quantification of acetylation and phosphorylation of the histone variant H2AX upon ionizing radiation reveals distinct cellular responses in two cancer cell lines," *Radiation and Environmental Biophysics*, vol. 54, no. 4, pp. 403–411, 2015.
- [124] M. Herberg, S. Siebert, M. Quaas et al., "Loss of Msh2 and a single-radiation hit induce common, genome-wide, and persistent epigenetic changes in the intestine," *Clinical Epigenetics*, vol. 11, no. 1, p. 65, 2019.
- [125] X. Zhang, T. Kluz, L. Gesumaria, M. S. Matsui, M. Costa, and H. Sun, "Solar simulated ultraviolet radiation induces global histone hypoacetylation in human keratinocytes," *PLoS One*, vol. 11, no. 2, article e0150175, 2016.
- [126] D. P. Bartel, "MicroRNAs: target recognition and regulatory functions," *Cell*, vol. 136, no. 2, pp. 215–233, 2009.
- [127] B. Farhood, N. H. Goradel, K. Mortezaee et al., "Intercellular communications-redox interactions in radiation toxicity; potential targets for radiation mitigation," *Journal of Cell Communication and Signaling*, vol. 13, no. 1, pp. 3–16, 2019.
- [128] M. Najafi, R. Fardid, M. A. Takhshid, M. A. Mosleh-Shirazi, A. H. Rezaeyan, and A. Salajegheh, "Radiation-induced oxidative stress at out-of-field lung tissues after pelvis irradiation in rats," *Cell Journal*, vol. 18, no. 3, pp. 340–345, 2016.
- [129] S. S. Acharya, W. Fendler, J. Watson et al., "Serum microRNAs are early indicators of survival after radiation-induced hematopoietic injury," *Science Translational Medicine*, vol. 7, no. 287, article 287ra69, 2015.
- [130] M. Port, F. Herodin, M. Valente et al., "MicroRNA expression for early prediction of late occurring hematologic acute radiation syndrome in baboons," *PLoS One*, vol. 11, no. 11, article e0165307, 2016.
- [131] X. H. Li, C. T. Ha, D. Fu, and M. Xiao, "Micro-RNA30c negatively regulates REDD1 expression in human hematopoietic and osteoblast cells after gamma-irradiation," *PLoS One*, vol. 7, no. 11, article e48700, 2012.
- [132] X. H. Li, C. T. Ha, D. Fu, M. R. Landauer, S. P. Ghosh, and M. Xiao, "Delta-Tocotrienol suppresses radiation-induced microRNA-30 and protects mice and human CD34⁺ cells from radiation injury," *PLoS One*, vol. 10, no. 3, article e0122258, 2015.
- [133] M. E. Robbins, J. K. Brunso-Bechtold, A. M. Peiffer, C. I. Tsien, J. E. Bailey, and L. B. Marks, "Imaging radiation-induced normal tissue injury," *Radiation Research*, vol. 177, no. 4, pp. 449–466, 2012.
- [134] Y. Huang, Q. Hu, Z. Deng, Y. Hang, J. Wang, and K. Wang, "MicroRNAs in body fluids as biomarkers for non-small cell lung cancer: a systematic review," *Technology in Cancer Research & Treatment*, vol. 13, no. 3, pp. 277–287, 2014.
- [135] F. Gao, P. Liu, J. Narayanan et al., "Changes in miRNA in the lung and whole blood after whole thorax irradiation in rats," *Scientific Reports*, vol. 7, no. 1, article 44132, 2017.
- [136] L. Xie, J. Zhou, S. Zhang et al., "Integrating microRNA and mRNA expression profiles in response to radiation-induced injury in rat lung," *Radiation Oncology*, vol. 9, no. 1, p. 111, 2014.
- [137] S. P. Ghosh, R. Pathak, P. Kumar et al., "gamma-Tocotrienol modulates radiation-induced microRNA expression in mouse spleen," *Radiation Research*, vol. 185, no. 5, pp. 485–495, 2016.

Research Article

Lipoxin A4 Ameliorates Acute Pancreatitis-Associated Acute Lung Injury through the Antioxidative and Anti-Inflammatory Effects of the Nrf2 Pathway

Wen Ye ¹, Chenlei Zheng¹, Dinglai Yu ², Fan Zhang¹, Reguang Pan¹, Xiaofeng Ni¹, Zehao Shi¹, Zhongjing Zhang¹, Yukai Xiang ², Hongwei Sun ², Keqing Shi¹, Bicheng Chen ^{1,2}, Qiyu Zhang ², and Mengtao Zhou ^{1,2,3}

¹Key Laboratory of Diagnosis and Treatment of Severe Hepato-Pancreatic Diseases of Zhejiang Province, The First Affiliated Hospital, Wenzhou Medical University, Wenzhou, 325015 Zhejiang Province, China

²Department of Surgery, The First Affiliated Hospital, Wenzhou Medical University, Wenzhou, 325015 Zhejiang Province, China

³The Pancreatitis Treatment Center, The First Affiliated Hospital, Wenzhou Medical University, Wenzhou, 325015 Zhejiang Province, China

Correspondence should be addressed to Qiyu Zhang; qiyuz@126.com and Mengtao Zhou; zhoumengtao@wmu.edu.cn

Received 30 April 2019; Revised 8 August 2019; Accepted 12 September 2019; Published 6 November 2019

Guest Editor: Reggiani Vilela Gonçalves

Copyright © 2019 Wen Ye et al. This is an open access article distributed under the Creative Commons Attribution License, which permits unrestricted use, distribution, and reproduction in any medium, provided the original work is properly cited.

Acute lung injury (ALI) is a critical event involved in the pathophysiological process of acute pancreatitis (AP). Many methods have been widely used for the treatment of AP-ALI, but few are useful during early inflammation. Lipoxin A4 (LXA4), a potent available anti-inflammatory and novel antioxidant mediator, has been extensively studied in AP-ALI, but its underlying mechanism as a protective mediator is not clear. This research was conducted to identify the possible targets and mechanisms involved in the anti-AP-ALI effect of LXA4. First, we confirmed that LXA4 strongly inhibited AP-ALI in mice. Next, using ELISA, PCR, and fluorescence detection to evaluate different parameters, LXA4 was shown to reduce the inflammatory cytokine production induced by AP and block reactive oxygen species (ROS) generation *in vivo* and *in vitro*. In addition, TNF- α treatment activated the nuclear factor E2-related factor 2 (Nrf2) signaling pathway and its downstream gene heme oxygenase-1 (HO-1) in human pulmonary microvascular endothelial cells (HPMECs), and LXA4 further promoted their expression. This study also provided evidence that LXA4 phosphorylates Ser40 and triggers its nuclear translocation to activate Nrf2. Moreover, when Nrf2-knockout (Nrf2^{-/-}) mice and cells were used to further assess the effect of the Nrf2/HO-1 pathway, we found that Nrf2 expression knockdown partially eliminated the effect of LXA4 on the reductions in inflammatory factor levels while abrogating the inhibitory effect of LXA4 on the ROS generation stimulated by AP-ALI. Overall, LXA4 attenuated the resolution of AP-induced inflammation and ROS generation to mitigate ALI, perhaps by modulating the Nrf2/HO-1 pathway. These findings have laid a foundation for the treatment of AP-ALI.

1. Introduction

Acute pancreatitis (AP) is an inflammatory process characterized by local and systemic inflammatory response syndrome (SIRS) and high morbidity and mortality due to the activation of pancreatic zymogen, leading to autodigestion of pancreatic acinar cells [1, 2]. SIRS and multiorgan

dysfunction syndrome (MODS) follow after damage to pancreatic acinar cells. Most patients with AP experience a mild disease course, but 10–20% develop severe AP (SAP), which is a life-threatening condition [3, 4]. The lung is the most common susceptible organ. The primary cause of mortality in early-stage AP patients is frequently associated with acute lung injury (ALI) and acute respiratory distress syndrome

(ARDS) [5, 6]. Therefore, aggressive early intervention and optimized therapy for AP-ALI are very important to improve outcomes.

Several studies have demonstrated that the accumulation of a large number of neutrophils in the lungs is a common pathophysiological feature of ALI and that enhanced generation of reactive oxygen species (ROS) and increased production of proinflammatory cytokines play a crucial role in acute lung damage [7–10]. Therefore, AP-ALI can be attenuated by either inhibiting the generation of ROS or scavenging inflammatory factors such as TNF- α , IL-1 β , IL-6, and E-selectin.

Nuclear factor erythroid 2-related factor-2 (Nrf2) combined with a promoter antioxidant response element (ARE) is the key regulator of intracellular antioxidant enzymes and thus participates in eliminating ROS and preventing damage to cells caused by oxidative stress [11–13]. The Nrf2/ARE signaling pathway constitutes a pleiotropic cellular defense, and heme oxygenase-1 (HO-1) is one of the most important antioxidant enzymes triggered in this signaling pathway [12], which has received widespread attention in recent years due to its anti-inflammatory effects [14, 15].

Although many studies have focused on developing new clinical therapies for ALI and respiratory insufficiency, no particularly effective drugs are currently available beyond routine life-support treatment. Lipoxin A4 (LXA4), one of the most important physiological lipoxins, is a member of the family of endogenous anti-inflammatory molecules generated from arachidonic acid during the onset of the inflammatory response [16]. Notably, studies have demonstrated that LXA4 can play a role in blocking the generation of proinflammatory cytokines and preventing oxidative stress-mediated tissue injury [17, 18]. However, the mechanism of protection has not yet been entirely elucidated.

In the present study, we explored whether the administration of LXA4 can protect lung tissue against oxidative and proinflammatory molecule-mediated injury as well as whether LXA4 exerts beneficial effects on AP-ALI by activating the Nrf2/HO-1 pathway.

2. Materials and Methods

2.1. Animals. C57BL/6 wild-type (WT) mice were obtained from the Laboratory Animal Center of Wenzhou Medical University (Wenzhou, CN). Nrf2-knockout (Nrf2^{-/-}) mice were obtained from the Jackson Laboratory (Bar Harbor, ME, USA) and bred by the Institute of Model Animals (Nanjing, CN) [19]. Offspring were bred with Nrf2^{-/-} male and female mice, and genotypes were identified by PCR before the experiment. All the mice used in the present research were 6-week-old male mice weighing 20–25 g, and the experiments were performed in full compliance with the guidelines of the Institutional Animal Committee of Wenzhou Medical University. WT and knockout animals were randomly assigned to three experimental groups: the control group (control)—0.9% saline (ip); the AP group (AP)—caerulein (50 μ g/kg, 7 times, ip)+LPS (10 mg/kg, ip); and the AP+LXA4 group (AP+LXA4)—LXA4 (0.1 mg/kg, ip)+caerulein (50 μ g/kg, 7 times, ip)+LPS (10 mg/kg, ip).

Each group included six mice. All animals were killed 24 h after drug injection.

2.2. Histopathological Analysis. Pancreatic and pulmonary tissue samples were collected and immediately fixed in paraformaldehyde for 48 h, followed by dehydration with graded alcohol and embedding in paraffin. The tissues were semiseriably cut into 5 μ m sections, and the tissue samples were deparaffinized twice for 15 min using xylene and rehydrated for 5 min, respectively, in 100, 95, 90, 80, and 75% ethanol. Then, the sections were stained with hematoxylin-eosin (HE; G1120, Solaibio, CN). After observation under a light microscope, pancreatic pathological scores and lung injury scores were assessed as previously described [20, 21]. Each slide was divided into five equal areas at 400x magnification to estimate the histopathological alterations. If discrepancies arose between the two examiners, a conclusive agreement was reached with the involvement of the third investigator.

2.3. Amylase Activity Estimation. Serum amylase activity in the groups treated with different solutions was quantified using iodine-amylum colorimetry following the manufacturer's protocol (1530511002, Jon Ln, CN).

2.4. Wet-to-Dry Weight (W/D) Ratios. The right lung was excised and blotted with a filter paper to absorb the surface water. Then, its weight was measured on an electronic scale and recorded as the wet weight (*W*). The right lung was then dried at 70°C in an oven for 48–72 h, and its dry weight (*D*) was measured until the weight was constant. The *W/D* ratio was calculated using the following formula: $W/D = (\text{wet weight} - \text{dry weight})/\text{dry weight}$.

2.5. ELISA Quantification. The serum levels of TNF- α , IL-1 β , and E-selectin in mice were determined by ELISA using quantikine ELISA kits according to the manufacturer's instructions (ab208348, ab100704, and ab201279; Abcam, USA).

2.6. Immunohistochemical (IHC) Analysis. Immunohistochemistry was used to qualitatively analyze the expression of phenotypic markers. To examine the expression of IL-6 in lung tissue samples, an IHC examination was carried out with formalin-fixed, paraffin-embedded sections (4 μ m) mounted on adhesion microscope slides (80312-3161, Citotest, CN). The sections were deparaffinized and rehydrated using xylene and graded concentrations of alcohol. The samples were boiled in antigen retrieval buffer containing citrate-hydrochloric acid (0.01 mol/l) using a microwave unit at full power for 15 min. Then, blocking with hydrogen peroxide (3% H₂O₂) was performed for 10 min to reduce the influence of endogenous peroxidases. Nonspecific proteins were blocked with 5% donkey serum at 37°C for 1 h. The sections were incubated with an anti-IL-6 antibody (1 : 500, ab6672, Abcam, USA) overnight at 4°C. The sections were further processed by an indirect immunoperoxidase technique using secondary antibodies, and the immunocomplexes were visualized as a brown color with diaminobenzidine (DAB, P0202, Beyotime, CN). Negative control sections were processed similarly, but the primary antibody

TABLE 1: Sequences of the primers used for quantitative real-time PCR.

Gene	Forward primer (5'–3')	Reverse primer (5'–3')
β -Actin	CCTGGCACCCAGCACAAAT	GGGCCGGACTCGTCATAC
IL-1 β	GCGGCATCCAGCTACGAATCTC	AACCAGCATCTTCCTCAGCTTGTC
IL-6	CCTCCAGAACAGATTTGAGAGTAGT	GGGTCAGGGGTGGTTATTGC
E-selectin	GAAGAGGTTCTTCCTGCCAAGTG	CAGAGCCATTGAGCGTCCATCC
Nrf2	ACCTCCCTGTTGTTGACTT	CACTTTATTCTTACCCCTCCT

was replaced with the antibody diluent. The slides were stained with Harris hematoxylin (G1120, Solaibio, CN). Representative images were captured with a microscope (Leica, Jena, GER).

2.7. Flow Cytometry. Lung tissue samples were cut into pieces, continuously agitated, and gently ground to extract cells, and ROS were quantified by the ROS-sensitive fluorophore DCFH-DA using the ROS Assay Kit (S0033, Beyotime, CN) according to the manufacturer's protocol [22, 23]. Then, cells from the lung tissue were incubated with DCFH-DA and analyzed for fluorescence intensity using a FACSCalibur flow cytometer (BD Biosciences, USA). The data were analyzed with FlowJo (version 10.0.7).

2.8. Cell Culture. Human pulmonary microvascular endothelial cells (HPMECs) were obtained from ScienCell Research Laboratories (San Diego, CA, USA). Cells were grown in endothelial cell medium (1001, ScienCell Research Laboratories, USA) containing 10% fetal bovine serum (0025, ScienCell Research Laboratories, USA), endothelial cell growth supplement (1052, ScienCell Research Laboratories, USA) and 5 ml of penicillin/streptomycin solution (0503, ScienCell Research Laboratories, USA). Experiments were performed when the HPMECs reached 80%-90% confluence.

2.9. RNA Extraction and qRT-PCR. RNA was extracted from HPMECs by Trizol Reagent (15596026, Thermo Fisher Scientific, USA) according to the manufacturer's instructions. The RNA expression of IL-1 β , IL-6, and E-selectin was detected by RT-PCR with mRNA-specific primers (Sangon Biotech, CN). One microgram of RNA was reverse-transcribed into cDNA using the Reverse Transcription System (4374966, Thermo Fisher Scientific, USA). RT-PCR was performed with SYBR Green Supermix with ROX (A25742, Thermo Fisher Scientific, UK) using a PCR detection system (7500fast, Applied Biosystems, CA). Ct values were used to quantify the mRNA levels, and the Ct value of each target mRNA was standardized to the Ct value of β -actin using the $2^{-\Delta\Delta Ct}$ method. The primer pairs used are listed in Table 1.

2.10. Measurement of Intracellular ROS Levels. Intracellular levels of ROS were quantified with dehydroergosterol (DHE) (S0063, Beyotime, CN) according to the manufacturer's recommendation [24, 25]. HPMECs were seeded in 6-well plates and incubated with drugs. Then, they were incubated with DHE for 15 min, and the fluorescence intensity was observed using a Nikon Eclipse TI fluorescence micro-

scope (Nikon Corporation, Tokyo, JP). Next, trypsinization was used to collect the cells, which were resuspended in PBS. To detect fluorescence, a C6 flow cytometer (BD Biosciences, USA) was used.

2.11. Western Blot (WB) Analysis. HPMECs were washed with phosphate-buffered saline (PBS) (20012500BT, Gibco, Thermo Fisher Scientific, USA). Then, the cells were lysed with radio immunoprecipitation assay (RIPA) buffer (P0013B, Beyotime, CN) containing protease (ST506, Beyotime, CN) and phosphatase inhibitors for 20 min. The lysates were then sonicated and centrifuged at 12,000 rpm for 15 min at 4°C to obtain the total protein supernatant. Protein concentrations were determined by a commercial BCA kit (P0010, Beyotime, CN). The samples were denatured for 5 min by heating at 95°C. β -Actin was used as the reference for the total cell proteins, and Lamin B was used as the reference for the nuclear fractions. Equal amounts of protein were separated by SDS-PAGE, transferred to PVDF membranes, and blocked with 5% skim milk for 2 h on a rocker. The membranes were then incubated with a primary antibody overnight at 4°C. The following primary antibodies were used: an anti-Nrf2 (ab62352, Abcam, USA), anti-Nrf2 (phosphoS40) (ab76026, Abcam, USA), anti-HO-1 (ab13243, Abcam, USA), anti- β -actin (ab76026, Abcam, USA), and anti-Lamin B (ab151735, Abcam, USA). The membranes were then incubated with the appropriate secondary antibodies (Biosharp, CN) for 1 h. The immunoreactive bands were detected by chemiluminescence methods, and densitometry analysis was performed using VisionWorks imaging software (Eastman Kodak Company, Rochester, NY).

2.12. Nuclear Protein Extraction. Nuclear fractions were extracted from HPMECs using a nuclear protein extraction kit (P0028, Beyotime, CN) according to the manufacturer's instructions.

2.13. Immunofluorescence. HPMECs were seeded at a density of 100,000 cells/well on 20 mm glass coverslips (WHB-12-CS, WHB, CN) and grown to 80% confluence. The cells were incubated with 4% paraformaldehyde for 15 min and permeabilized for 30 min at 37°C with 0.1% Triton X-100 (T8200, Solarbio Life Sciences, CN). Then, the cells were blocked with PBS containing 5% donkey serum for 1 h. The cells were then treated with the anti-Nrf2 antibody overnight at 4°C. The coverslips were incubated for 2 h with an Alexa Fluor 488-conjugated AffiniPure Goat Anti-Rabbit IgG (33106ES60, YEASEN, CN) secondary antibody in the dark. Then, the

cells were counterstained with DAPI (36308ES20, YEASEN, CN) for 10 min. The coverslips were visualized using a laser confocal microscope (Leica TCS SP8, Jena, GER).

2.14. Transient Transfection and Luciferase Assay. Based on the binding sites KB, ARE, and TRE in the HO-1 protein gene promoter sequence targeted by the AP-1, NF- κ B, and Nrf2 pathways, we constructed gene silencing plasmids. HPMECs were cotransfected with the AP-1, NF- κ B, or Nrf2 and AP-1+NF- κ B plasmids using Lipofectamine 3000. Luciferase activity was measured using a microplate reader (Tecan, Männedorf, CH).

2.15. Lentiviral Transfection. Nrf2 lentivirus and negative control lentivirus were chemically synthesized by GeneChem (Shanghai, CN). The lentiviruses were transfected into HPMECs according to the manufacturer's instructions. Nrf2 mRNA expression was detected 72 h later, and Nrf2 expression knockdown cells were used to evaluate the generation of inflammatory factors and ROS.

2.16. Statistical Analysis. Values are presented as the mean \pm standard deviation (SD). Statistical analysis was performed using GraphPad Prism 7.0 (GraphPad Software, San Diego, CA). Comparisons between two groups were performed by Student's *t*-tests, and Fisher's exact tests were used to determine differences among more than two groups. The results were calculated using data from three independent experiments. $P < 0.05$ was considered statistically significant.

3. Results

3.1. LXA4 Propagates the Resolution of AP and the Associated ALI Inflammation. Samples were stained with HE and observed under an optical microscope. Histological evaluation of the pancreatic tissue showed acinar cell vacuolation, interstitial tissue edema, inflammatory cell infiltration, hemorrhage, and necrosis in the AP group, indicating the successful induction of pancreatitis [26]. Almost no obvious pathological changes were noted in the control group. Compared with the AP group, the AP+LXA4 group exhibited reduced pathology (Figure 1(a)). Pancreatitis severity was estimated by measuring the pathology score. Compared with that in the AP group, the histological score of the pancreas in the AP+LXA4 group was largely attenuated (Figure 1(b)). The levels of amylase were significantly increased in the AP group, whereas they were slightly decreased in the AP+LXA4 treatment group (Figure 1(c)). As shown in Figure 1(d), the control group showed normal pulmonary architecture, while the AP group exhibited an increased alveolar septum thickness caused by alveolar collapse, multiple inflammatory cell infiltrates, and hyperemia in the pulmonary architecture, and the LXA4 treatment group showed an obvious improvement in pulmonary architecture. Histological analyses were performed, and the W/D ratio of the lungs was calculated. Lung injury scores of the AP+LXA4 group were less severe than those of the AP group (Figure 1(e)). The lung W/D ratio results agreed with the lung injury scores (Figure 1(f)). These results indicated that

LXA4 administration can attenuate injury to the pancreas and lungs.

3.2. LXA4 Attenuates the Levels of Proinflammatory Cytokines and Oxidative Stress in Lung Tissue. As shown by the results of the ELISA analysis in Figures 2(a)–2(c), TNF- α , IL-1 β , and E-selectin levels in serum were significantly increased in the AP group compared with those in the control group. These proinflammatory cytokine levels were reduced by LXA4 treatment. Examples of lung tissue sections stained for IL-6 are shown in Figure 2(d). The results of IHC analyses indicated that IL-6 levels were markedly increased in the AP group. When treated with LXA4, mice showed alleviated damage with weaker IL-6 staining in the lung tissue. Then, we detected the level of ROS in lung tissue homogenates. As shown in Figure 2(e), compared with the control group, the levels of ROS in the AP and AP+LXA4 groups were dramatically enhanced. LXA4 reduced the level of ROS compared with that in the AP group. The numerical statistical histogram is shown in Figure 2(f). The administration of LXA4 markedly reduced the production of inflammatory factors and ROS, thereby inhibiting AP-ALI.

3.3. The Inhibitory Effect of LXA4 on HPMEC Inflammation and the Redox State. To validate our findings *in vivo*, we established an inflammatory model in HPMECs stimulated with TNF- α . As shown in Figures 3(a)–3(c), the RT-PCR results demonstrated that TNF- α treatment obviously induced the expression of IL-1 β , IL-6, and E-selectin at the mRNA level, while LXA4 attenuated this induction in HPMECs. Next, the effect of LXA4 on the redox state of HPMECs under oxidative stress was explored. Fluorescence images (Figures 3(d) and 3(e)) stained with DHE to detect ROS revealed that compared with control treatment, TNF- α treatment resulted in a large increase in ROS. LXA4 inhibited the effect of TNF- α on ROS generation to some degree. As shown in Figures 3(f) and 3(g), the flow cytometric analysis verified these results. These data indicated that LXA4 may play a role in protecting HPMECs from inflammation and oxidative stress.

3.4. LXA4 Promotes Nrf2/HO-1 Pathway Activation in HPMECs. The Nrf2 pathway is a pathway closely related to oxidative stress and inflammatory responses [27–29]. To test the activation of Nrf2 in HPMECs, we detected the expression of Nrf2 and pSer40 Nrf2 by Western blotting. As shown in Figures 4(a) and 4(b), the expression levels of Nrf2 and pSer40 Nrf2 were significantly upregulated after TNF- α treatment. Moreover, the expression levels in the TNF- α +LXA4 group were even higher than those in the other two groups. These results suggested that Nrf2 can be activated by phosphorylation at Ser40. To further understand the molecular mechanisms underlying the effect of LXA4 on Nrf2, we performed WB and immunofluorescence experiments using HPMECs. TNF- α treatment increased the Nrf2 protein level in the nucleus. In addition, when LXA4 was administered simultaneously, the nuclear Nrf2 level was even higher (Figures 4(c) and 4(d)). The effect of LXA4 on Nrf2 activation was further demonstrated by confocal microscopy.

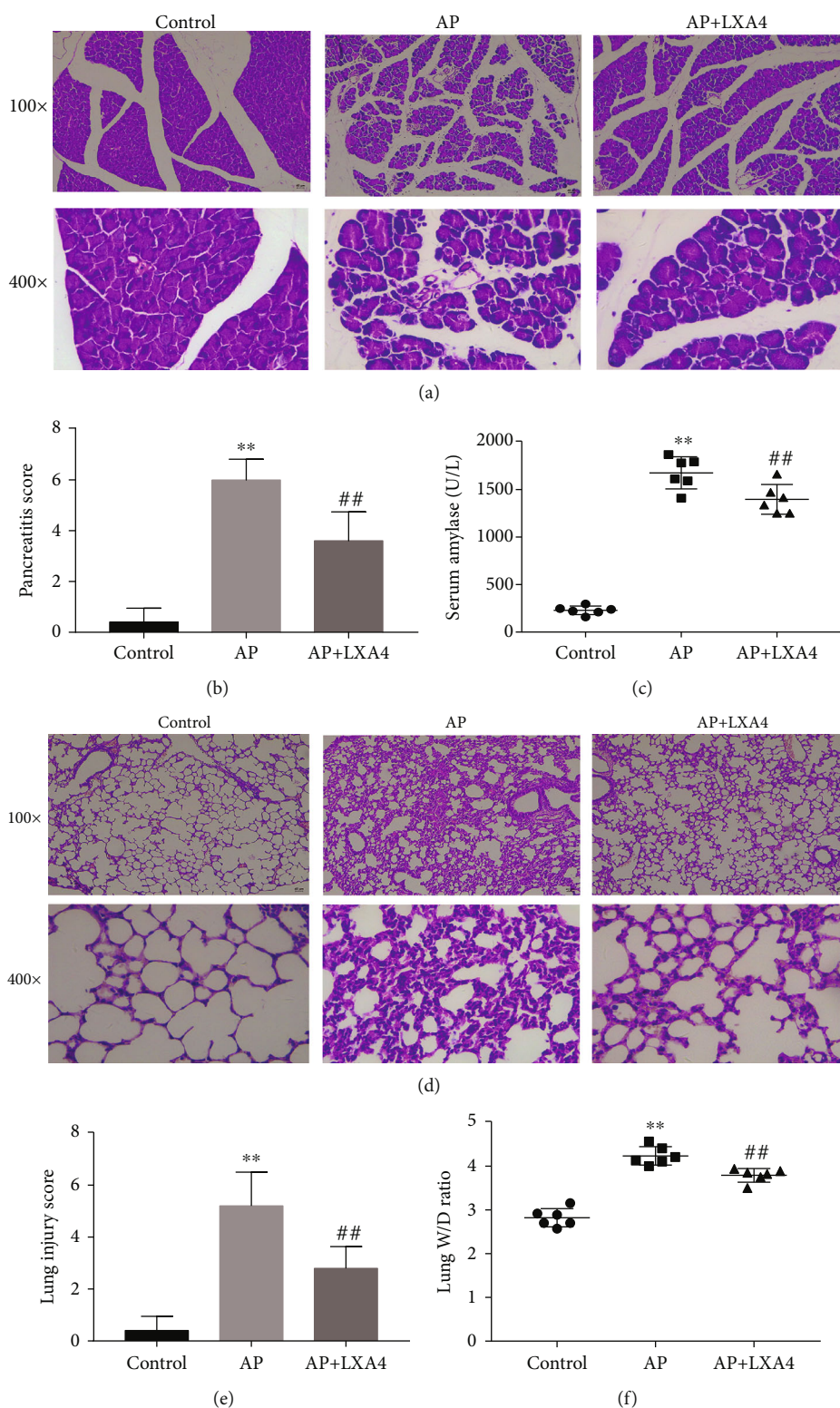


FIGURE 1: LXA4 effectively inhibited pancreatitis and AP-ALI in mice. Animals were randomly divided into three experimental groups: the AP group (AP) treated with caerulein (50 μ g/kg, 7 times, ip)+LPS (10 mg/kg, ip); the AP+LXA4 group treated with LXA4 (0.1 mg/kg, ip)+caerulein+LPS; and the control group treated with 0.9% saline (ip). (a) Representative pathological images of the pancreas (100x and 400x) and (b) histological scores were obtained to evaluate the degree of injury. Slides were evaluated by two independent investigators in a blinded manner. (c) Serum amylase levels were measured by means of iodine-amylum colorimetry. (d) Representative pathological images of the lung (100x and 400x), (e) lung injury scores, and (f) the lung wet/dry weight ratio are shown. ** $P < 0.01$ vs. the control group. ## $P < 0.01$ vs. the AP group. AP: the acute pancreatitis group; AP+LXA4, the acute pancreatitis+Lipoxin A4 group; AP-ALI: the acute pancreatitis-induced acute lung injury; LPS: lipopolysaccharide.

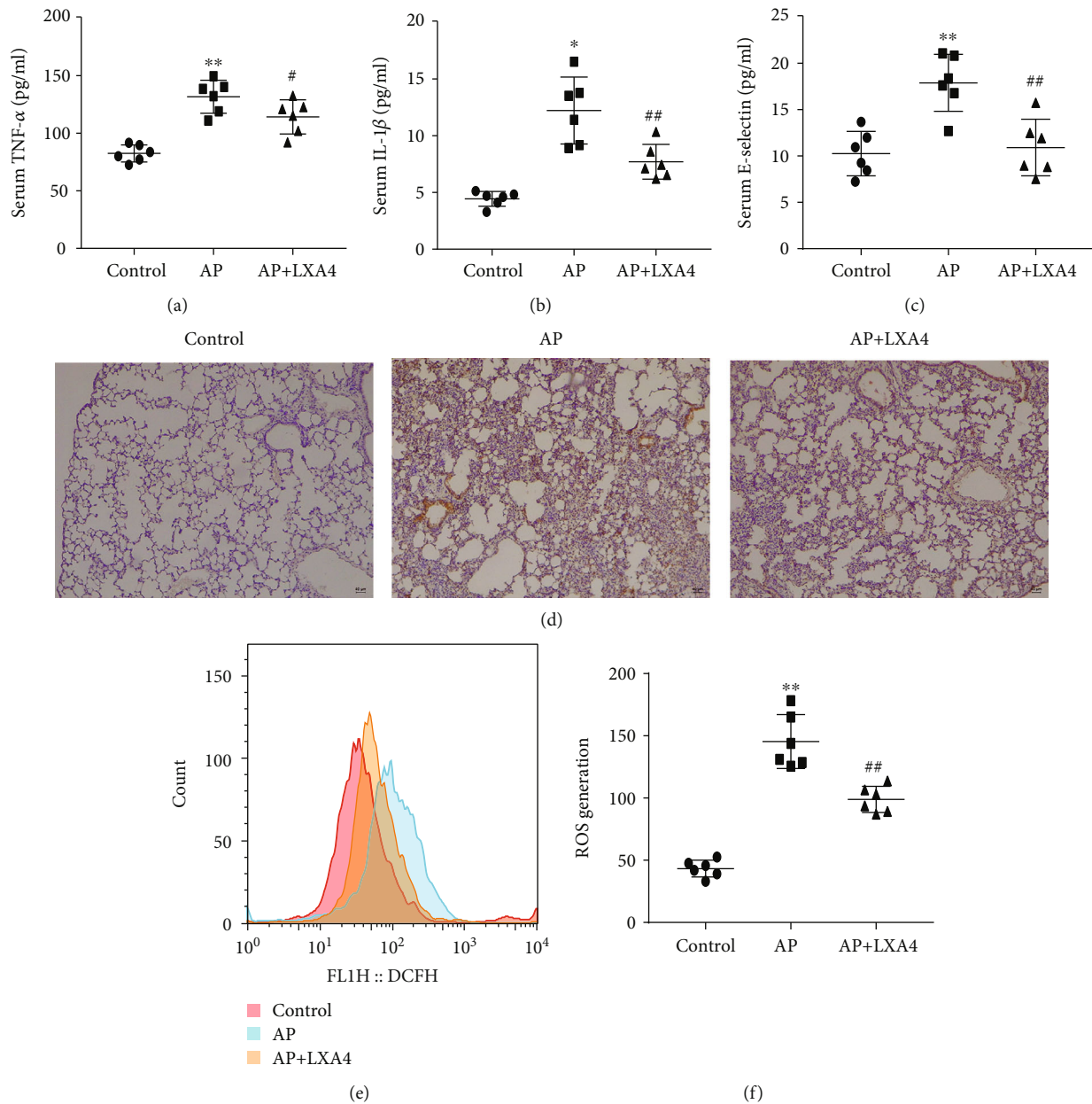


FIGURE 2: LXA4 inhibited proinflammatory cytokine and ROS generation in AP-ALI mice. Mouse serum and lung tissue samples were collected to evaluate injury 24 h after modeling. (a–c) The serum levels of the inflammatory factors TNF- α , IL-1 β , and E-selectin were measured by ELISA. (d) Immunohistochemistry micrographs of lung tissue sections show the expression of IL-6. (e) Flow cytometric analysis of the cellular ROS in lung tissues in different experimental mouse groups was performed. (f) The quantitative mean fluorescence intensity in each treatment group is shown. * $P < 0.05$ and ** $P < 0.01$ vs. the control group. # $P < 0.05$ and ## $P < 0.01$ vs. the AP group. AP: the acute pancreatitis group; AP+LXA4: the acute pancreatitis+Lipoxin A4 group; AP-ALI: the acute pancreatitis-induced acute lung injury; ROS: reactive oxygen species.

As demonstrated by the results of the immunofluorescence analysis shown in Figure 4(e), weak and diffuse Nrf2 staining in the cytoplasm was observed in the control group. Following TNF- α treatment, Nrf2 was activated and translocated into the cell nucleus, and staining in the cytoplasm and nucleus became stronger. In the LXA4 group, these changes were more obvious, and the activation of Nrf2 was significantly increased in the LXA4 group compared with that in the TNF- α group, indicating that the nuclear translocation of Nrf2 can be further promoted by LXA4.

Next, immunoblot analysis (Figures 4(a) and 4(b)) showed that the expression of HO-1 was efficiently increased in the TNF- α +LXA4 group compared with that in both the control and TNF- α groups. We further tested relative luciferase activities in HPMECs. The results of the luciferase reporter assay in Figure 4(f) showed that Nrf2 more effectively regulated HO-1 than NF- κ B, AP-1, and NF- κ B combined with AP-1. We speculated that the Nrf2/HO-1 pathway may play a role in the protective effects of LXA4.

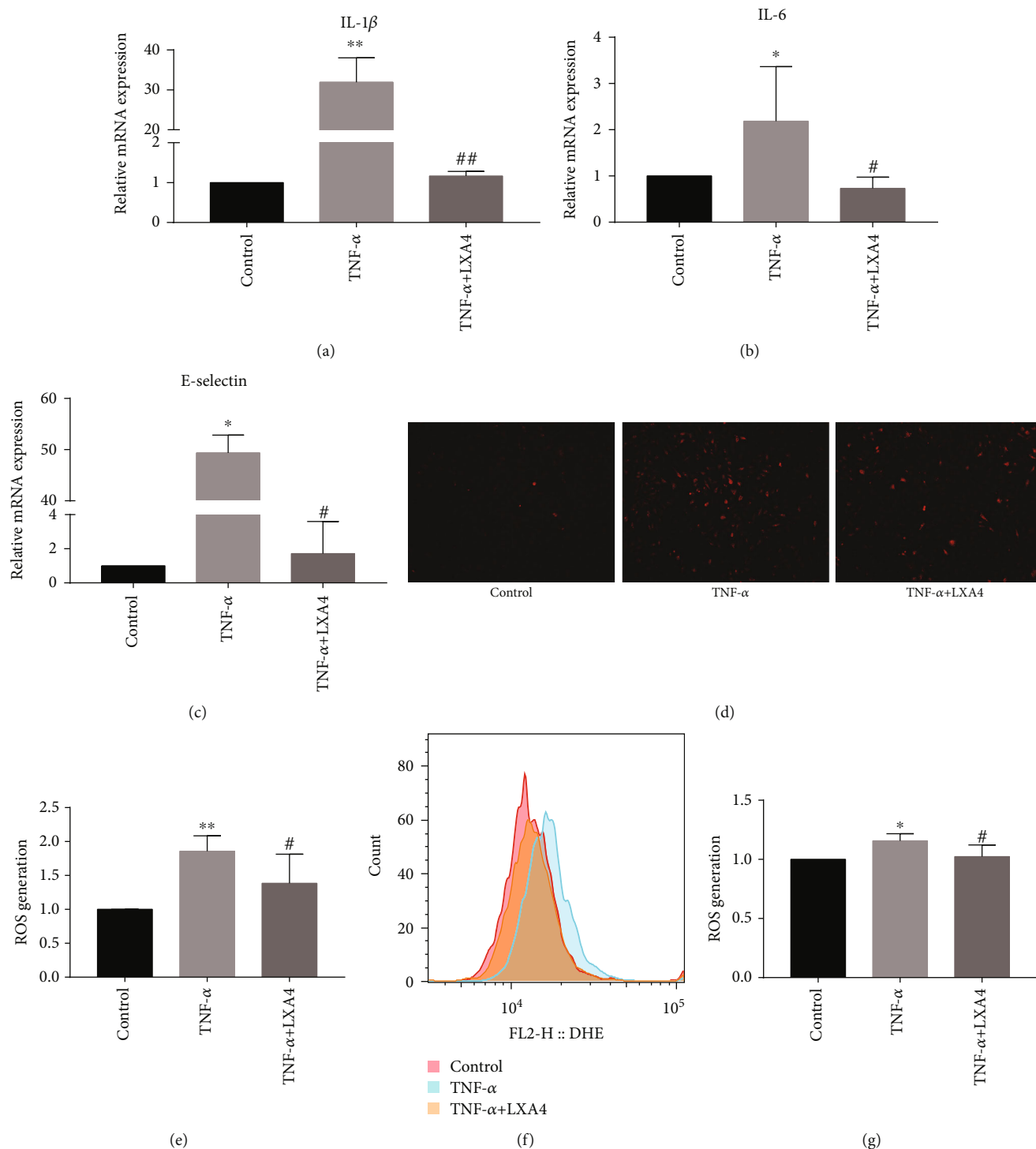


FIGURE 3: LXA4 alleviated TNF- α -induced damage and inhibited ROS generation in vitro. TNF- α has been commonly used for AP-ALI experimental modeling in vitro, and we used the concentration established in our previous study. HPMECs were pretreated with 50 ng/ml LXA4 for 1 h, followed by stimulation with 50 ng/ml TNF- α for 24 h. (a–c) Fold changes in the mRNA expression of IL-1 β , IL-6, and E-selectin in HPMECs were calculated. The mRNA levels of IL-1 β , IL-6, and E-selectin were measured by RT-PCR. (d) Cellular ROS were observed by fluorescence microscopy. (e) The quantitative mean fluorescence intensity in each treatment group is shown. (f) The levels of ROS were determined by flow cytometric analysis. (g) Flow cytometric analysis results are presented as a histogram. * P < 0.05 and ** P < 0.01 vs. the control group. # P < 0.05 and ## P < 0.01 vs. the TNF- α group. TNF- α : the TNF- α group; TNF- α +LXA4: the TNF- α +Lipoxin A4 group; ROS: reactive oxygen species; AP-ALI: the acute pancreatitis-induced acute lung injury; HPMECs: human pulmonary microvascular endothelial cells.

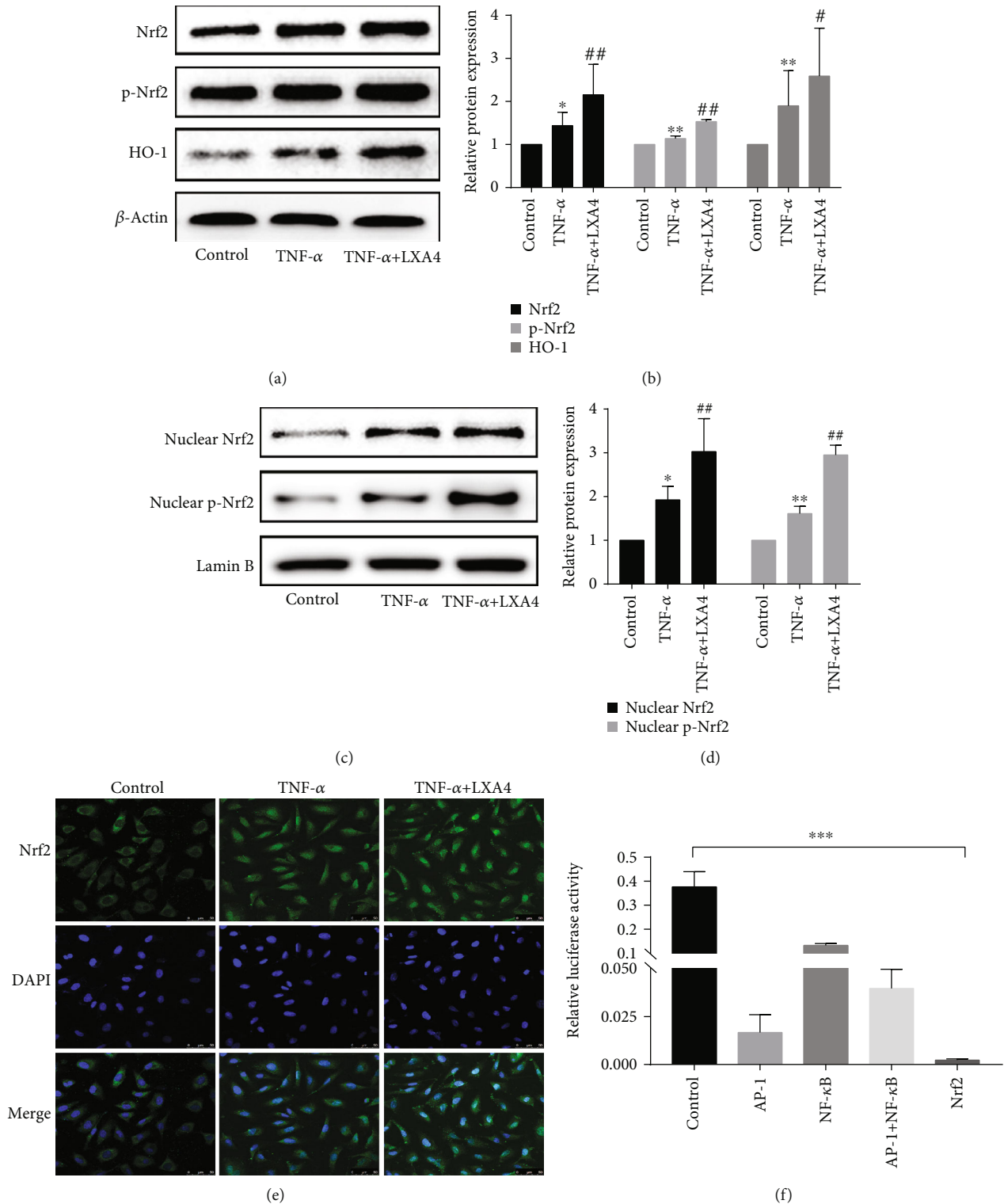


FIGURE 4: LXA4 activated the Nrf2 pathway and upregulated HO-1 expression. (a) The total protein levels of Nrf2, pSer40-Nrf2, and HO-1 in HPMECs were determined by Western blotting. β -Actin was used as an internal control. (b) Relative band densities were quantified, and the normalized values are indicated in the histogram. (c) The nuclear Nrf2 and pSer40-Nrf2 levels were assessed by Western blot analysis. For the internal control, Lamin B was used. (d) The blots were analyzed by densitometry, and the results are expressed in the histogram. (e) Nrf2 nuclear translocation in HPMECs was determined using immunofluorescence analysis. (f) A luciferase reporter assay showed that Nrf2 was the gene that most effectively regulated HO-1. All experiments were performed at least three times. * $P < 0.05$, ** $P < 0.01$ and *** $P < 0.001$ vs. the control group. # $P < 0.05$ and ## $P < 0.01$ vs. the TNF- α group. TNF- α : the TNF- α group; TNF- α +LXA4, the TNF- α +Lipoxin A4 group; Nrf2: the nuclear factor E2-related factor 2; p-Nrf2: phosphorylated Nrf2; HO-1: heme oxygenase-1; AP-1: activator protein-1; NF- κ B: nuclear factor kappa B.

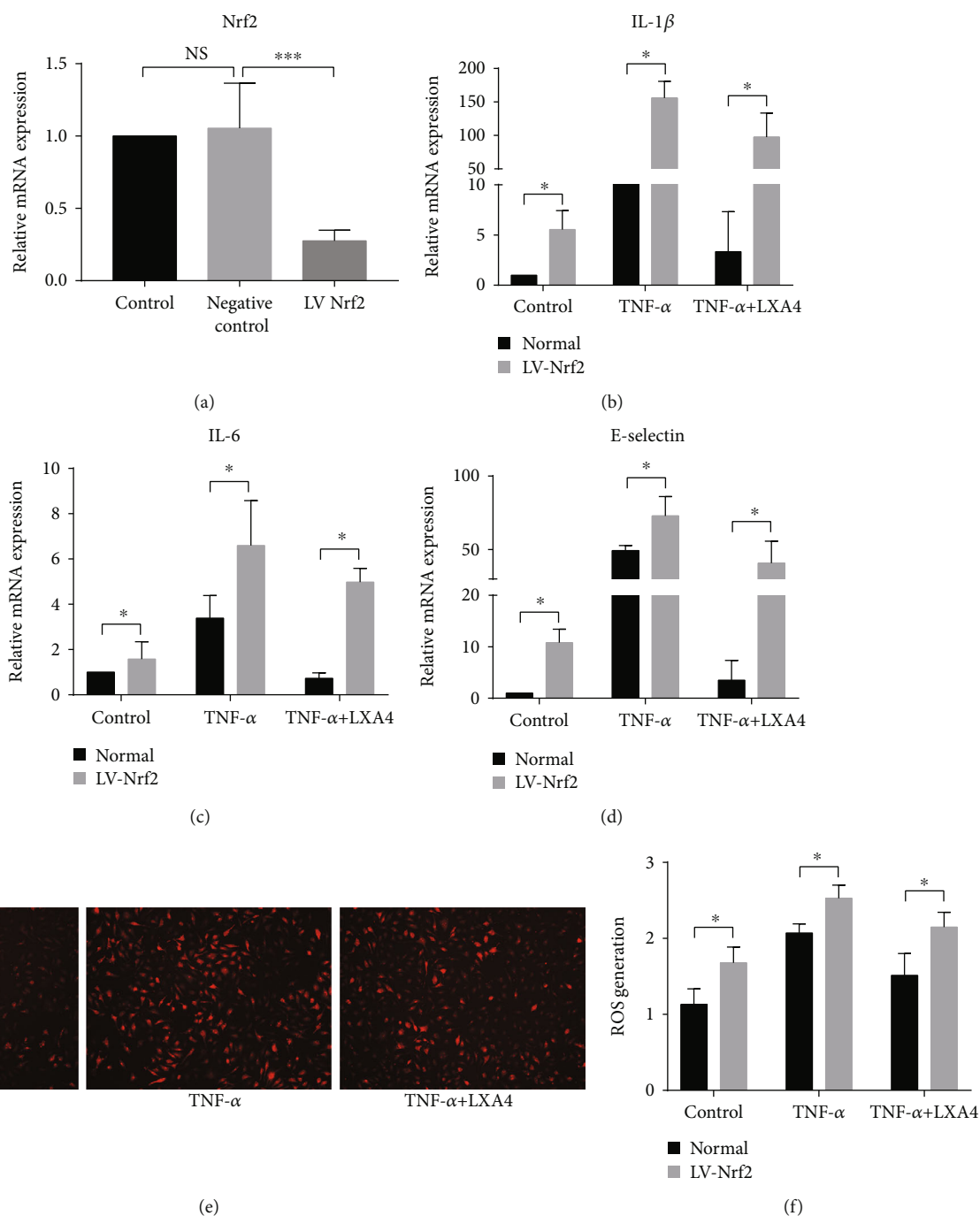


FIGURE 5: Knocking down Nrf2 expression attenuated the effects of LX4 on the regulation of proinflammatory factors and ROS in HPMECs. (a) Nrf2 mRNA levels in HPMECs. The cells were transfected with a Nrf2 lentivirus for 72 h. The mRNA levels of Nrf2 were determined by RT-PCR. (b–d) Determination of IL-1 β , IL-6, and E-selectin mRNA expression by RT-PCR. β -Actin served as an internal control. (e) Cellular ROS levels in the Nrf2 knockout HPMECs, measured using DHE. This experiment was independently repeated three times with 3 wells per time. (f) The quantitative mean fluorescence intensity in each treatment group is shown (* $P < 0.05$, *** $P < 0.001$). TNF- α : the TNF- α group; TNF- α +LXA4: the TNF- α +Lipoxin A4 group; LV Nrf2: the Nrf2 lentivirus-transfected group.

3.5. Inhibition of Nrf2 with a Lentivirus Attenuates the Anti-Inflammatory and Antioxidative Effects of LX4 on HPMECs. To further determine whether Nrf2 is involved in the beneficial effect of LX4, we observed the effect of LX4 on Nrf2-deficient cells. A specific lentivirus was used to knock down Nrf2 expression. The Nrf2 LV-treated group expressed lower levels of Nrf2 than the negative control and

control groups (Figure 5(a)). As shown in Figures 5(b)–5(d) and 5(f), without stimulation, Nrf2 inhibition increased the expression of inflammatory factors and ROS in HPMECs. When HPMECs were challenged with TNF- α in the presence or absence of LX4, Nrf2 LV-transfected cells generated higher IL-6, IL-1 β , and E-selectin levels than normal cells. Similarly, ROS levels showed a considerable increase after

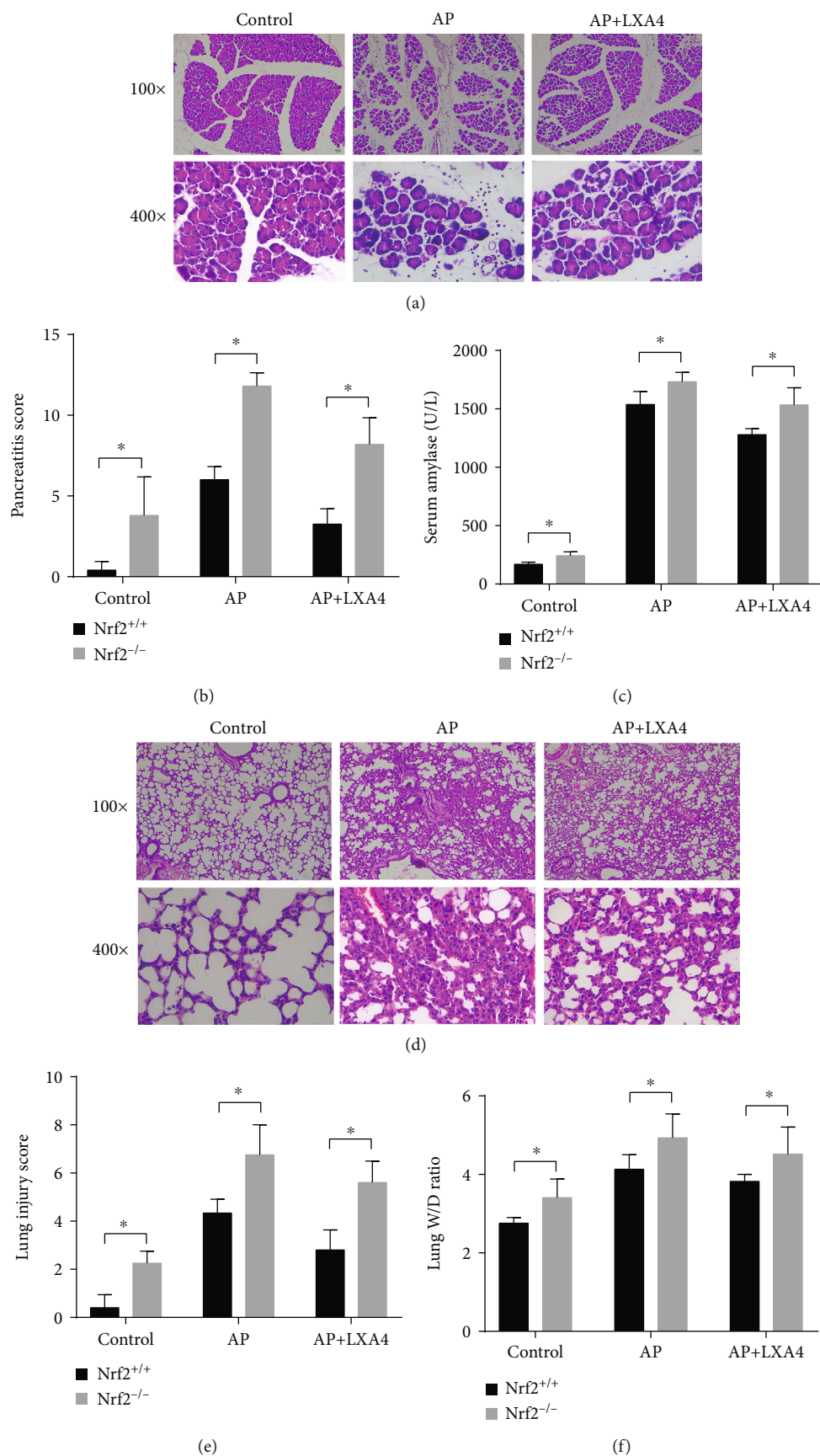


FIGURE 6: Continued.

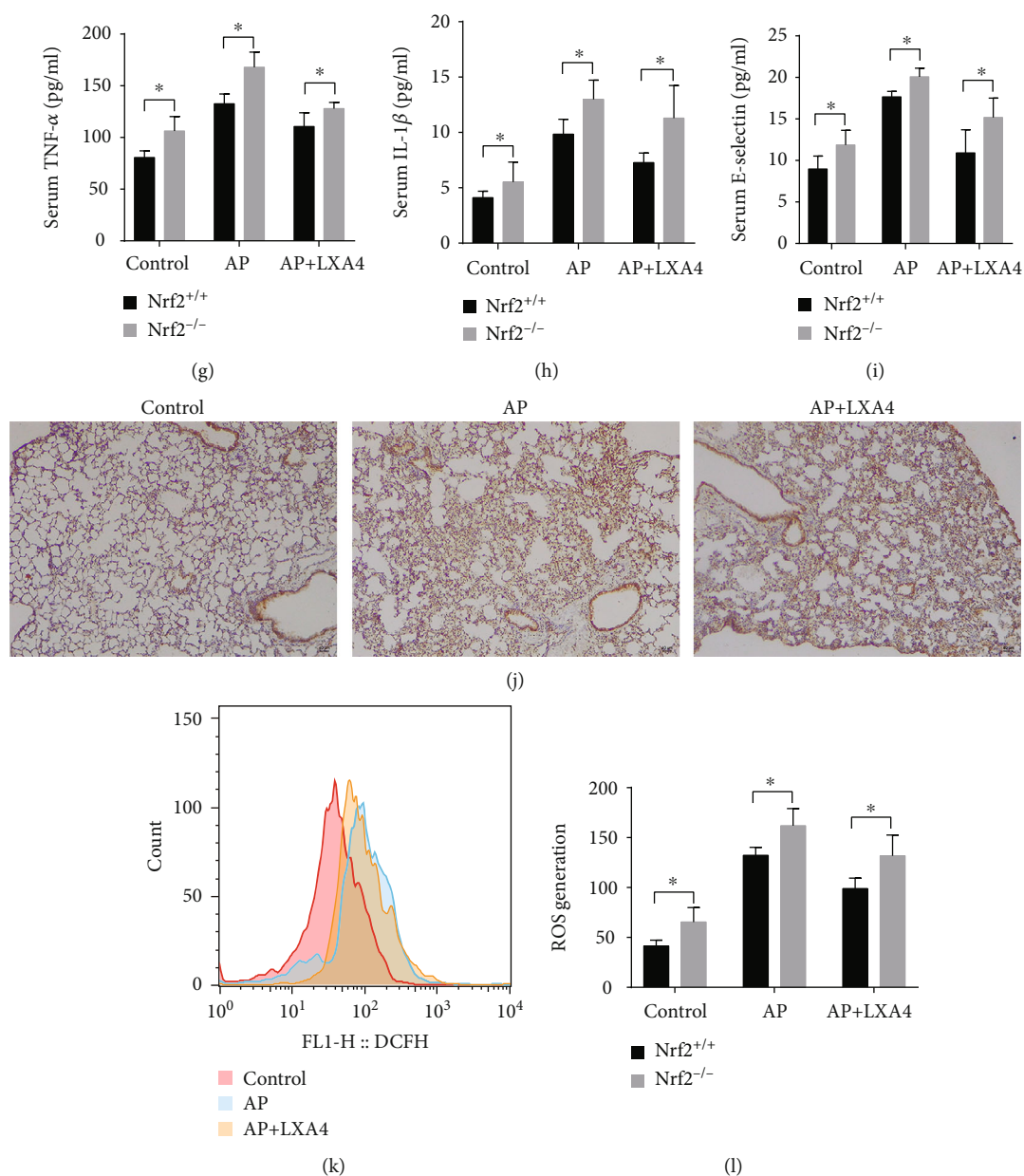


FIGURE 6: Knocking out Nrf2 partially abolished the anti-inflammatory and antioxidative effects of LXA4 on mice. Nrf2^{-/-} mice in the AP group were intraperitoneally injected with caerulein (50 μ g/kg, 7 times, ip) and LPS (10 mg/kg, ip), and those in the AP+LXA4 group were injected with LXA4 (0.1 mg/kg) before caerulein+LPS administration following the same protocol used for the Nrf2^{+/+} mice. (a, d) Representative morphological analysis of the pancreas and lung tissue of the Nrf2^{-/-} mice in the control, AP, and AP+LXA4 groups, (b, e) histological scores of the pancreas and lungs, (c) serum amylase levels, and (f) lung wet/dry weight ratios. (g–i) The levels of TNF- α , IL-1 β , and E-selectin in the serum of mice measured by ELISA. (j) Images of IL-6 expression in lung tissue sections assessed by immunohistochemistry. (k) Representative images of the flow cytometric evaluation of cellular ROS levels in lung tissue from each treatment group. (l) Fluorescence signals detected using a flow cytometer. The mean fluorescence intensity values are graphed (* $P < 0.05$). AP: the acute pancreatitis group; AP+LXA4: the acute pancreatitis+Lipoxin A4 group.

either TNF- α or TNF- α +LXA4 stimulation compared with control treatment (Figures 5(e) and 5(f)). These results confirmed that LXA4 protects cells through Nrf2 activation.

3.6. Knocking Out Nrf2 Partially Abolishes the Protective Effect of LXA4 on Mice. Nrf2^{-/-} mice were injected with or without caerulein+LPS or LXA4 following the same protocol used for Nrf2^{+/+} mice. The results in Figures 6(a)–6(c)

showed that histological changes in the pancreas and serum amylase activity were largely increased in Nrf2^{-/-} mice compared with those in Nrf2^{+/+} mice in all groups. The results shown in Figures 6(d)–6(f) suggested that Nrf2^{-/-} mice had more obvious lung injury characteristics and damage than Nrf2^{+/+} mice. The protective effects of LXA4 on pancreatic and lung tissue damage in AP-ALI were reduced in Nrf2^{-/-} mice. Similarly, the decreased levels of proinflammatory

cytokines, including TNF- α , IL-1 β , and E-selectin, observed after LXA4 administration following AP were partially reversed in Nrf2^{-/-} mice (Figures 6(g)–6(i)). In addition, IHC staining for IL-6 in the lung tissues of Nrf2^{-/-} and WT mice (Figures 6(j)) and 2(d) confirmed that Nrf2 mediates the effect of LXA4 on IL-6 expression. We next investigated whether the beneficial effect of LXA4 on AP-induced ROS production is Nrf2 dependent. Our results showed that the protective effect of LXA4 on AP-ALI was abolished in Nrf2^{-/-} mice (Figures 6(k) and 6(l)). Thus, the positive effect of LXA4 on AP-ALI may depend on Nrf2 activation.

4. Discussion

AP is the most common and devastating inflammatory disorder of the pancreas. AP remains a challenging clinical problem, and its detrimental effects can extend beyond the pancreas, resulting in local and systemic complications and a high mortality rate ranging from 20 to 30% in the most severe cases [30, 31]. The pathophysiology of AP is always considered in two phases. In the early stages, intrapancreatic activation of trypsin in acinar cells leads to autodigestion as well as the activation of various injurious inflammatory factors [32–34]. As AP progresses, acinar cell necrosis activates further pancreatic inflammation, which leads to SIRS or even organ damage, including ALI [32].

ALI, a common and severe complication of AP, usually occurs during the early phase and dramatically increases the risk of mortality associated with uncontrolled pancreatitis [35]. Many studies have attempted to identify effective therapies for AP, but this disease is still poorly treated outside of supportive care, highlighting the demand for new therapies targeting the underlying mechanism of AP.

LXA4 is an endogenous lipid mediator that displays an anti-inflammatory effect and has been extensively studied in a growing list of inflammation-related disease models [16], including fat embolism syndrome-induced lung injury [36], lipopolysaccharide-induced BV2 microglial activation and differentiation [16], and inflammation in diabetes-associated atherosclerosis [37]. Our group revealed that LXA4 can alleviate the symptoms of ALI associated with AP [38, 39]. However, the detailed mechanism by which this improvement occurs remains unclear.

AP-ALI is characterized by severe pulmonary edema and inflammation [38]. To determine the potential mechanism of the effect of LXA4, we employed HPMECs, the cells that form the interior barrier of the alveolocapillary membrane, as a convenient *in vitro* model to study [40]. Simultaneously, an experimental work in mouse models significantly increased our understanding of the pathophysiological links between AP and ALI. The present study indicated that histopathological changes, pathological injury scores, serum amylase levels, and lung W/D ratios in the AP group were significantly higher than those in the control group, which demonstrated that the mouse model of AP-ALI was successfully established. Mice pretreated with LXA4 exhibited obviously reduced serum amylase levels and lung W/D ratios and improved histopathological inflammatory damage in the

lungs and pancreas. These results suggested that LXA4 can ameliorate the severity of AP and ALI.

In AP-ALI, the inflammatory response and inflammatory cytokines play pivotal roles and exert major influences on the outcome of the disease [5, 41]. The intricate balance of cytokine production relates to the degree of tissue damage [42]. Generally, lung edema due to the overexpression of inflammatory mediators is accepted as one of the major prerequisites for AP-ALI pathogenesis. HPMECs are attacked by inflammatory mediators, resulting in increased HPMEC permeability and barrier dysfunction [43]. After the alveolar barrier is damaged, a substantial amount of tissue fluid infiltration aggravates pulmonary edema, and the damaged lung function causes the blood oxygen saturation level to drop sharply, thus causing the body to be in a serious anoxic state and increasing the risk of mortality [6]. The well-known proinflammatory cytokines TNF- α , IL-1 β , and IL-6 are considered pivotal promoters for initiating and perpetuating lung injury. TNF- α and IL-6 can recruit leukocytes into the lung tissue, while IL-1 β can accelerate the process of lung damage by inducing monocytes and macrophages [44–46]. Meanwhile, E-selectin, which belongs to the selectin family of adhesion molecules, is expressed only on the surface of activated vascular endothelial cells, initiates the adhesion of leukocytes to vascular endothelial cells, and is increasingly important to judge the criticality and prognosis of ALI [47, 48]. In this study, our results confirmed that TNF- α treatment of HPMECs influenced the mRNA expression of IL-6, IL-1 β , and E-selectin as measured by PCR and that these changes can be partly ameliorated in the presence of LXA4. Next, an ELISA demonstrated that LXA4 significantly reduced the serum TNF- α , IL-1 β and E-selectin levels that were increased in the mice in the AP group. In addition, the IL-6 level in the lung tissue was increased in the mice in the AP group but mitigated by LXA4 pretreatment. LXA4 efficiently inhibited proinflammatory cytokine release to attenuate local and systemic inflammatory responses.

Recent research indicates that disruption of the balance between oxidation and reduction is believed to play a vital role in the occurrence and development of ALI [49, 50], especially in early AP-ALI. Excessive amounts of ROS can be produced by activated neutrophils, resulting in severe oxidative stress damage and irreversible injury to tissues and cells [51, 52]. Reductions in the production of the important oxidants of ROS are protective against AP-ALI. We frequently noticed that LXA4 can inhibit ROS generation. On this basis, we explored the influence of LXA4 on oxidative stress *in vitro* and *in vivo*. Similar to others' previous work [53], very low ROS levels could be detected in normal mice and cells. As popularly accepted, ROS production was enhanced in the mice in the AP group. This finding was in line with our expectation that HPMECs would also produce ROS locally after TNF- α stimulation. In our study, LXA4 produced an excellent effect to block AP-triggered ROS accumulation in lung tissue, which agreed with the result in HPMECs.

Nrf2, which is responsible for the regulation of the cellular redox balance and protective antioxidants, has emerged as a therapeutic target for oxidative stress [54–56]. Activating Nrf2 is a crucial strategy for inhibiting ROS generation and

controlling oxidative stress. In addition, Nrf2 is known to be an important regulator in ALI [57–59]. Our results showed that TNF- α stimulation upregulated Nrf2 expression, and LXA4 further enhanced Nrf2 activation and decreased injury in HPMECs. Normally, Nrf2 is located in the cytoplasm and translocates into the nucleus after stimulation. Evidence from Western blotting and cellular immunofluorescence in our current investigation showed that the total and nuclear Nrf2 protein levels markedly improved after LXA4 treatment. Moreover, TNF- α -induced phosphorylation of Ser40 in Nrf2 was further enhanced by LXA4. Our results showed that LXA4 increased the Nrf2 level in the nucleus and the phosphorylation of Ser40 in Nrf2.

Nrf2 binds to AREs in the nucleus and enhances the expression of downstream target genes, including HO-1 [60]. HO-1 is a cytoprotective antioxidant enzyme that plays a protective role under both physiological and pathological conditions [61]. The present results agree with those for Nrf2; LXA4 has the ability to switch the activity of HO-1 in TNF- α -treated HPMECs from a high expression state to a much higher expression state. The mechanism by which LXA4 activates HO-1 remains to be further studied. A luciferase assay was employed to show the major role of Nrf2 in the activation of HO-1 by recording the fluorescence intensity of HPMECs transfected with NF- κ B, AP-1, and Nrf2.

Moreover, to determine the role of the Nrf2 signaling pathway in the LXA4-mediated mitigation of AP-ALI, HPMECs were transfected with a Nrf2 gene knockout lentivirus. Here, IL-1 β , IL-6, and E-selectin mRNA levels were higher in the Nrf2-knockout HPMECs than those in normal cells in all three groups. In TNF- α -stimulated Nrf2-knockout cells, ROS production was significantly increased, and the preventive effect of LXA4 was not obvious, suggesting that LXA4 displays Nrf2-dependent antioxidant activity. To further assess the function of Nrf2 in the antioxidant response, we compared Nrf2^{-/-} mice with WT mice. Pathological damage was compared in the pancreas and lungs of WT and Nrf2^{-/-} mice after modeling and treatment, and more intense inflammatory cell infiltration, edema, and even necrosis were found, as expected, in the Nrf2^{-/-} mice compared to observations in the WT mice. Mice with AP-ALI also showed increasing W/D ratios, which were greater in Nrf2^{-/-} mouse lungs than those in WT mouse lungs. In turn, higher levels of inflammatory cytokines were observed in the Nrf2^{-/-} mice than those in the WT mice. A decrease in ROS production was observed in WT mice pretreated with LXA4 compared with WT mice in the AP group. Furthermore, a higher increase in ROS production was observed in the Nrf2^{-/-} mice than that in the WT mice under every condition.

In summary, our study showed that LXA4 played a protective role against AP-ALI and exhibited anti-inflammatory properties in TNF- α -stimulated HPMECs. LXA4 also displayed significant antioxidant effects, thus reducing ROS levels. LXA4 attenuated AP-ALI, which was mediated at least in part by the Nrf2/HO-1 pathway. Of course, some limitations exist, and further studies are needed to clarify the mechanism in greater detail.

Data Availability

The data used to support the findings of this study are included within the article.

Conflicts of Interest

The authors have declared no conflicts of interest.

Authors' Contributions

Wen Ye and Chenlei Zheng contributed equally to this work.

Acknowledgments

This work was supported by grants from the National Natural Sciences Foundation of China (81570583, 81770630, 81800567, and 81700568).

References

- [1] A. S. Gukovskaya, I. Gukovsky, H. Algül, and A. Habtezion, "Autophagy, inflammation, and immune dysfunction in the pathogenesis of pancreatitis," *Gastroenterology*, vol. 153, no. 5, pp. 1212–1226, 2017.
- [2] S. D. Crockett, S. Wani, T. B. Gardner et al., "American Gastroenterological Association Institute Guideline on initial management of acute pancreatitis," *Gastroenterology*, vol. 154, no. 4, pp. 1096–1101, 2018.
- [3] S. M. van Dijk, N. D. L. Hallensleben, H. C. van Santvoort et al., "Acute pancreatitis: recent advances through randomised trials," *Gut*, vol. 66, no. 11, pp. 2024–2032, 2017.
- [4] M. M. Lerch, "Classifying an unpredictable disease: the revised Atlanta classification of acute pancreatitis," *Gut*, vol. 62, no. 1, pp. 2–3, 2013.
- [5] H. Guo, D. W. Suo, H. P. Zhu, X. M. Sun, and J. Chen, "Early blood purification therapy of severe acute pancreatitis complicated by acute lung injury," *European Review for Medical and Pharmacological Sciences*, vol. 20, no. 5, pp. 873–878, 2016.
- [6] C. M. Pastor, M. A. Matthay, and J. L. Frossard, "Pancreatitis-associated acute lung injury: new insights," *Chest*, vol. 124, no. 6, pp. 2341–2351, 2003.
- [7] A. P. Wheeler and G. R. Bernard, "Acute lung injury and the acute respiratory distress syndrome: a clinical review," *The Lancet*, vol. 369, no. 9572, pp. 1553–1564, 2007.
- [8] K. Jiang, S. Guo, C. Yang et al., "Barbaloin protects against lipopolysaccharide (LPS)-induced acute lung injury by inhibiting the ROS-mediated PI3K/AKT/NF- κ B pathway," *International Immunopharmacology*, vol. 64, pp. 140–150, 2018.
- [9] Y.-F. Tsai, S.-C. Yang, W.-Y. Chang et al., "Garcinia multiflora inhibits FPR1-mediated neutrophil activation and protects against acute lung injury," *Cellular Physiology and Biochemistry*, vol. 51, no. 6, pp. 2776–2793, 2018.
- [10] B. Li, X. Han, X. Ye et al., "Substance P-regulated leukotriene B4 production promotes acute pancreatitis-associated lung injury through neutrophil reverse migration," *International Immunopharmacology*, vol. 57, pp. 147–156, 2018.
- [11] J. Kim and Y.-S. Keum, "NRF2, a key regulator of antioxidants with two faces towards cancer," *Oxidative Medicine and Cellular Longevity*, vol. 2016, Article ID 2746457, 7 pages, 2016.

- [12] K.-A. Jung and M.-K. Kwak, "The Nrf2 system as a potential target for the development of indirect antioxidants," *Molecules*, vol. 15, no. 10, pp. 7266–7291, 2010.
- [13] Y. Zhang, K. A. Ahmad, F. U. Khan, S. Yan, A. U. Ihsan, and Q. Ding, "Chitosan oligosaccharides prevent doxorubicin-induced oxidative stress and cardiac apoptosis through activating p38 and JNK MAPK mediated Nrf2/ARE pathway," *Chemico-Biological Interactions*, vol. 305, pp. 54–65, 2019.
- [14] L. Haodang, Q. Lianmei, L. Ranhui et al., "HO-1 mediates the anti-inflammatory actions of sulforaphane in monocytes stimulated with a mycoplasmal lipopeptide," *Chemico-Biological Interactions*, vol. 306, pp. 10–18, 2019.
- [15] C.-C. Lin, L.-D. Hsiao, R.-L. Cho, and C.-M. Yang, "CO-releasing molecule-2 induces Nrf2/ARE-dependent heme oxygenase-1 expression suppressing TNF- α -induced pulmonary inflammation," *Journal of Clinical Medicine*, vol. 8, no. 4, p. 436, 2019.
- [16] J. Wu, D.-H. Ding, Q.-Q. Li, X.-Y. Wang, Y.-Y. Sun, and L.-J. Li, "Lipoxin A4 regulates lipopolysaccharide-induced BV2 microglial activation and differentiation via the notch signaling pathway," *Frontiers in Cellular Neuroscience*, vol. 13, p. 19, 2019.
- [17] J. Mai, W. Liu, Y. Fang et al., "The atheroprotective role of lipoxin A₄ prevents oxLDL-induced apoptotic signaling in macrophages via JNK pathway," *Atherosclerosis*, vol. 278, pp. 259–268, 2018.
- [18] R. M. Martinez, V. Fattori, P. Saito et al., "Lipoxin A4 inhibits UV radiation-induced skin inflammation and oxidative stress in mice," *Journal of Dermatological Science*, vol. 91, no. 2, pp. 164–174, 2018.
- [19] K. Chan, R. Lu, J. C. Chang, and Y. W. Kan, "NRF2, a member of the NFE2 family of transcription factors, is not essential for murine erythropoiesis, growth, and development," *Proceedings of the National Academy of Sciences of the United States of America*, vol. 93, no. 24, pp. 13943–13948, 1996.
- [20] G. Matute-Bello, R. K. Winn, M. Jonas, E. Y. Chi, T. R. Martin, and W. C. Liles, "Fas (CD95) induces alveolar epithelial cell apoptosis *in vivo*: implications for acute pulmonary inflammation," *The American Journal of Pathology*, vol. 158, no. 1, pp. 153–161, 2001.
- [21] J. Schmidt, D. W. Rattner, K. Lewandrowski et al., "A better model of acute pancreatitis for evaluating therapy," *Annals of Surgery*, vol. 215, no. 1, pp. 44–56, 1992.
- [22] J.-K. Dong, H.-M. Lei, Q. Liang et al., "Overcoming erlotinib resistance in EGFR mutation-positive lung adenocarcinomas through repression of phosphoglycerate dehydrogenase," *Theranostics*, vol. 8, no. 7, pp. 1808–1823, 2018.
- [23] Y. Teng, Y. Cai, W. Pi, L. Gao, and C. Shay, "Augmentation of the anticancer activity of CYT997 in human prostate cancer by inhibiting Src activity," *Journal of Hematology & Oncology*, vol. 10, no. 1, p. 118, 2017.
- [24] L. Chaudhuri, E. H. Sarsour, and P. C. Goswami, "2-(4-Chlorophenyl)benzo-1,4-quinone induced ROS-signaling inhibits proliferation in human non-malignant prostate epithelial cells," *Environment International*, vol. 36, no. 8, pp. 924–930, 2010.
- [25] J. Gatliff, D. East, J. Crosby et al., "TSPO interacts with VDAC1 and triggers a ROS-mediated inhibition of mitochondrial quality control," *Autophagy*, vol. 10, no. 12, pp. 2279–2296, 2014.
- [26] S. Wang, H. M. Ni, X. Chao et al., "Impaired TFEB-mediated lysosomal biogenesis promotes the development of pancreatitis in mice and is associated with human pancreatitis," *Autophagy*, vol. 15, no. 11, pp. 1954–1969, 2019.
- [27] Y. Zhang, X. Wang, C. Chen et al., "Regulation of TBBPA-induced oxidative stress on mitochondrial apoptosis in L02 cells through the Nrf2 signaling pathway," *Chemosphere*, vol. 226, pp. 463–471, 2019.
- [28] L. Subedi, J. H. Lee, S. Yumnam, E. Ji, and S. Y. Kim, "Anti-inflammatory effect of sulforaphane on LPS-activated microglia potentially through JNK/AP-1/NF- κ B inhibition and Nrf2/HO-1 activation," *Cell*, vol. 8, no. 2, p. 194, 2019.
- [29] Y. Qu, C. Wang, N. Liu, C. Gao, and F. Liu, "Morin exhibits anti-inflammatory effects on IL-1 β -stimulated human osteoarthritis chondrocytes by activating the Nrf2 signaling pathway," *Cellular Physiology and Biochemistry*, vol. 51, no. 4, pp. 1830–1838, 2018.
- [30] C. E. Forsmark, S. Swaroop Vege, and C. M. Wilcox, "Acute pancreatitis," *New England Journal of Medicine*, vol. 375, no. 20, pp. 1972–1981, 2016.
- [31] P. Pavlidis, S. Crichton, J. Lemmich Smith et al., "Improved outcome of severe acute pancreatitis in the intensive care unit," *Critical Care Research and Practice*, vol. 2013, Article ID 897107, 5 pages, 2013.
- [32] M. G. T. Raraty, S. Connor, D. N. Criddle, R. Sutton, and J. P. Neoptolemos, "Acute pancreatitis and organ failure: pathophysiology, natural history, and management strategies," *Current Gastroenterology Reports*, vol. 6, no. 2, article 35, pp. 99–103, 2004.
- [33] P. A. Banks, T. L. Bollen, C. Dervenis et al., "Classification of acute pancreatitis—2012: revision of the Atlanta classification and definitions by international consensus," *Gut*, vol. 62, no. 1, pp. 102–111, 2012.
- [34] F. S. Gorelick and E. Thrower, "The acinar cell and early pancreatitis responses," *Clinical Gastroenterology and Hepatology*, vol. 7, no. 11, pp. S10–S14, 2009.
- [35] T. Dombernowsky, M. Ø. Kristensen, S. Rysgaard, L. L. Gluud, and S. Novovic, "Risk factors for and impact of respiratory failure on mortality in the early phase of acute pancreatitis," *Pancreatology*, vol. 16, no. 5, pp. 756–760, 2016.
- [36] N. Gan, R. Zhang, X. Xu et al., "Effects of the ALX/FPR2 receptors of lipoxin A₄ on lung injury induced by fat embolism syndrome in rats," *Biomedicine & Pharmacotherapy*, vol. 112, p. 108595, 2019.
- [37] E. P. Brennan, M. Mohan, A. McClelland et al., "Lipoxins protect against inflammation in diabetes-associated atherosclerosis," *Diabetes*, vol. 67, no. 12, pp. 2657–2667, 2018.
- [38] Z. Shi, W. Ye, J. Zhang et al., "LipoxinA4 attenuates acute pancreatitis-associated acute lung injury by regulating AQP-5 and MMP-9 expression, anti-apoptosis and PKC/SSeCKS-mediated F-actin activation," *Molecular Immunology*, vol. 103, pp. 78–88, 2018.
- [39] W. Lv, C. Lv, S. Yu et al., "Lipoxin A4 attenuation of endothelial inflammation response mimicking pancreatitis-induced lung injury," *Experimental Biology and Medicine*, vol. 238, no. 12, pp. 1388–1395, 2013.
- [40] J. Xu, G. Wei, J. Wang et al., "Glucagon-like peptide-1 receptor activation alleviates lipopolysaccharide-induced acute lung injury in mice via maintenance of endothelial barrier function," *Laboratory Investigation*, vol. 99, no. 4, article 170, pp. 577–587, 2019.
- [41] Y. Zhang, L. Yan, and W. Han, "Elevated level of miR-551b-5p is associated with inflammation and disease progression in

- patients with severe acute pancreatitis," *Therapeutic Apheresis and Dialysis*, vol. 22, no. 6, pp. 649–655, 2018.
- [42] J. Xu, H.-b. Li, L. Chen et al., "BML-111 accelerates the resolution of inflammation by modulating the Nrf2/HO-1 and NF- κ B pathways in rats with ventilator-induced lung injury," *International Immunopharmacology*, vol. 69, pp. 289–298, 2019.
- [43] L. Yi, X. Huang, F. Guo, Z. Zhou, M. Chang, and J. Huan, "GSK-3 β -dependent activation of GEF-H1/ROCK signaling promotes LPS-induced lung vascular endothelial barrier dysfunction and acute lung injury," *Frontiers in Cellular and Infection Microbiology*, vol. 7, p. 357, 2017.
- [44] Y. Liu, J. Mei, L. Gonzales et al., "IL-17A and TNF- α exert synergistic effects on expression of CXCL5 by alveolar type II cells in vivo and in vitro," *Journal of Immunology*, vol. 186, no. 5, pp. 3197–3205, 2011.
- [45] L. Yao, T. Yago, B. Shao et al., "Elevated CXCL1 expression in gp130-deficient endothelial cells impairs neutrophil migration in mice," *Blood*, vol. 122, no. 23, pp. 3832–3842, 2013.
- [46] L. Chávez-Sánchez, K. Chávez-Rueda, M. Legorreta-Haquet et al., "The activation of CD14, TLR4, and TLR2 by mLDL induces IL-1 β , IL-6, and IL-10 secretion in human monocytes and macrophages," *Lipids in Health and Disease*, vol. 9, no. 1, p. 117, 2010.
- [47] F. Jin, D. Liu, H. Yu et al., "Sialic acid-functionalized PEG-PLGA microspheres loading mitochondrial-targeting-modified curcumin for acute lung injury therapy," *Molecular Pharmaceutics*, vol. 16, no. 1, pp. 71–85, 2018.
- [48] J.-P. Cao, X.-Y. He, H.-T. Xu, Z. Zou, and X.-Y. Shi, "Autologous transplantation of peripheral blood-derived circulating endothelial progenitor cells attenuates endotoxin-induced acute lung injury in rabbits by direct endothelial repair and indirect immunomodulation," *Anesthesiology*, vol. 116, no. 6, pp. 1278–1287, 2012.
- [49] M. Ren, Y.-M. Wang, J. Zhao et al., "Metallothioneins attenuate paraquat-induced acute lung injury in mice through the mechanisms of anti-oxidation and anti-apoptosis," *Food and Chemical Toxicology*, vol. 73, pp. 140–147, 2014.
- [50] I. Lee, C. Dodia, S. Chatterjee, S. I. Feinstein, and A. B. Fisher, "Protection against LPS-induced acute lung injury by a mechanism-based inhibitor of NADPH oxidase (type 2)," *American Journal of Physiology-Lung Cellular and Molecular Physiology*, vol. 306, no. 7, pp. L635–L644, 2014.
- [51] P. Sacco, E. Decleva, F. Tentor et al., "Butyrate-loaded chitosan/hyaluronan nanoparticles: a suitable tool for sustained inhibition of ROS release by activated neutrophils," *Macromolecular Bioscience*, vol. 17, no. 11, article 1700214, 2017.
- [52] B. D. Levy, L. Hickey, A. J. Morris et al., "Novel polyisoprenyl phosphates block phospholipase D and human neutrophil activation *in vitro* and murine peritoneal inflammation *in vivo*," *British Journal of Pharmacology*, vol. 146, no. 3, pp. 344–351, 2005.
- [53] X. Cheng, S. He, J. Yuan et al., "Lipoxin A₄ attenuates LPS-induced mouse acute lung injury via Nrf2-mediated E-cadherin expression in airway epithelial cells," *Free Radical Biology and Medicine*, vol. 93, pp. 52–66, 2016.
- [54] J. Yao, S. Peng, J. Xu, and J. Fang, "Reversing ROS-mediated neurotoxicity by chlorogenic acid involves its direct antioxidant activity and activation of Nrf2-ARE signaling pathway," *BioFactors*, vol. 45, no. 4, pp. 616–626, 2019.
- [55] M. Jin, J. Wang, X. Ji et al., "MCUR1 facilitates epithelial-mesenchymal transition and metastasis via the mitochondrial calcium dependent ROS/Nrf2/Notch pathway in hepatocellular carcinoma," *Journal of Experimental & Clinical Cancer Research*, vol. 38, no. 1, p. 136, 2019.
- [56] Y. Dai, J. Zhang, J. Xiang, Y. Li, D. Wu, and J. Xu, "Calcitriol inhibits ROS-NLRP3-IL-1 β signaling axis via activation of Nrf2-antioxidant signaling in hyperosmotic stress stimulated human corneal epithelial cells," *Redox Biology*, vol. 21, article 101093, 2019.
- [57] H. Lv, Q. Liu, Z. Wen, H. Feng, X. Deng, and X. Ci, "Xanthohumol ameliorates lipopolysaccharide (LPS)-induced acute lung injury via induction of AMPK/GSK3 β -Nrf2 signal axis," *Redox Biology*, vol. 12, pp. 311–324, 2017.
- [58] W. Yao, G. Luo, G. Zhu et al., "Propofol activation of the Nrf2 pathway is associated with amelioration of acute lung injury in a rat liver transplantation model," *Oxidative Medicine and Cellular Longevity*, vol. 2014, Article ID 258567, 9 pages, 2014.
- [59] G. Zheng, H. Ren, H. Li et al., "*Lycium barbarum* polysaccharide reduces hyperoxic acute lung injury in mice through Nrf2 pathway," *Biomedicine & Pharmacotherapy*, vol. 111, pp. 733–739, 2019.
- [60] J. Lee, K. Song, E. Huh, M. S. Oh, and Y. S. Kim, "Neuroprotection against 6-OHDA toxicity in PC12 cells and mice through the Nrf2 pathway by a sesquiterpenoid from *Tussilago farfara*," *Redox Biology*, vol. 18, pp. 6–15, 2018.
- [61] N. Li, J. Alam, M. I. Venkatesan et al., "Nrf2 is a key transcription factor that regulates antioxidant defense in macrophages and epithelial cells: protecting against the proinflammatory and oxidizing effects of diesel exhaust chemicals," *Journal of Immunology*, vol. 173, no. 5, pp. 3467–3481, 2004.

Review Article

Alcohol Intake and Abnormal Expression of Brf1 in Breast Cancer

Chenghao Huang ¹, Yanmei Zhang ^{2,3} and Shuping Zhong ³

¹State Key Laboratory of Molecular Vaccinology and Molecular Diagnostics, National Institute of Diagnostics and Vaccine Development in Infectious Diseases, School of Public Health, Xiamen University, China

²Department of Pharmacology of Shantou University Medical College, China

³Department of Medicine, Keck School of Medicine, University of Southern California, Los Angeles, CA, USA

Correspondence should be addressed to Shuping Zhong; szhong@usc.edu

Received 27 July 2019; Accepted 28 September 2019; Published 31 October 2019

Guest Editor: Reggiani Vilela Gonçalves

Copyright © 2019 Chenghao Huang et al. This is an open access article distributed under the Creative Commons Attribution License, which permits unrestricted use, distribution, and reproduction in any medium, provided the original work is properly cited.

Breast cancer is the most common malignant disease of females. Overall, one woman in every nine will get breast cancer at some time in her life. Epidemiological studies have indicated that alcohol consumption has most consistently been associated with breast cancer risk. However, the mechanism of alcohol-associated breast cancer remains to be addressed. Little is known about the effects of alcohol consumption on Brf1 (TFIIIB-related factor 1) expression and RNA Pol III gene (RNA polymerase III-dependent gene) transcription, which are responsible for protein synthesis and tightly linked to cell proliferation, cell transformation, and tumor development. Emerging evidences have indicated that alcohol induces deregulation of Brf1 and Pol III genes to cause the alterations of cell phenotypes and tumor formation. In this paper, we summarize the progresses regarding alcohol-caused increase in the expression of Brf1 and Pol III genes and analysis of its molecular mechanism of breast cancer. As the earlier and accurate diagnosis approach of breast cancer is not available yet, exploring the molecular mechanism and identifying the biomarker of alcohol-associated breast cancer are especially important. Recent studies have demonstrated that Brf1 is overexpressed in most ER+ (estrogen receptor positive) cases of breast cancer and the change in cellular levels of Brf1 reflects the therapeutic efficacy and prognosis of this disease. It suggests that Brf1 may be a potential diagnosis biomarker and a therapeutic target of alcohol-associated breast cancer.

1. Introduction

Alcohol intake is consistently associated with an increased risk of breast cancer [1–4]. Alcohol is known to promote mammary tumorigenesis [5–7]. Alcohol consumption is associated with ER+ (estrogen receptor positive) cases of breast cancer much more than with ER- cases of this disease [8–10]. Although the exact mechanism by which alcohol causes breast cancer is still unclear, alcohol consumption is thought to induce breast carcinogenesis through various mechanisms, such as the perturbation of estrogen metabolism and response, mutagenesis by the ethanol metabolite acetaldehyde, and oxidative damage, as well as by affecting the one-carbon metabolic pathways through reduced folic acid intake and use [11]. Previous studies have shown that chronic alcohol consumption results in the production of acetaldehyde and induction of CYP2E1. Acetaldehyde is a by-product of alcohol

metabolism catalyzed by ADH (alcohol dehydrogenase), which has direct mutagenic and carcinogenic effects *in vitro* and *in vivo* studies [12]. CYP2E1 is associated with the release of ROS (reactive oxygen species) and conversion of procarcinogens to carcinogens. Alcohol exposure increases cellular production of ROS and induces cellular stress, resulting in tissue injury and ALD (alcoholic liver disease).

However, little is known about the role of alcohol in Brf1 (TFIIIB-related factor 1) expression and Pol III gene (RNA polymerase III-dependent gene) transcription during breast tumor development. Pol III genes are responsible for protein synthesis and tightly linked to cell proliferation, cell transformation, and cancer development. RNA polymerase III is responsible for the synthesis of a variety of small untranslated RNAs, including tRNAs and 5S rRNA [12]. Brf1 is a subunit of the TFIIIB complex of Pol III gene transcription machinery. Brf1 specifically regulates tRNAs and 5S rRNA

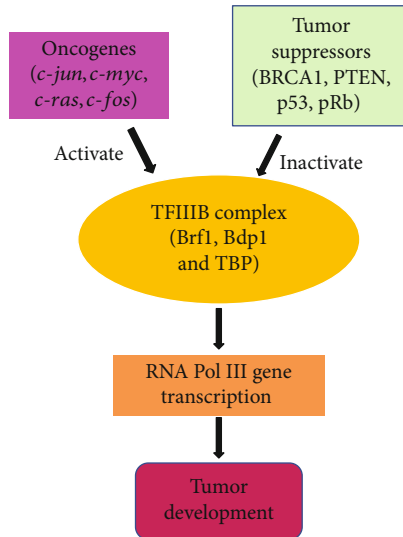


FIGURE 1: The alteration of the TFIIB complex of transcription machinery. TFIIB is a complex of the transcription machinery of RNA Pol III genes; TFIIB includes Brf1, Bdp1, and TBP. Oncogenic proteins, such as c-Jun, c-Myc, Ras, and c-Fos activate TFIIB to enhance RNA Pol III gene transcription, resulting in tumorigenesis. In contrast, tumor suppressors, such as BRCA1, PTEN, p53, and pRb, inactivate its activity to decrease the transcription of Pol III genes, leading to repression of tumor development.

transcription. The PNCs (perinucleolar compartments) are dependent on the continuation of RNA Pol III gene transcription and more prevalent in cancer cells than in normal cells [13]. PNC prevalence significantly correlates with the progression of breast cancer [14]. Accumulation of Pol III gene transcripts around the nucleolus is especially evident in transformed cells [15]. Consistent with the idea that a high translational capacity is necessary for rapid growth and proliferation of tumor cells, Pol III gene transcripts have been found to be increased in human cancers [10, 16, 17]. Furthermore, expression of the Pol III gene, BC200, was elevated in breast squamous cell carcinoma tissues [18]. Our studies using both cell culture models and animal models have revealed that alcohol induces transcription of tRNA^{Leu} and 5S rRNA [19, 20]. This induction in mice fed with alcohol is associated with tumor development [19]. Alcohol-induced tRNA and 5S rRNA transcription in a breast cancer cell line is in an ER α -dependent manner [20]. These evidences support the idea that ER α may mediate the modulation of alcohol-induced Brf1 expression and Pol III gene transcription in breast cells.

Genome-wide studies have demonstrated that many RNA Pol II transcription factors are associated with RNA Pol III transcribed genes and overlap the occupancy of RNA Pol III [21]. Initial studies suggest that tRNAs are differentially expressed in a tissue-specific manner and that induction of RNA Pol III-dependent transcription may not uniformly increase all tRNA isoacceptors [22]. It implies that the differences of Pol III gene transcription levels match the diversities in various physiological and pathological conditions. The transcription machinery of tRNA genes is com-

posed of RNA Pol III, TFIIB, and TFIIC complexes to control tRNA transcription, whereas, the 5S rRNA gene transcription machinery consists with the complexes of RNA Pol III, TFIIB, TFIIC, and TFIIA. The complex of TFIIB consists of TBP and its associated factors, Brf1 (or Brf2) and Bdp1. Brf1 and Bdp1 are specifically utilized in the Pol III gene transcription process. TBP is required for transcription by all three nuclear polymerases, Pol I, II, and III, in gene transcription [23]. The tumor suppressors, BRCA1, p53, pRb, and PTEN, repress, whereas oncogenes, such as Ras, c-Jun, c-Myc, and c-Fos, increase Pol III gene transcription [24–26] (Figure 1). An increase in TBP levels to induce Pol III gene transcription is required for its transforming function [27–29]. Studies have demonstrated that change in TBP expression is able to alter the cellular level of Bdp1, but not Brf1 [30]. It suggests that Brf1 is more specific and critically important in the regulation of tRNA and 5S rRNA genes. A recent study indicates that alcohol-induced TBP transcription is not significantly associated with ER α expression in ER+ breast cancer cells [20]. In contrast, alteration of alcohol-induced ER α expression significantly changes cellular levels of Brf1 in these cells [20]. This implies that this TFIIB subunit, Brf1, may be involved in the ER-mediated induction of Pol III genes caused by alcohol. In the review, we will mainly focus on the role of alcohol-induced changes in Brf1 expression and deregulation of Pol III genes.

2. Alcohol-Caused Alteration of Brf1 Expression and Breast Cancer

In terms of the difference in regulation regions of RNA Pol III genes, these genes are divided into three types. Type I of Pol III genes is 5S rRNAs, and Type II of the genes is tRNAs, whereas Type III is composed of other small Pol III genes except type I and type 2 of these genes. Brf1 and Brf2 (TFIIB-related factor 2) are subunits of TFIIB. Brf1 takes part in the regulation of Type 1 (5S rRNAs) and Type 2 (tRNAs) Pol III gene transcription, whereas Brf2 mainly modulates the transcription of Type III genes, such as U6, 7SL, and 7SK genes, and other small RNAs. As 5S rRNA and tRNAs function protein synthesis, they are required to cell growth, cell transformation, and tumor development. Brf1 gene IDs of human, mouse, and rat are 2972, 72308, and 299347, respectively. Human Brf1 gene (ID: 2972) primarily codes a 90 kD protein. At the review, we primarily focus on the discussions of abnormal Brf1 expression in the cases of human breast cancer and alcohol-induced Brf1 expression in breast cancer cells.

2.1. Abnormal Expression of Brf1 and Its Significance in Breast Cancer. As mentioned above, Brf1 specifically regulates transcription of tRNAs and 5S rRNA genes, while the deregulation of the Pol III genes is tightly linked to cell transformation and tumor development. This suggests that Brf1 plays a critically important role in breast cancer. However, the status of Brf1 expression in patients of breast cancer has been determined until recently. The studies report that, for the first time, 218 samples of human breast cancer have been collected to measure the levels of Brf1 expression by

immunohistochemistry method. 102 of 218 cases (46.8%) display strong Brf1 staining in lesion tissues, which is classified in the high Brf1 expression group [10]. The other 116 cases (53.2%) of breast carcinoma include moderate, weak, or negative staining of Brf1 in the lesion tissues, which is classified as the low Brf1 expression group [10]. The staining signals of Brf1 in most of the breast cancer cases primarily accumulate in the nucleus, while its localization in the cytoplasm is only 3.7% (8/218) [10]. The most clinically pathological characteristic of 218 cases is not the significant correlation between Brf1 expression and other clinic pathological features, such as patient age, paucimonia, histological type, clinical stage, tumor size, lymph node, and metastasis [10]. In contrast, there is a significant correlation between high Brf1 expression and high ER expression ($p = 0.012$), high PR expression ($p = 0.035$) or non-triple-negative status ($p = 0.012$), but not Her2 expression ($p = 0.357$) [10]. These studies reveal that the levels of Brf1 expression of the human breast cancer are associated with their hormone statuses. The results are consistent with an early study, which demonstrates that ER α mediates alcohol-induced Brf1 expression [20]. More interestingly, the OS (overall survival) times of the patients with low Brf1 expression (118.7 ± 5.4 months, $n = 116$) are significantly shorter than with the cases of high Brf1 expression (137.5 ± 4.4 months, $n = 102$, $p = 0.004$) [10]. Furthermore, the DFS (disease-free survival) periods in the high Brf1 expression group (135.3 ± 5.0 months) are markedly longer than those in the low Brf1 expression group (112.8 ± 6.4 months, $p = 0.004$) [10]. Therefore, these studies show that patients with high Brf1 expression have better prognosis after hormone therapy. It looks strange, as high Brf1 expression in cancer patients should possess short survival times usually [17].

Approximately 80% cases of breast cancer are ER+ [4, 5, 31]. The ER+ patients were treated by hormone therapy after they were diagnosed as breast cancer and performed surgery resection, whereas a preferred drug of hormone therapy is Tam (tamoxifen), which is an antagonist of the estrogen receptor in breast tissue and has been widely used for the treatment for both early and advanced ER+ breast cancers in women [32]. We have demonstrated that high expression of Brf1 in hepatocellular carcinoma cases displays short OS period [17]. We also found the trend that the patients with high Brf1 expression reveal short OS period in other cancers (unpublished). More interestingly, our early studies have found that Tam significantly inhibits the induction of Brf1 caused by alcohol in ER+ breast cancer cells [33]. As Tam is able to repress Brf1 expression, the cellular levels of Brf1 in the ER+ patients are actually at low levels during hormone treatment. This explains why high Brf1 expression has longer survival periods in the ER+ cases than ER- cases with the disease. It suggests that cellular levels of Brf1 are not only as a diagnosis marker but also as an indicator of prognosis under hormone treatment.

2.2. Alcohol Increases Brf1 Expression to Promote Breast Tumor Development. Emerging evinces indicate that alcohol consumption is an established risk factor for breast cancer [1–4]. The relative increase in risk ranges from 5 to 10%

(~1 drink/10 grams/day) to 40–50% (~3 drinks/day) [34, 35]. Studies have demonstrated that alcohol feeding prompted mammary tumor formation in mice [36, 37]. Mechanism analysis indicates that alcohol-promoted breast cancer development may be through its effect on the expression of aromatase and PPAR- γ with resulting increases in estrogen (ER ligand) levels [38, 39]. However, Brf1 overexpression in human cases of breast cancer is a direct evidence [10]. Mechanism studies demonstrate that alcohol increases Brf1 expression in ER+ breast cancer cells [20]. Alcohol induces transformation of nontumor breast cells, and it also increases the rates of colony formation of human breast cancer cells [20]. However, once knocking down Brf1 expression by its siRNA, the rates of colony formation will be significantly reduced. This indicates that alcohol-increased Brf1 expression is critically important in cell transformation and tumor development.

2.3. ER α and Runx2 Mediate Alcohol-Induced Brf1 Expression. Studies have demonstrated that alcohol increases the activity of the ERE-Luc promoter in ER+ MCF-7 cells [20] and alcohol intake enhances the transcriptional activity of ER α and activates the E2 signaling pathway (37.40). Alcohol increases cellular levels of Brf1 in ER+ breast cancer cells [20]. This implies that ER α has potential to mediate Brf1 expression. Studies support the idea that E2, a ligand of ER α , augments cellular levels of Brf1 mRNA and proteins. In contrast, ER α siRNA significantly represses Brf1 expression in ER+ breast cancer cells [20]. The capacity of ER α in Brf1 expression is not for another subunit, TBP, of TFIIB complex.

Runx2 (Runt-related transcription factor 2) is a component of ER α downstream and is modulated by ER α . Runx2 is expressed in ER+ human breast cancer cell lines and participates in mammary gland development. Studies have indicated that Runx2 plays important roles in tumor cell growth and migration, as well as in bone metastasis of breast cancer. However, it remains to be investigated whether Runx2 mediates Brf1 expression. Recently, we have determined the role of Runx2 in Brf1 expression. The results indicate that Runx2 is overexpressed in human biopsies of breast cancer (unpublished). Alcohol enhances Runx2 expression in ER+ breast cancer cell line, MCF-7. Repression of Runx2 decreases Brf1 expression (unpublished). ER α mediates alcohol-induced Runx2 expression in the cells (unpublished). Together, these studies demonstrate that Runx2 modulates Brf1 expression through the ER α pathway induced by alcohol. Alcohol-increased Runx2 expression may play a crucial role in alcohol-associated breast cancer development.

2.4. Alcohol Induces Signal Events Which Mediate Brf1 Expression. Brf1 is a phosphorylated protein. Plk1 (polo-like kinase 1) phosphorylates Brf1 on serine 450 to directly promote tRNA and 5S rRNA transcription in cell interphase [40]. This stimulatory modification is overridden at mitosis, when elevated Plk1 activity causes Brf1 phosphorylation on threonine 270, which prevents RNA polymerase III recruitment to the transcription machinery [40]. Studies have indicated that PKB (protein kinase B) phosphorylates Brf1 at serine 92, resulting in binding to 14-3-3 and impairment of

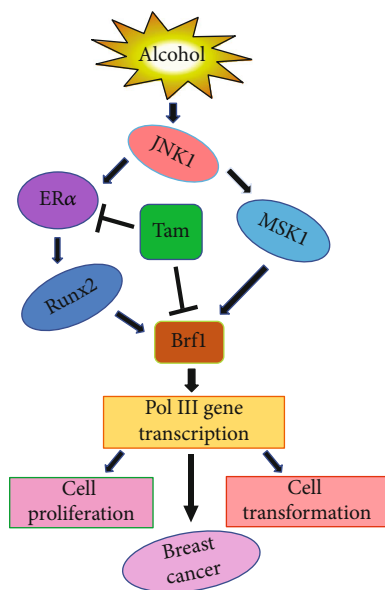


FIGURE 2: The alcohol-induced modulation of Brf1 expression. Alcohol increases Brf1 expression through two ways in breast cells. One is that alcohol activates JNK1 and MSK1 to upregulate Brf1 expression; another way is that alcohol activates JNK1 to enhance ER α and Runx2 expression, leading to augmenting Brf1 expression. The two pathways increase RNA Pol III gene, eventually resulting in cell proliferation and transformation and mammary tumor development, while Tam inhibits ER α activity and decreases the cellular level of Brf1.

mRNA decay activity [41]. Further analysis reveals that an additional regulatory site of Brf1 is at serine 203, which cooperates with its serine 92 *in vivo* [42]. Brf1 serine 203 is also phosphorylated by PKB. Mutation of both serine 92 and serine 203 to alanine uncouples Brf1 from PKB regulation, leading to constitutive mRNA decay even in the presence of stabilizing signals [42]. The deregulation of Pol III gene transcription has been linked to cancer, whereas germline mutations of genes encoding RNA polymerase III subunits or tRNA processing factors cause neurogenetic disorders in humans, such as hypomyelinating leukodystrophies and pontocerebellar hypoplasia [43]. Studies indicate that disease-causing mutations reduce Brf1 occupancy at tRNA genes to decrease Pol III gene transcription and impair cell growth [43].

Although PIK and PKB are able to phosphorylate Brf1 [40–42], our studies indicate that alcohol activates JNK1, but not JNK2 [19], while JNK1 indeed mediates alcohol-induced Brf1 expression in both hepatocellular carcinoma and breast cancer cells [19, 20]. In the ER+ breast cancer cell line, MCF-7, alcohol activates JNK1 and enhances ER α activity to elevate Brf1 expression [20]. The increase in Brf1 and Pol III genes by alcohol in ER+ breast cancer cell lines is significantly higher than those in ER- breast cancer cell lines and nontumor breast cell lines [20]. This finding is consistent with an early study, in which Brf1 expression in ER+ human breast cancer cases is higher than that in ER- cases [44]. Interestingly, inhibition of JNK1 signaling by its chemical inhibitor or siRNA significantly reduces ER α activity, result-

ing in the decrease in Brf1 expression [20]. In contrast, enhancing JNK1 expression augments ER α activity to elevate cellular levels of Brf1 [20]. Further analysis indicates that the decrease in ER α attenuates alcohol-caused induction of Brf1 expression [20]. Together, these studies indicate that different phosphorylation of Brf1 reveals various functions in Pol III genes. Alcohol increases ER α activity to enhance Brf1 expression through the JNK1 pathway (Figure 2).

2.5. Alcohol Increases Expression of Brf1 Causing the Alterations of Cellular Phenotypes. Studies have demonstrated that carcinogens are able to increase Brf1 expression in cell culture models. EGF (epidermal growth factor) stimulates Brf1 expression in mouse epidermal cell line to augment the rates of cell growth and cell transformation [45]. Repressing Brf1 expression inhibits the EGF-stimulated cell transformation [45], whereas DEN (diethylnitrosamine), a potent chemical hepatocarcinogen, has widely been used to induce HCC (hepatocellular carcinoma) in rodents. DEN administration caused HCC in 100% of male mice [46]. A study has indicated that DEN dramatically elevates Brf1 expression in liver cells [47]. DEN-induced cell proliferation is inhibited by decreasing the cellular level of Brf1 [47]. These studies demonstrate that carcinogens are indeed able to increase Brf1 expression [45, 47]. Alcohol has been classified as carcinogenic to humans by the IACR (International Agency for Research on Cancer) [31, 48, 49]. It implies that alcohol has potential to increase Brf1 expression, resulting in alteration of cellular phenotypes. Alcohol may be a good reagent to study the mechanism of breast cell proliferation, cell transformation, and tumor development.

Studies have demonstrated that alcohol dramatically increases Brf1 expression in ER+ breast cancer cell lines [20]. Recent studies further indicate that Brf1 is overexpressed in human HCC biopsies [17]; the high Brf1 expression of the HCC patients displays shorter survival times [17]. This indicates that the abnormal expression of Brf1 links to human cancers and high Brf1 expression predicts worse prognosis of HCC. Although alcohol significantly enhances Brf1 expression in ER+ breast cancer cells, low dose (25mM) of alcohol alone is hard to induce transformation of nontumor breast cells (MCF-10A) [20], while the MCF-10A cells treated with EGF are able to cause colony formation in soft agar assay. But, the treatment of EGF plus alcohol significantly increases the rates of cell transformation [20]. However, once Brf1 expression is repressed in MCF-10A cells, the rates are dramatically reduced in this condition. And also, the rates of cell proliferation are enhanced under alcohol treatment in both liver cells and breast cells [17, 20]. Inhibition of Brf1 expression decreases alcohol-caused rates of cell growth. These studies demonstrate that alcohol-increased Brf1 expression causes the changes in cell phenotypes.

The above studies indicate that carcinogens increase Brf1 expression *in vitro* and abnormal expression of Brf1 is associated with human cancers, such as breast cancer and HCC [10, 17]. Brf1 is overexpressed in human biopsies of liver and breast cancer cases. These evidences support the idea that abnormal expression of Brf1 is tightly linked to cell transformation and breast cancer.

2.6. Epigenetic Regulation of Brf1 Expression by Alcohol-Induced Histone H3 Phosphorylation. Gene expression is epigenetically regulated through DNA methylation and covalent chromatin modifications, such as phosphorylation (H3ph), acetylation (H3ac), and methylation (H3me) of histone H3 and other histones. Emerging evidences suggest that histone modifications, such as methylation, are a dynamic process that modulates transcriptional activity in both normal and tumor cells [50–54]. Histone modifications are the consequence of a balance of the enzymes, which involve histone modifications. Histone methylation is a result of a coordinated interplay between histone lysine methyltransferases [such as EZH2 (enhancer of zeste homolog 2)] and demethylases [such as LSD (lysine-specific demethylase) or KDM (lysine demethylase)] at specific gene promoters, thereby contributing to normal development or occurring disease [52, 55]. Triple methylation of histone H3 lysine 27 (H3K27me_{2/3}) and lysine 9 (H3K9me₃) is a hallmark of silenced chromatin [56]. In contrast, triple methylation of histone H3 lysine 4 (H3K4me₃) is an activating histone mark [57, 58]. Histone H3 phosphorylation (H3ph) is mediated by protein kinase, such as JNK1 and MSK1, and phosphatases [59, 60], whereas histone H3 acetylation is modulated by histone acetyltransferases and deacetylases, such as HDAC1 and HDAC2. We have reported that H3ph at serine 10 and serine 28 increases Pol III gene transcription to cause cell transformation (46.48). Inhibition of the H3ph decreases Pol III gene transcription and represses cell transformation (46.48). However, increasing H3ph occupancy in the Brf1 promoter reduces H3K27me₃ binding to them, leading to the enhancement of Pol III gene transcription (46.48). Previous studies have demonstrated that MSK1 mediates H3ph [60]. Very recent studies further indicate that alcohol activates MSK1 and induces H3ph (unpublished). Inhibition of MSK1 signaling by its chemical inhibitor, SB-747651A, represses the induction of Brf1 expression caused by alcohol (unpublished). Together, the above studies show that alcohol induces Brf1 expression through the JNK1-MSK1-H3ph-ER α and Runx2 pathway to cause phenotypic alterations of breast cells (Figure 3).

3. Deregulation of RNA Pol III Genes and Breast Cancer

As mentioned above, RNA polymerase III transcribes a variety of untranslated RNAs and the Pol III gene products include tRNAs, 5S rRNAs, 7SL RNA, 7SK RNA, and U6 RNA [61–63]. Since the tRNAs and 5S rRNAs control the translational and growth capacity of cells and link to tumor development [64, 65], it is especially important to explore alcohol's role in the deregulation of Pol III genes and tumor development. An animal study has demonstrated that alcohol increases the transcription of Pol III genes [19]. The levels of tRNA and 5S rRNA transcription in the liver tumor tissues of HCV NS5A transgenic mice are much higher than that in nontumor liver tissues [19]. Alcohol feeding of mice promotes mammary tumorigenesis [36, 37]. Cell culture studies have demonstrated that the transcription products of RNA Pol III genes were elevated in both transformed and tumor

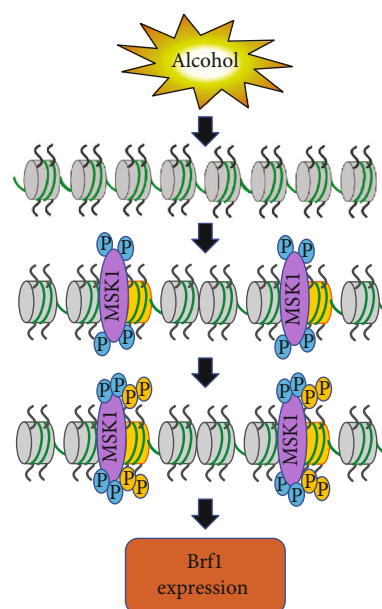


FIGURE 3: Alcohol-induced histone H3 phosphorylation which upregulates Brf1 expression. Alcohol induces activation of MSK1, which binds to the sites of chromatin of the target genes. Activated MSK1 mediates histone H3 phosphorylation (H3ph) to cause chromatin remodeling at local, leading to increases in Brf1 transcription. P: the phosphorylation group.

cells [19, 20, 29, 33, 66–69], while the inductions of Pol III genes by alcohol in tumor cells were much higher than those in nontumor cells [33]. Consistent with this idea, enhanced Pol III gene transcription is required for oncogenic transformation of cells [19, 20, 29]. It suggests that alcohol-induced deregulation of Pol III genes play a crucial role in cell transformation and tumorigenesis [19, 20, 29, 33, 36, 37].

3.1. The Feature of Alcohol-Enhanced Transcription of Pol III Genes in Breast Cells. Breast cancer has become the most common cancer and leading cause of cancer mortality in women in the United States [70]. In terms of the status of ER expression, the patients of breast cancer were divided into ER+ cases and ER- cases. Approximately 80% cases of human breast cancers are ER+, and ~20% cases are ER- [2, 5, 6]. The latter include the cases of ER-, PR-, and Her-, which are called triple-negative breast cancer (TNBC). Clinical studies indicate that ER+ cases of breast cancer have good prognosis after hormone treatment, while ER- cases display worse prognosis.

As alcohol intake is associated with ER+ cases of breast cancer much more than with ER- cases of this disease [8, 9], the mechanism analysis of alcohol-associated breast cancer indicates that cellular levels of Pol III gene transcription are significantly different in ER- breast cell lines, not ER- nontumor breast cell lines (MCF-10A, MCF-10F, and MCF12A) or ER- breast cancer cell lines (MDA-MB235 and SKRB-3), from ER+ breast cancer cell lines (MCF-7 and TDT477) [20]. Interestingly, the alcohol-increased amounts of precursor tRNA^{Leu} and 5S rRNA transcript in ER+ breast cancer cells (MCF-7 and TDT477) are dramatically higher than those in ER- cells (MCF-10A, MCF12A, MDA-MB235, and SKRB-3) [10, 20, 66–69]. The

induction of Pol III genes caused by alcohol in ER+ MCF-7 cells is 5-6 higher than that in ER- breast cells (MCF-10A, MCF-10F, MCF-12A, MDA-MB235, and SKRB-3). It suggests that alcohol-induced deregulation of Pol III genes is in an ER-dependent manner. The feature of alcohol-caused deregulation of Pol III genes in ER+ breast cells is consistent with that of alcohol intake which is associated with ER+ cases of breast cancer.

3.2. Molecular Mechanism of Alcohol-Increased RNA Pol III Gene Transcription in Breast Cancer Cells. As alcohol enhances the activity of ER α and activates the E2 signaling pathway in breast cells [37, 71], it suggests that ER α may be involved in the modulation of alcohol-induced transcription of Pol III genes. Alcohol treatment increases the activity of the ERE-Luc promoter [20, 72]. E2, a ligand of ER α , elevates 3-fold of the ERE-Luc activity, while alcohol plus E2 produces 4.5-fold of its activity in ER+ breast cancer cells [20]. In addition, alcohol strongly increases the cellular levels of ER α mRNA or protein [20]. These studies demonstrated that alcohol indeed enhances ER α expression in ER+ breast cancer cells. To establish whether ER α expression affects Pol III gene transcription, ER+ breast cancer cells (MCF-7) were treated with alcohol. The results indicate that E2 alone elevated (~2-fold) tRNA^{Leu} and 5S rRNA transcription, while alcohol plus E2 produces 11-14-fold of the increase in the transcription of Pol III genes [20]. However, inhibiting expression of ER α by its siRNA reduces the levels of ER α mRNA and protein and also decreases the transcription of tRNA^{Leu} and 5S rRNA [20]. These studies support the conclusion that ER α modulates alcohol-induced transcription of Pol III genes.

Tam is an estrogen receptor antagonist. Tam competitively binds to ER in tumors and other tissue targets to inhibit estrogen effects [32]. The traditional concept of Tam efficacy in breast cancer therapy is known through the ER α pathway. Recent studies demonstrate that Tam is able to directly inhibit alcohol-induced transcription of Brf1 and Pol III genes [33]. This function of Tam may explain its efficacy in ER+ cases of breast cancer, but not TNBC cases. This new finding provides the possibility that inhibition of Pol III gene transcription may be a potential approach to repress alcohol-promoted cell transformation and breast cancer development and to elevate the efficacy in Tam-resistant cases of ER+ breast cancer.

In addition, very recent studies indicate that Runx2 is overexpressed in human biopsies of breast cancer (unpublished). Alcohol enhances Runx2 expression in ER+ breast cancer cells. Repression of Runx2 decreases Brf1 expression and Pol III gene transcription. Further analysis indicates that Runx2 and Brf1 colocalize in the nucleus and they synergistically modulate Pol III gene transcription. Because ER α mediates alcohol-induced Runx2 expression in ER+ MCF-7 cells, the above studies demonstrate that Runx2 modulates Brf1 expression and Pol III gene transcription through the ER α pathway induced by alcohol.

3.3. Brf1 Plays a Critical Role in Alcohol-Induced Deregulation of Pol III Genes. As Brf1 is a key transcription

factor to directly regulate Pol III gene activity, once the levels of Brf1 are changed in any physiological and pathological conditions, the cellular levels of tRNAs and 5S rRNAs would be altered, resulting in changes in cellular phenotype or occurrence of diseases, even tumor development. As mentioned above, these factors, such as signaling molecules (such as JNK1 and MSK1), hormone receptor (such as ER α), transcription factors (such as Runx2, BRCA1), epigenetic modifications (such as histone H3 phosphorylation), carcinogens (such as alcohol, EGF, DEN), medicine (Tam), and others [[20, 31, 33, 66-69, 73] and (unpublished)], which impact Brf1 expression, lead to deregulation of Pol III genes and cause cell proliferation, cell transformation, and eventually breast cancer development. The alcohol-induced deregulation of RNA Pol III genes is a consequence of Brf1 expression change in ER+ breast cells. In terms of the feature of Brf1 in breast tissue, it strongly implies that developing an inhibitor to repress Brf1 expression may reach to the therapeutic purpose of human breast cancer.

4. Summary and Prospects

Alcohol is a liquid diet and widely used as consumption drink in daily life. Alcohol has been classed as a carcinogen to human by IACR in 2011 [31, 48, 49]. Alcohol intake-associated diseases have caused more and more attention. It has especially shown solicitude for that alcohol consumption is consistent with the risk of breast cancer in women. Studies have demonstrated that Brf1 is overexpressed in ER+ cases of breast cancer. High expression of Brf1 in ER+ cases of this disease shows better prognosis under the hormone treatment. Further studies indicate that a hormone drug, Tam, is able to directly repress Brf1 expression, causing the reduction of Pol III gene transcription except Tam competitively binding to ER. Mechanism studies have demonstrated that ER α affects the TFIIB subunit and Brf1 expression, but not TBP, in breast cells. This feature of Brf1 in breast cancer provides a possibility to develop a new approach by inhibiting Brf1 expression for therapy of the patients of breast cancer. Brf1 is not only a therapeutic target of breast cancer but also a biomarker of prognosis of the disease. In the future, more and more attention should be immersed into the studies of the Brf1 inhibitor as a novel approach of breast cancer therapy. It will be of huge interest for both basic science and clinical communities to investigate this mechanism of alcohol-associated breast cancer and identify whether reducing Brf1 expression and Pol III gene transcription by direct or indirect manners represses mammary tumor development.

Abbreviations

Brf1:	TFIIB-related factor 1
TBP:	Tata-box binding protein
Pol III gene:	RNA polymerase III-dependent gene
IARC:	International Agency for Research on Cancer
PNCs:	Perinucleolar compartments
RNA Pol:	RNA polymerase
OS:	Overall survival
DFS:	Disease-free survival

TNBC: Triple-negative breast cancer
 Tam: Tamoxifen
 ALD: Alcoholic liver disease
 ROS: Reactive oxygen species.

Conflicts of Interest

The authors declare that they have no conflict of interest.

Authors' Contributions

S Zhong conceived the idea. CH Huang, YM Zhang, and S Zhong prepared this manuscript. Chenghao Huang and Yanmei Zhang have contributed equally to the present study.

Acknowledgments

The studies summarized in this paper were partly supported by National Institute on Alcohol Abuse and Alcoholism/NIH grants AA017288, AA021114, AA023247, and AA04169 to S. Zhong. We want to thank Drs. M. R. Stallcup, Danial Levy, and Neil Kaplowitz (University of Southern California) for scientific discussions.

References

- [1] Collaborative Group on Hormonal Factors in Breast Cancer, "Alcohol, tobacco and breast cancer - collaborative reanalysis of individual data from 53 epidemiological studies, including 58 515 women with breast cancer and 95 067 women without the disease," *British Journal of Cancer*, vol. 87, no. 11, pp. 1234–1245, 2002.
- [2] B. MacMahon, "Epidemiology and the causes of breast cancer," *International Journal of Cancer*, vol. 118, no. 10, pp. 2373–2378, 2006.
- [3] A. L. Petri, A. Tjønneland, M. Gamborg et al., "Alcohol Intake, Type of Beverage, and Risk of Breast Cancer in Pre- and Postmenopausal Women," *Alcoholism Clinical Experimental Research*, vol. 28, no. 7, pp. 1084–1090, 2004.
- [4] K. W. Singletary and S. M. Gapstur, "Alcohol and breast cancer: review of epidemiologic and experimental evidence and potential mechanisms," *JAMA*, vol. 286, no. 17, pp. 2143–2151, 2001.
- [5] S. Deandrea, R. Talamini, R. Foschi et al., "Alcohol and breast cancer risk defined by estrogen and progesterone receptor status: a case-control study," *Cancer Epidemiology Biomarkers & Prevention*, vol. 17, no. 8, pp. 2025–2028, 2008.
- [6] R. Suzuki, N. Orsini, L. Mignone, S. Saji, and A. Wolk, "Alcohol intake and risk of breast cancer defined by estrogen and progesterone receptor status—A meta-analysis of epidemiological studies," *International Journal of Cancer*, vol. 122, no. 8, pp. 1832–1841, 2008.
- [7] K. W. Singletary, M. Q. McNary, A. M. Odoms, J. Nelshoppen, and M. A. Wallig, "Ethanol consumption and DMBA-induced mammary carcinogenesis in rats," *Nutrition and Cancer*, vol. 16, no. 1, pp. 13–23, 1991.
- [8] K. Singletary, J. Nelshoppen, and M. Wallig, "Enhancement by chronic ethanol intake of N-methyl-N-nitrosourea-induced rat mammary tumorigenesis," *Carcinogenesis*, vol. 16, no. 4, pp. 959–964, 1995.
- [9] T. Watabiki, Y. Okii, T. Tokiyasu et al., "Long-Term Ethanol Consumption in ICR Mice Causes Mammary Tumor in Females and Liver Fibrosis in Males," *Alcoholism: Clinical and Experimental Research*, vol. 24, pp. 117S–122S, 2000.
- [10] Z. Fang, Y. Yi, G. Shi et al., "Role of Brf1 interaction with ER α , and significance of its overexpression, in human breast cancer," *Molecular Oncology*, vol. 11, no. 12, pp. 1752–1767, 2017.
- [11] R. G. Dumitrescu and P. G. Shields, "The etiology of alcohol-induced breast cancer," *Alcohol*, vol. 35, no. 3, pp. 213–225, 2005.
- [12] V. Purohit, J. Khalsa, and J. Serrano, "Mechanisms of alcohol-associated cancers: introduction and summary of the symposium," *Alcohol*, vol. 35, no. 3, pp. 155–160, 2005.
- [13] S. Huang, T. J. Deerinck, M. H. Ellisman, and D. L. Spector, "The dynamic organization of the perinucleolar compartment in the cell nucleus," *The Journal of Cell Biology*, vol. 137, no. 5, pp. 965–974, 1997.
- [14] R. V. Kamath, A. D. Thor, C. Wang et al., "Perinucleolar compartment prevalence has an independent prognostic value for breast cancer," *Cancer Research*, vol. 65, no. 1, pp. 246–253, 2005.
- [15] C. Wang, J. C. Politz, T. Pederson, and S. Huang, "RNA polymerase III transcripts and the PTB protein are essential for the integrity of the perinucleolar compartment," *Molecular Biology of the Cell*, vol. 14, no. 6, pp. 2425–2435, 2003.
- [16] A. G. Winter, G. Sourvinos, S. J. Allison et al., "RNA polymerase III transcription factor TFIIC2 is overexpressed in ovarian tumors," *Proceedings of the National Academy of Sciences*, vol. 97, no. 23, pp. 12619–12624, 2000.
- [17] Q. Zhong, S. Xi, J. Liang et al., "The significance of Brf1 overexpression in human hepatocellular carcinoma," *Oncotarget*, vol. 7, no. 5, pp. 6243–6254, 2016.
- [18] W. Chen, W. Bocker, J. Brosius, and H. Tiedge, "Expression of neural BC200 RNA in human tumours," *The Journal of Pathology*, vol. 183, no. 3, pp. 345–351, 1997.
- [19] S. Zhong, K. Machida, H. Tsukamoto, and D. L. Johnson, "Alcohol induces RNA polymerase III-dependent transcription through c-Jun by co-regulating TATA-binding protein (TBP) and Brf1 expression," *Journal of Biological Chemistry*, vol. 286, no. 4, pp. 2393–2401, 2011.
- [20] Q. Zhang, J. Jin, Q. Zhong, X. Yu, D. Levy, and S. Zhong, "ER α mediates alcohol-induced deregulation of Pol III genes in breast cancer cells," *Carcinogenesis*, vol. 34, no. 1, pp. 28–37, 2013.
- [21] D. Raha, Z. Wang, Z. Moqtaderi et al., "Close association of RNA polymerase II and many transcription factors with Pol III genes," *Proceedings of the National Academy of Sciences*, vol. 107, no. 8, pp. 3639–3644, 2010.
- [22] K. A. Dittmar, J. M. Goodenbour, and T. Pan, "Tissue-specific differences in human transfer RNA expression," *PLoS Genetics*, vol. 2, no. 12, article e221, 2006.
- [23] N. Hernandez, "TBP, a universal eukaryotic transcription factor?," *Genes & Development*, vol. 7, no. 7b, pp. 1291–1308, 1993.
- [24] H. D. Wang, A. Trivedi, and D. L. Johnson, "Regulation of RNA polymerase I-dependent promoters by the hepatitis B virus X protein via activated Ras and TATA-binding protein," *Molecular and Cellular Biology*, vol. 18, no. 12, pp. 7086–7094, 1998.
- [25] A. Woiwode, S. A. S. Johnson, S. Zhong et al., "PTEN represses RNA polymerase III-dependent transcription by targeting the

- TFIIIB complex,” *Molecular and Cellular Biology*, vol. 28, no. 12, pp. 4204–4214, 2008.
- [26] I. Veras, E. M. Rosen, and L. Schramm, “Inhibition of RNA polymerase III transcription by BRCA1,” *Journal of Molecular Biology*, vol. 387, no. 3, pp. 523–531, 2009.
- [27] S. A. S. Johnson, L. Dubeau, and D. L. Johnson, “Enhanced RNA polymerase III-dependent transcription is required for oncogenic transformation,” *Journal of Biological Chemistry*, vol. 283, no. 28, pp. 19184–19191, 2008.
- [28] S. Zhong, J. Fromm, and D. L. Johnson, “TBP is differentially regulated by c-Jun N-terminal kinase 1 (JNK1) and JNK2 through Elk-1, controlling c-Jun expression and cell proliferation,” *Molecular and Cellular Biology*, vol. 27, no. 1, pp. 54–64, 2007.
- [29] S. Zhong, C. Zhang, and D. L. Johnson, “Epidermal growth factor enhances cellular TATA binding protein levels and induces RNA polymerase I- and III-dependent gene activity,” *Molecular and Cellular Biology*, vol. 24, no. 12, pp. 5119–5129, 2004.
- [30] S. Zhong and D. L. Johnson, “The JNKs differentially regulate RNA polymerase III transcription by coordinately modulating the expression of all TFIIIB subunits,” *Proceedings of the National Academy of Sciences of the United States of America*, vol. 106, no. 31, pp. 12682–12687, 2009.
- [31] G. Shi and S. Zhong, “Alcohol-associated cancer and deregulation of Pol III genes,” *Gene*, vol. 612, pp. 25–28, 2017.
- [32] V. C. Jordan, “A current view of tamoxifen for the treatment and prevention of breast cancer,” *British Journal of Pharmacology*, vol. 110, no. 2, pp. 507–517, 1993.
- [33] Q. Zhong, G. Shi, Q. Zhang, L. Lu, D. Levy, and S. Zhong, “Tamoxifen represses alcohol-induced transcription of RNA polymerase III-dependent genes in breast cancer cells,” *Oncotarget*, vol. 5, no. 23, pp. 12410–12417, 2014.
- [34] H. K. Seitz, C. Pelucchi, V. Bagnardi, and C. La Vecchia, “Epidemiology and pathophysiology of alcohol and breast cancer: update 2012,” *Alcohol Alcohol*, vol. 47, no. 3, pp. 204–212, 2012.
- [35] W. Demark-Wahnefried and P. J. Goodwin, “To your health: how does the latest research on alcohol and breast cancer inform clinical practice?,” *Journal of Clinical Oncology*, vol. 31, no. 16, pp. 1917–1919, 2013.
- [36] S. Wang, M. Xu, F. Li et al., “Ethanol promotes mammary tumor growth and angiogenesis: the involvement of chemoattractant factor MCP-1,” *Breast Cancer Research and Treatment*, vol. 133, no. 3, pp. 1037–1048, 2012.
- [37] A. W. Wong, S. M. Dunlap, V. B. Holcomb, and N. P. Nunez, “Alcohol Promotes Mammary Tumor Development via the Estrogen Pathway in Estrogen Receptor Alpha-Negative HER2/neu Mice,” *Alcoholism: Clinical and Experimental Research*, vol. 36, no. 4, pp. 577–587, 2012.
- [38] R. K. Petersen, S. B. Larsen, D. M. Jensen et al., “PPARGgamma-PGC-1alpha activity is determinant of alcohol related breast cancer,” *Cancer Letters*, vol. 315, no. 1, pp. 59–68, 2012.
- [39] U. Vogel, J. Christensen, B. A. Nexø, H. Wallin, S. Friis, and A. Tjønneland, “Peroxisome proliferator-activated [corrected] receptor-gamma2 [corrected] Pro12Ala, interaction with alcohol intake and NSAID use, in relation to risk of breast cancer in a prospective study of Danes,” *Carcinogenesis*, vol. 28, no. 2, pp. 427–434, 2007.
- [40] J. A. Fairley, L. E. Mitchell, T. Berg et al., “Direct regulation of tRNA and 5S rRNA gene transcription by Polo-like kinase 1,” *Molecular Cell*, vol. 45, no. 4, pp. 541–552, 2012.
- [41] M. Schmidlin, M. Lu, S. A. Leuenberger et al., “The ARE-dependent mRNA-destabilizing activity of BRF1 is regulated by protein kinase B,” *The EMBO Journal*, vol. 23, no. 24, pp. 4760–4769, 2004.
- [42] D. Benjamin, M. Schmidlin, L. Min, B. Gross, and C. Moroni, “BRF1 protein turnover and mRNA decay activity are regulated by protein kinase B at the same phosphorylation sites,” *Molecular and Cellular Biology*, vol. 26, no. 24, pp. 9497–9507, 2006.
- [43] G. Borck, F. Hög, M. L. Dentici et al., “BRF1 mutations alter RNA polymerase III-dependent transcription and cause neurodevelopmental anomalies,” *Genome Research*, vol. 25, no. 2, pp. 155–166, 2015.
- [44] P. K. Julka, R. T. Chacko, S. Nag et al., “A phase II study of sequential neoadjuvant gemcitabine plus doxorubicin followed by gemcitabine plus cisplatin in patients with operable breast cancer: prediction of response using molecular profiling,” *British Journal of Cancer*, vol. 98, no. 8, pp. 1327–1335, 2008.
- [45] Q. Zhang, Q. Zhong, A. G. Evans, D. Levy, and S. Zhong, “Phosphorylation of histone H3 serine 28 modulates RNA polymerase III-dependent transcription,” *Oncogene*, vol. 30, no. 37, pp. 3943–3952, 2011.
- [46] W. E. Naugler, T. Sakurai, S. Kim et al., “Gender disparity in liver cancer due to sex differences in MyD88-dependent IL-6 production,” *Science*, vol. 317, no. 5834, pp. 121–124, 2007.
- [47] Q. Zhong, G. Shi, Q. Zhang, Y. Zhang, D. Levy, and S. Zhong, “Role of phosphorylated histone H3 serine 10 in DEN-induced deregulation of Pol III genes and cell proliferation and transformation,” *Carcinogenesis*, vol. 34, no. 11, pp. 2460–2469, 2013.
- [48] V. J. Coglianò, R. Baan, K. Straif et al., “Preventable exposures associated with human cancers,” *JNCI Journal of the National Cancer Institute*, vol. 103, no. 24, pp. 1827–1839, 2011.
- [49] IARC Working Group on the Evaluation of Carcinogenic Risks to Humans, “A Review of Human Carcinogens,” in *IARC Monographs on the Evaluation of Carcinogenic Risks to Humans*, vol. 100, pp. 100:v-vii–100:1–412, IARC: Distributed for the International Agency for Research on Cancer by the Secretariat of the World Health Organization, Lyon, France, 2011.
- [50] C. Lu, P. S. Ward, G. S. Kapoor et al., “IDH mutation impairs histone demethylation and results in a block to cell differentiation,” *Nature*, vol. 483, no. 7390, pp. 474–478, 2012.
- [51] F. De Santa, M. G. Totaro, E. Prosperini, S. Notarbartolo, G. Testa, and G. Natoli, “The histone H3 lysine-27 demethylase Jmjd3 links inflammation to inhibition of polycomb-mediated gene silencing,” *Cell*, vol. 130, no. 6, pp. 1083–1094, 2007.
- [52] K. Jepsen, D. Solum, T. Zhou et al., “SMRT-mediated repression of an H3K27 demethylase in progression from neural stem cell to neuron,” *Nature*, vol. 450, no. 7168, pp. 415–419, 2007.
- [53] F. Lan, P. E. Bayliss, J. L. Rinn et al., “A histone H3 lysine 27 demethylase regulates animal posterior development,” *Nature*, vol. 449, no. 7163, pp. 689–694, 2007.
- [54] G. van Haaften, G. L. Dalgliesh, H. Davies et al., “Somatic mutations of the histone H3K27 demethylase gene *UTX* in human cancer,” *Nature Genetics*, vol. 41, no. 5, pp. 521–523, 2009.
- [55] G. L. Sen, D. E. Webster, D. I. Barragan, H. Y. Chang, and P. A. Khavari, “Control of differentiation in a self-renewing

- mammalian tissue by the histone demethylase JMJD3,” *Genes & Development*, vol. 22, no. 14, pp. 1865–1870, 2008.
- [56] A. H. F. M. Peters, J. E. Mermoud, D. O’Carroll et al., “Histone H3 lysine 9 methylation is an epigenetic imprint of facultative heterochromatin,” *Nature Genetics*, vol. 30, no. 1, pp. 77–80, 2002.
- [57] H. Santos-Rosa, R. Schneider, A. J. Bannister et al., “Active genes are tri-methylated at K4 of histone H3,” *Nature*, vol. 419, no. 6905, pp. 407–411, 2002.
- [58] R. Schneider, A. J. Bannister, F. A. Myers, A. W. Thorne, C. Crane-Robinson, and T. Kouzarides, “Histone H3 lysine 4 methylation patterns in higher eukaryotic genes,” *Nature Cell Biology*, vol. 6, no. 1, pp. 73–77, 2004.
- [59] S. Zhong, Y. Zhang, C. Jansen, H. Goto, M. Inagaki, and Z. Dong, “MAP kinases Mediate UVB-induced Phosphorylation of histone H3 at serine 28,” *Journal of Biological Chemistry*, vol. 276, no. 16, pp. 12932–12937, 2001.
- [60] S. Zhong, C. Jansen, Q. B. She et al., “Ultraviolet B-induced phosphorylation of histone H3 at serine 28 is mediated by MSK1,” *Journal of Biological Chemistry*, vol. 276, no. 35, pp. 33213–33219, 2001.
- [61] E. Ullu and C. Tschudi, “*Alu* sequences are processed 7SL RNA genes,” *Nature*, vol. 312, no. 5990, pp. 171–172, 1984.
- [62] G. Dieci, G. Fiorino, M. Castelnovo, M. Teichmann, and A. Pagano, “The expanding RNA polymerase III transcriptome,” *Trends in Genetics*, vol. 23, no. 12, pp. 614–622, 2007.
- [63] G. M. Borchert, W. Lanier, and B. L. Davidson, “RNA polymerase III transcribes human microRNAs,” *Nature Structural & Molecular Biology*, vol. 13, no. 12, pp. 1097–1101, 2006.
- [64] R. J. White, “RNA polymerase III transcription and cancer,” *Oncogene*, vol. 23, no. 18, pp. 3208–3216, 2004.
- [65] S. J. Goodfellow, F. Innes, L. E. Derblay, W. R. MacLellan, P. H. Scott, and R. J. White, “Regulation of RNA polymerase III transcription during hypertrophic growth,” *The EMBO Journal*, vol. 25, no. 7, pp. 1522–1533, 2006.
- [66] Q. Zhong, G. Shi, Y. Zhang, L. Lu, D. Levy, and S. Zhong, “Alteration of BRCA1 expression affects alcohol-induced transcription of RNA Pol III-dependent genes,” *Gene*, vol. 556, no. 1, pp. 74–79, 2015.
- [67] Y. Yi, J. Lei, G. Shi et al., “The effects of liquor spirits on RNA Pol III genes and cell growth of human cancer lines,” *Food and Nutrition Sciences*, vol. 09, no. 3, pp. 208–220, 2018.
- [68] S. Chen, Y. Yi, T. Xia et al., “The influences of red wine in phenotypes of human cancer cells,” *Gene*, vol. 702, pp. 194–204, 2019.
- [69] J. Lei, S. Chen, and S. Zhong, “Abnormal expression of TFIIB subunits and RNA Pol III genes is associated with hepatocellular carcinoma,” *Liver Research*, vol. 1, no. 2, pp. 112–120, 2017.
- [70] R. L. Siegel, K. D. Miller, and A. Jemal, “Cancer statistics, 2017,” *CA: A Cancer Journal for Clinicians*, vol. 67, no. 1, pp. 7–30, 2017.
- [71] Y. Yi, C. Huang, Y. Zhang et al., “Exploring a common mechanism of alcohol-induced deregulation of RNA Pol III genes in liver and breast cells,” *Gene*, vol. 626, pp. 309–318, 2017.
- [72] S. Fan, Q. Meng, B. Gao et al., “Alcohol stimulates estrogen receptor signaling in human breast cancer cell lines,” *Cancer Research*, vol. 60, no. 20, pp. 5635–5639, 2000.
- [73] Q. Zhong, G. Shi, Y. Zhang, D. Levy, and S. Zhong, “Elk1 and AP-1 sites in the TBP promoter mediate alcohol-induced deregulation of Pol III-dependent genes,” *Gene*, vol. 526, no. 1, pp. 54–60, 2013.

Research Article

Resveratrol Reverses Thioacetamide-Induced Renal Assault with respect to Oxidative Stress, Renal Function, DNA Damage, and Cytokine Release in Wistar Rats

Seema Zargar ¹, Mona Alonazi,¹ Humaira Rizwana ², and Tanveer A. Wani ³

¹Department of Biochemistry, College of Science, King Saud University, P.O. Box 22452 Riyadh 11451, Saudi Arabia

²Department of Microbiology, College of Science, King Saud University, P.O. Box 22452 Riyadh 11451, Saudi Arabia

³Department of Pharmaceutical Chemistry, College of Pharmacy, King Saud University, P.O. Box 2457, Riyadh 11451, Saudi Arabia

Correspondence should be addressed to Seema Zargar; szargar@ksu.edu.sa

Received 11 April 2019; Revised 30 June 2019; Accepted 10 August 2019; Published 10 September 2019

Guest Editor: Reggiani Vilela Gonçalves

Copyright © 2019 Seema Zargar et al. This is an open access article distributed under the Creative Commons Attribution License, which permits unrestricted use, distribution, and reproduction in any medium, provided the original work is properly cited.

Background. Thioacetamide (TAA), a class 2B-type carcinogen, is a potent toxicant. Toxicities caused by this compound in various tissues due to oxidative stress, increase of proinflammatory markers, and apoptosis have been reported; however, reports on kidney toxicity are negligible. Resveratrol (RSV), on the other hand, has demonstrated antioxidant and anti-inflammatory effects in different cases. Resveratrol's protective effects against TAA kidney toxicity were investigated in four rat groups. **Methodology.** Four groups of rats were studied as follows ($n = 8$): control group, where rats were fed normal diet and water; TAA group, where rats received 0.3% TAA in water for two weeks; RSV group, where rats received 10 mg/kg body weight (bw) of RSV as oral suspension for two weeks; and treated group, where rats orally received 10 mg/kg bw RSV and simultaneously received 0.3% TAA for two weeks. Kidney homogenates from all groups were analyzed for cytokine release (IL-4, TNF- α , and IFN- γ) and oxidative stress (lipid peroxidation, catalase, and 8-OHdG). The serum of rats was analyzed for the quantification of renal function markers (blood urea nitrogen (BUN), creatinine, and creatine kinase). **Result.** A significant increase in the renal function markers (BUN, 240%; creatinine, 187%; and creatine kinase, 117%), oxidative stress parameters (lipid peroxidation, 192% increase; catalase, 30.5% decrease), cytokines (IL-4, 120%; TNF- α , 129%; and IFN- γ , 133%), and DNA damage was observed in the TAA-treated group. All changes were significantly reversed in the group treated with RSV and TAA ($P < 0.05$) in combination, with no significant difference compared to the control group. **Conclusion.** We conclude that resveratrol shows protection against TAA toxicity in rat kidney with respect to DNA damage, oxidative stress, renal function and cytokine release.

1. Introduction

Thioacetamide (TAA; CH_3CSNH_2), an organosulfur compound, is commonly used as a fungicide [1, 2] owing to its generation of sulfide ions that prevent the germination of fungal spores. TAA is also widely used as an *in situ* source of sulfide ions in qualitative inorganic analysis to replace hydrogen sulfide in the pharmaceutical and chemical industries [3, 4]. The routes of human exposure to TAA include the generation of toxic fumes inhaled/ingested or absorbed through the skin. TAA is a model toxicant of choice due to its water-soluble nature and remarkable ability to induce assault [5]. TAA belongs to the class 2B-type carcino-

gens and results in acute liver and cytomegaly [6]. Acute exposure to TAA leads to necrosis as well as changes in chronic calcium permeability to the membrane due to an imbalance in calcium uptake, leading to apoptosis in the liver tissue [6–8]. TAA affects the ending of the proximal renal tubule by causing cell death [9]. When TAA is bioactivated, thioacetamide S-oxide is formed which leads to the generation of peroxide radicals further leading to the generation of reactive oxygen species (ROS) [1]. ROS initiates oxidation reactions such as lipid peroxidation to unsaturated lipids or triggers other reactions with sulfhydryl compounds, leading to liver injury [6, 10–12]. The metabolites generated are later distributed among several organs including the liver, kidney,

adrenals, bone marrow, plasma, and other tissues [13], hence can modify amine lipids and proteins leading to further systemic oxidative stress, cytokine release, and altered kidney function that remain poorly understood. Resveratrol (RSV) (3,5,4'-trihydroxy-trans-stilbene), a natural polyphenolic compound found in grapes, berries, and many other plant species, is well known for its antioxidant properties [14]. RSV has demonstrated its protective activity against many oxidative stresses and inflammation [15, 16]. In addition, it has exhibited many health benefits including antioxidant [17], antimutagenic [18], anti-inflammatory [19], estrogenic [20], antiplatelet [21], anticancer [22], and cardioprotective [23] properties.

In the present study, we administered RSV- to TAA-treated rats to examine its effect on the levels of cytokine release, oxidative stress, and kidney function.

2. Materials and Methods

All chemicals required in this study including TAA were from Sigma-Aldrich (St. Louis, MO, USA) and RSV from EMD Millipore (Calbiochem, Billerica, MA, USA).

2.1. Experimental Protocol. 32 male Wistar rats (4 weeks old; 70–80 g) were randomly divided into four different groups with eight rats each. The groups were categorized as control group; TAA group, rats receiving TAA; RSV group, rats receiving RSV; and TAA+RSV group, rats simultaneously receiving RSV and TAA.

TAA dosage was based on a previous literature [12]. Since RSV is insoluble in water, the suspension of 10 mg per mL stock was prepared and 10 mg/kg bw of the stock administered to rats by oral gavage.

All groups were sacrificed by carbon dioxide asphyxiation. The study was approved by the institutional review board for animal ethics (protocol no. 6828/2017), and every attempt was made to follow the guidelines. The control group was fed standard laboratory chow and water for two weeks, while in the TAA group, rats drank water containing 0.3% for two weeks. For the RSV group, rats were given 10 mg/kg/body weight (bw) of RSV as an oral suspension (the suspension was prepared as 10 mg/mL in water) for two weeks; rats in the TAA+RSV group were orally given a simultaneous 10 mg/kg bw RSV suspension with 0.3% TAA in water for 2 weeks.

2.2. Sample Preparation. Blood was drawn from the tail vein and the serum extracted and stored in a -80°C freezer for future use. The kidneys were dissected, washed, weighed, homogenized, and sonicated in normal saline using an ultrasonic cell disrupter from Vibra cell 72434 (Bioblock, Illkrich Cedex) [24]. All homogenates were centrifuged at 4,000 rpm for 5 min at 4°C . The resulting suspension was sonicated four times and stored in a -70°C freezer after centrifuging at 5000 rpm for 6 min at 4°C . Prior to performing the assay, all samples were diluted to 0.01 mol/L in PBS.

2.3. Assay of Cytokines (TNF- α , IL-4, and IFN- γ). TNF- α was measured using the Sea-133ra ELISA kit from Cloud-Clone

Corporation (CCC, USA) according to the method of Zargar et al. [11]. A precoated 96-well microplate with polyclonal antibody specific to TNF- α was added to the samples and standards. The unbound solution was removed via several rounds of washing. Avidin-conjugated horseradish peroxidase (HRP) was added and the plate washed. TMB substrate was added for the development of enzyme color and the reaction terminated by the addition of sulfuric acid. The change in color was measured at 450 nm. Each sample was measured in duplicate and the level of TNF- α determined by comparing the optical density (OD) of samples using the standard curve. Concentration of TNF- α was presented as pg/100 mg protein.

IL-4 and IFN- γ were measured using an ELISA kit from Cloud-Clone Corporation. Briefly, the 96-well microplates were pre-coated with the respective polyclonal antibody. The kit standards and samples were added according to the manufacturer's instructions and the unbound solutions removed via washing. Avidin-conjugated horseradish peroxidase (HRP) was later added to the plate. The unbound material was washed after the addition of the substrate solution and the reaction terminated by adding sulfuric acid. The change in absorbance was measured at 450 nm. Each sample was measured in duplicate and the concentrations of IL-4 were determined by comparing the OD of samples using a standard curve. Concentration of IL-4 was presented as pg/100 mg protein. For IFN- γ measurement, IFN- γ precoated antibody plates were treated with kit standards and the homogenates incubated for 1 h at 37°C . Following the addition of detection reagent, the plate was again incubated at 37°C for 1 h. After washing, the detection reagent B was added and the plate incubated for 30 min. Finally, the substrate solution was added, and after a 20 min incubation, the stop solution was added to terminate the reaction; absorbance was then recorded at 450 nm. Each sample was measured in duplicate and the level of IFN- γ presented in pg/100 mg of protein after comparison to the standard curve.

2.4. Assay of DNA Damage and Oxidative Stress. To examine DNA damage in cells, we assessed 8-hydroxy-2-deoxyguanosine (8-OHdG), a global marker of oxidative stress. The 8-OHdG was measured using an ELISA kit from Abnova Corporation, Taipei City (Taiwan). Briefly, 50 μL of homogenate followed by 50 μL of the detection solution was added to each precoated well and the plate incubated at 37°C for 1 h. The plate was then washed several times and inverted on dry tissue towels. A volume of 100 μL of the working solution, reagent B (detection reagent), was added to each well. The plate was then incubated for 45 min at 37°C and washed five times. A volume of 90 μL of substrate was later added to each well. The plate was incubated again at 37°C in the dark for 15–30 min. Finally, 50 μL of the stop solution was added and the change in color determined at 450 nm. The level of 8-OHdG was determined in duplicate against a standard curve using a four-parameter logistic (4-PL) curve-fit software. The 8-OHdG was presented as ng/100 mg of DNA.

For lipid peroxide formation, 1.5 mL of 20% trichloroacetic acid was added to the preincubated tissue homogenates

and centrifuged at 600 *g* for 10 min at 4°C. Further, 0.67% of thiobarbituric acid was added and the reaction mixture boiled for 15 min. Absorbance was recorded upon cooling at 535 nm using a blank reagent [25].

For catalase (CAT) activity, the homogenate was added to produce a final volume of 1.8 mL with sodium phosphate buffer (0.4 M; pH 7.2). At a later time, 1.2 mL of H₂O₂ was added to initiate the reaction and change in absorbance recorded at 240 nm for 2 min. One unit of CAT represents the amount in μ moles of H₂O₂ decomposed in 1 min with 43.6 M⁻¹ cm⁻¹ as the molar absorbance of H₂O₂ [26].

Total protein levels from homogenates were measured using bovine serum albumin as the standard [27]. The protein amount was calculated from a standard curve. Protein values are expressed as mg/g of fresh tissue.

2.5. Assay of Kidney Function Markers. The following parameters were measured using colorimetric kits from Human (Diagnostics Worldwide) (Wiesbaden, Germany): blood urea nitrogen (BUN), serum creatinine, and creatine kinase. To measure BUN, 10 μ L serum was added to 1 mL of the working reagent and the samples were incubated at 37°C for 30 s; absorbance was immediately recorded at 340 nm and after 1 min to determine the serum urea concentration. The BUN concentration was later determined by dividing serum urea concentration with the conversion factor 2.14, evaluated based on molecular weights of both BUN and urea. For serum creatinine and creatine kinase estimation, 10 μ L serum was added to 1 mL of the working reagent and incubated at 37°C for 30 s.

The absorbance of creatinine was immediately recorded at 500 nm and after 2 min; change in absorbance was directly proportional to creatinine in the sample. The absorbance of creatine kinase was recorded at 450 nm.

Histological analysis of the middle third part of non-clipped kidney was performed by modern enclosed tissue processor (Leica Biosystems, US); sections of 5–6 μ m thickness were stained with hematoxylin-eosin (HE). Images of at least five randomly selected areas of each sample were photographed at 40x magnification and analyzed for kidney injury by an expert pathologist who was blinded to the sample assignment in the experiment.

2.6. Statistical Analysis. All results are expressed as mean \pm SD. The data statistically represented by number, mean, and SD were recorded. Comparison of different groups was performed using one-way ANOVA with Tukey's multiple comparison test. Comparison of all treatment groups was performed against the control group. A probability value (*P* value) ≤ 0.05 was deemed significant. All statistical calculations were performed using SPSS program (Statistical Package for Social Science version 11.0).

3. Results

The TAA group that received 0.3% TAA dissolved in water for two weeks experienced a significant increase in IL-4. Rats administered with a simultaneous treatment of the same amount of TAA and 10 mg/kg/bw of RSV dissolved in water

for two weeks experienced a significant decrease when compared to the TAA-treated group (*P* < 0.05) (Figure 1). TNF- α was also significantly increased with TAA; however, a significant reversal occurred in the rat group that received simultaneous treatment of TAA and RSV (*P* < 0.05). A significant difference was not found when the RSV group was compared to the control group (Figure 2). Similarly, IFN- γ levels were significantly increased by TAA treatment and this effect was reversed by simultaneous RSV treatment with TAA. RSV treatment also resulted in a significant increase in IFN- γ levels when compared to the control group (*P* < 0.05) (Figure 3).

The marker, 8-OHdG, is considered ideal for genotoxicity. The genotoxic effect in cells was increased by TAA and the increased levels of 8-OHdG significantly reduced in the rat group simultaneously treated with RSV (*P* < 0.05) (Figure 4). RSV treatment did not exhibit any significant difference with respect to the control group. Lipid peroxidation was also significantly increased by TAA treatment while RSV treatment significantly decreased the level of lipid peroxides. When both were simultaneously used, the increase caused by TAA was significantly and completely reversed (*P* < 0.05). Catalase was also significantly decreased by TAA treatment; however, combined therapy with RSV completely reversed the altered levels (*P* < 0.05) (Table 1). Separately and combined, TAA and RSV also altered the biochemical markers of kidney function (Table 1). BUN was significantly increased with TAA treatment while RSV treatment resulted in no significant alteration in the BUN level. When both the TAA and RSV drinks were simultaneously ingested, the increase in BUN caused by TAA ingestion was completely reversed (*P* < 0.05). Creatinine levels were significantly increased by TAA treatment while in the combination therapy, TAA and RSV treatment significantly reversed the increased level compared to the TAA-treated group. Creatine kinase levels were also significantly increased by TAA treatment when compared to control; RSV treatment had no effect on creatine kinase concentration. When both RSV and TAA were simultaneously ingested, the levels of creatine kinase were significantly reversed to normal (*P* < 0.05).

TAA insult led to a distortion in the glomerulus with significant congestion; RSV treatment, however, preserved the glomerular structure. Treatment with RSV before TAA preserved glomerular structure but the congestion of tubules could not be protected (Figure 5).

4. Discussion

TAA, an organosulfur fungicide, is a famous carcinogen that causes centrilobular hepatic necrosis in rats. RSV has been demonstrated to protect against the occurrence of many diseases such as diabetes, coronary heart diseases, tumor and obesity, and some oxidative stresses [28, 29]. In this study, RSV was demonstrated to exert protective effects against TAA-induced assault with respect to oxidative stress, renal function, DNA damage, and cytokine release on kidney tissue.

Renal function markers (BUN, creatinine, and creatine kinase) and the free radical scavenging (lipid peroxidation,

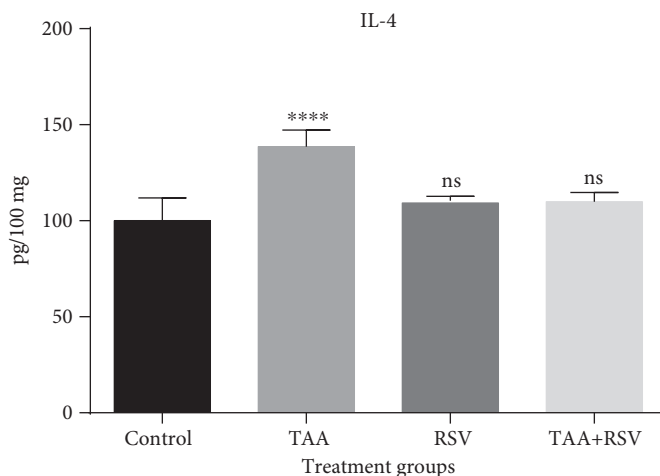


FIGURE 1: Effect of thioacetamide and resveratrol on the IL-4. IL-4 concentrations are expressed as pg/mg protein ($n = 8$) for the treated groups compared to the control group. **** $P < 0.0001$; ns: nonsignificant.

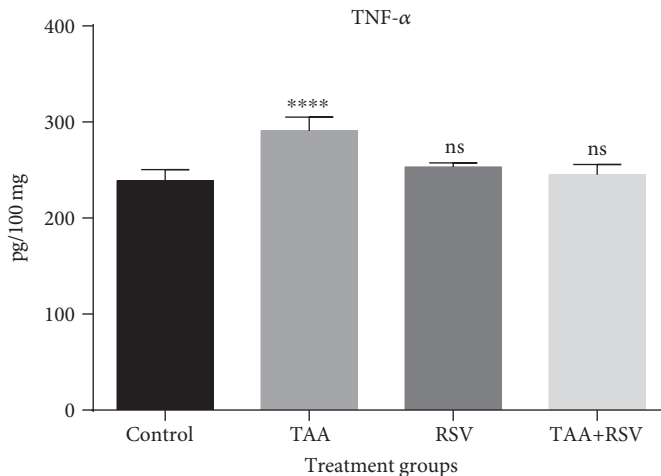


FIGURE 2: Effect of thioacetamide and resveratrol on TNF- α . TNF- α concentrations are expressed as pg/mg protein ($n = 8$) for the treated groups compared to the control group. **** $P < 0.0001$; ns: nonsignificant.

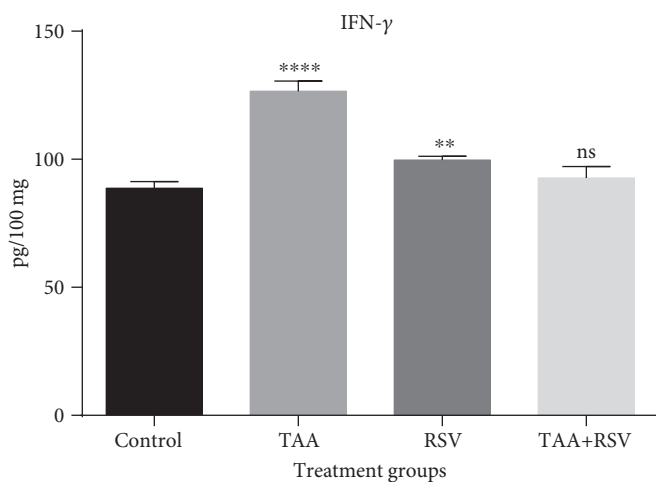


FIGURE 3: Effect of thioacetamide and resveratrol on IFN- γ . IFN- γ concentrations are expressed as pg/mg protein ($n = 8$) when treated groups are compared to the control group. **** $P < 0.0001$; ** $P < 0.01$; ns: nonsignificant.

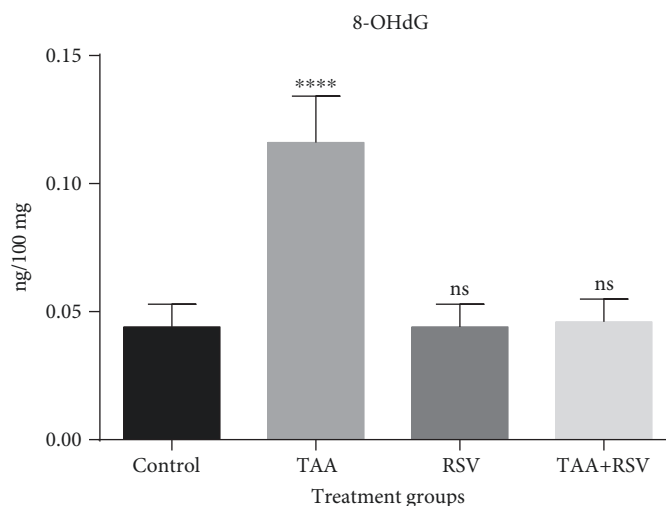


FIGURE 4: Effect of thioacetamide and resveratrol on 8-OHdG. 8-OHdG concentrations ($n = 8$) are expressed as ng/100 mg tissue when treated groups are compared to control group. **** $P < 0.0001$; ns: nonsignificant.

TABLE 1: Effect of thioacetamide-induced changes alone and combined with resveratrol on the levels of kidney function and oxidative stress markers. Data are represented as mean \pm SD of three independently performed experiments; each group had 8 rats for all experiments conducted: TAA-treated, 0.3% for two weeks; RSV-treated, 10 mg/kg bw for 2 weeks; and TAA+RSV-treated, 0.3%+10 mg/kg bw simultaneously for 2 weeks.

Parameters	Control	TAA-treated	RSV-treated	TAA+RSV-treated
BUN (mg/mg protein)	18.31 \pm 2.9 ^b	44.03 \pm 1.9 ^{acd}	20.7 \pm 1.6 ^b	17.88 \pm 2.0 ^b
Creatinine (mg/mg protein)	0.31 \pm 0.06 ^{bcd}	0.58 \pm 0.03 ^{ac}	0.44 \pm 0.02 ^{bd}	0.37 \pm 0.03 ^{bc}
Creatine kinase (U/mg protein)	57.71 \pm 2.6 ^b	67.66 \pm 1.6 ^{ac}	58.26 \pm 1.8 ^b	60.28 \pm 5.9 ^b
Lipid peroxidation (mmoles/mg protein)	2.20 \pm 0.537 ^{bc}	4.24 \pm 0.57 ^{acd}	1.81 \pm 0.71 ^{abd}	2.38 \pm 0.12 ^b
Catalase (U/mg protein)	1.08 \pm 0.46 ^{bd}	0.33 \pm 0.06 ^{ad}	0.98 \pm 0.22 ^b	1.33 \pm 0.23 ^b

^aSignificant ($P < 0.05$) compared to control; ^bsignificant ($P < 0.05$) compared to TAA-treated group; ^csignificant ($P < 0.05$) compared to with the RSV-treated group; ^dsignificant ($P < 0.05$) compared to simultaneous treatment of TAA+RSV-treated group.

catalase, and 8-OHdG) protection of RSV were assessed along with the relevant cytokine markers (IL-4, TNF- α , and IFN- γ). An increase in BUN, creatinine, and creatine kinase in the TAA-treated group indicated insufficiency in renal function. Previous studies reported that in acute tubular necrosis, tubular injury is mainly responsible for the reduced glomerular filtration. It was also suggested that the tubular abnormalities involved are blockage of tubules causing backward flow of glomerular filtrate [30]. Thus, renal insufficiency in TAA-treated rats might be secondary to ROS [31]. Reduced catalase activity was observed in the TAA group (Table 1) when compared to the control group, suggesting a decreased antioxidant potential in the TAA group. In addition, the catalase levels observed in the RSV- and TAA-treated group were similar to that of the control group, suggesting a reversal of the reduced antioxidant activity due to RSV treatment. It was found that the inflammatory markers, IL-4, TNF- α , and IFN- γ , were significantly reversed in the rat group simultaneously treated with TAA and RSV when compared to the increased levels observed in the TAA-treated group. Oxidative stress in other tissues caused by TAA has been reported in many studies; however, studies on kidney tissue are almost negligible [1, 32–34]. Many

reports suggest that the oxidative stress caused by TAA may cause many diseases and pathologies. In this study, we found an increase in IL-4 expression in the TAA-treated kidney of rats, which was completely reversed by RSV treatment. Oxidative stress is an essential trigger for the activation of NF κ B in ischemia reperfusion injury. This results in the activation of p38 MAPK, which may be involved in the NF κ B activation that leads to TNF- α production [35]. Other studies have reported the induction of IL-6 expression during the development of acute kidney injury both in humans [36] and in experimental animal models [37, 38]; however, a study of IL-4 expression was not performed. IL-4 is a cytokine that can affect the activity of many types of tissues and can possess both proinflammatory and anti-inflammatory properties. Its upregulation leads to the infiltration of neutrophils in the renal tissue, hence the progression of renal injury [39]. In this study, we found that TAA treatment increased IFN- γ levels with respect to the control (i.e., inflammation at selected dose (10 mg/kg bw)). The primary function of IFN- γ is to limit damage to tissues in inflammation that would activate macrophages and NK cells to name a few that play major roles in tissue repair. Many studies have reported that IFN- γ induction increases ROS production in cells and increased

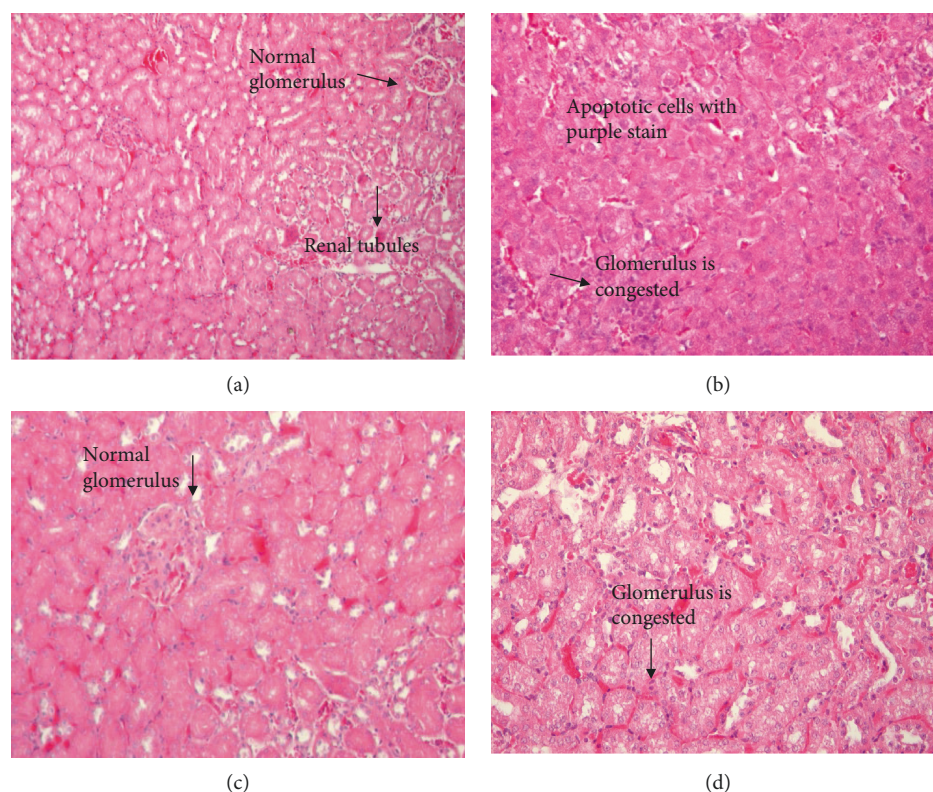


FIGURE 5: HE staining of thioacetamide and resveratrol treatments in kidney tissue sections at 40x. (a) Control group: having normal glomerulus and kidney tubules. (b) TAA-treated group: TAA treatment led to distortion of the glomerulus with apoptotic cells. (c) RSV-treated group: having normal glomerulus and tubules. (d) RSV+TAA-treated group: treatment with RSV before TAA preserved glomerular congestion while congestion of tubules and apoptotic cells were completely treated.

ROS production contributes to IFN- γ -induced cell apoptosis to serve as a preventive measure in tissue injury [40, 41].

TAA increased DNA damage with increased 8-OHdG generation; however, treatment with RSV reversed this change. 8-OHdG is one of the markers induced by ROS that reflect oxidative damage [42]. Increased levels of 8-OHdG in cells is the best indicator of oxidative stress caused by degenerative diseases such as cancer [43]. Consistently, Zhang et al. [44] found induced level of 8-OHdG in urine sample from subjects exposed to formaldehyde. In addition, increased levels of 8-OHdG due to oxidative DNA damage based on urine samples of children with acute leukemia have been reported [45]. Increase in lipid peroxidation has been reported in many oxidative stress-induced renal injuries [46–48]. In our study, TAA also caused an increase in lipid peroxidation, and the effect was reversed in the group simultaneously treated with RSV and TAA. We emphasize its simultaneous use with TAA exposure, if any.

Data Availability

The data used to support the findings of this study are available from the corresponding author upon request.

Conflicts of Interest

The authors declare no conflicts of interest.

Acknowledgments

The authors would like to extend their sincere appreciation to the Deanship of Scientific Research at King Saud University (no. RG-1438-042) for funding the research.

References

- [1] S. Ghosh, A. Sarkar, S. Bhattacharyya, and P. C. Sil, "Silymarin protects mouse liver and kidney from thioacetamide induced toxicity by scavenging reactive oxygen species and activating PI3K-Akt pathway," *Frontiers in Pharmacology*, vol. 7, p. 481, 2016.
- [2] F. A. Kadir, F. Othman, M. A. Abdulla, F. Hussan, and P. Hassandarvish, "Effect of *Tinospora crispa* on thioacetamide-induced liver cirrhosis in rats," *Indian Journal of Pharmacology*, vol. 43, no. 1, pp. 64–68, 2011.
- [3] H. E. Gunning, "Thioacetamide as a sulfide precipitant in qualitative and quantitative analysis," *Journal of Chemical Education*, vol. 32, no. 5, p. 258, 1955.
- [4] L. Lehrman, "Thioacetamide as a source of hydrogen sulfide in qualitative analysis," *Journal of Chemical Education*, vol. 32, no. 9, p. 474, 1955.
- [5] M. T. Pritchard and U. Apte, "Models to study liver regeneration," in *Liver Regeneration, Basic Mechanisms, Relevant Models and Clinical Applications*, pp. 15–40, Academic Press, 2015.

- [6] S. Zargar, T. A. Wani, A. A. Alamro, and M. A. Ganaie, "Amelioration of thioacetamide-induced liver toxicity in Wistar rats by rutin," *International Journal of Immunopathology and Pharmacology*, vol. 30, no. 3, pp. 207–214, 2017.
- [7] E. Moreira, L. Fontana, J. L. Periago, F. S. de Medina, and Á. Gil, "Changes in fatty acid composition of plasma, liver microsomes, and erythrocytes in liver cirrhosis induced by oral intake of thioacetamide in rats," *Hepatology*, vol. 21, no. 1, pp. 199–206, 1995.
- [8] S. Zargar, N. J. Siddiqi, S. K. Al Daihan, and T. A. Wani, "Protective effects of quercetin on cadmium fluoride induced oxidative stress at different intervals of time in mouse liver," *Acta Biochimica Polonica*, vol. 62, no. 2, pp. 207–213, 2015.
- [9] E. A. Barker and E. A. Smuckler, "Nonhepatic thioacetamide injury. II. The morphologic features of proximal renal tubular injury," *The American Journal of Pathology*, vol. 74, no. 3, pp. 575–590, 1974.
- [10] H. Hajovsky, G. Hu, Y. Koen et al., "Metabolism and toxicity of thioacetamide and thioacetamide S-oxide in rat hepatocytes," *Chemical Research in Toxicology*, vol. 25, no. 9, pp. 1955–1963, 2012.
- [11] S. Zargar, A. R. A. Al-Majed, and T. A. Wani, "Potentiating and synergistic effect of grapefruit juice on the antioxidant and anti-inflammatory activity of aripiprazole against hydrogen peroxide induced oxidative stress in mice," *BMC Complementary and Alternative Medicine*, vol. 18, no. 1, pp. 106–113, 2018.
- [12] S. Zargar, N. J. Siddiqi, T. H. Khan, and I. E. Elredah, "Effect of cadmium fluoride and quercetin on *in vivo* activity of indoleamine 2,3-dioxygenase in mice liver and kidney," *Fluoride*, vol. 47, pp. 31–42, 2014.
- [13] S. Ogura and T. Shimosawa, "Oxidative stress and organ damages," *Current Hypertension Reports*, vol. 16, no. 8, p. 452, 2014.
- [14] J. A. Baur and D. A. Sinclair, "Therapeutic potential of resveratrol: the *in vivo* evidence," *Nature Reviews Drug Discovery*, vol. 5, no. 6, pp. 493–506, 2006.
- [15] P. K. Bagul, N. Deepthi, R. Sultana, and S. K. Banerjee, "Resveratrol ameliorates cardiac oxidative stress in diabetes through deacetylation of NFkB-p65 and histone 3," *The Journal of Nutritional Biochemistry*, vol. 26, no. 11, pp. 1298–1307, 2015.
- [16] U. Hoda, N. B. Agarwal, D. Vohora, S. Parvez, and S. Raisuddin, "Resveratrol suppressed seizures by attenuating IL-1 β , IL1-Ra, IL-6, and TNF- α in the hippocampus and cortex of kindled mice," *Nutritional Neuroscience*, vol. 20, no. 9, pp. 497–504, 2017.
- [17] S. S. Leonard, C. Xia, B. H. Jiang et al., "Resveratrol scavenges reactive oxygen species and effects radical-induced cellular responses," *Biochemical and Biophysical Research Communications*, vol. 309, no. 4, pp. 1017–1026, 2003.
- [18] F. Uenobe, S. Nakamura, and M. Miyazawa, "Antimutagenic effect of resveratrol against Trp-P-1," *Mutation Research*, vol. 373, no. 2, pp. 197–200, 1997.
- [19] A. A. Bertelli, F. Ferrara, G. Diana et al., "Resveratrol, a natural stilbene in grapes and wine, enhances intraphagocytosis in human promonocytes: a co-factor in antiinflammatory and anticancer chemopreventive activity," *International Journal of Tissue Reactions*, vol. 21, pp. 93–104, 1999.
- [20] S. Soylemez, H. Gurdal, A. Sepici, and F. Akar, "The effect of long-term resveratrol treatment on relaxation to estrogen in aortae from male and female rats: role of nitric oxide and superoxide," *Vascular Pharmacology*, vol. 49, no. 2-3, pp. 97–105, 2008.
- [21] B. Olas and B. Wachowicz, "Resveratrol, a phenolic antioxidant with effects on blood platelet functions," *Platelets*, vol. 16, no. 5, pp. 251–260, 2005.
- [22] B. B. Aggarwal, A. Bhardwaj, R. S. Aggarwal, N. P. Seeram, and S. Y. Shishodia, "Role of resveratrol in prevention and therapy of cancer: preclinical and clinical studies," *Anticancer Research*, vol. 24, no. 5A, pp. 2783–2840, 2004.
- [23] S. Das and D. K. Das, "Resveratrol: a therapeutic promise for cardiovascular diseases," *Recent Patents on Cardiovascular Drug Discovery*, vol. 2, no. 2, pp. 133–138, 2007.
- [24] J. M. Yousef, G. Chen, P. A. Hill, R. L. Nation, and J. Li, "Melatonin attenuates colistin-induced nephrotoxicity in rats," *Antimicrobial Agents and Chemotherapy*, vol. 55, no. 9, pp. 4044–4049, 2011.
- [25] H. G. Utey, F. Bernheim, and P. Hochstein, "Effect of sulfhydryl reagents on peroxidation in microsomes," *Archives of Biochemistry and Biophysics*, vol. 118, no. 1, pp. 29–32, 1967.
- [26] H. Aebi, "[13] Catalase *in vitro*," *Methods in Enzymology*, vol. 105, pp. 121–126, 1984.
- [27] M. A. K. Markwell, S. M. Haas, L. L. Bieber, and N. E. Tolbert, "A modification of the Lowry procedure to simplify protein determination in membrane and lipoprotein samples," *Analytical Biochemistry*, vol. 87, no. 1, pp. 206–210, 1978.
- [28] S. M. Van der Made, J. Plat, and R. P. Mensink, "Resveratrol does not influence metabolic risk markers related to cardiovascular health in overweight and slightly obese subjects: a randomized, placebo-controlled crossover trial," *PLoS One*, vol. 10, no. 3, article e0118393, 2015.
- [29] O. Vang, N. Ahmad, C. A. Baile et al., "What is new for an old molecule? Systematic review and recommendations on the use of resveratrol," *PLoS One*, vol. 6, no. 6, 2011.
- [30] A. Whelton and K. Solez, "Pathophysiologic mechanisms in aminoglycoside nephrotoxicity," *Journal of Clinical Pharmacology*, vol. 23, no. 10, pp. 453–460, 1983.
- [31] P. Leena and B. R. Alaraman, "Effect of green tea extract on cisplatin induced oxidative damage on kidney and testes of rats," *Ars Pharmaceutica*, vol. 46, pp. 5–18, 2005.
- [32] N. A. Bayomy, E. Z. Abdelaziz, M. A. Said, M. S. Badawi, and R. H. el-Bakary, "Effect of pycnogenol and spirulina on vancomycin-induced renal cortical oxidative stress, apoptosis, and autophagy in adult male albino rat," *Canadian Journal of Physiology and Pharmacology*, vol. 94, no. 8, pp. 838–848, 2016.
- [33] G. R. Romualdo, T. F. Grassi, R. L. Goto et al., "An integrative analysis of chemically-induced cirrhosis-associated hepatocarcinogenesis: histological, biochemical and molecular features," *Toxicology Letters*, vol. 281, pp. 84–94, 2017.
- [34] I. M. Sabler, M. Berkovitch, J. Sandbank et al., "Exposure to hyperbaric oxygen intensified vancomycin-induced nephrotoxicity in rats," *PLoS One*, vol. 11, no. 4, article e0152554, 2016.
- [35] N. S. Dhalla, L. Golfman, S. Takeda, N. Takeda, and M. Nagano, "Evidence for the role of oxidative stress in acute ischemic heart disease: a brief review," *The Canadian Journal of Cardiology*, vol. 15, pp. 587–593, 1999.
- [36] E. M. Simmons, J. Himmelfarb, M. T. Sezer et al., "Plasma cytokine levels predict mortality in patients with acute renal

- failure," *Kidney International*, vol. 65, no. 4, pp. 1357–1365, 2004.
- [37] S. Lemay, H. Rabb, G. Postler, and A. K. Singh, "Prominent and sustained up-regulation of gp130-signaling cytokines and of the chemokine MIP-2 in murine renal ischemia-reperfusion injury," *Transplantation*, vol. 69, no. 5, pp. 959–963, 2000.
- [38] V. S. Vaidya, K. Shankar, E. A. Lock, D. Dixon, and H. M. Mehendale, "Molecular mechanisms of renal tissue repair in survival from acute renal tubule necrosis: role of ERK1/2 pathway," *Toxicologic Pathology*, vol. 31, no. 6, pp. 604–618, 2003.
- [39] Y. Nechemia-Arbely, D. Barkan, G. Pizov et al., "IL-6/IL-6R axis plays a critical role in acute kidney injury," *Journal of the American Society of Nephrology*, vol. 19, no. 6, pp. 1106–1115, 2008.
- [40] R. J. Thapa, S. H. Basagoudanavar, S. Nogusa et al., "NF- κ B protects cells from gamma interferon-induced RIP1-dependent necroptosis," *Molecular and Cellular Biology*, vol. 31, no. 14, pp. 2934–2946, 2011.
- [41] D. Yang, S. G. Elner, Z. M. Bian, G. O. Till, H. R. Petty, and V. M. Elner, "Pro-inflammatory cytokines increase reactive oxygen species through mitochondria and NADPH oxidase in cultured RPE cells," *Experimental Eye Research*, vol. 85, no. 4, pp. 462–472, 2007.
- [42] B. Halliwell and J. M. C. Gutteridge, "Free radicals, other reactive species and disease," in *Free Radicals in Biology and Medicine*, B. Halliwell and J. M. C. Gutteridge, Eds., pp. 617–783, Oxford University Press, New York, NY, U.S.A., Third edition edition, 1999.
- [43] Q. H. Yao, S. R. Mei, Q. F. Weng et al., "Determination of urinary oxidative DNA damage marker 8-hydroxy-2'-deoxyguanosine and the association with cigarette smoking," *Talanta*, vol. 63, no. 3, pp. 617–623, 2004.
- [44] B. Y. Zhang, Y. Q. Shi, X. Chen et al., "Protective effect of curcumin against formaldehyde -induced genotoxicity in A549 cell lines," *Journal of Applied Toxicology*, vol. 33, no. 12, pp. 1468–1473, 2013.
- [45] A. Valavanidis, T. Vlachogianni, and C. Fiotakis, "8-hydroxy-2'-deoxyguanosine (8-OHdG): a critical biomarker of oxidative stress and carcinogenesis," *Journal of Environmental Science and Health, Part C*, vol. 27, no. 2, pp. 120–139, 2009.
- [46] R. Dhanarajan, P. Abraham, and B. Isaac, "Protective effect of ebselen, a selenoorganic drug, against gentamicin-induced renal damage in rats," *Basic & Clinical Pharmacology & Toxicology*, vol. 99, no. 3, pp. 267–272, 2006.
- [47] B. R. Guidet and S. V. Shah, "In vivo generation of hydrogen peroxide by rat kidney cortex and glomeruli," *American Journal of Physiology-Renal Physiology*, vol. 256, no. 1, pp. F158–F164, 1989.
- [48] G. Sener, A. O. Sehirli, H. Z. Altunbas et al., "Melatonin protects against gentamicin-induced nephrotoxicity in rats," *Journal of Pineal Research*, vol. 32, no. 4, pp. 231–236, 2002.

Research Article

Danhong Injection Alleviates Postoperative Intra-abdominal Adhesion in a Rat Model

Yunhua Wu ¹, Guangbing Wei,¹ Junhui Yu,¹ Zilu Chen,¹ Zhengshui Xu,¹ Rui Shen,¹ Ting Liang,^{2,3} Lu Zheng,⁴ Kang Wang,¹ Xuejun Sun ¹, and Xuqi Li ¹

¹Department of General Surgery, The First Affiliated Hospital of Xi'an Jiaotong University, Xi'an, 710061 Shaanxi, China

²Department of Radiology, The First Affiliated Hospital of Xi'an Jiaotong University, Xi'an, 710061 Shaanxi, China

³Department of Biomedical Engineering, the Key Laboratory of Biomedical Information Engineering of the Ministry of Education, School of Life Science and Technology, Xi'an Jiaotong University, Xi'an, 710061 Shaanxi, China

⁴Department of Physical Examination, The First Affiliated Hospital of Xi'an Jiaotong University, Xi'an, 710061 Shaanxi, China

Correspondence should be addressed to Xuejun Sun; sunxy@mail.xjtu.edu.cn and Xuqi Li; lixuqi@163.com

Received 25 April 2019; Accepted 1 July 2019; Published 19 August 2019

Guest Editor: Reggiani Vilela Gonçalves

Copyright © 2019 Yunhua Wu et al. This is an open access article distributed under the Creative Commons Attribution License, which permits unrestricted use, distribution, and reproduction in any medium, provided the original work is properly cited.

Background. Among all the common complications that occur after abdominal surgery, intestinal adhesion is perhaps the most unpleasant one. However, current methods to treat and prevent intestinal adhesion are limited; thus, exploring new methods to prevent and treat intestinal adhesion is greatly needed. In this study, we demonstrated that Danhong injection (DHI) may be used as a promising method to prevent and treat intra-abdominal adhesion in a rat model. **Materials and Methods.** Forty-eight rats were randomly divided into six groups. Except for the sham-operated group, all rats underwent cecal abrasion to establish an adhesion model. After the operation, the rats in the DHI-treated groups received different doses of DHI via the tail vein daily, while the other group was treated with the same volume of saline solution. Seven days after the operation, all rats were sacrificed, and the degree of adhesion was evaluated by Nair's scoring system. The extent of inflammation in the adhesion tissue was detected by HE staining and the expression of tumor necrosis factor- α (TNF- α) and transforming growth factor- β (TGF- β). The collagen deposition was assessed by Sirius red staining and α -SMA, MMP9, t-PA, and PAI-1 levels. Oxidative stress was indicated by the level of reactive oxygen species (ROS) in adhesion tissues and by immunohistochemical labeling of Nrf2. Furthermore, rat primary peritoneal mesothelial cells (RPMCs) were treated with H₂O₂ and DHI, and NF- κ B phosphorylation was detected to illustrate the effect of DHI on oxidative stress. **Results.** The intra-abdominal adhesion scores were significantly decreased in the groups treated with a high dose of DHI compared with the control groups, and the degree of inflammation, fibrosis, and oxidative stress was also significantly decreased. DHI treatment significantly reduced the levels of TNF- α , TGF- β 1, and PAI and increased the expression levels of MMP9, Nrf2, and t-PA in the adhesion tissues. ROS levels and NF- κ B phosphorylation were significantly reduced in DHI-treated RPMCs compared with the control RPMCs. **Conclusion.** DHI alleviates the formation of postoperative intra-abdominal adhesions by inhibiting inflammation, collagen deposition, and oxidative stress in a rat model and may serve as a promising drug to prevent intra-abdominal adhesions.

1. Introduction

Intra-abdominal adhesion is one of the most common complications after abdominal surgery [1]. After this operation, injury or trauma can cause inflammation, which in turn leads to collagen deposition and the development of intra-abdominal adhesion [2]. Adhesion formation is a process that involved the repair of injured peritoneal tissue; if the

damaged tissue is repaired in time, adherence will not occur or limited adhesion will occur; otherwise, adhesion will occur [3]. Even though various methods have attempted to prevent postoperative adhesion, their effects are far from satisfactory. Surgeons continue to attempt to discover effective ways to prevent and treat adhesion formation [4].

Oxidative stress is used to describe the abnormal condition in which the balance between reactive oxygen

species (ROS) or reactive nitrogen species (RNS) and antioxidant systems, including enzymes and nonenzyme particles, is destroyed [5]. After abdominal surgery, both an increase in ROS/RNS production and the suppression of the antioxidant system result in the development of adhesion via oxidative stress [6]. The loss of balance between these systems will not only lead to an exacerbated inflammation reaction but can also harm peritoneal tissue repair. Thus, alleviating ROS may be a potential way to prevent postoperative adhesion.

Danhong injection (DHI), a traditional Chinese medicine, was extracted from *Salviae miltiorrhizae* Radix and *Carthami tinctorii* Flos. The main bioactive constituents in DHI include salvianic acid A, salvianic acid B, protocatechuic aldehyde, and rosmarinic acid [7]. In a previous study, DHI was demonstrated to exert many effects, such as anti-inflammatory, antioxidant, anticoagulatory, hypolipidemic, antiapoptotic, vasodilatory, and angiogenesis-promoting actions [8, 9], and DHI is widely used in the treatment of cerebral ischemia and cardiovascular diseases [10]. The postoperative adhesion develops through interactions between inflammation and collagen deposition; thus, we hypothesize that DHI may have a protective effect on postoperative abdominal adhesion. Based on this hypothesis, our study was designed and conducted to show the ability of DHI to prevent postoperative adhesion by reducing inflammation, collagen deposition, and oxidative stress.

2. Materials and Methods

2.1. Experimental Animals and Reagents. Forty-eight Sprague-Dawley (SD) rats weighing 200 g to 250 g were obtained from the Experimental Animal Center of Xi'an Jiaotong University. These rats were freely housed in a thermostatic room at approximately $22 \pm 2^\circ\text{C}$. DHI was purchased from Heze Buchang Pharmaceutical Co. Ltd. (Heze, China) and diluted in 0.9% saline.

2.2. Experimental Preparation and Design. Abdominal hair was removed one day before the operation. Anesthesia was performed by the intraperitoneal injection of 50 mg/kg phenobarbital sodium (GuideChem, Shanghai, China). Then, the skin was sterilized with pyrrolidone iodine three times. A 2 to 3 centimeter incision was created at the middle of the abdomen. Except for the sham-operated group, an intra-abdominal adhesion model was established in all the rats by scraping the abdominal and bilateral intestinal wall as described in previous studies [11]. The rats in the sodium hyaluronate (HA) group were then treated with 2 mL of HA gel (Qingdao Haitao Biochemical Co. Ltd., Qingdao, China) before the abdomen was closed. After the skin was disinfected again, the abdominal cavity was closed by an intermittent suture in two layers. Within one week after the operation, the rats in the DHI group received an intravenous injection in the tail of 0.8 mL of different doses of DHI. The doses for the DHI1 group, DHI2 group, and DHI3 group were 1 mL/kg, 2 mL/kg, and 4 mL/kg, respectively. The rats in the other three groups were injected with 0.8 mL of saline daily.

2.3. Assessment of General Adhesion in the Specimens. Seven days later, the rats were anesthetized as previously described and sacrificed [11]. The abdominal cavity was opened by a U-incision. The status of intra-abdominal adhesion was evaluated by Nair et al.'s [12] scoring system (Supplemental Table 1). Then, samples of adhesion tissues were removed and divided into two parts: one part was fixed in 4% formalin, and the other part was stored at -80°C for ROS detection. Specifically, the cecum and abdominal tissues were collected from the sites with the most severe adhesion, whereas the cercal lesions and corresponding peritoneal tissues were collected from nonadhesion tissues.

2.4. Pathological Assessment. Twenty-four hours after soaking in formalin, the specimen was embedded in paraffin and sliced into $4\ \mu\text{m}$ thick pathological sections. Four incisions were randomly selected from each pathological tissue for hematoxylin and eosin (HE) staining, and the results were observed by light microscopy. Samples were evaluated based on the scoring system used in previous studies [13]. The inflammatory response was scored as follows (Supplemental Table 2): 0 for cases with no inflammatory cells; 1 for cases with observable macrophages, lymphocytes, and plasma cells; 2 for cases with macrophages, plasma cells, eosinophils, and neutrophils; and 3 for cases with inflammatory cell infiltration and microabscess formation. All scores were evaluated by two pathologists from our university. Five fields under high-magnification microscopy were randomly selected from each pathological section for scoring, and the average score of each rat was used as the final score.

2.5. Sirius Red Picric Acid Staining. More than 5 pathological sections were randomly selected for Sirius red picric acid staining using the experimental method. Staining was performed with 0.1% Sirius red picric acid (Direct Red 80; Sigma-Aldrich, St. Louis, MO, USA), followed by counterstaining with hematoxylin. Five high-magnification fields were randomly selected from each pathological section to measure the width of collagen tissue by using Image-Pro Plus 5.0 software (Leica Qwin. Plus, Leica Microsystem Imaging Solutions Ltd., Cambridge, UK). The average thickness of the adhesive area of each tissue was considered the thickness of the adhesive area of each tissue.

2.6. Immunohistochemistry. In this study, immunohistochemistry was performed with a SABC kit (Maxim, Fuzhou, China). All experimental procedures were performed following the operation manual's instructions. The sections were incubated with an α -SMA primary antibody (GB13044, Servicebio, Hubei, China, 1:200), MMP9 primary antibody (GB13044, Servicebio, Hubei, China, 1:200), and Nrf-2 primary antibody (GB13044, Servicebio, Hubei, China, 1:200) at 4°C overnight. Subsequently, the sections were incubated with a ubiquitinated secondary antibody at room temperature for 30 min, followed by streptavidin peroxidase for 30 min at the same temperature. Then, DAB development, hematoxylin counterstaining, further dehydration, and mounting were performed. Five high-magnification fields were randomly selected from each section for

immunohistochemistry scoring to obtain the average of all the sections of each tissue as the final score. The sections were scored as follows: 0 represented tissues with no expression, 1 represented tissues with weakly positive expression, 2 represented tissues with positive expression, 3 represented tissues with strongly positive expression, and 4 represented tissues with extremely abundant expression.

2.7. Western Blot. Protein extraction from tissue samples was performed using the RIPA Protein Extraction Kit (Thermo Fisher Scientific, USA) following the operation manual. Western blotting was performed as described in the literature [11]. The extracted proteins were subjected to 12% sodium dodecyl sulfate polyacrylamide gel electrophoresis and then transferred to a PVDF membrane. After blocking with 5% milk for 1 h, the membrane was incubated with the primary antibody at 4°C overnight. The primary antibodies included anti-NF- κ B (catalog no. Ab16502, Abcam, Cambridge, UK, 1:1000 dilution), anti-NF- κ B (phospho S536) (catalog number ab86299, Abcam, Cambridge, 1:1000 dilution), and anti-b-GAPDH (sc-47778, Santa Cruz Biotechnology, 1:1000 dilution). After incubation, the PVDF membrane was rinsed and then incubated with the secondary antibody for 1 h at room temperature. Then, the protein expression was detected by using a chemiluminescence detection system (Millipore, Billerica, MA, USA).

2.8. ELISA. Enzyme-linked immunosorbent assay (ELISA) was performed according to the manufacturer's description. The indexes included tissue-type plasminogen activator (t-PA) (CSB-E07917r, Shanghai Ximei Chemical Co. Ltd., Shanghai, China), plasminogen-activating inhibitor (PAI-1) (CSB-E07948r, Shanghai Ximei Chemical Co. Ltd., Shanghai, China), TNF- α (88-7340, Thermo Fisher Scientific, Waltham, America), and TGF- β 1 (CSB-E04727r, Shanghai Ximei Chemical Co. Ltd., Shanghai, China).

2.9. Isolation and Culture of RPMCs and of ROS. The isolated and cultured rat primary peritoneal mesothelial cells (RPMCs) were performed as previously described [14]. Male SD rats weighing 150-250 g were intraperitoneally injected with 25 mL of 0.25% trypsinase-0.02% EDTA-Na₂. The fluid in the abdominal cavity was collected after 30 min and centrifuged at 1000 rpm for 10 min. The cells were cultured in 15% (v/v) FBS DMEM/F12 medium in 25 cm² tissue culture flasks at 37°C in a humidified 5% CO₂ atmosphere. The cells were passaged every 3-5 days, and RPMCs from the second and third passages at 80% confluence were used for the following experiments. Before quantifying the ROS levels, the RPMCs (5 × 10⁶) were grown on cover slips. Then, the cells in the DHI-treated group were kept in 2% DHI solutions for 24 hours, while the control group was treated with the same dose of PBS. Then, both groups were treated with 50 μM/L H₂O₂ (Sigma Chemical Co., St. Louis, MO, USA) for 1 hour. ROS detection experiments were performed as previously described [15] by a ROS assay kit (KGT010-1, Nanjing KeyGen Biotech. Co. Ltd, China). After washing three times, the cover slips were incubated with 10 μM/L DCFH-DA serum-free DMEM/F12 medium for 30 min in a

37°C environment in the dark. Then, the cells were washed again and mounted on a microslide. The intracellular ROS levels were then detected by a confocal ultraspectral Leica microscope at an excitation wavelength of 488 nm and an emission wavelength of 525 nm.

2.10. The Detection of ROS in Adhesion Tissues. The tissues stored at -80°C were prepared into consecutive frozen sections. At least four sections were used to detect the ROS in each tissue. After the sections were slightly dehydrated, the ROS dyeing solution (catG0002, Wuhan Servicebio Technology Co. Ltd., China) was added to the sectioned tissue, and the sections were incubated in a 37°C environment in the dark for 30 min. After washing three times, the slices were incubated in DAPI dyeing solution (catG1012, Wuhan Servicebio Technology Co. Ltd., China) for 10 min at room temperature. Then, the slices were washed three additional times and dried with resistance to fluorescence quenching after sealing seal tablets. These slices were observed by fluorescence microscopy, and images were collected. The ROS expression was calculated as the ratio of ROS-positive nuclei to total nuclei.

2.11. Statistical Methods. All data in this study were analyzed using SPSS 18.0 (Chicago, IL, USA), and all data are expressed as the mean ± standard deviation. The normally distributed data were compared with a *t* test or one-way ANOVA and LSD, and the data without a normal distribution were analyzed using the Kruskal-Wallis test. The counting data were processed using Fisher's exact test. A *P* value less than 0.05 was considered statistically significant.

3. Results

3.1. DHI Treatment Alleviates Intra-abdominal Adhesion. No rat died or had severe postoperative complications during the experiment. Seven days after the operation, intra-abdominal adhesion was assessed by Nair's scoring system, and the results are presented in Figure 1. The rats in the control group had extensive adhesion, and the adhesion bands were thick. Compared to the control group, both the HA- and DHI-treated groups had a moderate degree of adhesion, and the adhesion bands appeared smaller and looser in the HA- and DHI-treated groups than the control group (Figure 1(a)). Although the adhesion score exhibited a decreasing tendency in the HA- and DHI-treated groups compared with the control group, only the DHI3 group showed a statistically significant difference (Figure 1(b); *P* < 0.05). However, the preventive effect of DHI was not significantly different from the HA group. Only two rats had loose incision adhesion in the sham group, while only one rat in the DHI2 group and two rats in the DHI3 group had no adhesion. All rats in the other groups had adhesion (Figure 1(c)).

3.2. DHI Inhibits the Inflammatory Response in Adhesion Tissue. To determine the possible mechanism by which DHI reduces postoperative abdominal adhesion, we detected inflammation-related indicators. HE staining showed that the inflammation score of the DHI treatment groups that

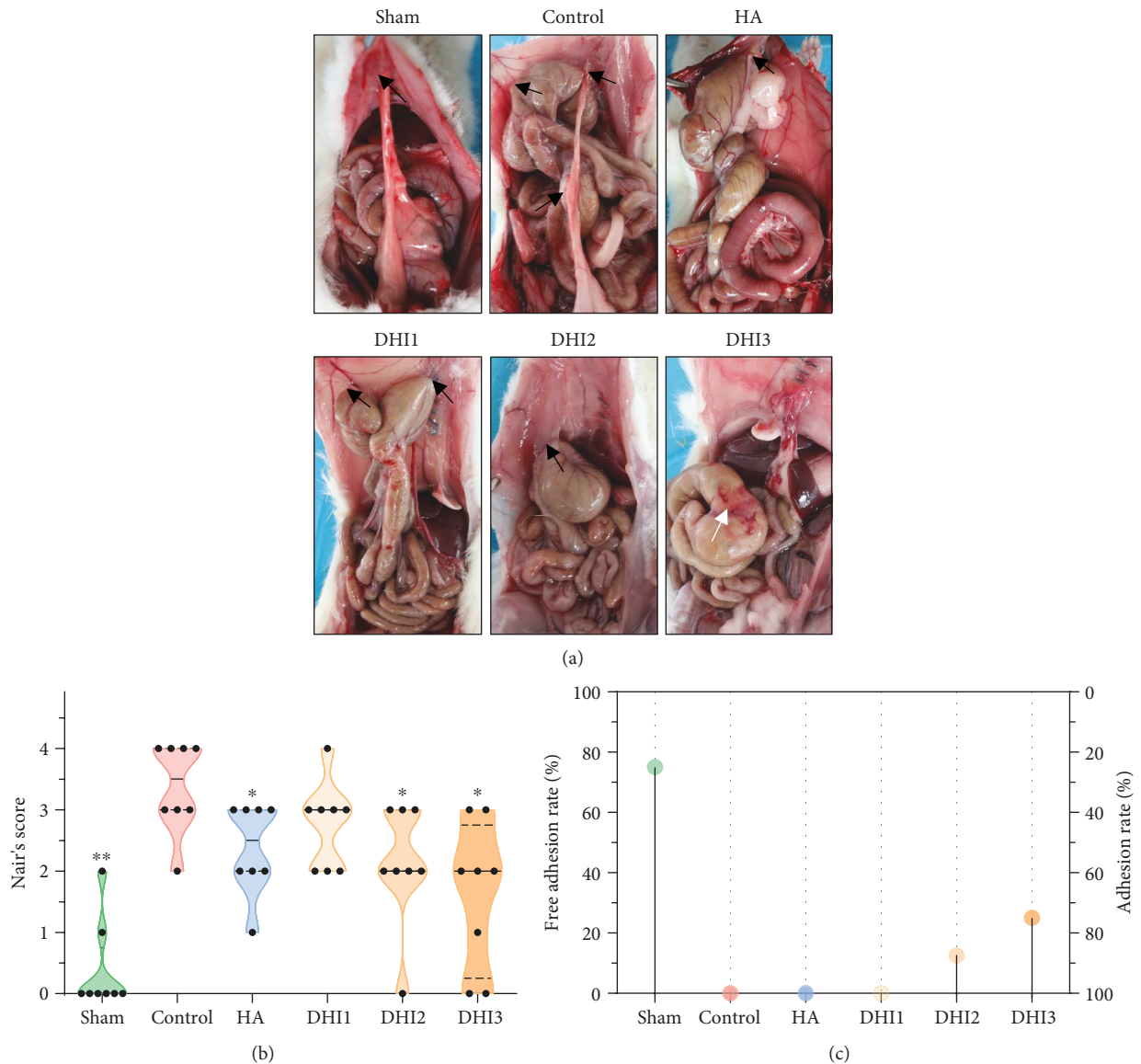


FIGURE 1: The adhesion formation conditions of different groups ($n = 8$). (a) In the sham-operated group, intra-abdominal adhesions occurred in two rats only. All rats in the control group exhibited severe adhesion. All rats in the HA-treated and DHI1 groups had moderate and loose adhesion bands. The adhesions of the rats in the DHI2 and DHI3 groups were lighter than those in the control group. One rat in the DHI2 group and two rats in the DHI3 group had no adhesion formation. The black arrows indicate adhesion on the abdominal wall. The white arrows indicate the injured serosal surface of the cecum without adhesion formation. (b) The Nair score for each group (compared with the control group, $*P < 0.05$ and $**P < 0.01$, abnormal distribution, Kruskal-Wallis test). (c) The nonadhesion rate of each group.

administered the highest doses of DHI was decreased compared with that of the control group (Figures 2(a) and 2(b)). ELISA detection of TNF- α and TGF- β 1 levels in the adhesion tissue showed that TNF- α was significantly decreased in the DHI- and HA-treated groups compared with the control group (Figure 2(c); $P < 0.05$), while TGF- β 1 was decreased in the HA- and middle- and high-DHI-treated groups compared with the control group (Figure 2(d); $P < 0.05$).

3.3. DHI Could Decrease Collagen Deposition and Promote Fibrinolysis in the Adhesion Tissue. Collagen deposition

is one of the most important reasons for adhesion formation. Sirius red staining, which reflects the collagen density of adhesion tissues, demonstrated that the fibrin thickness of the adhesion tissue in the DHI3 group was decreased compared with the control group (Figures 3(a) and 3(c); $P < 0.05$). Immunohistochemical staining of α -SMA (marker of myofibroblasts) showed that the α -SMA levels in the HA-treated group, DHI2 group, and DHI3 group were reduced compared with the control group (Figures 3(b) and 3(d); $P < 0.05$). To investigate the mechanism by which DHI reduced collagen deposition, we quantified the matrix metalloproteinase system indicator MMP9 and

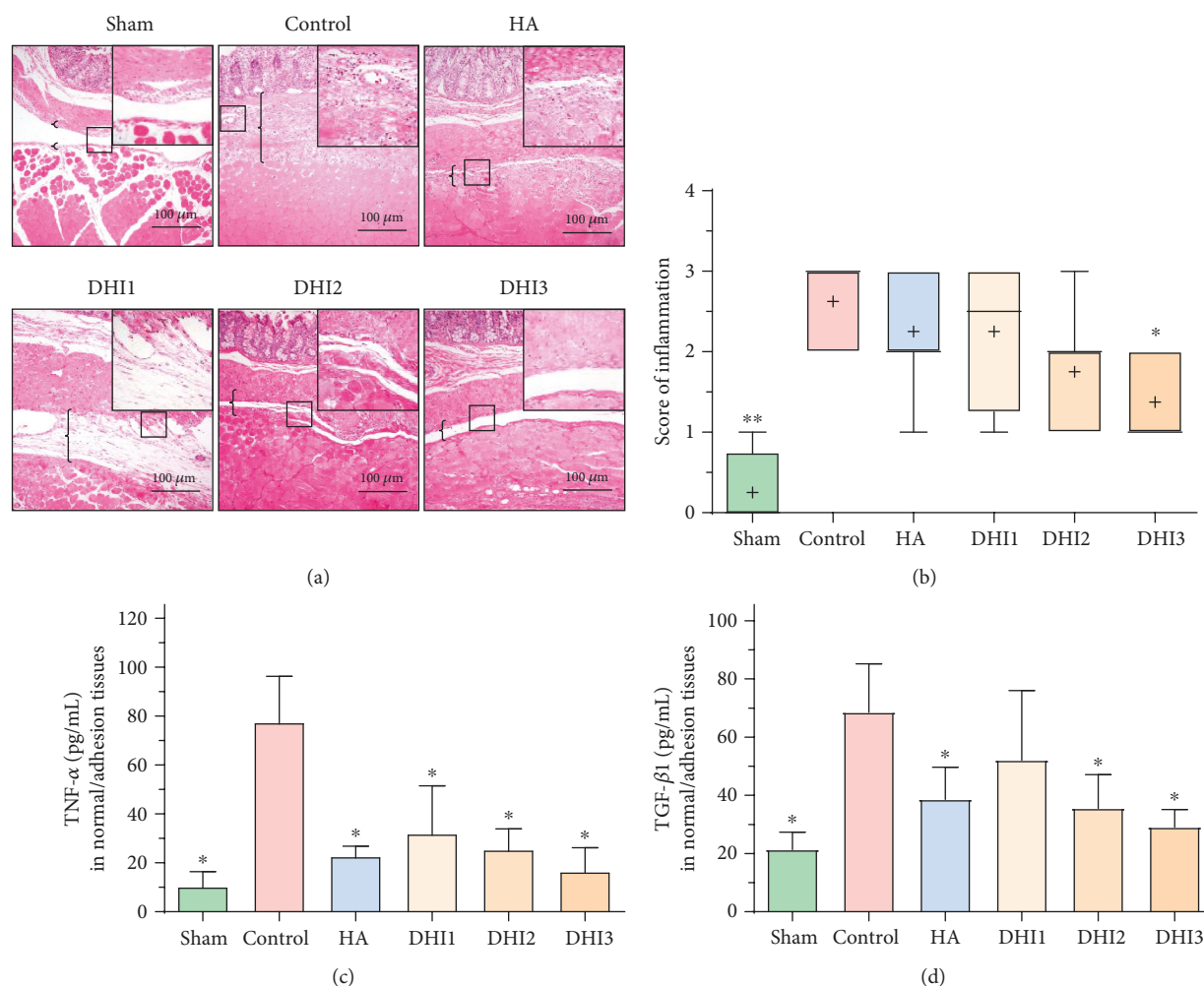


FIGURE 2: DHI treatment can reduce inflammation in adhesion tissue in the rat model 7 days after operation ($n = 8$; compared with the control group, $*P < 0.05$ and $**P < 0.01$). (a) HE staining of each group at 100x magnification. The top right corner is shown at 200x magnification. The brackets indicate tissue with adhesion. (b) The inflammatory score of each group based on HE staining (compared with the control group, $*P < 0.05$ and $**P < 0.01$, normal distribution, one-way ANOVA). (c) The TNF- α expression in each group (compared with the control group, $*P < 0.05$, abnormal distribution, Kruskal-Wallis test). (d) The TGF- β expression in each group (compared with the control group, $*P < 0.05$, abnormal distribution, Kruskal-Wallis test).

the fibrinogenolysis system indexes t-PA and PAI-1. The results demonstrated that the expression of MMP9 and t-PA in the adhesion tissues was increased in the DHI2 and DHI3 groups compared with the control group (Figures 4(a)–4(c); $P < 0.05$), whereas the level of PAI-1 was decreased in the DHI2 and DHI3 groups compared with the control group (Figure 4(d); $P < 0.05$).

3.4. DHI Reduces Oxidative Stress in Adhesion Tissues. ROS levels play an important role in adhesion formation [16]; thus, we measured a ROS-related index in vivo. The ROS level in the adhesion tissues was remarkably reduced in the DHI3 group (Figures 5(a) and 5(c); $P < 0.05$). Furthermore, we detected the expression of the antioxidative stress index Nrf2 in the adhesion tissues and found that the Nrf2 level was also increased in the DHI3 group compared with the control group (Figures 5(b) and 5(d); $P < 0.05$).

3.5. DHI Reduces Oxidative Stress in RPMCs. To further verify that DHI reduces ROS in adhesion tissue, we detected the ROS expression in RPMCs, as shown in Figures 6(a) and 6(b). When the samples were treated with the same dose of H_2O_2 , the 2% (v/v) DHI-treated group had a lower ROS level than the control group (Figures 6(a) and 6(b); $P < 0.05$). To further illustrate the mechanism by which DHI decreased ROS levels, we detected the NF- κ B expression in each group. The level of phosphorylated NF- κ B was significantly decreased in the DHI-treated groups compared with the control group (Figures 6(c) and 6(d); $P < 0.05$).

4. Discussion

The traditional Chinese medicine DHI is extracted from *S. miltiorrhizae* Radix and *C. tinctorii* Flos, and various studies have demonstrated that DHI can be used to treat

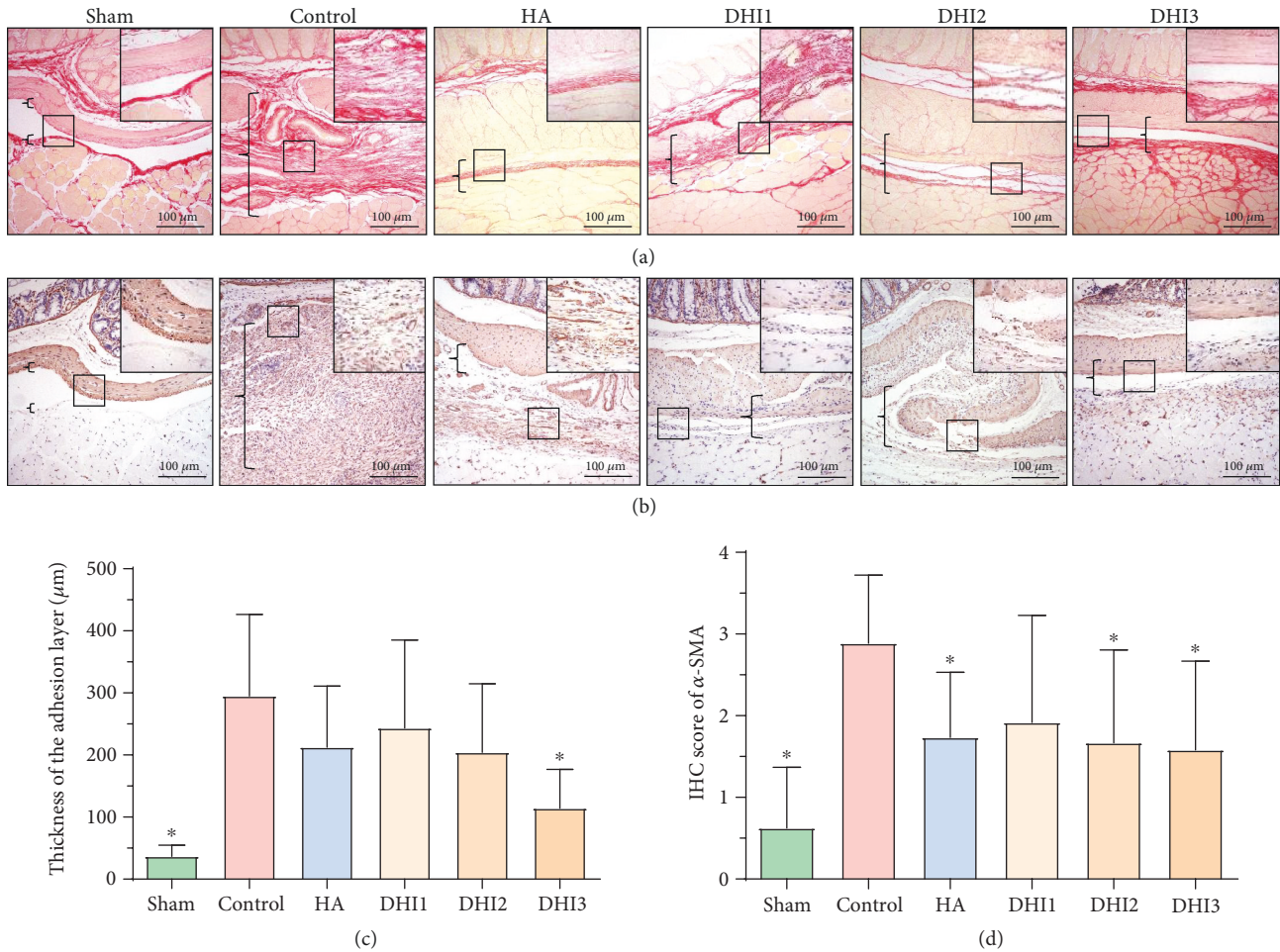


FIGURE 3: DHI treatment attenuated collagen deposition in the adhesion tissue of the rat model 7 days after operation ($n = 8$; compared with the control group, $*P < 0.05$ and $**P < 0.01$). (a) Sirius red picric acid staining of each group at 100x magnification. The top right corner is shown at 200x magnification. The brackets indicate tissue in the adhesion area. (b) α -SMA staining of each group at 100x magnification. The top right corner is shown at 200x magnification. The brackets indicate tissue in the adhesion area. (c) Adhesion thickness in each group as assessed by Sirius red picric acid staining (compared with the control group, $*P < 0.05$, abnormal distribution, Kruskal-Wallis test). (d) α -SMA staining scores of each group (compared with the control group, $*P < 0.05$, normal distribution, one-way ANOVA).

cerebral ischemia and heart diseases [17], as well as ischemia-reperfusion injury [18]. Herein, we demonstrated that DHI can be used as a potential drug to prevent postoperative adhesion by reducing inflammatory reactions, decreasing fibrosis, and alleviating oxidative stress.

The formation of intestinal adhesion is complex. Initially, injury causes and amplifies inflammation, followed by collagen deposition and adhesion [19]. In this process, the repair of the local peritoneal tissue repair also plays an important role; if the injured area can be repaired in a timely manner, limited adhesion develops. Thus, preventing the formation of abdominal adhesion after surgery requires all of these factors to be considered, and simple physical barriers may not be satisfactory. This problem has been verified in many clinical studies [20].

It is widely acknowledged that postoperative adhesion formation is stimulated by inflammation and oxidative damage [5, 21]. Trauma and injury after operation will inevitably lead to oxidative stress reactions and inflammation, and the increase in ROS can accelerate the amplification of

inflammation and damage mesothelial cells [22]. To determine whether the anti-inflammatory activity of DHI exerts a protective role in adhesion formation in a rat model, this prospective study was designed. HE staining was used as an index for inflammation. The results demonstrated that DHI treatment reduced inflammation. Additionally, the levels of cytokines such as TGF- β 1 and TNF- α in adhesion tissues were measured, and the results demonstrated that the DHI-treated groups had lower levels of TGF- β 1 and TNF- α expression in adhesion tissues than the control group. These results suggest that DHI alleviates the formation of abdominal adhesion by reducing inflammation in the adhesion tissue.

The interaction between oxidative stress and inflammation plays a critical role in adhesion formation; high concentrations of ROS can injure peritoneal mesothelial cells and promote inflammation. A previous study demonstrated that DHI reduces oxidative stress by activating superoxide dismutase (SOD) and reducing the production of malondialdehyde (MDA) in both myocardial ischemia/reperfusion

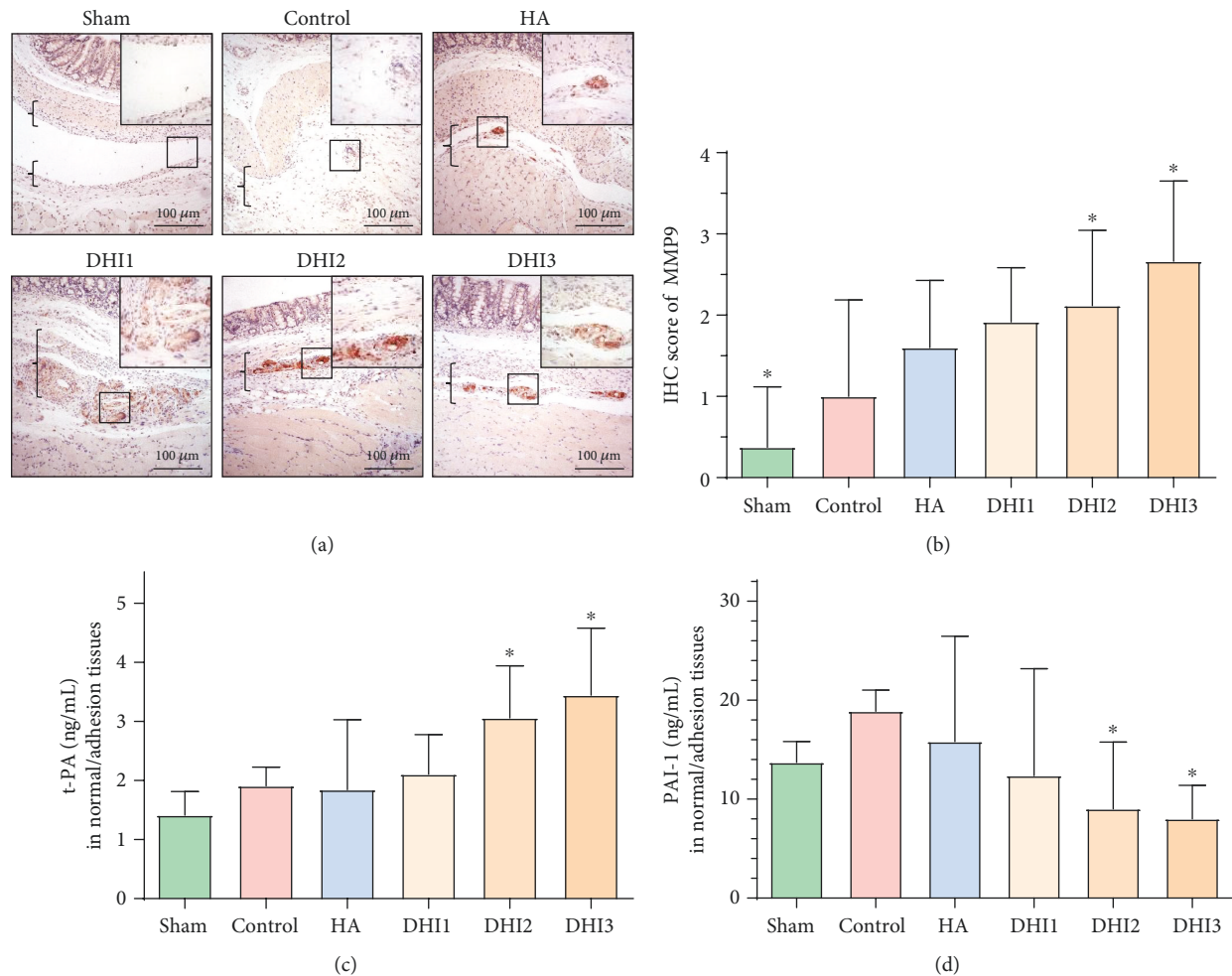


FIGURE 4: DHI treatment promoted fibrinogenolysis in the adhesion tissue of the rat model 7 days after operation ($n = 8$; compared with the control group, $*P < 0.05$). (a) MMP9 staining of each group at 100x magnification; the top right corner is shown at 200x magnification. The brackets indicate tissue in the adhesion area. (b) MMP9 staining scores of each group (compared with the control group, $*P < 0.05$, normal distribution, one-way ANOVA). (c) The t-PA expression in the adhesion tissue of each group (compared with the control group, $*P < 0.05$, abnormal distribution, Kruskal-Wallis test). (d) The PAI-1 expression in the adhesion tissue of each group (compared with the control group, $*P < 0.05$, abnormal distribution, Kruskal-Wallis test).

(MI/R) and acute lung injury (ALI) mouse models [23]. Here, we demonstrated that DHI can reduce the level of ROS in both adhesion tissue and H_2O_2 -treated mesothelial cells. To further illustrate this effect in adhesion tissue, we quantified the expression of Nrf2, which is a transcription factor that regulates an expansive set of antioxidant-related genes and acts in synergy to remove ROS through sequential enzymatic reactions [24]. We found that the expression of Nrf2 in the adhesion tissue of DHI-treated rats was increased compared with that of control rats. To explore its mechanism, we detected the expression of the important inflammation factor NF- κ B in H_2O_2 - and DHI-treated RPMCs. The results showed that DHI treatment can decrease the NF- κ B expression in mesothelial cells. This effect was consistent with previous studies [10, 25]. Therefore, these results suggest that one possible mechanism for the DHI-mediated reduction of inflammation in adhesion tissue is the inhibition of ROS via a decrease in NF- κ B phosphorylation.

Another explanation for the DHI-mediated prevention of adhesion formation may be the reduction of collagen deposition and promotion of fibrinolysis in adhesion tissues. Within seven days after operation, the balance between fibrin deposition and degradation determines whether normal peritoneal healing or adhesion formation occurs. After the operation, inflammation increased, which resulted in fibrinous exudate and fibrin formation. Fibrin forms as a result of the activation of a coagulation cascade. However, owing to the activation of the fibrinolytic and extracellular matrix system (MMPs), any intra-abdominal fibrin deposits must be lysed. t-PA is a major plasminogen activator and has a high affinity for fibrin, while MMP9 is an important enzyme classified as an MMP. Plasminogen activation is impaired by PAI-1 and its analog through the formation of inactive complexes [26]. Many studies have demonstrated that DHI can reduce collagen deposition [27]. In our study, we found that DHI increased the t-PA expression and decreased the

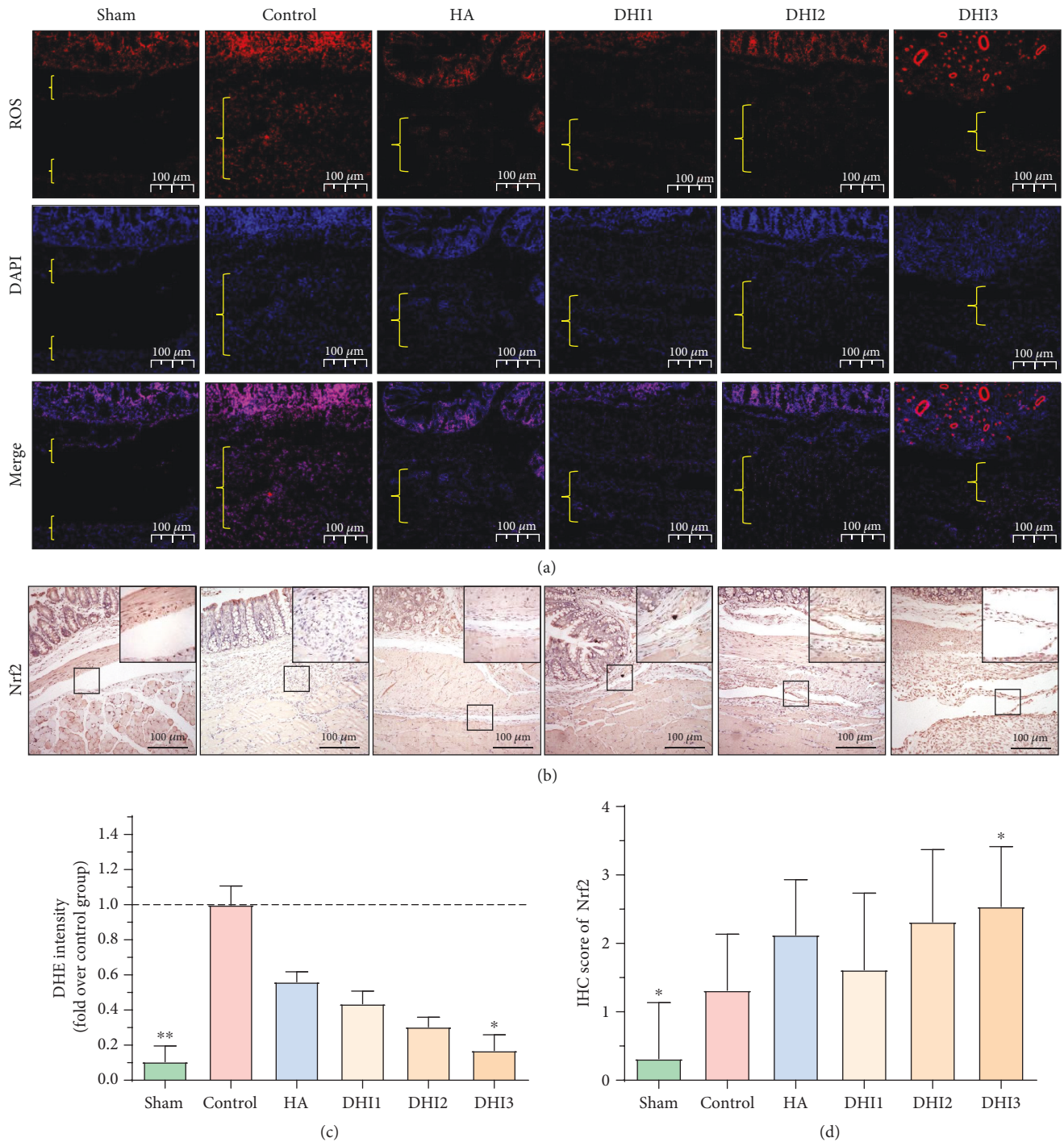


FIGURE 5: DHI treatment reduces oxidative stress in the adhesion tissues of the rat model 7 days after operation ($n = 8$; compared with the control group, $*P < 0.05$). (a) Representative ROS level of each group at 100x magnification, and the area between the bracket indicates the tissue in the adhesion area. (b) Nrf2 staining scores of each group at 100x magnification. The top right corner is shown at 200x magnification. (c) Relative ROS expression in the adhesion tissue of each group (compared with the control group, $*P < 0.05$, abnormal distribution, Kruskal-Wallis test). (d) Nrf2 staining scores of each group (compared with the control group, $*P < 0.05$, normal distribution, one-way ANOVA).

PAI-1 expression in adhesion tissue. In addition, DHI treatment promoted the MMP9 expression, which resulted the enhancement of the fibrinolytic and MMP systems.

The strategies for the prevention and treatment of postoperative adhesion are various [3]. While base on the

mechanism for adhesion development, these methods can be mainly classified as the following. The first one is using the physical barrier such as membrane or gel; these barriers can separate the injured peritoneal tissue which can reduce the adhesion formation [19, 28]. The second way for

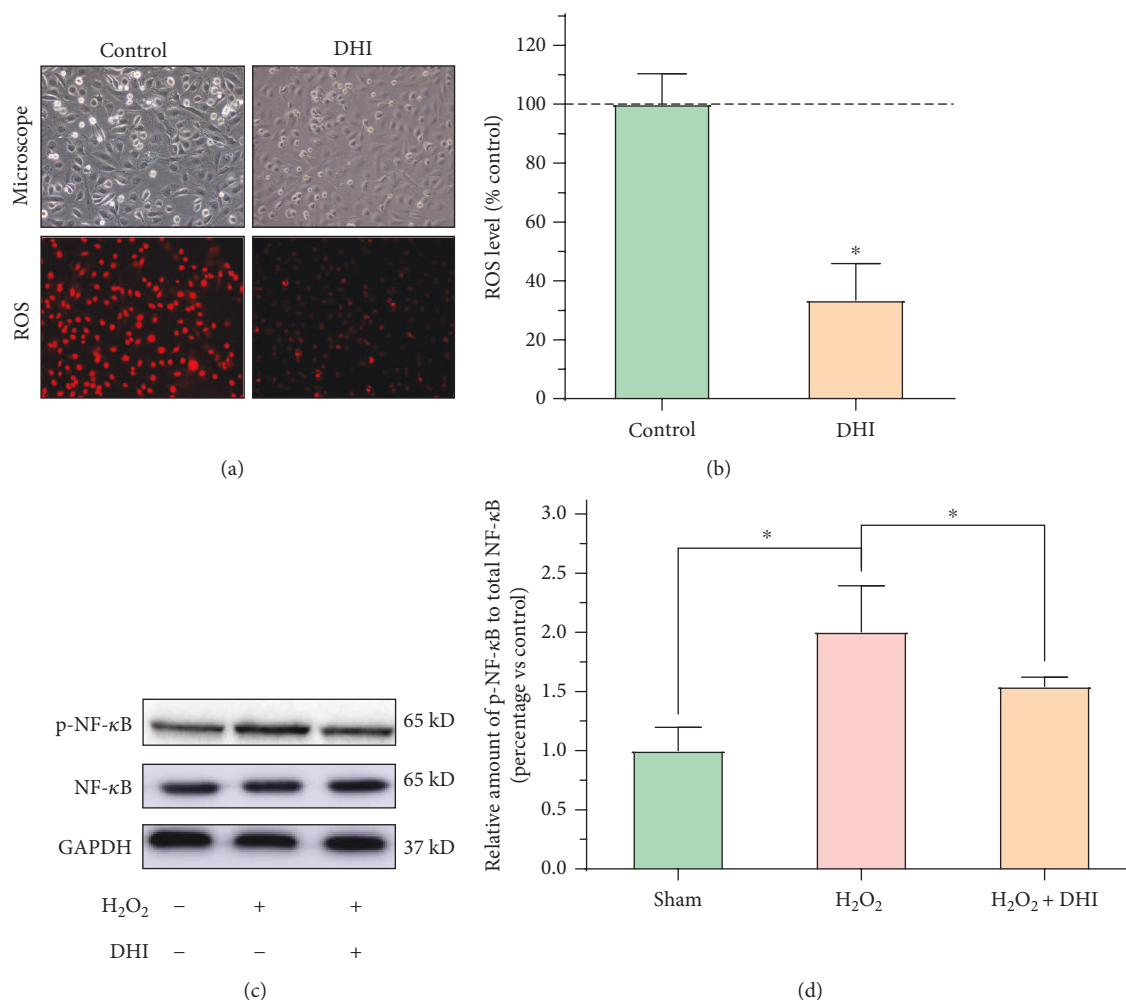


FIGURE 6: DHI treatment reduces oxidative stress in RPMCs (compared with the control group, * $P < 0.05$ and ** $P < 0.01$). (a) Representative cellular morphology and ROS expression in DHI-treated and control cells at 100x magnification. (b) The ROS level in DHI-treated and control cells (compared with the control group, * $P < 0.05$, normal distribution, t test). (c) Western blot detection of NF- κ B and phosphorylated NF- κ B expression in the different DHI- and H₂O₂-treated groups. (d) The ratio of the relative expression of phosphorylated NF- κ B to total NF- κ B in each group (compared with the control group, * $P < 0.05$, ** $P < 0.01$, normal distribution, one-way ANOVA).

postoperative adherence prevention is alleviating the inflammation and its enlargement; controlling the inflammation reaction can reduce the vascular permeability and tissue damage [29]. Thirdly, reducing the fiber deposition or promoting adhesion tissue fiber dissolving is very important, especially during 3 to 5 days after the operation [30]. The fourth one is protection of peritoneal mesothelial cells. After the operation, the mesothelial cells will not only be injured or dead, it can also be transferred into fibroblasts thus promote the adhesion formation; moreover, the lack of peritoneal mesenchymal cell and exposure of subperitoneal collagen tissue can promote the formation of adhesion [31, 32]. Lastly and the most important methods to prevent adhesion is reduction of surgical damage, exact hemostasis, and removal of blood clots during the operation; besides, surgeons should avoid residual foreign substance [33].

In this study, we demonstrated that DHI can potentially be used as a drug to prevent the formation of postoperative adhesion. However, there are several limitations in our study.

First, this study is based on an animal model, and the effect of DHI on human adhesion formation requires further investigation. The other limitation is that because of the complexity of DHI, the pharmacological action and toxicity of DHI are not fully understood; thus, additional studies investigating the individual components of DHI on adhesion prevention are required.

5. Conclusion

DHI can inhibit the formation of intra-abdominal adhesion in a rat model by inhibiting inflammation, collagen deposition, and oxidative stress. DHI may serve as a promising drug for preventing intra-abdominal adhesion.

Data Availability

The data used to support the findings of this study are included within the article.

Conflicts of Interest

The authors declare that they have no conflicts of interest.

Authors' Contributions

Yunhua Wu and Guangbing Wei contributed equally to this work.

Acknowledgments

This study was supported by the National Natural Science Foundation of China (No. 81770521 and No. 81572734) and the Joint Foundation of the First Affiliated Hospital of Xi'an Jiaotong University and Buchang Biological Co. LTD (No. BC2017-10). This experimental study was finished in the Department of Experimental Animal Center of Xi'an Jiaotong University and Translation Medicine Center of the First Affiliated Hospital of Xi'an Jiaotong University.

Supplementary Materials

Supplemental Table 1: Nair et al. scoring system. Supplemental Table 2: histopathological criteria for inflammatory score. (*Supplementary Materials*)

References

- [1] R. T. Beyene, S. L. Kavalukas, and A. Barbul, "Intra-abdominal adhesions: anatomy, physiology, pathophysiology, and treatment," *Current Problems in Surgery*, vol. 52, no. 7, pp. 271–319, 2015.
- [2] D. Brüggmann, G. Tchartchian, M. Wallwiener, K. Münstedt, H. R. Tinneberg, and A. Hackethal, "Intra-abdominal adhesions: definition, origin, significance in surgical practice, and treatment options," *Deutsches Ärzteblatt International*, vol. 107, no. 44, pp. 769–775, 2010.
- [3] G. Wei, C. Zhou, G. Wang, L. Fan, K. Wang, and X. Li, "Keratinocyte growth factor combined with a sodium hyaluronate gel inhibits postoperative intra-abdominal adhesions," *International Journal of Molecular Sciences*, vol. 17, no. 10, p. 1611, 2016.
- [4] M. Javaherzadeh, A. Shekarchizadeh, M. Kafaei, A. Mirafshrieh, N. Mosaffa, and B. Sabet, "Effects of intraperitoneal administration of simvastatin in prevention of postoperative intra-abdominal adhesion formation in animal model of rat," *Bulletin of Emergency and Trauma*, vol. 4, no. 3, pp. 156–160, 2016.
- [5] A. O. Awonuga, J. Belotte, S. Abuaneh, N. M. Fletcher, M. P. Diamond, and G. M. Saed, "Advances in the pathogenesis of adhesion development: the role of oxidative stress," *Reproductive Sciences*, vol. 21, no. 7, pp. 823–836, 2014.
- [6] H. Nakagawa, Y. Matsumoto, Y. Matsumoto, Y. Miwa, and Y. Nagasaki, "Design of high-performance anti-adhesion agent using injectable gel with an anti-oxidative stress function," *Biomaterials*, vol. 69, pp. 165–173, 2015.
- [7] J. Chen, J. Wei, Y. Huang et al., "DanHong injection enhances the therapeutic efficacy of mesenchymal stem cells in myocardial infarction by promoting angiogenesis," *Frontiers in Physiology*, vol. 9, p. 991, 2018.
- [8] X. Feng, Y. Li, Y. Wang et al., "DanHong injection in cardiovascular and cerebrovascular diseases: pharmacological actions, molecular mechanisms, and therapeutic potential," *Pharmacological Research*, vol. 139, pp. 62–75, 2019.
- [9] J. Wan, H. Wan, R. Yang et al., "Protective effect of DanHong injection combined with Naoxintong capsule on cerebral ischemia-reperfusion injury in rats," *Journal of Ethnopharmacology*, vol. 211, pp. 348–357, 2018.
- [10] Z. L. Guo, Y. Zhu, X. T. Su et al., "DanHong injection dose-dependently varies amino acid metabolites and metabolic pathways in the treatment of rats with cerebral ischemia," *Acta Pharmacologica Sinica*, vol. 36, no. 6, pp. 748–757, 2015.
- [11] G. Wei, Y. Wu, Q. Gao et al., "Gallic acid attenuates postoperative intra-abdominal adhesion by inhibiting inflammatory reaction in a rat model," *Medical Science Monitor*, vol. 24, pp. 827–838, 2018.
- [12] S. K. Nair, I. K. Bhat, and A. L. Aurora, "Role of proteolytic enzyme in the prevention of postoperative intraperitoneal adhesions," *Archives of Surgery*, vol. 108, no. 6, pp. 849–853, 1974.
- [13] Q. Gao, G. Wei, Y. Wu et al., "Paeoniflorin prevents postoperative peritoneal adhesion formation in an experimental rat model," *Oncotarget*, vol. 8, no. 55, pp. 93899–93911, 2017.
- [14] Q. Liu, Y. Zhang, H. Mao et al., "A crosstalk between the Smad and JNK signaling in the TGF- β -induced epithelial-mesenchymal transition in rat peritoneal mesothelial cells," *PLoS One*, vol. 7, no. 2, article e32009, 2012.
- [15] Y. Y. Zhang, M. Yi, and Y. P. Huang, "Oxymatrine ameliorates doxorubicin-induced cardiotoxicity in rats," *Cellular Physiology and Biochemistry*, vol. 43, no. 2, pp. 626–635, 2017.
- [16] G. Wei, Y. Wu, Q. Gao et al., "Effect of emodin on preventing postoperative intra-abdominal adhesion formation," *Oxidative Medicine and Cellular Longevity*, vol. 2017, Article ID 1740317, 12 pages, 2017.
- [17] K. Wang, D. Zhang, J. Wu, S. Liu, X. Zhang, and B. Zhang, "A comparative study of DanHong injection and Salvia miltiorrhiza injection in the treatment of cerebral infarction: a systematic review and meta-analysis," *Medicine*, vol. 96, no. 22, article e7079, 2017.
- [18] J. B. Zou, X. F. Zhang, J. Wang et al., "The therapeutic efficacy of DanHong injection combined with percutaneous coronary intervention in acute coronary syndrome: a systematic review and meta-analysis," *Frontiers in Pharmacology*, vol. 9, p. 550, 2018.
- [19] L. X. Lin, F. Yuan, H. H. Zhang, N. N. Liao, J. W. Luo, and Y. L. Sun, "Evaluation of surgical anti-adhesion products to reduce postsurgical intra-abdominal adhesion formation in a rat model," *PLoS One*, vol. 12, no. 2, article e0172088, 2017.
- [20] H. Tang, D. Liu, H. F. Qi et al., "Effect of retension sutures on abdominal pressure after abdominal surgery," *Chinese Journal of Traumatology = Zhonghua Chuang Shang Za Zhi*, vol. 21, no. 1, pp. 20–26, 2018.
- [21] S. J. Forrester, D. S. Kikuchi, M. S. Hernandez, Q. Xu, and K. K. Griending, "Reactive oxygen species in metabolic and inflammatory signaling," *Circulation Research*, vol. 122, no. 6, pp. 877–902, 2018.
- [22] Z. Liu, S. Cheng, C. Gu, H. Pei, and X. Hong, "Effect of hydrogen-rich saline on postoperative intra-abdominal adhesion bands formation in mice," *Medical Science Monitor*, vol. 23, pp. 5363–5373, 2017.

- [23] Y. Guan, Y. Yin, Y. R. Zhu et al., "Dissection of mechanisms of a Chinese medicinal formula: Danhong injection therapy for myocardial ischemia/reperfusion injury *in vivo* and *in vitro*," *Evidence-Based Complementary and Alternative Medicine*, vol. 2013, Article ID 972370, 12 pages, 2013.
- [24] I. Bellezza, P. Scarpelli, S. V. Pizzo, S. Grottelli, E. Costanzi, and A. Minelli, "ROS-independent Nrf2 activation in prostate cancer," *Oncotarget*, vol. 8, no. 40, pp. 67506–67518, 2017.
- [25] X. Jiang, B. Lv, P. Li et al., "Bioactivity-integrated UPLC/Q-TOF-MS of Danhong injection to identify NF- κ B inhibitors and anti-inflammatory targets based on endothelial cell culture and network pharmacology," *Journal of Ethnopharmacology*, vol. 174, pp. 270–276, 2015.
- [26] W. Arung, M. Meurisse, and O. Detry, "Pathophysiology and prevention of postoperative peritoneal adhesions," *World Journal of Gastroenterology*, vol. 17, no. 41, pp. 4545–4553, 2011.
- [27] M. Lyu, C. L. Yan, H. X. Liu et al., "Network pharmacology exploration reveals endothelial inflammation as a common mechanism for stroke and coronary artery disease treatment of Danhong injection," *Scientific Reports*, vol. 7, no. 1, article 15427, 2017.
- [28] D. Poehnert, L. Grethe, L. Maegel et al., "Evaluation of the effectiveness of peritoneal adhesion prevention devices in a rat model," *International Journal of Medical Sciences*, vol. 13, no. 7, pp. 524–532, 2016.
- [29] J. Bi, S. Zhang, Z. du et al., "Peripheral serotonin regulates postoperative intra-abdominal adhesion formation in mice," *Scientific Reports*, vol. 7, no. 1, article 10001, 2017.
- [30] M.-T. G. Lee, C.-C. Lee, H.-M. Wang et al., "Hypothermia increases tissue plasminogen activator expression and decreases post-operative intra-abdominal adhesion," *PLoS One*, vol. 11, no. 9, article e0160627, 2016.
- [31] S. E. Mutsaers, K. Birnie, S. Lansley, S. E. Herrick, C. B. Lim, and C. M. Prêle, "Mesothelial cells in tissue repair and fibrosis," *Frontiers in Pharmacology*, vol. 6, p. 113, 2015.
- [32] P. Sandoval, J. A. Jiménez-Heffernan, G. Guerra-Azcona et al., "Mesothelial-to-mesenchymal transition in the pathogenesis of post-surgical peritoneal adhesions," *The Journal of Pathology*, vol. 239, no. 1, pp. 48–59, 2016.
- [33] A. Hindocha, L. Beere, S. Dias, A. Watson, and G. Ahmad, "Adhesion prevention agents for gynaecological surgery: an overview of Cochrane reviews," *The Cochrane Database of Systematic Reviews*, vol. 1, article CD011254, 2015.

Research Article

miR-200c Modulates the Pathogenesis of Radiation-Induced Oral Mucositis

Jingjing Tao ¹, Mengjing Fan,¹ Difan Zhou,² Yiyang Hong,¹ Jing Zhang,¹ Hai Liu,³ Sherven Sharma,⁴ Guanyu Wang ², and Qinghua Dong ^{1,5}

¹Biomedical Research Center, Sir Run Run Shaw Hospital, School of Medicine, Zhejiang University, Hangzhou, Zhejiang, China

²Department of General Surgery, Sir Run Run Shaw Hospital, School of Medicine, Zhejiang University, Hangzhou, Zhejiang, China

³Department of Radiotherapy, Sir Run Run Shaw Hospital, School of Medicine, Zhejiang University, Hangzhou, Zhejiang, China

⁴David Geffen School of Medicine at UCLA and the Veterans Affairs, Los Angeles, CA, USA

⁵Key Laboratory of Cancer Prevention and Intervention, China National Ministry of Education, China

Correspondence should be addressed to Guanyu Wang; wangguanyu@zju.edu.cn and Qinghua Dong; dongqinghua@zju.edu.cn

Received 3 March 2019; Accepted 28 April 2019; Published 27 June 2019

Guest Editor: Reggiani Vilela Gonçalves

Copyright © 2019 Jingjing Tao et al. This is an open access article distributed under the Creative Commons Attribution License, which permits unrestricted use, distribution, and reproduction in any medium, provided the original work is properly cited.

Radiation-induced oral mucositis (RIOM) is one of the most common side effects of radiotherapy in cancer patients, especially in almost all head and neck cancer patients. It presents as severe pain and ulceration. The development of RIOM is composed of five stages: initiation, primary damage response, signal amplification, ulceration, and healing. However, the key regulators involved in the RIOM pathogenesis remain largely unknown. In this study, we reveal a novel role of miR-200c, a member of the miR-200 family, in modulating RIOM pathogenesis. Using a mouse model mimicking RIOM, we found that the miR-200 family numbers (miR-141, miR-200a, miR-200b, and miR-200c) except miR-429 were significantly induced during the RIOM formation. Besides, in RIOM mice, miR-200c expression level was also increased dramatically in the normal human keratinocytes (NHKs) after irradiation. Knockdown of miR-200c expression with miR-200c-3p-shRNA significantly reduced senescence phenotype and enhanced cell proliferation in NHKs after irradiation. The generation of reactive oxygen species (ROS) and p47 enzyme involved in ROS production was increased after irradiation but both were markedly reduced in NHKs by miR-200c inhibition. Knockdown of miR-200c expression in NHKs increased DNA double-strand break repair after irradiation compared with control NHKs. Furthermore, miR-200c inhibition repressed the production of proinflammatory cytokines (TGF- β , TNF- α , and IL-1 α) via inhibiting NF- κ B and Smad2 activation in NHKs exposed to IR. Additionally, miR-200c inhibition promoted NHK migration and increased the expression of molecules that regulate epithelial to mesenchymal transition, including Snail, Vimentin, Zeb1, and Bmi-1. These results not only identify the key role of miR-200c in the pathogenesis of RIOM but also provide a novel therapeutic target to treat RIOM.

1. Introduction

Radiation-induced oral mucositis (RIOM) is one of the main adverse events of radiotherapy (RT). Approximately 80–100% of patients receiving RT for head and neck cancer develop RIOM. RIOM is characterized by ulceration and results in severe pain, interference in treatment administration, and can even worsen the quality of life, also affects patient survival [1]. Though the key regulators involved in RIOM pathogenesis remain largely unknown, a five-stage model was proposed to explain the development of RIOM:

initiation, primary damage response, signal amplification, ulceration, and healing [2]. IR injury results in lethal DNA damage (mainly DNA double-strand breaks, DSB) with generation of reactive oxygen species (ROS). This is followed by NF- κ B activation, releasing large amounts of proinflammatory cytokines [3]. These cytokines not only damage the tissue but also provide a positive-feedback loop to amplify the primary damage initiated by radiation. For example, TNF- α acts through the TNF- α receptor family and can activate NF- κ B signaling again. Then, the mucosal ulcerations form. During the last healing stage, the basal epithelial cells

can migrate, proliferate, and differentiate to heal the ulcer. Traditional treatments, such as pain control, nutritional support, antibiotic administration, or immune modulation, targeting a single pathogenic process, may reduce symptoms of RIOM, but these treatments are not sufficient to cure the disease and also have various side effects [4]. Therefore, it is essential to identify the key regulators that control the pathogenic processes of RIOM and to develop alternative therapeutic strategies to treat RIOM.

MicroRNAs are small noncoding RNAs that regulate posttranscriptionally by mRNA cleavage or translational repression [5]. Because a single miRNA targets hundreds of mRNAs, miRNA plays an important regulatory role in the initiation of various diseases. The miR-200 family contains five homologous miRNAs including miR-200a, miR-200b, miR-200c, miR-141, and miR-429. Extensive research have demonstrated that miR-200 family inhibits the epithelial-to-mesenchymal transition (EMT) and tumor metastasis, represses cancer stem cell self-renewal, reverses chemoresistance, and enhances radiosensitivity in some types of cancer [6]. It has previously been observed that miR-200 family is involved in the response to oxidative stress across multiple species [7]. miR-200c overexpression regulates the oxidative stress response genes and increases cellular radiosensitivity in lung cancer cells [6]. Nonetheless, the function of miR-200c in the regulation of RIOM is still unclear.

Bmi-1 and Zeb1 are two key genes targeted by miR-200c and miR-141 [8]. Bmi-1 is known to mitigate IR-induced genotoxicity and protects normal human keratinocytes (NHKs) after IR [9]. Zeb1 is a crucial regulator in EMT which promotes wound healing [10]. Recent study showed that increased miR-200c expression in the skin is related to age-associated delay in wound healing and compromises skin repair in chronic wounds [11]. Thus, we postulated that miR-200c could modulate the RIOM pathogenesis. In this study, we investigated the role of miR-200c in modulating the pathogenesis of RIOM and found that miR-200a, miR-200b, miR-200c, and miR-141 were induced during RIOM in the mouse model. We also identified that the most significantly expressed miR-200 was miR-200c in normal NHKs after IR. We further demonstrated that miR-200c inhibition decreased the IR-induced senescence, ROS generation, and production of proinflammatory cytokines, molecularly through inhibiting p16, p47 expression and activating Smad2 and NF- κ B signaling. Meanwhile, miR-200c inhibition enhanced cell proliferation and DNA damage repair and promoted cell wound healing ability and EMT-related gene expressions. Collectively, our studies not only identify the novel functional role of miR-200c in modulating pathogenic processes of RIOM but also provide a potential therapeutic target for RIOM treatment.

2. Materials and Methods

2.1. Radiation-Induced Oral Mucositis Mouse Model. All animal care and experimental procedures strictly followed the recommendations in the Guide for the Care and Use of Laboratory Animals of Zhejiang University and were approved by the Committee on the Ethics of Animal

Experiments of Zhejiang University. We developed the RIOM mouse model by exposing the head and neck area of C57/BL6 mice (6-8 weeks old) to radiation from X-RAD 160 (Precision X-ray, New Haven, CT) with a lead shield covering the rest of the body [12]. We treated the mice with different single doses (15, 18, 20, 25, and 30 Gy) in preliminary experiments and selected 25 Gy as the optimal dosage to rapidly induce radiogenic mucositis. Mice were anesthetized during irradiation. At 7 days posttreatment, the excised tongues were stained with 1% toluidine blue (TB) in 10% acetic acid till there were no further staining and washed with 1% acetic acid [13]. Increased TB staining and a change in epithelial thickness were used as markers of oral mucositis. At 3, 4, 5, 6, and 7 days posttreatment, the tongues ($n = 5$ in each group) were frozen at -80°C and used for qPCR analysis for miR-200 family and inflammation cytokines.

2.2. Immunohistochemistry (IHC) and Hematoxylin-Eosin (H&E) Staining. The tongues were fixed with 4% paraformaldehyde and embedded in paraffin, which was used in $5\ \mu\text{m}$ sections to conduct histologic analysis. For H&E staining, tissue samples were sectioned from the middle of the wounds, then stained with hematoxylin and eosin. In order to visualize Bmi-1 and Zeb1 in the tongues, standard immunoperoxidase procedures were used and the sections from the tongues ($n = 5$ in each group) were incubated with primary antibodies overnight at 4°C , then were further incubated with horseradish peroxidase-linked secondary antibodies for 2 hours at room temperature.

2.3. Cell Culture. This study was performed strictly according to the recommendations from the Guide for Clinical Research which were provided by Sir Run Run Shaw Hospital, Zhejiang University. This protocol was approved and monitored by the Ethics Committee of Sir Run Run Shaw Hospital, Zhejiang University (No. 20170222-26). Informed consent was obtained from all patients. Primary NHKs were isolated from human foreskins according to protocols described elsewhere [14]. NHKs were cultured in serum-free EpiLife™ medium with calcium supplied with defined growth supplement (Invitrogen, Carlsbad, CA). To generate NHK/Control and NHK/miR-200c- cells, NHKs were infected with lentivirus carrying control vector (hU6-MCS-CMV-EGFP) or miR-200c-3p-shRNA (Genechem, Shanghai) and further selected by puromycin. To generate the irradiation experiments, NHKs were exposed to varying irradiation doses with X-RAD 160 irradiator.

2.4. Clone Formation Assay. NHKs were cultured at 6-well plates with 1000-6000 cells per well and treated correspondingly with 0, 4, 6, 8, and 10 Gy irradiation. Cells were further cultured for 10 days after irradiation. 0.5% crystal violet was used for staining, then the colonies were counted. The surviving fraction was calculated by the proportion of seeded cells after being irradiated to form colonies relative to untreated cells. To further calculate the cellular radiosensitivity (mean lethal dose, D_0) and the capacity for sublethal damage repair (quasithreshold dose, Dq), the equation $\text{SF} = 1 - (1 - e^{-D/D_0})^N$ was applied. Those values

were then used to calculate the sensitization enhancement ratio (SER) [15].

2.5. Senescence-Associated β Galactosidase (SA- β -Gal) Activity Assay. After being washed in PBS twice, NHKs were further fixed in 2% formaldehyde, 0.2% glutaraldehyde solution. SA- β -Gal staining solution (Beyond Biotech, China) was used for staining, then incubated at 37°C for 16 h.

2.6. Western Blot Analysis and Immunofluorescence Staining. Protein extraction and the assay were carried out as described in our previous study [9]. The antibodies used in this study are listed in Table S1.

For immunofluorescence staining, we fixed cells in 4% paraformaldehyde at room temperature for 15 min, then permeabilized in 0.25% TritonX-100 for 15 min, blocked with 5% goat serum for 1 hour. We used mouse monoclonal anti-phospho- γ -H2AX and Alex Fluor®549 goat anti-mouse IgG (Thermo Fisher A-11005) as primary and secondary antibodies. Nuclei were stained with DAPI in SlowFade® Gold Antifade Mountant (Thermo Fisher, S36942). Images were captured with a Zeiss HBO-100 fluorescence microscope (Carl Zeiss, Germany).

2.7. Reverse Transcription qPCR. Total RNA were extracted by using TRIzol™ Reagent (Invitrogen™). Reverse transcription was performed with a reverse transcription system (Promega, Madison, WI, USA) according to the manufacturer's instructions. qPCR was carried out three times for each sample using FastStart Universal SYBR Green Master (Roche Diagnostics, Rotkreuz, Switzerland) to determine the mRNA level of cytokines. To detect mir-200 family expression, All-in-One miRNA RT-PCR Detection Kit (GeneCopoeia, Rockville, MD) was used according to the manufacturer's instructions. Reverse transcription reaction was performed with All-in-One cDNA Synthesis SuperMix (Bimake, B24403); qPCR was performed using SYBR Green qPCR Master Mix (Bimake, B21202). Primer sequences are listed in Table S2.

2.8. Determination of Intracellular ROS Level. NHKs were stained with 5 μ M dihydroethidium (DHE) (Beyotime Biotech, China) at room temperature for 30 min. We use FACSCalibur using CellQuest software (Becton Dickinson, San Jose, CA) to quantify fluorescence intensity of DHE.

2.9. Neutral Comet Assay. A neutral comet assay was performed to detect the level of DNA DSBs, using the CometAssay Kit (Trevigen, Gaithersburg, MD) [16]. After being exposed to 5 Gy IR, cells were harvested at 10 h after irradiation and were further electrophoresed in the CometSlides. GelRed was used for staining. Images were obtained by the Zeiss HBO-100 fluorescence microscope. Degree of DNA damage was compared in the groups by measuring the DNA containing ratio of head/tail using comet assay software project (CASP). The threshold of CASP parameters was adjusted: head center threshold (HCT) = 0.8, tail threshold (TT) = 0.05, head threshold (HT) = 0.05, and comet threshold (CT) = 0.05. The tail DNA was measured

by the sum of intensities of pixels in the tail according to the online protocol.

2.10. Wound Healing. NHKs were seeded in 6-well plates (5×10^5 cells/well) until they reached 90% confluence, a linear wound was created by scratching using the pipette tip [17]. After 5 Gy IR, photos were taken at 0, 24, and 30 hours.

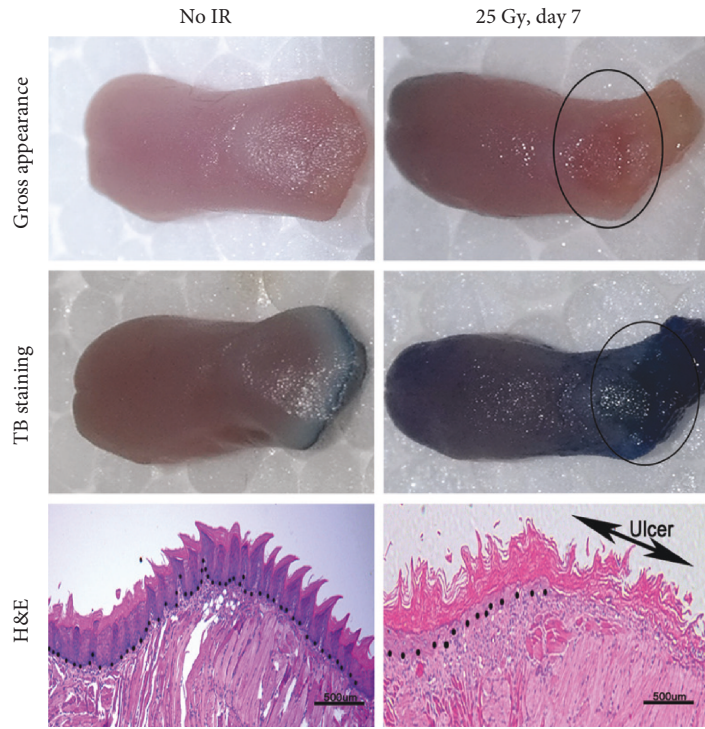
2.11. Statistical Analysis. To detect the differences among various treatments, one-way analysis of variance (ANOVA) was used; the paired Student's *t*-test was used for evaluation of the differences between two groups. Differences with $P < 0.05$ were considered significant.

3. Results

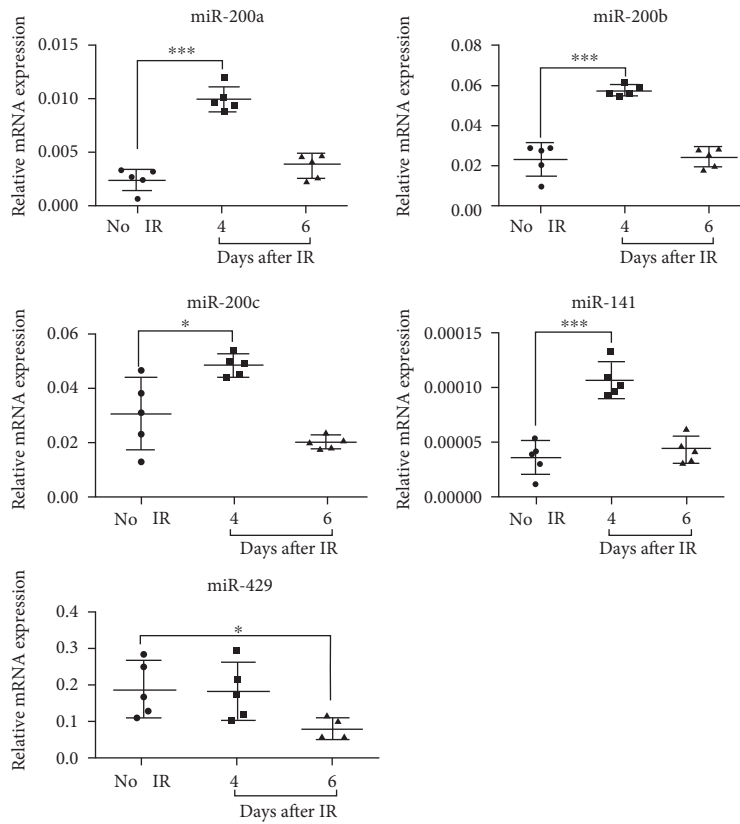
3.1. miR-200 Family Numbers Are Induced during RIOM. To determine if miR-200 family was involved in RIOM, we generated the RIOM mouse model by exposing the mouse to 25 Gy irradiation. Ulcers were seen at the posterior surface of the tongue, and the TB-stained ulcers were evident at day 7 after irradiation. Histological analyses showed complete depletion of the stratified squamous keratinized epithelium (Figure 1(a)). We checked miR-200 family expression in the tongues at days 4 and 6 (during RIOM ulcer formation) after irradiation. Most members of miR-200s (miR-141, miR-200a, miR-200b, and miR-200c) were significantly increased at day 4 after irradiation compared to the nonirradiated group, then decreased to the normal level at day 6 after irradiation. Only miR-429 expression level did not change at day 4 but decreased obviously at day 6 after irradiation (Figure 1(b)).

Cytokine-induced excessive inflammation is the key feature of RIOM [18]. We thus investigated the expression levels of 5 proinflammatory cytokines in the tissue of oral mucositis at different time points after irradiation. TNF- α , MIP-1 β , and IL-1 α were dramatically increased at day 7 after irradiation. IL-6 was increased obviously from days 3, 5, and 7 after irradiation. TGF- β was increased from day 3 to day 5 but decreased at day 7 after irradiation (Figure 1(c)). Consistent with the increased miR-200s, mRNA and protein expression levels of their target genes Bmi-1 and Zeb1 were substantially reduced in RIOM tongues (Figures 1(d) and 1(e)). These data indicate that RIOM is associated with the miR-200s expression.

3.2. miR-200c Modulates Proliferation and Senescence in NHKs Exposed to IR. To investigate if the miR-200 family was also upregulated by IR *in vitro*, NHKs were exposed to 5 Gy IR. miR-141 was undetectable in NHKs, and miR-429 expression had no change compared with nonirradiated cells. However, miR-200a, miR-200b, and miR-200c were increased significantly even at 48 h after irradiation (Figure 2(a)). Among them, miR-200c was the most significantly induced miR-200 in NHKs and increased as early as 6 h after irradiation. Therefore, we selected miR-200c for our following investigations. To determine if miR-200c contributes to RIOM in NHKs, we generated miR-200c knock-down NHKs (NHK/miR-200c-) by infecting lentiviruses

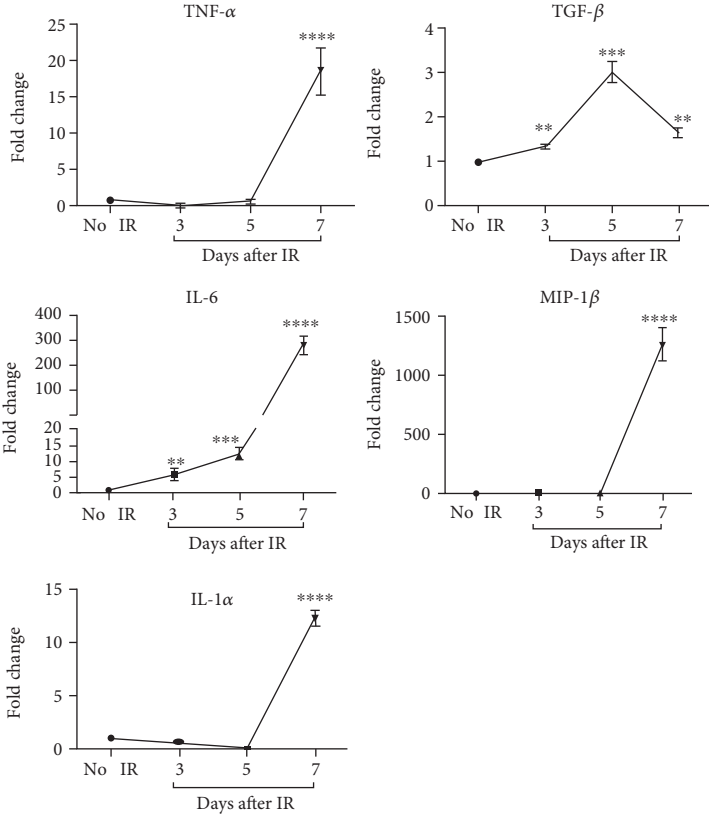


(a)

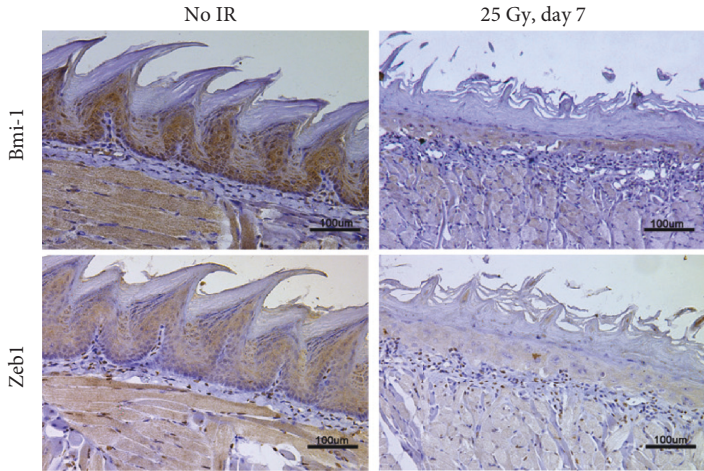


(b)

FIGURE 1: Continued.



(c)



(d)

FIGURE 1: Continued.

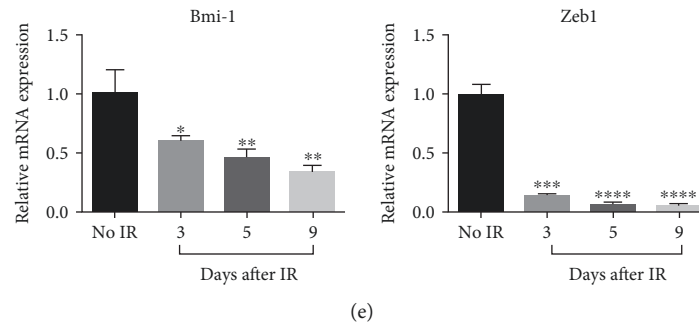


FIGURE 1: miR-200 family numbers are induced during RIOM. (a) Representative images of RIOM gross appearance, toluidine blue (TB) staining, and HE staining of tongue tissues from nonirradiated and irradiated C57BL/6 mice at day 7 after 25 Gy IR. Arrows show the areas of ulcer. The dot lines refer to epithelial-stromal boundary. (b) The tongues of C57BL/6 mice were harvested at days 0, 4, and 6 postirradiation; the expression level of miR-200 family was measured by qPCR ($n=5$ per group). $*P < 0.05$ and $***P < 0.001$ vs. nonirradiated control mice. (c) The tongues of C57BL/6 mice were harvested at days 0, 3, 5, and 7 postirradiation, then the mRNA levels of TNF- α , TGF- β , IL-6, IL-1 α , and MIP-1 β were measured by qPCR (mean \pm S.D.). The proinflammatory cytokines were induced during RIOM formation. $**P < 0.01$, $***P < 0.001$, and $****P < 0.0001$ vs. nonirradiated control mice. (d) IHC staining of Bmi-1 and Zeb1 of tongue tissues from nonirradiated and irradiated mice at day 7 after 25 Gy IR. (e) The mRNA level of Bmi-1 and Zeb1 in the tongues of C57BL/6 mice harvested at days 0, 3, 5, and 9 postirradiation was analyzed by qPCR. $*P < 0.05$, $**P < 0.01$, $***P < 0.001$, and $****P < 0.0001$ vs. nonirradiated control mice.

encoding miR-200c-specific shRNA sequence. miR-200c expression increased dramatically at days 2, 3, and 7 after IR in the NHK/Control cells, but it was inhibited in the NHK/miR-200c- cells (Figure 2(b)). Previous study has demonstrated that stress-induced premature senescence is the main cellular response of NHKs to irradiation [9]. We found that the knockdown of miR-200c notably suppressed SA- β -gal activity in irradiated NHKs. Furthermore, the NHK/miR-200c- cells maintained being active for cell proliferation when NHK/Control cells became nonreplicative at day 7 after IR (Figure 2(c)). Radiation response of NHKs was further evaluated with the colony-forming assay, a gold standard for determining radiosensitivity [19]. As expected, we observed that the ability of clone formation and the plating efficiency of NHK/miR-200c- cells were much higher than those of NHK/Control cells after IR (Figure 2(d)). miR-200c inhibition decreased the radiosensitivity of NHK, with a SER of 0.23 (Table S3). In addition, miR-200c inhibition notably suppressed IR-induced expression of cell cycle molecule p16^{INK4A}, which mediate telomere-independent senescence (Figure 2(e)). Thus, miR-200c inhibition promoted cell proliferation while it prevented senescence of NHKs after IR. These data support our hypothesis that miR-200c may modulate the pathogenesis of RIOM.

3.3. miR-200c Regulates ROS Generation and DNA Repair in NHKs after Irradiation. In the initiation stage of RIOM, radiotherapy induces a direct and lethal DNA damage and ROS generation in epithelial cells. We first investigated the effect of miR-200c on ROS generation. DHE staining showed that ROS was obviously generated in the NHK/Control cells at 4 and 6 days after irradiation, but it was markedly suppressed in the NHK/miR-200c- cells (Figure 3(a)). Accordingly, p47-phox, an important enzyme involved in ROS generation, was increased in the NHK/Control cells at 2, 5, and 7 days post IR, but the induction was inhibited in the NHK/miR-200c- cells (Figure 3(b)).

Then, we further determined whether miR-200c inhibition affects DNA damage response in NHKs by the comet assay and γ -H2AX staining, which are the standard methods to detect DSB formation. NHK/miR-200c- cells exhibited shorter comet tails and less DNA containing ratio of head/tail than NHK/Control cells at 10 hours after irradiation, suggesting less DSB formation (Figure 3(c)). Furthermore, irradiation notably increased γ -H2AX foci formation in the NHK/Control cells, whereas the formation level was markedly reduced in NHK/miR-200c- cells after irradiation (Figure 3(d)). Consistent to the γ -H2AX foci formation, the protein levels of γ -H2AX and p-p53 in NHK/miR-200c- cells were markedly reduced after IR compared with NHK/Control cells (Figure 3(e)). These data indicate that miR-200c inhibition mitigates the genotoxic effects of IR by suppressing ROS generation and enhancing repair of damaged DNA.

3.4. miR-200c Regulates Proinflammatory Cytokine Induction and TGF- β /NF- κ B Activation in NHKs after Irradiation. During the primary damage response stage of RIOM, NF- κ B is one of the most significantly activated pathways, which stimulates proinflammatory cytokine release from cells. We next determined the involvement of miR-200c in the regulation of cytokine release and NF- κ B activation induced by IR. We first evaluated the production of proinflammatory cytokines after irradiation by qPCR. TNF- α , TGF- β , and IL-1 α were significantly induced in 5 Gy irradiated NHK/Control cells, but they were much less in the NHK/miR-200c- cells (Figure 4(a)).

We further examined IR-induced activation of NF- κ B by immunofluorescence staining. NF- κ B translocation into the nucleus was significantly increased as early as 15 minutes post IR and prolonged till 60 min in the NHK/Control cells. In contrast, the translocation of NF- κ B was reduced in the NHK/miR-200c- cells after IR (Figure 4(b)). Accordingly, IR rapidly increased levels of p-NF- κ B and p-I κ B in NHK/Control cells. miR-200c inhibition prevented the

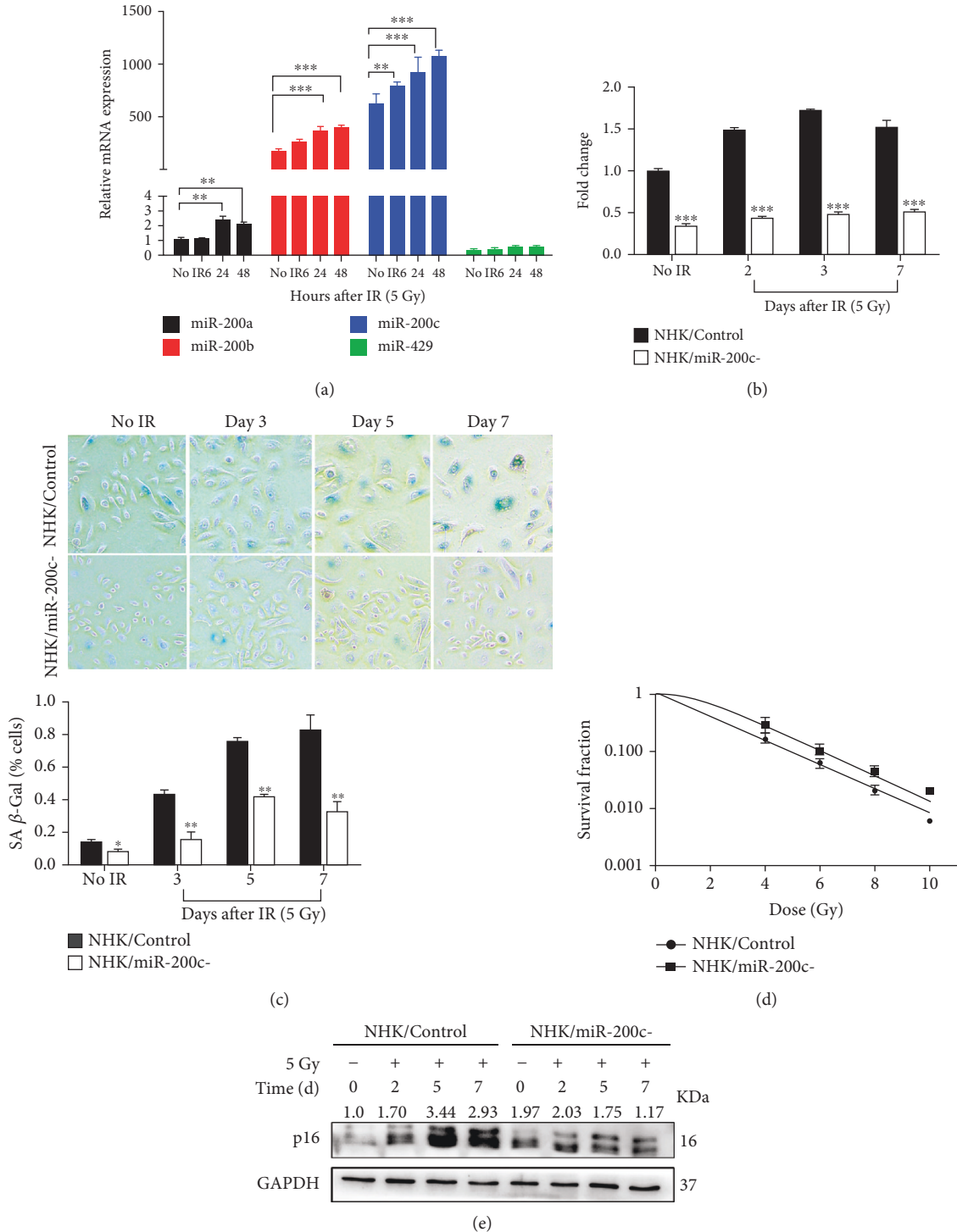


FIGURE 2: miR-200c modulates proliferation and senescence in NHKs exposed to IR. (a) The expression level of miR-200 family was measured by qPCR (mean ± S.D.) at indicated time after being exposed to 5 Gy. 5S rRNA was used as an internal control. ** $P < 0.01$ and *** $P < 0.001$ vs. nonirradiated cells. (b) NHKs were infected with sh-miR-200c (NHK/miR-200c-) or a scrambled negative control (NHK/Control); miR-200c expression was measured by qPCR (mean ± S.D.) at days 2, 3, and 7 after being exposed to 5 Gy. 5S rRNA was used as an internal control. *** $P < 0.001$ vs. NHK/Control. (c) SA-β-Gal assay was performed in NHK/Control and NHK/miR-200c- cells at days 0, 3, 5, and 7 postirradiation; the numbers of positive cells were counted (mean ± S.D.). IR-induced senescent cells were much less in NHK/miR-200c- compared with NHK/Control cells. * $P < 0.05$ and ** $P < 0.01$ vs. NHK/Control. Scale bar 200 μm. (d) NHK/Control and NHK/miR-200c- cells were cultured in 6-well plates for 24 hours before being irradiated with the indicated doses. Cells were further cultured for 10 days, then the colonies were counted; surviving fractions were determined by the number of colonies divided by the number of seeded cells × plating efficiency. (e) Western blotting was performed for p16^{INK4A} and GAPDH (internal control) in NHK/Control and NHK/miR-200c- cells at indicated time after being exposed to 5 Gy.

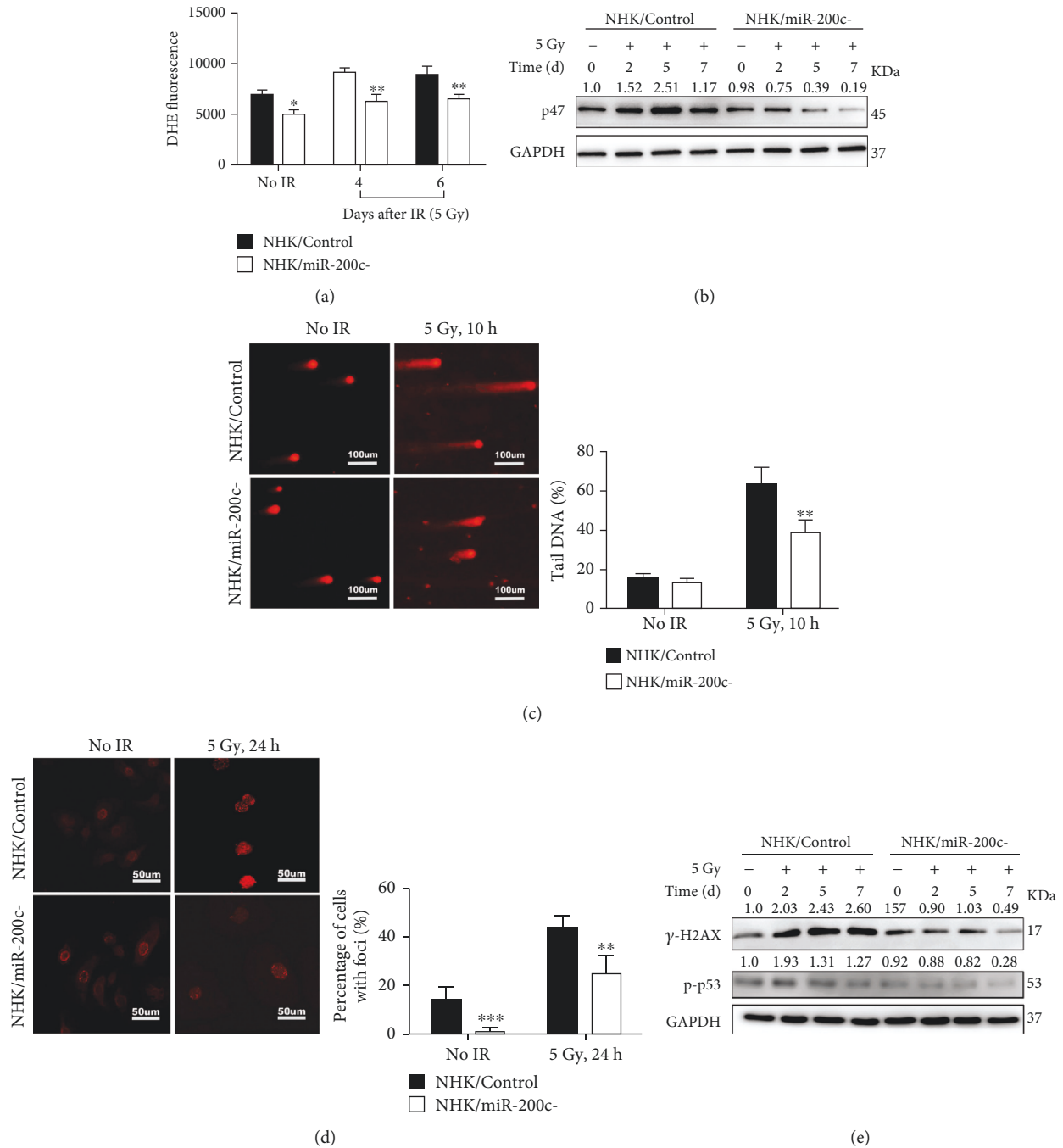


FIGURE 3: miR-200c regulates ROS generation and DNA repair in NHKs after irradiation. (a) NHK/Control and NHK/miR-200c- cells were exposed to 5 Gy IR and stained with DHE. Fluorescence intensity was quantitatively determined by flow cytometry. * $P < 0.05$ and ** $P < 0.01$ vs. NHK/Control cells. (b) Western blotting was performed for p47 and GAPDH (internal control) in NHK/Control and NHK/miR-200c- cells at indicated time after being exposed to 5 Gy. (c) NHK/Control and NHK/miR-200c- cells were exposed to 5 Gy radiation and neutral comet assay was performed. Photos were taken at 0 and 10 h postirradiation, and DNA DSB was quantitated by DNA containing ratio of head/tail (mean \pm S.D.). ** $P < 0.01$ vs. NHK/Control cells. (d) NHK/Control and NHK/miR-200c- cells were irradiated at 5 Gy; cells were further stained with the γ -H2AX antibody 24 h after radiation. Representative images were taken; the percentage of γ -H2AX foci positive cells (>5 intranuclear foci) was statistically analyzed (mean \pm S.D.). ** $P < 0.01$ and *** $P < 0.001$ vs. NHK/Control cells. (e) Western blotting was performed for γ -H2AX, p-p53, and GAPDH (internal control) in NHK/Control and NHK/miR-200c- cells at indicated time after being exposed to 5 Gy.

IR-induced NF- κ B and I κ B activation. The total I κ B levels had no significant change in both cells (Figure 4(c)). It has been reported that the NF- κ B-dependent gene expression

in irradiated NHKs is dependent on the TGF- β pathway [20]. We then tested if miR-200c affects Smad-dependent TGF- β pathway. Phosphorylated Smad2 level was increased

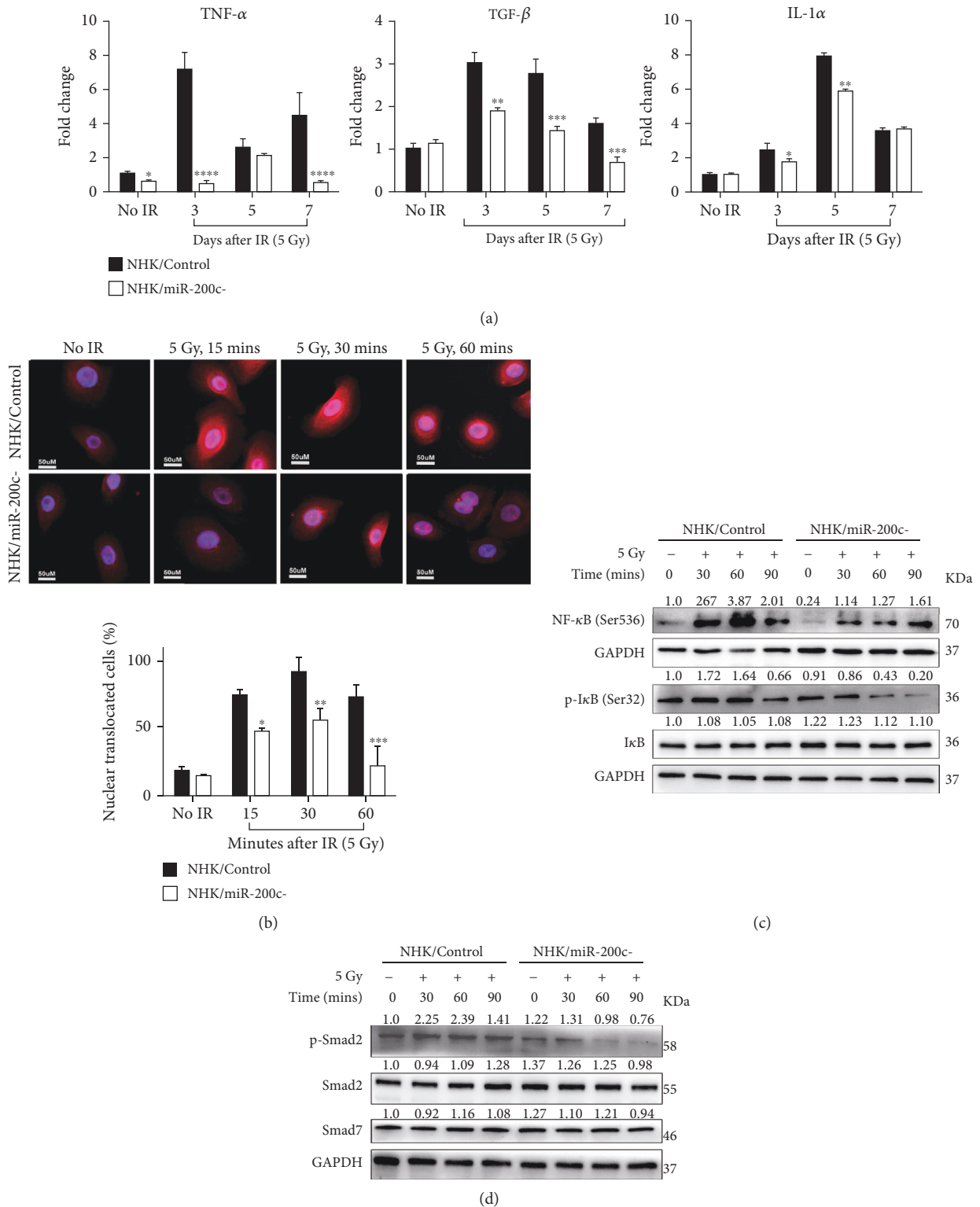


FIGURE 4: miR-200c regulates proinflammatory cytokine induction and TGF- β /NF- κ B activation in NHKs after irradiation. (a) NHK/Control and NHK/miR-200c- cells were exposed to 5 Gy IR; the expression of TNF- α , TGF- β , and IL-1 α was measured by qPCR at 0, 3, 5, and 7 days postirradiation. * $P < 0.05$, ** $P < 0.01$, and *** $P < 0.001$ vs. NHK/Control cells. (b) NHK/Control and NHK/miR-200c- cells were exposed to 5 Gy radiation; the immunofluorescent images of NF- κ B (phosphor S 536) were taken at 0, 15, 30, and 60 min postirradiation. The NF- κ B nuclear translocated cell numbers were counted. (c) Western blotting was performed for NF- κ B (phosphor S536), I κ B (phosphor S32), I κ B, and GAPDH (internal control) in NHK/Control and NHK/miR-200c- cells at indicated time after being exposed to 5 Gy. (d) Western blotting was performed for p-Smad2, Smad2, Smad7, and GAPDH (internal control) in NHK/Control and NHK/miR-200c- cells at indicated time after being exposed to 5 Gy.

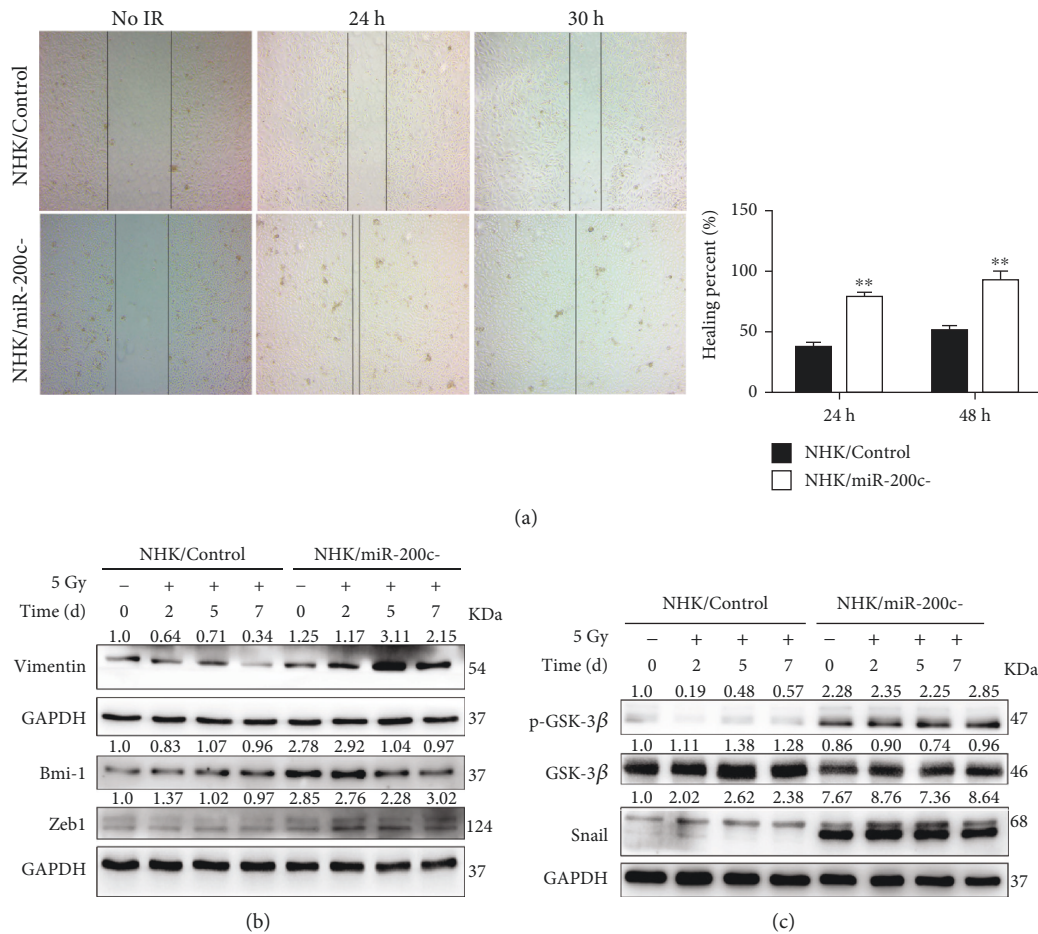


FIGURE 5: miR-200c regulates NHK migration after irradiation. (a) Wound healing assay was performed in NHK/Control and NHK/miR-200c- cells at indicated time after being exposed to 5 Gy. Left panel: images were taken at 0, 24, and 30 h after irradiation. Right panel: quantification of the healing percent (mean \pm S.D.) of cells. $^{**}P < 0.01$ vs. NHK/Control cells. (b) Western blotting was performed for Vimentin, Zeb1, and Bmi-1 in NHK/Control and NHK/miR-200c- cells at indicated time after being exposed to 5 Gy. (c) Western blotting was performed for p-GSK-3 β , GSK-3 β , Snail, and GAPDH (internal control) in NHK/Control and NHK/miR-200c- cells at indicated time after being exposed to 5 Gy. miR-200c inhibition activated GSK-3 β /Snail pathway.

in irradiated NHK/Control cells, but it was diminished in NHK/miR-200c- cells (Figure 4(d)). We also checked the expression level of Smad7, a negative feedback inhibitor of TGF- β /Smad signaling, after IR. However, miR-200c inhibition had no effect on Smad7 level in both nonirradiated and irradiated NHKs (Figure 4(d)). These results indicate that miR-200c inhibition represses IR-induced production of proinflammatory cytokines through inhibiting NF- κ B and TGF- β signaling pathways.

3.5. miR-200c Regulates NHK Migration after Irradiation. Migrating keratinocytes promote the epithelium reepithelialization in the healing stage of RIOM. To test the effect of miR-200c in tissue healing, we examined the migration ability of NHKs after IR by the wound healing assay. miR-200c inhibition significantly promoted cell migration compared to the NHK/Control cells, and the healing percentage almost reached 100% at 30 hours after IR (Figure 5(a)). EMT is a key process in wound healing [21]. We then checked the expression levels of Zeb1 and Bmi-1, which are the target genes of miR-200c and can promote EMT. Bmi-1 level

was much higher in NHK/miR-200c- cells compared with NHK/Control cells. Furthermore, miR-200c inhibition increased Zeb1 expression while it maintained Bmi-1 at a similar level after IR (Figure 5(b)). Meanwhile, Vimentin, a mesenchymal marker, was significantly increased in the irradiated NHK/miR-200c- cells. Given that GSK-3 β /Snail signal pathway is importantly involved in modulating EMT process [21, 22], we further checked if miR-200c inhibition-induced EMT was also regulated by this pathway. miR-200c inhibition decreased the total amount of GSK-3 β in irradiated NHKs, while it upregulated p-GSK-3 β and Snail expression level in NHKs (Figure 5(c)). These results indicate that miR-200c inhibition promotes NHK migration through enhancing EMT.

4. Discussion

The pathobiology of RIOM is complex and multifaceted; thus, the key regulator of RIOM pathogenesis has not been fully understood. In this study, we show for the first time that

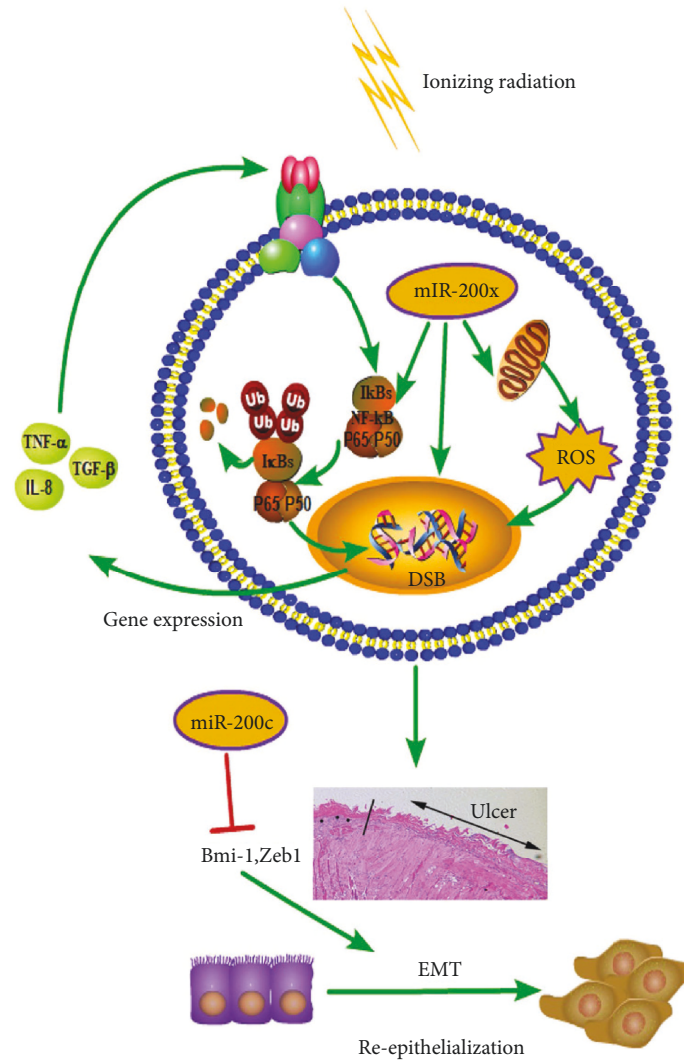


FIGURE 6: The potential role of miR-200c in regulating the pathogenesis of RIOM. miR-200c promoted radiation-induced NF- κ B signaling by increasing the phosphorylation level of I κ B α at the position ser32 and phosphorylation at position ser536 of p65 as well as nuclear translocation level, which led to overproduction of proinflammatory cytokines. miR-200c increased the DNA DSB level and ROS generation induced by radiation and caused more severe senescence phenotype. miR-200c decreased the expression of Bmi-1 and Zeb1, which led to downregulation of p-GSK-3 β and Snail, thus inhibited NHK cell EMT. miR-200c mediated increased inflammation, DNA DSB, and ROS generation as well as decreased EMT capacity of NHK during the pathogenesis of RIOM.

miR-200c is the key regulator in modulating pathogenic processes of RIOM.

The pathogenesis of RIOM is similar in humans and mice. RIOM starts as an acute inflammation after RT exposure and lasts between 7 and 98 days in cancer patients [23, 24]. Using a mouse model mimicking RIOM, we found that miR-200s were significantly increased in tongue epithelium at day 4 after irradiation. Irradiated mice developed oral ulcer with epithelial ablation and overproduction of proinflammatory cytokines at day 7 post IR, consistent with the other reports [25]. Unlike in mice, miR-200c expression was the earliest and highest among miR-200s in NHKs. miR-200c inhibition protected NHKs from IR-induced senescence and maintained cell proliferation. These data demonstrated that miR-200c was involved in the pathogenesis of RIOM.

ROS is an important early trigger resulting in RIOM and in turn induced oxidative stress-associated DNA damage [26]. miR-200c inhibition reduced IR-induced cellular ROS generation and p47 protein expression. By analyzing γ -H2AX and comet assay, we found reduced DSB damage and more efficient repair of DNA in irradiated NHK/miR-200c- cells. Thus, miR-200c regulates ROS generation and DSB repair at the initiation stage of RIOM.

NF- κ B is one of the major signaling pathways activated by IR, which promotes proinflammatory cytokine (such as TGF- β) release from cells [27]. Signal amplification during RIOM is an important step in IR-induced injury; overproduced proinflammatory cytokines restimulate and amplify mucosal damage. In this study, miR-200c inhibition reduced NF- κ B nuclear translocation, I κ B activation, and

proinflammatory cytokine production in irradiated NHKs, effectively alleviating inflammation. Besides NF- κ B, TGF- β signaling is also activated in oral mucositis [28]. TGF- β plays a key role in normal epidermal inflammatory responses; NF- κ B-dependent gene expression in keratinocytes after irradiation requires intact TGF- β signaling [20]. The key mediators in the TGF- β signaling pathway are the Smads [29]. Phosphorylated Smad2/3 is involved in the activation of TGF- β signaling. Smad7 is a negative feedback inhibitor which competes with Smad2/3 for binding to activated TGFR1 [30]. We found that IR-induced p-Smad2 was inhibited in NHK/miR-200c- cells, while Smad7 level was not changed. These results demonstrated that miR-200c inhibition reduced TGF- β activation through pSmad2 inhibition but not Smad7 promotion. Thus, miR-200c reduces inflammation by antagonizing NF- κ B and TGF- β activation.

Wound healing is associated with cellular proliferation, migration, and tissue remodeling [31]. In the healing stage of RIOM, keratinocytes migrate and proliferate to reepithelialize the epithelium [32]. EMT is a process required in wound healing after injury. Transcription factors Zeb1/2, Bmi-1, and Snail are master EMT regulators and also targets of miR-200c [33]. Zeb1 can efficiently inhibit the cell-cell adhesion molecule E-cadherin and promote EMT [34]. Bmi-1 can regulate Snail and promote EMT [35]. Studies show that inhibition of GSK-3 β activity can subsequently suppress p-Snail and induce Snail protein nuclear localization, then promotes EMT [36, 37]. In this work, we showed that miR-200c inhibition increased the expression of p-GSK-3 β and Snail in irradiated NHKs. Zeb1 and Bmi-1 expression levels were decreased in the tongue during RIOM. miR-200c inhibition increased Zeb1 and Bmi-1 levels in NHKs. Thus, miR-200c inhibition promotes NHK migration after IR through regulating EMT-related protein expressions and GSK-3 β /Snail pathways.

Bmi-1 plays a role in some biological functions including senescence, self-renewal, DNA damage response (DDR), and cancer [38, 39]. Bmi-1 can maintain mitochondrial function and redox homeostasis [40]. Bmi-1 also protects NHKs from IR-induced DNA damage [9]. Bmi-1 is a crucial component in DDR, as it is required to recruit the DDR machinery to DSB sites after irradiation [40, 41]. Thus, the upregulation of Bmi-1 in irradiated NHK/miR-200c- cells may play a key role in reducing DNA damage and promoting DSB repair.

TGF- β promotes EMT in cancer cells [42], but it induces growth inhibition and apoptosis in keratinocytes. Knock-down of TGF- β signaling axis reduces skin scarring [43]. Bmi-1 reduces senescence of NHKs by inhibiting TGF- β signaling pathway [44]. Bmi-1 inhibits senescence and extends the lifespan of normal cells by suppressing p16^{INK4A} [45]. Thus, Bmi-1 may also play a key role in reducing senescence and promoting cell proliferation in irradiated NHK/miR-200c- cells.

In summary, we provide evidence that miR-200c modulates the pathogenesis of RIOM. Potential mechanisms for the context-specific effects of miR-200c are as follows: in the initiation stage of RIOM, miR-200c inhibition reduces radiation-induced ROS generation and DNA

damage. In the primary damage response and signaling amplification stages, miR-200c inhibition attenuates TGF- β - and NF- κ B-mediated inflammation. In the healing stage, miR-200c inhibition promotes NHK migration through regulating the EMT process by upregulating its targets Zeb1 and Bmi-1 and activating GSK-3 β /Snail signal pathways (Figure 6). Bmi-1 may play the most important role in miR-200c-modulated pathogenesis of RIOM.

Abbreviations

DHE:	Dihydroethidium
DSB:	DNA double-strand break
EMT:	Epithelial-mesenchymal transition
GAPDH:	Glyceraldehyde-3-phosphate dehydrogenase
IR:	Ionizing radiation
IL6:	Interleukin 6
IL-1 α :	Interleukin-1 α
NHK:	Normal human keratinocyte
NF- κ B p65:	Nuclear translocation factor 65 subunit
qPCR:	Quantitative real-time polymerase chain reaction
RIOM:	Radiation-induced oral mucositis
ROS:	Reactive oxygen species
TGF- β :	Transforming growth factor- β
TNF α :	Tumor necrosis factor alpha.

Data Availability

The data used to support the findings of this study are available from the corresponding authors upon request.

Conflicts of Interest

The authors declare that they have no conflict of interest.

Authors' Contributions

G. W. and Q. D. conceived the project and designed the experiments; J. T., M. F., D. Z., Y. H., J. Z., and L. L. performed the experiments; J. T., G. W., S. S., and Q. D. analyzed the data and wrote the paper.

Acknowledgments

This work was supported by the National Natural Science Foundation of China (81272493 and 81472213), the Zhejiang Provincial Natural Science Foundation of China (LY17H220001), the Health Commission of Zhejiang Province (2019331258 and 2019335600), the Science Technology Department of Zhejiang Province (2015C33134 and 2015C37112), and the Basic Public Welfare Research Program of Zhejiang Province (LGD19H160005).

Supplementary Materials

Supplementary 1. Table S1: primary antibodies for western blot, IF, and IHC.

Supplementary 2. Table S2: primer sequences for quantitative RT-PCR.

Supplementary 3. Table S3: clonogenic survival parameters fitting the data to a multitarget model.

References

- [1] A. Trotti, L. A. Bellm, J. B. Epstein et al., “Mucositis incidence, severity and associated outcomes in patients with head and neck cancer receiving radiotherapy with or without chemotherapy: a systematic literature review,” *Radiotherapy and Oncology*, vol. 66, no. 3, pp. 253–262, 2003.
- [2] S. T. Sonis, “Pathobiology of mucositis,” *Seminars in Oncology Nursing*, vol. 20, no. 1, pp. 11–15, 2004.
- [3] S. T. Sonis, “Oral mucositis,” *Anti-Cancer Drugs*, vol. 22, no. 7, pp. 607–612, 2011.
- [4] S. T. Sonis and A. Villa, “Phase II investigational oral drugs for the treatment of radio/chemotherapy induced oral mucositis,” *Expert Opinion on Investigational Drugs*, vol. 27, no. 2, pp. 147–154, 2018.
- [5] D. P. Bartel, “MicroRNAs: genomics, biogenesis, mechanism, and function,” *Cell*, vol. 116, no. 2, pp. 281–297, 2004.
- [6] M. A. Cortez, D. Valdecanas, X. Zhang et al., “Therapeutic delivery of miR-200c enhances radiosensitivity in lung cancer,” *Molecular Therapy*, vol. 22, no. 8, pp. 1494–1503, 2014.
- [7] A. Magenta, C. Cencioni, P. Fasanaro et al., “miR-200c is upregulated by oxidative stress and induces endothelial cell apoptosis and senescence via ZEB1 inhibition,” *Cell Death and Differentiation*, vol. 18, no. 10, pp. 1628–1639, 2011.
- [8] U. Burk, J. Schubert, U. Wellner et al., “A reciprocal repression between ZEB1 and members of the miR-200 family promotes EMT and invasion in cancer cells,” *EMBO Reports*, vol. 9, no. 6, pp. 582–589, 2008.
- [9] Q. Dong, J. E. Oh, W. Chen et al., “Radioprotective effects of Bmi-1 involve epigenetic silencing of oxidase genes and enhanced DNA repair in normal human keratinocytes,” *The Journal of Investigative Dermatology*, vol. 131, no. 6, pp. 1216–1225, 2011.
- [10] C. P. Bracken, P. A. Gregory, N. Kolesnikoff et al., “A double-negative feedback loop between ZEB1-SIP1 and the microRNA-200 family regulates epithelial-mesenchymal transition,” *Cancer Research*, vol. 68, no. 19, pp. 7846–7854, 2008.
- [11] E. Aunin, D. Broadley, M. I. Ahmed, A. N. Mardaryev, and N. V. Botchkareva, “Exploring a role for regulatory miRNAs in wound healing during ageing: involvement of miR-200c in wound repair,” *Scientific Reports*, vol. 7, no. 1, article 3257, 2017.
- [12] G. Han, L. Bian, F. Li et al., “Preventive and therapeutic effects of Smad7 on radiation-induced oral mucositis,” *Nature Medicine*, vol. 19, no. 4, pp. 421–428, 2013.
- [13] P. Güneri, J. B. Epstein, A. Kaya, A. Veral, A. Kazandı, and H. Boyacioglu, “The utility of toluidine blue staining and brush cytology as adjuncts in clinical examination of suspicious oral mucosal lesions,” *International Journal of Oral and Maxillofacial Surgery*, vol. 40, no. 2, pp. 155–161, 2011.
- [14] S. Zare, M. A. Zarei, T. Ghadimi, F. Fathi, A. Jalili, and M. S. Hakhamaneshi, “Isolation, cultivation and transfection of human keratinocytes,” *Cell Biology International*, vol. 38, no. 4, pp. 444–451, 2014.
- [15] Q. Qin, H. Cheng, J. Lu et al., “Small-molecule survivin inhibitor YM155 enhances radiosensitization in esophageal squamous cell carcinoma by the abrogation of G₂ checkpoint and suppression of homologous recombination repair,” *Journal of Hematology & Oncology*, vol. 7, no. 1, p. 62, 2014.
- [16] Q. Dong, L. Chen, Q. Lu et al., “Quercetin attenuates doxorubicin cardiotoxicity by modulating Bmi-1 expression,” *British Journal of Pharmacology*, vol. 171, no. 19, pp. 4440–4454, 2014.
- [17] Z. Xu, J. Tao, P. Chen et al., “Sodium butyrate inhibits colorectal cancer cell migration by downregulating Bmi-1 through enhanced miR-200c expression,” *Molecular Nutrition & Food Research*, vol. 62, no. 6, article e1700844, 2018.
- [18] M. Yoshizumi, T. Nakamura, M. Kato et al., “Release of cytokines/chemokines and cell death in UVB-irradiated human keratinocytes, HaCaT,” *Cell Biology International*, vol. 32, no. 11, pp. 1405–1411, 2008.
- [19] E. Nuryadi, T. B. M. Permata, S. Komatsu, T. Oike, and T. Nakano, “Inter-assay precision of clonogenic assays for radiosensitivity in cancer cell line A549,” *Oncotarget*, vol. 9, no. 17, pp. 13706–13712, 2018.
- [20] K. A. Hogan, A. Ravindran, M. A. Podolsky, and A. B. Glick, “The TGF β 1 pathway is required for NF κ B dependent gene expression in mouse keratinocytes,” *Cytokine*, vol. 64, no. 3, pp. 652–659, 2013.
- [21] R. C. Stone, I. Pastar, N. Ojeh et al., “Epithelial-mesenchymal transition in tissue repair and fibrosis,” *Cell and Tissue Research*, vol. 365, no. 3, pp. 495–506, 2016.
- [22] R. Kalluri and R. A. Weinberg, “The basics of epithelial-mesenchymal transition,” *The Journal of Clinical Investigation*, vol. 119, no. 6, pp. 1420–1428, 2009.
- [23] S. Al-Ansari, J. A. E. M. Zecha, A. Barasch, J. de Lange, F. R. Rozema, and J. E. Raber-Durlacher, “Oral mucositis induced by anticancer therapies,” *Current Oral Health Reports*, vol. 2, no. 4, pp. 202–211, 2015.
- [24] S. T. Sonis, “Mucositis: the impact, biology and therapeutic opportunities of oral mucositis,” *Oral Oncology*, vol. 45, no. 12, pp. 1015–1020, 2009.
- [25] O. M. Maria, A. Syme, N. Eliopoulos, and T. Muanza, “Single-dose radiation-induced oral mucositis mouse model,” *Frontiers in Oncology*, vol. 6, p. 154, 2016.
- [26] T. Kuilman, C. Michaloglou, W. J. Mooi, and D. S. Peeper, “The essence of senescence,” *Genes & Development*, vol. 24, no. 22, pp. 2463–2479, 2010.
- [27] P. Viatour, M. P. Merville, V. Bours, and A. Chariot, “Phosphorylation of NF- κ B and I κ B proteins: implications in cancer and inflammation,” *Trends in Biochemical Sciences*, vol. 30, no. 1, pp. 43–52, 2005.
- [28] S. L. Lu, D. Reh, A. G. Li et al., “Overexpression of transforming growth factor β 1 in head and neck epithelia results in inflammation, angiogenesis, and epithelial hyperproliferation,” *Cancer Research*, vol. 64, no. 13, pp. 4405–4410, 2004.
- [29] R. Derynck and Y. E. Zhang, “Smad-dependent and Smad-independent pathways in TGF- β family signalling,” *Nature*, vol. 425, no. 6958, pp. 577–584, 2003.
- [30] L. Bian, G. Han, C. W. Zhao, P. J. Garl, and X. J. Wang, “The role of Smad7 in oral mucositis,” *Protein & Cell*, vol. 6, no. 3, pp. 160–169, 2015.
- [31] S. A. Eming, P. Martin, and M. Tomic-Canic, “Wound repair and regeneration: mechanisms, signaling, and translation,” *Science Translational Medicine*, vol. 6, no. 265, article 265sr6, 2014.

- [32] P. A. Coulombe, "Wound epithelialization: accelerating the pace of discovery," *The Journal of Investigative Dermatology*, vol. 121, no. 2, pp. 219–230, 2003.
- [33] R. Perdígão-Henriques, F. Petrocca, G. Altschuler et al., "miR-200 promotes the mesenchymal to epithelial transition by suppressing multiple members of the Zeb2 and Snail1 transcriptional repressor complexes," *Oncogene*, vol. 35, no. 2, pp. 158–172, 2016.
- [34] H. Peinado, D. Olmeda, and A. Cano, "Snail, Zeb and bHLH factors in tumour progression: an alliance against the epithelial phenotype?," *Nature Reviews Cancer*, vol. 7, no. 6, pp. 415–428, 2007.
- [35] B. H. Guo, Y. Feng, R. Zhang et al., "Bmi-1 promotes invasion and metastasis, and its elevated expression is correlated with an advanced stage of breast cancer," *Molecular Cancer*, vol. 10, no. 1, p. 10, 2011.
- [36] P. Stock, O. Akbari, G. Berry, G. J. Freeman, R. H. DeKruyff, and D. T. Umetsu, "Induction of T helper type 1-like regulatory cells that express Foxp3 and protect against airway hyper-reactivity," *Nature Immunology*, vol. 5, no. 11, pp. 1149–1156, 2004.
- [37] B. P. Zhou, J. Deng, W. Xia et al., "Dual regulation of Snail by GSK-3 β -mediated phosphorylation in control of epithelial-mesenchymal transition," *Nature Cell Biology*, vol. 6, no. 10, pp. 931–940, 2004.
- [38] X. Lin, D. Ojo, F. Wei, N. Wong, Y. Gu, and D. Tang, "A novel aspect of tumorigenesis-BMI1 functions in regulating DNA damage response," *Biomolecules*, vol. 5, no. 4, pp. 3396–3415, 2015.
- [39] I. K. Park, S. J. Morrison, and M. F. Clarke, "Bmi1, stem cells, and senescence regulation," *The Journal of Clinical Investigation*, vol. 113, no. 2, pp. 175–179, 2004.
- [40] J. Liu, L. Cao, J. Chen et al., "Bmi1 regulates mitochondrial function and the DNA damage response pathway," *Nature*, vol. 459, no. 7245, pp. 387–392, 2009.
- [41] S. Facchino, M. Abdouh, W. Chatoo, and G. Bernier, "BMI1 confers radioresistance to normal and cancerous neural stem cells through recruitment of the DNA damage response machinery," *The Journal of Neuroscience*, vol. 30, no. 30, pp. 10096–10111, 2010.
- [42] R. Derynck, B. P. Muthusamy, and K. Y. Saetern, "Signaling pathway cooperation in TGF- β -induced epithelial-mesenchymal transition," *Current Opinion in Cell Biology*, vol. 31, pp. 56–66, 2014.
- [43] M. W. J. Ferguson and S. O'Kane, "Scar-free healing: from embryonic mechanisms to adult therapeutic intervention," *Philosophical Transactions of the Royal Society B: Biological Sciences*, vol. 359, no. 1445, pp. 839–850, 2004.
- [44] R. H. Kim, M. B. Lieberman, R. Lee et al., "Bmi-1 extends the life span of normal human oral keratinocytes by inhibiting the TGF- β signaling," *Experimental Cell Research*, vol. 316, no. 16, pp. 2600–2608, 2010.
- [45] J. J. L. Jacobs, K. Kieboom, S. Marino, R. A. DePinho, and M. van Lohuizen, "The oncogene and Polycomb-group gene bmi-1 regulates cell proliferation and senescence through the ink4a locus," *Nature*, vol. 397, no. 6715, pp. 164–168, 1999.

Review Article

Noncoding RNAs in Cardiac Autophagy following Myocardial Infarction

Annie Turkieh, Henri Charrier, Emilie Dubois-Deruy, Sina Porouchani, Marion Bouvet, and Florence Pinet 

Univ. Lille, Inserm, Institut Pasteur de Lille, U1167-RID-AGE, FHU-REMOD-VHF, F-59000 Lille, France

Correspondence should be addressed to Florence Pinet; florence.pinet@pasteur-lille.fr

Received 7 March 2019; Accepted 23 April 2019; Published 3 June 2019

Guest Editor: Reggiani Vilela Gonçalves

Copyright © 2019 Annie Turkieh et al. This is an open access article distributed under the Creative Commons Attribution License, which permits unrestricted use, distribution, and reproduction in any medium, provided the original work is properly cited.

Macroautophagy is an evolutionarily conserved process of the lysosome-dependent degradation of damaged proteins and organelles and plays an important role in cellular homeostasis. Macroautophagy is upregulated after myocardial infarction (MI) and seems to be detrimental during reperfusion and protective during left ventricle remodeling. Identifying new regulators of cardiac autophagy may help to maintain the activity of this process and protect the heart from MI effects. Recently, it was shown that noncoding RNAs (microRNAs and long noncoding RNAs) are involved in autophagy regulation in different cell types including cardiac cells. In this review, we summarized the role of macroautophagy in the heart following MI and we focused on the noncoding RNAs and their targeted genes reported to regulate autophagy in the heart under these pathological conditions.

1. Introduction

Myocardial infarction (MI) is a cardiovascular event caused by obstruction of one or more arteries supplying the heart. This area of the heart is therefore no longer supplied with oxygen and nutrients leading to the death of cardiomyocytes. Coronary reperfusion is the only recognized method to reduce the size of the infarct if it is performed within hours after MI. Despite its beneficial effect, several deleterious events such as increased oxidative stress and cell death are observed during the reperfusion process. If the infarcted zone is very extensive, there is a decrease in the contractile function of the heart. In order to compensate for this loss and maintain normal blood flow, the heart will undergo structural changes such as thinning of the infarcted zone, fibrosis, cardiomyocyte hypertrophy, and left ventricle (LV) dilatation [1]. Left ventricle remodeling (LVR) is initially a protective mechanism but in the long term can lead to heart failure (HF) [2–4]. Despite current therapy, acute MI and HF remain the leading causes of death and disability worldwide. New therapeutic strategies are therefore required to protect

the heart against the detrimental effects of acute ischemia/reperfusion (I/R) injury, in order to prevent cardiomyocyte death and reduce myocardial infarct size, preserve LV function, and prevent the onset of HF.

Macroautophagy is an important and nonselective proteolytic mechanism that regulates the homeostasis of long-lived proteins, macromolecules including lipids and cell organelles, by surrounding them in a double-membrane vesicle known as autophagosome in order to deliver them to the lysosome for degradation [5]. It plays an essential role for maintaining heart structure and function under baseline conditions [6–8]. Several studies showed that macroautophagy is upregulated in the heart following MI and suggested that this process may protect the heart against MI effects [9–11]. Recently, it was shown that noncoding RNAs (microRNAs (miRNA) and long noncoding RNAs (lncRNA)) are involved in autophagy regulation in different cell types including cardiac cells [12–14]. In this review, we summarized the role of macroautophagy in the heart following MI and we focused on the noncoding RNAs and their targeted genes reported to regulate autophagy in the heart under pathological conditions.

2. Macroautophagy Mechanism

Macroautophagy proceeds in several successive steps and involves different proteins as previously described [5]. In summary, autophagy induction is mainly regulated by the ULK (unc-51-like kinase) complex which is composed of ULK1/2, ATG13 (autophagy-related gene 13), ATG101, and FIP200 (focal adhesion kinase family interacting protein with a 200 kDa mass). Activation of the PI3K complex contributes to the vesicle nucleation, the first step of autophagosome formation. This complex is composed of Beclin-1, ATG14, VPS34 (phosphatidylinositol 3-kinase vacuolar protein sorting 34), and VPS15. Finally, two ubiquitin-like protein conjugation systems are required for the vesicle elongation, the first to form ATG12-ATG5-ATG16L1 complex and the second to form LC3II (microtubule-associated protein 1 light chain II), the lipidated form of LC3. For this latter step, ATG4 cleaves pro-LC3 to LC3I before its conjugation to phosphatidylethanolamine by ATG7, ATG3, and ATG12-ATG5-ATG16L1 complex. Several pathways were shown to regulate autophagy by activation or inactivation of one of these ATG proteins. For example, mTOR (mammalian target of rapamycin) activation inhibited autophagy by decreasing ULK1 activity [15] and ATG14/VSP34-35 complex formation [16]. AMPK (adenosine monophosphate-activated protein kinase) positively regulated autophagy by increasing Beclin-1 phosphorylation leading to its interaction with VSP34 [17]. However, Bcl-2 interacts with Beclin-1 for blocking its interaction with VSP34 [18].

2.1. Macroautophagy during Ischemia/Reperfusion. The regulation of autophagy is different during ischemia and reperfusion [10]. During heart ischemia, nutrient and oxygen supplies to the cardiac cells decrease, inducing mitochondrial and cellular dysfunction that lead to cell death. To protect them, the cardiac cells induce autophagy via the AMPK/mTOR pathway in order to degrade/eliminate damaged organelles and proteins and provide the substrates necessary for their survival. During reperfusion, there is an increase of reactive oxygen species (ROS) production inducing a strong expression of Beclin-1 which on the one hand promotes the formation of autophagosomes and on the other hand inhibits the expression of genes involved in the fusion of autophagosomes with lysosomes [19]. In addition, ROS inhibit the expression of LAMP-2, a protein involved in the fusion of autophagosomes with lysosomes. Autophagy is then induced excessively during reperfusion but is inactive. Blocking the degradation of the contents of autophagosomes promotes oxidative stress, decreases mitochondrial permeability, and causes cell death. Partial inhibition of Beclin-1 expression (heterozygous mice) has been shown to protect against apoptosis induced during reperfusion while its total deletion is deleterious [10]. These data showed that autophagy is a protective mechanism during ischemia but its excessive induction during reperfusion is deleterious.

2.2. Macroautophagy during LVR in Post-MI. The activity of autophagy and its role in LVR post-MI have been studied in murine models with permanent ligation of the left coronary

artery. Autophagy is induced in noninfarcted area of the heart during the subacute (1 week) and chronic (3 weeks) stages after MI [11]. Inhibition of autophagy by bafilomycin (a pharmacological agent that blocks the fusion of the autophagosome with the lysosome) promoted LVR and worsens cardiac dysfunction. In contrast, administration of trehalose (a nonnaturally reduced disaccharide) in mice after ligation activated autophagy, reduced LVR, and improved cardiac function at 4 weeks post-MI [20]. However, this protective effect of trehalose on the heart was not observed in mice invalidated for the Beclin-1 gene, but an increase in the activity of mTOR was observed in the noninfarcted area of the heart. It has been shown that the inhibition of mTOR activity induced autophagy leading to a decrease of LVR and an improvement in cardiac function in post-MI [21]. All these data showed a protective role of autophagy in later stages in post-MI but its activity remained insufficient to prevent LVR and cardiac dysfunction.

3. Macroautophagy Regulation by Noncoding RNAs during and following MI

About 99% of the human genome do not encode proteins but are transcriptionally highly active and give rise to a broad spectrum of noncoding RNAs (ncRNAs) with regulatory and structural functions. Based on the size criteria of 200 nucleotides (nt), ncRNAs are divided into long (>200 nt) and short ncRNAs (<200 nt).

The ncRNAs are modulated in some cardiovascular diseases including MI [22, 23]. The significant changes in their expression pattern upon MI highlighted their contribution in the regulation of pathogenesis of MI. Furthermore, it was shown that ncRNAs could regulate autophagy in some cardiac disorders including MI, hypertrophy, and HF [12–14]. In this part, we summarized the noncoding RNAs which have been reported to regulate cardiac autophagy during and following MI and highlighted their specific autophagic targets and their importance as new therapeutic targets to protect the heart against I/R injury and prevent cardiac remodeling and dysfunction (Figure 1).

3.1. Macroautophagy Regulation by mRNAs. MiRNAs are defined as single-stranded noncoding RNAs around 22 nucleotides and are highly conserved between species [22]. Once synthesized and matured through several steps, these miRNAs bind to the complementary 3'UTR of their target mRNA and either degrade or silence them. A near-perfect match between the seed region of the miRNA (8 nucleotides at its 5'UTR end) and its target leads to complete degradation of mRNA, while a partial complementary results in the suppression of the gene expression. MiRNAs may have one or multiple mRNA targets and are involved in the regulation of numerous biological processes in the heart including autophagy.

3.1.1. Antiautophagic miRNAs with Protective Effects. Several miRNAs were modulated during I/R and seem to have a protective effect by decreasing excessive autophagy-induced cell apoptosis by targeting one of the ATG genes. MiR-188-3p

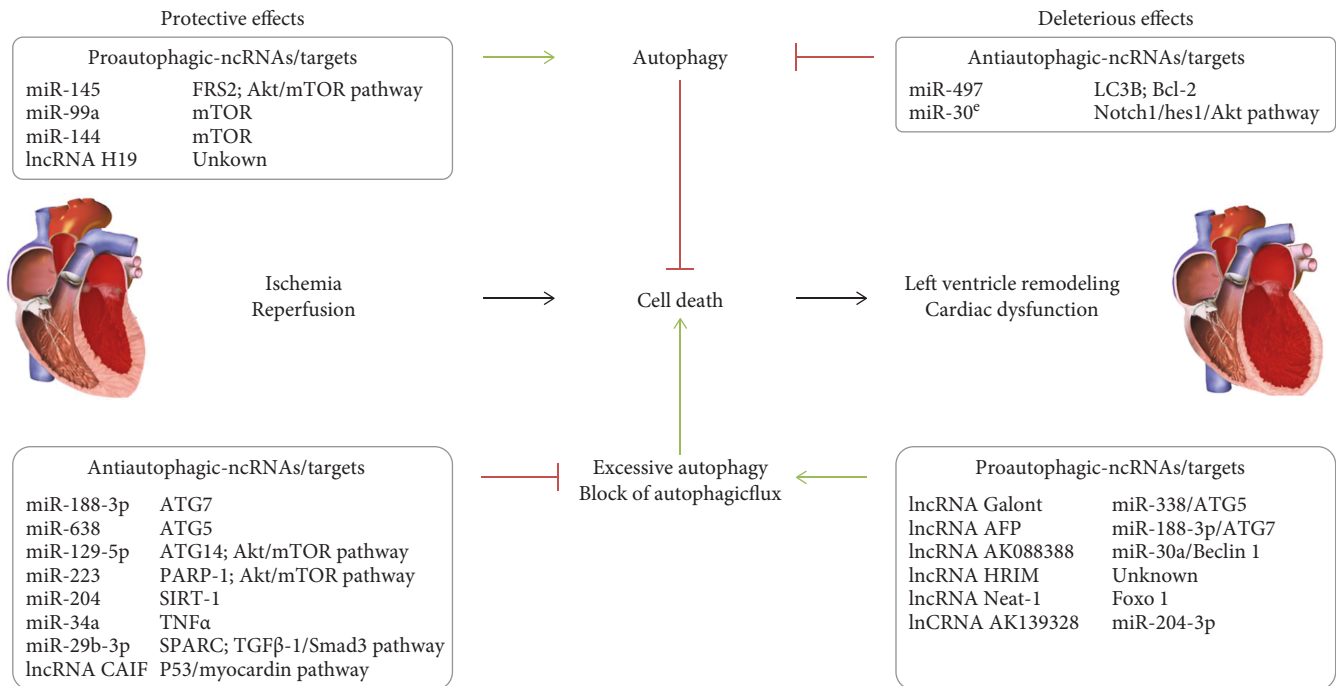


FIGURE 1: Outline summarizing the noncoding RNAs regulating cardiac autophagy and their targets and function. Green and red arrows indicate activation and inhibition, respectively.

levels are reduced in cardiomyocytes treated with anoxia/reoxygenation and in MI mice. Overexpression of miR-188-3p in MI mice attenuated autophagy by targeting autophagy mediator Atg7 and decreased the infarcted area size [24]. It was shown that miR-638 suppressed the expression of Atg5 by targeting its 3'UTR region. It is downregulated in human cardiomyocytes after hypoxia/reoxygenation (H/R), and its overexpression improves the viability of these cells. However, enforced expression of Atg5 reversed the effect of miR-638 on autophagy and cell apoptosis suggesting that miR-638 attenuated the effects of H/R treatment by regulating ATG5-mediated autophagy in human cardiomyocytes [25]. Also, overexpression of miR-129-5p in H9c2 cells treated by hydrogen peroxide inhibited autophagy by targeting the Atg14 gene and activating the PI3K/AKT/mTOR pathway resulting in decreased cell apoptosis [26].

Other miRNAs play their protective effect by regulating one of the pathways involved in autophagy regulation. The levels of miR-223 are significantly upregulated in the heart of post-MI HF rats and in hypoxia-treated neonatal rat cardiomyocytes (NRCMs) and H9c2 cells. The increased miR-223 levels protect NRCMs and H9c2 cells from hypoxia-induced apoptosis whereas decreasing miR-223 expression had contrasting effects. This protective effect of miR-223 is explained by the decrease of its target gene expression PARP-1 (poly(ADP-ribose) polymerase 1) resulting in inhibition of excessive autophagy via the Akt/mTOR pathway [27]. However, miR-204 expression is decreased in the heart of rat upon I/R injury associated with increased autophagy as observed by the increased LC3II levels [28]. Also, it was shown that transfection of miR-204 in H9c2 cells attenuated cell apoptosis induced by H/R treatment. The protective effect of miR-

204 is explained by targeting SIRT1-mediated autophagy [29]. The expression of miR-34a is also decreased during I/R and overexpression of this miR decreased TNF α expression resulting in reduced autophagy and apoptosis levels on NRCMs after H/R [30]. Lower miR-29b-3p levels were found in HF patients and in hypoxia-stimulated H9c2 cells. The overexpression of miR-29b-3p inhibited autophagy and apoptosis induced in hypoxic-induced H9c2 cells through targeting SPARC and inhibiting TGF β -1/Smad3 pathway [31].

3.1.2. Antiautophagic miRNAs with Deleterious Effects. Some miRNAs contribute to ischemic/reperfusion injury by inhibiting the autophagy process. miR-497 is dramatically downregulated in the infarcted heart and in hypoxic cardiomyocytes, and its overexpression in murine MI model increased the infarcted size. It was shown that miR-497 inhibited autophagy by targeting the LC3B gene and induced cell apoptosis by targeting the Bcl-2 gene suggesting that decreasing miR-497 levels is a protective mechanism of the heart in response to MI [32]. The expression of miR-30e was also decreased after myocardial I/R. Its silencing in H9c2 cells increased autophagy and attenuated oxidative stress and cell apoptosis that are reversed by treating the cells with 3-methyladenine, an inhibitor of macroautophagy. These results suggest that decreasing the miR-30e levels protected the heart against I/R injury by autophagy induction [33].

3.1.3. Proautophagic miRNAs with Protective Effects. Higashi et al. [34] showed that 30 min of coronary occlusion followed by 2 days of reperfusion caused a significant decrease in the rabbit cardiac tissue expression of miR-145 in the border

and infarcted areas of the myocardium compared to the remote noninfarcted area. Injection of liposomes containing miR-145 after the beginning of reperfusion reduced the infarcted area size and improved the LV function and remodeling; these beneficial effects were abolished by chloroquine treatment. Further study showed that miR-145 promoted autophagy in cardiomyocyte by directly targeting FRS2 (fibroblast growth factor receptor substrate 2) mRNA resulting in the acceleration of the transition of LC3I to LC3II, an important step of autophagosome maturation [34]. The protective effect of miR-145 is also observed in H9c2 cells after H/R. In this study, the authors demonstrated that miR-145 inhibited H/R-induced apoptosis by promoting autophagy via the Akt3/mTOR signaling pathway [35]. miR-99a was shown to be downregulated in the infarcted heart and in neonatal mice ventricle myocytes exposed to hypoxia. Lentivirus-mediated overexpression of miR-99a in the infarcted heart inhibited cardiac remodeling and improved heart function at 1 and 4 weeks after its administration. It was shown that miR-99a decreased mTOR protein levels without any effect on its mRNA levels suggesting that miR-99a regulated mTOR expression at a posttranscriptional level. Consequently, the autophagy induced was associated with a decrease of cell apoptosis. This study demonstrated that overexpression of miR-99a improved post-MI cardiac function by upregulating autophagy via targeting mTOR pathways, inhibiting apoptosis, and attenuating pathological remodeling [36]. The miR-144 levels were reduced in the heart of MI mice with permanent left anterior descending artery (LAD) ligation. The miR-144 k/o mice showed a worse HF phenotype with ventricular dilatation and impaired contractility after LAD ligation. However, miR-144 administration decreased myocardial infarcted size and improved post-MI remodeling. Further study allowed authors to conclude that miR-144 increased autophagy and decreased fibrosis and apoptosis by targeting mTOR [37].

3.2. Macroautophagy Regulation by lncRNAs. lncRNAs are noncoding RNAs longer than 200 nucleotides that regulate both gene expression and protein translation [22]. Nuclear localized lncRNAs can regulate gene expression at both the epigenetic and transcriptional levels. Cytosol-based lncRNAs can modify protein translation by blocking, stabilizing/destabilizing, or sponging miRNAs. The lncRNAs are involved in the regulation of numerous biological processes including autophagy in cardiac and noncardiac cells.

3.2.1. Antiautophagic lncRNA with Protective Effects. Liu et al. [38] showed that the expression of lncRNA CAIF (cardiac autophagy inhibitory factor) was significantly decreased in a mice model of I/R injury and in cardiomyocytes treated with H₂O₂. Conversely, overexpression of CAIF inhibited autophagy inducing cardiomyocyte cell death and cardiac dysfunction caused by I/R. In this study, the authors demonstrate that CAIF directly binds to p53 protein and blocks its interaction with the myocardin promotor. Myocardin, a smooth muscle and cardiac muscle-specific transcriptional activator, is upregulated after I/R and H₂O₂ treatment and is involved in autophagy regulation in cardiomyocytes by

increasing Beclin-1 expression. These data suggest CAIF-P53-myocardin pathway as a novel regulator of autophagy in cardiomyocytes and as a potential therapeutic target in order to inhibit excessive autophagy and improve cardiac function after I/R [38].

3.2.2. Proautophagic lncRNA with Protective Effects. On the other hand, it was shown that the lncRNA H19 expression was decreased in a mice model of acute MI and that its overexpression decreased infarcted size and improved cardiac function associated with autophagy upregulation; however, the mechanisms by which autophagy is regulated by H19 are still unknown. These results suggest that H19 protects the heart from MI by increasing cardiac autophagy [39].

3.2.3. Proautophagic lncRNAs with Deleterious Effects. Some lncRNAs are upregulated after I/H and enhanced autophagy target gene expression by inhibiting miRNA expression. Yin et al. [40] showed that lncRNA Galont (GATA1 activated lncRNA) is upregulated in neonatal mice cardiomyocytes in response to anoxia/reoxygenation; however, miR-338 expression is downregulated. Overexpression of miR-338 directly decreased the formation of autophagic vesicles and induced cell death after anoxia/reoxygenation treatment without any effect on control cells. The antiautophagic effect of miR-338 is explained by its direct targeting of the autophagic mediator Atg5. It was shown that Galont directly bound to miR-338 and decrease its expression. Consequently, Atg5 expression is increased resulting in excessive cardiac autophagy and cell death [40]. Also, the lncRNA APF (autophagy-promoting factor) enhances cardiac autophagy and cell death by inhibiting miR-188-3p expression resulting in the increase of its target gene expression, Atg7 [24]. Furthermore, lncRNA AK088388 is upregulated during reoxygenation in mouse cardiac myocytes associated with the decreased miR-30a expression. Overexpression of miR-30a decreased the expression of its target gene Beclin-1 resulting in inhibition of autophagy induction and decreased cell death. The cooverexpression of lncRNA AK088388 inhibited the protective effect of miR-30a. However, the mutation of the miR30-a binding site in AK088388 failed to block the effect of this miRNA on autophagy and cell survival. These results suggest that lncRNA AK088388 regulates autophagy through miR-30a/Beclin-1 pathway to affect cardiomyocyte injury [41]. The lncRNA HRIM (hypoxia/reoxygenation injury-related factor in myocyte) was upregulated after H/R in H9c2 cells. HRIM silencing prevented death of cells by suppressing the autophagic activity in H/R-treated cells. However, the target genes of this lncRNA and the detailed mechanism of its autophagic effect need to be elucidated [42]. Other lncRNAs were highly expressed in diabetic murine heart and contributed to I/R injury by regulating autophagy. It was shown that Neat-1 (nuclear-enriched abundant transcript 1) and AK139328 seemed to induce autophagy by upregulating Foxo1 expression and decreasing miR-204-3p levels, respectively [43, 44].

lncRNA MALAT1 (metastasis-associated lung adenocarcinoma transcript 1) is expressed at high levels in patients with acute MI [45] and is closely associated with the

pathogenesis of myocardial I/R injury [46, 47]. It was shown, on the one hand, that MALAT1 contained binding site for miR-204 [48] and, in the other hand, that miR-204 protected the cardiomyocytes against I/R injury via inhibiting autophagic cell death [28]. Also, MALAT1 targeted miR-558 to enhance ULK1-mediated autophagy in isoproterenol-treated cardiomyocytes [49]. It will be important to know if lncRNA MALAT1 increased cardiomyocyte autophagy and myocardial injury during I/R by negatively regulating miR-204 or miR-558 expression.

4. Conclusion

Despite current therapies, acute MI and HF which often follow remain the leading causes of death and disability worldwide. New therapeutic strategies are therefore required to protect the heart against the detrimental effects of acute ischemia/reperfusion injury. Inhibition of macroautophagy during reperfusion prevented cardiomyocyte death and reduced myocardial infarct size; however, its induction during LVR preserved LV function and prevented the onset of HF. Most pharmacological agents used up to date for regulating macroautophagy are not specific and may interfere with other cellular processes, so it will be necessary to identify new therapeutic approaches to regulate autophagy. Several noncoding RNAs were shown to be modulated during I/R and involved on cardiac autophagy regulation. The tissue-specific expression of some noncoding RNAs and their easy manipulation show their potential as novel targets for clinical developments to treat autophagy-related diseases. Identification of specific cardiac noncoding RNAs that regulate autophagy could be a good opportunity to protect the heart from MI injury without affecting the autophagy activity in other organs.

Conflicts of Interest

The authors declare no conflict of interest.

Acknowledgments

AT received a fellowship from Agence Nationale de la Recherche (ERA-NET Co-fund action ERA-CVD JTC2016 No. 680969) and EDD from “Fondation Lefoulon Delalande.” FP is a MC substitute member of European Cooperation in Science and Technology Action Transautophagy (CA15138) and is a MC member of European Cooperation in Science and Technology Action cardioRNA (CA1229).

References

- [1] M. A. Pfeffer and E. Braunwald, “Ventricular remodeling after myocardial infarction. Experimental observations and clinical implications,” *Circulation*, vol. 81, no. 4, pp. 1161–1172, 1990.
- [2] M. St John Sutton, M. A. Pfeffer, T. Plappert et al., “Quantitative two-dimensional echocardiographic measurements are major predictors of adverse cardiovascular events after acute myocardial infarction. The protective effects of captopril,” *Circulation*, vol. 89, no. 1, pp. 68–75, 1994.
- [3] P. de Groote, M. Fertin, A. Duva Pentiah, C. Goéminne, N. Lamblin, and C. Bauters, “Long-term functional and clinical follow-up of patients with heart failure with recovered left ventricular ejection fraction after β -blocker therapy,” *Circulation. Heart Failure*, vol. 7, no. 3, pp. 434–439, 2014.
- [4] C. Bauters, E. Dubois, S. Porouchani et al., “Long-term prognostic impact of left ventricular remodeling after a first myocardial infarction in modern clinical practice,” *PLoS One*, vol. 12, no. 11, article e0188884, 2017.
- [5] Y. Ohsumi, “Historical landmarks of autophagy research,” *Cell Research*, vol. 24, no. 1, pp. 9–23, 2014.
- [6] A. Nakai, O. Yamaguchi, T. Takeda et al., “The role of autophagy in cardiomyocytes in the basal state and in response to hemodynamic stress,” *Nature Medicine*, vol. 13, no. 5, pp. 619–624, 2007.
- [7] B. Gan, X. Peng, T. Nagy, A. Alcaraz, H. Gu, and J.-L. Guan, “Role of FIP200 in cardiac and liver development and its regulation of TNF α and TSC-mTOR signaling pathways,” *The Journal of Cell Biology*, vol. 175, no. 1, pp. 121–133, 2006.
- [8] T. Kaizuka and N. Mizushima, “Atg13 is essential for autophagy and cardiac development in mice,” *Molecular and Cellular Biology*, vol. 36, no. 4, pp. 585–595, 2016.
- [9] L. Yan, D. E. Vatner, S.-J. Kim et al., “Autophagy in chronically ischemic myocardium,” *Proceedings of the National Academy of Sciences*, vol. 102, no. 39, pp. 13807–13812, 2005.
- [10] Y. Matsui, H. Takagi, X. Qu et al., “Distinct roles of autophagy in the heart during ischemia and reperfusion: roles of AMP-activated protein kinase and Beclin 1 in mediating autophagy,” *Circulation Research*, vol. 100, no. 6, pp. 914–922, 2007.
- [11] H. Kanamori, G. Takemura, K. Goto et al., “The role of autophagy emerging in postinfarction cardiac remodeling,” *Cardiovascular Research*, vol. 91, no. 2, pp. 330–339, 2011.
- [12] S. K. Gupta and T. Thum, “Non-coding RNAs as orchestrators of autophagic processes,” *Journal of Molecular and Cellular Cardiology*, vol. 95, pp. 26–30, 2016.
- [13] L. Yang, H. Wang, Q. Shen, L. Feng, and H. Jin, “Long non-coding RNAs involved in autophagy regulation,” *Cell Death & Disease*, vol. 8, no. 10, p. e3073, 2017.
- [14] T. Sun, M.-Y. Li, P.-F. Li, and J.-M. Cao, “MicroRNAs in cardiac autophagy: small molecules and big role,” *Cells*, vol. 7, no. 8, p. 104, 2018.
- [15] J. Kim, M. Kundu, B. Viollet, and K.-L. Guan, “AMPK and mTOR regulate autophagy through direct phosphorylation of Ulk1,” *Nature Cell Biology*, vol. 13, no. 2, pp. 132–141, 2011.
- [16] H.-X. Yuan, R. C. Russell, and K.-L. Guan, “Regulation of PIK3C3/VPS34 complexes by MTOR in nutrient stress-induced autophagy,” *Autophagy*, vol. 9, no. 12, pp. 1983–1995, 2013.
- [17] J. Kim, Y. C. Kim, C. Fang et al., “Differential regulation of distinct Vps34 complexes by AMPK in nutrient stress and autophagy,” *Cell*, vol. 152, no. 1–2, pp. 290–303, 2013.
- [18] R. Kang, H. J. Zeh, M. T. Lotze, and D. Tang, “The Beclin 1 network regulates autophagy and apoptosis,” *Cell Death and Differentiation*, vol. 18, no. 4, pp. 571–580, 2011.
- [19] X. Ma, H. Liu, S. R. Foyil et al., “Impaired autophagosome clearance contributes to cardiomyocyte death in ischemia/reperfusion injury,” *Circulation*, vol. 125, no. 25, pp. 3170–3181, 2012.
- [20] S. Sciarretta, D. Yee, N. Nagarajan et al., “Trehalose-induced activation of autophagy improves cardiac remodeling after myocardial infarction,” *Journal of the American College of Cardiology*, vol. 71, no. 18, pp. 1999–2010, 2018.

- [21] S. J. Buss, S. Muenz, J. H. Riffel et al., "Beneficial effects of mammalian target of rapamycin inhibition on left ventricular remodeling after myocardial infarction," *Journal of the American College of Cardiology*, vol. 54, no. 25, pp. 2435–2446, 2009.
- [22] A. Das, A. Samidurai, and F. N. Salloum, "Deciphering Non-coding RNAs in cardiovascular health and disease," *Front Cardiovasc Med.*, vol. 5, p. 73, 2018.
- [23] W. Poller, S. Dimmeler, S. Heymans et al., "Non-coding RNAs in cardiovascular diseases: diagnostic and therapeutic perspectives," *European Heart Journal*, vol. 39, no. 29, pp. 2704–2716, 2018.
- [24] K. Wang, C.-Y. Liu, L.-Y. Zhou et al., "APF lncRNA regulates autophagy and myocardial infarction by targeting miR-188-3p," *Nature Communications*, vol. 6, no. 1, 2015.
- [25] P. Zhao, B.-L. Zhang, K. Liu, B. Qin, and Z.-H. Li, "Overexpression of miR-638 attenuated the effects of hypoxia/reoxygenation treatment on cell viability, cell apoptosis and autophagy by targeting ATG5 in the human cardiomyocytes," *European Review for Medical and Pharmacological Sciences*, vol. 22, no. 23, pp. 8462–8471, 2018.
- [26] H. Zhang, X. Zhang, and J. Zhang, "MiR-129-5p inhibits autophagy and apoptosis of H9c2 cells induced by hydrogen peroxide via the PI3K/AKT/mTOR signaling pathway by targeting ATG14," *Biochemical and Biophysical Research Communications*, vol. 506, no. 1, pp. 272–277, 2018.
- [27] X. Liu, Y. Deng, Y. Xu, W. Jin, and H. Li, "MicroRNA-223 protects neonatal rat cardiomyocytes and H9c2 cells from hypoxia-induced apoptosis and excessive autophagy via the Akt/mTOR pathway by targeting PARP-1," *Journal of Molecular and Cellular Cardiology*, vol. 118, pp. 133–146, 2018.
- [28] J. Xiao, X. Zhu, B. He et al., "MiR-204 regulates cardiomyocyte autophagy induced by ischemia-reperfusion through LC3-II," *Journal of Biomedical Science*, vol. 18, no. 1, p. 35, 2011.
- [29] R. Qiu, W. Li, and Y. Liu, "MicroRNA-204 protects H9C2 cells against hypoxia/reoxygenation-induced injury through regulating SIRT1-mediated autophagy," *Biomedicine & Pharmacotherapy*, vol. 100, pp. 15–19, 2018.
- [30] H. Shao, L. Yang, L. Wang, B. Tang, J. Wang, and Q. Li, "MicroRNA-34a protects myocardial cells against ischemia-reperfusion injury through inhibiting autophagy via regulating TNF α expression," *Biochemistry and Cell Biology*, vol. 96, no. 3, pp. 349–354, 2018.
- [31] S. Zhou, D. Lei, F. Bu, H. Han, S. Zhao, and Y. Wang, "MicroRNA-29b-3p targets SPARC gene to protect cardiocytes against autophagy and apoptosis in hypoxic-induced H9c2 cells," *Journal of Cardiovascular Translational Research*, 2018.
- [32] X. Li, Z. Zeng, Q. Li et al., "Inhibition of microRNA-497 ameliorates anoxia/reoxygenation injury in cardiomyocytes by suppressing cell apoptosis and enhancing autophagy," *Oncotarget*, vol. 6, no. 22, pp. 18829–18844, 2015.
- [33] J. Zheng, J. Li, B. Kou, Q. Yi, and T. Shi, "MicroRNA-30e protects the heart against ischemia and reperfusion injury through autophagy and the Notch1/Hes1/Akt signaling pathway," *International Journal of Molecular Medicine*, vol. 41, no. 6, pp. 3221–3230, 2018.
- [34] K. Higashi, Y. Yamada, S. Minatoguchi et al., "MicroRNA-145 repairs infarcted myocardium by accelerating cardiomyocyte autophagy," *American Journal of Physiology. Heart and Circulatory Physiology*, vol. 309, no. 11, pp. H1813–H1826, 2015.
- [35] L. Yan, N. Guo, Y. Cao et al., "miRNA-145 inhibits myocardial infarction-induced apoptosis through autophagy via Akt3/mTOR signaling pathway in vitro and in vivo," *International Journal of Molecular Medicine*, vol. 42, no. 3, pp. 1537–1547, 2018.
- [36] Q. Li, J. Xie, R. Li et al., "Overexpression of microRNA-99a attenuates heart remodelling and improves cardiac performance after myocardial infarction," *Journal of Cellular and Molecular Medicine*, vol. 18, no. 5, pp. 919–928, 2014.
- [37] J. Li, S. X. X. Cai, Q. He et al., "Intravenous miR-144 reduces left ventricular remodeling after myocardial infarction," *Basic Research in Cardiology*, vol. 113, no. 5, 2018.
- [38] C.-Y. Liu, Y.-H. Zhang, R.-B. Li et al., "LncRNA CAIF inhibits autophagy and attenuates myocardial infarction by blocking p53-mediated myocardial transcription," *Nature Communications*, vol. 9, no. 1, p. 29, 2018.
- [39] M. Zhou, Y.-G. Zou, Y.-Z. Xue et al., "Long non-coding RNA H19 protects acute myocardial infarction through activating autophagy in mice," *European Review for Medical and Pharmacological Sciences*, vol. 22, no. 17, pp. 5647–5651, 2018.
- [40] G. Yin, X. Yang, Q. Li, and Z. Guo, "GATA1 activated lncRNA (Galnt) promotes anoxia/reoxygenation-induced autophagy and cell death in cardiomyocytes by sponging miR-338," *Journal of Cellular Biochemistry*, vol. 119, no. 5, pp. 4161–4169, 2018.
- [41] J. Wang, Z. Bie, and C. Sun, "Long noncoding RNA AK088388 regulates autophagy through miR-30a to affect cardiomyocyte injury," *Journal of Cellular Biochemistry*, vol. 120, no. 6, pp. 10155–10163, 2019.
- [42] Z. Huang, B. Ye, Z. Wang et al., "Inhibition of lncRNA-HRIM increases cell viability by regulating autophagy levels during hypoxia/reoxygenation in myocytes," *Cellular Physiology and Biochemistry*, vol. 46, no. 4, pp. 1341–1351, 2018.
- [43] M. Ma, J. Hui, Q. Zhang, Y. Zhu, Y. He, and X. Liu, "Long non-coding RNA nuclear-enriched abundant transcript 1 inhibition blunts myocardial ischemia reperfusion injury via autophagic flux arrest and apoptosis in streptozotocin-induced diabetic rats," *Atherosclerosis*, vol. 277, pp. 113–122, 2018.
- [44] S. Yu, B. Dong, Z. Fang, X. Hu, L. Tang, and S. Zhou, "Knockdown of lncRNA AK139328 alleviates myocardial ischemia/reperfusion injury in diabetic mice via modulating miR-204-3p and inhibiting autophagy," *Journal of Cellular and Molecular Medicine*, vol. 22, no. 10, pp. 4886–4898, 2018.
- [45] M. Vausort, D. R. Wagner, and Y. Devaux, "Long noncoding RNAs in patients with acute myocardial infarction," *Circulation Research*, vol. 115, no. 7, pp. 668–677, 2014.
- [46] Z.-H. Zhao, W. Hao, Q.-T. Meng, X.-B. Du, S.-Q. Lei, and Z.-Y. Xia, "Long non-coding RNA MALAT1 functions as a mediator in cardioprotective effects of fentanyl in myocardial ischemia-reperfusion injury," *Cell Biology International*, vol. 41, no. 1, pp. 62–70, 2017.
- [47] H. Hu, J. Wu, D. Li, J. Zhou, H. Yu, and L. Ma, "Knockdown of lncRNA MALAT1 attenuates acute myocardial infarction through miR-320-Pten axis," *Biomedicine & Pharmacotherapy*, vol. 106, pp. 738–746, 2018.
- [48] J. Li, J. Wang, Y. Chen et al., "LncRNA MALAT1 exerts oncogenic functions in lung adenocarcinoma by targeting miR-204," *American Journal of Cancer Research*, vol. 6, no. 5, pp. 1099–1107, 2016.
- [49] X. Guo, X. Wu, Y. Han, E. Tian, and J. Cheng, "LncRNA MALAT1 protects cardiomyocytes from isoproterenol-induced apoptosis through sponging miR-558 to enhance ULK1-mediated protective autophagy," *Journal of Cellular Physiology*, vol. 234, no. 7, pp. 10842–10854, 2018.

Research Article

Hypoxia-Inducible Factor-1 α Knockdown Plus Glutamine Supplementation Attenuates the Predominance of Necrosis over Apoptosis by Relieving Cellular Energy Stress in Acute Pancreatitis

Liang Ji ¹, Xiaoyu Guo ¹, Jiachen Lv ², Fan Xiao ¹, Wangjun Zhang ¹, Jie Li ¹, Zhitao Lin ¹, Bei Sun ¹ and Gang Wang ¹

¹The Department of General Surgery, The No. 1 Affiliated Hospital of Harbin Medical University, Harbin, 150001 Heilongjiang Province, China

²The Department of General Surgery, The No. 3 Affiliated Hospital of Harbin Medical University, Harbin, 150001 Heilongjiang Province, China

Correspondence should be addressed to Gang Wang; wgilu79@163.com

Received 9 March 2019; Accepted 9 May 2019; Published 2 June 2019

Guest Editor: Reggiani Vilela Gonçalves

Copyright © 2019 Liang Ji et al. This is an open access article distributed under the Creative Commons Attribution License, which permits unrestricted use, distribution, and reproduction in any medium, provided the original work is properly cited.

The present study was conducted to investigate the effect and potential mechanism of hypoxia-inducible factor-1 α (HIF-1 α) genetic inhibition plus glutamine (Gln) supplementation on necrosis-apoptosis imbalance during acute pancreatitis (AP), with a specific focus on the regulations of intracellular energy metabolism status. Wistar rats and AR42J cells were used to establish AP models. When indicated, a HIF-1 α knockdown with or without a Gln supplementation was administered. *In vivo*, local and systemic inflammatory injuries were assessed by serum cytokine measurement, H&E staining, and transmission electron microscope (TEM) observation of pancreatic tissue. *In vitro*, intracellular energy metabolism status was evaluated by measuring the intracellular adenosine triphosphate (ATP), lactic acid, and Ca²⁺ concentrations and the mitochondrial potential. In addition, changes in the apoptotic activity were analyzed using TUNEL staining *in vivo* and an apoptosis assay *in vitro*. HIF-1 α knockdown alleviated AP-related inflammatory injury as indicated by the measurements of serum cytokines and examinations of TEM and H&E staining of pancreatic tissues. HIF-1 α knockdown played an antioxidative role against AP-related injuries by preventing the increase in the intracellular Ca²⁺ concentration and the decrease in the mitochondrial membrane potential and subsequently by suppressing the glycolysis pathway and increasing energy anabolism in AR42J cells after AP induction. Apoptosis was significantly upregulated when HIF-1 α was knocked down before AP induction due to an attenuation of the translocation of nuclear factor-kappa B to the nuclei. Furthermore, these merits of HIF-1 α knockdown in the relief of the metabolic stress and upregulation of apoptosis were more significant when Gln was administered concomitantly. In conclusion, Gln-supplemented HIF-1 α knockdown might be promising for the future management of AP by relieving the intracellular energy stress, thereby attenuating the predominance of necrosis over apoptosis.

1. Introduction

Acute pancreatitis (AP) may present as a mild self-limiting condition or as a lethal gastrointestinal disorder. The mechanisms of AP remain elusive, and no specific cure has yet been developed [1–6]. The progression and prognosis of AP

mainly depend on the dominant death mode of the acinar cells. During the natural course of AP, the injured acinar cells are directed towards two major cell death pathways, namely, necrosis and apoptosis. Unlike apoptosis which acts as a self-defense mechanism against AP-related injuries, necrosis usually correlates positively with the severity of AP [7].

Therefore, relieving the predominance of necrosis over apoptosis by attenuating the necrosis and/or promoting apoptosis is a promising direction in the management of AP.

Recent studies have indicated that apoptosis and necrosis of pancreatic acinar cells during AP are interconvertible rather than being completely fixed under certain circumstances. The level of adenosine triphosphate (ATP), an index of intracellular energy metabolism, is pivotal in regulating the switching and interactions between apoptosis and necrosis [8]. Stress might induce overconsumption of intracellular ATP, which would facilitate necrosis. However, high levels of ATP tend to upregulate cellular apoptosis [9]. Thus, numerous studies have been conducted to investigate the role of energy metabolism in the pathogenesis of AP. Up to the present, there have been no reports regarding the interconversion of cellular necrosis-apoptosis through the regulation of energy metabolism status in AP.

Hypoxia-inducible factor-1 (HIF-1), a unique regulatory transcriptional factor which can be activated and highly expressed in response to hypoxia, has gained a worldwide attention due to its dominant role in the regulation of intracellular energy metabolism in some inflammatory and immune diseases. HIF-1 is a heterodimer composed of α and β subunits. Unlike HIF-1 β , which demonstrates stable intracellular expression, HIF-1 α is regulated by the incubated oxygen exposure concentration and acts as the major active unit of HIF-1 [10, 11]. By regulating the transcription and expression of target genes, HIF-1 α has the inverse effects of shutting down the tricarboxylic acid cycle and facilitating the glycolysis pathway. These processes inhibit the ATP production and activate the inflammatory response [12, 13]. Gomez et al. [14] found that 8-12 hours after establishing a mouse model of AP, the level of HIF-1 α in the pancreatic tissue was significantly increased.

Metabolically, glutamine (Gln) has long been known to be a nonessential amino acid. However, it serves as a conditionally essential amino acid in response to stress and injury [15]. Gln is a source of fuel for lymphocytes and enterocytes and might play an antioxidative role as a precursor for glutathione and a cytoprotective role by upregulating heat shock proteins [16]. It has been shown that Gln supplementation during AP maintains gut integrity, improves the immune response, and decreases the release of some proinflammatory mediators by inhibiting the activation of nuclear factor-kappa B (NF- κ B) and p38 mitogen-activated protein kinase [17-19]. On the basis of the solubility and instability of Gln, L-alanyl-L-glutamine is usually administered as a donor *in vivo* because it is a dipeptide that dissociates into free Gln soon after entry into the circulatory system [20].

We therefore performed the present study to investigate the effect and potential mechanism of HIF-1 α genetic inhibition plus Gln supplementation on necrosis-apoptosis imbalance during AP with a specific focus on the regulation of intracellular energy metabolism status.

2. Materials and Methods

2.1. Animals and Reagents. A total of 60 male Wistar rats (200-220 g) were supplied by the Animal Research Center,

the First Clinical College of Harbin Medical University (Harbin, China). The rats were fed with rodent chow and water *ad libitum* in an environmentally controlled room (18-21°C, 40-60% relative humidity, and 12 h light/dark cycle). After an acclimatization for one week, the rats were fasted overnight before the experiments. All surgical procedures and cares administered to the rats were approved by the Institutional Animal Care and Use Committee of Harbin Medical University (No. 2011BS001).

Sodium taurocholate (Na-TC) and L-alanyl-L-glutamine were purchased from Sigma-Aldrich (St. Louis, MO, USA). A commercial lentivirus-mediated small interfering RNA (siRNA) kit was purchased from Genecopia (San Francisco, MO, USA) to silence HIF-1 α . Antibodies used in the present study are cleaved PARP (Asp214), cleaved caspase-3 (Asp175), cleaved caspase-9 (Asp353), and nuclear factor- κ B p65 purchased from Cell Signaling Technology (Danvers, MA, USA); β -actin purchased from Santa Cruz Biotechnology (Santa Cruz, CA, USA); and HIF-1 α purchased from Novus (Littleton, CO, USA).

2.2. Experimental Design In Vivo. A model of AP in rats was induced as described previously [21]. Briefly, the rats were anesthetized by an intraperitoneal injection of sodium pentobarbital (30 mg/kg). Then, a midline laparotomy was performed and the distal pancreaticobiliary duct was ligated. AP was induced by a retrograde infusion of 3.5% Na-TC (0.15 mL/100 g) into the pancreaticobiliary duct.

The rats were allocated into four groups ($n = 10$): sham, AP, HIF-1 α siRNA, and HIF-1 α siRNA+Gln groups. AP was induced in the rats in AP, HIF-1 α siRNA, and HIF-1 α siRNA+Gln groups, whereas the rats in the sham group were subjected only to laparotomy. Based on our preliminary experiments, an injection of lentivirus-mediated HIF-1 α siRNA (Lv-siHIF-1 α) particles [10^6 TU/mL in 200 μ L of phosphate-buffered saline (PBS)] through the caudal vein 5 d before the experiment was performed to silence HIF-1 α in rats. In sham and AP groups, an equivalent level of negative control (Lv-siNC) particles was administered instead. Additionally, the rats in the HIF-1 α siRNA+Gln group received an intravenous injection of L-alanyl-L-glutamine (0.4 g/kg) through the caudal vein immediately after AP induction [18, 22, 23]. The rats were sacrificed at 24 h after AP induction, and blood and pancreatic samples were collected. The serum was obtained after a centrifugation at 3000 rpm for 15 min and then stored at -80°C until assay. The pancreatic tissue was prepared for three different purposes: (1) rinsed in saline buffer and snap-frozen in liquid nitrogen at -80°C for Western blot, (2) fixed in 4% buffered paraformaldehyde for 48 h and then embedded in paraffin for hematoxylin-eosin (H&E) staining and terminal deoxynucleotidyl transferase-mediated dUTP nick end labeling (TUNEL) staining, and (3) fixed in 2 mL of 2.5% glutaraldehyde and then postfixed in 1% osmium tetroxide solution for transmission electron microscopy (TEM).

2.3. Measurement of Parameters in Serum and Pancreas. The serum levels of amylase and C-reactive protein (CRP) were spectrophotometrically measured using a biochemical

autoanalyzer (Toshiba, Japan) as previously described [24]. The serum and pancreatic levels of tumor necrosis factor- α (TNF- α) and interleukin-1 β (IL-1 β) were measured using enzyme-linked immunosorbent assay kits (R&D Systems, Minneapolis, MN, USA) according to the manufacturer's instructions.

2.4. H&E Staining. H&E staining was performed to examine the level of inflammation and tissue damage under a light microscope (40x). Two experienced pathologists who were blinded to the experimental protocol scored the pancreatic tissue on a scale from 0 to 4 for the degrees of edema, inflammation, hemorrhage, and necrosis respectively in 20 randomized high-power fields according to the histological scoring criteria as Kusske et al. reported [25]. Then, the final score was totaled for each group.

2.5. TEM. The fixed samples were dehydrated through a graded series of ethanol and embedded in epoxy resin. Ultrathin sections (80 nm) were collected on copper grids, double-stained with uranyl acetate and lead citrate, and then examined under a Hitachi H-7100 transmission electron microscope (Hitachinaka, Japan) at 80 kV.

2.6. Measurement of Myeloperoxidase (MPO) and Lipid Peroxidase (LPO) in the Pancreas. The pancreatic levels of MPO and LPO were measured with the specific kits (Jiancheng Bioengineering Institute, Nanjing, China) according to the manufacturer's instructions. The former was expressed as units per gram of pancreatic homogenates, and the latter was expressed as micromoles per gram of pancreatic homogenates.

2.7. TUNEL Staining. The apoptosis of pancreatic acinar cells was determined using a TUNEL Apoptosis Detection Kit (Beyotime Biotechnology, Shanghai, China) according to the manufacturer's instructions [26]. Cellular nuclei with the presence of a dark reddish-brown chromogen were identified as positive. The TUNEL-positive cells were counted in 10 randomly selected high-power fields under a light microscope and expressed as a percentage of the total cell counts (apoptosis index).

2.8. Electrophoretic Mobility Shift Assay (EMSA). A nuclear extraction kit and an EMSA kit were purchased from Thermo Fisher Scientific (Rockford, IL, USA) to determine the DNA binding activities of NF- κ B and HIF-1 α . Briefly, 2 μ L of nuclear extract (at a concentration of 2 μ g/ μ L) was incubated with 1 μ L of biotin-labeled probe containing the NF- κ B- (5'-AGTTGAGGGGACTTCCAGGC-3') or HIF-1 α - (5'-TCTGTACGTGACCACACTCACCTC-3') binding domain for 30 min at 15°C. The reaction mixtures were separated on 6% nondenaturing polyacrylamide gels in 0.5x *tris*-borate ethylenediamine tetraacetic acid at 120 V for 60 min at 4°C and transferred onto a presoaked membrane at 300 mA for 30 min at 4°C. The membranes were subjected to ultraviolet light-induced cross-linking for 3 min and then incubated with blocking buffer containing a stabilized streptavidin-horseradish peroxidase conjugate (1:1 000) for 30 min. The bands on the membranes were

detected with a Chemiluminescent Nucleic Acid Detection Module Kit (Thermo Fisher Scientific).

2.9. Cell Cultures. The rats pancreatic exocrine cell line AR42J was purchased from the American Type Culture Collection (Manassas, VA, USA) and cultured in Dulbecco's modified Eagle's medium (Gibco, Grand Island, NY, USA) supplemented with 10% fetal bovine serum (ScienCell, San Diego, CA, USA), 100 U/mL of penicillin, and 100 mg/mL of streptomycin (Invitrogen, Carlsbad, CA, USA) at 37°C in a 5% CO₂-humidified incubator.

2.10. Experimental Design In Vitro. There were four groups *in vitro*: control, AP, HIF-1 α siRNA, and HIF-1 α siRNA +Gln groups. AR42J cells in control and AP groups were transfected with Lv-siNC particles whereas the counterparts in the HIF-1 α siRNA and HIF-1 α siRNA+Gln groups were transfected with Lv-siHIF-1 α . AR42J cells were plated in 6-well plates (5 \times 10⁴ per well) until 70% confluent so that appropriate volumes of lentivirus could be added to achieve the multiplicity of the infection value recommended by the manufacturer. To simulate AP, the Lv-siHIF-1 α or Lv-siNC particle-pretreated cells were incubated with 500 μ M of NATC for 12 h [27, 28]. When indicated, L-alanyl-L-glutamine (2 mM) was administered together with AP stimulation [29, 30]. The culture medium supernatants were collected to evaluate lactate dehydrogenase (LDH) release and glucose uptake with a biochemical autoanalyzer (Toshiba, Tokyo, Japan) as previously described [24].

2.11. Measurements of Intracellular ATP and Lactic Acid. The intracellular levels of ATP and lactic acid were measured with specific kits (Jiancheng Bioengineering Institute) according to the manufacturer's instructions and then normalized to the protein concentrations, which were determined using the bicinchoninic acid method. The former was expressed as nmol/mg, and the latter was expressed as mmol/g.

2.12. Measurement of Intracellular Ca²⁺ Concentration. The method for the measurement of intracellular Ca²⁺ concentration has been described previously [31]. In brief, the cells were preloaded with 5 μ M of Fura-2 AM (Beyotime, Shanghai, China) in HEPES buffer for 1 h at room temperature. Images of the Fura-2-loaded cells were captured using a laser confocal microscope (LSM 510, Carl Zeiss, Oberkochen, Germany) and analyzed using Image-Pro Plus v6.0 software (Media Cybernetics, Crofton, MA, USA). Background-subtracted fluorescent images for excitation at 340 nm and 380 nm were captured. The intracellular Ca²⁺ concentration was estimated from the ratio of Fura-2 fluorescence emitted at 510 nm after excitation at 340 nm to that after excitation at 380 nm, according to the Grynkiewicz equation [32].

2.13. Intracellular Mitochondrial Potential. Intracellular mitochondrial potential (MP) was determined using a dual-emission mitochondrial dye 5,5',6,6'-tetrachloro-1,1',3,3'-tetraethylbenzimidazolocarboyanine iodide (JC-1, Beyotime) as detailed elsewhere [33]. In short, staining was performed using 2.5 μ g/mL of JC-1 for 15 min at 37°C. After staining, the cells were rinsed 3 times with PBS. Dye

equilibration was allowed for 10 min at room temperature prior to imaging. Fluorescent images of the emissions at 529 nm and 590 nm were captured using a laser confocal microscope (Carl Zeiss). JC-1 exhibits a fluorescence emission shift upon aggregation from 529 nm (green monomer, indicative of low MP) to 590 nm (red "J-aggregates," indicative of high MP). Thus, a reduced ratio of red/green fluorescence indicates mitochondrial depolarization.

2.14. Apoptosis Assay. Apoptosis was determined by Annexin V and propidium iodide staining (BD Biosciences, Shanghai, China) as described previously [24]. Theoretically, Annexin V and propidium iodide double-staining indicates necrosis whereas Annexin V single-staining indicates apoptosis. The images were acquired using a confocal laser scanning microscope (Carl Zeiss), and the average percentages of apoptotic cells were calculated in 5 randomly selected high-power fields.

2.15. Western Blot Analysis. The protocol for Western blot has been described previously [24, 27, 28]. In brief, pancreatic tissue or cells were homogenized in a protein lysis buffer (Beyotime, Shanghai, China) that contained the protease inhibitor (Roche) and phosphatase inhibitor (Roche) and centrifuged at 10 000g for 10 min at 4°C. The samples containing 50 µg of total protein were separated using 10% polyacrylamide SDS gels and electrophoretically transferred to polyvinylidene difluoride membranes. The membranes were blocked with 5% skim milk then incubated with appropriate primary antibodies (dilution for all: 1:1000) and horseradish peroxidase-conjugated secondary antibodies. The immunostained protein bands were detected using an enhanced chemiluminescence kit (Pierce Chemical, Rockford, IL, USA). β -Actin was used as the protein loading control, and the level of protein expression was corrected using the band density relative to that of β -actin.

2.16. Statistical Analysis. The data are presented as the mean \pm standard deviation (SD) of three independent experiments and analyzed using SAS 9.1 for Windows (SAS Institute, Cary, NC, USA). Comparisons between multiple groups were performed using a one-way ANOVA followed by Dunnett's *t*-test. A *P* value of <0.05 was taken to be statistically significant.

3. Results

3.1. The Upregulation of HIF-1 α after AP Induction Was Prevented by Prior HIF-1 α Knockdown. As Figure 1(a) shows, the HIF-1 α -DNA binding activity was significantly increased in the AP group compared to that of the sham group. However, the HIF-1 α DNA-binding activity associated with AP induction was significantly reduced by prior HIF-1 α knockdown. The detectable levels of HIF-1 α expression among these groups also confirmed these results (Figure 1(b)). That is, the level of HIF-1 α expression was increased by AP induction and this increase was significantly inhibited when HIF-1 α was knocked down before AP induction.

3.2. HIF-1 α Knockdown Alleviated AP-Related Inflammatory Injury, and This Therapeutic Effect Was Enhanced by the Additional Administration of Gln. AP induction, with or without any intervention, was associated with a range of levels of edema, necrosis, inflammatory cell infiltration, and hemorrhage whereas there was no evident ectopic in rats that had undergone a sham operation. The histological scoring indicated that the morphological alterations were most severe in the AP group, followed by the HIF-1 α siRNA group and HIF-1 α siRNA+Gln group (Figure 2(a)). The same results were obtained for the measurements of the serum levels of amylase and CRP (Figure 2(b)) as well as the levels of TNF- α and IL-1 β both in sera and pancreatic tissues (Figures 2(c) and 2(d)). Thus, these results indicated that HIF-1 α knockdown alleviated AP-related inflammatory injuries, and this therapeutic effect was further enhanced by the additional administration of Gln.

3.3. HIF-1 α Silencing Played an Antioxidative Role against AP-Related Injuries, and This Effect Was Enhanced by the Additional Administration of Gln. To evaluate the levels of oxidative stress response among the animals treated with the various procedures, the pancreatic levels of MPO and LPO were measured. AP induction was significantly associated with increases in the levels of both MPO and LPO compared to those in the sham group. HIF-1 α silencing before AP induction significantly decreased the levels of MPO and LPO when compared with those in the AP group. Moreover, the levels of MPO and LPO in the HIF-1 α siRNA+Gln group were significantly decreased compared to those in the HIF-1 α siRNA group (Figure 3(a)). Such effects on the oxidative stress response due to HIF-1 α silencing, with or without Gln supplementation before AP induction, were also suggested by the ultrastructural alterations that were observed using TEM. As shown in Figure 3(b), AP induction was associated with mitochondrial swelling, endoplasmic reticulum disorder, and nuclear fragmentation. Notably, these ultrastructural alterations were most severe in the AP group, followed by those in the HIF-1 α siRNA group and those in the HIF-1 α siRNA+Gln group.

3.4. Apoptosis Was Significantly Upregulated when HIF-1 α Knockdown Was Administered before AP Induction, and This Effect Was Enhanced by a Concurrent Administration of Gln. TUNEL staining of the pancreatic sections was observed under a light microscope (Figure 4(a)). The results showed that HIF-1 α knockdown before AP induction increased the apoptosis index compared with that in the AP group. Moreover, a concurrent administration of Gln with HIF-1 α knockdown significantly increased the apoptosis index than that in the HIF-1 α knockdown group (Figure 4(b)).

3.5. HIF-1 α Knockdown Attenuated NF- κ B Nuclear Translocation Induced by AP, and This Effect Was Enhanced by a Concurrent Administration of Gln. As the most important regulator in the pathogenesis of AP, the activation of NF- κ B might upregulate the expression of proinflammatory factors, antiapoptotic proteins, and other important mediators that account for the local and systemic responses to AP induction.

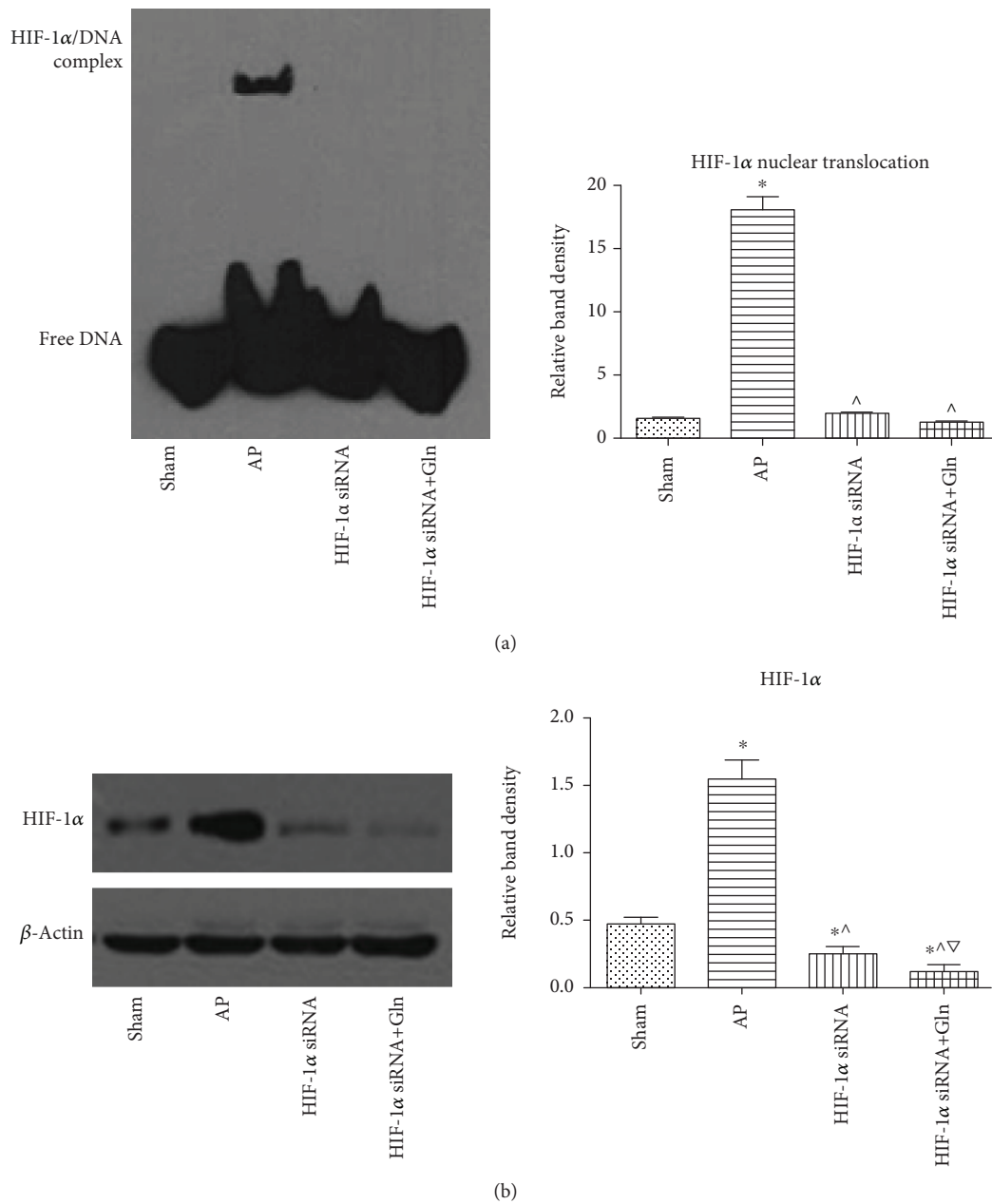


FIGURE 1: The upregulation of HIF-1 α after AP induction was prevented by prior HIF-1 α knockdown. (a) Representative EMSA blots (left) and quantifications (right) of HIF-1 α DNA-binding activity in pancreatic tissues harvested from the rats that were subjected to sham operation, AP, HIF-1 α siRNA, and HIF-1 α siRNA+Gln for 24 h since AP induction. (b) Representative immunoblot images (left) and quantifications (right) of HIF-1 α protein expression in pancreatic tissues harvested from the rats as described above. β -Actin was used as the protein loading control. Data were presented as mean \pm SD ($n = 3$). * $P < 0.05$ versus sham, ^ $P < 0.05$ versus AP, and $\nabla P < 0.05$ versus HIF-1 α siRNA. Abbreviations: AP: acute pancreatitis; EMSA: electrophoretic mobility shift assay; Gln: glutamine; HIF-1 α : hypoxia inducible factor-1 α ; SD: standard deviation.

It was shown that the nuclear translocation of HIF-1 α was significantly increased by AP induction compared to that in the sham group (Figure 1(a)). Moreover, HIF-1 α knockdown before AP induction significantly ameliorated the level of NF- κ B nuclear translocation compared with that induced by AP induction alone. In addition, the level of NF- κ B nuclear translocation was significantly lower in the HIF-1 α siRNA+Gln group than that in the HIF-1 α siRNA group (Figures 5(a) and 5(b)).

3.6. HIF-1 α Knockdown Suppressed the Glycolysis Pathway and Increased Energy Anabolism in AR42J Cells, and These Effects Were Enhanced when Gln Was Administered Concomitantly. After HIF-1 α silencing, the levels of ATP and lactic acid in each group were measured (Figure 6(a)). AP induction was significantly associated with a decrease in ATP level and an increase in lactic acid level compared with those in the control group. HIF-1 α silencing, which was conducted before AP induction, was significantly associated with

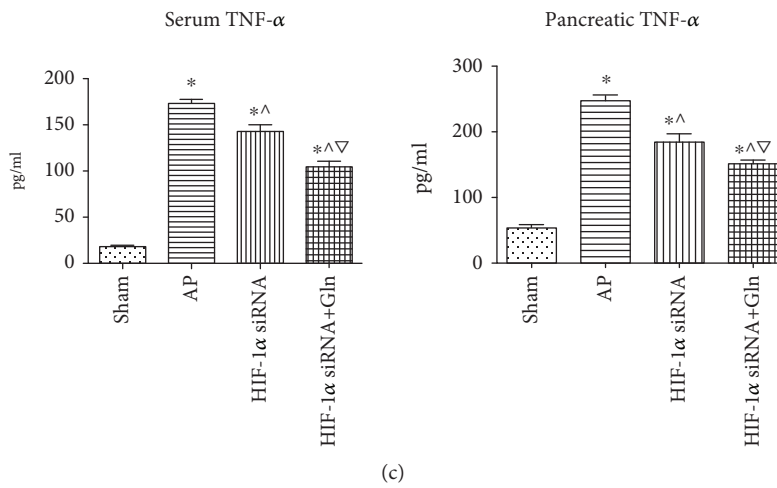
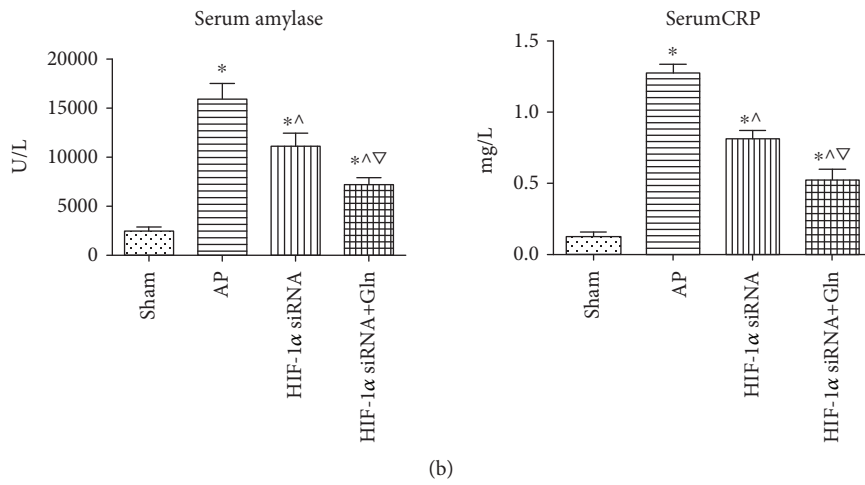
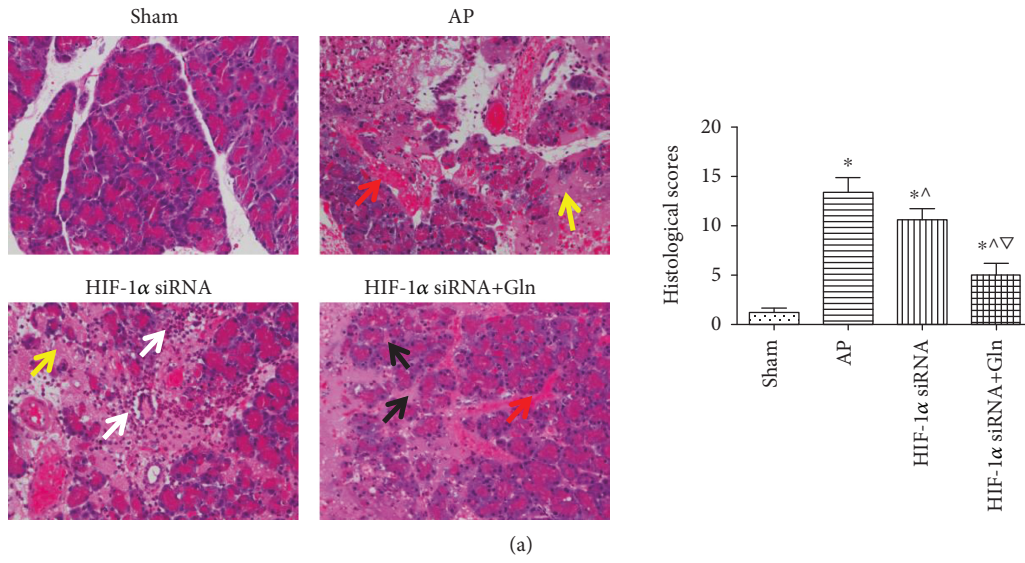


FIGURE 2: Continued.

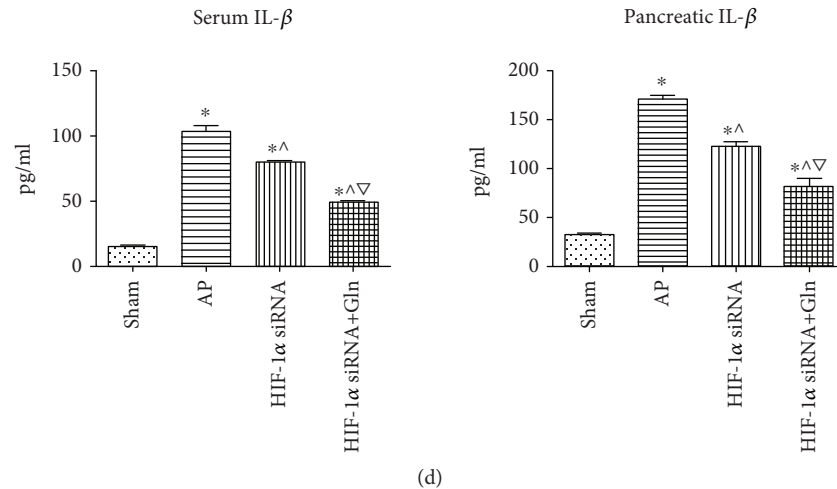


FIGURE 2: HIF-1 α knockdown alleviated AP-related inflammatory injury, and this therapeutic effect was enhanced by the additional administration of Gln. (a) Representative photos (40 \times) and histological scores of H&E-stained pancreatic tissues harvested from the rats as described in Figure 1(a). Black arrow indicates edema, white arrow indicates inflammatory infiltration, yellow arrow indicates necrosis, and red arrow indicated hemorrhage. (b) The serum levels of amylase and CRP in rats as described in Figure 1(a). (c) The serum (left) and pancreatic (right) levels of TNF- α in rats as described in Figure 1(a). (d) The serum (left) and pancreatic (right) levels of IL-1 β in rats as described in Figure 1(a). Data were presented as mean \pm SD ($n = 3$). * $P < 0.05$ versus sham, ^ $P < 0.05$ versus AP, and $\nabla P < 0.05$ versus HIF-1 α siRNA. Abbreviations: AP: acute pancreatitis; CRP: C-reactive protein; Gln: glutamine; H&E: hematoxylin-eosin; HIF-1 α : hypoxia inducible factor-1 α ; IL-1 β : interleukin-1 β ; SD: standard deviation; TNF- α : tumor necrosis factor- α .

an increase in ATP level and a decrease in lactic acid level compared with those in the AP group. In addition, a concomitant administration of Gln with HIF-1 α silencing was significantly correlated with an increase in ATP level compared with that in the HIF-1 α siRNA group. In accordance with previous intracellular findings, the measurement of supernatant glucose and LDH also indicated that HIF-1 α knockdown suppressed the glycolysis pathway and increased energy anabolism in AR42J cells, and these effects were enhanced when Gln was administered concomitantly (Figure 6(b)).

3.7. HIF-1 α Knockdown Prevented the Increase in the Intracellular Ca²⁺ Concentration and the Decrease in the Mitochondrial Membrane Potential in AR42J Cells after AP Induction, and These Effects Were Enhanced when Gln Was Administered Concomitantly. As shown in Figures 7(a) and 7(b), a certain degree of mitochondrial depolarization developed after AP induction was indicated by the significant decreased red/green fluorescence ratio compared to that in the control group. HIF-1 α knockdown before AP induction significantly corrected the mitochondrial membrane potential that resulted from AP induction alone, and this effect was enhanced when Gln supplementation was administered together with HIF-1 α knockdown. In addition, a prior HIF-1 α knockdown corrected the increase in the intracellular Ca²⁺ concentration that resulted from AP induction alone, and this effect was enhanced when Gln was administered concomitantly (Figure 7(c)).

3.8. HIF-1 α Knockdown Decreased Necrosis and Increased Apoptosis within AR42J Cells after AP Induction, and These Effects Were Enhanced when Gln Was Administered Concomitantly with HIF-1 α Knockdown. The apoptosis assay was conducted using Annexin V and PI staining. Various

levels of apoptosis were identified within AR42J cells after AP induction compared to those in the control group. Figures 8(a) and 8(c) show that HIF-1 α knockdown before AP induction decreased necrosis and increased apoptosis relative to that caused by AP induction alone. Moreover, HIF-1 α knockdown plus Gln supplementation before AP induction resulted in decreased necrosis and increased apoptosis compared to that in the HIF-1 α siRNA group. The cytoplasmic expression of cleaved caspase-3, caspase-9, and PARP, which was evaluated by Western blot, also confirmed the previous findings. The levels of active caspase-3, caspase-9, and PARP in the HIF-1 α siRNA group were significantly increased than those in the AP group. In addition, the levels of activated caspase-3, caspase-9, and PARP were significantly increased when Gln was administered together with HIF-1 α knockdown compared to that in the HIF-1 α siRNA group (Figures 8(b) and 8(d)–8(f)).

4. Discussion

AP continues to be a clinical challenge, and no specific therapy has yet been developed. Although there are some common early-phase characteristics such as abnormal activation of pancreatic enzymes within acinar cells, AP might present as a mild self-limited course or even an eventful life-threatening one. Accordingly, the secondary response of the acinar cells to early intracellular damage, namely, the mode of cell death, becomes a critical factor that determines the degree of the inflammatory response and the occurrence and development of subsequent complications in AP [34].

Apoptosis is an active form of programmed cell death that is characterized by an intact cell membrane and the formation of apoptotic bodies. These cells are eventually digested by phagocytes without inducing inflammation or

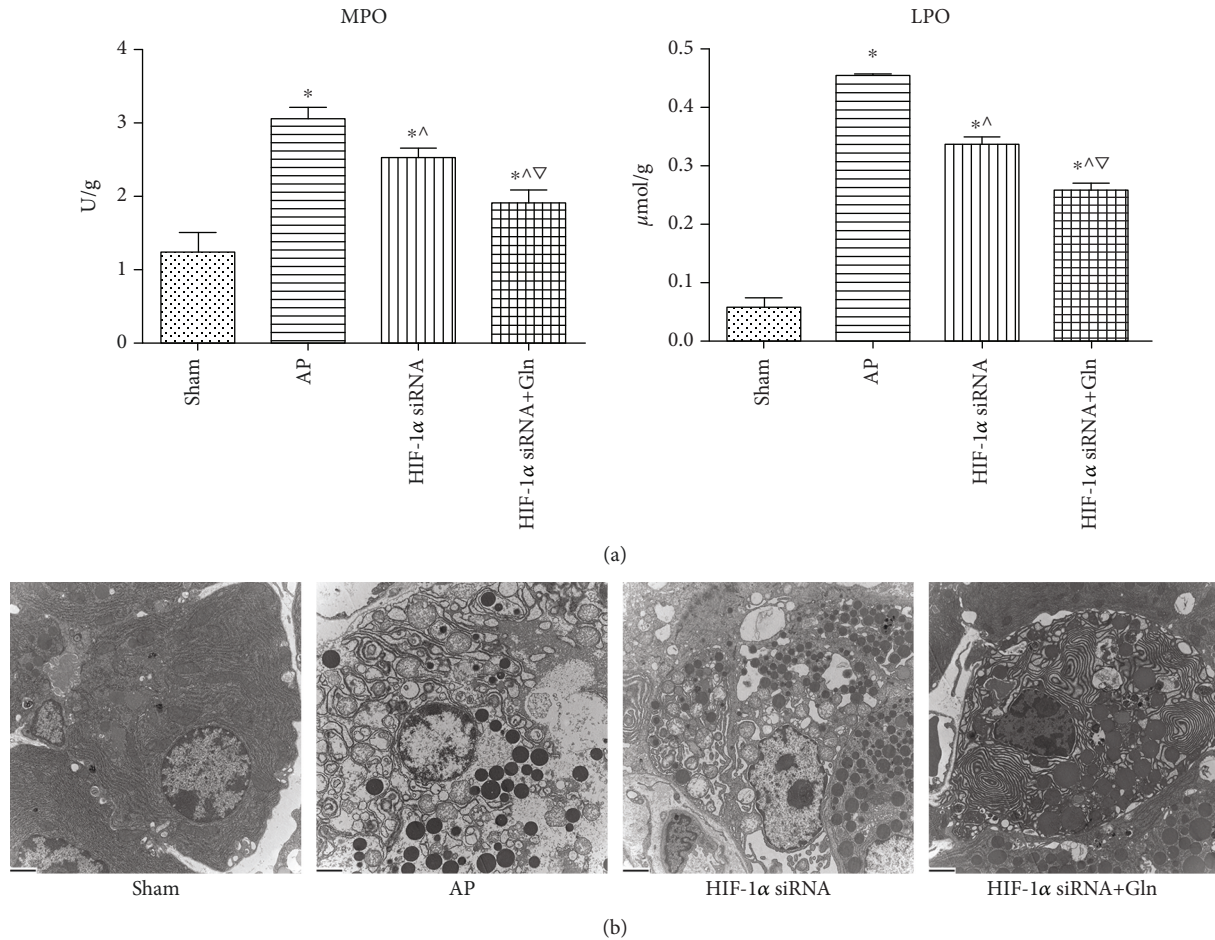


FIGURE 3: HIF-1 α silencing played an antioxidative role against AP-related injuries, and this effect was enhanced by the additional administration of Gln. (a) The pancreatic levels of MPO (left) and LPO (right) in rats as described in Figure 1(a). (b) Representative TEM photos of pancreatic tissues harvested from the rats as described in Figure 1(a), bar = 2 μm . Data were presented as mean \pm SD ($n = 3$). * $P < 0.05$ versus sham, ^ $P < 0.05$ versus AP, and $\nabla P < 0.05$ versus HIF-1 α siRNA. Abbreviations: AP: acute pancreatitis; Gln: glutamine; HIF-1 α : hypoxia-inducible factor-1 α ; LPO: lipid peroxidase; MPO: myeloperoxidase; SD: standard deviation; TEM: transmission electron microscope.

damage to adjacent cells. Necrosis is a passive cell death process that features severe cell membrane rupture accompanied by a massive release of cellular contents, which triggers a strong inflammatory response. In AP, apoptosis might result in the acinar cells being in a relatively stable or “dormant” condition with no further violent inflammation, which might significantly improve AP prognosis. In patients with pancreatitis that causes detectable necrosis in $\geq 50\%$ of the pancreas, the mortality rate can approach 20% [35]. It has been confirmed that acinar cell apoptosis is a self-protective phenomenon in AP, and inducing acinar cell apoptosis could significantly alleviate the severity of AP and its progression [7, 35]. Our study showed that the HIF-1 α siRNA+Gln group demonstrated the highest proportion of acinar cell apoptosis and the least damage to the pancreatic tissue, which further helped to verify the significance of acinar cell apoptosis in AP development.

The mitochondrion not only is the major site of cellular oxidative phosphorylation and energy supply but also plays a crucial role in modulating necrosis and apoptosis [36, 37]. Recently, a few reports have emphasized the mitochondrion

and its alterations in the pathogenesis of AP [38–40]. Injury-related stress factors associated with AP could induce dysfunction of the Ca²⁺-ATP kinase (Ca²⁺ pump) of the acinar cells, which would eventually lead to intracellular Ca²⁺ overload. This phenomenon is considered to be an early key event in AP and contributes extensively to the exacerbation of its progress [4, 41–45]. Intracellular Ca²⁺ overload triggers the constant Ca²⁺ ingestion of mitochondria [46], which accelerates the loss of the mitochondrial membrane potential due to mitochondrial membrane permeabilization as the result of the opening of the mitochondrial membrane permeability transition pore (PTP). These processes directly induce adverse changes in the mitochondrial structure and function as well as disordered energy metabolism [36, 47–49].

It has been shown that mitochondrial membrane permeabilization is the common onset pathway to cell necrosis and apoptosis, and the intracellular ATP level following mitochondrial membrane permeabilization has been proven to play a key role in determining the death mode of the cells [50]. In our opinion, maintenance of a high ATP level in

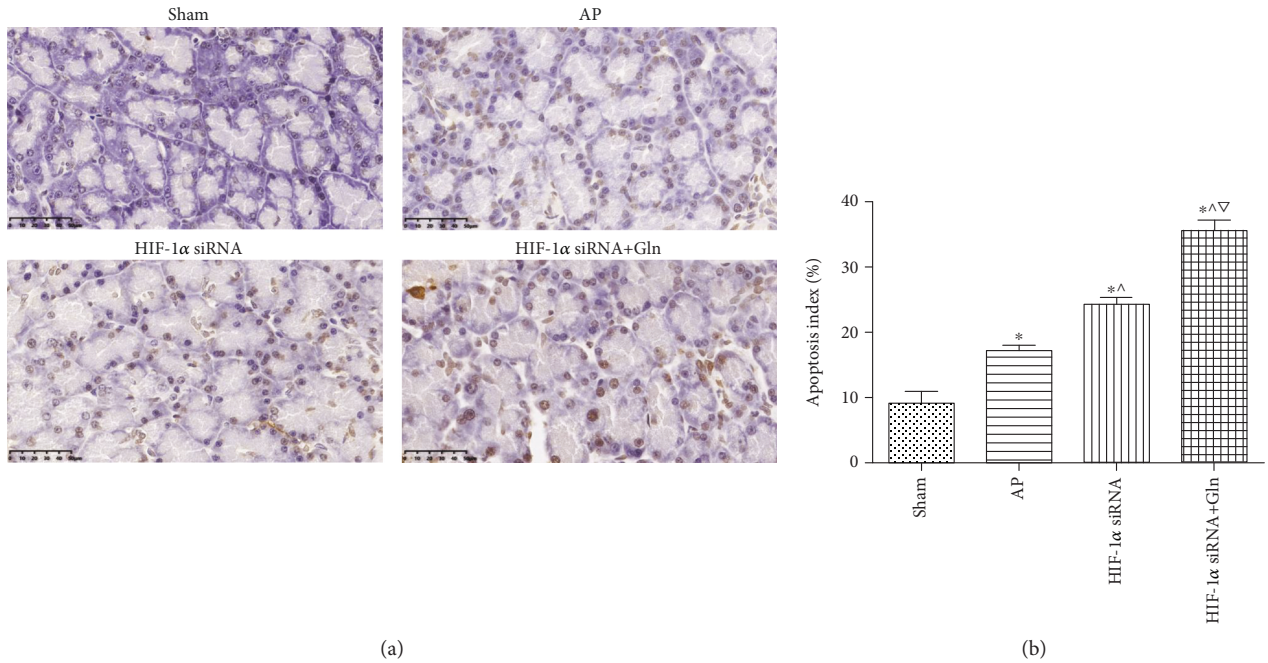


FIGURE 4: Apoptosis was significantly upregulated when HIF-1 α knockdown was administered before AP induction, and this effect was enhanced by a concurrent administration of Gln. (a) Representative TUNEL photos of pancreatic tissues harvested from the rats as described in Figure 1(a), bar = 50 μ m. (b) The ratio of TUNEL-positive cell counts to total cell counts was calculated to yield an apoptosis index in each group. Data were presented as mean \pm SD ($n = 3$). * $P < 0.05$ versus sham, ^ $P < 0.05$ versus AP, and $\nabla P < 0.05$ versus HIF-1 α siRNA. Abbreviations: AP: acute pancreatitis; Gln: glutamine; HIF-1 α : hypoxia inducible factor-1 α ; SD: standard deviation; TUNEL: terminal deoxynucleotidyl transferase-mediated dUTP nick end labeling.

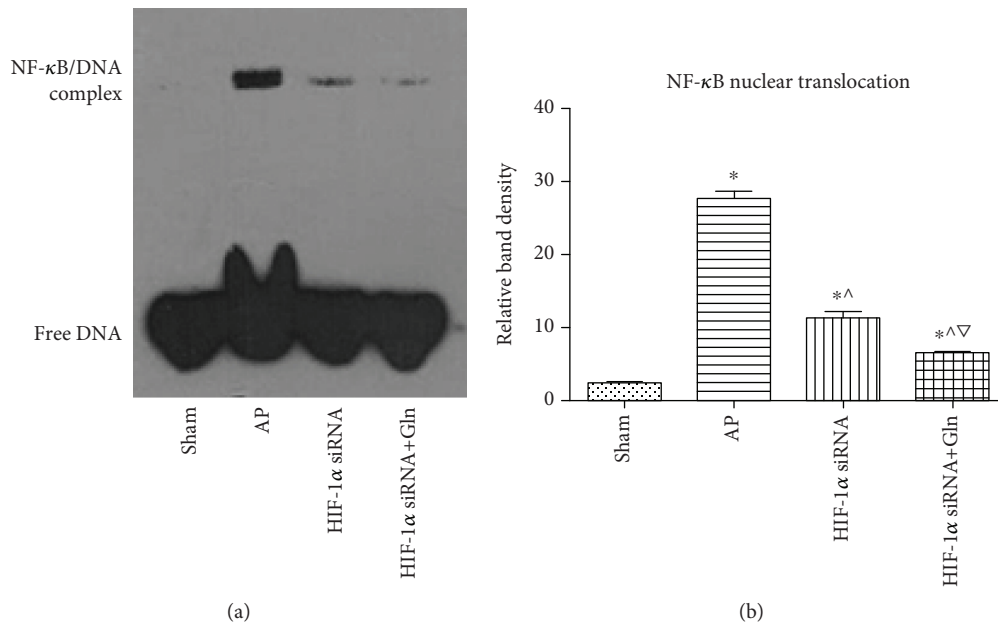


FIGURE 5: HIF-1 α knockdown attenuated NF- κ B nuclear translocation induced by AP, and this effect was enhanced by a concurrent administration of Gln. (a and b) Representative EMSA blots (a) and quantifications (b) of NF- κ B DNA-binding activity in pancreatic tissues harvested from the rats as described in Figure 1(a). Data were presented as mean \pm SD ($n = 3$). * $P < 0.05$ versus sham, ^ $P < 0.05$ versus AP, and $\nabla P < 0.05$ versus HIF-1 α siRNA. Abbreviations: AP: acute pancreatitis; EMSA: electrophoretic mobility shift assay; Gln: glutamine; HIF-1 α : hypoxia-inducible factor-1 α ; NF- κ B: nuclear factor-kappa B; SD: standard deviation.

the impaired acinar cells after AP induction might promote the cellular necrosis-to-apoptosis transformation by the following mechanisms: ① Ca²⁺-ATP kinase is a highly ATP-

dependent enzyme system that consumes much energy. ATP could enhance the Ca²⁺-ATP kinase activity of the cell membrane and endoplasmic reticulum, thus resulting in the

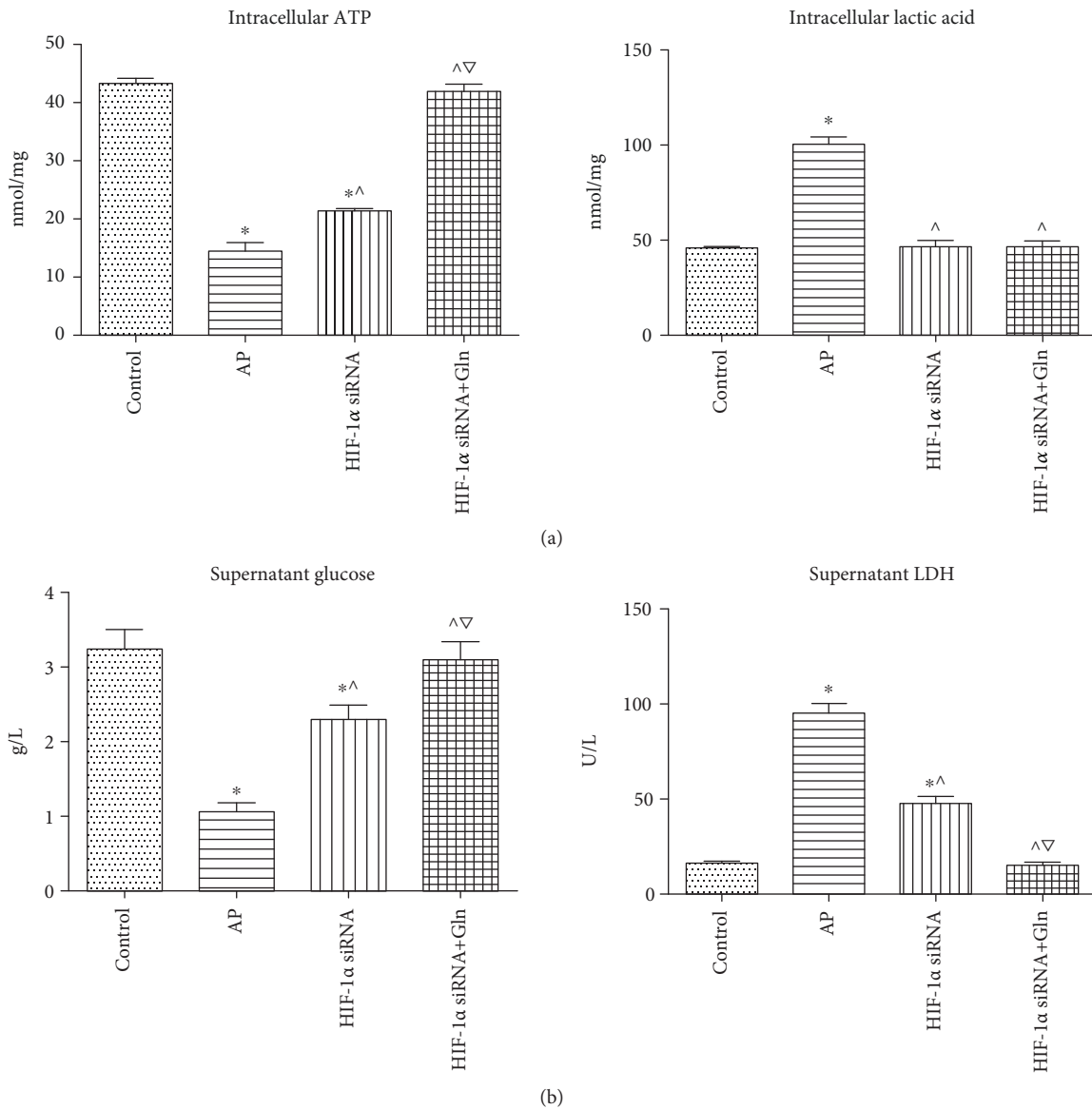


FIGURE 6: HIF-1 α knockdown suppressed the glycolysis pathway and increased energy anabolism in AR42J cells, and these effects were more profound if Gln was administered concomitantly. (a) The intracellular levels of ATP (left) and lactic acid (right) in AR42J cells that were subjected to control, AP, HIF-1 α siRNA, and HIF-1 α siRNA+Gln for 12 h since AP simulation. (b) The supernatant levels of glucose (left) and LDH (right) when AR42J cells were subjected to control, AP, HIF-1 α siRNA, and HIF-1 α siRNA+Gln for 12 h since AP simulation. Data were presented as mean \pm SD ($n = 3$). * $P < 0.05$ versus sham, ^ $P < 0.05$ versus AP, and $\nabla P < 0.05$ versus HIF-1 α siRNA. Abbreviations: AP: acute pancreatitis; ATP: adenosine triphosphate; Gln: glutamine; HIF-1 α : hypoxia-inducible factor-1 α ; LDH: lactate dehydrogenase; SD: standard deviation.

pumping of the overloaded Ca^{2+} out of the cell or into the endoplasmic reticulum, which would further reduce the intramitochondrial Ca^{2+} level and the degree of PTP opening. When the PTP opening is effectively suppressed, the massive loss of mitochondrial membrane potential and constant depletion of ATP could be reversed, which would allow the cellular energy metabolism balance to recover so that the necrosis is prevented [36]. ② ATP is the trigger for caspase activation which has a cascade amplification effect [32, 35]. The caspase pathway plays a critical role in regulating the cellular necrosis/apoptosis balance. Caspase activation can not only induce cellular apoptosis but also prevent necrosis by

inhibiting the activation of polyadenosine diphosphate ribosomal polymerase [7, 32, 35]. However, inactivation of caspase commonly aggravates the cellular necrosis as well as the severity of lesion [35]. Furthermore, chromatin condensation, apoptotic body formation, and other key aspects of apoptosis all require a certain level of ATP [51]. Our results showed that HIF-1 α siRNA+Gln could decrease the intracellular Ca^{2+} level and the sustained loss of mitochondrial membrane potential by increasing the ATP contents within acinar cells, further increasing the cellular expression of caspase-3 and -9 and PARP, which would promote the transformation of acinar cell necrosis to apoptosis.

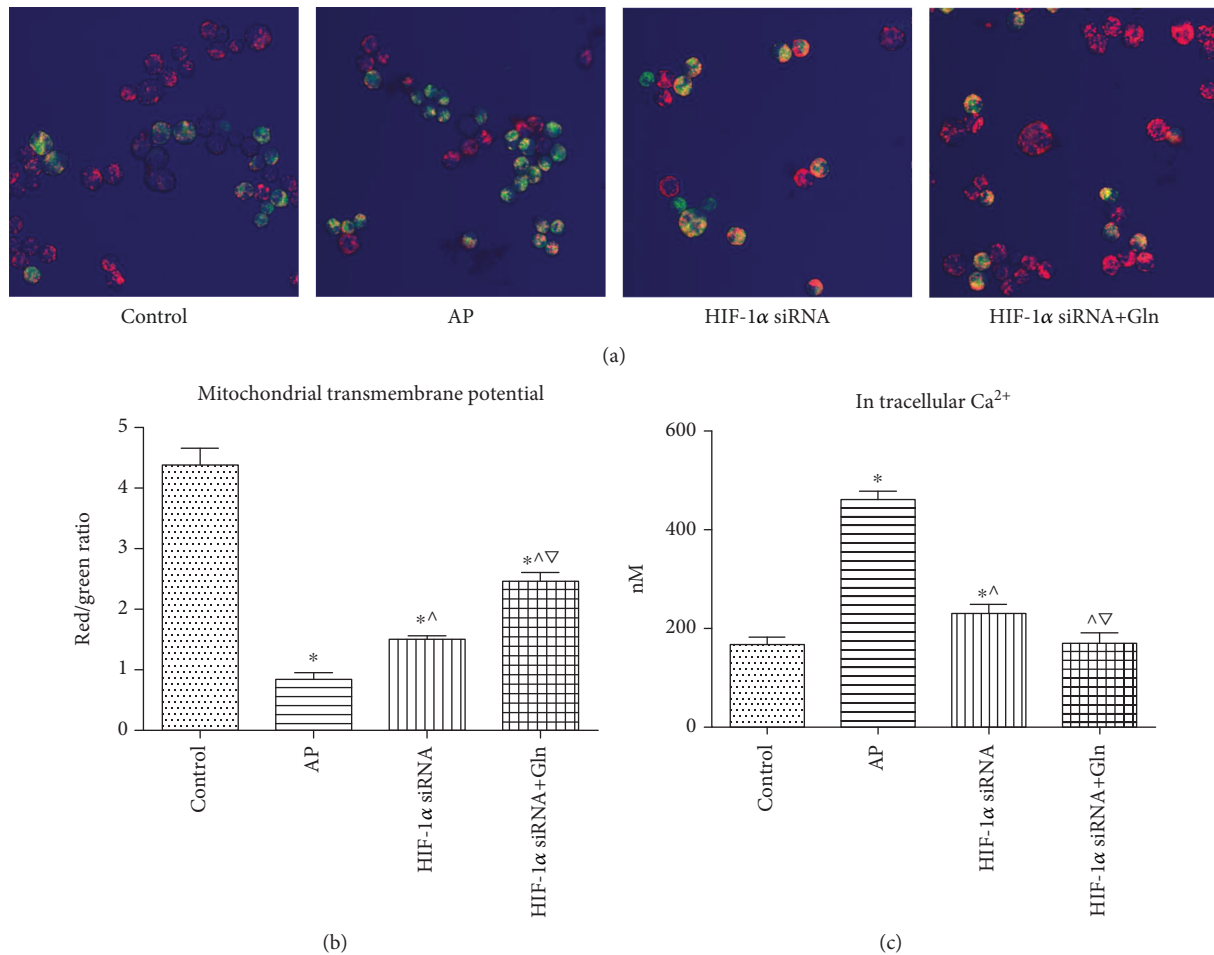


FIGURE 7: HIF-1 α knockdown prevented the increase in the intracellular Ca²⁺ concentration and the decrease in the mitochondrial membrane potential in AR42J cells after AP induction, and these effects were enhanced when Gln was administered concomitantly. (a and b) Representative fluorescent images (a, 20x) indicative of intracellular mitochondrial potential by JC-1 staining in AR42J cells as described in Figure 6(a), and the ratio of red/green fluorescence (b) was calculated to indicate intracellular mitochondrial potential. (c) The intracellular concentration of Ca²⁺ in AR42J as described in Figure 6(a). Data were presented as mean \pm SD ($n = 3$). * $P < 0.05$ versus sham, ^ $P < 0.05$ versus AP, and $\nabla P < 0.05$ versus HIF-1 α siRNA. Abbreviations: AP: acute pancreatitis; Gln: glutamine; HIF-1 α : hypoxia-inducible factor-1 α ; SD: standard deviation.

Recently, accumulating evidence has suggested that the balance between apoptosis and necrosis influences the severity of AP [40, 52]. The promotion of apoptosis ameliorates AP-related injuries and *vice versa* [7, 53]. We therefore considered that the energy metabolism pathway within pancreatic acinar cells might be a promising focus in the pathogenesis of AP.

There are two main aspects to the function of HIF-1 α [54]. First, HIF-1 α modulates intracellular glucose metabolism by promoting glycolysis and inhibiting oxidative phosphorylation. Second, HIF-1 α enhances the tissue oxygen concentration through vasodilation by the induction of inducible nitric oxide synthetase (iNOS) and endothelin-1 (ET-1) and by increasing the erythrocyte concentration through the upregulation of erythropoietin (EPO) [55]. Both our present results and previous findings suggested that the expression of HIF-1 α was upregulated within acinar cells after AP induction [43, 56]. However, the regulatory effects of HIF-1 α in AP are poorly understood. In

the present study, HIF-1 α knockdown ameliorated the acinar cell injuries, suppressed the overwhelming inflammatory response, and diminished the necrotic area in the pancreas, but increased the acinar cells apoptotic rate *in vivo*. Moreover, HIF-1 α knockdown ameliorated the cellular energy metabolism stress and maintained the concentration of Ca²⁺ and the stability of the mitochondria *in vitro*. In general, our results indicated that HIF-1 α knockdown attenuated the predominance of necrosis over apoptosis after the attack of AP.

Gln is an important energy substance in the body. It has a powerful glycemic effect which can provide sufficient substrates for oxidative phosphorylation of the cells. Gln can be administered to maintain gut integrity and ameliorate the inflammatory response in AP [17–19]. Our results indicated that Gln supplementation in addition to HIF-1 α knockdown was more protective for the acinar cells from AP-related injuries than HIF-1 α knockdown alone was. Therefore, the combination of Gln supplementation and

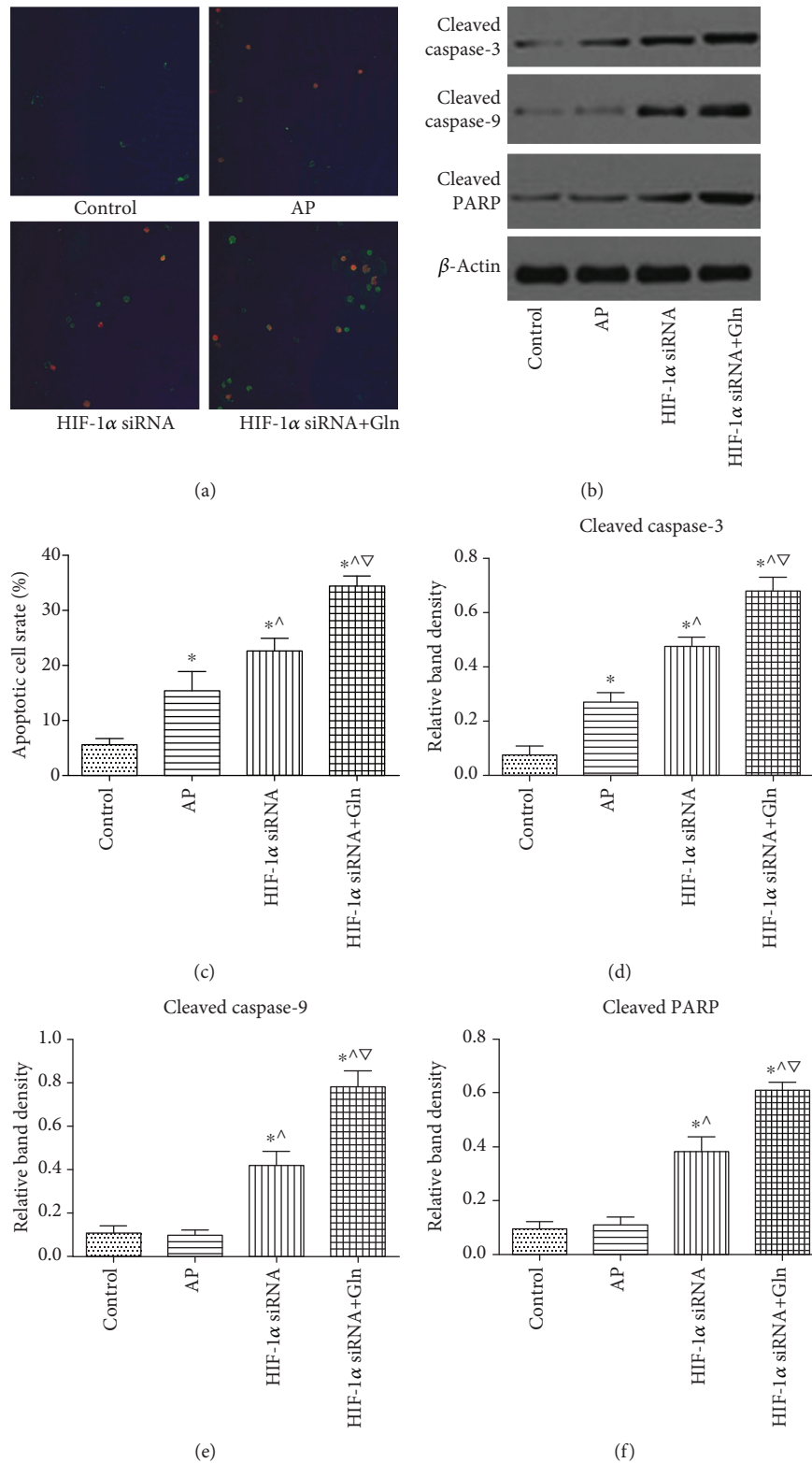


FIGURE 8: HIF-1 α knockdown decreased necrosis and increased apoptosis within AR42J cells after AP induction, and these effects were enhanced when Gln was administered concomitantly with HIF-1 α knockdown. (a and c) Representative fluorescent images (a, 10x) indicative of apoptotic activity by Annexin V and propidium iodide double-staining in AR42J cells as described in Figure 6(a), and the percentage of green cells (c) was calculated to assess the apoptotic cells rate. (b and d-f) Representative immunoblot images (b) and quantifications of cytoplasm cleaved caspase-3 (d), caspase-9 (e), and PARP (f) expression in AR42J cells as described in Figure 6(a). β -Actin was used as the protein loading control. Data were presented as mean \pm SD ($n = 3$). * $P < 0.05$ versus sham, ^ $P < 0.05$ versus AP, and $\nabla P < 0.05$ versus HIF-1 α siRNA. Abbreviations: AP: acute pancreatitis; Gln: glutamine; HIF-1 α : hypoxia-inducible factor-1 α ; SD: standard deviation.

HIF-1 α knockdown might be a promising strategy in the future management of AP.

In this study, the application of HIF-1 α silencing combined with Gln supplementation could regulate the energy metabolism of the inflammatory acinar cells and promote their necrosis-to-apoptosis transformation, which has a potential clinical value for improving the prognosis of AP. In our opinion, the significance and advantages of this experiment are as follows: ①glycogenic oxidative phosphorylation is the main means by which acinar cells obtain ATP to maintain their physiological function. However, the massive activation of HIF-1 α during AP significantly inhibits the cellular oxidative phosphorylation of glycogen. Consequently, glycolysis becomes the major pathway for acinar cells to obtain ATP. Glycolysis is a form of energy metabolism with high consumption and low output, which can only maintain the cell energy supply over a limited time course. Continuous and excessive glycolysis leads to the accumulation of its end-product, lactic acid, which causes cellular acidosis and further significant damages to the structure and function of the cells. In addition, the disturbance of the pancreatic microcirculation in AP leads to the lack of adequate supply of glycogen in local pancreatic tissues, which accelerates the depletion of glycogen in acinar cells and eventually induces the depletion of ATP as the result of an increased anaerobic glycolysis capacity associated with “no glucose for glycolysis.” Therefore, it is not the best compensatory mechanism to regulate energy metabolism through enhancing glycolysis of the acinar cells by activated HIF-1 α . Inhibiting the activation of HIF-1 α to avoid the waste of glycogen and permit the limited glycogen supply to undergo oxidative phosphorylation may turn out to be more favorable by allowing the acinar cells to continuously produce enough ATP and thus accelerate the necrosis-to-apoptosis transformation. ② HIF-1 α can not only inhibit the mitochondrial tricarboxylic acid cycle by activating pyruvate dehydrogenase kinase-1 [30] but also suppress the mitochondrial respiratory function by upregulating iNOS to induce massive synthesis of NO [9, 57]. Therefore, inhibition of HIF-1 α activation could allow the full use of a limited oxygen supply to enhance mitochondrial oxidative phosphorylation which would result in the production of sufficient ATP. ③ Downregulation of HIF-1 α expression could effectively improve pancreatic microcirculatory dysfunction by suppressing the synthesis of EPO and ET-1, which would increase the glycogen supply and oxygen content in acinar cells with the results that the mitochondrial oxidative phosphorylation process would be enhanced. ④ Traditional apoptosis inducers are nonselective and might simultaneously induce apoptosis of both damaged and normal acinar cells. Clearly, inducing normal acinar cell apoptosis would further impair the physiological function of the pancreas and aggravate AP. In this study, on the one hand, the acinar cells in which we increased the ATP contents by the combination of HIF-1 α silencing and Gln supplementation were mainly the injured acinar cells, and this treatment had no harmful effect on the normal cells. Therefore, this therapy could protect the physiological function of the pancreas to the maximum extent by endowing the apoptosis induction with certain selectivity, thus avoiding excessive

apoptosis and extra damage to the pancreas. On the other hand, obtaining sufficient ATP in the normal acinar cells is an important guarantee to maintain their physiological function, which can enhance their ability to resist inflammatory attack. Therefore, the design of this study might achieve the dual effects of “treatment and prevention.”

5. Conclusion

In conclusion, the present study highlights the promising effects of Gln-supplemented HIF-1 α knockdown in the management of AP. The underlying mechanisms may be attributed to the amelioration of intracellular energy stress through the maintenance of mitochondrial homeostasis and prevention of intracellular Ca²⁺ overload, which result in the attenuation of the predominance of necrosis over apoptosis.

Data Availability

The data used to support the findings of this study are included within the article.

Conflicts of Interest

The authors declare that there is no conflict of interest regarding the publication of this paper.

Authors' Contributions

Liang Ji, Xiaoyu Guo, and Jiachen Lv contributed equally to this article.

Acknowledgments

This paper was supported by grants from the National Natural Science Foundation of China (Nos. 81100314 and 81770639), innovative research funds of the No. 1 Affiliated Hospital of Harbin Medical University (2018BS013), Heilongjiang Postdoctoral Fund (LBH-Z18131), and Heilongjiang Scientific Fund for Institutions of Higher Education (hosted by Liang Ji, no grant number available yet).

References

- [1] J. E. Everhart and C. E. Ruhl, “Burden of digestive diseases in the United States Part III: liver, biliary tract, and pancreas,” *Gastroenterology*, vol. 136, no. 4, pp. 1134–1144, 2009.
- [2] I. Gukovsky, S. J. Pandol, and A. S. Gukovskaya, “Organellar dysfunction in the pathogenesis of pancreatitis,” *Antioxidants & Redox Signaling*, vol. 15, no. 10, pp. 2699–2710, 2011.
- [3] R. P. Sah, P. Garg, and A. K. Saluja, “Pathogenic mechanisms of acute pancreatitis,” *Current Opinion in Gastroenterology*, vol. 28, no. 5, pp. 507–515, 2012.
- [4] W. Huang, D. M. Booth, M. C. Cane et al., “Fatty acid ethyl ester synthase inhibition ameliorates ethanol-induced Ca²⁺-dependent mitochondrial dysfunction and acute pancreatitis,” *Gut*, vol. 63, no. 8, pp. 1313–1324, 2014.
- [5] D. E. Goldenberg, S. R. Gordon, and T. B. Gardner, “Management of acute pancreatitis,” *Expert Review of Gastroenterology & Hepatology*, vol. 8, no. 6, pp. 687–694, 2014.

- [6] P. G. Lankisch, M. Apte, and P. A. Banks, "Acute pancreatitis," *The Lancet*, vol. 386, no. 9988, pp. 85–96, 2015.
- [7] O. A. Mareninova, K. F. Sung, P. Hong et al., "Cell death in pancreatitis: caspases protect from necrotizing pancreatitis," *Journal of Biological Chemistry*, vol. 281, no. 6, pp. 3370–3381, 2006.
- [8] A. Iida, H. Yoshidome, T. Shida et al., "Does prolonged biliary obstructive jaundice sensitize the liver to endotoxemia?," *Shock*, vol. 31, no. 4, pp. 397–403, 2009.
- [9] D. M. Booth, J. A. Murphy, R. Mukherjee et al., "Reactive oxygen species induced by bile acid induce apoptosis and protect against necrosis in pancreatic acinar cells," *Gastroenterology*, vol. 140, no. 7, pp. 2116–2125, 2011.
- [10] M. Ripoli, A. D'Aprile, G. Quarato et al., "Hepatitis C virus-linked mitochondrial dysfunction promotes hypoxia-inducible factor 1 α -mediated glycolytic adaptation," *Journal of Virology*, vol. 84, no. 1, pp. 647–660, 2010.
- [11] T. Sakamoto and M. Seiki, "A membrane protease regulates energy production in macrophages by activating hypoxia-inducible factor-1 via a non-proteolytic mechanism," *Journal of Biological Chemistry*, vol. 285, no. 39, pp. 29951–29964, 2010.
- [12] J. Mateo, M. García-Lecea, S. Cadenas, C. Hernández, and S. Moncada, "Regulation of hypoxia-inducible factor-1 α by nitric oxide through mitochondria-dependent and -independent pathways," *Biochemical Journal*, vol. 376, no. 2, pp. 537–544, 2003.
- [13] G. Wang, J. C. Iv, L. F. Wu, L. Li, D. L. Dong, and B. Sun, "From nitric oxide to hyperbaric oxygen: Invisible and Subtle but Nonnegligible Gaseous Signaling Molecules in Acute Pancreatitis," *Pancreas*, vol. 43, no. 4, pp. 511–517, 2014.
- [14] G. Gomez, E. W. Englander, G. Wang, and G. H. Greeley Jr, "Increased expression of hypoxia-inducible factor-1 α , p48, and the Notch signaling cascade during acute pancreatitis in mice," *Pancreas*, vol. 28, no. 1, pp. 58–64, 2004.
- [15] S. C. Blass, H. Goost, R. H. Tolba et al., "Time to wound closure in trauma patients with disorders in wound healing is shortened by supplements containing antioxidant micronutrients and glutamine: a PRCT," *Clinical Nutrition*, vol. 31, no. 4, pp. 469–475, 2012.
- [16] P. E. Wischmeyer, "Glutamine: mode of action in critical illness," *Critical Care Medicine*, vol. 35, no. 9, pp. S541–S544, 2007.
- [17] E. Alhan, A. Usta, S. Türkyılmaz, B. V. Kural, and C. Ercin, "Effects of glutamine alone on the acute necrotizing pancreatitis in rats," *Journal of Surgical Research*, vol. 193, no. 1, pp. 161–167, 2015.
- [18] T. Han, X. L. Li, D. L. Cai, Y. Zhong, and S. S. Geng, "Effects of glutamine-supplemented enteral or parenteral nutrition on apoptosis of intestinal mucosal cells in rats with severe acute pancreatitis," *European Review for Medical and Pharmacological Sciences*, vol. 17, no. 11, pp. 1529–1535, 2013.
- [19] B. A. Mizock, "Immunonutrition and critical illness: an update," *Nutrition*, vol. 26, no. 7-8, pp. 701–707, 2010.
- [20] K. A. Kudsk, "Glutamine: more evidence, more promise," *Journal of Parenteral and Enteral Nutrition*, vol. 32, no. 4, pp. 492–494, 2008.
- [21] G. Wang, B. Han, H. Zhou et al., "Inhibition of hydrogen sulfide synthesis provides protection for severe acute pancreatitis rats via apoptosis pathway," *Apoptosis*, vol. 18, no. 1, pp. 28–42, 2013.
- [22] J. Fan, G. Li, L. Wu et al., "Parenteral glutamine supplementation in combination with enteral nutrition improves intestinal immunity in septic rats," *Nutrition*, vol. 31, no. 5, pp. 766–774, 2015.
- [23] J. Fan, L. Wu, G. Li et al., "Effects of enteral nutrition with parenteral glutamine supplementation on the immunological function in septic rats," *British Journal of Nutrition*, vol. 113, no. 11, pp. 1712–1722, 2015.
- [24] X. Bai, Z. Song, Y. Zhou et al., "The apoptosis of peripheral blood lymphocytes promoted by hyperbaric oxygen treatment contributes to attenuate the severity of early stage acute pancreatitis in rats," *Apoptosis*, vol. 19, no. 1, pp. 58–75, 2014.
- [25] A. M. Kusske, A. J. Rongione, S. W. Ashley, D. W. McFadden, and H. A. Reber, "Interleukin-10 prevents death in lethal necrotizing pancreatitis in mice," *Surgery*, vol. 120, no. 2, pp. 284–289, 1996.
- [26] K. Kang, M. Zhao, H. Jiang, G. Tan, S. Pan, and X. Sun, "Role of hydrogen sulfide in hepatic ischemia-reperfusion-induced injury in rats," *Liver Transplantation*, vol. 15, no. 10, pp. 1306–1314, 2009.
- [27] L. Ji, L. Li, F. Qu et al., "Hydrogen sulphide exacerbates acute pancreatitis by over-activating autophagy via AMPK/mTOR pathway," *Journal of Cellular and Molecular Medicine*, vol. 20, no. 12, pp. 2349–2361, 2016.
- [28] K. A. Muili, D. Wang, A. I. Orabi et al., "Bile acids induce pancreatic acinar cell injury and pancreatitis by activating calcineurin," *Journal of Biological Chemistry*, vol. 288, no. 1, pp. 570–580, 2013.
- [29] B. W. Carey, L. W. S. Finley, J. R. Cross, C. D. Allis, and C. B. Thompson, "Intracellular α -ketoglutarate maintains the pluripotency of embryonic stem cells," *Nature*, vol. 518, no. 7539, pp. 413–416, 2015.
- [30] M. M. Rogero, P. Borelli, R. A. Fock et al., "Effects of glutamine on the nuclear factor-kappaB signaling pathway of murine peritoneal macrophages," *Amino Acids*, vol. 39, no. 2, pp. 435–441, 2010.
- [31] C. S. K. Lee, B. C. K. Tong, C. W. H. Cheng, H. C. H. Hung, and K. H. Cheung, "Characterization of two-pore channel 2 by nuclear membrane electrophysiology," *Scientific Reports*, vol. 6, no. 1, article 20282, 2016.
- [32] G. Grynkiewicz, M. Poenie, and R. Y. Tsien, "A new generation of Ca²⁺ indicators with greatly improved fluorescence properties," *Journal of Biological Chemistry*, vol. 260, no. 6, pp. 3440–3450, 1985.
- [33] A. Korenić, J. Boltze, A. Deten, M. Peters, P. Andjus, and L. Radenović, "Astrocytic mitochondrial membrane hyperpolarization following extended oxygen and glucose deprivation," *PLoS One*, vol. 9, no. 2, article e90697, 2014.
- [34] M. Bhatia, F. L. Wong, Y. Cao et al., "Pathophysiology of acute pancreatitis," *Pancreatology*, vol. 5, no. 2-3, pp. 132–144, 2005.
- [35] A. S. Gukovskaya, O. A. Mareninova, I. V. Odinkova et al., "Cell death in pancreatitis: effects of alcohol," *Journal of Gastroenterology and Hepatology*, vol. 21, Supplement 3, pp. S10–S13, 2006.
- [36] I. V. Odinkova, K. F. Sung, O. A. Mareninova, K. Hermann, I. Gukovsky, and A. S. Gukovskaya, "Mitochondrial mechanisms of death responses in pancreatitis," *Journal of Gastroenterology and Hepatology*, vol. 23, Supplement 1, pp. S25–S30, 2008.

- [37] H. Ardehali, "Cytoprotective channels in mitochondria," *Journal of Bioenergetics and Biomembranes*, vol. 37, no. 3, pp. 171–177, 2005.
- [38] J. Maleth, V. Venglovecz, Z. Razga, L. Tiszlavicz, Z. Rakoncay, and P. Hegyi, "Non-conjugated chenodeoxycholate induces severe mitochondrial damage and inhibits bicarbonate transport in pancreatic duct cells," *Gut*, vol. 60, no. 1, pp. 136–138, 2011.
- [39] P. Golstein and G. Kroemer, "Cell death by necrosis: towards a molecular definition," *Trends in Biochemical Sciences*, vol. 32, no. 1, pp. 37–43, 2007.
- [40] A. S. Gukovskaya and S. J. Pandol, "Cell death pathways in pancreatitis and pancreatic cancer," *Pancreatology*, vol. 4, no. 6, pp. 567–586, 2004.
- [41] W. Halangr, R. Matthias, L. Schild, F. Meyer, H. U. Schulz, and H. Lippert, "Effect of supramaximal cerulein stimulation on mitochondrial energy metabolism in rat pancreas," *Pancreas*, vol. 16, no. 1, pp. 88–95, 1998.
- [42] D. N. Criddle, J. Murphy, G. Fistetto et al., "Fatty acid ethyl esters cause pancreatic calcium toxicity via inositol trisphosphate receptors and loss of ATP synthesis," *Gastroenterology*, vol. 130, no. 3, pp. 781–793, 2006.
- [43] S. Orrenius, B. Zhivotovsky, and P. Nicotera, "Regulation of cell death: the calcium-apoptosis link," *Nature Reviews Molecular Cell Biology*, vol. 4, no. 7, pp. 552–565, 2003.
- [44] J. V. Gerasimenko, O. V. Gerasimenko, A. Palejwala, A. V. Tepikin, O. H. Petersen, and A. J. Watson, "Menadione-induced apoptosis: roles of cytosolic Ca^{2+} elevations and the mitochondrial permeability transition pore," *Journal of Cell Science*, vol. 115, Part 3, pp. 485–497, 2002.
- [45] G. Hajnoczky, L. D. Robb-Gaspers, M. B. Seitz, and A. P. Thomas, "Decoding of cytosolic calcium oscillations in the mitochondria," *Cell*, vol. 82, no. 3, pp. 415–424, 1995.
- [46] R. F. Feissner, J. Skalska, W. E. Gaum, and S. S. Sheu, "Cross-talk signaling between mitochondrial Ca^{2+} and ROS," *Frontiers in Bioscience*, vol. 14, no. 1, pp. 1197–1218, 2009.
- [47] S. G. Voronina, S. L. Barrow, A. W. M. Simpson et al., "Dynamic changes in cytosolic and mitochondrial ATP levels in pancreatic acinar cells," *Gastroenterology*, vol. 138, no. 5, pp. 1976–1987.e5, 2010.
- [48] J. Marx, E. Pretorius, and M. J. Bester, "Effects of *Urginea sanguinea*, a traditional asthma remedy, on embryo neuronal development," *Journal of Ethnopharmacology*, vol. 104, no. 3, pp. 315–321, 2006.
- [49] D. N. Criddle, J. V. Gerasimenko, H. K. Baumgartner et al., "Calcium signalling and pancreatic cell death: apoptosis or necrosis?," *Cell Death & Differentiation*, vol. 14, no. 7, pp. 1285–1294, 2007.
- [50] J. Marx, E. Pretorius, and M. Bornman, "The neurotoxic effects of prenatal cardiac glycoside exposure: a hypothesis," *Neurotoxicology and Teratology*, vol. 28, no. 1, pp. 135–143, 2006.
- [51] N. Miyoshi, H. Oubrahim, P. B. Chock, and E. R. Stadtman, "Age-dependent cell death and the role of ATP in hydrogen peroxide-induced apoptosis and necrosis," *Proceedings of the National Academy of Sciences of the United States of America*, vol. 103, no. 6, pp. 1727–1731, 2006.
- [52] M. Bhatia, "Apoptosis of pancreatic acinar cells in acute pancreatitis: is it good or bad?," *Journal of Cellular and Molecular Medicine*, vol. 8, no. 3, pp. 402–409, 2004.
- [53] M. Bhatia, M. A. Wallig, B. Hofbauer et al., "Induction of apoptosis in pancreatic acinar cells reduces the severity of acute pancreatitis," *Biochemical and Biophysical Research Communications*, vol. 246, no. 2, pp. 476–483, 1998.
- [54] C. J. Schofield and P. J. Ratcliffe, "Oxygen sensing by HIF hydroxylases," *Nature Reviews Molecular Cell Biology*, vol. 5, no. 5, pp. 343–354, 2004.
- [55] J. Schödel, D. R. Mole, and P. J. Ratcliffe, "Pan-genomic binding of hypoxia-inducible transcription factors," *Biological Chemistry*, vol. 394, no. 4, pp. 507–517, 2013.
- [56] X. Bai, B. Sun, S. Pan et al., "Down-regulation of hypoxia-inducible factor-1alpha by hyperbaric oxygen attenuates the severity of acute pancreatitis in rats," *Pancreas*, vol. 38, no. 5, pp. 515–522, 2009.
- [57] P. Nicotera and G. Melino, "Regulation of the apoptosis-necrosis switch," *Oncogene*, vol. 23, no. 16, pp. 2757–2765, 2004.